THE MECHANICS OF CONTINUOUS ROLLER BENDING OF PLATES

MENG HUA

DOCTOR OF PHILOSOPHY

Faculty of Engineering

Department of Mechanical and Production Engineering

The University of Aston in Birmingham

August, 1986

THE UNIVERSITY OF ASTON IN BIRMINGHAM
Department of Mechanical and Production Engineering

THE MECHANICS OF CONTINUOUS ROLLER BENDING OF PLATES

Submitted in fulfilment of the requirements
for the degree of Doctor of Philosophy

Author : MENG HUA Year : 1986

Summary

This research initiates a study of the mechanics of four roll plate bending and provides a methodology to investigate the process experimentally. To carry out the research a suitable model bender was designed and constructed. The model bender was comprehensively instrumented with ten load cells, three torquemeters and a tachometer.

A rudimentary analysis of the four roll pre-bending mode considered the three critical bending operations. The analysis also gave an assessment of the model bender capacity for the design stage. The analysis indicated that an increase in the coefficient of friction in the contact region of the pinch rolls and the plate would reduce the pinch resultant force required to bend a plate to a particular bend radius.

The mechanisms involved in the four roll plate bending process were investigated and a mathematical model evolved to determine the mechanics of four roll thin plate bending.

A theoretical and experimental investigation was conducted for the bending of HP30 aluminium plates in both single and multipass bending modes. The study indicated that the multipass plate bending mechanics of the process varied according to the number of bending passes executed and the step decrement of the anticipated finished bend radius in any two successive passes (i.e. the bending route).

Experimental results for single pass bending indicated that the rollers normally exert a higher bending load for the steady-continous bending with the pre-inactive side roll operative. For the pre-bending mode and the steady-continous bending mode with the pre-active side roll operative, the former exerted the higher loads. The single pass results also indicated that the force on the side roll, the torque and power steadily increased as the anticipated bend radius decreased.

Theoretical predictions for the plate internal resistance to accomplish finished bend radii of between 2500mm and 500mm for multipass bending HP30 aluminium plates, suggested that there was a certain bending route which would effectively optimise the bender capacity.

Key words : **Continuous roller plate bending,
Bender design and instrumentation,
Elastic-elastoplastic deformation.
Single / multi pass bending modes.**

CONTENTS

CHAPTER THREE

DESIGN OF MODEL BENDER

CHAPTER FOUR

INSTRUMENTATION AND CALIBRATIONS

CHAPTER FIVE

THEORETICAL ANALYSIS AND RESULTS

CHAPTER SIX

MATERIAL PROPERTIES AND PERIPHERAL INVESTIGATION

CHAPTER SEVEN

EXPERIMENTAL PROCEDURE AND RESULTS

CHAPTER EIGHT

OBSERVATION AND DISCUSSION

CHAPTER NINE

CONCLUSIONS

CHAPTER TEN

SUGGESTIONS FOR FURTHER WORK

APPENDIX 3.1

PART DETAIL DESCRIPTIONS AND ITEM DRAWINGS OF THE MODEL BENDER UNIT

APPENDIX 6.1

SURFACE FINISH MEASUREMENTS FOR ROLLERS AND BEND PLATE SPECIMENS

APPENDIX 7.1

DERIVATION OF THE EMPIRICAL EXPRESSIONS FOR SPRINGBACK AND BEND RADIUS ANALYSIS FOR THIN PLATE BENDING MODES

LIST OF FIGURES

LIST OF DRAWING ITEMS FOR MODEL BENDER

LIST OF TABLES

NOMENCLATURE

General symbols

a, b = Constants for the equation of the torque calibraion.

a, h = Semi-thickness of a plate.

a_0 = $(\sqrt{3})/2$

= Pre-springback local bend radius at the commencement of the first yield in the longitudinal direction of a plate.

a_1, a_2 = Constants in equation (2.8).

a, b, c, d = Respective parametric functions, for each bending mode, in the plate deflection function, $W(x)$.

$\mathring{a}$ = Dimensionless ratio of plate/beam deflection, δ, to its bend radius R (see equation (3.1))

A = $\int_{elastic} \sigma_x z dz$, the internal elastic bending resistance per unit plate width for the single and first pass bending operation.

A_1 = Fully internal elastic bending resistance per unit width in the plate central core at the top roll contact (multipass bending).

A_2 = Internal elatoplastic bending resistance per unit width in the thickness of the plate at the top roll contact (multipass bending).

A_r = Reduction of the cross-sectional area of a plate.

A, C_{ijkl}, D_{ijklmn} = Coefficients of an anisotropic material as used in equation (A2.5).

b = breadth of a beam or indentation platen, or the width of a bendplate

B = $\int_{elastoplastic} \sigma_x z dz$, i.e. the internal elastoplastic bending reistance per unit width for the first and single pass bending analysis.

β = Rotational angle of a plate during bending.
= A variable in equation (A2.18).
= Displacement (positional powering) angle of the side roll hydraulic cylinder for a critical operation in fig 3.2.

c = Distance of elastic-plastic interface from plate/beam neutral or central axis as defined in Chapter 3.

c, d = Constants for the equation of the top roll speed calibration.

c_i = Distance of the elastic-elastoplastic interface from the neutral (or central) plane of a bendplate for the first and single pass bending analysis.

c_{i0} = Distance of the elastic-elastoplastic interface from the neutral (or cental) plane of a bendplate for the second and subsequent pass bending analysis.

c_0 = $[(\bar{\sigma}_e - \sigma_0)/H]^{1/n}$ for the second and subsequent pass bending analysis.

d = Depth of a beam or diameter of a rod/roll.

D_{ti} = Depth of the plastic deformation of a bendplate, where i=1,2.. etc..

D_T = Total increment of the platstic deformation depth in the thickness of a bendplate.

δ = Deflection of a beam/rod.
= Small increment of a variable.

δ_{ij} = Kronecker delta

e = Engineering strain.

e_1, e_2, e_3, e_4 = Strain measured in the strain gauge number 1, 2, 3 and 4, respectively.

e_x, e_y, e_z = Engineering and elastic strain in the x, y and z direction, respectively, in the co-ordinate system of a bendplate.

$_xe_0, e_{x0}$ = Longitudinal engineering and elastic strain at the yield point.

e_{ij}, ε_{ij} = Engineering and true strain tensor, respectively.

ε = True strain or effective (uniaxial tensile) strain.

$\varepsilon^p_{ij}, \varepsilon_i{}^p$ = Plastic strain tensor.

$\varepsilon^e_{ij}, \varepsilon_i{}^e$ = Elastic strain tensor, where i=x,y,z and j=1,2,3, ...

$\varepsilon_0, \varepsilon_0{}^e$ = Effective (or uniaxial tensile) strain at the first yield.

$\varepsilon_x, \varepsilon_y, \varepsilon_z$ = True strain in X, Y and Z direction, respectively, of a bendplate

ε_{x10} = Longitudinal strain on the fibre layer at the elastic-elastoplastic interface.

ε_{x0} = Longitudinal yield strain corresponding to σ_{x0}.

ε_t = Total effective (uniaxial tensile) strain.

$\delta\varepsilon_i$ = Tensor for incremental strain, where i=x, y and z.

$\delta\varepsilon_i^e$ = Tensor for incremental elastic strain, where i=x, y and z.

$\delta\varepsilon_i^p$ = Tensor for incremental plastic strain, where i=x, y and z.

$\Delta\varepsilon_t$, $\Delta\varepsilon$ = Discrete total incremental strain.

$\Delta\varepsilon^e$, $\Delta\varepsilon_e^e$ = Discrete incremental effective elastic strain.

$\Delta\varepsilon^p$, $\Delta\varepsilon_e^p$ = Discrete incremental effective plastic strain.

E = Young's modulus.
= Electric potential.

E_{bd} = Potential difference across the junctions b and d in an electric circuit.

F = Force (applied load), or strain gauge factor.

F_a, F_b = Component of the axial and bending force respectively.

F_h, F_v = Horizontal and vertical force component respectively.

F_p = Pinch force.

F_s, F_t, F_b = Resultant-bending force on the operative top and bottom roll, respectively.

$F_1, F_2, F_3, F_4, \ldots$ = Gauge factor for the strain gauge 1, 2, 3, and 4, ..., respectively.

F,G,H,L,M,N = Parametric characteristics of an anisotropic material at the current loading state [see equation (6.2)].

f = A yield function.

f_0 = $(r_f/R)-1$

for the second and subsequent pass bending mode.

$f(\sigma_{ij})$ = Stress-strain relationship defined as in equation (6.2) for the anisoptropic material

g = $[(1-\nu^2)\bar{\sigma}]/[E(1-\nu+\nu^2)^{1/2}]$

for the first and single pass bending mode.

= $[(1-\nu^2)\bar{\sigma}_e]/[E(1-\nu+\nu^2)^{1/2}$

$-\{[3(1-\nu)/2(1-\nu+\nu^2)^{1/2}-(\sqrt{3}/2)]\{\bar{\sigma}_e-\sigma_0)/E\}$

for the second and subsequent pass bending mode.

G = Modulus of rigidity of a material.

γ, τ = Shear strain and stress respectively.

h = Semi-thickness of a bendplate.
= Depth of a sectorial base as in equation (4.8).

H = Material hardening constant

$H(\sigma_1, \sigma_2, \sigma_3)$ = A function of the principal stresses, σ_1, σ_2 and σ_3.

H_b, V_b = Component of the horizontal and vertical force , respectively, measured by the bottom loadcell.

H_s, V_s = Component of the horizontal and vertical force , respectively, measured by the side roll loadcell.

H_t, V_t = Component of the horizontal and vertical force , respectively, measured by the top roll loadcell

i = Electical current in a strain gauge bridge.

I, I = Second moment of the cross-sectional area of a beam/plate and loadcell.

J_2, J_3 = Second and third invariants of the stresses.

k = Shear stress at yield.

K, K_1 = $(H/E)\{[3(1-\nu)/2(1-\nu+\nu^2)^{1/2}]-(\sqrt{3})/2\}$

K = A dimensionless ratio defined as used in equation 3.11)

L = Length of a beam/plate, rod and the base of a sector, respectively.

L_a, L_s, L_d = Length of the u.v. traces during the period of the acceleration, the steadily driving condition and the deceleration, respectively.

L_g = Bending arm of the counter bending moment.

M = Bending moment

M_i = Internal bending resistance of the plate at the top roll contact.

M_e, M_t = External bending moment about the top roll contact.

M_x = Bending moment in any cross sectional area x away from the origin of the co-ordinate system.

μ = Coefficient of friction

μ, ν = Lode variables defined as in equations (A2.17) and (A2.18) respectively

n = Material hardening index.
= An integer in a summation series.

N_s = Bending load measured by the side roll loadcell

ν = Poisson's ratio.

O_t, O_b, O_s = Centre of the top, the bottom and the side roll, respectively, in the co-ordinate system

O_p = Centre of the positional powering direction of the side roll hydraulic cylinder.

O_c = centre of the contact of the side roll and the bendplate.

ω = Rotational speed of the top roll

ω_0 = Chart length at the reference point for the tachometer signal.

ω_r = Chart length for the tachometer signal.

P = Power.

P_m = Measured power at the mean torque.

P_s = Axial load measured by the side roll loadcell

ϕ = Stress function

q = Unit load on the top surface of a plate.

θ = Angle subtended by the arc of a bend.
= Contact angle between the rollers and the bendplate.
= Angle of rotation.

θ_{si} = Initial side roll contact angle with a curved plate.
= Positional powering angle of the operative side roll.

θ_{sm} = Maximum contact angle of the side roll and the bendplate.

r = Radius of the rolls (or rod and loadcell).

r_f = Finshed bend radius of the single/first pass bending operation.
= Initial radius of a bendplate before commencing the second, the third and the subsequent bending pass.

r_{ff} = Finished plate bent radius of the second, the third and the subsequent bending pass.

r_{fi} = Finished inner bend radius of the bentplate.

r_i, r_0 = Inner and outer radius, respectively, of a cylinder (or tube).

r_t, r_b, r_s = Radius of the top roll, the bottom roll and the side roll, respectively.

R = Instantaneous local bend radius of a plate/beam.
= Resistance in an electrical circuit.

R_{bj} = Equivalent resistance in each strain gauge bridge

R_y = Radius of curvature as yield first occurs on the outer fibre of a bend beam/plate.

R_1, R_2, R_3, R_4, R_5, R_6, R_7, R_8 = Resistance for the strain gauge 1, 2, 3, 4, 5, 6, 7 and 8, respectively, in a bridge circuit.

R_1, R_{1st} = Bend radius at the first yield for the second and the subequent pass bending mode.

S = Length of an arc or a curve
= Surface area of a body

σ = Stress.

σ_{ij} = Stress tensor

σ_x, σ_y, σ_z = Stress in the respective x, y and z direction.

σ_{x0} = Longitudinal stress at the first yield condition

$\bar{\sigma}$ = Effective (uniaxial tensile) stress

$\bar{\sigma}_e$ = Instantaneous first yield stress for the second and the subsequent passes bending mode.

$\bar{\sigma}_{em}$ = Mean instantaneous first yield stress in the elastoplastic deformation zone of a bendplate.

σ_0 = Uniaxial tensile (effective) stress at the commencement of the first yield.

$\Delta\bar{\sigma}$ = Discrete incremental stress

t = Plate thickness
= Time.

T = Torque.

T_b = Equivalent driving torque.

T_d = Driving torque.

T_l = Maximum position of the measured torque signal on a u.v. chart

T_m, T_{max} = Mean and maximum torque, respectively, measured by the torquemeter

T_r = Mean position of the u.v. chart oscilation for the torque signal.

T_0 = Initially set u.v. chart reference point for the torque signal.

u = Longitudinal displacement function of a bendplate.
= Velocity.

U = Strain energy in a deformed plate

v = Displacement function along the direction of the plate width.

V = Volume of a body.
= Velocity.
= Voltage.

V_{bj} = Individual bridge voltage supply

V_c = Chart speed of the u.v. recorder.

V_m = Main voltage supply

x, y, z = Length, width and thickness in the plate co-ordinate system.

x_i = Corresponding distance of x_{0i} after or at any instant of the bending

x_0 = Initial distance of the side roll centre to the origin of the bender co-ordinate system.

x_{0i} = Horizontal distance between the centres of the bottom pinch roll and the nominated active side roll prior to the bending operation.

Δx = Horizontal displacement of the nominated active side roll.

Y = Uniaxial tensile yield stress of a perfect plastic material.

y_i = Corresponding distance of the y_{0i} after or at any instant of the bending operation.

y_{0i} = Vertical distance from the centre of the active side roll to the bottom face of the model bender top beam prior to the bending operation.

y_∂ = Vertical distance of the initial centre of the active side roll to its contact point with the bendplate.

$y_{\partial n}$ = Net vertical displacement of the side roll.

Δy = Vertical displacement of the active side roll.

Δy_s = Measured value of Δy.

ψ, ψ' = Displacement (positional powering) angle of the side roll hydraulic cylinder.

W, W(x), W(x,y) = Deflection function of a plate.
= Displacement function in the thickness of a plate.

W_j = Displacement function as defined in (A2.30)

W = Work done.

z = Distance of a fibre layer from the neutral (or central) plane in the thickness of the plate.

dz = Change of the fibre distance from the neutral (or central) plane in the thickness of the plate.

Subscripts :

b = Bottom roll or bending
d = Driving
h = Horizontal component
m = Model
p = Prototype
s = Side roll
t = Top roll
v = Vertical component

Note :
Other symbols used in this thesis are defined as they appear

CHAPTER ONE

INTRODUCTION

1.1. Introduction

Cylindrical tube sections are widely used in most engineering structures, such as : pressure vessels, heat exchanger shells, boiler chambers, etc.. They also form the major structural skeleton of oil and gas rigs. Over the last few decades, the engineering application of tubular and semi-tubular structures has greatly increased. Further examples are where the civil engineering and building industries have utilised them in the construction of tunnels, commercial and industrial buildings etc..

Metal forming to produce a cylindrical tube is an art that has existed over a century. In general, the production of seamless tube can be carried out by punching or rotary piercing ingots or billets, followed by elongation of the formed hollow. However, this process is only suitable for producing small and medium diameter tubes. The manufacture of large diameter tubes usually involves a substantial tool inventory. Moreover, the initial piercing is neither economical nor practical for producing medium and large size tubulars. A more economical production process for the manufacture of various sizes of tubes is to fabricate them by welding together plates which have been bent to form cylindrical sections.

There are a number of existing techniques available for the bending of plates, such as : stamp-bending [73], stretch-bending [151] and pressbrake bending [103,115]. All the aforementioned techniques normally demand relatively heavy investments in tooling in order to bend the plate into tube sections of various radii. Another shortcoming of the above bending processes is the prolonged setting up time required for successive bending of two plates into different bend radii. Furthermore, their operational principles, the physical geometry of the toolings and the spring-back phenomenon are

such that these bending processes do not generally achieve a uniform bend radius in a finished bend sector. Consequently, a substantial amount of edge material may have to be machined off, which increases the cost of production. In addition, a completed tube, formed by any of the above processes, normally has two or more welded seams. These restrictions clearly indicate the deficiencies of the existing processes.

In plate forming industry, one of the most versatile pieces of equipment, particularly for bending tubular sections, is the roller bender.

The advantages of the roller bender over other plate bending equipment are as follows:

a- It can be used to bend a plate into many different sectional shapes, such as : elliptical, cylindrical, "rectangular", "square" and "triangular" tubulars.
b- It can bend plate to different diameter with a minimum diameter just larger than that of the top roll of the bender, for different plate thicknesses and widths.

By operating a roller bender, at its designed capacity, the necessity of using dies and punches, which are the basic requirements in most other bending processes, are eliminated. In addition, much greater finished dimensional accuracy can be achieved than that produced by the hammer and anvil method. Moreover, the machines only occupy a relatively small space on the shop-floor.

The appreciation of the advantages of the roller bending process, has seen the development of various types of these machines [37,38]. The three-roll pyramid bender appears to be the most common roll configuration. Due to the increasing demand for roller benders in the plate bending industry, numerous designs of the roller bender are now available. These

range from the various three-roll symmetrical and/or assymmetrical initial pinch machines, to different capacities of the four roll double-initial pinch machines. Each roll configuration of the bender is designed to perform a particular forming process. The four roll bender was developed to minimise the straight edge which often remains on bentplate, formed in the three-roll bending process. However, the three-roll bender can bend a thicker plate [37,38], etc.. It is noted that the evolution of the roller bender has also led to a number of two-roll benders being developed [143]. The practicability of the two-roll bender is still questionable, as it may require the installation of a number of bottom rollers.

The science of the roller bending of plates is out of step with the art of the roller bending machines. Despite the many varieties of benders, the normal practice of plate roller bending still relies heavily on the experience and the skill of the operator. Working to templates, or trial and error, still remains common practice in the industry. For this reason, most plate bending manufacturers experience low productivity, and are not able to make full use of the available equipment.

The increase in the use of tubular items and other similar engineering components, which are formed by roller benders, and the increasing competition from overseas, initiated this study of the mechanics of the process.

1.2. The objectives of the research

The mechanics of the roller bending of plates may include studies of the metallurgical aspect of a bendplate before and after the roller bending, the metallurgical interaction in the bendplate during bending, the forces on the rolls, the power

required to bend the plates for various working conditions, and the roll deflection phenomena and its effect on the finished product. Details of the residual stress distributions in the bentplate, its deviation during bending, and the springback characteristics of a bent plate may also be studied. However, it must be recognised that any successful research study must have its objectives clearly defined.

The objectives of the present research are as follows :

a- To produce a theory which will predict the forces and torques on the rolls, for bending plates with different thicknesses, widths and dissimilar yield stresses, and to different bend radii in the pre-bending and continuous bending condition. It also requires the derivation of a mathematical model which will predict the power required for each pass and for the complete bending process. The theories will also account for the deformation depth in each bending operation.

b- To collect systematically the bending data from the roller bending process in order to provide an insight into the actual mechanics of the process.

c- To design a satisfactory model bender for carrying out the experimental studies so as to achieve (b).

d- To produce a computer programme which may include all the parameters stated in (a).

In the plate bending production environment, the ultimate goals of these objectives are :

1- To optimise the bending process by reducing the passes required to bend a particular bend-radius of a plate.

2- To increase the product yield from the process.

3- To reduce the cost of the products by decreasing the overhead and operational costs.

4- To reduce the dependence on skilled labour for the

bending machine operation.

1.3. Outline of the research

The research began with the design and construction of a model bender (Chapter 3), which simulated most features of a four-roll Verrina bender at Head Wrightson Teesdale (HWT). The design of the model will also facilitate the investigation of the general mechanics of other roll bender configurations (See section 3.2). The design of the model bender was carried out after studies of the specifications of the Verrina bender at HWT, the preliminary analysis in pre-bending mode of the three assumed critical operations (See sections 3.3-3.4) of the bender and the model making analysis. The analyses provided a basis for estimating the parameters through a series of studies of the specifications of the Verrina bender at HWT.

Following the design of the model bender the appropriate instrumentation to measure the respective parameters was investigated and setup (Chapter 4). A series of preliminary calibrations (Chapter 4) and material property investigations (Chapter 6) were then performed . Subsequently, experiments to bend HP30 aluminium plates of 8 mm and 10.09 mm thick for 80 mm, 120 mm and 240 mm wide specimens, mostly in multipasses were carried out (Chapter 7). The main parameters to be investigated in the experimental study were the forces and the torques required to bend the plates to various finished bend radii. The corresponding length of the straight edge needed in the pre-bending for each bend was also measured for certain plate specimens.

A mathematical analysis was performed (Appendix 7.1) for studying empirically the springback after bending the thin plates. The empirical study will require the extraction of measurements from the experiment.

Prior to the mathematical modelling of the bending process, the mechanisms involved in the roller bending of plates were assessed (Chapter 5). This provided a means to produce an appropriate mathematical theory. A mathematical theory to confirm the objective (a), in section 1.2, for thin plate bending was also evolved (Chapter 5 and Appendix 5.1), and a corresponding computer programmes for

(i) predicting the internal resistance to external bending moment about the top roll nominal contact,

(ii) predicting the local bend radius at the top roll nominal contact,

and,

(iii) predicting the depth of elastoplastic deformation at the top roll contact, related to any expected finished bend radius of a bent plate, were produced.

1.4. Summary of research findings

The study clearly demonstrated the complexity of the mechanics of the roller bending of plates. Theoretical prediction and experimental data indicate that the multipass plate bending mechanics of the process varies according to the number of bending passes executed and the step decrement of the anticipated finished bend radius in any two successive passes. This is mainly due to the effect of initial geometry of a bend plate, the various degrees of springback curvature, the different magnitudes of plastic depth penetration through the plate thickness in successive bending passes, and the dissimilar propagation of the plastic deformation zone in the effective deformation zone during bending.

Experimental results confirmed the different bending mechanisms as visualised for the pre-bending active side roll operative mode and the pre-bending inactive side roll operative mode (see Chapter five).

Theoretical prediction, for multipass bending of HP30 aluminium plate specimens, suggests that there is a certain combination of number of pass and step decrement in the finished bend radius, in two successive bending passes, which is the most efficient.

CHAPTER TWO

LITERATURE SURVEY

2.1 Introduction

Although there is little research information on the roller bending of plates in the existing literature, numerous investigations on associated topics are available.

According to the proposed mechanisms of roller bending (section 5.2), the bending operation (fig 5.2) is closely related to the areas of :

(1) conventional plate bending analysis
and
(2) surface contact of a roller with
  i. a flat plate,
  ii. a curved plate.

Since a bent metal plate will only retain the required profile if permanent deformation has occurred, a knowledge of plasticity is thus required. Consequently, a systematic analysis of the bending process would necessitate a review of the following topics :

1. Introduction to plasticity (which is briefly reviewed in Appendix 2.1)
2. Roll bending
3. Plate/beam bending
4. Surface contact stress/friction

2.2. Roll Bending

When the versatility of the roller bender was recognised, numerous types were developed to meet the various production specifications. Their categories can basically be classified [38] as follows :

(a) three-roll symmetrical or asymmetrical pinch benders,

(b) four roll-pinch benders, and
(c) two-roll benders.

The arrangement of the rolls can further be grouped as
(1) horizontal, and
(2) vertical.

Various methods of driving the rolls are also available. It normally depends on the size of the bender or its load rating. The power may either be supplied manually, hydraulic-mechanically, electromechanically, wholly hydraulic, or a combination of manual and electromechanical.

Winship [38] described most of the geometrically different types of three and four roll benders, i.e. their operation and bending procedures, their design considerations (such as roll geometries, frame, general arrangements and roll control) and the bendpiece handling system, etc.. He also briefly discussed the effect of the bendpiece length at its finishing stage, and comparisons of the three/four roll benders in the plate bending operation. In general, the three-roll benders are used to bend thick plate, while the four-roll benders provide improvements in material handling and productivity, and greater flexibility. They are also able to operate in any of the three roll configurations. Another advantage of the four-roll bender over the three-roll variety is that the bending process [37, 38] is more efficient.

Roggendorf and Haeusler [37] traced the evolution and the operational characteristics of a three-roll symmetrical pyramid bender produced in 1948 by Dornach in Switzerland. They went on to describe the development and evolution of various Haeusler bending machines during the period 1948 to 1979. The evolution of the Haeusler roll bending machines is a good example of the development of the roll benders in the metal industry.

The implementation of computer technology into machine engineering has created the universal acceptance of NC machined tools. Its application in metal forming however is still in its infancy. To introduce CNC for the roll bending process, a series of studies to develop the interactive program system for the numerical simulation of roll bending of sheets and profiles has been carried out by Ludowig and Zicke [35, 36], at Dortmund University, West Germany.

The study of Ludowig and Zicke [35, 36] has resulted in several versions of interactive program systems for CNC roll bending, e.g. ROBEND, being produced. Accordingly, ROBEND can be applied to the following types of bending machines :

(1) the asymmetrical three-roll bender
(2) the symmetrical three-roll bender
(3) the symmetrical four-roll bender
(4) the asymmetrical three-roll bender, applied to conical roll bending.

It has been stated [35,36] that the ROBEND programs enable the roll positions to be determined, taking into consideration the contour of the bendplate as well as the elastic behaviour of the plate material. The programmes also allowed for the geometry of the bender to be controlled. The ROBEND method approximates the complex contour of the bendpiece by means of a sequence of circular arcs with different radii. ROBEND was claimed to be capable of accommodating changes in the material properties during the determination of the bending curvature. It could also correct the errors caused by the rigidity of the machine, bendplate dimensions, etc., by means of a diameter sensor. The program allows the operator to visualise the bending contour of the bendpiece on the computer screen. It is unfortunate that the details of their analysis, to the present knowledge of the author, are not available.

The contribution of Ludowig and Zicke [35, 36] undoubtedly advanced the science and the art of the roll bending in thin and medium plate forming. The science of roller plate bending, especially in the heavy plate bending, is still not fully explored due to the complex nature of the problem and the frictional conditions [17] of the rolls and plates. From the literature studied, it appears that analysis to determine the mechanics of roller bending has only been confined to the three roll pyramid bender [33, 34].

Bassett and Johnson [33] analysed the top roll vertical force (F_{tv}) and torque (T) required in the three-roll pyramid bending process by using the following two methods :

(a) a geometrical analysis based on the assumption that deflection from the plate is in the arc of a circle.
(b) a load analysis using the uni-axial stress-strain relation for the material.

Their prediction and experimental data, on bending aluminium alloy, indicate that their geometrical analysis predicted the upper roll vertical force and the torque to an acceptable level of accuracy. This was done by considering only the tensile stress strain properties of the material. The load-analysis of Bassett and Johnson generally gave less accurate approximation than the former one. The reason might be due to the increased induced error of the assumed stress-strain relative to the actual properties of the material and their assumption of the negligible plate slope. The study of Basset and Johnson concluded that some other parameters , such as the distance between the upper and lower rolls, etc., require either the introduction of a constant factor or further modification . Furthermore the analysis was only applicable for single pass bending.

Hansen and Jannerup [34] also modelled the single pass elastic-plastic bending of a beam using three-roll pyramid bender. They commenced with a geometrical analysis and assumed a triangular moment distribution between the rollers. They also considered the stress-strain relationship of the actual material. The calculation from the model of Hansen and Jannerup led to a curvature function, which differs somewhat from that assumed by Bassett and Johnson [33] ; i.e. a circle. The geometrical analysis of Hansen et al accounts for the offset of the contact point of the plate and the upper roll from the vertical centre line of the roll. It also considered the variation of the geometrical shape of the workpiece from the in-bending roll to the out-bending roll. The model also computes the bending force and bending moment. Experimental measurements and evaluation from the model for a special case of constant curvature [34] showed good experimental and theoretical agreement.

Though the analyses of both Bassett and Johnson [33] and Hansen and Jannerup [34] seem to produce data agreeable with experimental measurements, the variation of the geometrical set up and drive arrangement of the bender always changes the bending mechanics of the process [34] . Also, certain assumptions, such as the ignoring of friction etc, may need further investigation. Moreover, the above two studies are only applicable to the particular set up of a three roll bender in the single pass bending mode.

In the recent study of Bata and Malik [32], the effects on the plate formability of the tensile stress and the UTS, impact and surface hardness values, and surface flows were studied. Through their investigation of the systemmatical elongation of the plates, Bata et al concluded that thick steel plate could be roll formed to strain levels greater than 5 %, i.e. ranging between 7 - 9.4 %. Bata et al also found the

stress relieving treatment lowered the yield strength and UTS of the roll formed plates and in some cases restored these properties to those of the "as-received" plates.

It appears from the literature available that the actual analysis on the forces and torques, for either single or multipass bending mode, in four roll benders has not been carried out.

2.3. Plate/Beam Bending

2.3.1. Elastic bending

This is a popular subject in engineering research due to the extensive use of plate/beam in structural engineering. A representative text on this subject, i.e. the analysis of plate bending, is by Timoshenko and Woinowsky-Krierger [108]. Szillard [105] also generalised the classical and numerical methods of the plate bending analysis. Besides the existing texts, numerous research articles are also available in the current literature.

2.3.1.1 Small deflections of plate in bending

Under the conditions of small plate deflection, i.e. the deflection is smaller than the thickness of the plate, conventional elastic analysis of most plate bending problems solves Lagrange's (biharmonic) differential equation of plate,

$$\nabla^4 W = -(q/D) \qquad (2.1)$$

where W is the vertical displacement profile of the plate's middle surface, q is the uniformly distributed load on the plate, D is the flexural rigidity (which is expressed as

$D=\{2Et/12(1-\nu^2)\}$) of the plate, and t is the thickness of the plate.

The solution of equation (2.1) to satisfy the respective static or dynamic boundary conditions normally produces a complete solution.

In plate bending, equation (2.1) is traditionally solved by the use of the Fourier's trigonometric series for most rectangular plate bending problems. Some of the circular plate bending problems involve the adoption of the Bessel functions etc..

With the exception of certain simply supported and edge clamped examples, and a few other boundary conditions [105, 108] which give an exact solution, most problems in plate bending are difficult to solve exactly. Throughout the last few decades, techniques, such as :

(1) variational energy methods, which includes Rayleigh Ritz [105, 108], the perturbational solution [114] and Reissner's method [88, 91, 92, 94].
(2) Muskhelishvilli method, which is a complex variable solution for two-dimensional problems of linear elasticity [55]
(3) Boundary integral equation method [64]
    - The solution of the biharmonic equation is expressed as a boundary integral in terms of the stress function or the transverse deflection.
(4) Collocation (point matching) method [49, 81, 107].
(5) Finite difference method [67, 68, 81].
(6) Finite element method [112]. etc.,

have been developed to solve the plate bending problems either exactly or approximately. Some of the literature concerning the application of these techniques will now be mentioned

A. Reissner's method

Reissner [91] assumed a linear distribution for the bending and shear stresses σ_x, σ_y and τ_{xy} to obtain expressions for the transverse shear stresses (τ_{zx} and τ_{zy}) and the normal stress component σ_z, by means of the differential equations of equilibrium and the consideration of the shear stress results V_i in terms of the stress couples M and H. Through the application of Castigliano's theorem of least work, Reissner established a system of differential equations of the sixth order. These equations are related to linear examples of bending thin elastic plates, and took into account the transverse deformability of the plate.

By introducing the stress function for the shear stress resultants V_i, Reissner [92] applied the derived system equations [91] to analyse the torsional problem of a rectangular plate, and the bending-twisting problem of an infinite plate with a circular hole in the middle.

In 1946, Reissner [93] generalised the derivations [91, 92], to a simpler form. He then further applied the technique to solve bending problem of a cantilever plate due to a torsional transverse load.

Plass et al [88] modified Reissner's variational principle to a form applicable to small deflection problems for thin plates. The modified principle was then used to obtain the approximate analysis of the static deflection and vibration problems of two plates : a squared plate and a 45-degree swept back plate. They also compared the data with Rayleigh Ritz

technique. The results were comparable. However, the Reissner principle allows the selection of moment functions which satisfy the desired boundary conditions without having to rely on the selected deflection function forms. This selection is difficult for satisfying the free edge conditions.

By treating a narrow rectangular cantilever beam as a plane stress problem, Reissner [94] proposed a method for obtaining upper and lower bound results for the end deflection of the beam using elementary polynomial solutions of Airy's differential equation and approximate boundary conditions.

B. Muskhelishvilli's method

Deverall [55] applied Muskhelishvilli's complex variable method to the problem of small deflections due to bending of a thin, isotropic, homogeneous clamped plate with transverse load. He solved the functional equation involved in Muskhelishivilli's method by means of series expansions.

C. Boundary integral equation method

Grover and Chou [64] developed a method for the direct solution of the problems of plane stress and plate bending in an infinite sheet with a curvilinear hole. They solved the biharmonic equation as a boundary integral in terms of the stress function or the transverse deflection. The stress function or transverse deflection was then found by integration of the boundary integral. The method eliminates unknown boundary values of the stress function or transverse deflection, as Green's function is made to satisfy the boundary conditions at the hole.

D. Collocation method

Inspired by the Ritz approach and through the observation that most structural plates are either spot-welded or rivetted, i.e. being supported only at a few small areas around the periphery, Thorne [107] proposed a point matching method to solve the plate problem with fixing point along the edge, subjected to uniform load (or a centralled load). The method involved an algebraic polynomial, which satisfied the Lagrange equation and the boundary conditions around a square plate.

Conway [49] extended the point matching method to other boundary value problems governed by Laplace's or the biharmonic differential equation. He suggested the use of an algebraic trigonometric polynomial to satisfy the differential equation. He showed that the method was very convenient to use and gave accurate results.

Leissa and Niedenfuhr [74] applied Conway's algebraic trigonometric polynomial to a problem of the cantilever square plate with uniform transverse load. The comparison with the Rayleigh Ritz solution for the same problem indicated a good agreement. Applying the same technique, Leissa and Niedenfuhr [75] solved the bending problem of the square plate with two adjacent edges free and the others clamped or simply supported. It was found that it gave results close to the exact solutions for the same problem.

In comparing the approximate analysis of the bending of a rectangular cantilever plate, having a span to chord ratio of $^1/2$, subject to a uniform normal pressure, Nash [81] used the collocation method with algebraic and hyperbolic trigonometric polynomials to solve the problem. He chose polynomials to satisfy exactly the deflection and slope conditions along the clamped edge.

E. Finite difference method

Holl [67] expressed the relevant differential equations of the plate bending problem in finite difference forms. Utilising the principle of superposition of deflection surfaces or equivalent stress systems both by difference and differential methods, Holl solved a series of square plate problems. His thick plate theory allowed the determination of the correct critical stress at the centre of the lower surface of the plates.

Noticing the scarcity of analyses for the deflection and strength of finite cantilever plates, Holl [68] in 1937 applied the finite difference method to analyse the problem of a cantilever plate with a concentrated edge load. The method overcame the difficulty encounted in solving the boundary condition of the third derivatives of deflection at a free corner.

F. Finite element method

The finite element method is a powerful approximate technique in solving most engineering problems. It is especially useful in dealing with irregular and complex boundary condition problems. A great number of publications, on the theory and application of this method is currently available.

Westbrook et al [112] proposed a three-dimensional finite element method for plate bending. Their method of derivation was based on the theorem of minimum potential energy. The method approximates the solution of the variational problem. It accounts for the transverse shear and thickness effects. It is also applicable to thick plate bending. Numerical results, using the derived finite element equations, for square plates under point or distributed load, and with either simply supported or clamped boundaries, showed a good convergence and was comparable with other existing results.

G. Other techniques of analysis

There are numerous other techniques available for plate bending analysis in literature. Examples can be found in references 107, 108 etc..

2.3.1.2. Bending of a cantilever plate

The elastic deflections of a cantilever plate, loaded by a simple concentrated force at the free edge, was first predicted by MacGregor [78] in 1934. MacGregor eliminated the difficulty of solving the boundary of the free corner formed by two free edges, in the exact solution, by assuming the rectangular cantilever plate to be infinitely long. His basic approach was to find the deflection function, $W=f(x,y)$, of the plate satisfying the biharmonic equation (2.1). For this purpose the deflection profile was represented by a Fourier integral of the form

$$W=\int_0^\infty \Gamma(\beta x)\cos\beta y\, dx \qquad (2.2)$$

where $\Gamma(\beta x)$ consists of four terms containing hyperbolic functions with four constants to be determined from the boundary conditions. MacGregor's prediction gave data closely agreeable with experimental result.

Jaramillo [70] further developed MacGregor's approach to evaluate the deflections and moments, due to a concentrated load which was acting at an arbitrary point, of an infinitely long rectangular plate. He solved the problem using improper Fourier integrals. The exact solution was transformed into a series form by means of contour integration.

Ramachandra-Rao [90] used generalised orthogonality relations, for the flexure of rectangular plates, to analyse the flexure of a semi-infinite cantilever plate loaded with a moment at infinity. The analysis accounted for the singularities in the shear force, which existed at the corners of the cantilever plate.

The deflections and moments of a finite cantilever plate, concentrately loaded at its free edge, was first analysed by Holl [68] using a finite difference method. Leissa and Niedenfuhr [74], and Nash [81] also analysed the problems of a cantilever plate, subjected to a uniformly transverse load, by means of a collocation method. They solved the problems using algebraic trigonometric polynomials and algebraic hyperbolic trigonometric polynomials respectively.

2.3.1.3. Large deflection of plate bending

The derivation of the Poisson Kirchoff (Lagrangian) equations for the problems of plate bending ignores the effect of the stretching of the middle surface and the possible shortening of the plate. The justification for neglecting this effect is questionable as the maximum deflection of any particle at the middle surface is no longer small in comparison with the thickness of the plate. Prescott [89] pointed out that the Poisson equation was very much in error when the deflection was in the same order as the thickness. The modified Poisson equation for large deflection is expressed in the following form

$$[(2Et^3)/(3(1-\nu^2))]\,\nabla^4 w - 2tE\{(\partial^2 w/\partial x^2)(\partial^2 \phi/\partial y^2) + (\partial^2 w/\partial x^2)(\partial^2 \phi/\partial x^2) - 2(\partial^2 w/\partial x \partial y)(\partial^2 \phi/\partial x \partial y)\} = q \qquad (2.3)$$

in which ϕ is a chosen stress function which has the following

properties

$$\tau_{xy} = -E(\partial^2\phi/\partial x\partial y) \qquad (2.4a)$$

$$\sigma_x = E(\partial^2\phi/\partial y^2), \quad \sigma_y = E(\partial^2\phi/\partial x^2) \qquad (2.4b)$$

The second term within the bracket in equation (2.3) is the total force per unit area in the direction of the z-axis due to all the mean stresses acting on the edges of an element dxdy.

Since there are two unknown functions, W and ϕ, in equation (2.3), the solution of the functions can only be obtained by simultaneously solving equation (2.3) and the following equilibrium equation of the plate.

$$\nabla^4 w = (\partial^2 w/\partial x\partial y)^2 - (\partial^2 w/\partial x^2)(\partial^2 w/\partial y^2) \qquad (2.5)$$

A complete analytical solution to equation (2.3) demands more boundary conditions than that for solving the normal Poisson equation. Generally, the exact number of boundary conditions is rather difficult to obtain in most plate bending problems. An easier approach is to assume a deflection function W in order to determine the load q.

According to Prescott [89], the modified middle surface membrane strain ε_x, ε_y and γ_{xy} are expressed as

$$\varepsilon_x = \partial u/\partial x + (1/2)(\partial w/\partial x)^2$$

$$\varepsilon_y = \partial v/\partial y + (1/2)(\partial w/\partial y)^2 \qquad (2.6)$$

and

$$\gamma_{xy} = \partial u/\partial x + \partial v/\partial y + (\partial w/\partial x)(\partial w/\partial y)$$

where, U, V and W are the plate displacement in X, Y and Z direction, respectively.

γ is the membrane shear strain.

Way [110] gave a general solution for the case of a circular plate bent to a figure of a revolution. He considered the polar forms of the radial and circumferential strains and stresses in the middle surface of the plate and also the corresponding additional depth strains and stresses at a distance Z from the middle surface. He solved the derived equations for the vertical and radial equilibrium by a number of equations of series form. He related the coefficients in the series by substituting them into the fundamental equations and employing the boundary conditions. Way's solution to the problem was an exact form and gave good correlation with experimental results.

Berger [44] simplified the non- linear equations for a flat plate with large deflections by assuming that the strain energy due to the second invariant of the middle surface can be neglected. Computations using the solution of these were also carried out for the deflection of uniformly loaded circular and rectangular plates with various boundary conditions. Berger further used the deflections found by this approach to determine the stresses for the circular plate. The accuracy of the Berger's approach was within the limits of normal engineering tolerance.

Tabarrok and Dost [106] briefly examined the four variational formulations, such as (i) the displacement formulation, (ii) the von Karman formulation, (iii) the stress function formulation and (iv) the complementary von Karman formulation, for the large deformation analysis of thin

plates. It was shown that by initially satisfying some of the governing equations the order and degree of the remaining set of the differential equations could be altered to facilitate the solutions.

Coan [47] presented a theory of large deflections orthotropic rectangular plates when the plate was initially curved. The boundaries were also subjected to the conditions of edge compression. The theorectical prediction was in good agreement with the experimental measurements.

2.3.1.4. Large deflection of beam bending

The bending curvature along a bent beam is normally governed by the fundamental Bernoulli Euler theorem.

$$1/R = d\theta/dS = (d^2y/dx^2)/[1+(dy/dx)^2]^{3/2} \qquad (2.7)$$

where, R is the local radius of curvature, S is the local arc length and θ is the subtend-angle of the arc.

In classical beam theory, the term of $(dy/dx)^2$ is always neglected. However, the evaluation of the large deflection problems of beam bending requires the retention of $(dy/dx)^2$ in equation (2.37). The existing solutions to this sort of problem generally involve a series combination of incomplete and complete elliptic integrals [42, 45, 48, 59].

Barten [42] assumed that the length of a cantilever beam, which had a uniform cross-section and was vertically loaded by a force at the free end, was constant. He solved the beam deflection and the length of its bending arm.

Bisshop and Drucker [45] developed a theory to account for

the shortening of the moment of a cantilever beam during bending. Frisch-Fay [59] further developed the theory to analyse the large deflections of a cantilever under two concentrated loads. It thus leads the way to the solution of multi-concentrated loads problems, where the principle of superposition cannot be applied as a result of non linearity of the cantilever.

Rohde [96] solved the problem of large deflections of a cantilever beam with a uniformly distributed load. Rohde's approach to the solution was different from the afore-mentioned investigators. He expressed θ as a series of S^n, i.e. $\theta=\sum_{n=0}^{\infty} a_n S^n$, in which a_n are the coefficients of the series and S is the local arc length.

Conway [48] analysed the two problems of large deflections of a simply supported beam with a centrally concentrated load. The two cases were :

(1) the reactions at the ends of the beam were assumed to act vertically,

and

(2) the reactions were assumed normal to the beam together with the tangential friction forces opposing the beam displacement.

A numerical method for calculating the large deflections of straight and curved beams was developed by Seames and Conway [98]. The method assumes that the elastic axis of a beam can be approximated to a number of circular arcs tangential to one another at their points of intersection. Seames et al applied the method to solve cantilever beams and rings subjected to concentrated or distributed loads. Predictions gave an excellent agreement with the exact solutions available [98].

2.3.2. Plastic Bending of Plates/Beams

2.3.2.1. Elastic-plastic and plastic bending

During bending, a beam/plate initially experiences elastic deformation until its outer fibre reaches the yield point. From then on the increase in bending load produces an elastic-plastic region in the beam/plate until complete plasticity occurs. Analysis of elastoplastic or plastic bending is rather complicated. However, most bending problems are analysed by assuming that material is perfectly plastic, or the bending is performed under pure bending etc..

Eason [57] solved the problem of elastic-plastic bending of a circular plate which was simply supported at its edge and carried a constant load over a central circular area. The solution was based on the von Mises yield condition and the associated flow rule. The analysis assumed that material was non work hardening, elastic-perfectly plastic, and incompressible.

By using von Mises' yield condition and Hencky's stress strain relation for a non work hardening material, Oshashi and Murakami [82] analysed the problem of the large deflection in elastic plastic bending of a simply supported circular plate under a uniform load. The analysis accounted for the membrane and bending strains.

Witmer et al [113] used the finite difference method to obtain the axisymmetric responses of plate to impulsive loading, involving both the elastic and plastic regions. Lin et al [76] also produced an analytical iteration method, adopting the incremental stress strain relationship, to predict the elastoplastic bending of rectangular plates with large deflections.

Oshashi and Kamiya [83] accounted for the effect of compressibility of the material in analysing the bending of thin plates having a non-linear stress strain relationship. The analysis, based on an empirical stress strain relation for pure aluminium was as follows :

$$\sigma = a_1[1-\exp(-a_2\varepsilon)] \qquad (2.8)$$

where, a_1 and a_2 are constants which are determined from experiment.

The analysis was mainly applicable to small deflections.

2.3.2.2. Pure moment bending

Due to the fact that pure bending produces a uniform curvature along the beam, a simplification of the complex plastic bending problem is utilised. A great number of investigations have been undertaken in this specific kind of bending [41, 51-53, 61, 66, 77, 79, 84-87, 97, 100, 109 etc.].

Osgood [84-86] analysed the problem of plastic bending for various geometrical cross section beams by assuming a stress strain relationship of $\varepsilon = \sigma/E + K(\sigma/E)^n$, in which K and n were constants. The relation between bending moment and curvature in a beam was thus worked out from equilibrium considerations.

Gaydon [61] treated the plastic bending of a thin strip as a generalised plane stress problem. Using the Levy-Mises stress-strain relation and the von Mises yield criterion, he solved the problem by a successive approximation method. His analysis also accounted for the variation in thickness and the movement of the neutral surface.

The problem of elastic plastic analysis of the bending of beams under the influence of an axial load for work hardening material was undertaken by El-Domiaty and Shabaik [58]. The analysis assumed a hardening stress strain relationship of the form $\sigma=K\varepsilon^n$. The variation of the applied bending moment with the axial force for fully elastic, elastoplastic, and fully plastic cases was given, both in analytical and graphical forms.

The gradual change in cross sectional contour of either a very wide or a very narrow bar with progressive bending was obtained by Hill [66] and Lubahn and Sachs [77]. The method developed by Lubahn and Sachs [77] was a successive approximation one. Its final solution showed not only the movement of the material axis towards the compression surface, but also the decrease in the radial co-ordinate. Denese [52] used the differential calculus theory to obtain a direct solution to the problem. He further devised a graphical method to assess the ultimate thickness/original-thickness ratio in terms of the inner curvature radius and the original thickness. Dadras and Majlessi [51] studied the problem for the bending of a rigid work hardening material. Dadras and Majlessi [51] modelled the effect of the σ-ε behaviour of the fibres in reversed loading. It was found that the variations of bending moment were greatly affected by the work hardening rate, but changed only slightly with yield stress level.

Verguts and Sowerby [109] extended the analysis to the problem of plastic bending of laminated sheet metals. They investigated the effects of the relative position of the strong and weak laminations in sheet to the overall sheet thickness. Their analyses provided means to determine whether the bending process was stable. The Bauschinger effect was also considered in the study. Majlessi and Dadras [79]

furthered the work of Verguts and Sowerby. They adopted a more realistic Bauschinger model to investigate the problem and studied the influence of laminate geometry in two-ply, as well as symmetric and non-symmetric three-ply laminates.

2.3.2.3. Pure bending of curved bar

Symmetrical pure plastic bending of a curved bar with an axial force was initially considered by Phillips [87]. His analytical approach was to approximate the stress strain curves for tension and compression by means of a series of straight lines. The axial load and bending moment were then found by the consideration of equilibrium at certain angular positions.

Shaffer and House [101] used the Airy stress function and Tresca yield criterion to determine for a wide curved bar the elastic stress distributions and the plastic stress distributions, in the radial and circumferential directions respectively. They also analysed the relevant displacements and strains [99, 100]. Their analysis was mainly for a perfectly plastic, incompressible material.

Shaffer et al's analysis [99-101] was relevant to the problem of analysing the curvature of the bar. Shepherd and Gaydon [102] used both the von Mises and Tresca yield criteria and the associated flow rules to determine the values of the couples necessary to produce plastic flow in a thin ring section plate.

2.3.3. Others

2.3.3.1. Some Practical bending processes

The forming operations of beam, plate and sheet have always been a major activity in the production of structural

components. One of the problems associated with an elasto-plastically deformed body under a system of deforming forces and constraining dies is the effect of friction between the workpiece and the constraining die. In 1966, Martin and Tsang [80] studied this problem theoretically and experimentally.

Assuming the conditions of both plane strain and plane stress, Martin et al [80] analysed the behaviour of a simple beam bent by a central load and freely supported by rollers at each end. It was concluded that, for beams whose lengths between supports were at least twenty five times their thickness, the load required to produce deflection was increased by the amount required to overcome friction. It did not, however, affect the circumferential strain at midspan.

Stelson and Gossand [103] analysed the force and displacement during the early part of the bending cycle in the pressbrake process. The analysis predicted the final punch position to produce the desired unloaded angle.

To examine the start of a pressbrake process in which thin plate strips began to deformed in order to plastically form V-shaped items, Johnson and Yu [73] analysed the large elastic deformation of strips in V-die bending. They obtained the relationship between the punch force and the punch displacement, and analysed the problem of the pressbrake bending of rigid/linear work hardening plates [115].

2.3.3.2. Springback

In precision metal forming, the final profile of a workpiece is often determined by the amount of springback after the loading is released. A knowledge of springback in each bending operation is therefore important in evaluating the required bending load and displacement. Botros [46] studied the springback in sheet metal forming after pressbrake

bending. He found that the degree of springback increased as the radius of bend increased. It decreased with increasing angle of bend and strip wall thickness. Johnson and Yu [71, 72] investigated the springback after the biaxial elastic-plastic pure bending of a rectangular plate. The latter analysis was based on (i) non-proportional loading for both the von Mises and Tresca criterion, and (ii) proportional loading for both the Mises and Tresca criteria. Yu and Johnson [116] also analysed the springback of a circular plate subjected to circumferential moments under the large elastic-plastic deflection condition.

2.3.3.3. Bendability

Plates of large width occasionally exhibit cracks across the width centre when bent to minimum radii which were otherwise successfully bent with smaller width plates. Gerard [62] studied the effect of bend width upon minimum bend radii. It was found that the stress condition existing at the centre of a large width revealed an unfavourable bi-axial tension stress that reduces the elongation from that experienced in simple tension.

Sangdahl et al [97] investigated the stress states occurring in bending rectangular sections by varying the rectangular dimensions. They found that the ductility was dimensionally dependent. It was generally increased by decreasing the breadth to thickness ratio of the section. Barlow [41] found that the ductility predicted at fracture of a wide beam in bending was also dependent on both the yield and fracture criteria and the amount of strain hardening. Barlow showed that the minimum bend radius of a wide beam was very sensitive to the yield criterion. Datsko and Yang [53] presented a simple equation $\{\varepsilon_f=\ln(100/(100-A_r))\}$ to correlate the minimum bend radius with

the reduction of material area, A_r.

2.3.3.4. Anticlastic curvature

Large deflections of a rectangular beam or plate in pure bending about a principal axis of its cross-section, depends on the curvature ratio $b^2/(Rd)$. Here, b is the breadth and d is the depth of the beam, and R is the radius of the neutral filament. If the ratio is small, as in the case of a beam where the breadth is comparable in magnitude with the depth, the cross section of the beam assumes an anticlastic curvature of radius R/ν. If $b^2/(Rd)$ is large, as in the case of a plate having b much greater than d, and bent to a considerable extent, the cross section remains substantially flat and the flexural rigidity of the plate is increased above that given by the usual beam theory by a factor $1/(1-\nu^2)$.

The above behaviour has been experimentally proved by Ashwell and Greenwood [39] and theoretically analysed by Ashwell [40]. Fung and Wittrick [60] furthered the anticlastic curvature analysis to take into account the lateral thickness variation of the strip. Conway and Farnham [50] considered the anticlastic nature of strips which had bevelling on either concave or convex side edges. It was found that a relatively small amount of bevelling on the concave side of the strips greatly reduced the anticlastic deformations.

A concise review on the analysis of anticlastic problems has been done by Horrocks and Johnson [69]. Horrocks and Johnson have also experimentally investigated the anticlastic curvature of plastically bent plates of varying widths and constant thickness, for mild steel and aluminium alloys.

2.4. Surface contact stresses/friction

Since Hertz introduced the study of contact stresses [138],

numerous investigations have concentrated on a number of elastic surface contact stress distribution problems with or without tangential forces [121, 131-134, 140]. The majority of these studies are highly mathematical.

Advances in the surface contact problem have been prominent within the last four decades. New insights and methods of analysis have been continuously appearing [120, 121, 128, 129, 139, 141].

Mindlin [131] analysed the contact compliance of elastic bodies under the conditions of (a) unstressed state, (b) pressed together with Hertzian force, and (c) tangential force and torsional couple on the contact surface. He expressed the compliance in terms of complete elliptic integrals. Mindlin found that the compliance was generally greater in the direction of the major axis of elliptic contact than in the direction of the minor axis for the case of the tangential force and within the practical range of Poisson's ratio.

Poristsky [133] analysed the two dimensional stresses and deflections, in terms of proper Airy functions, for cylindrical bodies in contact. Smith and Liu [134] used the two-dimensional approach to analyse the stresses due to tangential and normal loads on an elastic solid. The latter analysis assumed that both normal and tangential loads were distributed in a Hertzian fashion over the area of contact. It was found that the maximum shearing stress in the contact area was at the surface instead of beneath the surface for the application of combined loads.

Goodman [121] extended the Hertzian analysis of contact stresses to include the effects of friction on the interface between two elastic spheres compressed along the line connecting their centres. He also developed stress functions to analyse the shear loaded half-space in the linear theory of

elasticity. It was found that the distribution of shear stress needed to prevent the relative slip of surfaces, after modifying the contact region, was finite in the complete region.

The problem of the elastic contact of a plate with two axisymmetric bodies of disssimilar elastic properties and curvatures was considered by Tu and Gazis [140]. They truncated the solution of the resulting integral equations by a series of Legendre polynomials of even order whose coefficients were determined from a system of linear algebraic equations. O'Conner [132] numerically solved the formulated integral equations to calculate the surface shear traction and the torsional compliance of an elastic system comprising a plate between identical spheres.

After Archard [117] and Ling [129] had advanced the asperity contact theory, the concept of the plastic flow of the microcontact in sliding became well recognised. Statistical methods for estimating the area of contact of the asperities was introduced by Greenwood [123]. This led Tabor et al [122, 130, 137] to divide the total force resisting the sliding, into two components, i.e. ploughing and adhesion, to establish the connection between the surface contact nature and the friction condition [126, 127].

In supporting the close relation of contact asperities, friction and wear, Kragelsky and Demkin [128] analysed the problem of the contacting process of surfaces that were rough and wavy. They modelled a unit protrusion as a cone with a spherical top deforming elastically and plastically. On the basis of this model, calculations of the real contact area as a function of the load, the geometry of the surface, and the properties of the material were obtained.

Conway and Engel [120] applied a point-matching method to

find the contact stress distributions induced in an elastic slab indented by rough, rigid, spherical and cylindrical indenters. While Tsukizoe and Hisakado [139] analysed the mechanism of air leakage through the interstices between metal surfaces in contact, by assuming a normal distribution of the tips with higher asperities.

Yoshimoto and Tsukizoe [141] analysed the mechanism of wear between metal surfaces in terms of the real area of contact. The analysis allowed the number and size of individual areas of contact to be determined.

In the field of the rolling contact problem, Bentall and Johnson [118, 119] analysed the rolling contact stresses between rollers of unequal elastic constants [118], and when rolling an elastic strip [119] using a numerical method. The method provides a prediction of the contact stresses. It also allows the slip, the contact width and the speed to be studied as the strip passed through the grips.

Hahn and Levinson [124, 125] investigated the indentation of elastic layer(s) bonded to a rigid cylinder, for, (i) quasi-static without friction [124] and (ii) uni-directional slipping with Coulomb friction [125]. They used a stress function in the form of a trigonometrical series.

Soong and Li [136] studied the steady rolling contact of two dissimilar cylinders. One cylinder drove the other, with each cylinder bounded by a soft layer of arbitrary thickness. They used the point matching method to solve the formulated equations. Following the aforementioned study, they also investigated the effect of the asymmetric rolling contact in which a sheet driven in steady state through the nip of the rolls [135], was being pulled or pushed by a tangential force.

It has not been possible to find any analysis or

investigation in the available literature of the rolling contact problem, concerning an elastic strip or plate which experiences changes in the contact width and curvature, as it passes through two rollers.

CHAPTER THREE

DESIGN OF MODEL BENDER

3.1 Introduction

The objective of this research work is to evolve a reliable theory which will predict the mechanics of the roller bending process. Consequently, the theory must be compatible with experimental data. A model roller was therefore designed to fulfil this purpose. The initial conceptual specifications of the model were as follows :

(1) To simulate the Verrina roller bender at Head Wrightson Teesdale (HWT)
- this assists in appreciating the capacity and limitation imposed by the bender manufacturer. It also provides for the direct extraction of the experimental data, collected from the model, for application to the Verrina bender.

(2) To account for the physical features of the three/four roll plate benders
- this assists in the study of the mechanics of roller bending processes with either four- or three- roll configurations.

(3) To consider the effect of slip between the bendplate and the rollers on the bending mechanism.

(4) To study the effects of the roll size and interchangeability on the bending mechanism.

(5) To facilitate the ease of handling in the laboratory.

(6) To ensure that the cost of manufacturing the model plate bender is low.

It should be emphasized that the rigidity of the model is a prime concern of the design above all the aforementioned specifications. To meet these requirements, the designing of the model bender involved the following sequential studies.

3.2. Model making analysis

In the light of the first specification mentioned in section 3.1 and the principle of model making theory, the ideal simulation of the Verrina roller bender could be easily achieved if a geometric scale model was specified. This might be difficult to achieve, since the rigidity of each roll is inversely proportional to the fourth power of its diameter. In order to consider the possibility of adopting various ratios of independent parameters (obtained from model-making theory of the model and prototype), the following model-making analysis was thus carried out.

Another important reason which prompted the idea of the geometric analysis was that the model bender had to be designed before a full understanding of the roll bending mechanism had been obtained (see section 1.3), since the forces on each roll and the power required by the top pinch roll were unknown at this stage. The estimation of these quantities would only be possible by utilising the Verrina bender specifications available and applying them to the model making analysis.

3.2.1. The rolls of the model

It is important to point out here that the rolls of the Verrina bender are end clamped, and the simulation of end mounting for the model is impractical and difficult. It has been mentioned that the rigidity of the model is the main design criterion. From studies of textbooks on "Mechanics of Materials", it is known that the simply supported beam, with an equivalent concentrated load at the mid-span is a weakest structural system. Bearing in mind the encastre-nature of the bearings for the model, it was thus thought that the rolls of the model would be stiff enough to simulate the stiffness of

the Verrina prototype if the deflection of the roll was estimated on the basis of the simply supported arrangement.

The deflection, d, at the mid-span $L/2$ of a simply supported roll with a concentrated load, F, at the mid-span is as follows

$$\delta = FL^3/48EI$$

The substitution of I in terms of roll diameter, d, gives

$$\delta = 4FL^3/3\pi Ed^4$$

Let $\mathring{a}=\delta/R=4FL^3/3\pi Ed^4R$

where R=bent radius of the plate

$$\text{so } \mathring{a}_m/\mathring{a}_p=(F_m/F_p)(L_m/L_p)^3(E_p/E_m)(d_p/d_m)^4(R_p/R_m) \qquad (3.1)$$

Expression (3.1) is the ratio of the deflection of the model and the Verrina bender respectively. Thus, the value of $\mathring{a}_m$ or $\mathring{a}_p$ will be obtained if all the ratios of the dimensionless quantities on the r.h.s. and either $\mathring{a}_p$ or $\mathring{a}_m$ are known or assumed.

It may be appropriate to point out here that the deflection analysis for the end-clamped roll also gave the same expression as in (3.1).

Mathematically, any independent ratio can be transformed to a dependent ratio in expression (3.1). It thus allows F_m to be calculated from the extraction of the Verrina bender specifications.

3.2.2. Determination of the approximate ratio of the model and prototype "bending force", F_m/F_p.

From expression (3.1), it can be seen that the ratio of deflection may be determined, if all the dimensionless ratios on the r.h.s. are known. This is not possible since a reliable theory to determine the forces in the continuous roller bending of plates, for the four-roll bender, does not yet exist. Also, a full detailed analysis is rather complex (and not readily produced prior to the design of the model). Consequently a simplified analysis has been carried out using simple plate-bending theory.

It was noted that the end-presetting of the roll bending process for the four-roll bender could be considered as that of bending a plate with one edge clamped and the other edge uniformly loaded (fig 3.1(i)). For this case, the elastic strain stress relationship can be expressed as follows :

$$e_x=[\sigma_x - \nu(\sigma_y+\sigma_z)]/E$$
$$e_y=[\sigma_y - \nu(\sigma_z+\sigma_x)]/E \qquad (3.2)$$
$$e_z=[\sigma_z - \nu(\sigma_x+\sigma_y)]/E$$

The von Mises yield criterion for principal stresses σ_x, σ_y and σ_z is

$$(\sigma_x-\sigma_y)^2+(\sigma_y-\sigma_z)^2+(\sigma_z-\sigma_x)^2 = 2Y^2 \qquad (3.3)$$

where Y is the uniaxial tensile yield stress of the material.

For the plane strain and stress problem, i.e. $e_y=\sigma_z=0$, the

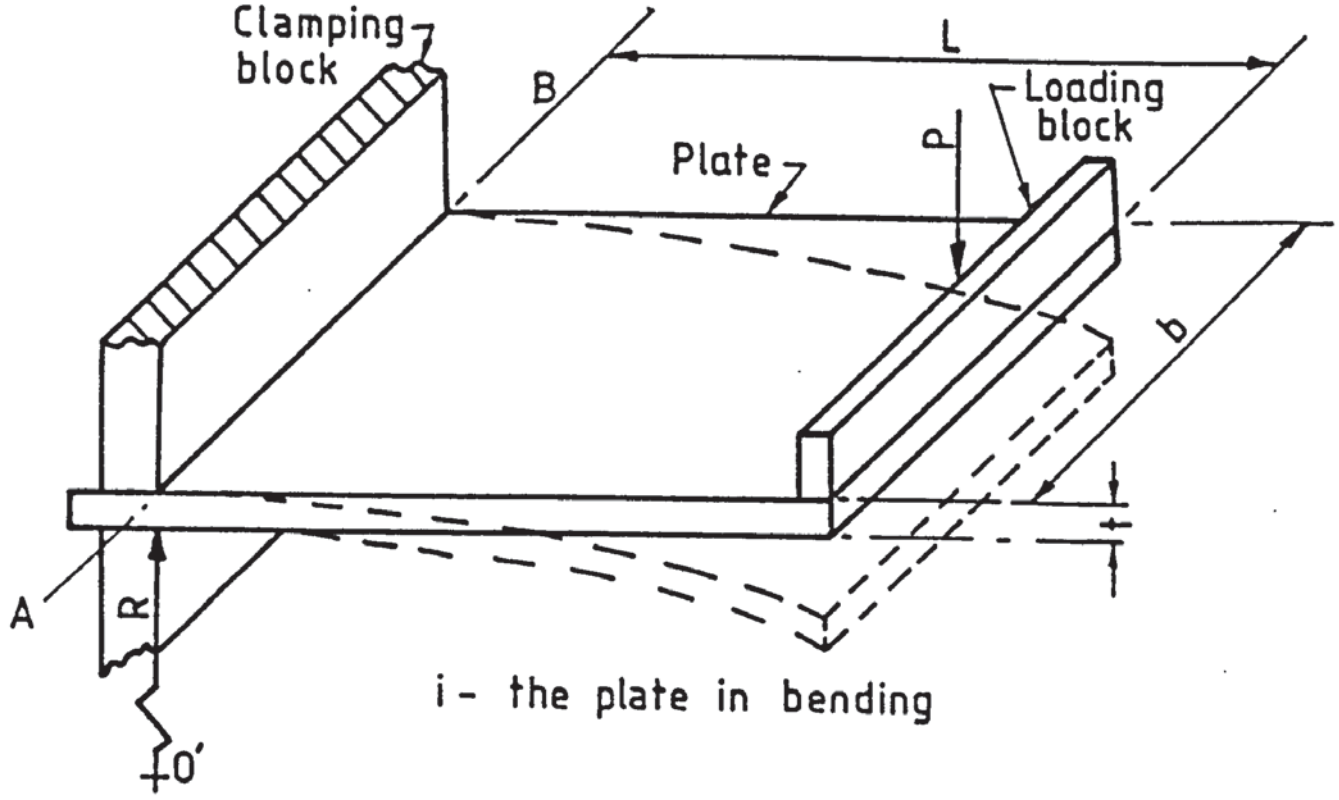

i - the plate in bending

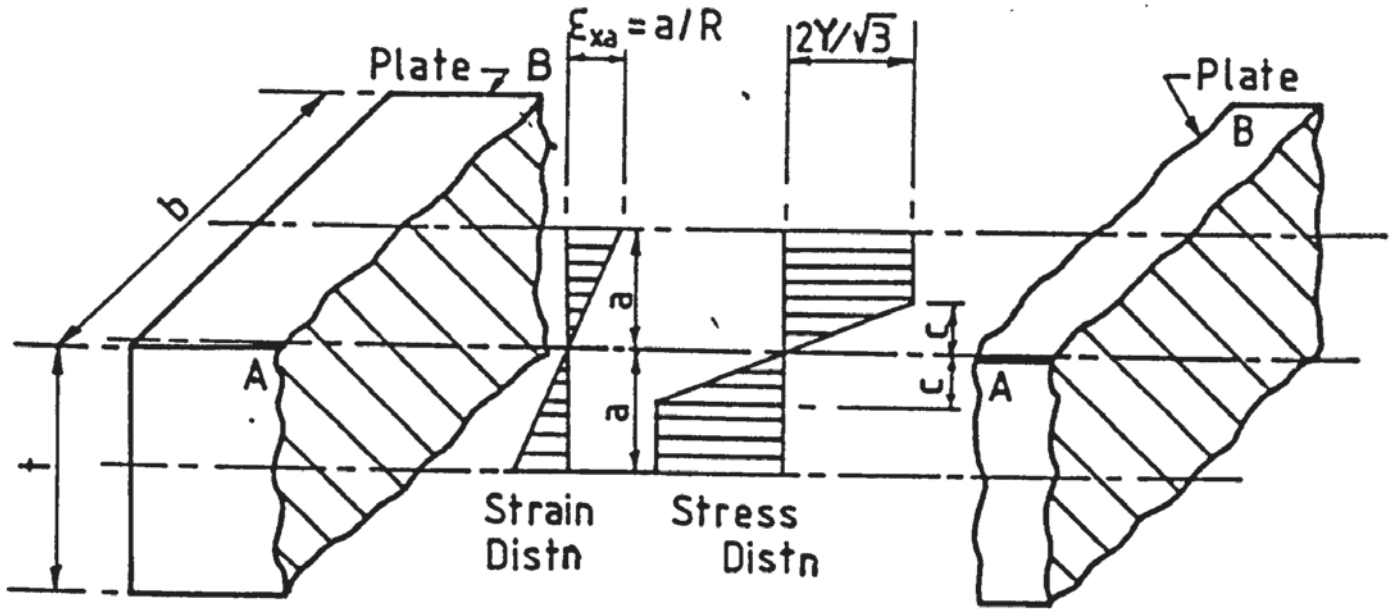

ii - Assumed strain and stress distn across the thickness of the plate in bending

FIG 3.1 PLATE BENDING WITH ONE EDGE CLAMPED AND THE OTHER LOADED

appropriate substitution into (3.2) and (3.3) gives

$$\sigma_{x0} = Y/\sqrt{(1-\nu+\nu^2)} \qquad (3.4)$$

Since yield generally starts at the outer fibre of the plate during
bending, the corresponding yield strain of the fibre can be expressed as

$$e_{x0} = (1-\nu^2)Y/E\sqrt{(1-\nu+\nu^2)} = a/R_y$$

where a = distance of the outer fibre from the neutral axis of the plate

R_y = radius of curvature as yield first occurs,

This assumes that there is no shift of neutral axis, i.e. it remains at the central axis of the plate. A further increase in the load, F, causes yielding to penetrate towards the neutral axis of the plate. Let c and R be the distance of the elastic-plastic interface from the neutral axis, and the new radius of curvature, respectively, of the bent plate. The assumption of perfect plastic material allows the yield strain at the interface to be expressed as

$$e_{x0} = c/R = a/R_y = (1-\nu^2)Y/E\sqrt{(1-\nu+\nu^2)} \qquad (3.6)$$

Assuming equal compressive and tensile properties of the bent material (fig 3.1(ii)), no residual stress, and that the lateral strain is negligible, (through the simplication of $\sigma_{x0}=(2/\sqrt{3})Y$ from (3.4) for $\nu=1/2$) the moment, M, due to the internal resistance of the cross-sectional area of the plate bend can be expressed as

$$M/2R^2b = \int_0^{\varepsilon_{x0}} (2/\sqrt{3})Ee^2\,de + \int_{\varepsilon_{x0}}^{a/R} (2/\sqrt{3})Y\,\varepsilon\,d\varepsilon \qquad (3.7)$$

After integration, rearrangement and appropriate substitution, the bending moment of the plate at the clamped edge (fig 3.1(i)) where deformation takes place, can be expressed as

$$M = (2/\sqrt{3})Yb(a^2 - c^2/3) \qquad (3.8)$$

This quantity is equal to the external bending moment along /about the edge of AB in fig 3.1(i);

thus, $M = FL$

Equating the above statement to expression (3.7) gives

$$F = [(2/\sqrt{3})Yb/L](a^2 - c^2/3) \qquad (3.9)$$

with the incorporation of expression (3.6) and (3.9), the load required to bend the plate to a radius of R can be determined.

The above analysis is a rough simulation of the plate roll-bending process. The load so obtained is considered to be approximate.

As mentioned in Chapter One, the production of an original theory for the roll bending of plates is complex and this work will therefore form a major part of the project, where most of the assumptions previously made should be eliminated. It should be appreciated that the bending effect due to the tangential force component (fig 3.2) is very significant and should be accounted for. The change of plate moment, the contact point between roll and plate, the contact frictional forces, the position of the neutral axis, the variation of the radii of curvature along the plate from the pinch rolls to the side roll, the springback quantities and the thickness of the plate will all contribute to the complexity of the theory. Additionally, neglection of the Bauschinger and work hardening

effects may not be possible. The inertia effect may also influence the bending process. Most of these effects await a full analysis to evaluate their relative contributions (some effects will be considered in the present developed theory : see Chapter Five).

3.2.3. Equivalent torque to bend the plate

Initially, this preliminary analysis was made to estimate the torque on the top roll at the transitional stage of the pre-bending and continuous bending modes.

3.2.3.1. One end clamped and the other end loaded

The change of the angle of rotation, $d\beta$, along the bent section, can be expressed as

$$d\beta = dx/R$$

If the bending moment, M, rotates the plate from an angle of 0 to β, the total strain energy, U, absorbed in the plate is thus :

$$U = \int_0^{\beta} M d\beta = \int_0^{L} (M/R) dx = \int_0^{L} (M^2/2EI) dx$$

By substituting $M=Fx$ and equation (3.9), this becomes

$$U = (1/2EI) \int_0^{L} [(2Yb/L\sqrt{3})(a^2 - c^2/3)\, x]^2 \, dx$$

After integration and rearrangement, it gives

$$U=[(2Y^2b^2L)/(9EI)](a^2 - c^2/3)^2 \qquad (3.10)$$

where E = modulus of elasticity for the material

If T_b is the equivalent torque and θ_d the angular displacement of the drive, then :

$$T_b\theta_d = U = [(2Y^2b^2L)/(9EI)](a^2 - c^2/3)^2$$

From this the following expression is obtained :

$$K = T_b/R = [2Y^2b^2L(a^2 - c^2/3)^2]/(9EI\theta_dR) = (2Y^2A^2Lb^2)/(9EI\theta_dR) \quad (3.11)$$

where $A = a^2 - c^2/3$

so :

$$K_m/K_p=(Y_m/Y_p)^2(A_m/A_p)^2(L_m/L_p)(I_p/I_m)(\theta_{dp}/\theta_{dm})(E_p/E_m)(R_p/R_m)(b_m/b_p)^2 \quad (3.12)$$

Expression (3.12) is regarded as the equivalent torque ratio for the condition of maximum bending moment at the clamped edge.

3.2.3.2. Plate bending under pure moment

If the plate is assumed to be bent under a pure bending moment at either plate edge, the strain energy expression remains in the form of :

$$U=\int_0^L [M^2/(2EI)]\, dx$$

In this case, the moment M applied across any section,

which assumes the equation (3.8), is constant along the bent arc. Through the appropriate substitution and using the procedures described in the last section, it can be shown that

$$K = T_b/R = [(2Y^2b^2L)/(3EI\theta_dR)](a^2 - c^2/3)^2$$

i.e. $$K = (2Y^2b^2LA^2)/(3EI\theta_dR) \qquad (3.13)$$

Expression (3.13) generates the same expression as (3.12) for the torque ratio.

In comparing (3.11) with (3.13), it is found that the equivalent torque in this case is greater than that in case (a) in the ratio of

$$T_{b\ (case\ b)}/T_{b\ (case\ a)} = 3/1$$

This is mainly due to the different bending mechanism of the two cases.

3.3. Estimation of roll force from the preliminary geometrical layout of the roller bender

In section (3.2), the bending force required on the side roll was very roughly estimated from a knowledge of simple plate bending theory. A more realistic estimation should also take the geometrical configuration of the rolls into consideration. It was realized that the strain energy required to bend the plate was mainly contributed by the side roll. The following description deals with this sort of problem (though it is also rather rudimentary). The subsequent description of the analysis ignores forces such as frictional, gravitational, inertia, etc..

3.3.1. Movement of the side roll with respect to the top roll

The two critical configurations as shown in fig 3.2 are assumed for the pre-bending condition.

3.3.1.1. Generation of the pre-bending of the plate (fig 3.2(i))

Considering the triangle ACD in figure 3.2(i), the angle, ß, can be expressed as

$$ß = \tan^{-1}[(r_t+r_s+t)/L]$$

A. Force on the side roll

Referring to figure 3.2(i), the effective bending force for this geometrical configuration is assumed only to be the vertical component, F_v, of the force F on the side roll. Assuming that the possible bending effect on the plate due to the horizontal force component, F_h, can be neglected, the force components can be expressed as follows

$$F_v = F\sin ß = F\sin\tan^{-1}[(r_t+r_s+t)/L] \qquad (3.14)$$

and $$F_h = F\cos ß = F\cos\tan^{-1}[(r_t+r_s+t)/L] \qquad (3.15)$$

By equating equations (3.9) and (3.14) and rearranging them, the force F on the side roll is thus obtained, i.e.

$$F = [2Yb(a^2 - c^2/3)]/\{(\sqrt{3})L\sin\tan^{-1}[(r_t+r_s+t)/L]\}$$

substituting $c=[(1-\nu^2)YR]/[E\sqrt{(1-\nu+\nu^2)}]$ gives

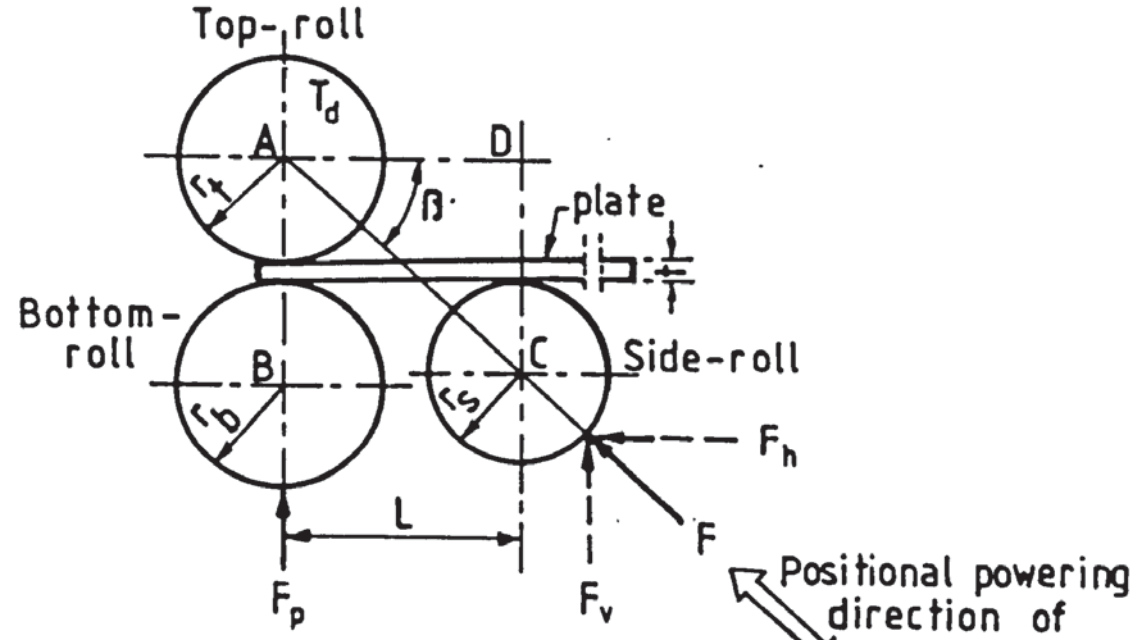

i - Initiation of pre-bending

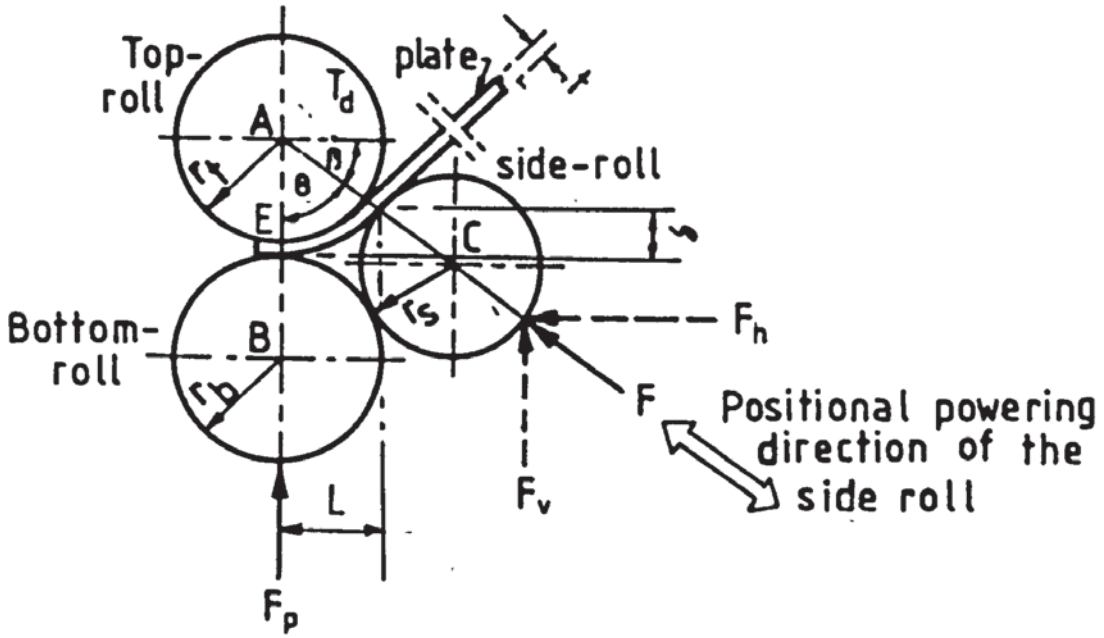

ii - Termination of pre-bending

FIG 3.2 THE ASSUMED CRITICAL CONFIGURATIONS OF THE ROLLERS

$$F = \{2Yb\{a^2-[(1-\nu^2)^2Y^2R^2]/[3E^2(1-\nu+\nu^2)]\}\}/\{(\sqrt{3})L\sin\tan^{-1}[r_t+r_s+t)/L]\} \quad (3.16)$$

At complete yielding, i.e. failure of the plate near the clamped edge $c=0$, F is expressed as

$$F = (2Yba^2)/\{(\sqrt{3})L\sin\tan^{-1}[(r_t+r_s+t)/L]\} \quad (3.17)$$

Equation (3.16) could be used as an approximation in order to estimate the force required to bend the plate to any radius of curvature, while (3.17) gives the maximum estimated force at the point of complete plastic penetration.

B. Force on the pinch roll

To prevent the plate moving backwards as bending proceeds, the generation of sufficient grip from the top and bottom rolls is required. If all other possible influential forces are ignored, the simplest configuration is for the pinch rolls to produce a tangential or frictional force, to oppose the tangential component, F_h, of the force F on the side roll.

Assuming the coefficient of friction μ is constant, the force F_p required on the pinch roll is thus :

$$F_p = F_h/\mu = F\cos\tan^{-1}[(r_t+r_s+t)/L]/\mu \quad (3.18)$$

After the substitution of F and simplification it gives

$$F_p = 2Yb(a^2 - c^2/3)\cot\tan^{-1}[(r_t+r_s+t)/L]/(\sqrt{3})L\mu$$

For bending any radius R of the plate, F_p is :

$$F_p=2Yb\{a^2-[(1-\nu^2)^2Y^2R^2/3E^2(1-\nu+\nu^2)]\cot \tan^{-1}[(r_t+r_s+t)/L]\}/(L\mu\sqrt{3}) \quad (3.19)$$

At the point of complete yielding F_p is :

$$F_p=2Yba^2\cot \tan^{-1}[(r_t+r_s+t)/L]/(L\mu\sqrt{3}) \quad (3.20)$$

Equations (3.19) and (3.20) are considered to be approximate estimations of the pinch force required for the pre-bending set up. For the purpose of the model design equation (3.20) is utilised. This gives the maximum force F_p.

C. Force on the top and bottom pinch roll

Equation (3.19) and (3.20) gives a reasonable but approximate estimation of the pinch force between the top and bottom rolls. It is difficult to apportion the force for each individual pinch roll, without a detailed analysis of the surface contact between each roll and the bent plate. In order to satify the design requirement, either one of the following two arbitrary choices is possible.

(1) Both the top and bottom rolls are arbitrarily taken to have the same force F_p.

(2) Only the bottom roll is arbitrarily taken to have the pinch force F_p. The pinch force F_t on the top roll is estimated as :

$$F_t = F_p + F_v = F(\sin\beta + \cos\beta/\mu) \quad (3.21)$$

for the equilibrium condition.

The second choice is a conservative estimate; it results in problems of bearing selection, as well as the mounting difficulty in relation to the cost and the size of the model.

The specifications of the Verrina bender revealed that the two rolls have almost the same cross-sectional area. Hence the adoption of the first choice is valid.

D. Torque required on the drive roll

Ignoring other possibly effective forces, the drive should generate sufficient torque, at least, to overcome the horizontal component, F_h, component of the force F on the side roll. This torque T_d is expressed as

$$T_d = F_h r_t \qquad (3.22)$$

After the substitution of the approximate terms and rearrangement, it gives the expression

$$T_d=\{2Ybr_t\{a^2-[(1-\nu^2)^2Y^2R^2/3E^2(1-\nu+\nu^2)]\}\text{cottan}^{-1}[(r_t+r_s+t)/L]\}/(L\sqrt{3}) \qquad (3.22)$$

for bending a plate to any radius of curvature R, and

$$T_d = \{2Ybr_t a^2\text{cottan}^{-1}[(r_t+r_s+t)/L]\}/(L\sqrt{3}) \qquad (3.23)$$

for a plate bent to the point of complete yielding at the pinch roll and plate contact region.

Physically, the torque obtained above is different from

that derived in section (3.2.3.). The former is required to overcome the tangential force F_h while the latter is purely the equivalent torque to bend the plate. For this reason, the total torque T_t required for a bend is approximately expressed as the sum of the two, i.e.

$$T_t = T_d + T_b \qquad (3.24)$$

As mentioned in section (3.2.3.), T_d (according to the analysis) might be partly due to the force F_v. Initially there was some uncertainty as to which torque, T_t or T_d, should be used as the drive torque. However, the numerical data analysis in section (3.4) has shown that the use of T_d, with an adequate factor, would be sufficient to simulate the drive in the Verrina bender. Naturally, T_t is the safe working torque for the model, but its acceptance increases the cost and size of the drive.

3.3.1.2. Termination of the pre-bending of the plate (fig 3.2(ii))

The critical condition, in this case, is that the bent plate almost touches the top roll. This is an unrealistic assumption since the surface contact is only limited in the region around the vertical central line of the pinch rolls and there is nothing to prevent movement of the bottom pinch roll towards the side roll.

Referring to figure 3.2(ii), it can be seen that the angle

β is equal to $90-\theta$.

From the triangle ABC, the following expression is obtained :

$$\cos\theta = (AB^2+AC^2-BC^2)/(2AB \cdot AC)$$

Since $AB = r_t+t+r_b$, $AC=r_t+t+r_s$ and $BC=r_b+r_s$, then :

$$\theta = \cos^{-1}\{[(r_t+t+r_b)^2+(r_t+t+r_s)^2-(r_b+r_s)^2]/[2(r_t+t+r_b)(r_t+t+r_s)]\}$$

Also from the triangle ABC, the moment arm, L, can be expressed as

$$L = (r_t+t)\sin\theta \qquad (3.25)$$

The substitution of θ above into equation (3.25) gives the complete expression for L.

The expression of the plate deflection, δ, at the contact point with the side roll can thus be expressed as

$$\delta = (r_t+t)(1-\cos\theta)$$

After the appropriate substitution of θ it gives :

$$\delta=(r_t+t)\{1-[(r_t+t+r_b)^2+(r_t+t+r_s)^2-(r_b+r_s)^2]/[2(r_t+t+r_b)(r_t+t+r_s)]\} \qquad (3.27)$$

A. Acting force on the side roll

The assumption of the maximum bending moment occurring at

the point E (fig 3.2(ii)) allows the external moment to be expressed as :

$$M = F(L\cos\theta + \delta\sin\theta) \qquad (3.28)$$

Equating this bending moment with equation (3.8) and the substitution of the expression for C gives :

$$F=\{2Yb\{a^2-[(1-\nu^2)^2Y^2R^2]/[3E^2(1-\nu+\nu^2)]\}\}/\{\sqrt{3}\{(r_t+t)\sin\{\cos^{-1}\{[(r_t+t+r_b)^2+(r_t+t+r_s)^2-(r_b+r_s)^2]/[2(r_t+t+r_b)(r_t+t+r_s)]\}\}\} \qquad (3.29)$$

for any particular bend radius R of a plate, and

$$F=(2Yba^2)/\sqrt{3}\{(r_t+t)\sin\{\cos^{-1}\{[(r_t+t+r_b)^2+(r_t+t+r_b)^2-(r_b+r_s)^2]/[2(r_t+t+r_b)(r_t+t+r_s)]\}\}\} \qquad (3.30)$$

at the point of complete yielding.

B. Force on the pinch rolls

For the reasons mentioned in section (3.3.1.1(b)), the choice of equal force on either pinch roll has been assumed. Thus the expressions at :

(1) any particular bend radius R of a plate, and at

(2) complete yielding of a plate C=0,

are as follows :

$$F_p= \{2Yb\{a^2-[(1-\nu^2)^2Y^2R^2]/[3E^2(1-\nu+\nu^2)]\}\}/\{\sqrt{3}[\mu(r_t+t)]\} \qquad (3.31)$$

and

$$F_p=(2Yba^2)/\{\sqrt{3}\mu(r_t+t)\} \quad (3.32)$$

C. Torque required from the drive to overcome the tangential force, F_h.

The torque required from the drive, in this case, is approximately equal to

$$\text{(i) } T=\{2Ybr_t\{a^2-[(1-\nu^2)^2Y^2R^2]/[3E^2(1-\nu+\nu^2)]\}\cot\theta\}/[\sqrt{3}(r_t+t)] \quad (3.33)$$

and

$$\text{(ii) } T=[2Ybr_ta^2\cot\theta]/[\sqrt{3}(r_t+t)] \quad (3.34)$$

D. The side roll moving with an angle, θ', relative to the pinch plane (see fig 3.3)

The geometrical configuration of the rolls (fig 3.3), in this case, is to simulate that of the Verrina bender. It should be noted that the angle, θ', is pre-set and remains constant throughout the bending process.

The main objectives of the approximate analysis in this section are

(1) to provide a basis for comparison between the estimated parameters of the model and those of the Verrina bender specifications,
(2) to study the variation of the estimated parameters of the

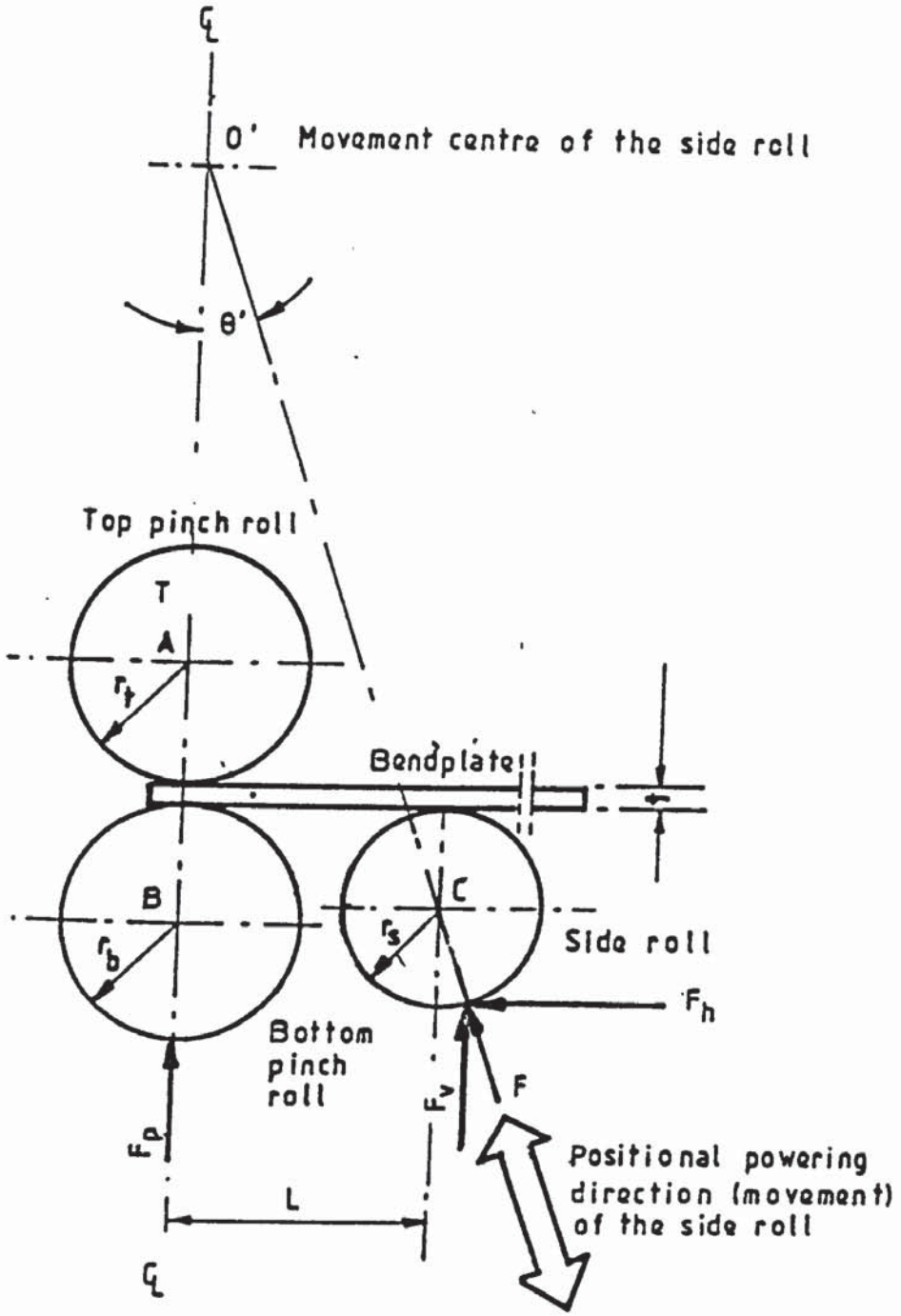

The critical configuration in pre-bending condition (initial condition)

FIG 3.3 THE CRITICAL CONFIGURATION OF THE SIMULATED BENDER ROLLERS

geometrical configuration with those in section (3.3.1), and to evaluate the workability of the model.

In this approximate analysis, most of the assumptions made in previous sections are again used.

3.3.1.3. Generation of the pre-bending (fig 3.3)

A. Acting force on the side roll

The acting force on the side roll may be estimated from the following expression :

$$F = F_v/\cos\theta' \qquad (3.35)$$

The substitution of equation (3.9) gives

$$F = \{2Yb\{a^2-\{(1-\nu^2)^2Y^2R^2]/[3E^2(1-\nu+\nu^2)]\}\}/[L\sqrt{3}\cos\theta'] \qquad (3.36)$$

for any particular radius R of bend, and

$$F = (2Yba^2)/(L\sqrt{3}\cos\theta') \qquad (3.37)$$

for complete yield through the plate thickness.

B. Acting force on the pinch rolls

The estimated force on both pinch rolls can be expressed as :

$$F_p = F\sin\theta'/\mu = (2Yb\tan\theta'/L\mu\sqrt{3})\{a^2-[(1-\nu^2)^2Y^2R^2]/\{3E^2(1-\nu+\nu^2)]\} \qquad (3.38)$$

for a particular bend radius R, and

$$F_p = F\sin\theta'/\mu = (2Yba^2\tan\theta'/L\mu\sqrt{3}) \quad (3.39)$$

for complete yielding through the plate thickness.

C. Torque required for the drive

The minimum torque required for the drive has the following expressions, i.e.

$$T=r_tF\sin\theta'=(2Ybr_t\tan\theta'/L\sqrt{3})\{a^2-[(1-\nu^2)^2Y^2R^2]/[3E^2(1-\nu+\nu^2)]\} \quad (3.40)$$

for any particular bend radius R of a plate, and

$$T=r_tF\sin\theta'=(2Ybr_ta^2\tan\theta'/L\sqrt{3}) \quad (3.41)$$

at complete yielding through the plate thickness.

3.4. Numerical data analysis of the model making

3.4.1. Data study

This section is mainly devoted to the analysis of the numerical data by the application of the above analysis. It also gives the reason for selecting the relative design parameters. The analysis is based on bending mild steel plate with $Y=235$ N/mm^2. With a model scale of 1/10, the application of expression (3.1), for $\mathring{a}_m/\mathring{a}_p=1$, gives the forces on the model side roll to be 85 kN, and on the pinch roll to be 167 kN. Also the application of the expression (3.12) gives the bending torque to be 98.1 kN m.

The above estimated data suggests that the torque is too high. In order to confirm the value obtained for the assumed drive torque, a direct calculation of the torque using

equation (3.13), for a model bending mild steel plate of b=305 mm, $A=a^2$=0.1 mm (i.e. c is assumed to be zero), L=99.4 mm and θ=4.12 mrad/s, has been carried out. The torque thus calculated is 143.8 kN m, which is in the same order as that obtained through the use of equation (3.12). A close study of the geometrical layout of the roll-bender indicates that this torque is a result primarily due to the nature of the applying force (However most work, in this case, is initially done by the side roll). It also seems to indicate that the drive torque required on the top roll may mainly be used to overcome the tangential component F_h of the force F on the side roll. It is thus an indication of the approximate analysis of the bender as shown in section (3.3).

A series of estimations was then performed using the expressions (3.36), (3.37), (3.38), (3.39), (3.40) and (3.41) for the Verrina bender when bending (see fig 3.3.) a full scale mild steel plate to the bend radius of 500 mm. The results indicated that the data calculated with c=0 and that with c pre-calculated with expression (3.6) were very close, i.e. within +2 %. For the former condition the data obtained (as tabulated in Table 3.1) showed good agreement with the original specification of the Verrina bender, though the estimated values were slightly higher (see Table 3.1). This shows that the model designed on the basis of the preliminary analysis can readily simulate the original prototype at HWT.

Subsequently, the model numerical data for the three critical geometric layouts, shown in figures 3.2 and 3.3. were also determined by using the appropriate expressions with c=0. The data generated is also tabulated in Table 3.1. The study of this data shows that the geometrical layout in figure 3.2(ii) gives the highest values, within +50 % of those for the layout in figure 3.2(i). The choice of the values has to

Table 3.1 Data Of The Model Bender Design Analysis

Data on the table was either extracted from the Verrina Bender at HWT or estimated from equations obtained from the preliminary rudimental analysis, in this chapter, for the pre-bending mode.

SPECIFICATIONS OF THE VERRINA FOUR ROLL BENDER AT HWT			
	Top Roll	Pinch Roll	Side Roll
Diameter (mm)	900	900	750
Maximum Roll Length (mm)	3050		
Daylight Between Pinch Roll (mm)	205		
Drive Torque (kN m)	981		
Drive Force (MN)		16.645	8.472

ESTIMATED DATA FROM THE APPROXIMATE ANALYSIS				
Layout	HWT Verrina Bender	HWT Verrina Simulation roll centre O' (fig 3.3)	Side Roll towards top roll centre A (fig 3.2i)	Side Roll towards top roll centre A (fig 3.2ii)
Pinch Roll Dia. (mm)	900	90	90	90
Side Roll Dia. (mm)	750	75	75	75
Max. Roll Length (mm)	3,050	305	305	305
Bend Radius (mm)	500	50	50	50
Plate Thickness (mm)	100	10	10	10
Side Roll Powering Angle, ψ^{o} (or ϕ^{o}).	20	20	47.06	49.43
Length of Roll (mm)	3100	310	310	310
Bending Arm (mm)	994	99.4	99.4	42.5
Top Roll Drive Torque (kN m)	136.16	1.362	4.017	5.556
Side Roll Drive Force (MN)	9.92	0.099	0.129	0.194
Pinch Roll Drive Force (MN)	16.93	0.169	0.445	0.615

take into consideration the cost to be incurred. Detailed enquiry for the selection of the motor indicated that the choice of a motor and gear-box to generate the torque of approximately 4 kN m substantially increases the cost of the drive unit to twice as much as that for generating the maximum torque of 2.5 kN m and they had to be specially ordered. However the study of the data shows that the selection of the latter will give a safety factor of 2.5 for the case in figure (3.3) and it is also possible to perform the bending tests for the case in figure (3.2). So, a compomise was made to select an existing Kopp variable speed drive which would generate a maximum torque of 2.5 kN m (at 4.5 rev/min) and run at a speed of from 4.5 to 40 rev/min.

3.4.2. Final choice of the parameters for the model

From the aforementioned study, the parameters for the model were finally decided as follows :

(1) Force on side roll to be 120 kN.
(2) Force on the top and bottom pinch rolls to be 450-500 kN.
(3) Torque of drive on the roll to be 2.5 kN m.
(4) The power of the side roll drive was arbitrarily taken as 2 kW
    - This drive arrangement facilitates the study of the slip, between the rolls and the bendpiece. Where the bending deformation zone of the bendpiece is between the pinch region the inlet or exit from the side roll.

The diameters of the top/bottom pinch roll and the side roll are 90 mm and 75 mm respectively. The full roll length is 310 mm.

The power drives and the rigidity of the rolls were designed to bend a mild steel plate of 235 N/mm^2 yield stress with a width of 305 mm, and thickness of 10 mm, to a minimum

bend radius of 50 mm before springback occurs

3.5. Formulae used in the component design of model bender

Most of the component dimensions of the model are calculated to give sufficient tensile and shear strengths at their maximum design loads. The normal safety factor used in the design ranges from 1.5 to 2, depending on the geometric constraint of the roll movement.

Below are some expressions used to calculate component dimensions with an assumed deflection.

(i) Cantilever beams/rods

(a) $\delta_{total} = 6FL/5btG + 4FL^3/Ebt^3$ for rectangular section

(b) $\delta_{total} = 10FL/9\pi r^2G + 4FL^3/3\pi Er^4$ for circular section

where δ is the free end deflection

(ii) End-supported beams

(a) $\delta_{total} = FL^3/16Ebt^3 + 3FL/10btG$ for built in beam

(b) $\delta_{total} = FL^3/4Ebt^3 + 3FL/10btG$ for simply supported beam

where δ is the mid-span deflection

3.6. The model bender

At the design stage the working principle of the model is first established to fulfil the design specifications (section 3.1). The following sub-section identifies the working principle of the model bender.

3.6.1. The working principle of the model bender

It was realised that the optimal condition of the side roll positional angle was significant in the assessment of the mechanics of the bending process. Furthermore a knowledge of the optimal bending arm in the initiation of the bending might lead to an improved design for a bender prototype for the metal forming industry. It was therefore useful to incorporate such investigations in the model in conjunction with the initial conceptual specifications of the model design mentioned in section (3.1).

The achievement of these design criteria requires the construction of a highly adaptable model, i.e. adjustment of the leg angles of ram (see fig 3.4). Hence, the general working principle of the model bender was as follows.

Referring to fig 3.4, the top roll A, with fixed centre, is the main power drive in the bender. The bottom roll B, which is free to rotate, is powered to move vertically to provide the pinch to the plate (This roll can be removed to simulate various types of three- roll symmetrical or asymmetrical benders). The side rolls, C and C', which are either free or driven to rotate, can move either along the axis of AC_0 and AC', or along the axis of $O'C_0$ and O'C', once the angle ϕ and ψ is pre-set. In the case where the former movement is chosen, the angle of ϕ can only be varied by suitably fixing the distance of X. If the latter movement is operative, the angle of ψ can be adjusted either by varying the distance of X or by rotating the axis about the points C_f and C_f' respectively.

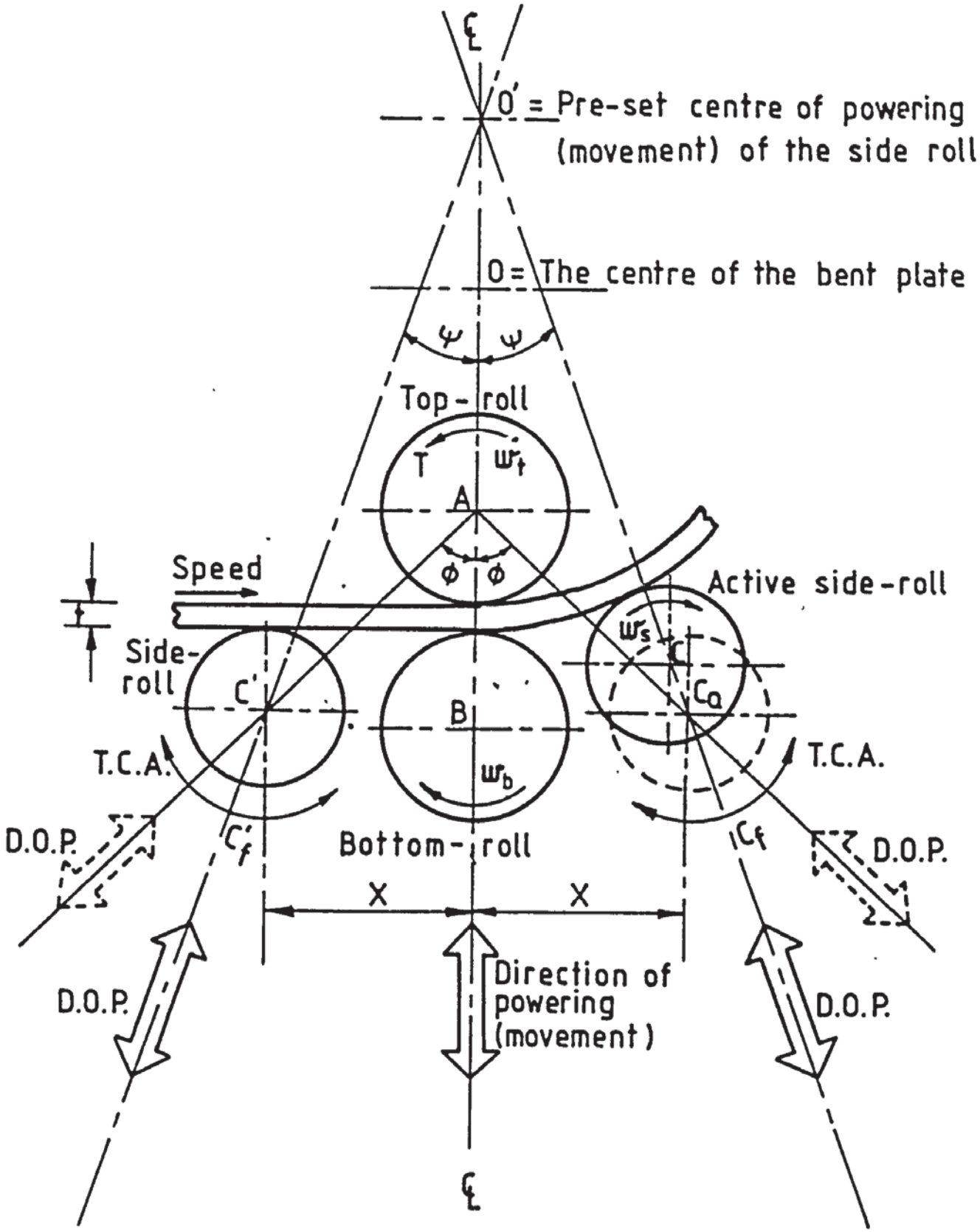

NOTE: T.C.A. = Top circular arc

D.O.P. = Direction of powering (movement)

FIG 3.4 THE WORKING PRINCIPLES OF THE MODEL BENDER

Working on these principles, the configuration of the Verrina bender can thus be simulated by suitably adjusting X and ψ. The slip effect can also be studied by driving the side rolls to rotate with different rotational speeds and directions. Most of the aforementioned design specifications are also accomplished with this principle.

The following describes the application of these principles to the actual design model.

3.6.2. The designed model bender

After an assessment of the design forces and torque for the model was made as mentioned in section 3.4, and the working principle as formulated in section 3.6.1, the design of a model bender was then formulated. Figure 3.5(a) shows the final assembly of the designed model bender.

The model bender can generally be divided into the following five major units, such as :

(a) the framework and detail of the bender (fig 3,5(b)),
(b) the hydraulic drives of the bottom pinch roll and the side rolls
(c) the base-bed of the bender,
(d) the motor drives of the top roll and the side rolls,
(e) the instrumentation of the model.

Details of the design considerations for units (a) to (d) will be described in the successive sections. Unit (e) will be dealt separately in Chapter Four.

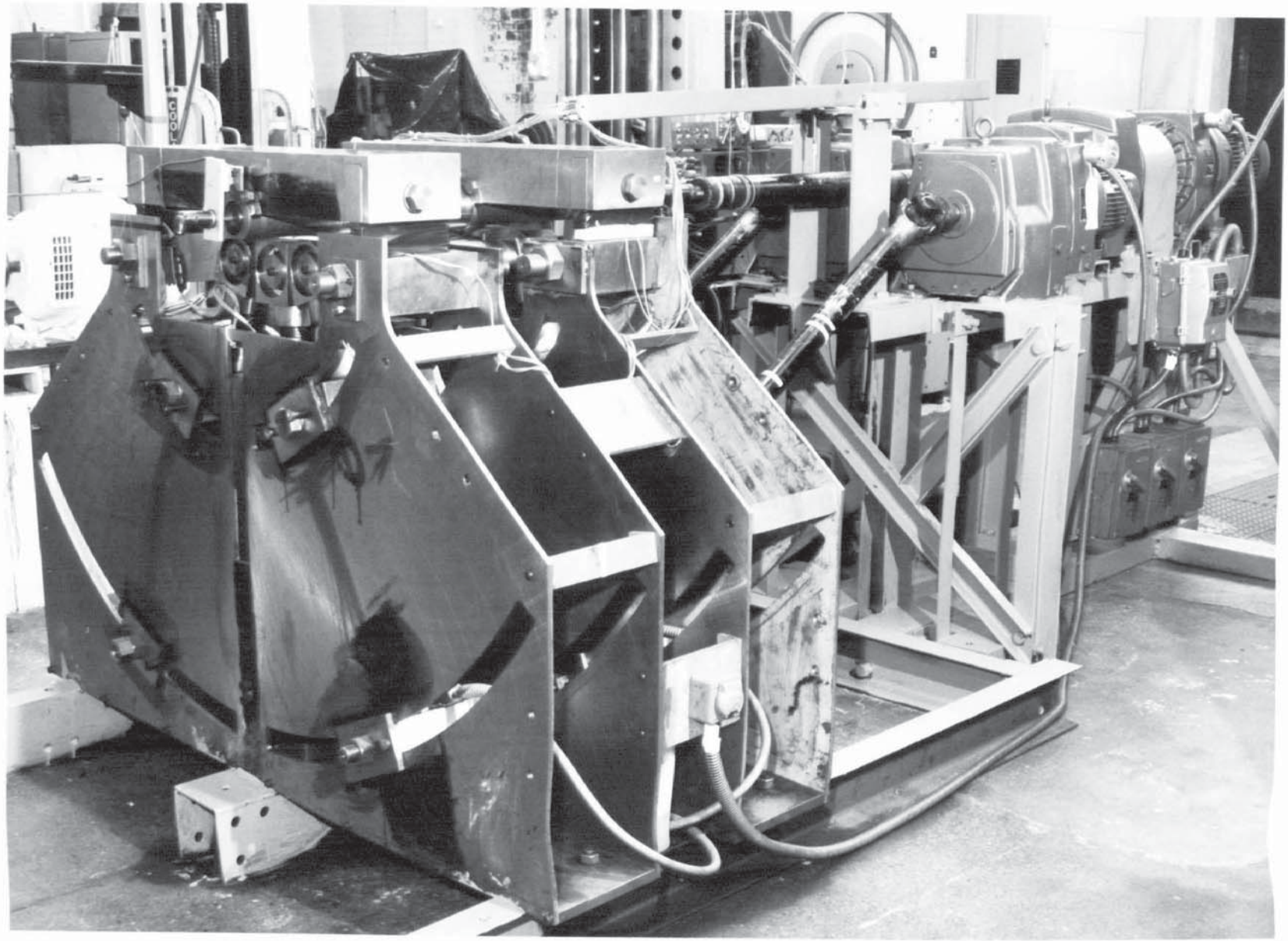

FIG 3.5(a) THE DESIGNED MODEL BENDER

3.6.2.1. Framework and details of the bending unit

The detailed description of the item and the relevant drawings are given in Appendix 3.1.

A. The framework of the bender

Referring to figure 3.5(b), the framework consisted of four 10 mm (thick) x 1060 mm (high) X 1700 mm (wide) mild steel end plates (item 1). Each end plate had two sets of sectorial slots, which had radii of 371 mm and 421 mm, and 950 mm and 1000 mm, respectively, with respect to the centre of the top roll (The centre of the top roll was at the position 100 mm above the top edge of the plate and on the plate centre line). A rectangular slot of 50 mm (wide) x 417 mm (high) was milled in the middle of each end plate. There was also a rectangular cut section of 525 mm (wide) x 180 mm (high) at the middle of the top edge of each end plate.

Each pair of the end plates was held together by a 10 mm (thick) x 240 mm (wide) x 1700 mm (long) mild steel holding plate (item 7), and four 10 mm (thick) x 50 mm (wide) x 240 mm (long) channel- shaped steel holding strips (item 4) along each vertical and inclining side edge as illustrated in figure 3.5(b). The end plates formed a sandwich unit for building up the mechanical parts of the hydraulic drives for each end of the bottom pinch and side rolls.

The two pairs of end plates (or sandwiching units) were held together by four 10 mm (thick) x 150 mm (wide) x 463 mm (long) mild steel cross-holding strips (item 5). The units were fastened to a base-bed (fig. 3.8).

On the top of each pair of end plates, there was a 110 mm (deep) x 194 mm (wide) x 780 mm (long) mild steel top beam (item 2) supported by a top loadcell (item 3) at either end. The loadcells were sandwiched and clamped to the pair of end

Fig 3.5(b) MODEL BENDER ASSEMBLY

ITEMS OF THE MODEL BENDER :-

1- End supporting plates
2- Top cross beam
3- Top roll loadcells
4- Holding strips for the end supporting plates
5- Cross holding strips
6- Bearing housing of the top roll
7- Bottom holding plates for the bending unit
8- Locking pins for the top roll loadcells
9- Clamping plates for the top beam loadcells
10- The top roll
11- The bottom pinch roll
12- Bearing Housing of the bottom roll
13- Connecting block of the bottom roll
14- Base block of the bottom roll hydraulic cylinder
15- Hydraulic cylinder retaining blocks for the bottom roll
16- Locking ring for the spherical bearing's inner raceway of the bottom roll
17- Torrington 20SF32 bearing housing locking rings
18- The side roll
19- Bearing housing of the side roll
20- Top clamping block of the side roll hydraulic cylinder
21- Locking plate for the side roll top clamping block
22- Connecting blocks for the side roll
23- Base-block for the side roll hydraulic cylinder
24- Bottom clamping block for the side roll hydraulic cylinder
25- Locking rods for the bottom clamping block of the side roll hydraulic cylinder
26- Locking plates for the side roll bottom clamping block
27- Torrington 17SF28 bearing housing locking ring
28- Locking ring for the side roll spherical bearing (inner raceway, free end)
29- Loadcell for the bottom pinch roll and the side rolls
30- Glacier MB100DU bearing locking ring
31- Locking ring for the side roll spherical bearing (inner raceway, driven end)
32- Loadcell cover for the bottom roll
33- Bush bearings for the side roll connecting block

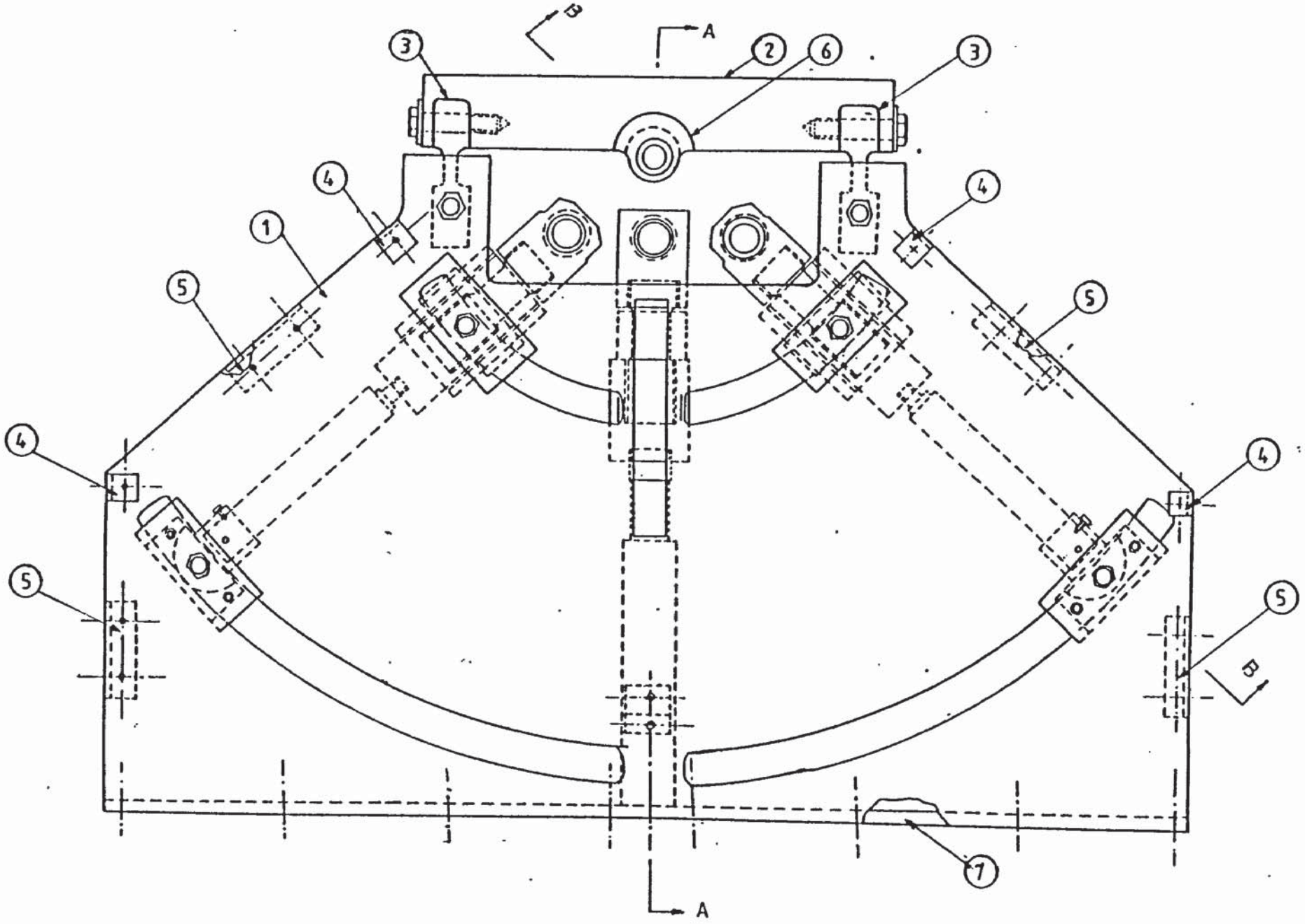

(i) End view

FIG 3.5(b) MODEL BENDER ASSEMBLY

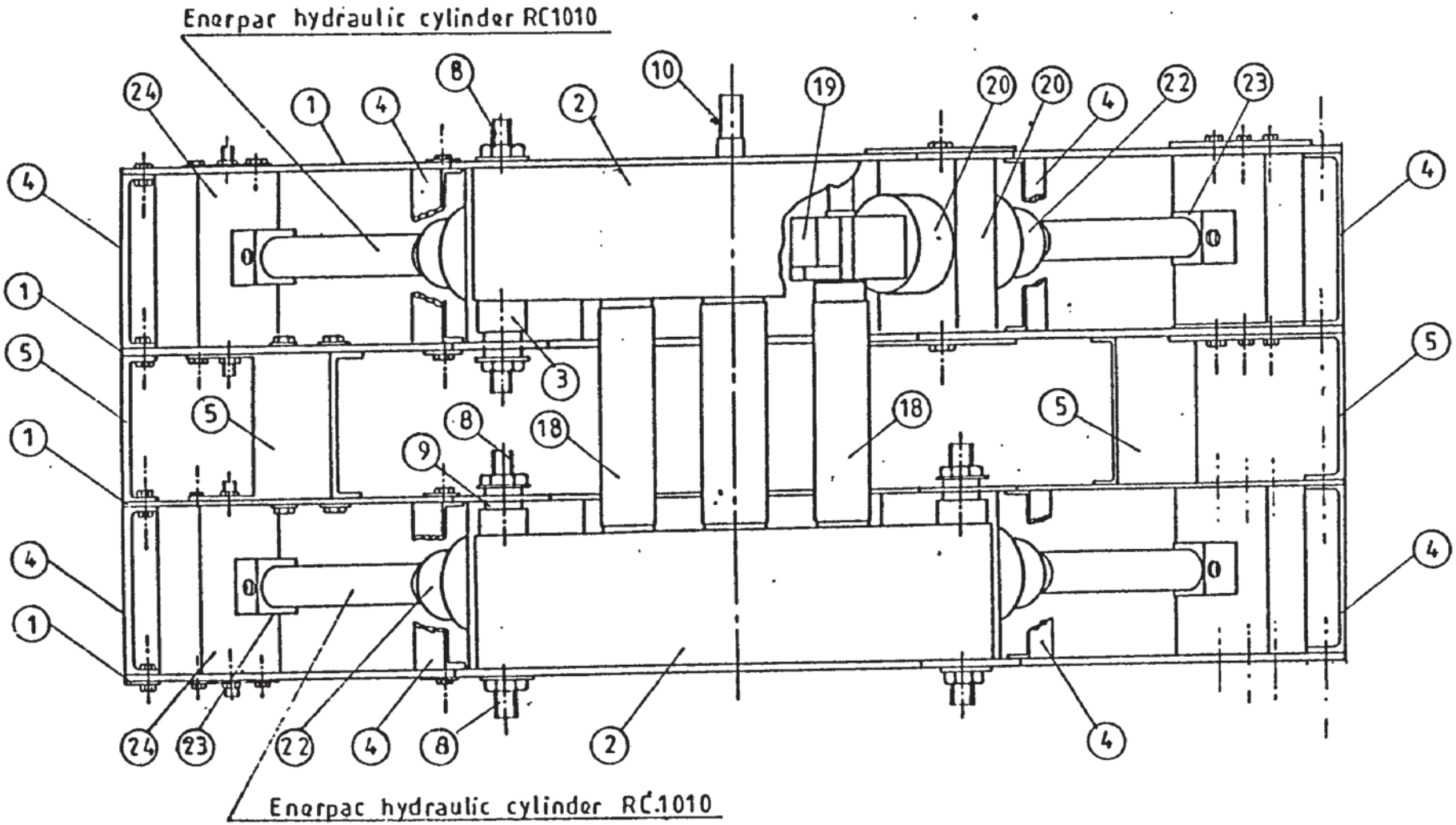

(ii) Plan view

FIG 3.5(b) MODEL BENDER ASSEMBLY

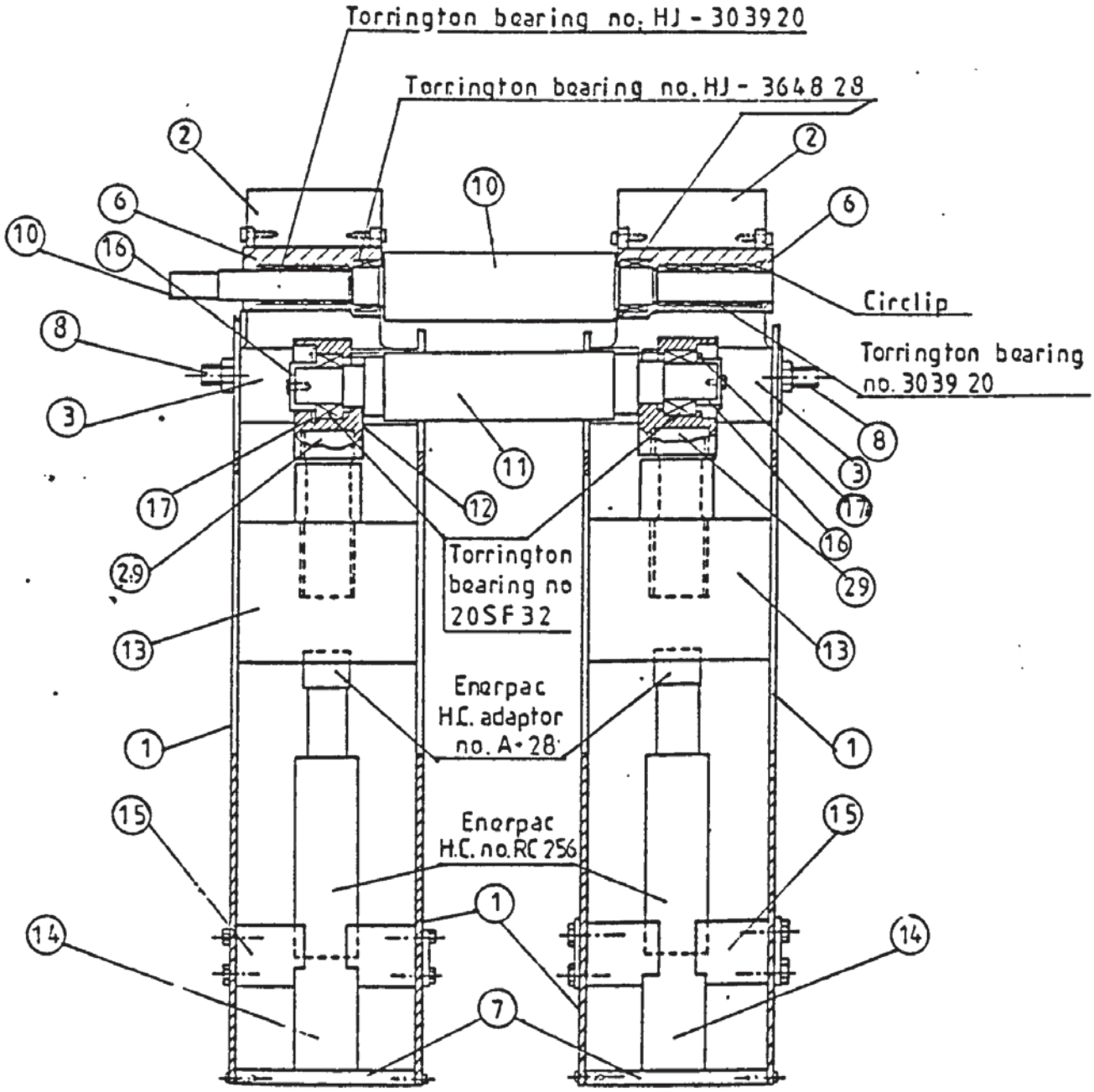

(iii) Sectional view of AA

FIG 3.5(b) MODEL BENDER ASSEMBLY

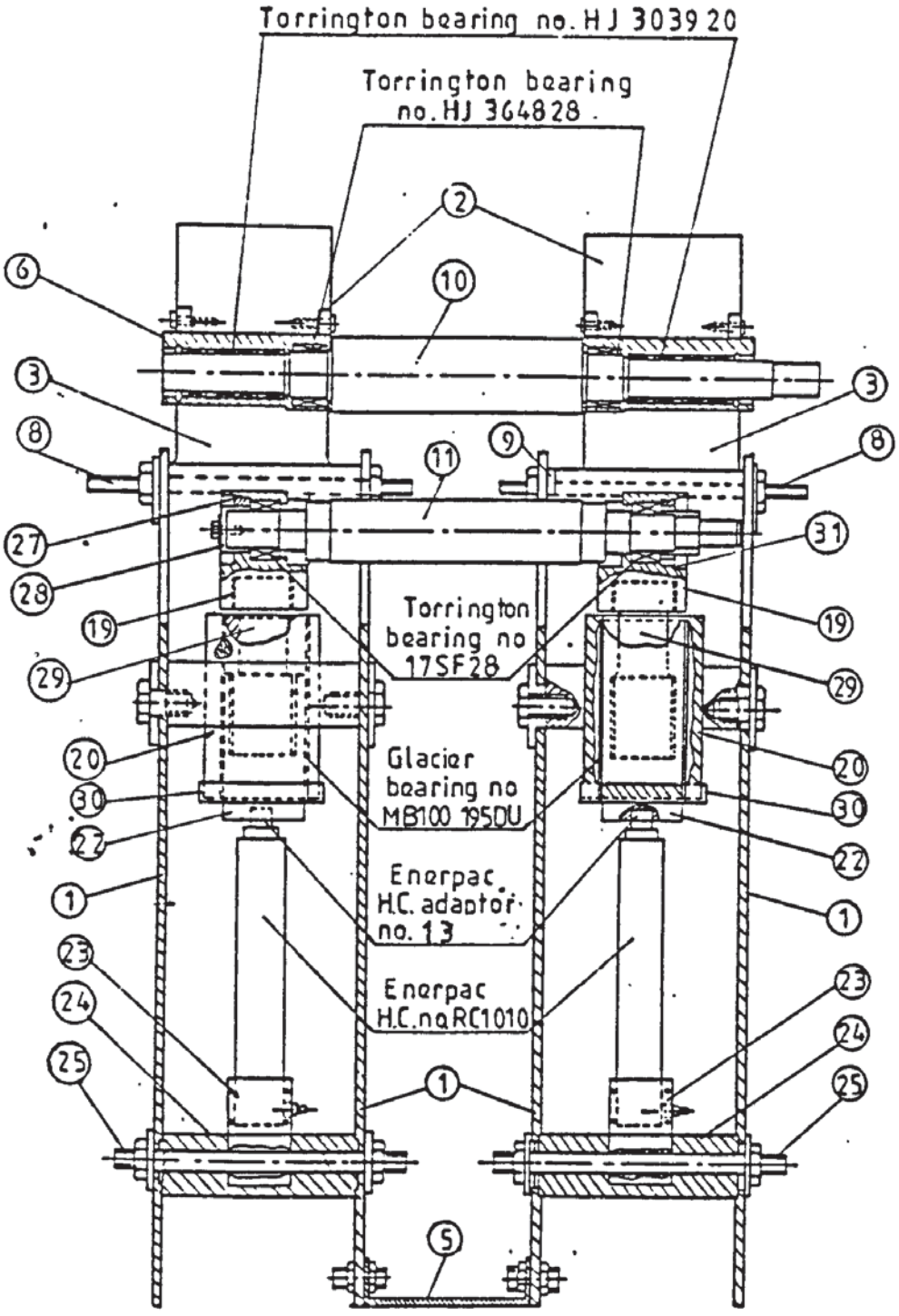

(iv) Sectional view of BB

FIG 3.5(b) MODEL BENDER ASSEMBLY

plates as shown in fig 3.5.

The circular slots in the end plates were made to locate the pre-set side roll hydraulic cylinders (i.e. the arced slots of radii 371 mm and 421 mm were for clamping the top retaining block of the side roll (item 20) while the sectorial slots of radii 950 mm and 1000 mm gave the access for clamping the bottom retaining block of the side rolls (item 24). The rectangular slot was made to hold the connecting blocks of the bottom roll (item 13) in position and to guide the vertical movement of the block.

The 525 mm x 180 mm rectangular section at the middle of the top edge on each end plate allowed access of the end drive to the side roll. It also allowed for free movement of the bottom and side rolls.

The circular trough on the bottom of each top beam was made for retaining the top roll housing bearing. The loadcells were located between the bearing housings and the corresponding connecting blocks, and then to the positioning Enerpac hydraulic cylinder (EHC) in the sandwiching partition of the sandwich unit. This provided a rigid framework for the bending section of the model.

B. The mounting of the rolls (fig 3.5(b))

All the rolls were made of Uddeholm tool steel (UHB Arne) with a specified hardness of 58-62 HRC. The rolls have a full roll length of 310 mm and a specified surface straightness of 0.8 μm/45 mm. The measurement of the surface finishes using a Talysurf have the following average values of CAL :

(i) 0.368 μm for side roll 1
(ii) 0.533 μm for side roll 2
(iii) 0.413 μm for bottom pinch roll

(iv) 0.418 μm for top pinch roll.

(a) The side roll

The side roll (item 18) had a diameter of 75 mm along its full rolling length. Each end of the full rolling section had stepped diameters of 72 mm and 50 mm; each 30 mm in length. A further section of 64 mm in length by 44.45 mm in diameter, at the ends facilitated the mounting of the Torrington spherical bearing no.17SF28 and its corresponding locking ring (item 28). At the driven end, a Torrington spherical bearing (no.17SF28) was mounted over a section, of length 54 mm and diameter 44.45 mm, partly threaded for a length of 30 mm to accommodate the locking ring (item 31). At the extreme ends of the driven shaft a 46.5 mm square section facilitated the coupling of the side roll torquemeters. The total length of the side roll, including the neck, was thus 624.5mm.

The bearing at each end of the side roll was mounted into a bearing housing (item 19) which was screwed to a loadcell (item 29). Attached to the loadcell was a 180 mm long circular connecting block (item 22) of diameter 100 mm, which was connected to an Enerpac hydraulic cylinder No.RC1010. The circular connecting block could slide within a top clamping block (item 20) of circular arc inner radius 370 mm. This was securely clamped to the end plates (item 1), which therefore absorbed most of the side load applied and prevents its rotation. The Enerpac hydraulic cylinder was sited in a base block (item 23) with a semi-circular male lug of diameter 120mm, which was located in the bottom clamping block (item 24) by the locking rod (item 25). The clamping block (item 24) was securely located in a sectorial slot of inner radius 950 mm in the end plate (item 1). It thus absorbed most of the axial load of the side roll (The semi-circular lug in item 23 allowed for the adjustment of the positional direction and the angle of the side roll with the bottom clamping block (item

24). To ensure the rigid clamping of the top and bottom clamping blocks on the end plates, M10 mm GKN cap screws were also employed, in addition to the main locking screws and pins (items 20 and 25), to reinforce the locational holding pressure on the clamping blocks. The positional locking plates (items 21 and 26) were used mainly to increase the surface contact area of the locking mechanism of the side roll and the end plate.

The mounting of the side roll in this way ensured the effective absorption of the force components on the side roll and allowed for flexible setting of the side roll. Hence the various design requisites in sections 3.1 were satisfied.

The mounted side roll deflected a maximum of 0.43 mm at its full load of 120 kN ; this was calculated by assuming that it was a simply supported stepped shaft.

All the mounting parts are designed to the maximum loaded strength with a safety factor of not less then 2, and positioned between the pair of end plates.

(b) The bottom pinch roll (ref to fig 3.5(b) and item drawing no. 11)

This roll had a total length of 564 mm. It consisted of a 310 mm full rolling length of diameter 90 mm with stepped end sections of 86 mm diameter by 30 mm in length, 57.15 mm diameter x 27.5 mm long, and 50.8 mm diameter x 67 mm long (This was for mounting the Torrington spherical bearing No.20SF32 and its locking ring, item 16), at either end of the full rolling length section.

The bearing at each end of the roll was mounted into a bearing housing (item 12), which was screwed to the top of a loadcell (item 29). The bottom of the loadcell was screwed to

the top of a connecting block (item 13). This was located in the rectangular slot within the end plates, and thus allowed for vertical movement. The bottom of the connecting block was connected to an Enerpac hydraulic cylinder (EHC) No.RC256 by an Enerpac hydraulic cylinder adaptor No.A28. The EHC was fixed on a base block (item 14) and located to prevent misalignment by a pair of holding blocks (item 15). The base block was positioned on the top of the bottom holding plate (item 7) of the sandwich unit.

The roll was tightly locked in the bearing housing by the outer raceway locking ring (item 16) and the inner raceway locking cap (item 17). It thus prevented side movement of the roll and ensured the alignment of the roll length with respect to the other rolls.

The roll gave a maximum deflection of 0.52 mm at its full load of 500 kN. This was calculated by considering it to be a simply supported stepped shaft.

(c) The top roll

The top roll had a total length of 819 mm. It consisted of a 310mm full roll length of diameter 90 mm and end sections of 62 mm diameter by 3 mm in length, 57.15 mm diameter by 49 mm in length (for mounting a Torrington bearing No.HJ384828), and 47.7 mm diameter by 160 mm in length (this was for mounting four Torrington bearings No.303920) at either end of the full roll length section. The sideways movement of the bearing (or the roll) was eliminated by a shoulder head and circlips. A 38 mm square section (55 mm long) at the end of the driven end facilitated the coupling of a torquemeter, which was connected to a propshaft and gear box of the main drive.

The bearings of the roll were mounted in a housing (item 6). This consisted of an off-centred, stepped-bore cylindrical

tube of 90 mm diameter and 205 mm length, with flanges at each end of the tube. The housing was bolted to the top beams (item 2). This arrangement enabled the extraction and replacement of the tube unit in the model.

The beam was designed to give a maximum deflection of 0.32 mm at its full load. The mounted roll gave a maximum deflection of 0.36 mm at its full load of 500 kN. This deflection was calculated by considering the roll to be simply-supported stepped shaft.

3.6.2.2. The hydraulic drive of the side rolls and the bottom pinch roll

The bottom pinch roll was powered by an Enerpac hydraulic cylinder (EHC) No.RC256 at each end. Each EHC provided a thrust of 230 kN and a maximum stroke of 159 mm.

The thrust of the side roll was supplied by an EHC No.1010. Each cylinder gave a force of 100 kN and a maximum stroke of 260 mm. The reason for over specifying the side roll drive was that it was difficult to obtain an appropriate small-sized cylinder to supply the power and at the same time give the required stroke.

It should be noted that the stroke of the hydraulic cylinders could either be kept to its maximum or be varied by a suitable choice of the height of each connecting block (item 13 or 22).

A. Connection and hydraulic circuitry of the side roll drive

Figure 3.5(b-iv) clearly illustrates the sequence of connection for each of the side roll drive components. From the sectional view BB of the model bender, it can be seen that

each end of the side roll was mounted to a Torrington spherical bearing No.17SF28, which in turn was housed in a bearing housing (item 19). The bearing was positioned on the roll by an end cap (item 28) and in the housing by a locking ring (item 27). The bottom of the housing was connected to a loadcell (item 29) which was in turn screwed on to the top of a connecting rod (item 22). The bottom of the connecting rod was then screwed to an Enerpac hydraulic cylinder (EHC) adaptor No.13 which was connected to an EHC No.RC1010. The cylinder slides in a base block (item 23) and can be locked. It was located in a bottom clamping block (item 24). The clamping block was sandwiched and locked by locking rod (item 25) into the arced slot of radii 950 mm and 1000 mm (with respect to the centre of the top roll) on the pair of end plates (item 1).

The mounted connecting push rod (item 22) and the loadcell were capable of moving vertically along the central line of the hydraulic cylinders in a bronze bush (item 34) in a top clamping block (item 20). The top clamping block was securely located and clamped in the sectorial slot of radii 371 mm and 421 mm.

The hydraulic circuitry of the side roll cylinders is shown in figure 3.6. The hydraulic cylinder was powered by an Enerpac hydraulic hand pump (EHHP) No.P80 type-2 speed, which was capable of providing the oil (220×10^4 mm^3) to the four EHCs during their full operating condition (i.e. 700 bar). The two way manual shut off valve was capable of operating at 700 bar from either port. The male thread fittings for the valve are 3/8 NPTF. All the fittings in the circuitry were made and recommended by Enerpac.

By suitably operating the pair of valves (1) and (2), or (3) and (4), respectively, with the hand pump on, the corresponding side roll No.1 or No.2 could be activated. The

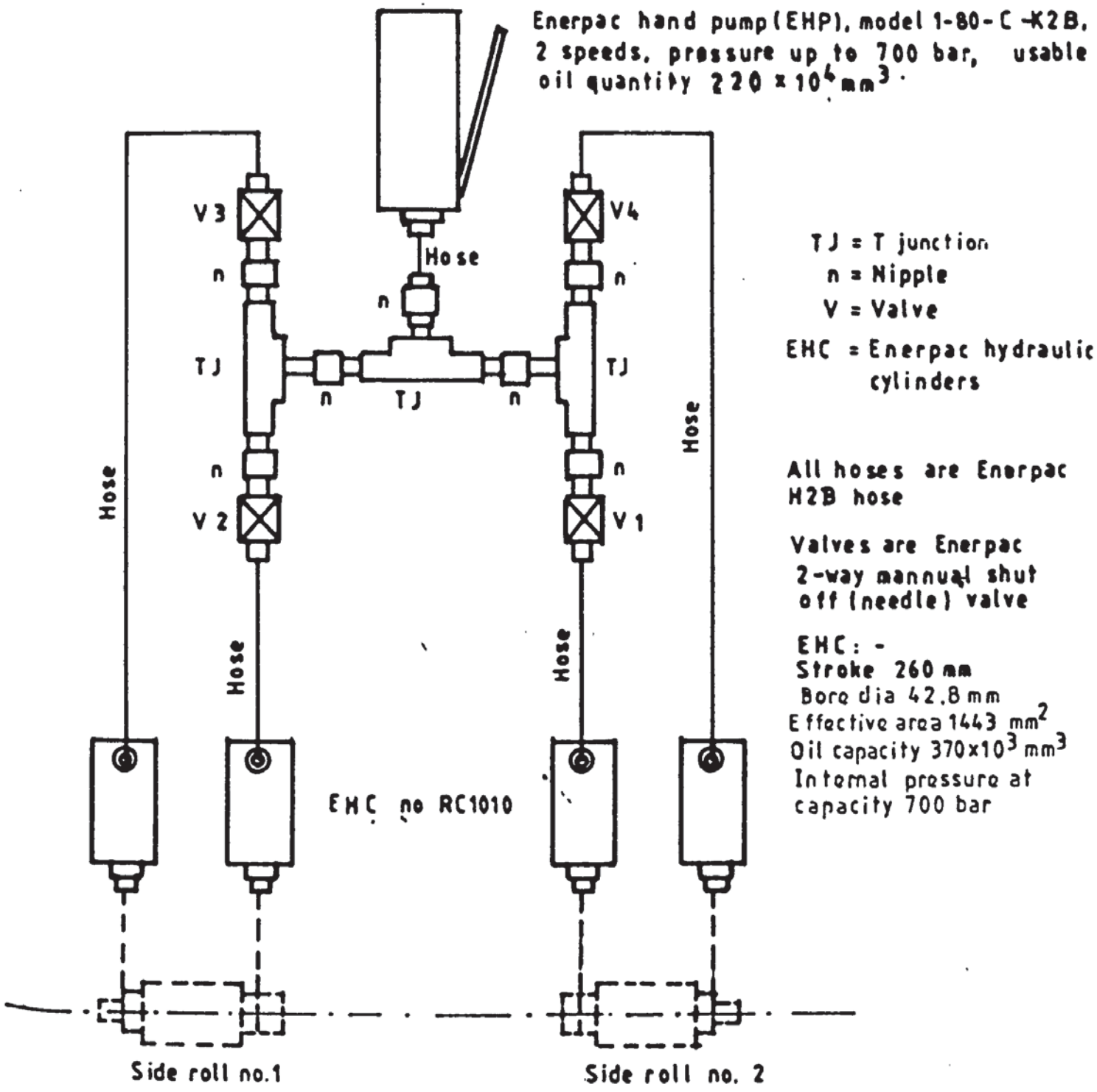

FIG 3.6 THE POWERING CIRCUITRY OF THE ENERPAC HYDRAULIC CYLINDER NO. RC1010 FOR THE SIDE ROLL OPERATION

levelling of the side roll in the bending process could be achieved by suitably adjusting the corresponding pair of valves (see fig. 3.6).

B. Connection and hydraulic circuitry of the bottom pinch roll drive

From the sectional view AA of the model bender in figure 3.5(b-iii), it can be seen that each end of the bottom pinch roll was mounted to a Torrington bearing No.20SF32, which in turn was housed in a bearing housing (item 12). The bearing was locked in the housing by an outer raceway locking ring (item 17) and the roll was prevented from lateral movement by a locking cap (item 16). The bottom of the bearing housing was screwed to the top of a loadcell (item 29). The loadcell was then screwed to a connecting block (item 13). The connecting block was located in, and allowed to move along a vertical square slot on the end plate (item 1). The bottom of the connecting block is connected to an Enerpac hydraulic cylinder (EHC) adaptor No.A28, which linked the connecting block to an Enerpac hydraulic cylinder No.RC256. The EHC was positioned on a base block (item 14) and was positionally clamped by a pair of holding blocks (item 15). The base block was placed on a bottom holding plate (item 7) of the sandwich unit.

The EHC was also powered by an Enerpac hydraulic hand pump with its circuitry as shown in fig 3.7. The hand pump had similar specification as that used for the side roll circuitry (fig 3.6). When the hand pump was operative, the levelling of the bottom pinch roll could be suitably adjusted by controlling the opening of the circuit valves (fig. 3.7).

3.6.3. The base-bed of the bender

The design specification (5) of the bender model as stated in section 3.1 implied the rejection of permanently mounting

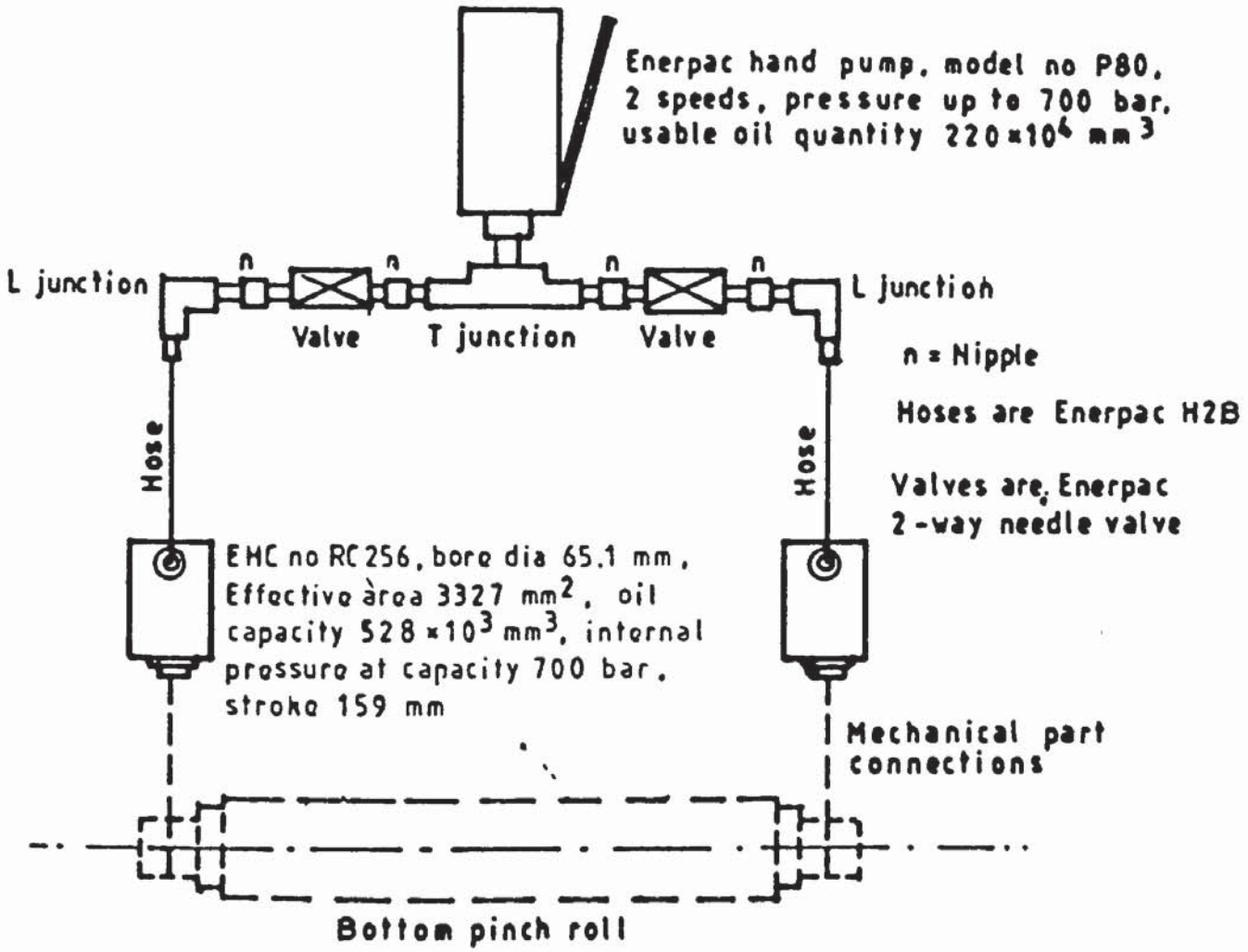

FIG 3.7 THE POWERING CIRCUITRY OF THE ENERPAC HYDRAULIC CYLINDER NO RC256 FOR THE BOTTOM PINCH ROLL

the bending unit on the floor. Furthermore, its rigidity precluded the placing of the bending unit and the motor drives on the floor. Consequently the required alignment and the rigidity of the model assembly confirmed the necessity of the base-bed.

Since ease of assembling and dismantling of the model bender was an important design criterion, the base bed was not welded. Instead, bolts were used in most parts of the assembly.

In designing the base frame, as illustrated in fig 3.8, the following factors were taken into consideration.

(1) the stability of the motor drive,
(2) the rigidity of the base frame,
(3) the accessibility of a stacker truck into the base bed to lift a heavy bendpiece after it has been formed,
(4) the freedom of the movement of the motor drive propshaft and the prevention of the blockage of the drive couplings, and
(5) the availability of materials.

Basically, the base bed consisted of two structures, i.e.

(a) The base frame for the bending unit
- this part was 152.4 mm high and was bolted together by 76.2 mm "L" sectional brackets. The bending unit was bolted onto the front of the bed. The two 152.4 mm wide mild steel plates, bolted across the edge channel sections and the middle channel 152.4 mm wide x 152.4 mm high at the front, provided access for the lift truck legs. It was bolted to a base frame of the motor drives at the rear of the bed.

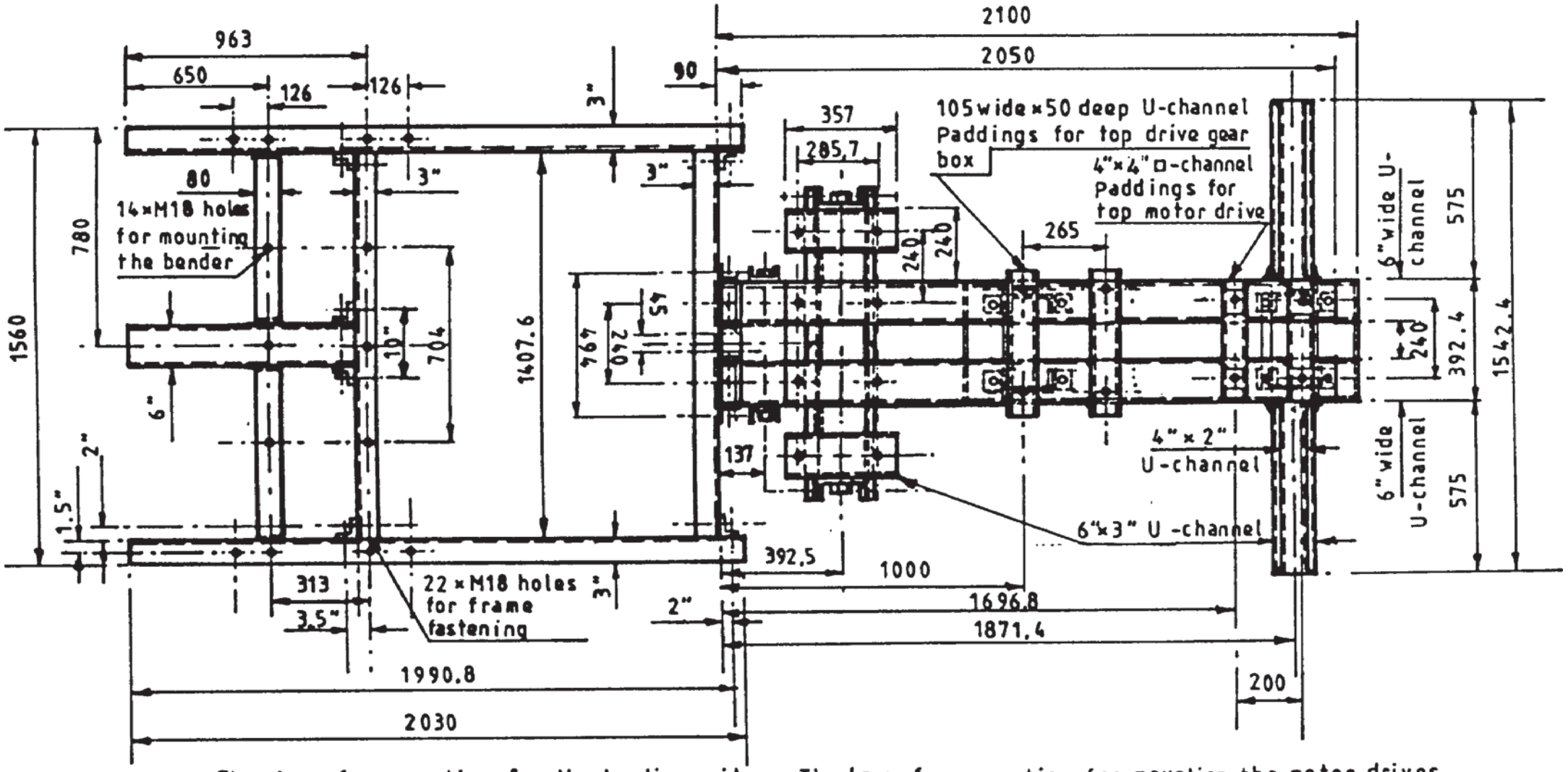

The base-frame section for the bending unit The base-frame section for mounting the motor drives

Material: ⊔-channels unless specified Dimensions in mm unless specified Scale: 1 to 20

(a) The plan view

FIG 3.8 THE DESIGN OF BENDER BASE BED

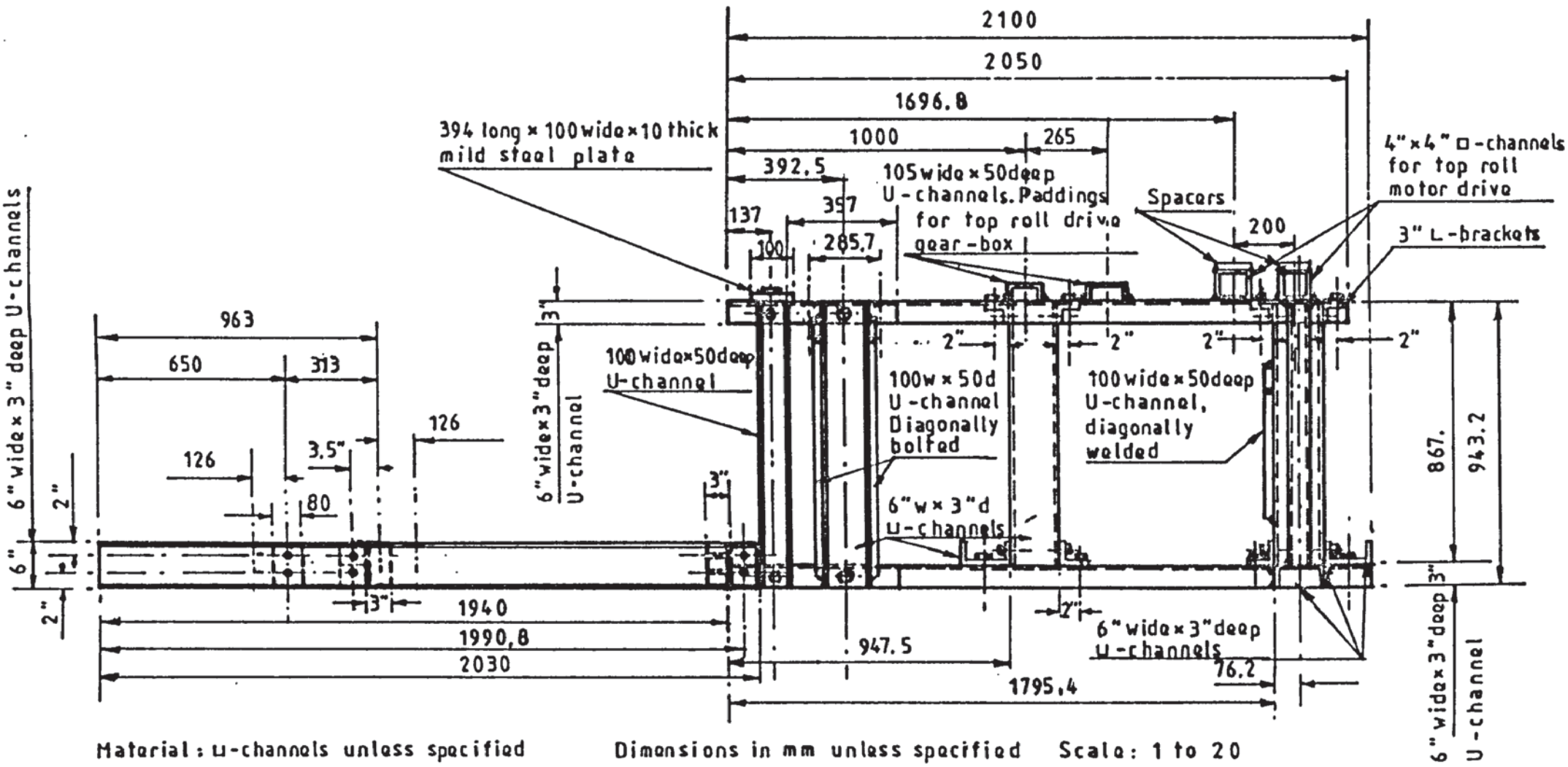

(b) The side view

FIG 3.8 THE DESIGN OF BENDER BASE BED

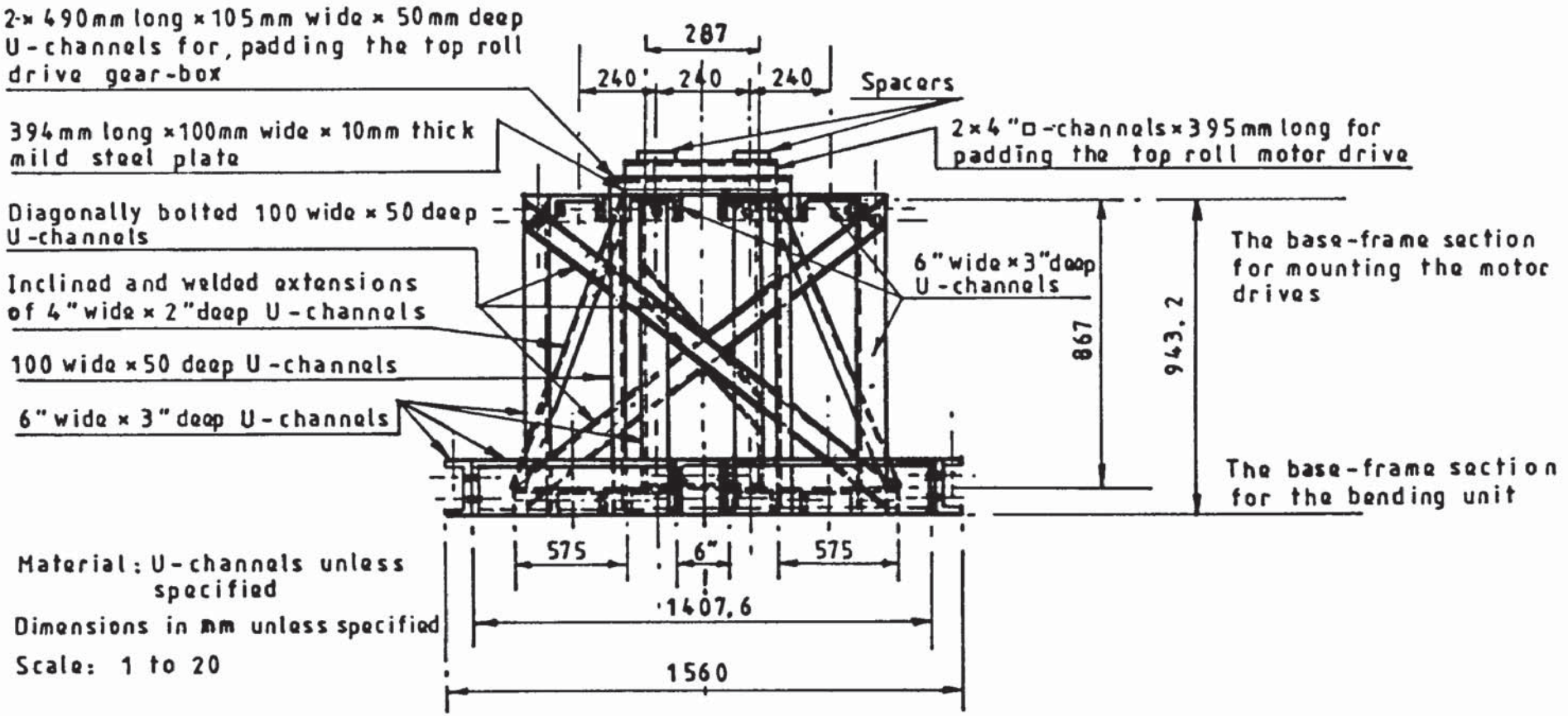

(c) The end view

FIG 3.8 THE DESIGN OF BENDER BASE BED

The overall dimensions of the base frame were 1560 mm wide x 2030 mm long x 152.4 mm high. The width and length were chosen to give sufficient stability to the bending unit when operating under working conditions.

(b) The base frame for mounting the motor drives
- this base frame was made of two layers, separated by three rows of 867 mm high channel columns. Each layer consisted of two 2050/2100 mm long x 152.4 mm wide channel sections with flange extension at the front section. At the front row columns, there were two pairs of channels diagonally bolted to the columns to stabilize the framework. For stability reason, at the rear row column, there was a channel section diagonally welded at an angle of 56° to the ground.

The nominal height of the frame work was 953 mm. The front flange extension at either side of the top layer was for mounting the side roll drive motors. The two main top parallel channel section (welded with suitable spacing channel) were for mounting the gear box and the Kopp variator which drove the top roll.

The base frame can easily be unbolted from the base frame of the bending unit. It can also be dismantled and stripped by simply unbolting the relevant connections. This facilitated handling of the rig.

This base bed gave the required rigidity and also met the design specification (5).

3.6.4. Motor drives for the model

3.6.4.1. The top roll drive

The maximum "daylight" in the pinch of the rig could be

suitably adjusted by altering the following parameters

(a) The height of the top loadcells.
(b) The height of the connecting block (item 13) of the bottom roll.

and

(c) The appropriate choice of a hydraulic cylinder to give the necessary stroke.

In the case of condition (a), it was essential to allow the top roll motor to accommodate a certain range of off-set in the driven shaft. It therefore led to the use of a prop-shaft in the top roll powering line. The prop-shaft also provided convenient handling of the bendpiece from the rig (i.e. to take off the bent plate by simply unbolting the top roll bearing housing from the top beam, without disturbing the couplings of the drive).

A 5.5 hp 321MS unit, coupled to a separate HT6R1 gear box by a Desch Conax RTW2 safety slip clutch, drove the top roll via a Kopp variator. The gear box was attached to a propshaft of nominal length 1564 mm, which was connected to a 200 mm long torquemeter (fig 3.9), at the square end of the top roll.

The propshaft, of length 150 mm, transmited a torque not less than 2.45 kN m at a minimum speed of 4 rev/min. This prop-shaft allowed the top roll to have a sufficient freedom of movement to cover an area of a conical base of diameter 400 mm. The outside diameter of the prop-shaft was 756.2 mm.

3.6.4.2. The side roll drive

Although the side rolls of the Verrina bender at HWT were free to rotate, the introduction of a motor drive to each side roll was needed in order to facilitate the study of the slip effect on the bending mechanics. One of the difficulties in

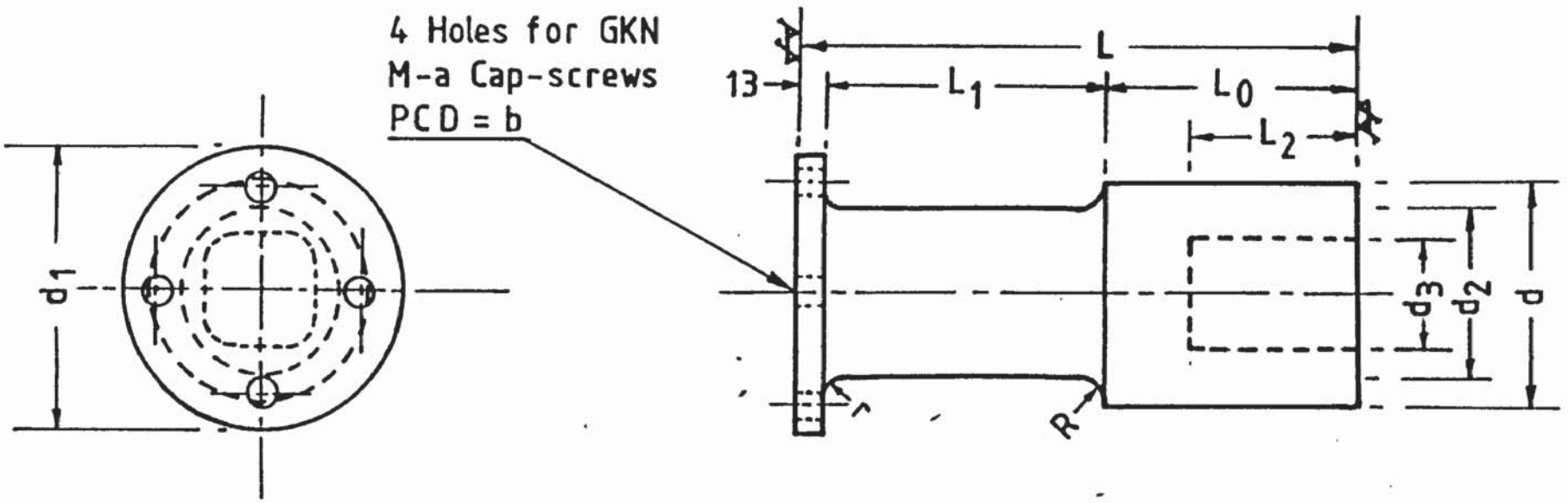

87

No. Off	a	b	d	d_1	d_2	d_3	L	L_0	L_1	L_2	R	r	
1	12	75	80	100	55	$38^{\pm .078}_{.000}$	200	90	97	60	6	4	TOP ROLL
2	10	65	70	80	45	$28^{\pm .078}_{.000}$	190	85	92	50	6	4	SIDE ROLL

Material : En8 Steel All Dimensions in mm

FIG 3.9 DESIGN OF TORQUEMETERS

the implementation of the side roll drive was that the position of the axis of the side roll changed as the bending proceeds. One solution was to drive the side roll through a prop-shaft.

To study the slip effect, the side rolls were be driven by a Kopp variator, size 318 type MSG5R1, through a 941 mm long propshaft of diameter 63.5 mm. The prop-shaft was coupled to a 190 mm long torquemeter by a mild steel coupling as shown in fig 3.10. The torquemeter located on the square end of the side roll thus completed the driving line. During normal tests the driving line was disconnected by simply isolating the torquemeter from the roll.

The Kopp variator was a three-phase, 6-pole drive. Its input power rating was 1.5 kW at a nominal motor speed of 930 rev/min.

Though the variator has a maximum output torque of 1.66 kNm, its actual magnitude was not a crucial factor since the plate was mainly driven through the pinch region of the bender by the top roll drive.

As for the top propshaft, the side roll propshaft had an axial movement of 150 mm. This also allowed the side roll freedom of movement to cover a conical base area of diameter 400 mm and it was capable of transmitting a torque not less than 1.23 kN m at 4 rev/min.

3.6.4.3. The electrical circuitry of the drives

Electrical power for the drive was through a 500 V and 30 A MEM mainstarter as shown in fig 3.11. The supply cables were subsequently led to an Allen-West starter, type SL2N, FL amp 20/35, through which an emergency stop was connected (the stop was mounted, for easy access, on a framework plate at the

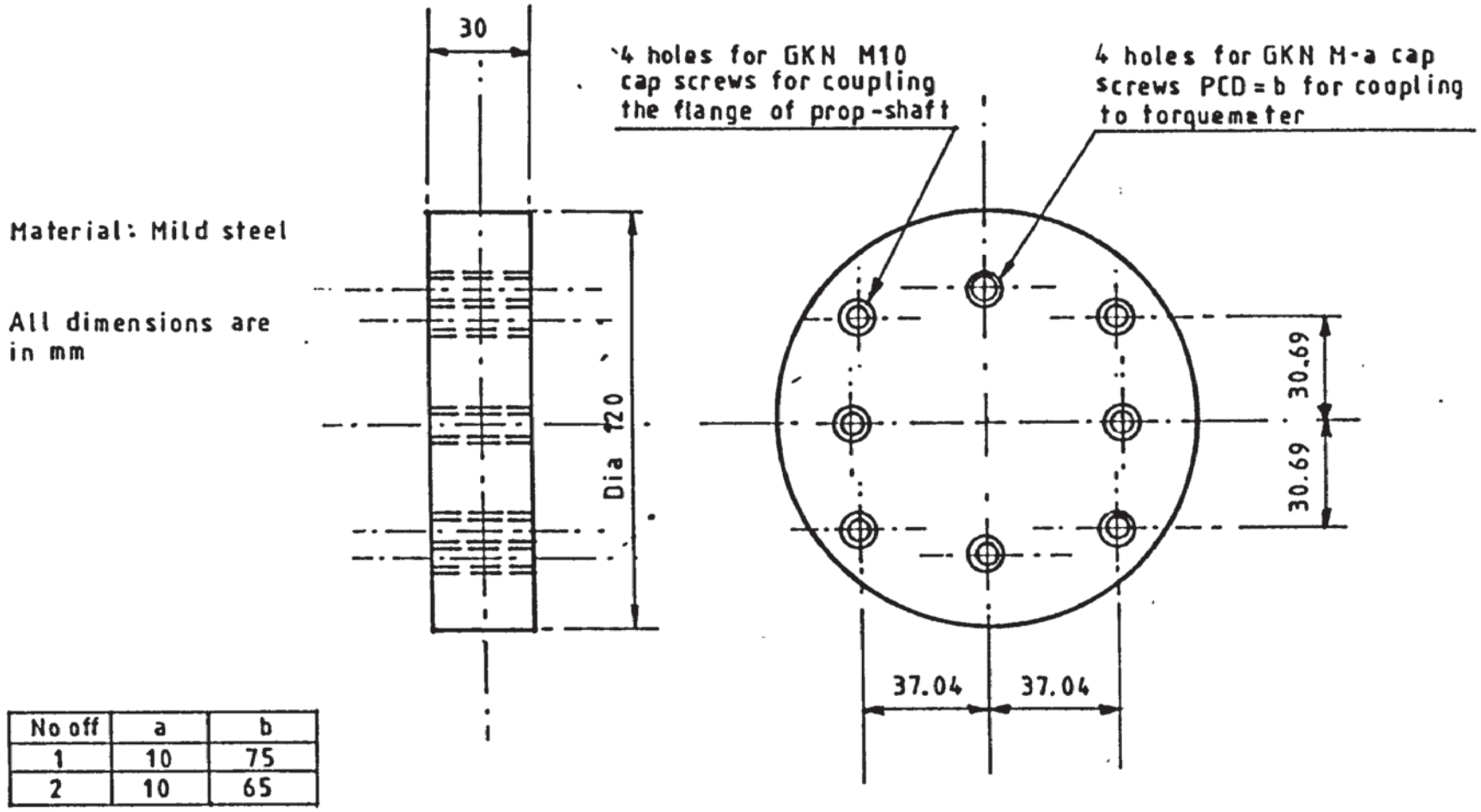

No off	a	b
1	10	75
2	10	65

FIG. 3.10 COUPLINGS OF THE TORQUEMETER AND PROP-SHAFT

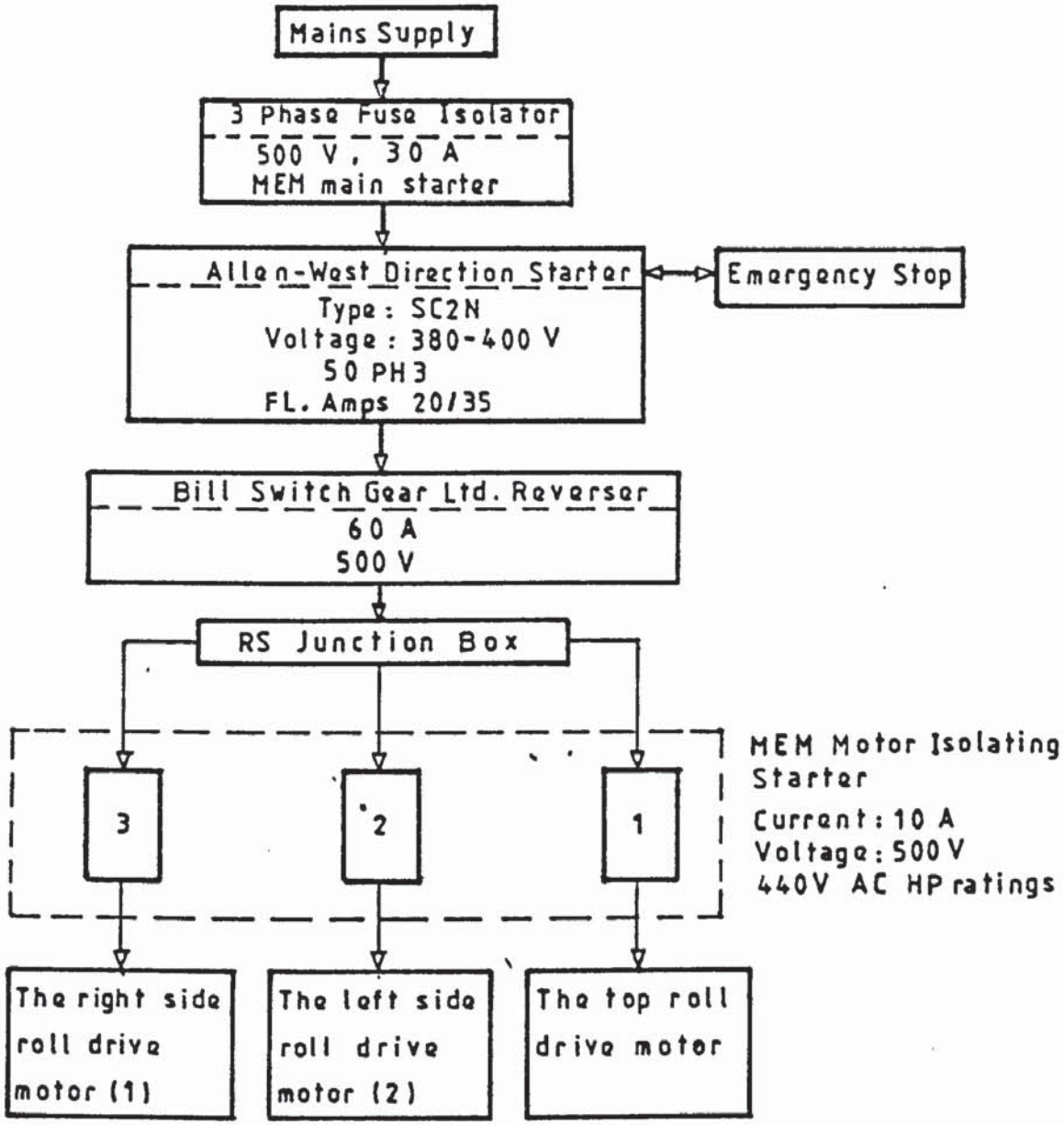

FIG 3.11 FLOW CHART OF THE ELECTRICAL POWER SUPPLY LINE

inlet of the bending unit). The cables were then led to a 60 A, 500 V Bill Switch reverser gear, which controlled the rotational direction of the driven rolls. The reverser unit supply cables were then connected to a junction box. The supply cables in the junction box were then branched to three MEM motor isolating switches. Each switch had a coil voltage of 380-400 V and 10 A. From the switch, supply cables branched to each corresponding motor.

Once in operation the reverser unit in the supply line altered, at the same time, the rotational direction of the three motors. It was desirable to have an isolated reverser for each individual motor so that the rotational direction of each motor could be controlled separately. This feature was discarded, partly due to cost, and also because the nominal rotation of the motor could be altered by changing the appropriate connection in either the isolating switch or the motor phase connection.

3.7. Summary on the model bender

The designed model bender therefore fulfilled most of its conceptual design specifications as mentioned in section 3.6.2. It could also accommodate changes in the operating parameters, such as : change of the roll diameters, and bending plates of different thicknesses and materials.

The prime objective of the model bender and its instrumentation (see Chapter Four) was to assess, under laboratory conditions, the torques and forces for bending various thicknesses of plate with different roll lengths. However the design also allowed for the study of the slip effect, the effect of the side roll positional angle and the length of the initial bending arm (so to optimize the setting geometry of the bender), and the surface friction of the plate etc.. In addition, it could be modified to allow for

investigation of the effect of the roll size and the roll surface texture on the mechanics of the bending process.

Furthermore, by referring to the mathematical analysis in Appendix 7.1, it can be seen that the model bender may also be used to investigate the springback characteristics in the thin plate bending mode. However investigation of springback in thick plate bending, using the model bender, required further detailed study.

CHAPTER FOUR

INSTRUMENTATION AND CALIBRATIONS

4.1. Introduction

Instrumentation is a necessary feature in all scientific and engineering research. Generally, reliable and representative data can only be collected if the instrumentation is properly and correctly installed. The principal measuring devices used in this research investigation were torquemeters and loadcells. This Chapter is mainly devoted to the design of these units, the circuitry of the sensing components, and their calibrations.

4.2. Pinch and side roll loadcell design

Normally, the design specification of a loadcell is o.1 $\%^{max}_{\Lambda}$ strain. The rigidity of the roll bender model is inadequate, since, under the estimated critical working conditions (see Chapter three), the installed loadcell will experience, due to the bending strain, lateral deflections of :

6.07 mm for the pinch bottom roll at a bending load of 60 kN, and
5.48 mm for the side roll at a bending load of 60 kN.

Also, in order to achieve good quality bent plate, the loadcell should be designed to exhibit minimum axial and bending strain. In the simulation study (see Chapter Three), it was recognized that the deflection produced by the bending strain component is much higher than that of the axial strain. Furthermore, owing to the difficulty of completely simulating the configurational feature of the push rods in the Verrina bender at HWT, the required rigidity may only be achieved if the bending strain due to the horizontal force component is reasonably small. The physical dimensions of the loadcells were also taken into account in the design process.

The ratio of the second moment of area of the loadcell in

square and circular cross-sectional area format is

$$I_s/I_c = (bd^3/12)/(\pi d^4/64) = 16b/3\pi d$$

where the assumption is made that the depth of the rectangular cross-sectional area of the loadcell is equivalent to the diameter of its circular counterpart.

It can be seen that the former (I_s), with $b=d$, is relatively stiffer than the latter (I_c). Furthermore, it is easier to alter its aspect ratio whilst still retaining the same structural rigidity. A suitable choice of the aspect ratio, maintaining a constant cross-sectional area, may also produce, for the square loadcell, a greater rigidity. Also, a strain gauge circuit installed on a square or rectangular cross-sectional area loadcell ensures the detection of the actual bending strain signal, provided it is mounted at 90° to the force component.

Although a rectangular or square loadcell offers structural advantages, machining costs are greater. Furthermore, since the push rods have axial freedom of movement, rectangular slots with adequate bearings in the mounting blocks are required. Consequently, the circular cross-section loadcell was chosen because it is more cost effective. This design is shown in drawing item 29 in Appendix 3.1, with an estimated maximum bending deflection of :

(i) 0.85 mm at bending arm 191 mm for the loadcell of the bottom pinch roll,

and

(ii) 0.77 mm at bending arm 184.5 mm for the loadcell of the side roll.

The corresponding maximum strains, at the critical operational condition were as follows :

(i) ε_a=460 x 10^{-6} in axial direction at load of 250 kN and

ε_b=1.0 x 10^{-3} in bending at 30 kN loading for the pinch roll loadcell.

(ii) ε_a=110 x 10^{-6} in axial direction at 60 kN loading and

ε_b= 1.0 x 10^{-3} in bending at 30 kN loading for the side roll loadcell

Each loadcell was directly screwed on to the top of the bearing housing (item 12 or 19, Apprendix 3.1) and collinear with the push rod (item 13 or 19, Appendix 3.1). This is connected to the hydraulic cylinder and is movable using the restraining rectangular slots of the end plate (item 1, Appendix 3.1) and the bottom retaining block (item 20, Appendix 3.1). The loadcells were carefully mounted to give a constant bending arm for all operating conditions.

4.3. Top roll loadcell design

To maintain the required structural rigidity of the model roll bender, the top roll loadcells (item 3, Apprendix 3.1) were designed to have the same stiffness criteria as the bottom pinch and the side roll loadcells. Each top loadcell was designed to give a maximum lateral deflection of 0.16 mm at a maximum total horizontal loading of 119.6 kN. The loadcell bending strain was a maximum of 420 x 10^{-6} at the middle for a load of 29.9 kN. The axial strain was 100 x 10^{-6} at a load of 124.6 kN.

The loadcells were situated at each end of the top beam (item 2 in fig. 3.5(b)), which supported the top roll bearing housing. Generally each loadcell experienced a quarter of the

axial load on the top roll (provided the axial loading was equally distributed at the centre of each beam).

4.4. Torquemeter design

According to Holman [145], the strain induced on a strain gauge attached at 45° angle on a hollow circular rod (with outside radius r_o and inner radius r_i) for a torque M, is given by

$$\varepsilon_{45} = Mr_o/[\pi G(r_o^4-r_i^4)] \qquad (4.1)$$

where $G=E/[2(1+\nu)]$ is the material modulus of rigidity.

Expression (4.1) was used as the basis of the torquemeter design.

The torquemeters, made from En8 steel, have the dimensions shown in figure 3.9. The end with an outside diameter d and a square hole d_3 of depth L_2 was directly connected to the square end of the rolls. The end with a flange of diameter d_1 was connected via a coupling, to the propshaft in the bender model (fig. 3.5). The section with a length L_1 and diameter d_2 is required for bonding the strain gauge elements. The torquemeter thus mounted enabled the torque, produced between the roll and the drive, to be measured.

The designed torquemeters give the following induced strains at 45° , i.e. (ε_{45}) :

(i) 483×10^{-6} for top roll torquemeter at a maximum torque of 2.45 kN m.

(ii) 441 x 10^{-6} for side roll torquemeter at a maximum torque of 1.2 kN m.

Their corresponding maximum shear stresses were :

(i) 75 N/mm^2 for the top roll torquemeter.

(ii) 68 N/mm^2 for the side roll torquemeter.

4.5. General strain gauge circuitry arrangement

For sensing purposes the strain gauge is a widely used element. Its principle of application is that of a change in its resistance when the strain gauge element is subjected to mechanical strain.

It is possible to illustrate its working principle by considering the circuitry in fig 4.1.

Let us assume that the strain gauge resistances R_1, R_2, R_3 and R_4 undergo small changes simultaneously. The effect on the potential difference E_{bd}, across the points of b and d can be expressed as the sum of each individual effect, i.e.

$$E_{bd}=E[(-R_2dR_1)/(R_1+R_2)^2+(R_1dR_2)/(R_1+R_2)^2-(R_4dR_3)/(R_3+R_4)^2 + (R_3dR_4)/(R_3+R_4)^2] \qquad (4.2)$$

Since the gauge factor tensor, F_i, is defined as

$$F_i=(dR_i/R_i)/\varepsilon_i$$

where, ε_i is the measured strain tensor, and

i=1, 2, 3, 4, ... etc..

Substituting it into equation (4.2) gives

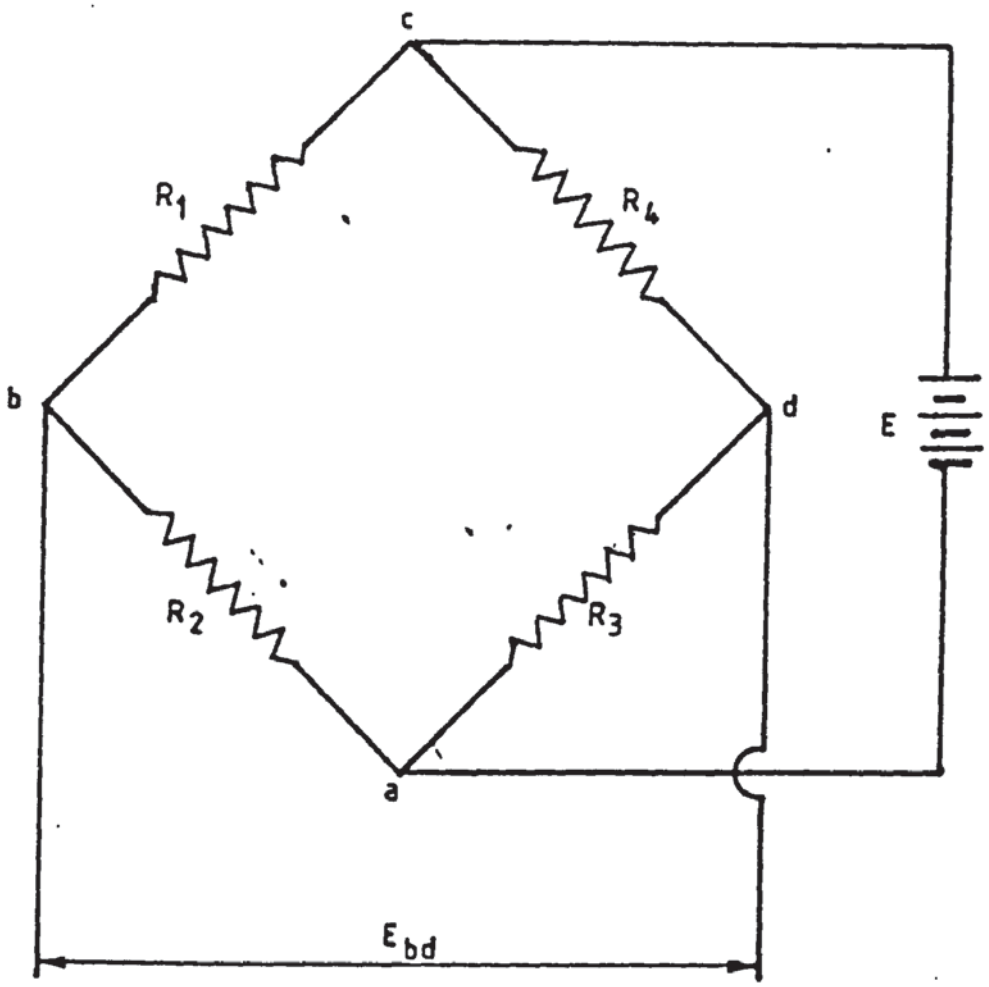

FIG 4.1 THE STANDARD WHEATSTONE BRIDGE CIRCUIT

$$E_{bd}=E[(-R_1R_2F_1\varepsilon_1)/(R_1+R_2)^2+(R_1R_2F_2\varepsilon_2)/(R_1+R_2)^2$$

$$-(R_3R_4F_3\varepsilon_3)/(R_3+R_4)^2+(R_3R_4F_4\varepsilon_4)/(R_3+R_4)^2] \quad (4.3)$$

Normally, a sensory bridge circuit is thus made up using strain gauges having equal resistance (preferently gauges from the same batch). This implies that $R_b=R_1=R_2=R_3=R_4$. For this special case, the bridge sensitivity, equation (4.3), can be reduced to :

$$E_{bd} = FE(-\varepsilon_1+\varepsilon_2-\varepsilon_3+\varepsilon_4)/4 \quad (4.4)$$

where, F is a common gauge factor.

By expressing the above equation in terms of current, i, to the bridge, it gives

$$E_{bd} = FiR_g(-\varepsilon_1+\varepsilon_2-\varepsilon_3+\varepsilon_4)/4 \quad (4.5)$$

where,

$$R_g = 1/[1/(R_1+R_2) + 1/(R_3+R_4)]$$

By a suitable arrangement of the strain gauges to produce the required ε_1, ε_2, ε_3 and ε_4 values in equation (4.5), many particular engineering parameters, such as the magnitude of axial load, or bending load, or torsional load, can be measured provided the process of calibration has previously been carried out.

4.6. Strain gauge circuitry for the bottom pinch and side roll loadcells and calibrations

4.6.1. Axial loading measurement

Usually, an axial load on a rod will produce a strain in the loading condition. A strain gauge orientated in the direction of the load will give an electrical signal. Because the ambient temperature can induce thermal strain in the strain gauge elements, some error in the output will be experienced. To accommodate the effect of changes, the dummy strain gauges are introduced in the bridge circuit (fig 4.1) to nullify the induced thermal strain in the active gauges.

Considering fig 4.1, if the two resistors connected to the point,a, are replaced by active and dummy strain gauges respectively, the bridge is called a half bridge. Its simplification in comparison with the full bridge (i.e. all elements in fig 4.1 are replaced by gauges) is that it is incapable of self-balancing. Generally a full bridge is recommended for most measurement circuitries.

In designing a bridge circuit it is necessary to eliminate all unwanted additive signals. In the axial loading case, the bending effect on a compressive strain gauge bridge should be totally isolated. By studying the resistance circuit in fig 4.2, this isolation can be achieved by bonding opposing active gauges, R_1 and R_2, R_5 and R_6 etc. on the surface of the loadcell. Generally, the arrangement will cancel out the bending strain signals within the bridge, as the bending force is applied to the cell. This is a consequence of the bending tensile strain in R_1 being cancelled out by an equivalent amount of the bending compressive strain in R_2. Likewise the

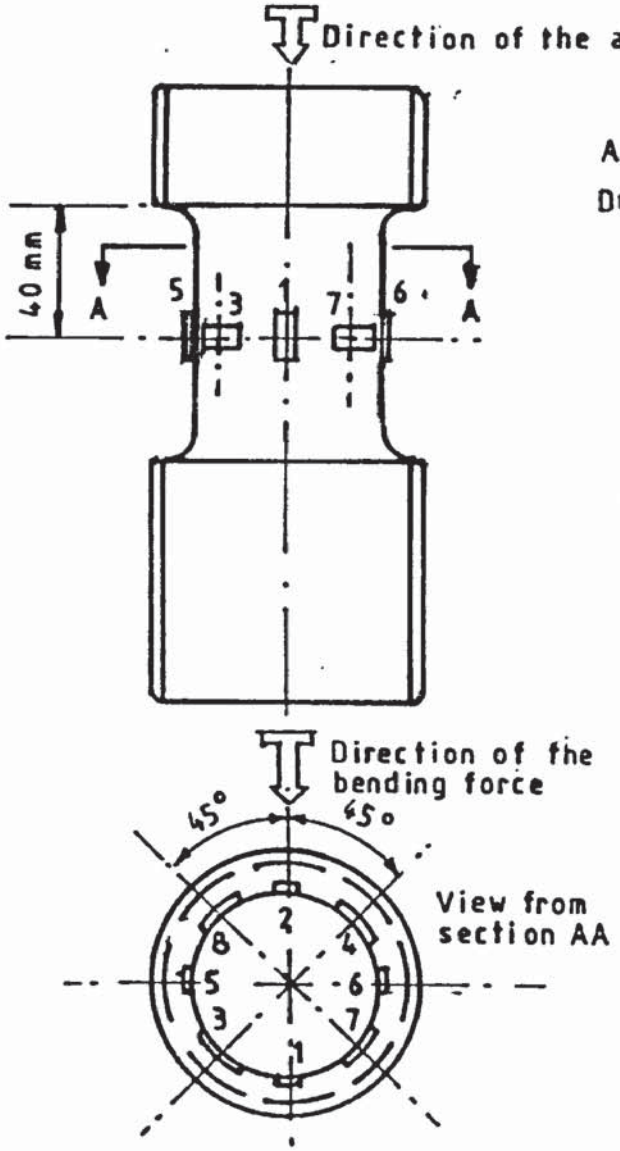

i- Strain gauge arrangement on the load cell

Active gauges: 1, 2, 5, 6
Dummy gauges: 3, 4, 7, 8

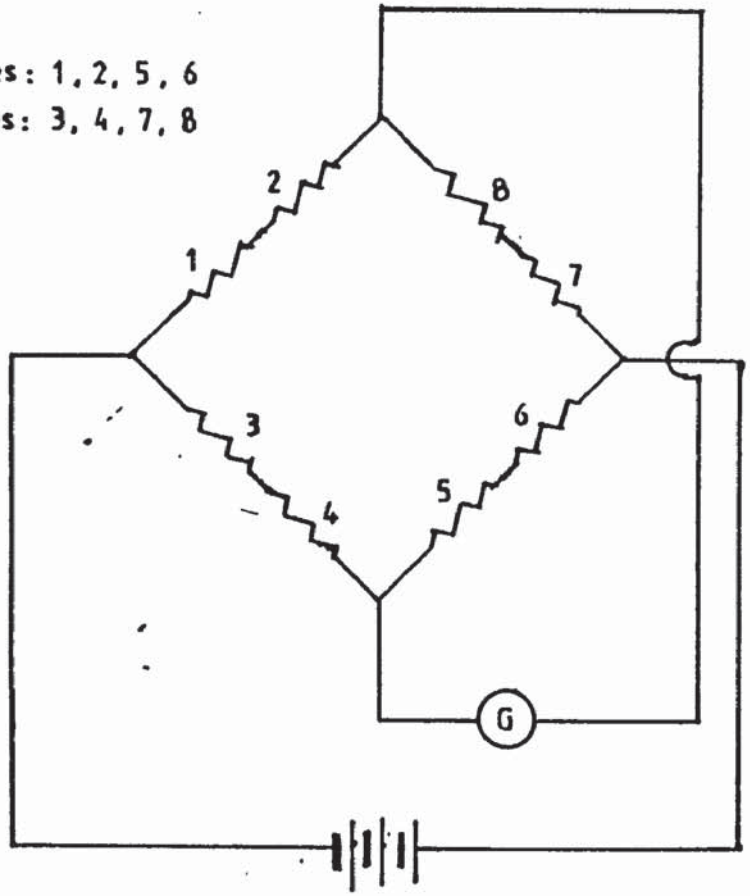

1, 2, 3, 4, 5, 6, 7, 8 are the strain gauges (resistors). All gauges are 100 ohm filaments.

ii- Bridge circuit arrangement

FIG 4.2 THE AXIAL BRIDGE CIRCUITRY ARRANGEMENT FOR ELIMINATING THE ADDITIVE SIGNAL DUE TO THE BENDING FORCE

same applies for R_3 and R_7, and R_6 and R_8 respectively. Thus the induced bending strain in strain gauges R_5 or R_6 is self-cancelling.

Each loadcell for the bottom roll or the side roll is screwed in the pressure block (rod) at the bottom and a bearing housing at the top. To ensure the proper installation of each strain gauge in the bridge relative to the bending force, F_b, dowel pins were initially considered for locating the position of the loadcell in its housings. Since the pressure block (rods) would operate vertically in its axial bearing housing, this would require precision dowel and holes, and thus incur additional manufacturing costs. Consequently to minimise costs, the concept of introducing dowel pins was abandoned.

Since it was recognised that the major bending force was in the direction orthogonal to the wall of the bearing housing, the technique employed to retain the relevant position of the bridge, for all loading conditions, was to bond the bridge on to the loadcell whilst the cell housing was tightly screwed down. Employing a Matrix angle divider the gauge element position was accurately marked in relation to the central line of the wall of the bearing housing. The marked lines were arranged to subtend an angle of 45° to each other, with a line along one of the central lines of the bearing housing walls as the initial datum. The axial load bridge was bonded to the cross-plot of the previously marked lines and the marked circumferential trace on the middle of the effective length of the load cell.

The appropriate bridge arrangement was utilised to remove any superfluous signals induced by other unwanted loading conditions. Two pairs of active gauges were installed, one

along the pair of central lines on the bearing housing walls, another along the orthogonal lines to the former (i.e. 1 and 2, and 5 and 6, respectively in fig 4.3). Fig 4.3 shows the appropriate circuitry which also amplified the bridge signal. Four temperature compensating gauges were also bonded at the cross lines of the 45° subtended angle to "℄", in the vicinity of the corresponding active gauges. These are also shown in the dummy arms in fig 4.3.

The resistance of each strain gauge element in the circuit was 100 Ω. Each element had a safe maximum current capacity of 20 mA. The bridge arrangement gave a measured resistance of 200 Ω across each arm and 199.3 Ω across each element.

4.6.1.1. Calibrations

On the basis of the preliminary analysis in the process of the model design (Chapter Three), it was estimated that the maximum bending load was :

(i) 250 kN on each pinch loadcell, and
(ii) 60 kN on each side loadcell,

for bending a 10 mm thick x 310 mm wide mild steel plate with strength of 235 N/mm^2 to 90 mm bend diameter before springback. As a consequence of the rigidity of the model bender the loadcell was designed to give maximum bending deflection as follows :

(i) 0.85 mm for the bottom pinch loadcell
(ii) 0.77 mm for the side roll loadcell.

This condition reduces the proportion of the axial strain of the loadcell in comparison with its design specification. Furthermore, aluminium plate, in the range 8 mm thick x 80 mm wide to 14.7 mm thick x 305 mm wide, would drastically reduce

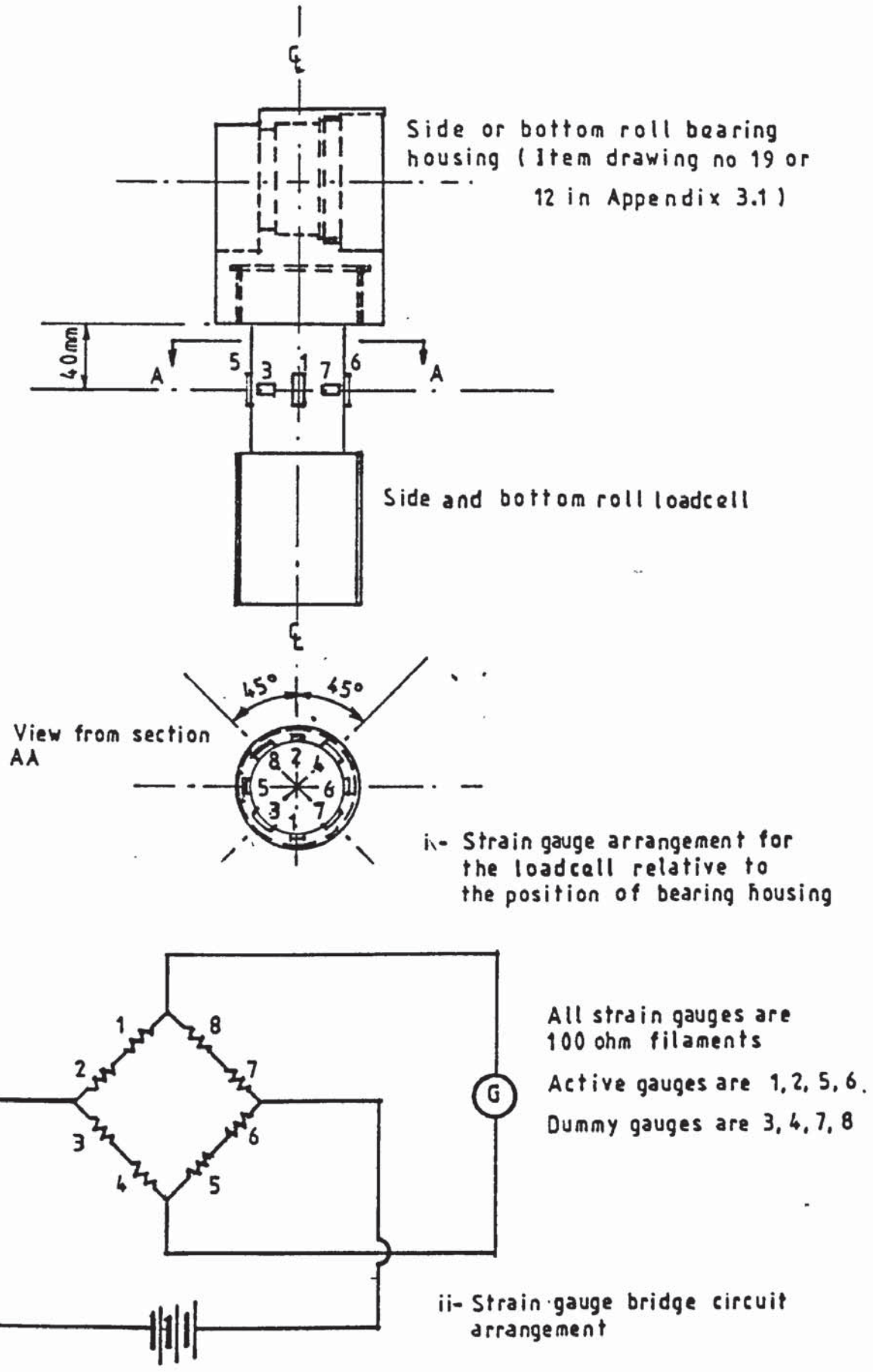

FIG 4.3 THE AXIAL STRAIN GAUGE AND BRIDGE CIRCUIT ARRANGEMENT RELATIVE TO THE POSITION OF BREARING HOUSING FOR THE SIDE AND BOTTOM ROLLS

the response of the output signal. Amplification of the bridge signal was necessary in order to cover the range of bend-plate sizes envisaged using the designed loadcell. The amplifier used in this particular purpose was a CIL conditioning unit series SGA 700-706. The circuitry diagram of the ampliflier, according to the manufacturer, is as shown in fig 4.4. The complete strain gauge circuitry is shown in fig 4.5. The introduction of the RS10kΩ potentiometer in the circuit (fig 4.5) facilitated the zero adjustment of the gauges bridge.

A. Main circuitry of the bridges

There are a total of 23 strain gauge bridges in the model. Consequently the supply of power to each individual bridge would be an expensive operation. Group powering was thus desirable. The method of grouping, i.e. series or parallel, mainly depended on isolating the effect of the variation of one bridge to another and the capacity of the main power pack.

Since the strain gauge bridge (S.G.B.) was connected in the circuit with a 10 kΩ RS potentiometer as shown in fig 4.5, the resistance ratio of the bridge to the potentiometer was only 1 %. The effect of the change of the strain gauge resistance to each individual circuit was thus negligible, i.e. for either the series or the parallel circuit. Circuit analysis showed that the former circuit required a main voltage supply, V_m, which is the sum of each individual bridge power supply V_{bj}, i.e.

$$V_m = \sum_{j=1}^{n} V_{bj} = i \sum_{j=1}^{n} R_{bj} \qquad (4.6)$$

An adequate supply for each individual bridge voltage V_{bj} was

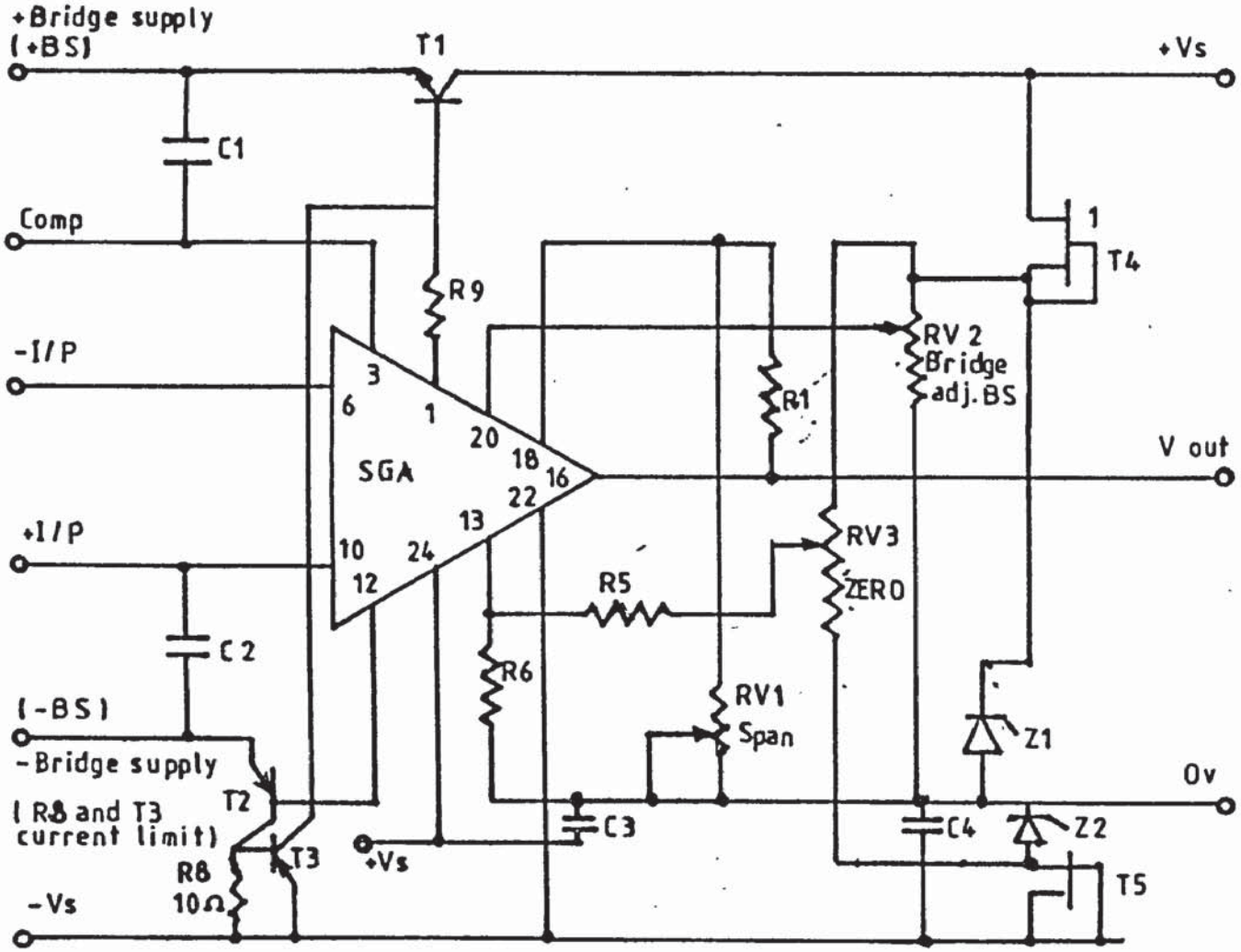

Specification:

Supply Vs = ± 12 V

Bridge supply current - AUTO LIMITS at 60 mA min.

Supply current = ± 20 mA

Span adjustable gain from 1 to 2000

Adjustable bridge supply from 1 to 12 V

FIG 4.4 THE CIRCUIT LAYOUT OF THE CIL MINIATURE CONDITIONING UNIT SERIES SGA 700 FOR STRAIN GAUGE AMPLIFIER

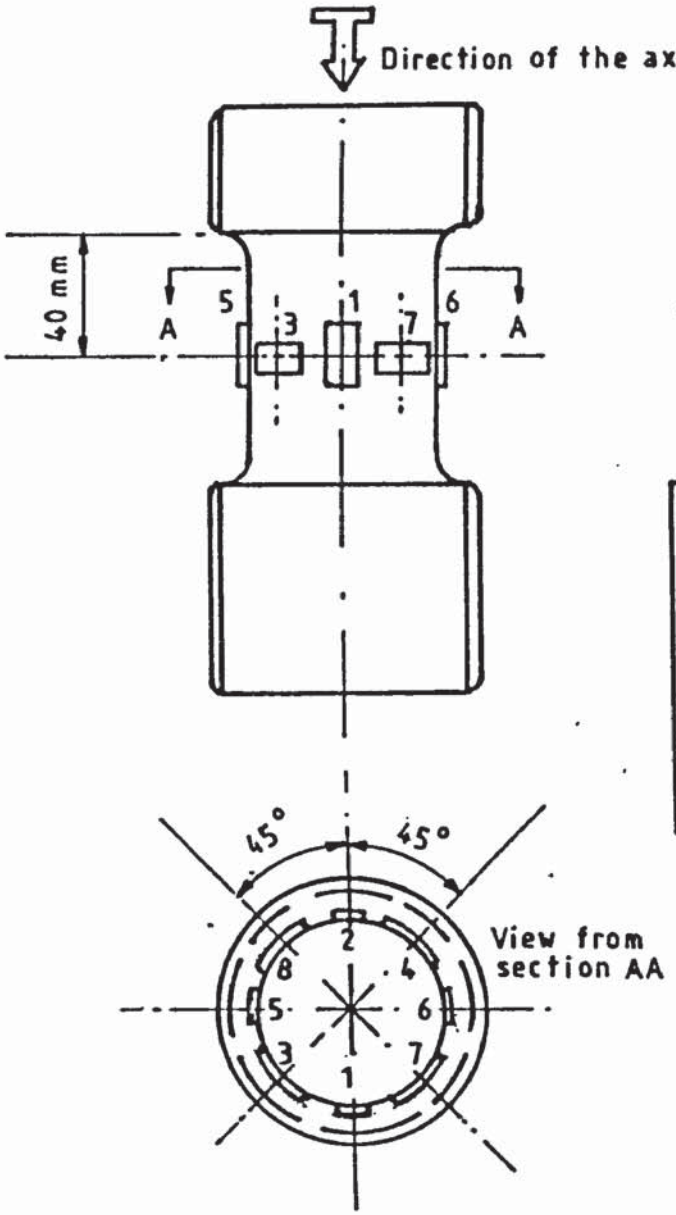

i - Strain gauge arrangement for the loadcell

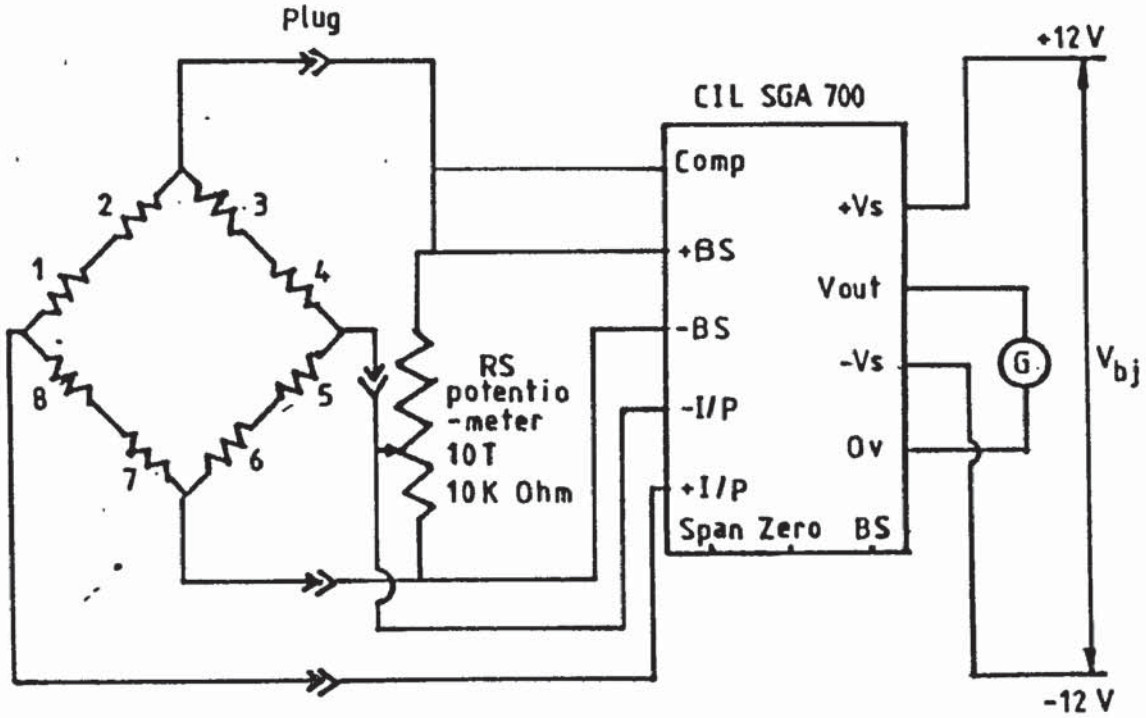

All strain gauges are 100 ohm filaments

Active gauges are 1, 2, 5, 6.

Dummy gauges are 3, 4, 7, 8.

ii - Strain gauge bridge circuit and CIL SGA 700 amplifier arrangement

FIG 4.5 THE STRAIN GAUGE BRIDGE CIRCUIT ARRANGEMENT FOR MEASURING THE LOADS ALONG THE AXIS OF THE SIDE AND BOTTOM LOADCELLS

required. The parallel circuit was chosen since this provided an equal power supply both in the main and in each individual circuit. The circuit of the amplifier and the bridge for the two pinch loadcells and the four side loadcells were then designed and are shown in figs 4.6 and 4.6A.

B. Preliminary calibration

The calibration was conducted using an Avery compression testing machine. The initial trial was performed to determine the appropriate galvanometers to be used. It was found that the Thorn EMI Datatech A1000 galvanometer, in conjunction with the CIL strain gauge amplifier SGA701-706, was suitable. It gave a steady output signal on the 200 mm span u.v. recorder chart.

C. Final calibrations

The calibration tests were conducted in such a manner as to simulate the mounting in the model bender. The calibration of the loadcell in situ was attempted. It was not successful because the required bending moment was rather difficult to achieve. This was mainly due to the nature of the loading which complicated the resolution of the bending load components for the side roll cells. Furthermore, the bending calibration for the pinch loadcells and the top loadcells required the availability of an additional rig. The design and manufacture of such a rig would require additional finance and time. To avoid the aforementioned problems, the calibration was performed using the Avery compression testing machine.

Each loadcell was completely mounted with the bearing housing and the corresponding connecting block (rod) in the clamping block. This arrangement was carefully positioned vertically on the base of the machine. In order to protect the spherical bearing in the housing from distortion a mild steel solid column was machined to fit the bearing bore. To ensure the complete direct transmission of the axial force to the

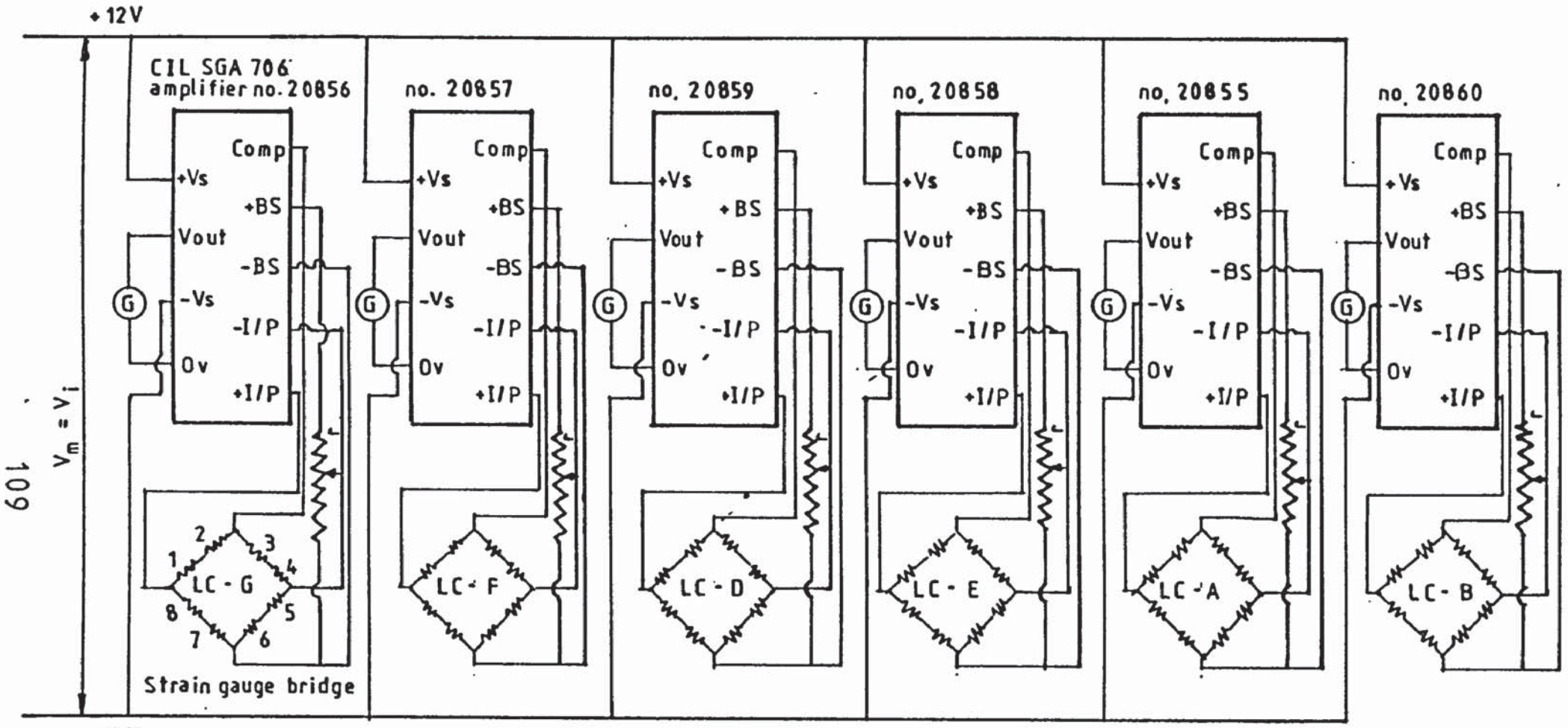

FIG 4.6 THE POWER SUPPLY ARRANGEMENT, CIL SGA 706 AMPLIFIERS AND THE AXIAL LOAD STRAIN GAUGE BRIDGES FOR THE BOTTOM PINCH AND SIDE ROLL LOADCELLS

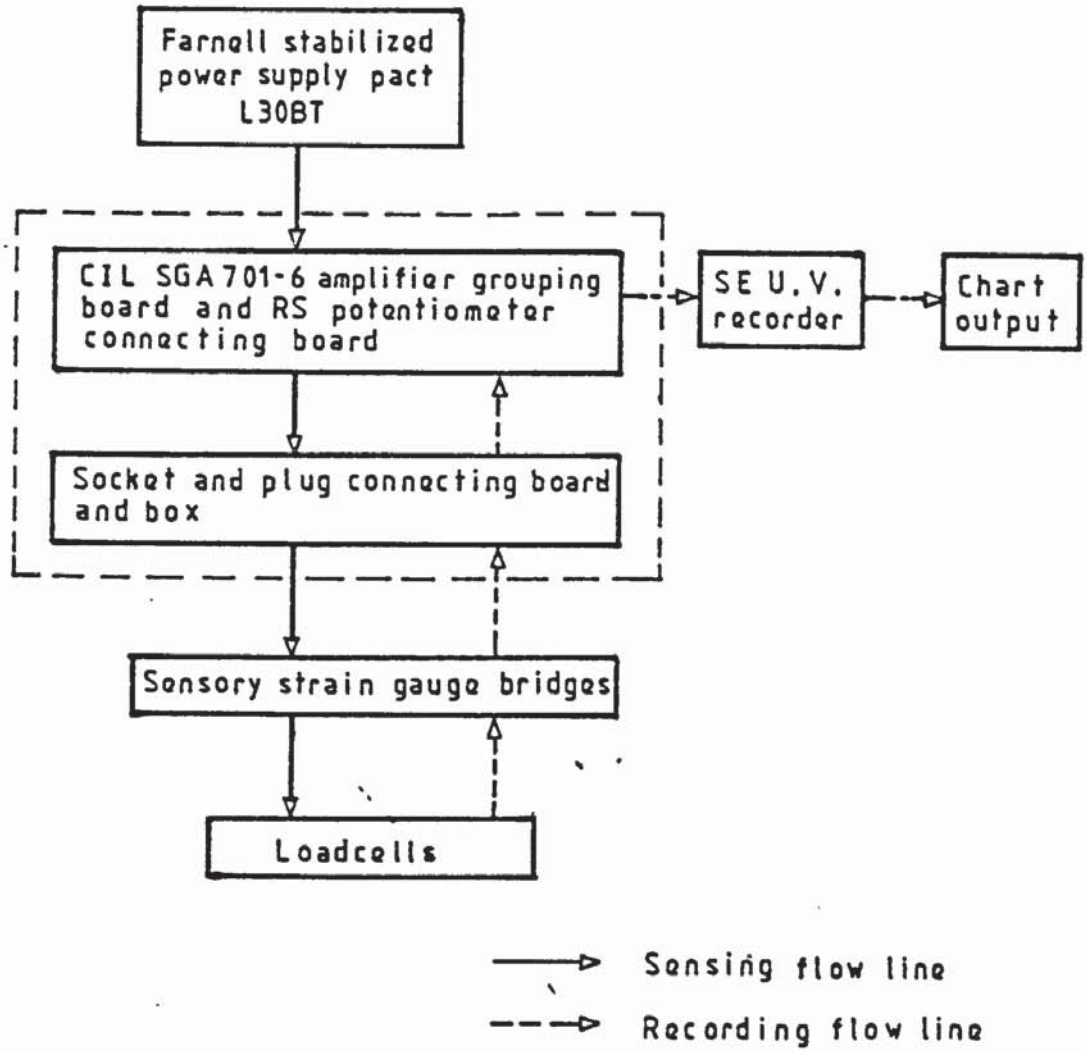

FIG 4.6A FLOW CHART FOR THE LAYOUT OF POWER STABILIZER AND THE RELEVANT RECORDING INSTRUMENTS

loadcell, a mild steel disc, with a small hole in the middle for locating a ball bearing, was placed on the top of the bearing housing (fig 4.7). Also a correctly machined cap was placed on the ball bearing to make proper contact with the platen of the Avery testing machine as the loading was applied.

The measuring output signal was in the form of chart traces. The layout of the recording instruments, the Farnell stabilised power supply L30BT and the strain gauge bridge circuits are shown in fig 4.6A. At the commencement of the calibration, all the relevant instruments were allowed to "warm up" and stabilise.

The voltage setting of the Farnell stabilised power supply was carefully measured by a Solartron d.v.m., which had an accuracy of ±10 mV. The calibrations were undertaken, with nearly full galvanometer deflection, for the calibration load ranges shown in Table 4.1.

The calibration ranges can be covered by either :

(1) Permanently setting a fixed bridge voltage supply and altering the gain ratio of the output from the strain gauge bridge, i.e. the ratio of the input signal to the amplifier and the corresponding output to the u.v. recorder.

or,

(2) Permanently setting a fixed gain ratio and merely altering the strain gauge bridge supply voltage.

The first setting worked successfully for a particular setting, i.e. a fixed range of calibration load range. The modification to the working load range, for bending different thickness and different materials of plates, required frequent changes in the bridge supply and galvanometer deflection. The

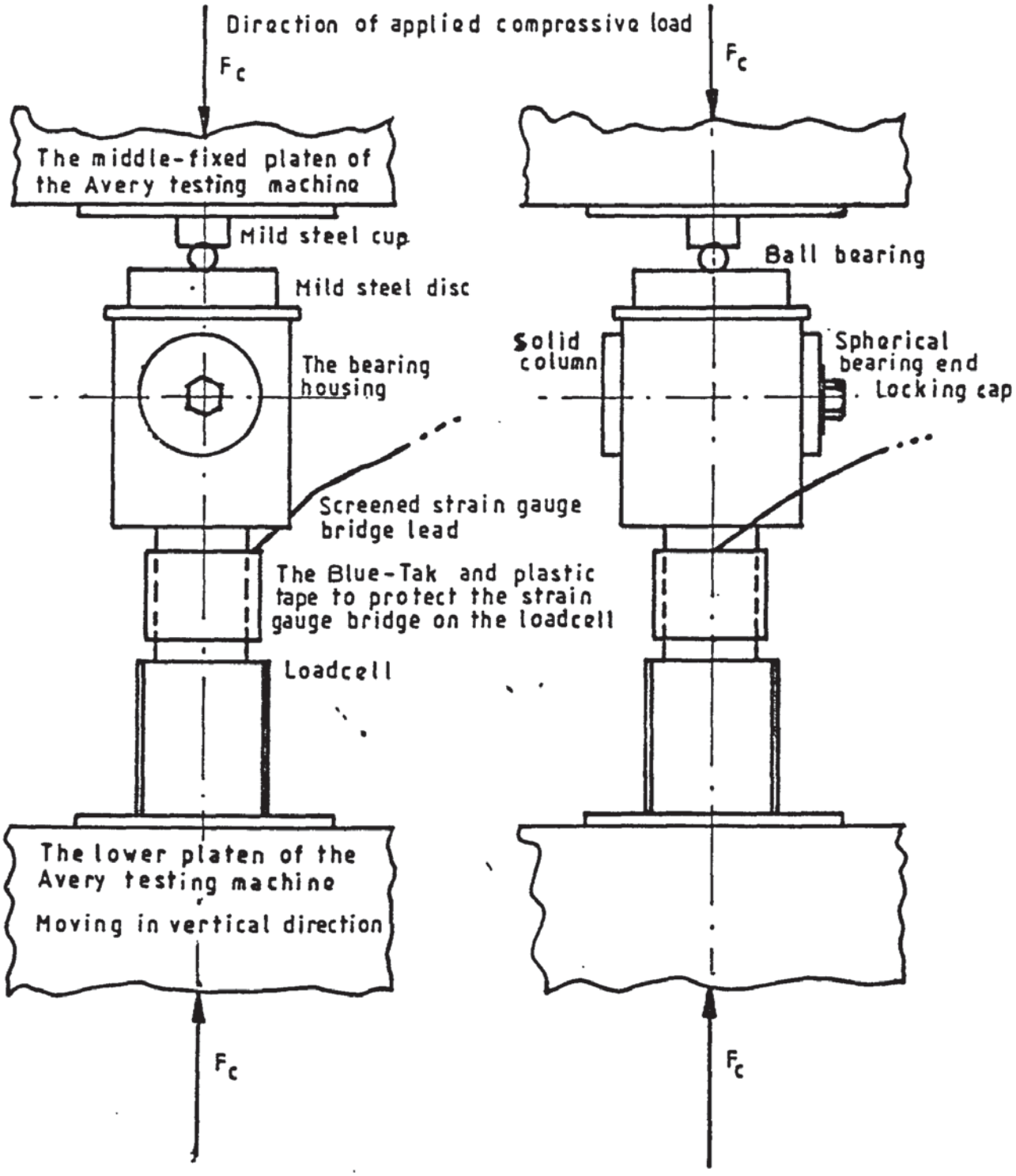

FIG 4.7 THE MOUNTING OF THE BOTTOM AND SIDE ROLL LOADCELL FOR THE AXIAL LOADING CALIBRATIONS

Table 4.1 Statistical Information Of the Calibration Results For the Sensory Devices

All the results obtained from the calibrations have been fed to an APPLE II statistical software. The equation of the linear regression for each set of the calibration data is thus expressed in the following form :

Force (F_j)= 9966.96(a_o+b_ox) N (A_f)

and,

Torque (T_j)=0.113125(a_o+b_ox) N m (A_t)

where, x is the u.v. chart reading in mm, related to its initial datum

This table tabulates the corresponding values of a_o and b_o, and the respective statistical data obtained from the statistical programme for the calibration results.

Load cell spec. letter/no.	Calibration		Calibrated statistical data from the linear regression programme				
	load range (tonf)	B.S voltage (V)	Constants in the equation A_f or A_t		Coeffts of determination	Coeffts of correlation	Standard error of estimation
			a_o	b_o			
(i) TOP ROLL LOAD CELL AXIAL LOADING CALIBRATIONS							
1	0-5	4.8	-0.0433	0.0368	0.9986	0.9993	0.0661
2		5.16	-0.0243	0.0374	0.9998	0.9999	0.0219
3		5.465	-0.0255	0.0504	0.9997	0.9998	0.0318
4		3.79	0.0498	0.4118	0.9995	0.9998	0.0375
1	0-10	2.51	-0.1823	0.0772	0.9986	0.9993	0.1328
2		2.60	-0.1882	0.0781	0.9992	0.9996	0.098
3		3.7	-0.2394	0.0781	0.9989	0.9994	0.1168
4		2.22	-0.019	0.0774	0.9999	1.	0.0304
1	0-13	1.96	-0.3820	0.1009	0.998	0.999	0.1954
2		2.06	-0.0229	0.0965	0.9999	1.	0.0393
3		3.08	-0.0702	0.0955	0.9999	0.9999	0.0459
4		1.87	-0.0728	0.0938	0.9999	0.9999	0.0509

Table 4.1 Statistical Information Of the Calibration Results For the Sensory Devices (Cont)

Load cell spec. letter/no.	Calibration		Calibrated statistical data from the linear regression programme				
	load range (tonf)	B.S voltage (V)	Constants in the equation A_f or A_t		Coeffts of determination	Coeffts of correlation	Standard error of estimation
			a_o	b_o			
(ii) TOP ROLL LOAD CELL BENDING CALIBRATIONS							
1	0-1	7.13	-0.0082	0.0055	0.9996	0.9998	0.0068
2			-0.0048	0.0059	0.9991	0.9995	0.0107
3			-0.0014	0.0048	0.9999	0.9999	0.0034
4			-0.001	0.0054	0.9997	0.9999	0.0057
1	0-2	3.56	-0.0408	0.0113	0.9989	0.9994	0.0232
2			-0.0341	0.0127	0.9983	0.9991	0.0288
3			-0.0101	0.0099	0.9998	0.9999	0.0094
4			-0.0113	0.0099	0.9996	0.9998	0.0127
1	0-3	2.37	-0.0066	0.0171	0.9999	0.9999	0.0109
2			-0.0471	0.0195	0.9992	0.9996	0.0271
3			-0.0132	0.0147	0.9992	1.	0.0086
4			-0.0443	0.0153	0.9994	0.9997	0.0228
1	0-4	1.78	-0.0575	0.0234	0.9995	0.9997	0.0317
2			-0.0857	0.0276	0.9993	0.9996	0.0375
3			-0.0215	0.0199	0.9999	1.	0.0115
4			-0.0556	0.0209	0.9995	0.9998	0.0294
(iii) SIDE ROLL LOAD CELL AXIAL LOAD CALIBRATIONS							
E	0-5	3.301	-0.0294	0.0281	0.9998	0.9999	0.0273
D		3.3	-0.0235	0.0407	0.9998	0.9998	0.0256
F		3.303	-0.0311	0.0346	0.9999	0.9999	0.0197
G		3.307	-0.0254	0.0360	0.9996	0.9998	0.0309
E	0-10	2.078	-0.0519	0.0474	0.9998	0.9999	0.0428
D		2.2	-0.0754	0.0608	0.9996	0.9998	0.0696
F		2.098	-0.0670	0.0548	0.9998	0.9999	0.0423
G		1.801	0.04971	0.0646	0.9955	0.9977	0.2227
E	0-14	1.299	0.14884	0.0750	0.9998	0.9999	0.0695
D		1.50	-0.2173	0.0906	0.9995	0.9997	0.1125
F		1.397	-0.0082	0.0818	1.	1.	0.0311
G		1.501	-0.2229	0.0803	0.9995	0.9998	0.0997

Table 4.1 Statistical Information Of the Calibration Results For the Sensory Devices (Cont)

Load cell spec. letter/no.	Calibration		Calibrated statistical data from the linear regression programme				
	load range (tonf)	B.S voltage (V)	Constants in the equation A_f or A_t		Coeffts of determination	Coeffts of correlation	Standard error of estimation
			a_o	b_o			
(iv) BOTTOM PINCH ROLL LOAD CELL AXIAL LOAD CALIBRATIONS							
A	0-10	3.3	-0.1043	0.0613	0.9997	0.9998	0.0613
B		3.412	0.07090	0.052	1.	0.9998	0.0573
A	0-20	1.911	-0.1192	0.1065	0.9998	0.9999	0.0938
B		1.941	0.15460	0.1003	0.9996	0.9998	0.1206
A	0-24	1.5	-0.3369	0.1363	0.9997	0.9998	0.1439
B		1.4	0.25786	0.1273	0.9996	0.9998	0.1732
(v) SIDE ROLL LOAD CELL BENDING LOAD CALIBRATIONS							
E	0-2	1.70	-0.0192	0.0114	0.9998	0.9999	0.0105
D			-0.0014	0.011	0.9999	1.	0.0056
F			-0.0106	0.0112	0.999	0.9999	0.0080
G			-0.0094	0.0106	0.9999	1.	0.0063
E	0-4	0.84	-0.0562	0.0233	0.9995	0.9998	0.0308
D			-0.0323	0.0224	0.9999	0.9999	0.0169
F			-0.0299	0.0238	0.9998	0.9999	0.0190
G			-0.0341	0.0211	0.9998	0.9999	0.0201
E	0-6	0.54	-0.0580	0.0361	0.9993	0.9997	0.0528
D			-0.0082	0.0347	0.9997	0.9999	0.0341
F			-0.0391	0.0363	0.997	0.9985	0.1055
E	0-10	0.36	0.00976	0.0520	0.9998	0.9999	0.0422
D			-0.1044	0.0503	0.9995	0.9998	0.0710
F			-0.0476	0.0544	0.9999	0.9999	0.0386
G			-0.045	0.0463	0.9999	1.	0.0261

Table 4.1 Statistical Information Of the Calibration Results For the Sensory Devices (Cont)

Load cell spec. letter/no.	Calibration		Calibrated stastical data from the linear regression programme				
	load range (tonf)	B.S voltage (V)	Constants in the equation A_f or A_t		Coeffts of determination	Coeffts of correlation	Standard error of estimation
			a_o	b_o			
(vi) BOTTOM PINCH ROLL LOAD CELL BENDING LOAD CALIBRATIONS							
A	0-2	1.70	0.0005	0.0096	0.9999	1.	0.0062
B			-0.0065	0.0098	0.9999	0.9999	0.0062
A	0-4	0.84	0.0025	0.0196	0.9999	0.9999	0.0137
B			-0.0604	0.0198	0.9995	0.9997	0.0298
A	0-6	0.54	-0.0313	0.0296	0.9998	0.9999	0.025
B			0.0442	0.0285	0.9993	0.9997	0.0498
A	0-10	0.36	-0.0895	0.0458	0.9992	0.9996	0.08
B			-0.0592	0.0482	0.9999	1.	0.0319
(vii) TOP ROLL ROTATIONAL SPEED CALIBRATION The calibrated linear regressional equation is expressed as $N=a_o+b_ox$ (rev/min), in which x is the u.v. chart length in mm related to its initial datum of zero rotation							
	0-30 R.P.M.		0.0486	0.5637	0.9999	1.	0.0875

problem posed by the latter method was the difficulty of measuring the output signal from the bridge supply. This was because for certain ranges the output signal was rather small and consequently difficult to measure accurately. Bearing in mind that the setting error band is normally cumulative it was therefore desirable to reduce the number of the measurements taken. Since the estimation of the maximum bridge voltage gave a value of 8 V, the maximum working strain gauge voltage supply was thus set at 3.3 V for the lowest load range in the calibration test. The amplification of the bridge output signal was suitably adjusted to give an acceptable galvanometer deflection in the lowest load range. The actual magnitude of the amplification of the bridge was not measured due to its low value, but it was permanently set. The subsequent calibrations for the other higher load ranges for each loadcell were performed by reducing the corresponding gauge bridge supply in the ratio of the maximum loads in each load range. For each load range calibration the calibration was repeated at least twice to ensure consistency and reliability of the results.

The results were analysed with the aid of a linear software package running on an Apple II microcomputer. The calibration equations and their corresponding coefficient of determination, the coefficient of correlation, and the standard error of estimation were thus obtained and tabulated in Table 4.1. An example of a calibration graph is shown in fig 4.8. All the graphs showed linear relationships and good correlation.

4.6.2. Bending loading

4.6.2.1. Strain gauge bridge arrangement and circuitry

The achievement of the maximum bending signals and the isolation of other induced superfluous signals depends on the

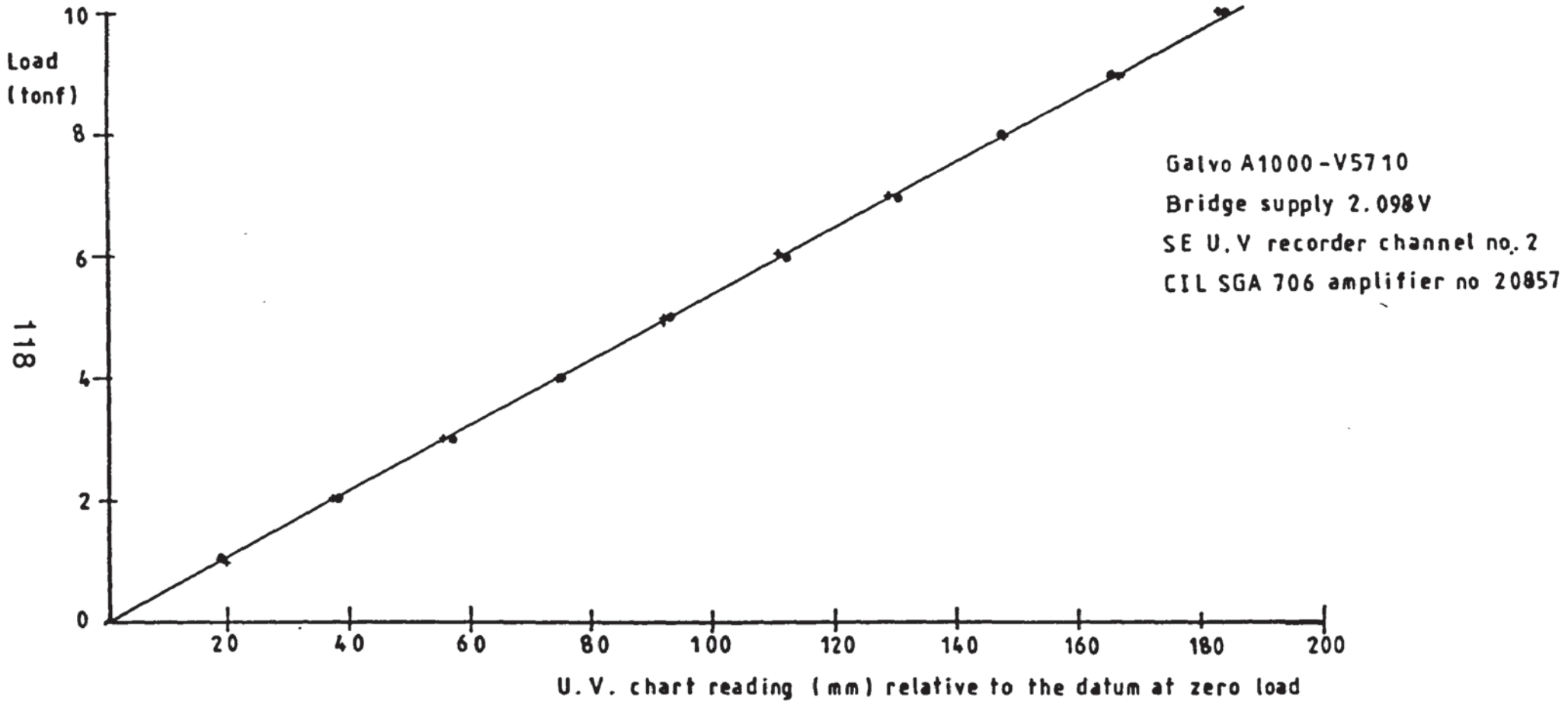

FIG 4.8 THE CALIBRATION GRAPH FOR AXIAL LOAD OF THE SIDE ROLL LOADCELL - F

arrangement of the strain gauge in the bridge and the position of the bridge on the loadcell surface. With reference to fig 4.1. and equation (4.2), it can be seen that any two balanced strain gauge responding to the axial loadcell will cancel out the signal output. This condition is obtained provided each gauge is in the bridge arrangement, containing a combination of either ab and ad, ab and bc, bc and cd, and ad and cd, respectively. For the two gauges arranged as 2-4 and 1-3 on the loadcell surface with the bending load in the direction as shown in fig 4.9. the nature of the bending allows $+\delta R_1$ and $-\delta R_2$ to be measured (if R_2 is in ab and R_1 is in either bc or ad). As in the previous case, a full strain gauge bridge is thus possible if another pair of gauges were arranged in a similar manner and connected in another arm pair.

4.6.2.2. Location of the strain gauge bridge

Because of the threads on the top and bottom connecting ends of the loadcells, and the lack of location pins in the circular cell, the position of the strain gauge bridge during the bending calibration may differ from its actual position in the rig. This situation created uncertainty between the calibration and the experimental results. The solution was to design a bridge circuit arrangement which would give a constant signal for all angular positions of the bridge, for any particular bending load vector. Various analyses of the strain gauge bridge set-ups and different circuit arrangements indicated that this objective was rather difficult to achieve. It was thus decided to bond the strain gauges on the loadcell surface along the central lines of either side wall of the bearing housing, with the housing screwed down. This was done because the bending load on the rolls was orthogonal to the wall. Consequently, the above gauge bridge arrangement will detect the maximum strain in each gauge.

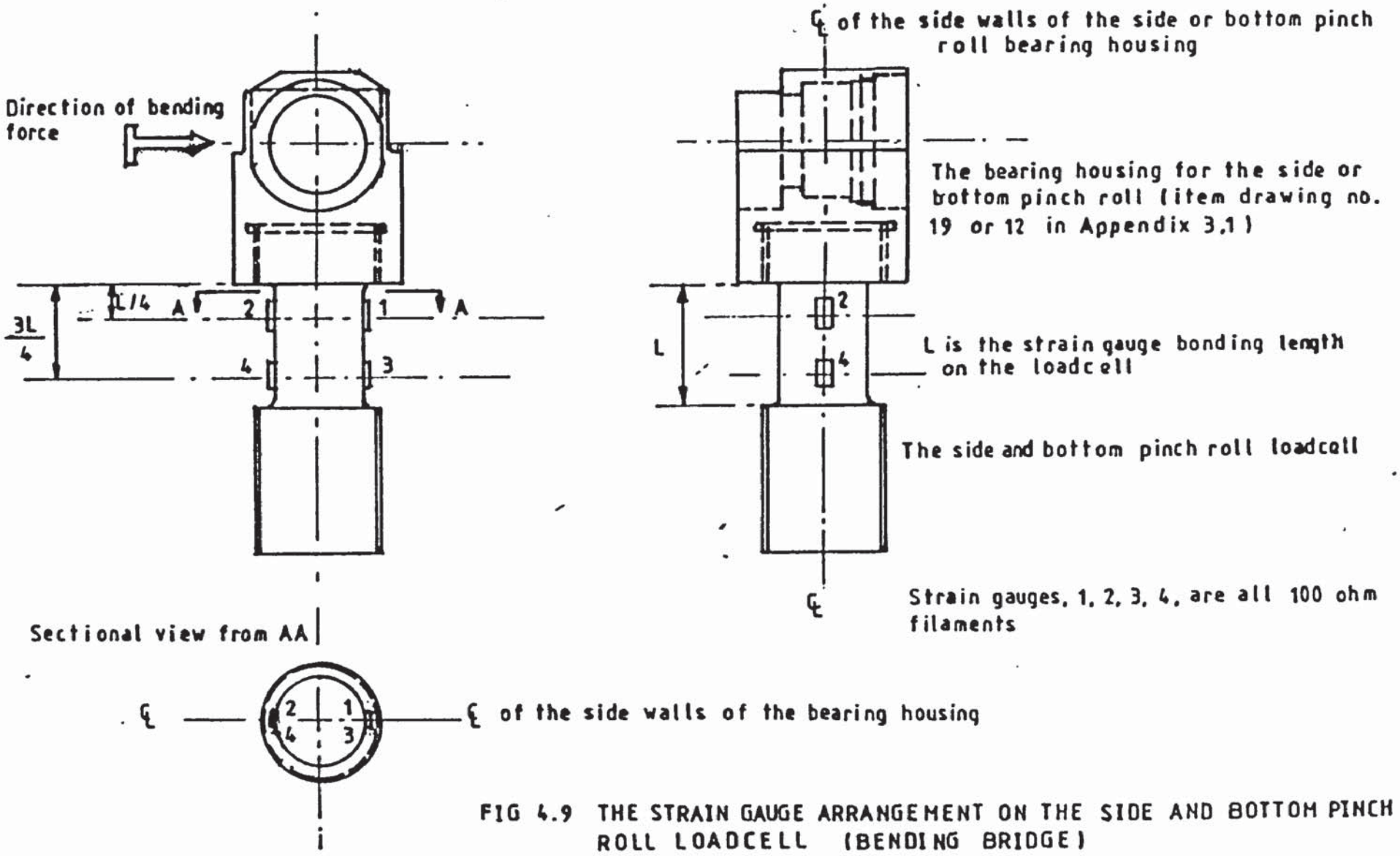

FIG 4.9 THE STRAIN GAUGE ARRANGEMENT ON THE SIDE AND BOTTOM PINCH ROLL LOADCELL (BENDING BRIDGE)

From the aforementioned considerations, the four gauges forming the full bridge were bonded on the "℄" of either side wall of the bearing housing : one pair was at the position one quarter of the gauge length, L, from the top of the cell and the other was three quarter of the gauge length from the same datum as shown in fig 4.9.

Each individual strain gauge bridge circuit is shown in fig 4.10. All the six bending bridges for the pinch and side roll loadcells were connected in parallel (fig. 4.11). A single d.c. Farnell L30B stabilizer power supply was used to provide a constant bridge voltage supply. RS10T-10kΩ potentiometers were introduced in the circuit for bridge balancing. The three-ways switches in the circuit, positioned between the output from each bridge and the recorder are mainly used to reverse the direction of the galvanometer deflection. This ensured that the bending output signal from the bridge, displayed on the u.v. chart, disregarded any bending influence on the loadcells.

4.6.2.3. Calibration

The calibration was carried out using the same Avery testing machine. For calibration purposes, in order to simulate the actual loadcell mounting condition, the loadcell , with its bearing housing secured on, was screwed into its push rod. These were then mounted in the retaining block. The retaining block, with the loadcell carefully positioned within it, was laid horizontally on to the bottom platen by a 25.4 mm x 300 mm x 615 mm mild steel plate and secured with six mild steel long screws of diameter 19.05 mm. Particular attention was also paid to the alignment of the blocks on the platen. When the central line of the bearing housing was aligned with the bending loading point, and the bending arm appropriately adjusted, a plate was laid on the bearing housing to

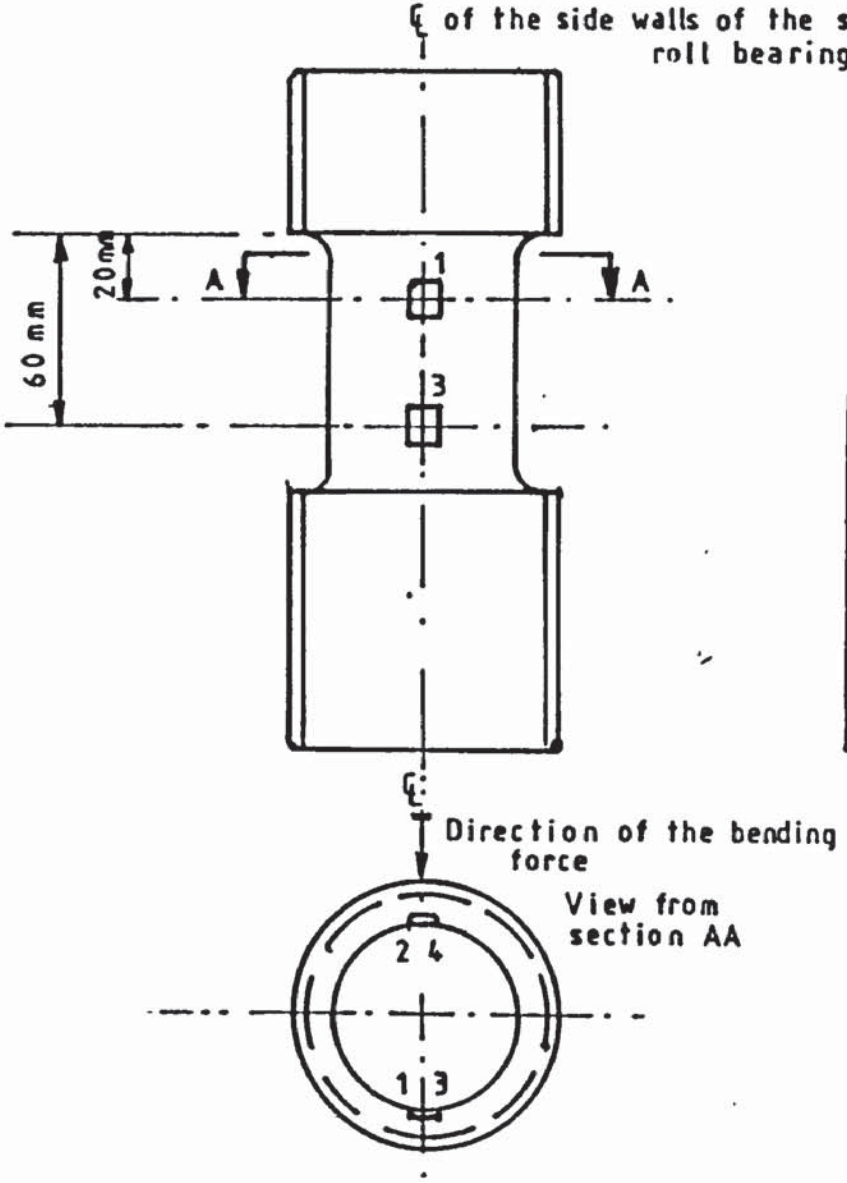

i- Strain gauge arrangement on the loadcell

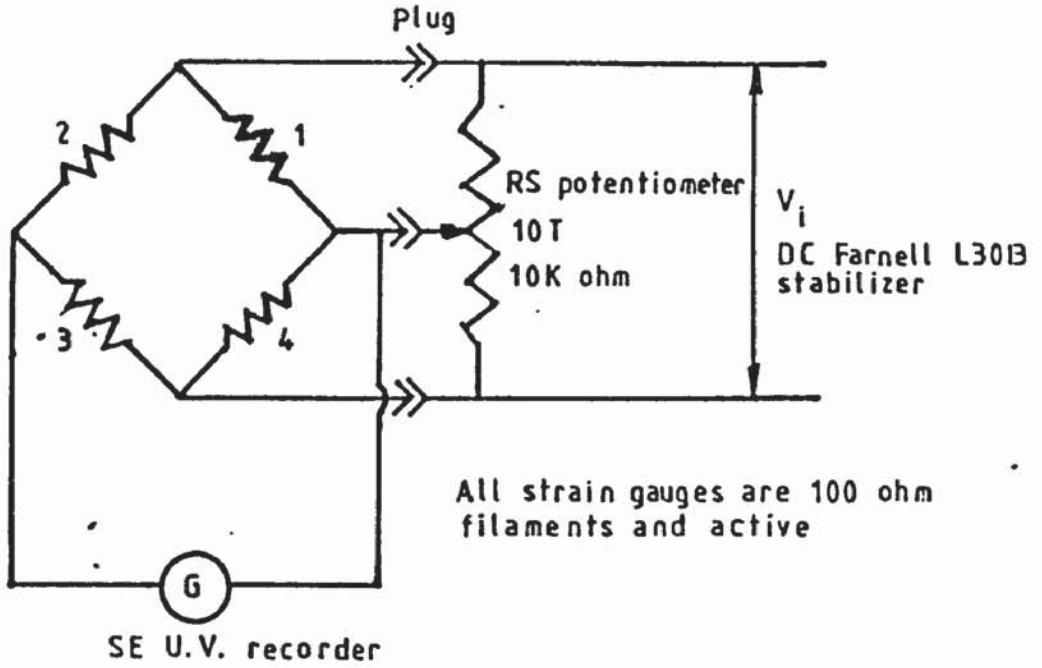

ii- Strain gauge bridge circuit arrangement

FIG 4.10 THE STRAIN GAUGE BRIDGE CIRCUIT ARRANGEMENT FOR MEASURING THE LOADS PERPENDICULAR TO THE AXIS OF THE SIDE AND BOTTOM LOADCELLS

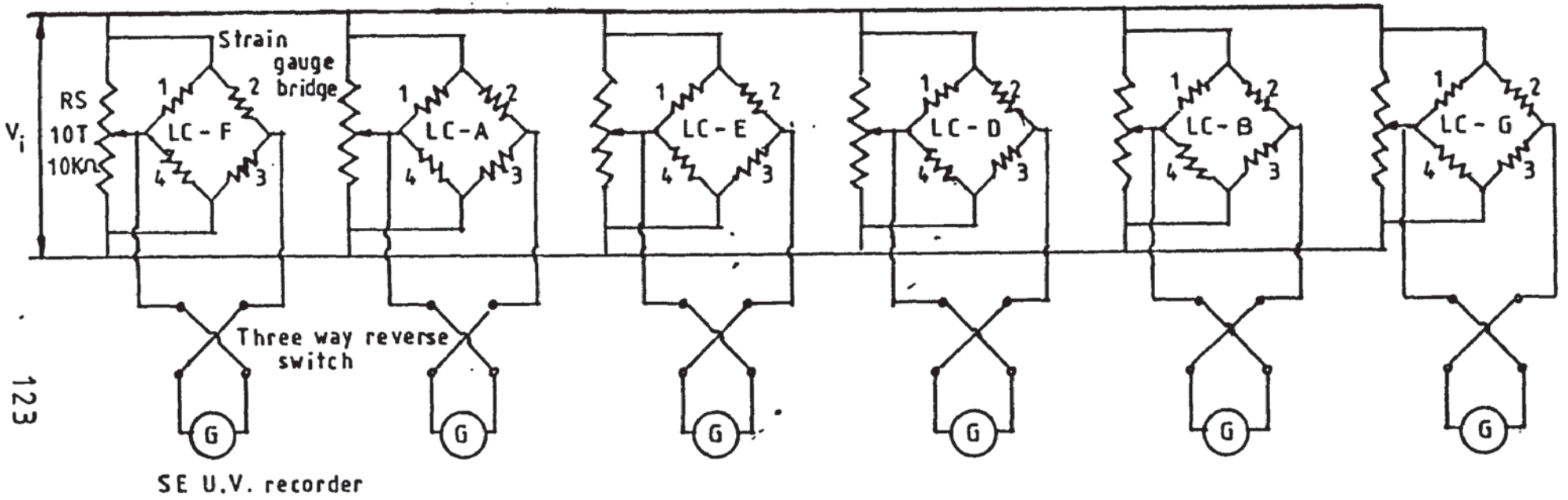

All strain gauges are 100 ohm filaments
1, 2, 3, 4 are all active gauges
V_i is a DC Farnell L30B power stabilizer
RS is RS potentiometer
LC represents load cells
A, B, D, E, F, G are the loadcells

FIG 4.11 THE POWERING CIRCUIT ARRANGEMENT FOR THE BENDING LOAD STRAIN GAUGE BRIDGES FOR THE BOTTOM PINCH AND SIDE ROLL LOADCELLS

distribute the transmission of the bending load. In order to avoid the shear effect, a ball bearing was introduced between the rod-column extension. The calibration thus set up is shown in fig 4.12.

In the same way as the other calibrations, the instruments were stabilised prior to the commencement of the calibration tests. The calibration for each loadcell was conveniently performed for four ranges, i.e.

(i) 0-20 kN with bridge supply voltage of 1.7 V
(ii) 0-40 kN with bridge supply voltage of 0.84 V
(iii) 0-60 kN with bridge supply voltage of 0.54 V
(iv) 0-100 kN with bridge supply voltage of 0.36 V.

The galvanometer and channel used for each loadcell, together with the corresponding information are shown in Table 4.1. For each range of calibration, the consistency of the results was confirmed by repeating the calibration at least twice. The linear regression equations and the coefficient of determination, the coefficient of correlation, and the standard error of estimation are also tabulated in Table 4.1.

4.7. Top loadcell bridge arrangement and circuitry

Unlike the pinch and side rolls, the top roll of the bender has no translational movement. This simplified the constraints of the loadcell design. The choice of a rectangular cross-sectional loadcell design, which allows for the modification of the thickness and width dimensions and, at the same time retain its original rigidity (see section 4.1), was thus appropriate. Furthermore, the flat surface of the rectangular loadcell aided installation of the strain gauges. The aforementioned characteristics, incorporating the consideration of the geometrical layout, and the operational nature of the model bender resulted in the top loadcell design

FIG 4.12 MOUNTING OF THE BENDING LOADING CALIBRATION OF A BOTTOM PINCH ROLL LOADCELL

as shown in fig 4.13.

4.7.1. Axial load strain gauge bridge and calibration

This bridge circuit is similar to the normal axial load bridge (fig. 4.2). The position of the strain gauges on the loadcell surface are shown in fig 4.14. A RS strain gauge amplifier (Type 308-815) was used. The circuitry of the bridge and the amplifier with its supplementary electronic components for each loadcell is shown in fig 4.15. The circuit gave a gain of (1+R1/R2), which was constantly set at 101. The changing of the output signal, at a particular load, can easily be achieved by simply adjusting the strain gauge bridge supply. This can be varied by adjusting the 10 kΩ zero setting potentiometer (a). The 10Tx10kΩ RS potentiometer (B) which was positioned across the positive and negative bridge supply, and connected to the positive bridge input, was mainly for balancing the bridge (fig.4.15).

The bridge amplifier system has a ±12 V supply at 20° C ambient temperature. In order to reduce the number of power packs, the four bridge amplifier system was connected in parallel as shown in fig 4.16.

Prior to calibration, all the instruments were "warmed up" to eliminate electrical drift. The calibration was again carried out using the Avery testing machine. The mounting of the calibration is as shown in fig 4.17.

Three load ranges, i.e. 0-50 kN, 0-100 kN and 0-130 kN set at their required bridge supply were considered. The reproducibility of the calibration results was confirmed by repeating each calibration twice. Detailed information and the linear regression equations of the results are shown in Table 4.1.

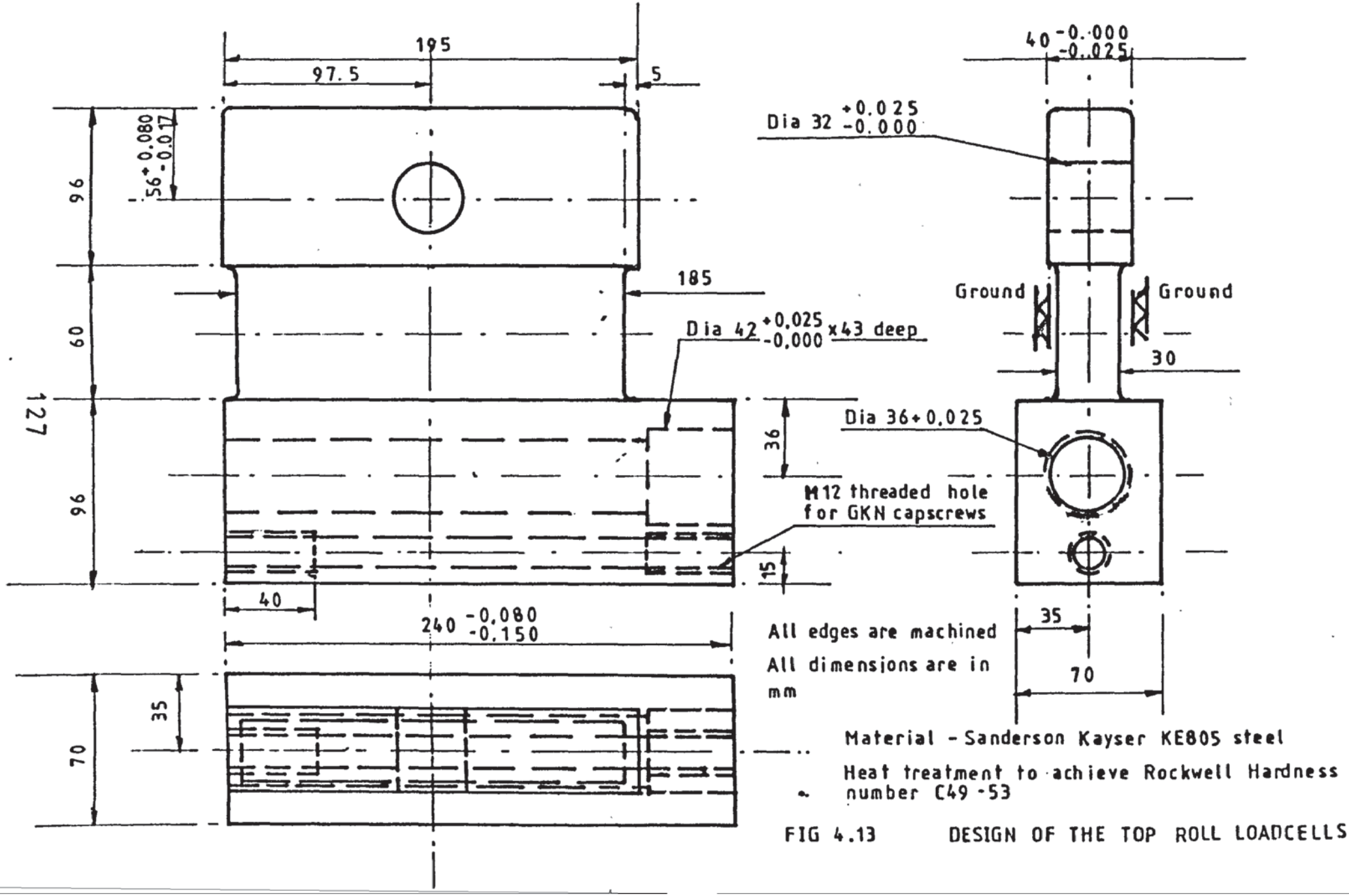

FIG 4.13 DESIGN OF THE TOP ROLL LOADCELLS

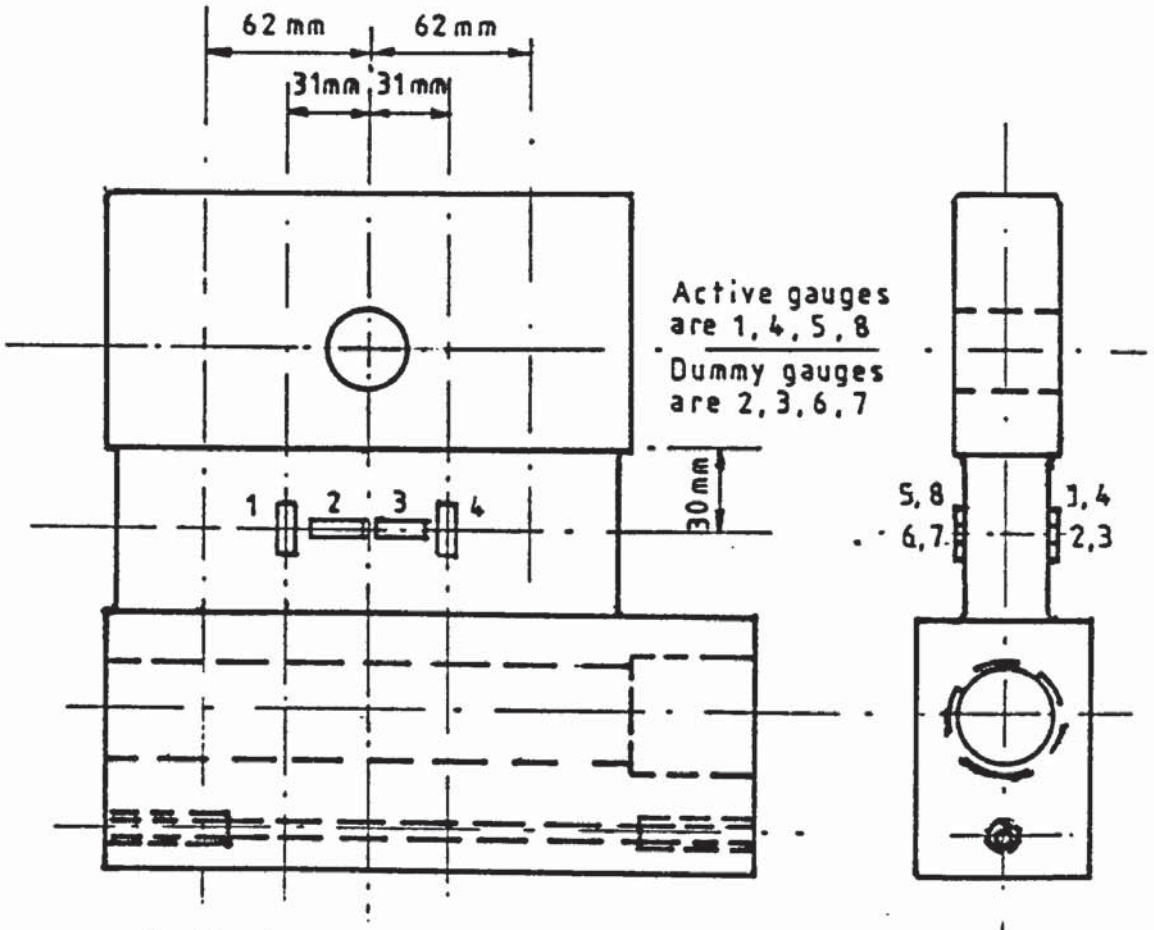

i- Strain gauge arrangement of the top load cell

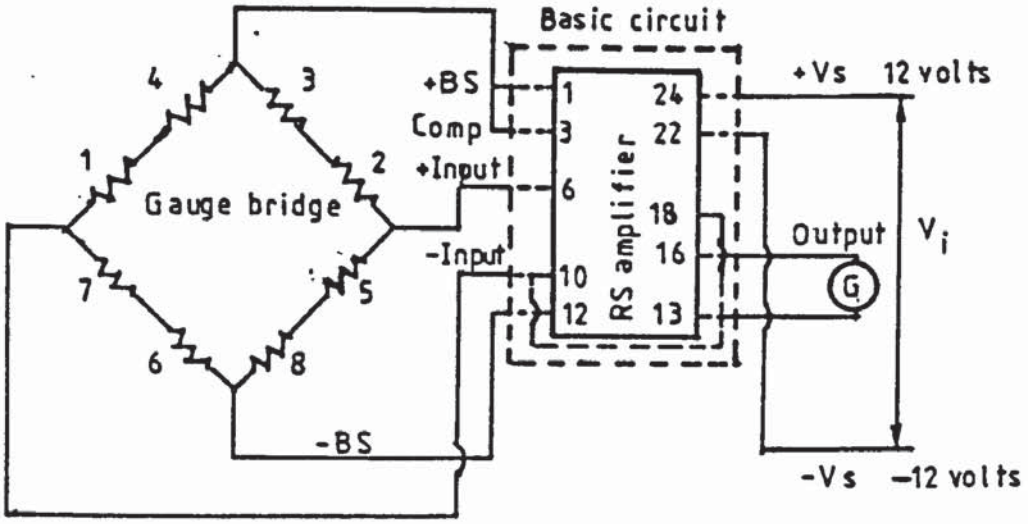

All strain gauges are 100 ohm filaments

ii - Strain gauge bridge circuit and RS amplifier type 308-815 arrangement

FIG 4.14 THE STRAIN GAUGE BRIDGE CIRCUIT ARRANGEMENT FOR MEASURING THE LOAD COMPONENT ALONG THE TOP ROLL LOADCELL AXIS

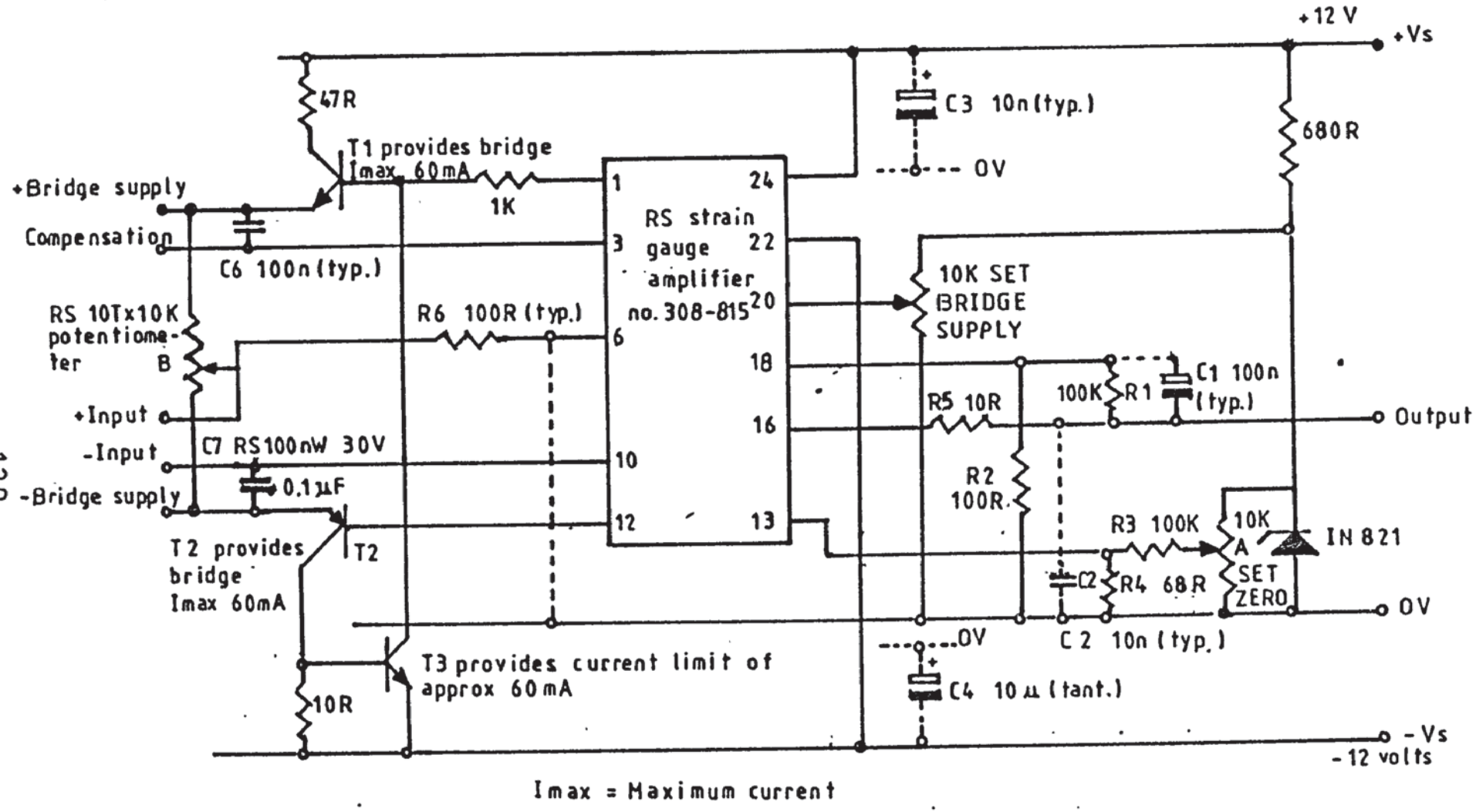

FIG 4.15 THE SUPPLEMENTARY CIRCUIT FOR THE RS STRAIN GAUGE AMPLIFIER FOR EACH TOP LOADCELL

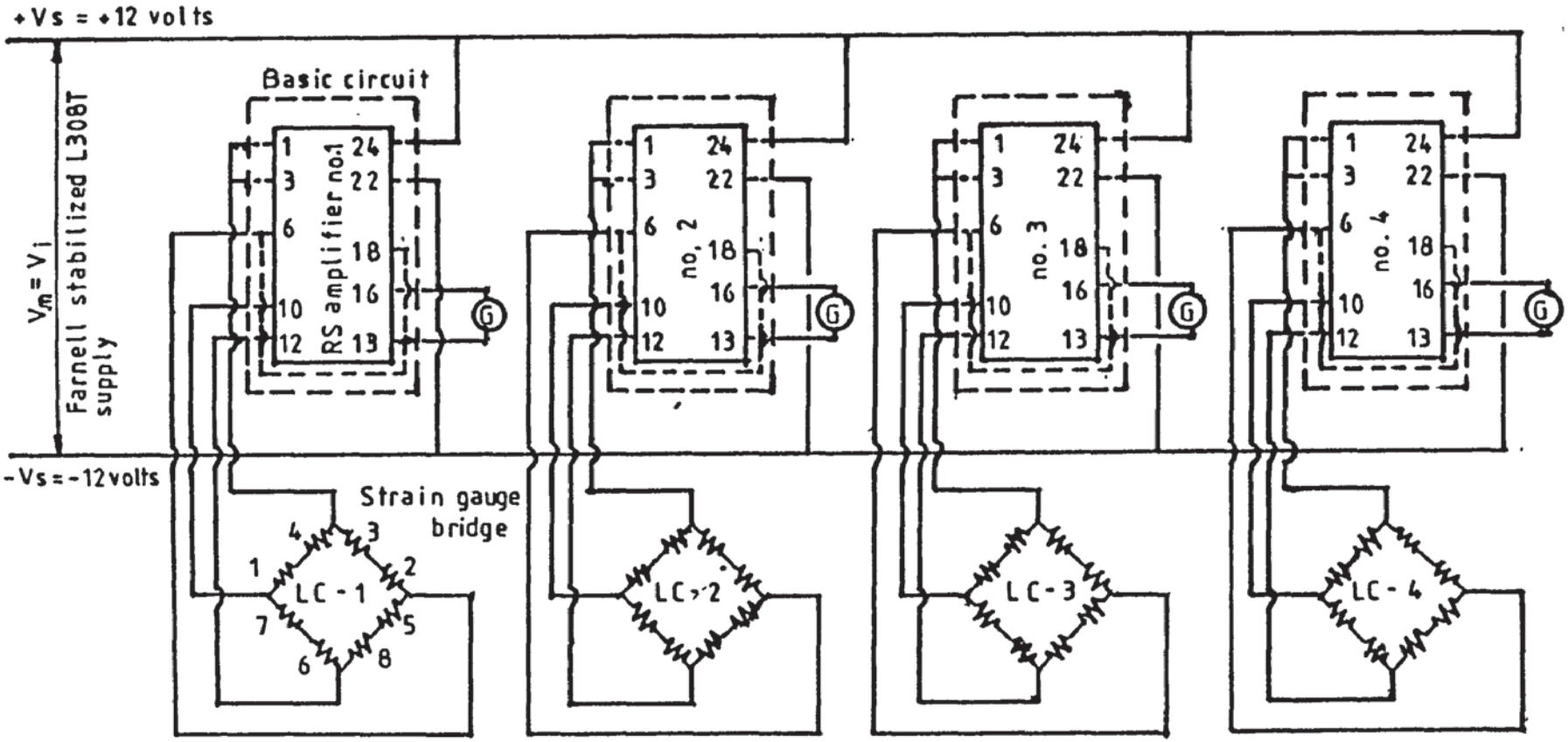

All strain gauges are 100 ohm filaments Active gauges are 1, 4, 5, 8.
Dummy gauges are 2, 3, 6, 7 LC indicates load cells
G are galvanometers in Southern Instruments U.V. recorder

FIG 4.16 THE POWERING CIRCUIT ARRANGEMENT OF THE RS STRAIN GAUGE AMPLIFIER TYPE 308 - 815 AND THE AXIAL LOAD STRAIN GAUGE BRIDGES FOR THE TOP LOADCELLS

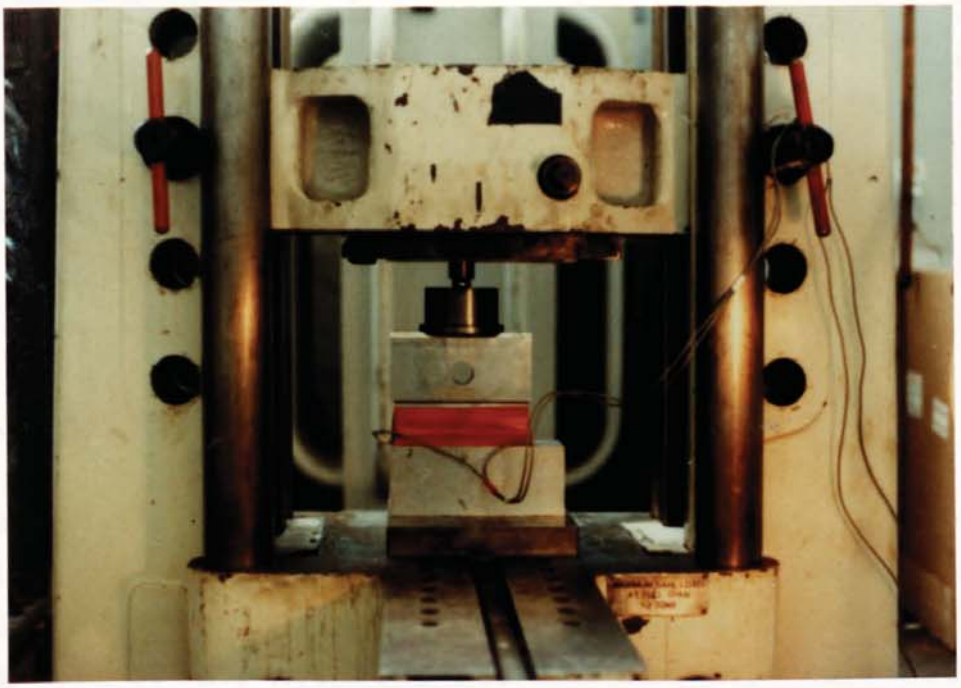

FIG 4.17 MOUNTING OF THE AXIAL LOADING CALIBRATION OF A TOP ROLL LOADCELL

4.7.2. Bending strain gauge bridge and calibration

4.7.2.1. Bridge position and circuitry

The rectangular cross-sectional shape of the loadcell facilitated the accurate sensing of the bending mode signal. The position of the strain gauges for this condition, the bridge circuit and its balancing potentiometer are shown in fig 4.18.

The four bridges in the bending mode are connected in a parallel circuit to a Farnell d.c. stabilizer L30B, as shown in fig 4.11.

4.7.2.2. Calibration

As previously the instruments were "warmed up" prior to calibration. The top loadcell was carefully clamped on the bottom platen of the Avery testing machine (fig 4.19) in a similar manner to the mounting for the bending calibration of the bottom pinch/side loadcells. The exclusion of the shear component effect, (probably caused by the friction between the surface contacts of the extension and other supplementary components in the loading condition), was carefully taken into consideration by the introduction of a ball bearing between the rod column extension and a metal strip. This again distributed the load transmitted to the loadcell. The metal strip was accurately located on the effective central line of the bending arm. Particular attention was also paid to the proper alignment of the extension pieces.

The calibration for each loadcell was performed for the four ranges, which were : 0-10 kN, 0-20 kN, 0-30 kN and 0-40 kN with a constant bridge supply of 7.13 V, 3.56 V, 2.37 V and 1.78 V respectively. The consistency of each set of the results was confirmed by twice repeating the calibration.

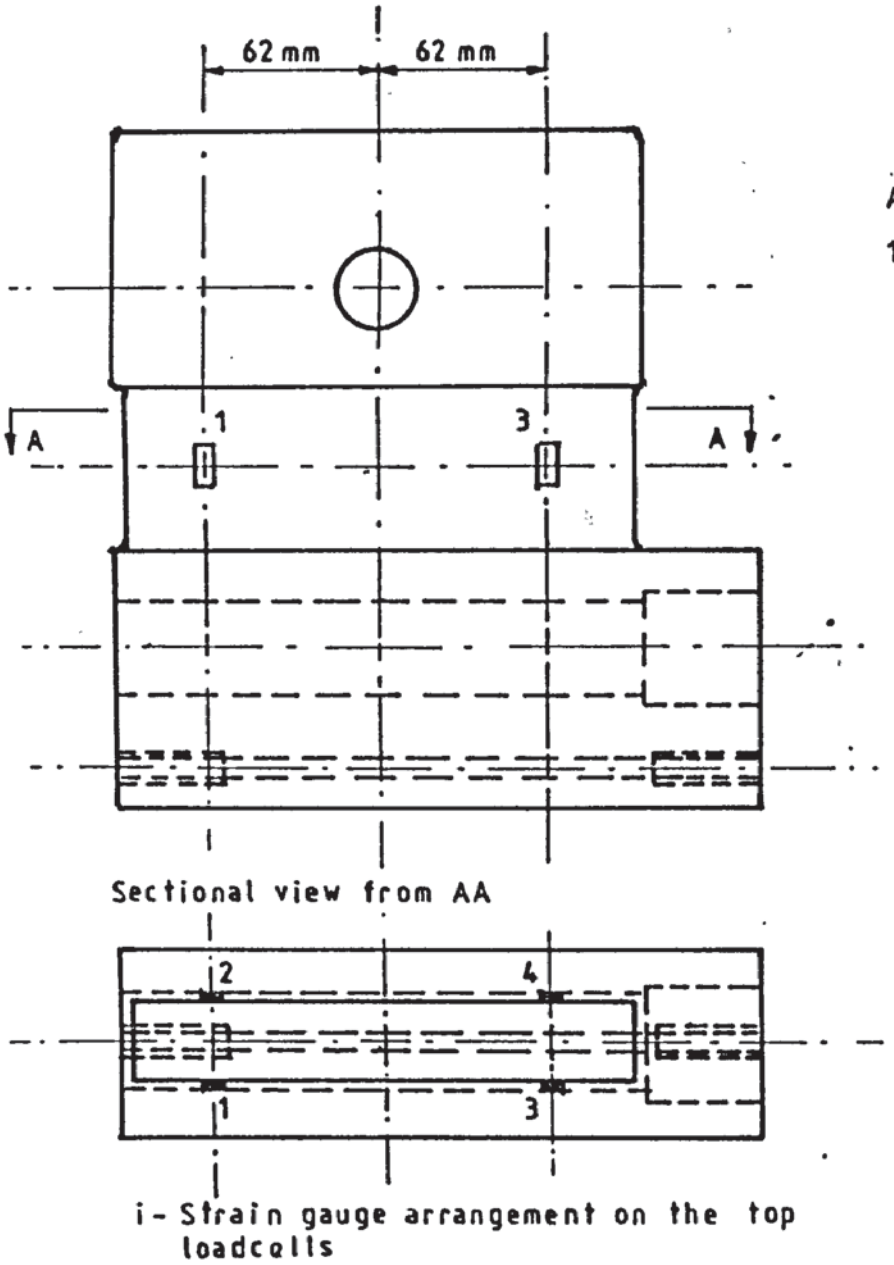

i- Strain gauge arrangement on the top loadcells

All strain gauges are 100 ohm filaments

1,2,3,4 are strain gauges

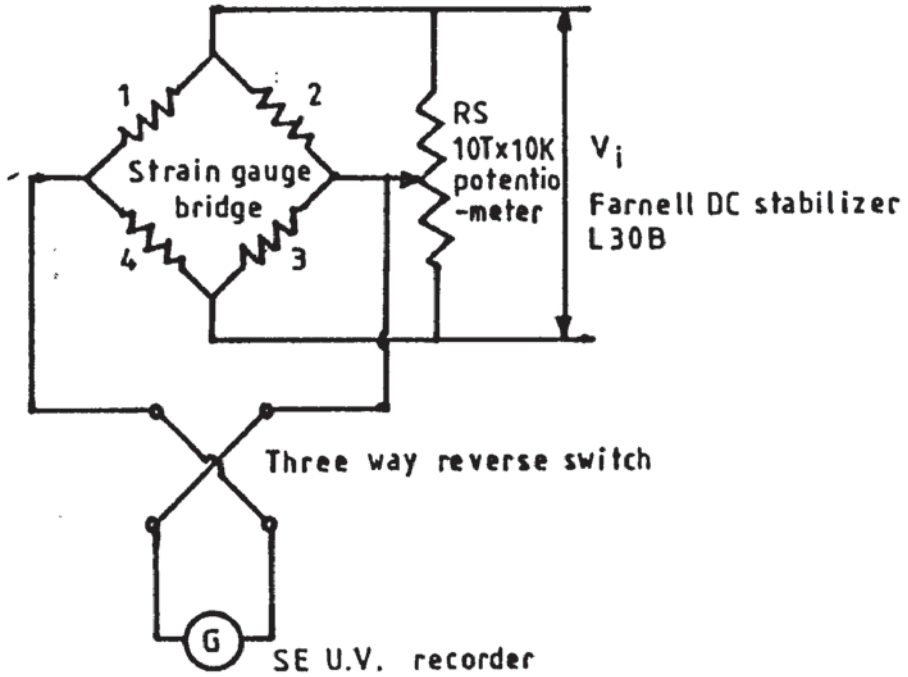

ii- Strain gauge bridge circuit arrangement

FIG 4.18 THE STRAIN GAUGE BRIDGE CIRCUIT ARRANGEMENT FOR MEASURING THE LOADS PERPENDICULAR TO THE AXIS OF THE TOP LOADCELLS

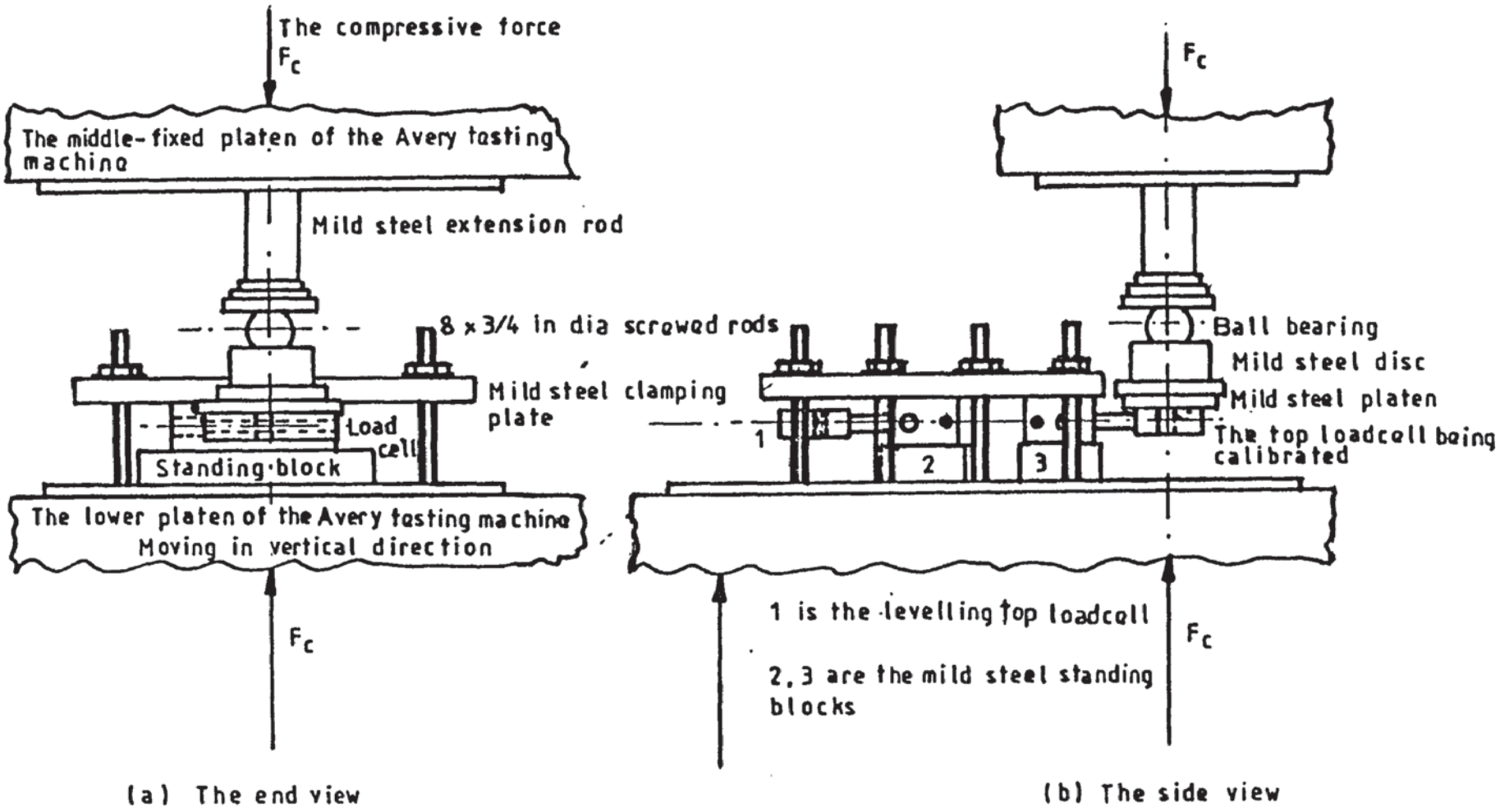

FIG 4.19 MOUNTING OF THE TOP LOADCELLS FOR THE BENDING CALIBRATIONS

Again the calibration results were transformed in the forms of linear regression equations as shown in Table 4.1. The corresponding coefficient of determination and the standard error of estimation are also shown in the table.

4.8. Torquemeter bridge arrangement and calibrations

In order to measure the driving torque in bending the plate, it was necessary to design a top roll torquemeter. Two side roll torquemeters were also required to study the slip effect, relative to the total power consumption.

The design principle of the torquemeter was based on equation (4.1) as mentioned in section 4.3. The designed torquemeters are shown in fig 3.9.

4.8.1. Strain gauge position and bridge circuitry

The torquemeter has a value of induced strain, ε_{45} at 45°, of almost half the recommended design specification, i.e. 0.1 %, at its maximum estimated torque. Consequently, its employment for the aluminium plate bending test is only possible if the bridge is either self-amplified, by increasing the number of gauges in the bridge with the suitable choice of a sensitive galvanometer, or, alternatively, with an additional amplifier to magnify the output signal from the bridge to the u.v. recorder.

The benefit of self amplification in a bridge, by increasing the number of gauges, is that it increases the maximum limit of the bridge supply. This increases the amplitude of the output signal.

Consideration of the relative high cost of an adequate amplifier, and the possible instability of gain adjustment in

the normal bridge amplifier, militates against its employment.

The position of the strain gauges on the torquemeter and its bridge circuitry are shown in fig 4.20. This bridge arrangement will automatically compensate against the thermal signal and attenuates other induced strain signals in the bridge.

4.8.2. Calibration

The calibration was carried out by using the Avery torsion testing machine. The mounting of the torquemeter in the machine is illustrated in fig 4.21.

Again, normal calibration procedures were carried out, the calibration for each torquemeter being performed for two load ranges :

(i) 0-452 N m and 0-904 N m with a bridge voltage supply of 4 V and 8 V, respectively, for the side roll torquemeters.
(ii) 0-904 N m and 0-1695 N m with a bridge voltage supply of 4 V and 8 V, respectively, for the top torquemeter.

The object of calibrating the torquemeters at the same two bridge supplies was to reduce the number of stabilised d.c. supplies.

Since the galvanometers utilized in the calibration are rather sensitive, i.e. 2.9 μV/mm, the zero balancing of the bridge was carefully carried out. The initial bridge balance was obtained by taking the output from the bridge to a Solartron A200 d.v.m. (this measures to 1 μV) and adjusting the RS10T-10kΩ potentiometer. The appropriate bridge supply was preliminarily established by referring to the bridge output voltage on the d.v.m.. This particular bridge output was considerably less than the corresponding value required

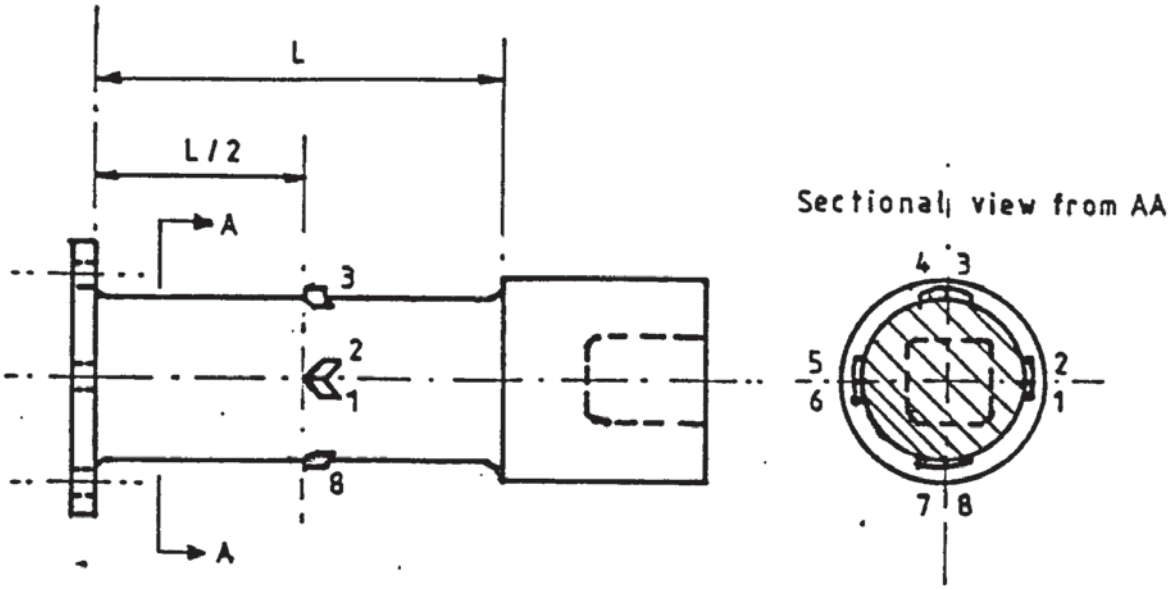

1, 2, 3, 4, 5, 6, 7 and 8 are all 100 ohm filament strain gauges

i - Strain gauge arrangement for torquemeters

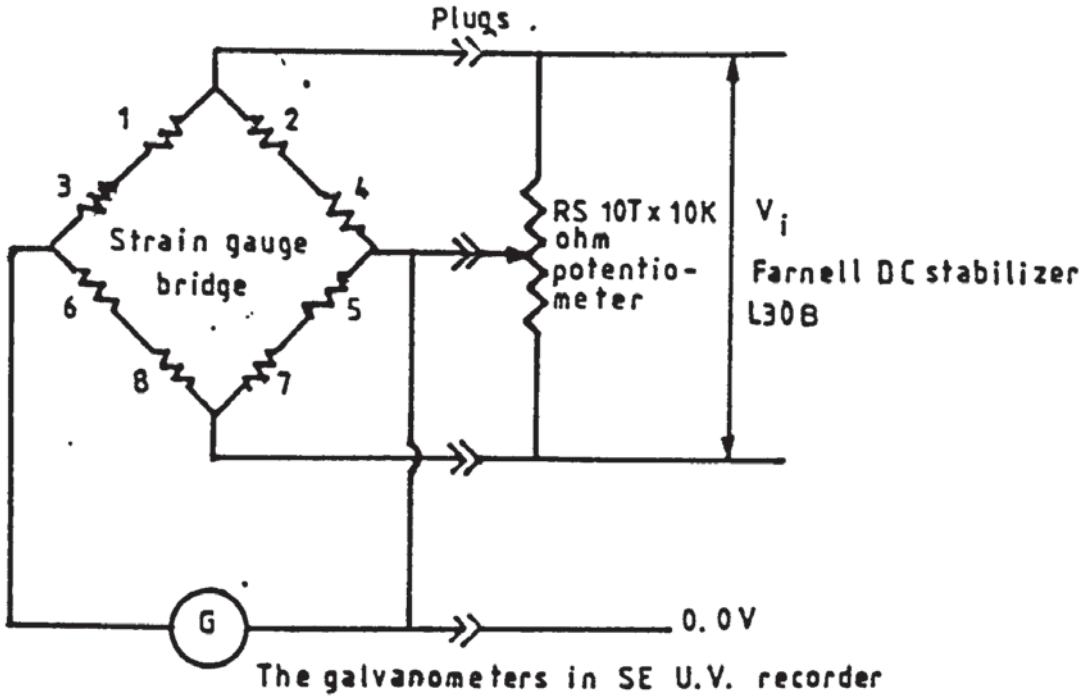

ii- Strain gauge bridge circuit arrangement

FIG 4.20 THE STRAIN GAUGE BRIDGE CIRCUIT ARRANGEMENT FOR TORQUE MEASUREMENTS

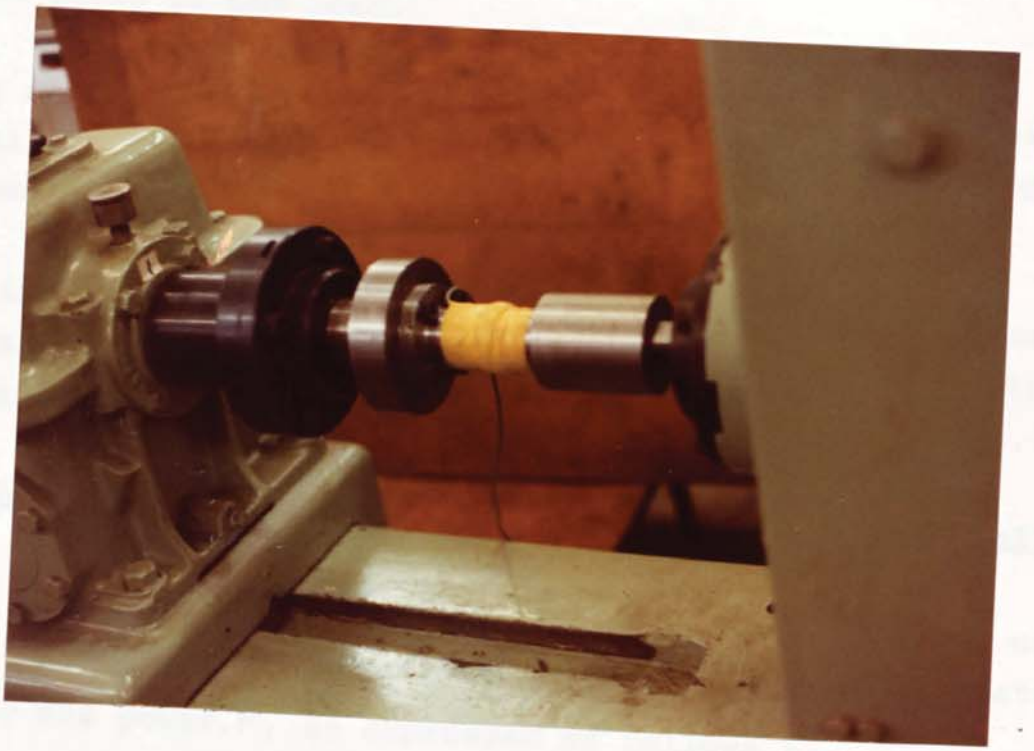

FIG 4.21 CALIBRATION MOUNTING OF A TORQUEMETER

for the full deflection of the galvanometer. The output was then connected to u.v. recorder and the final bridge supply was obtained by further adjustment of the bridge supply until the required galvanometer deflection was obtained in the initial stage. The subsequent bridge supply was taken as an inverse ratio of the load.

The reliability of the calibration was ensured by repeating the calibration twice and the results were plotted on a graph as shown in fig 4.22 to confirm their correlation.

As in the previous cases, the calibration data was keyed into an Apple II statistical software and the linear regression equations were obtained and shown in Table 4.1.

4.9. Measurement of the rotational speed of the rolls

The power needed to execute the continuous bending of a plate is one of the major parameter to be investigated. Normally the power, P, is expressed as follows :

$$P = T\omega = \pi TN/60 \qquad (4.7)$$

where ω is the angular velocity of the roll in rad/s.

T is the torque experienced on the roll in N m.

N is the rotational speed of the roll in rev/min.

Assessment of the rotational speed of the roll is therefore an important factor.

The speed of the drive line of the top roll, from the Allspeed Kopp R1-HT6 variable speed drive, was controlled and indicated approximately by a speed setting dial. Furthermore, the pinch action between the pinch rolls and the bend-plate in bending, may produce slight variations in the final rotational

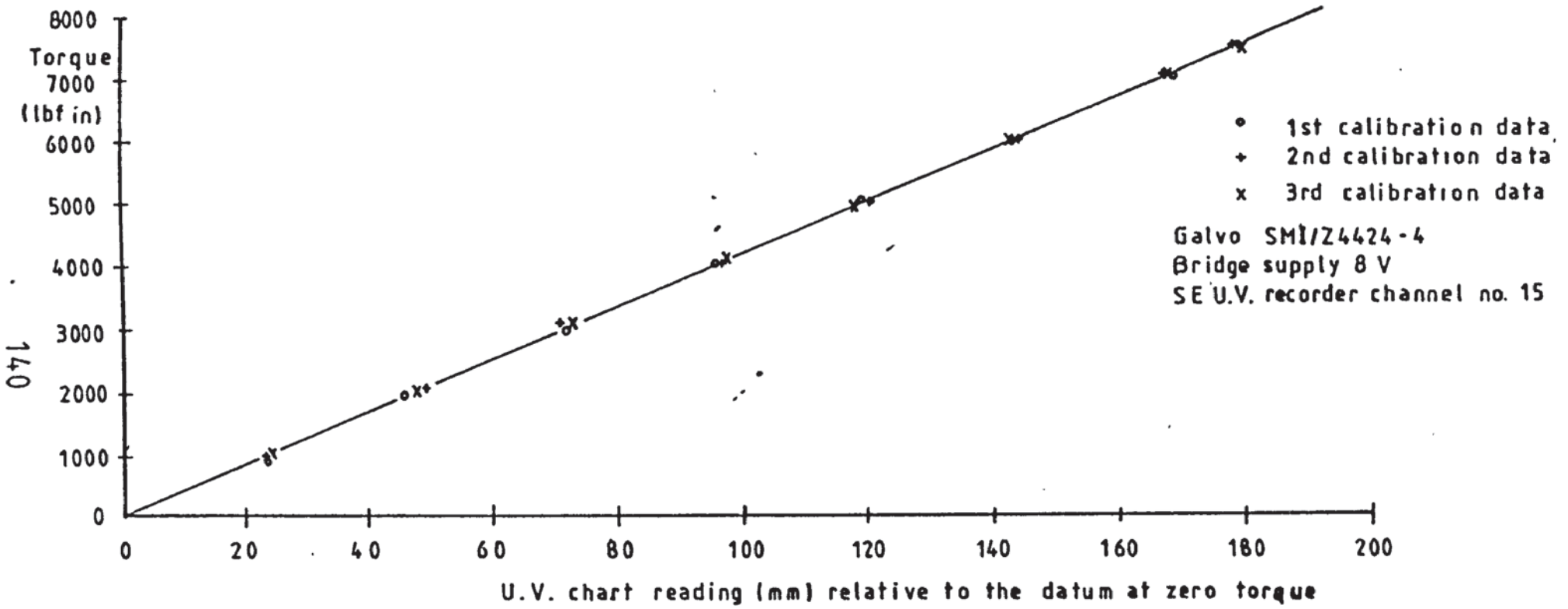

FIG 4.22 THE CALIBRATION GRAPH FOR TOP ROLL TORQUEMETER

speed of the top roll from that of the dial setting indicator. It was therefore decided to measure the rotational speed of the top roll directly. For this purpose, a Servo-Tek tachometer, rating of 20.8 V/1000 rev/min, was mounted at the free end of the top roll (fig 4.23). The tachometer was capable of generating a linear output signal corresponding to the number of the roll rotations.

Owing to the restrictive position of the side rolls, it was rather uneconomical to mount a tachometer at the free end of the side roll. With respect to performing the initial bending test, with free drive on the side roll, a knowledge of the side roll speed was not required. However, when the slip effect is investigated, instrumentation for this roll speed would be incorporated.

4.9.1. Circuitry and calibration of the top roll tachometer

The measuring circuit for the top roll tachometer is as shown in fig 4.24(i). The introduction of the 100 μF capacitor was to stabilise the output signal from the IME Thorn B160 galvanometer. It successfully attenuated the pick-up signal and thus gave satisfactory performance of the circuit arrangement.

In order to prevent the probable error introduced by misalignment of the tachometer in the top roll arrangement, the calibration was carried out in situ as follows :

A line was scribed on the propshaft of the top roll and a "L" shaped pointer was fastened on the frame, which was attached to the rig (fig 4.24(ii)). The calibration was carried out by noting the time for twenty revolutions of the propshaft. This was repeated for each of the five particularly

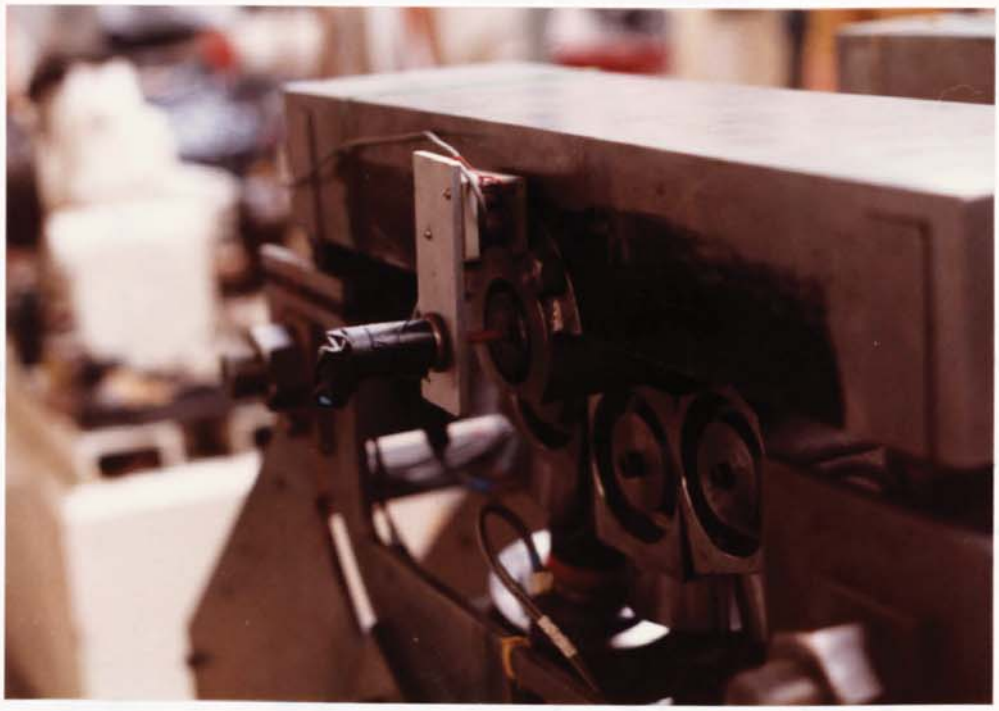

FIG 4.23 MOUNTING OF TACHOMETER FOR MEASURING THE ROTATIONAL SPEED OF THE TOP ROLL DRIVE

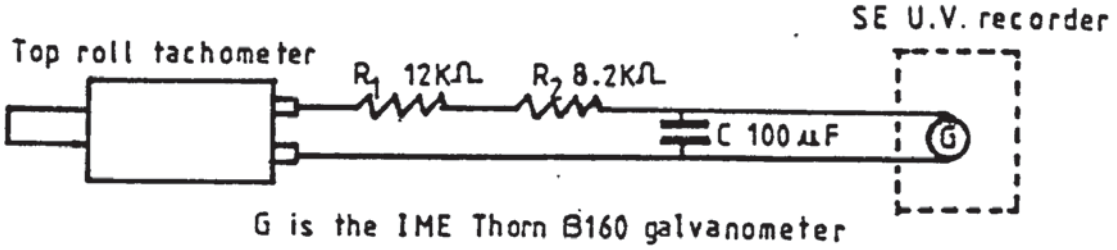

G is the IME Thorn B160 galvanometer

i - Circuit arrangement of the top roll tachometer

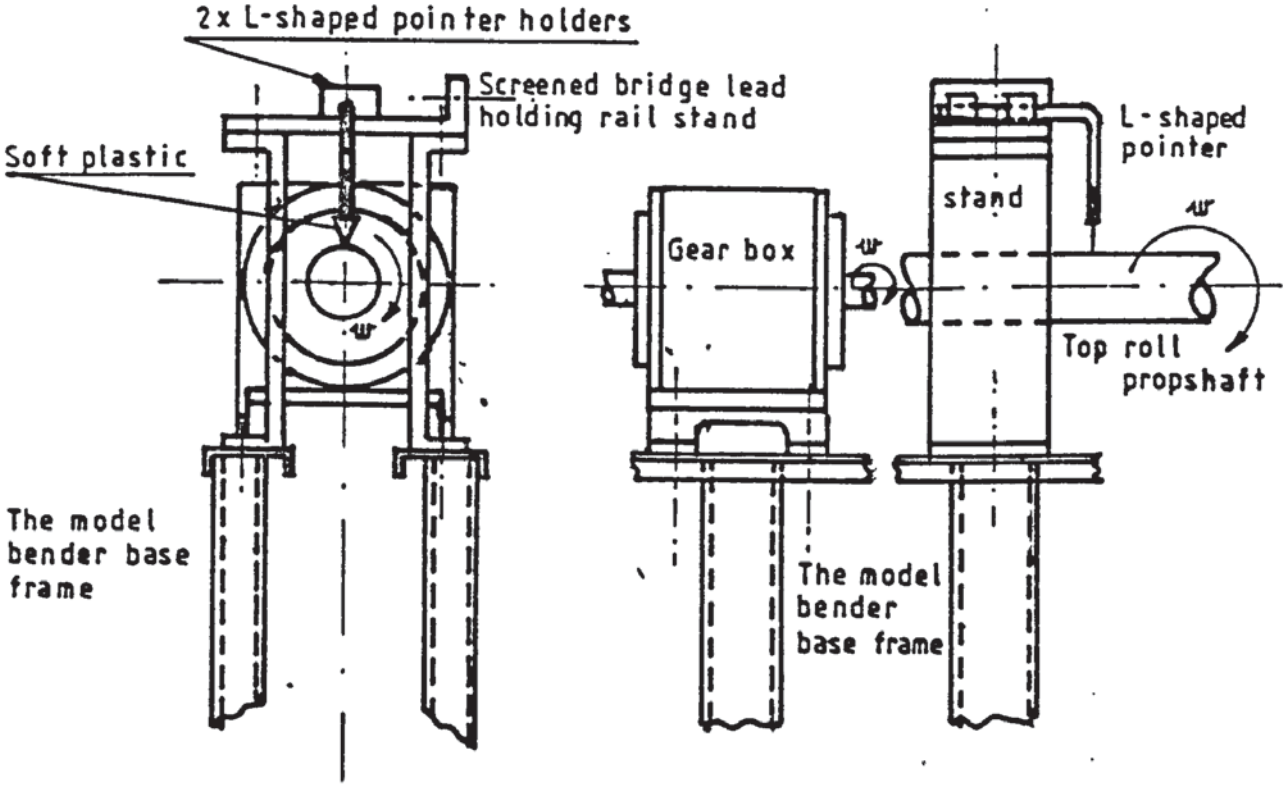

(a) The end. view (b) The side view

ii - The mounting of the L-shaped pointer for in situ calibration of the top roll tachometer

FIG 4.24 THE MEASURING CIRCUIT ARRANGEMENT AND THE MOUNTING OF THE SUPPLEMENTARY EQUIPMENT FOR IN SITU CALIBRATION OF THE TOP ROLL TACHOMETER

set rotational speeds. The corresponding trace amplitudes recorded on the u.v. chart were then plotted against the propshaft speed. The result of the calibration is shown in fig 4.25 and Table 4.1.

4.10. Device for measuring the inner radius of a bent plate

The measurement of roll forces and torques by itself will not provide any valuable information about the mechanics of the roll plate bending process. The data will only be useful provided the bent radius of the plate is measured. An arrangement for measuring the inner radius of curvature of a bent plate (fig 4.26) was thus designed.

The design of the device for measuring the inner radius of curvature (D.M.I.R.C.) is based on the evaluation of the diameter of a circle from a known sectoral base length, L, and its depth, h, from the midpoint of the sector (see Appendix 4.1). The expression for determining the bent diameter, d, in terms of L and h, of a bent plate is as follows :

$$d = (L^2/4 + h^2)/h \qquad (4.8)$$

The device consists of two mild steel beams of 12.7 mm x 37.5 mm x 100 mm and 12.7 mm x 37.5 mm x 150 mm respectively. The two beams were screwed together with their axial central line properly aligned. A 3 mm diameter hole was drilled through the central point of the two countersunk screwed beams. By a suitable choice of the contact points of the D.M.I.R.C. with the inner surface of the bent plate, the depth of the contact sector can be measured by the insertion of a depth gauge through the drilled hole. The application of this device is shown in fig 4.26.

4.11. Arrangement of the sensing components in the model bender

The layout of the sensing component arrangements in the model bender and the instruments are shown in fig 4.27 and fig 4.28, respectively. The specification of the loadcells and their corresponding sensory signals, the u.v. galvanometers and the channels used in the U.V. recorders are shown in Table 4.2.

4.12. Arrangement of the strain gauge bridge leads for the torquemeter

It has already been stated that the rigidity of the roll was the prime specification of the model design (section 3.2). Owing to the rolls being relatively long with small diameter end sections for the bearing housings, the drilling of a straight hole through the centre of the roll was considered impractical. Furthermore, it would also substantially weaken the rolls and their end sections. The introduction of slip rings as a device for transmitting the torque signals proved impractical for the present purpose. Consequently, an alternative way of wiring the torquemeter to the u.v. recorder was required. The detail of this method is as follows :

With reference to fig 4.29, it should be noted that the screened strain gauge bridge lead is of a length slightly greater than twice the length of the planned longest plate to be bent (i.e. 3813 mm). The lead is attached to a strong cord, which passes over a pulley fixed under a channel section member above the model bender. The other end of the cord is fixed to the channel bar. A weight of 0.4 N is hung at the middle of the cord. This controls the raising and lowering of the lead as it is wound and then released around the driven propshaft.

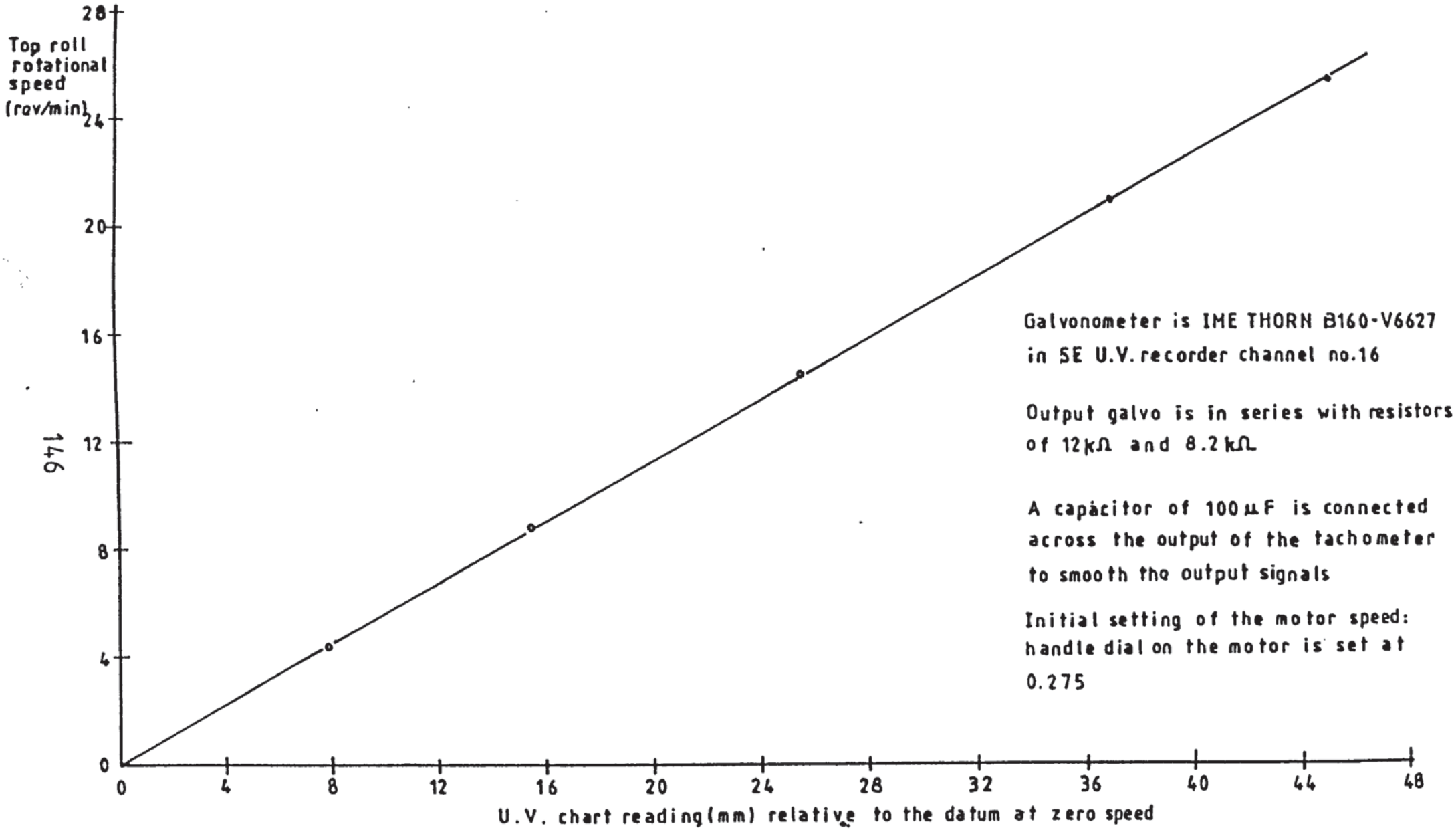

FIG 4.25 THE CALIBRATION GRAPH OF THE TACHOMETER FOR MEASURING TOP ROLL ROTATIONAL SPEEDS

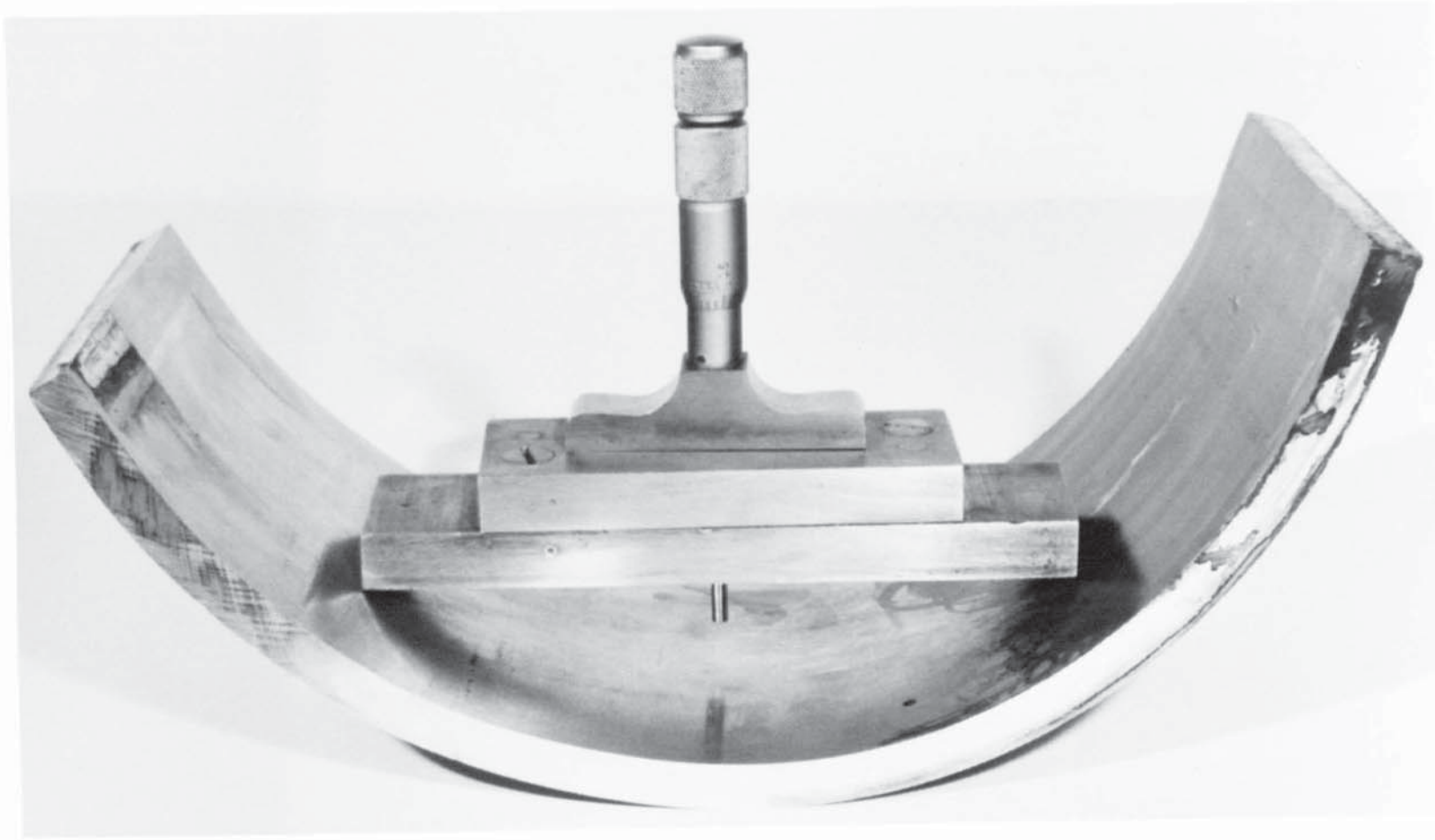

FIG 4.26 DEVICE TO MEASURE THE BEND RADIUS OF A BENT PLATE

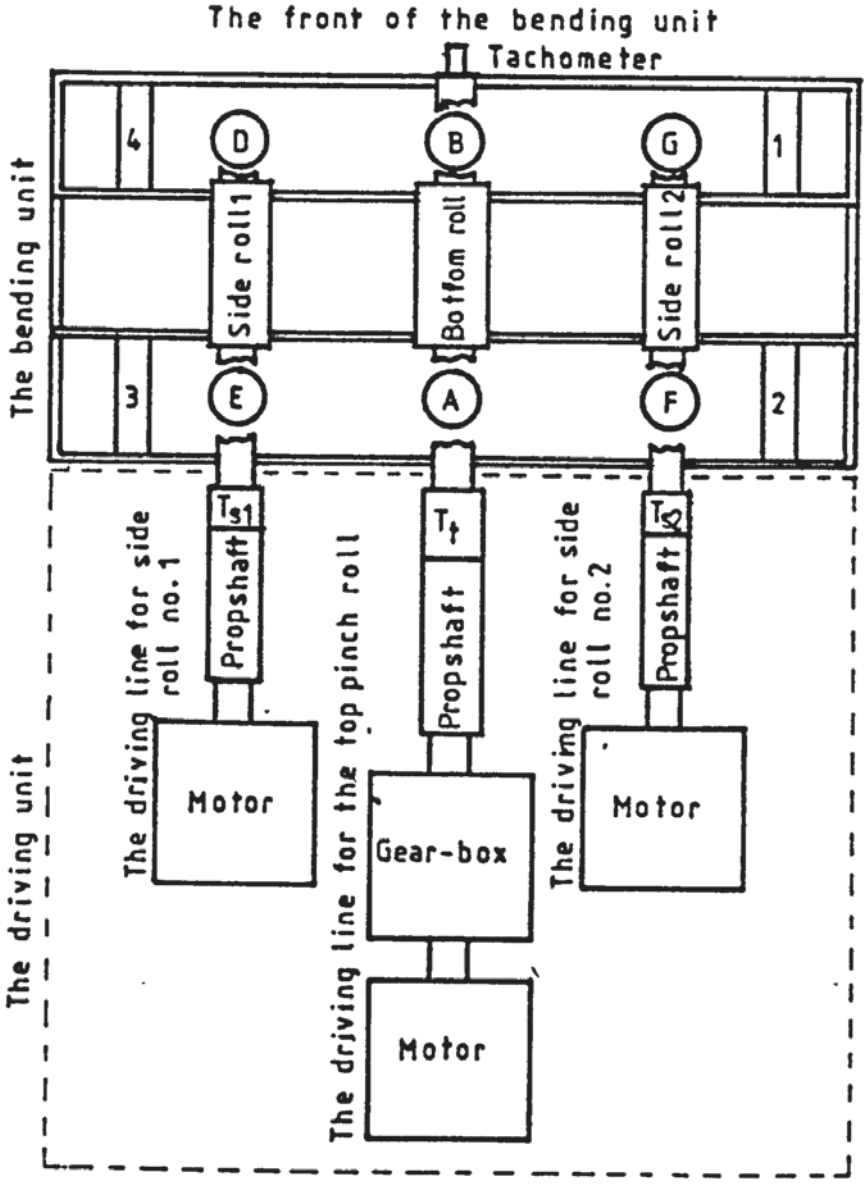

1, 2, 3, 4 are the specification numbers for the top loadcells

A, B are the specification letters for the bottom roll loadcells

D, E, F, G are the specification letters for the side roll loadcells

T_{s1} , T_{s2} are the torquemeters for the side roll number 1 and 2 respectively

T_t is the top roll torquemeter

FIG 4.27 PLAN ARRANGEMENT OF THE SENSING COMPONENTS IN THE MODEL BENDER

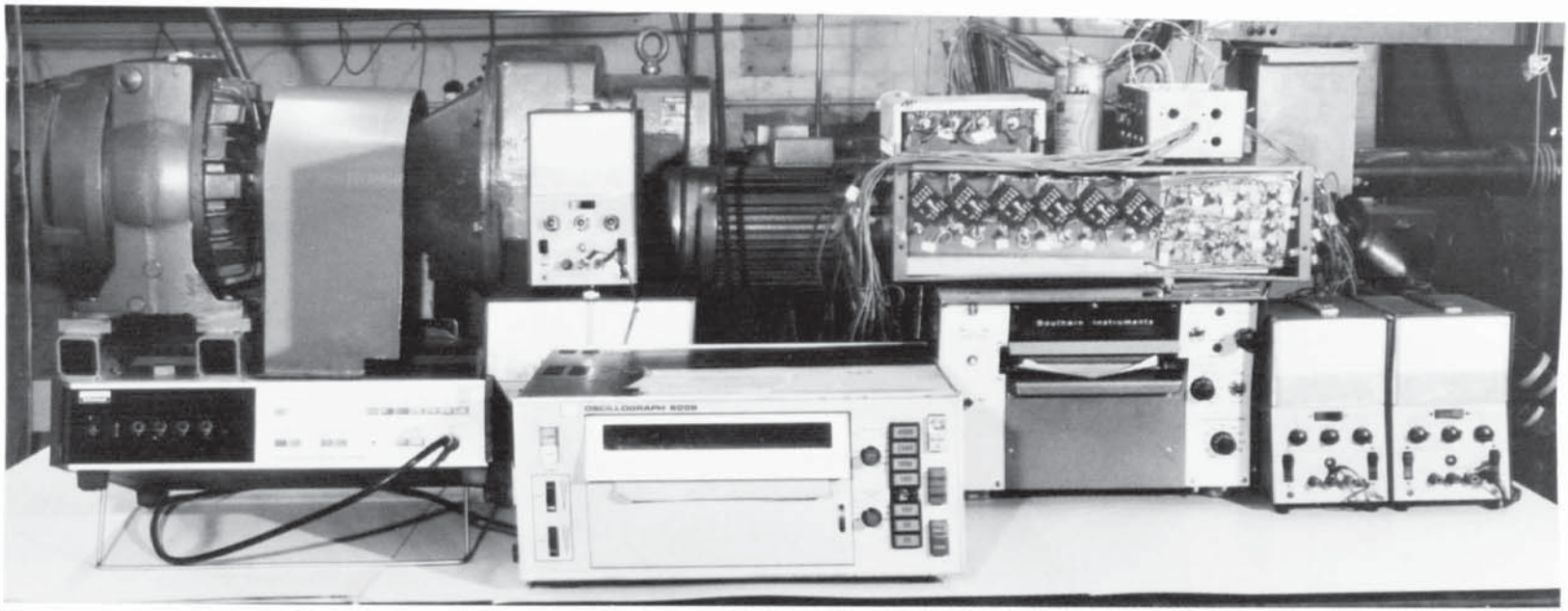

FIG 4.28 THE RECORDING INSTRUMENTS AND POWER SUPPLIES

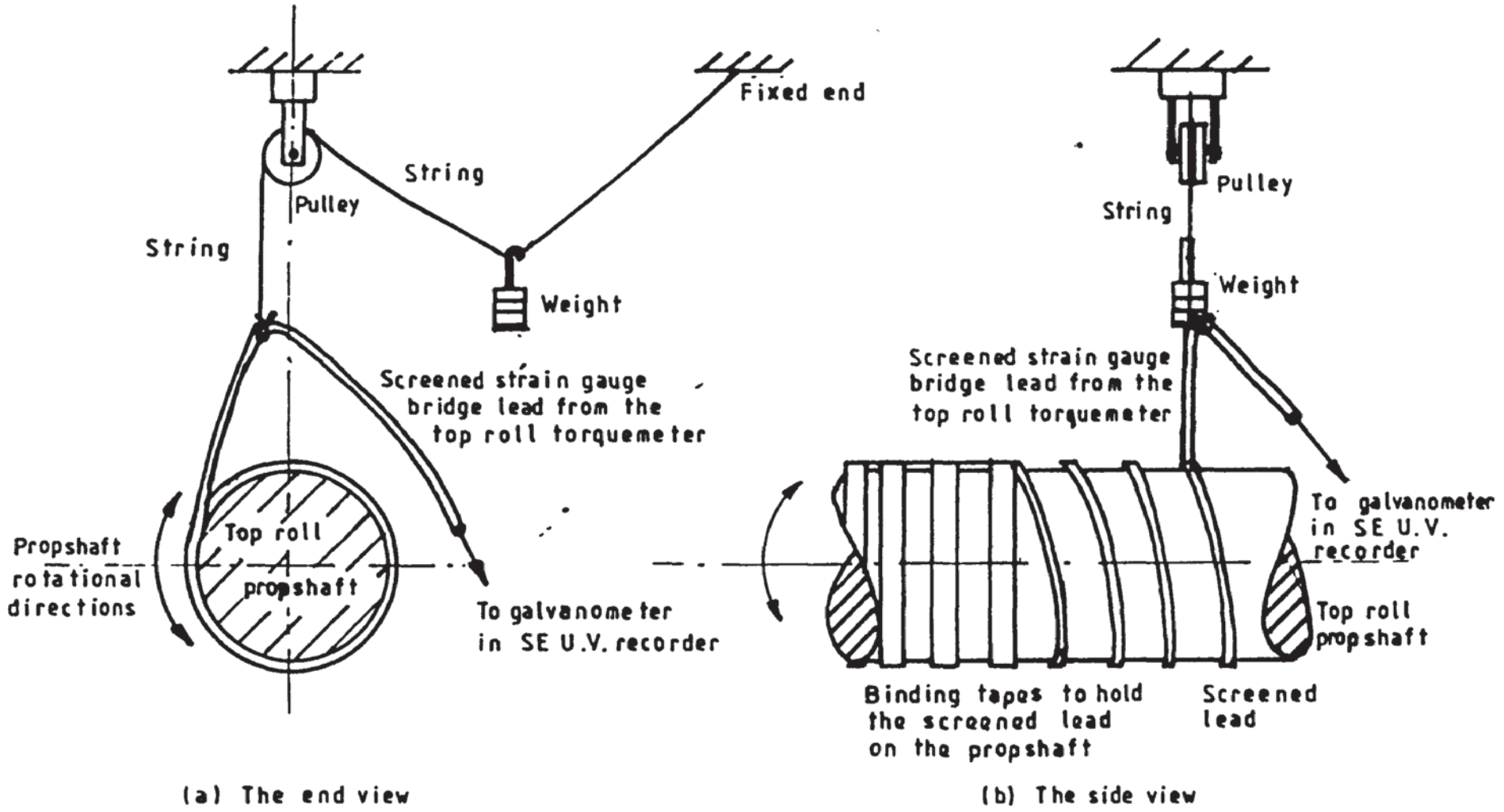

FIG 4.29 THE ARRANGEMENT OF THE STRAIN GAUGE BRIDGE LEADS FROM THE TORQUEMETERS

Table 4.2 The Respective Strain Gauge Bridges and Galvanometers in the U.V. Recorders

(i) Axial Load Bridges For the Ram loadcells

Loadcell		Amplifier no. (CIL SGA701)	Thorn EMI Galvanometer	SE U.V. Recorder Channel Number
Specification letter	Ram number			
G	6	20856	A1000-V5709	1
F	1	20857	A1000-V5710	2
D	4	20859	A1000-V5711	3
E	3	20858	A1000-V5714	4
A	2	20855	A1000-V5718	5
B	5	20860	A1000-V5660	6

(ii) Bending Load Bridges For the Ram Loadcells

Loadcell		Allocated RS Potentiometer Specification	Thorn EMI Galvanometer	SE U.V. Recorder Channel Number
Specification letter	Ram number			
F	1	RB1	A35-X9857	7
A	2	RB2	A35-X9858	8
E	3	RB3	A35-X9859	9
D	4	RB4	A35-X9861	10
B	5	RB5	A35-X9862	23
G	6	RB6	A35-X9864	12

Table 4.2 The Respective Strain Gauge Bridges and Galvanometers in the U.V. Recorders (cont)

(iii) Axial Load Bridges For the Frame Loadcells

Loadcell		RS Strain Gauge Amplifier	Galvanometer	U.V. Recorder Channel Number Southern Inst.nt
Specification letter	Frame number			
1	1	1	SMI/V779	3
2	2	2	SMI/V803	4
3	3	3	SMI/M100-9551	5
4	4	4	SMI/V4499-2	7

(iv) Bending Load Bridges For the Frame Loadcells

Loadcell		Allocated RS Potentiometer Specification	Thorn EMI Galvanometer	SE U.V. Recorde Channel Numbe
Specification letter	Frame number			
1	1	TB1	M20-9072	20
2	2	TB2	M20-9073	19
3	3	TB3	M20-9074	21
4	4	TB4	M20-9075	22

Table 4.2 The Respective Strain Gauge Bridges and Galvanometers in the U.V. Recorders (cont)

(v) Torquemeter Bridges

Torquemeter Specifiaction		Allocated RS Potentiometer Specification	Galvanometer	SE U.V. Recorder Channel Number
Specification cell	Spec. number			
Top roll	-	TT1	SMI/Z4424-4	15
Side roll	1	ST1	EMI/M20-9154	13
Side roll	2	ST2	SMI/Z4422-4	14

(vi) Top Roll Tachometer

Specifications	Thorn EMI Galvanometer	SE U.V. Recorder Channel Number
DC generation, Servo. Tek Product, Haw Horn NJ. Type : SA-740B-1 Rating : 20.8 V/1000 rev/min.	B160-V6627	16

CHAPTER FIVE

THEORETICAL ANALYSIS AND RESULTS

5.1. Introduction

This Chapter outlines the mechanism of the roller bending of plate using a four roll bender. It describes the first part of the mathematical analysis (to evaluate plate internal resistance to external bending moment about the top roll nominal contact) for bending thin plate to form cylindrical products. The second part of the analysis (i.e. to determine the relevant bending force, torque and power) will be continued in Appendix 5.1.

5.2. The roller bending sequences

Figure 5.1 shows the perspective configuration of the operational rolls and bendplate of a four roll bender. To manufacture a cylindrical finished product the geometrical profile in any zx plane may, in general, be identical, if the roll deflection is assumed zero. The detailed operational sequences are shown in figures 5.2(i) and 5.2(ii), for either thin or thick plate bending. They consists of :

(a) the pre-bending mode for the edge setting preparation (procedures 1 - 3, fig 5.2(i) for thick plate bending, and 1 - 2, fig 5.2(ii) for thin plate bending).
(b) The steady continuous bending mode to complete the cylindrical bend (procedures 8, fig 5.2(i) for thick plate bending, and procedures 3 - 6, fig 5.2(ii) for thin plate bending).

Figure 5.2 shows that the differences between the thin plate operation and the thick plate operation are as follows :

(a) a further pre-bending operation to prepare the finished end is needed for the thick plate bending mode, i.e. the procedures 3 - 7, fig 5.2(i).
(b) a steady continuous bending mode for thick plate bending can be carried out with either the pre-bending

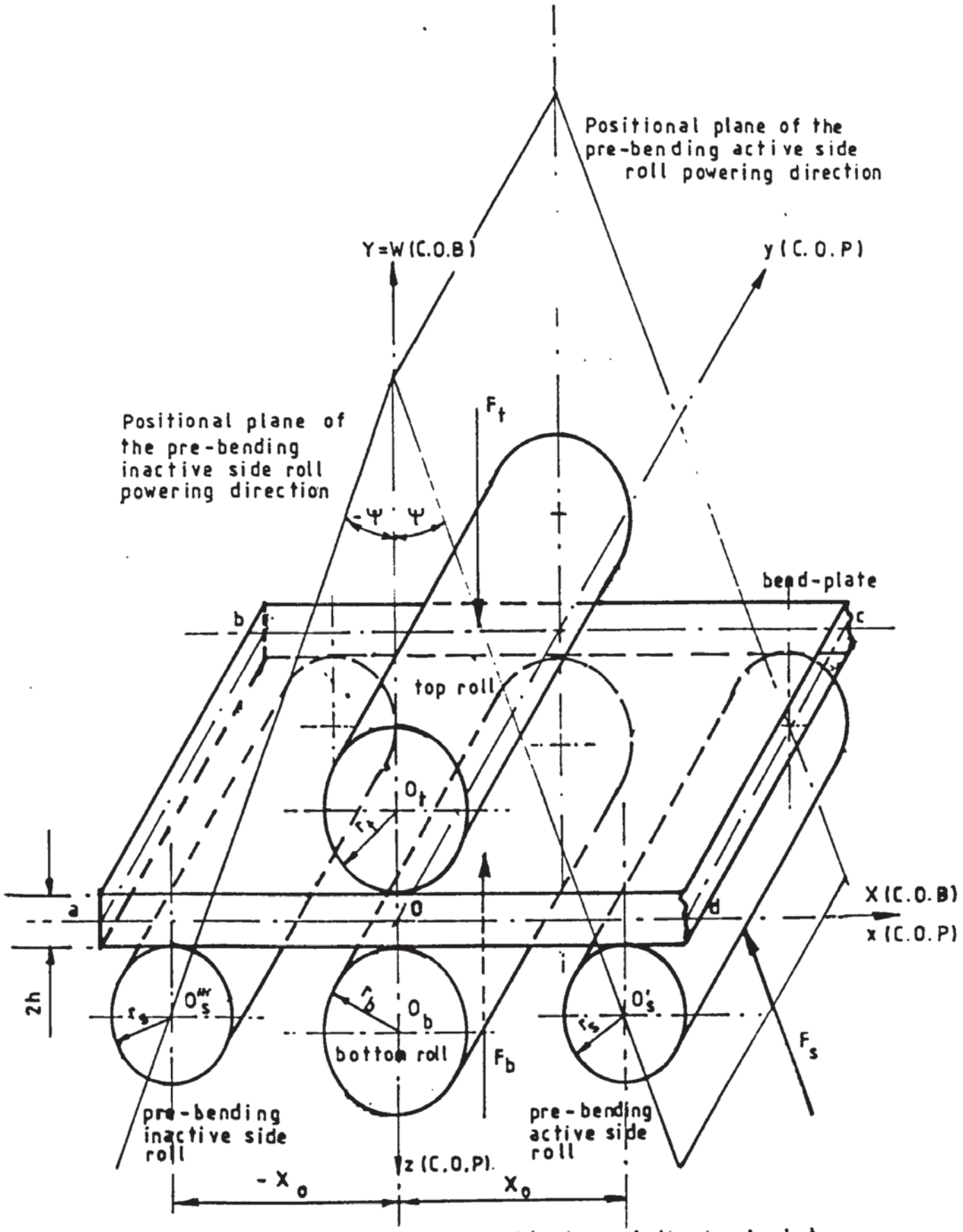

abcd is the central (neutral) plane of the bend-plate

C.O.B is the bender and plate co-ordinate system during bending

C.O.P is the plate co-ordinate system relative to plate itself

FIG 5.1 CO-ORDINATE FOR THE MODEL BENDER AND PLATE

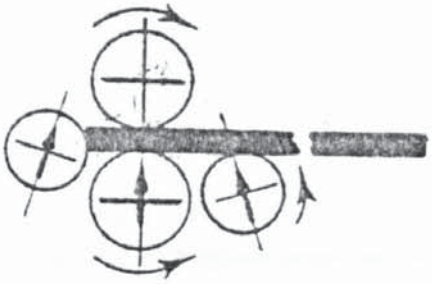

1.

5.

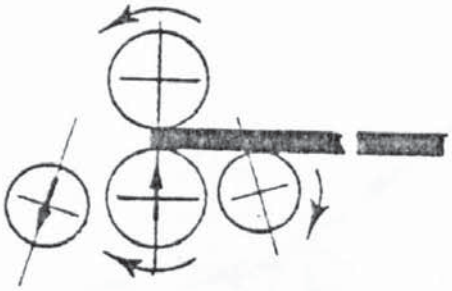

2.

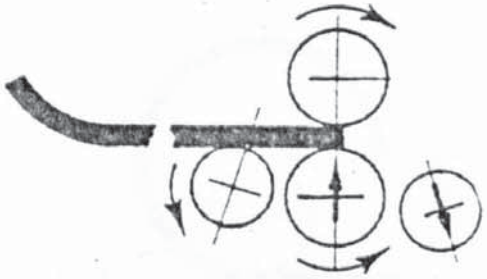

6.

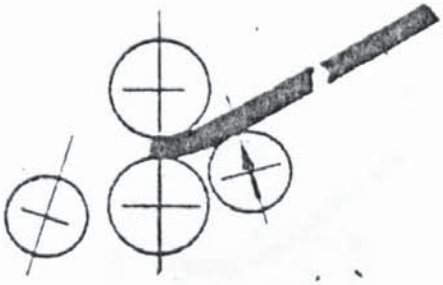

3.

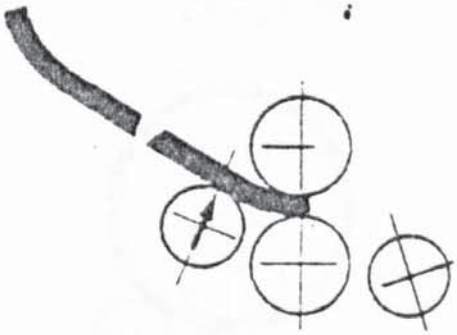

7.

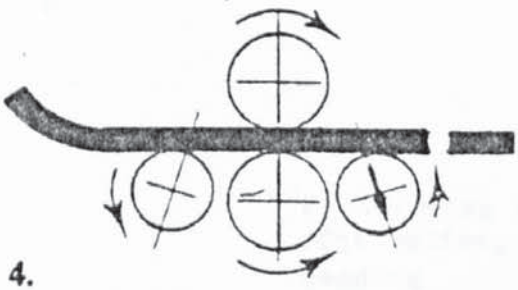

4.

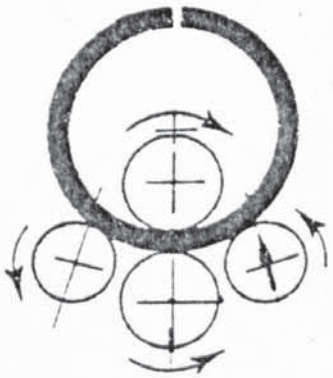

8.

Pre-bending operations
edge setting : 1, 2 and 5, 6.
bending : 3 and 7.
transporting : 4.

Steady-continuous bending operation : 8

(i) The roller bending sequence for thick plate

FIG 5.2 ROLLER PLATE BENDING OPERATIONS (FOUR ROLL BENDER)

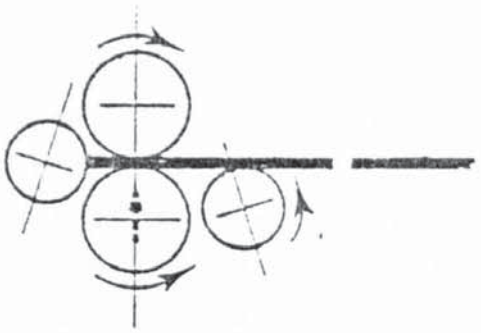

1.

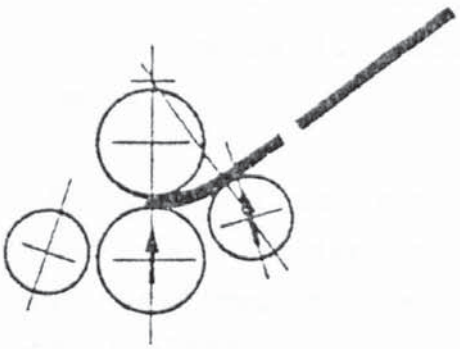

2.

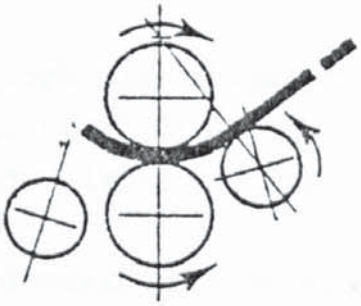

3.

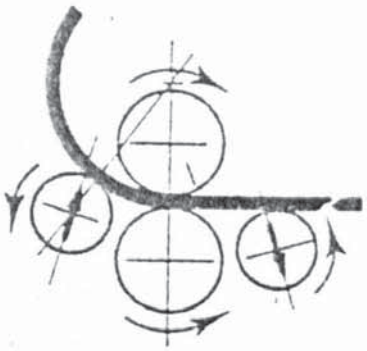

4.

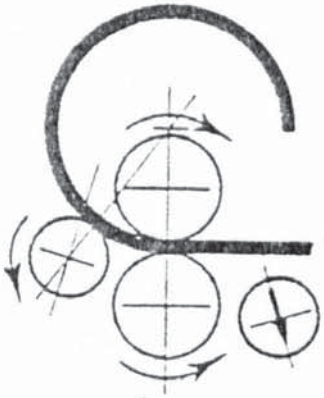

5.

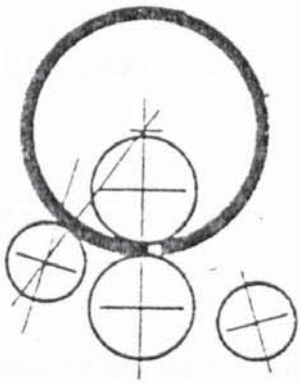

6.

Pre-bending operations
edge setting : 1
bending : 2

Steady-continuous operations: 3, 4, 5 and 6

(ii) The roller bending sequence for thin plate

FIG 5.2 ROLLER PLATE BENDING OPERATIONS (FOUR ROLL BENDER)

active side roll in operative (i.e. procedure 3, fig. 5.2(ii)) or the pre-bending inactive side roll in operative (i.e. procedure 5, fig 5.2(ii)).

(c) a steady continuous bending for thick plate operation is generally performed with both the pre-bending active and the pre-bending inactive side rolls (the former will be called pre-active side roll and the latter pre-inactive side roll in the following context) in operation (i.e. procedure 8, in fig 5.2(i))
- For most purposes both side rolls are in operation to optimise the bending effect by altering the top roll contact.

Although fig 5.2 illustrates the operational sequences for the four-roll plate bending process, the mechanism involved in the process requires to be fully visualised prior to the mathematical analysis.

5.3. Visualisation of the mechanism for the process

Although the mathematical modelling mainly concentrates on the roll bending of thin plates, the roller bending mechanism for thick plates is also generalised in this section.

The description of these mechanisms is classified into the following areas, i.e.

(i) The pre-bending mode,
(ii) The steady continuous bending mode, and
(iii) The surface contact between the bend plate and rolls,

for either thin or thick plate bending,

5.3.1. Pre-bending with a set active side roll angle, ψ.

From figure 5.3, the following particulars, for both thin

and thick plate roller pre-bending, are considered.

(a) The effective bending force, F_s, on the pre-active side roll is the resultant of the horizontal, F_{sh}, and the vertical, F_{sv}, components at the contact line, C_s, between the plate and the roll.

(b) The instantaneous contact line, C_s, of the active side roll and the plate varies as bending proceeds. Depending on :
(i) the radius of the finished bent plate,
(ii) the magnitude of the initial vertical bending arm, X_o,
(iii) the positional powering angle, ψ, of the side roll,
(iv) the capacity of the bender,
the instantaneous contact angle, θ_s, may be in the range of 0° to 180°. Normally, the maximum contact angle, θ_{sm}, occurs at the position where the movement of the operative side roll is blocked by the top roll (provided the bender has sufficient capacity).

(c) The instantaneous bending arms, i.e. X_s-X_t and W_s-W_t, of the two force components, i.e. F_{sv} and F_{sh}, respectively, on the operative side roll varies as the contact line changes.

(d) The force, F_t, on the top pinch roll is the resultant vectors of the loads on the side roll and the bottom pich roll, i.e. F_s and F_b respectively (fig 5.3).

(e) Maximum plastic deformation occurs in the contact region

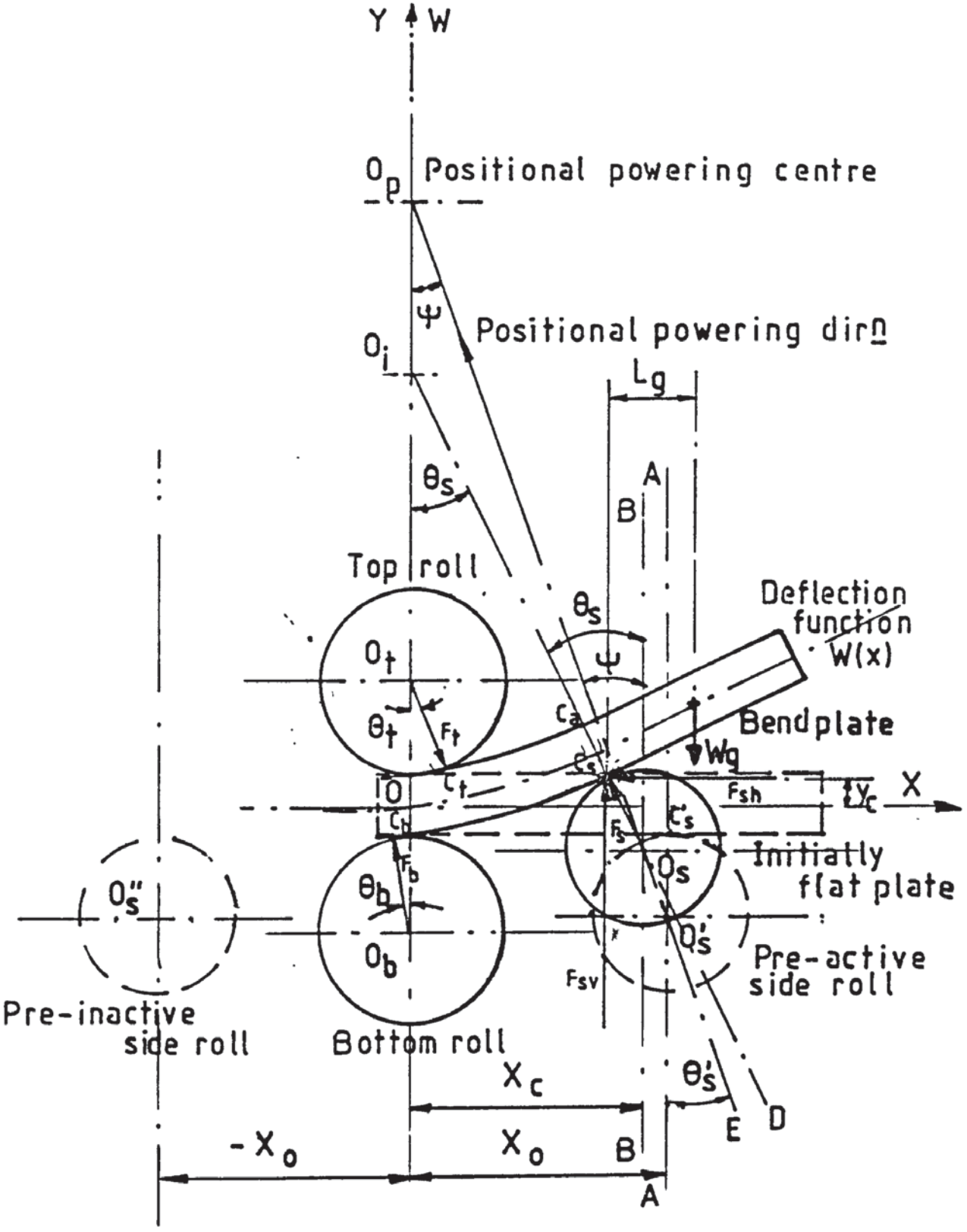

FIG 5.3 PRE-BENDING OF PLATE FOR A SET POSITIONAL POWERING ANGLE, Ψ.

between the top roll and the plate.

(f) Plastic deformation propagates from the pinch region towards some line, which is the first yield on the surface fibres, i.e. P_iP_o (fig 5.4) in the deformation zone. From this line, onwards to the inlet of the pre-active side roll, i.e. C_aC_s, complete elastic deformation is experienced (i.e. region E_t in fig 5.4).

(g) The top pinch roll may be driven in reverse or remain stationary as the pre-bending proceeds.
- An essential distinction between the driven and the stationary roll is that the top roll not only grips the plate by the pressure between the pinch rolls and plate, when it is driven , it also contributes to part of the braking effort generated by the driving torque. The latter merely opposes the force on the plate by the resultant of the pinch pressure.
- Though the former condition may reduce the resultant pinch force by the pinch rolls, there is the possibility of plate rejection.

(h) The resistance to the tangential force applied by the active side roll in the pre-bending depends on (i) the area of surface contact in pinch and (ii) the blockage by the bottom pinch roll to the plate end.
- It may indirectly determine the end setting and directly influence the pinch forces on the top and bottom rolls.

(i) The contact area of the pinch rolls on either side of the plate varies as the pre-bending proceeds.
- The nature of this variation is to increase the contact area with the top pinch roll and to diminish that with the bottom pinch roll, as the radius of curvature of bent plate increases. It is thought that the evaluation of the

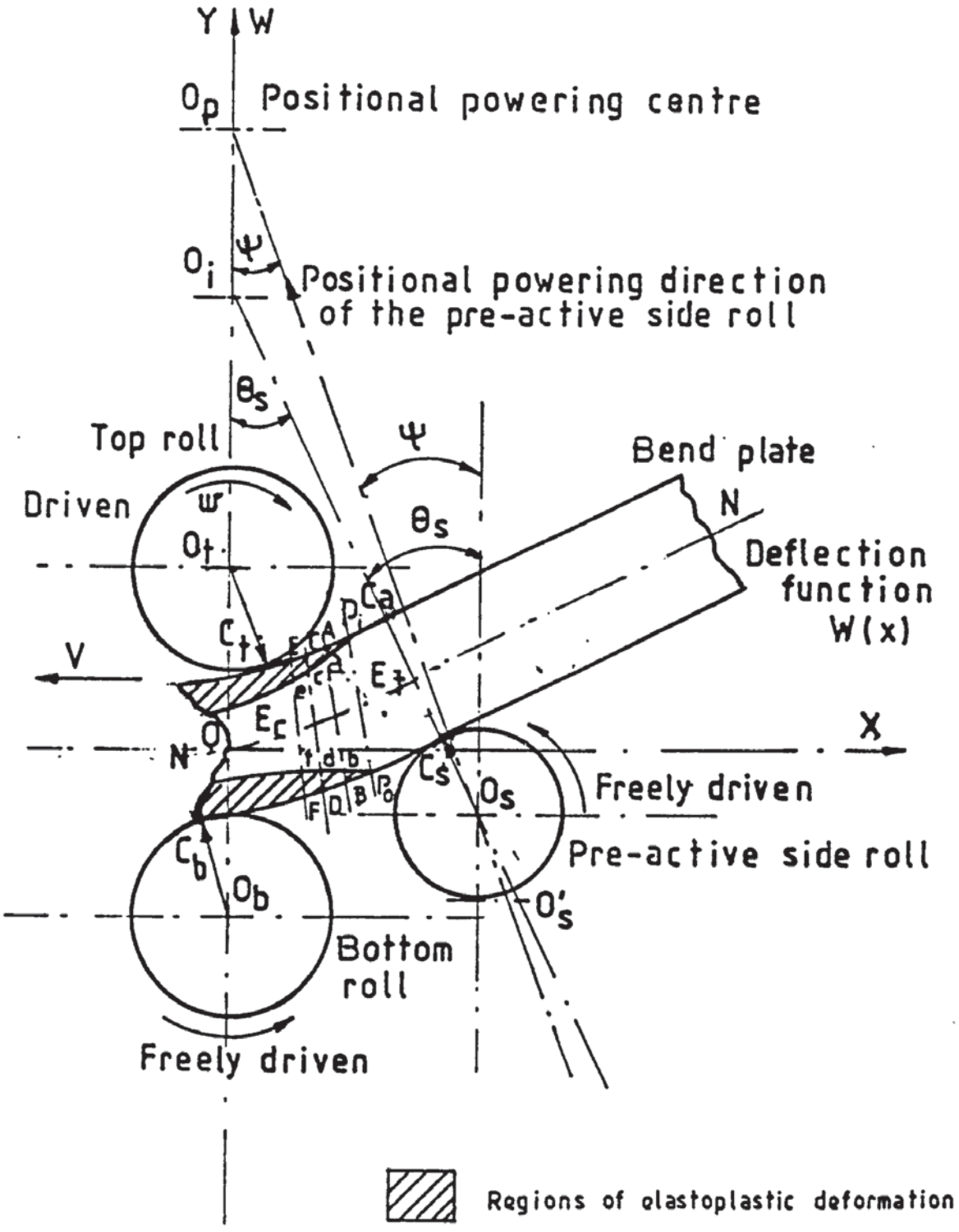

FIG 5.4 POSSIBLE DEFORMATION ZONE OF A PLATE IN STEADY-CONTINUOUS BENDING MODE

contact proportion, on each individual pinch roll, may provide a means to determine the magnitude of the roll load (although the mathematical modelling in this analysis does not employ this principle).

(j) The contact angle, θ_s, subtended by the instantaneous contact line of the operative side roll axis and the plate, and the vertical surface (AA or BB in fig 5.3), through the axis of the operative side roll, also varies continuously (see fig 5.5) as bending proceeds and as the position of the side roll changes. It is equal to ψ when the angle coincides with the positional angle, ψ, of the side roll (condition (ii) in fig 5.5)

(k) To pre-bend the edge of a bend plate to its necessary bend radius, the effective deformation zone assumes a series of different bend radii, from its minimum at the position, C_t, of maximum plastic deformation, to its maximum at the inlet, C_s, of the plate to the pre-active side roll (fig 5.3)

(l) For the bender with a horizontal bend axis, the weight of the overhanging plate before the inlet to the pre-active side roll generates a counter-bending moment, $W_g L_g$ (fig 5.3). The counter-bending moment reduces the effective curvature in the deformation zone, $C_t C_b C_s C_a$ (fig 5.4). It therefore increases the bending force on the operative side roll.
- Normally, the magnitude of the counter-bending moment is a direct function of the dimensions and density of the bendplate. However, its magnitude diminishes as the pre-bending proceeds. This is due to the upwards movement of the operative side roll tipping up the plate, thus

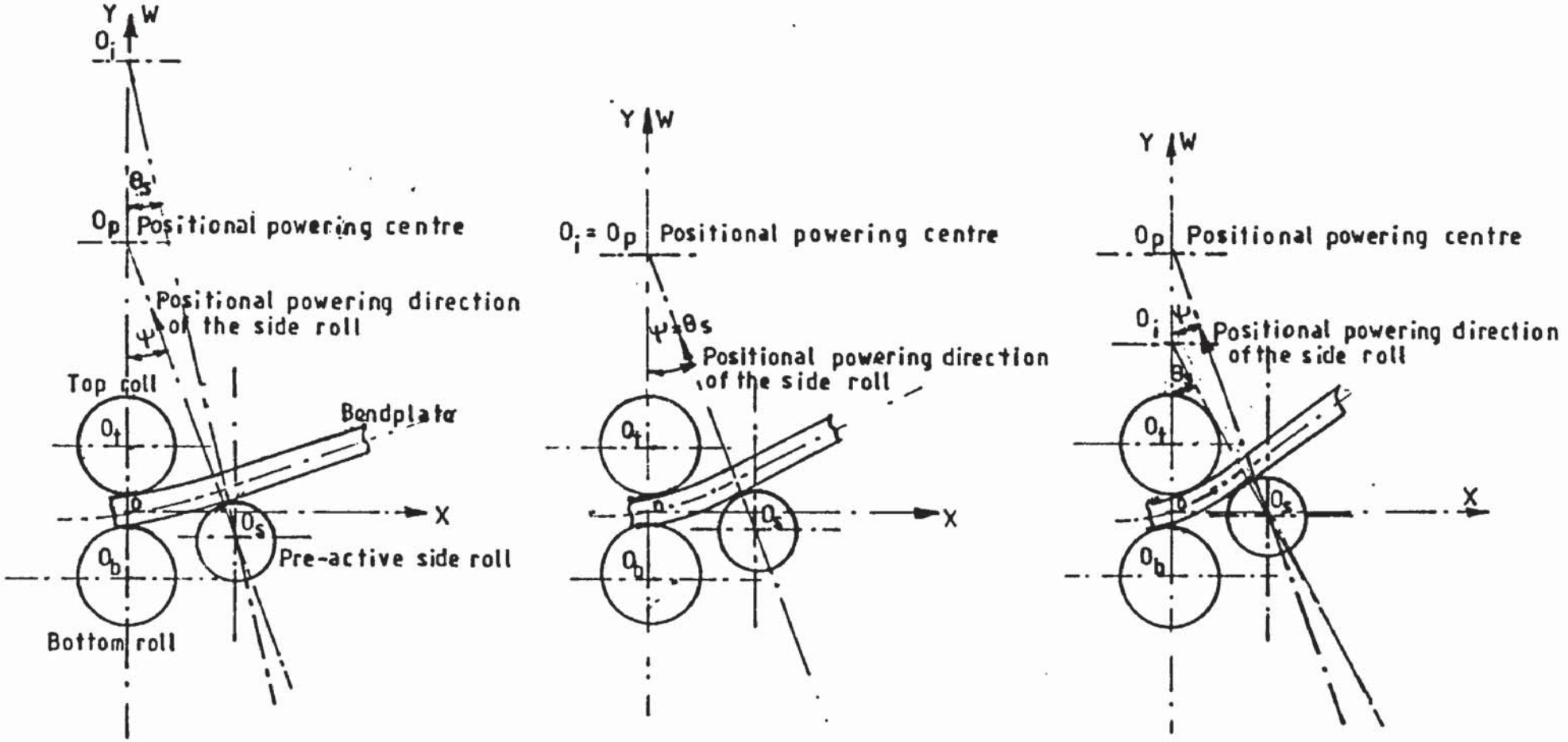

i- BENDING CONDITION FOR $0 \leq \theta_s < \psi$

Plate deflection function $W_0(x)$

ii- BENDING CONDITION FOR $\theta_s = \psi$

Plate deflection function $W_1(x)$

iii- BENDING CONDITION FOR $\theta_s > \psi$

Plate deflection function $W_2(x)$

FIG 5.5 THE THREE CONDITIONS OF THE SIDE ROLL CONTACT ANGLE, θ_s, RELATIVE TO ITS POSITIONAL POWERING ANGLE, ψ.

shortening the counter-bending moment arm, L_g.

(m) Roll deflection in bending may degrade the quality of the bent plate.
- The roll deflection normally depends upon the load distribution over the roll length of the roll. It is also a function of the plate flexural rigidity.

5.3.2. The steady continuous bending mode

As discussed in section 5.2, the steady continuous bending of thick plate is different from that of thin plate, consequently it will be dealt with separately.

5.3.2.1. Thin plate bending mechanism with an active side roll operative (ref to fig 5.2, 5.4 and 5.6)

From figures 5.2, 5.4 and 5.6, the following generalisations can be drawn.

(a) The plate is gradually deformed towards the pinch line as bending take place. The nature of the deformation is to decrease the radius of curvature progressively as the plate moves through the pinch gap. The deformation mechanism can simply be considered as a steady increase in the plastic deformation zone from the axis of the operative side roll to the pinch inlet.

The deformation region may consist of the following zones :

(1) A completely elastic deformation zone, in the region of the exit, from the operative side roll to an intermediate line on the plate surface (region $C_aC_sP_oP_l$, i.e. E_t in fig 5.4) where yield first occurs in its outer fibre layer

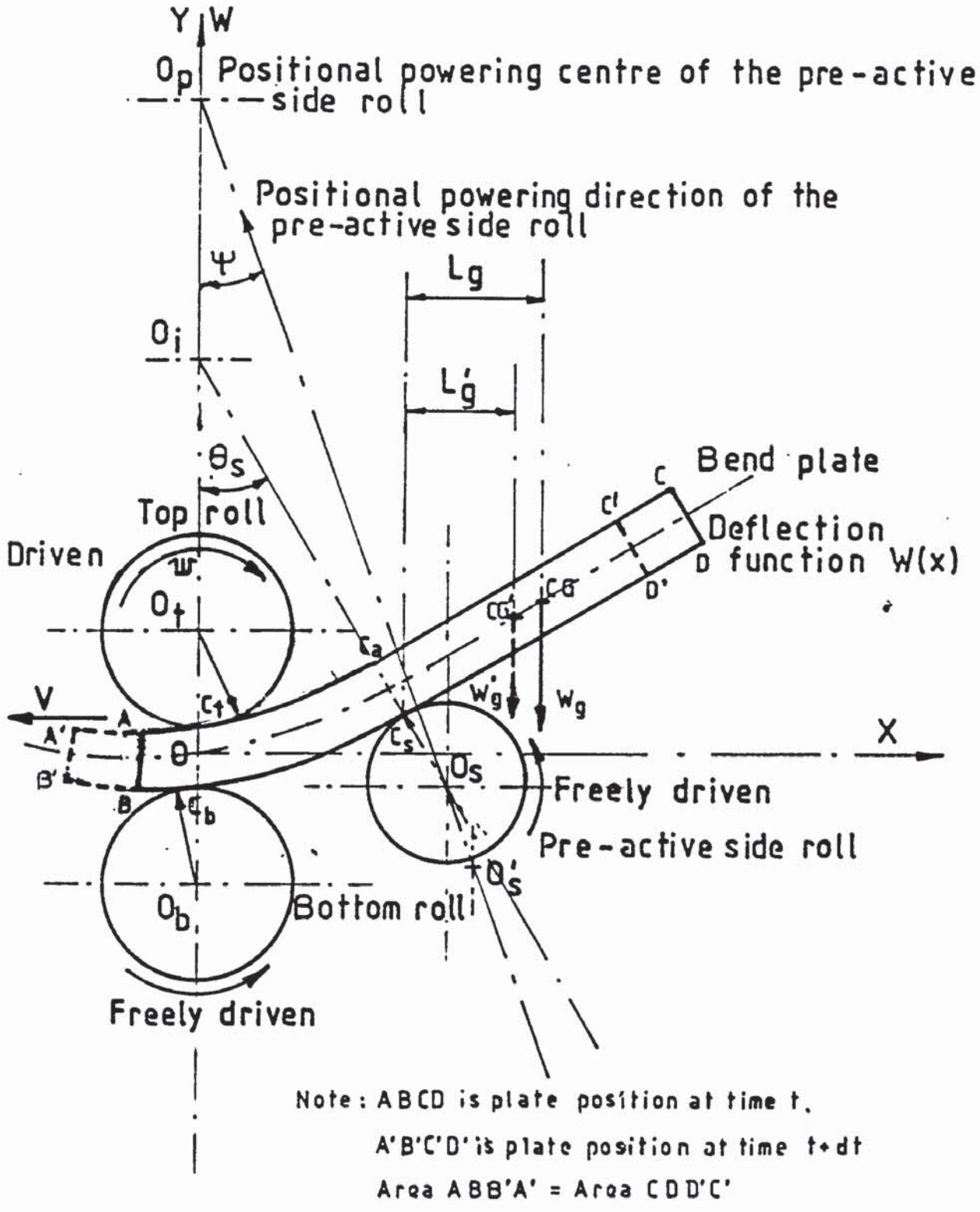

FIG 5.6 THE PRODUCTION OF THE COUNTER BENDING MOMENT

(i.e. at P_i and P_o respectively).

(2) An elastic-plastic deformation in the region from the first yield line to the pinch roll (in $P_iP_oC_bC_t$ in fig 5.4).

(3) A possibly complete yield region at or adjacent to the pinch roll.

In the region (2) the elastic layer at the core, E_c, of the plate is sandwiched by two elastoplastic deformation layers, on either side of the plate (fig 5.4). The depth of the elastoplastic deformation increases towards the pinch. Its deformation mechanism may be illustrated as follows.

With reference to figure 5.4. If the three equally spaced cross sections, such as : (i) $A_0a_0b_0B_0$ (i.e. AabB in fig 5.4), (ii) AabB (i.e. CcdD in fig 5.4) and (iii) $A_1a_1b_1B_1$ (i.e. EefF in fig 5.4), in which a certain amount of plastic deformation occurs, is considered, the total difference in the plastic depths, D_{ti}, with respect to $A_{i-1}B_{i-1}$ is

$$D_{t1} = (Aa+bB) - (A_0a_0+b_0B_0) \qquad (5.1a)$$

and

$$D_{t2} = (A_1a_1+b_1B_1) - (Aa+bB) \qquad (5.1b)$$

respectively.

Assuming the plate velocity is constant, A_0B_0 (i.e. AB in fig 5.4) will thus occupy the place of AB (i.e. CD in fig 5.4), while AB will take the next place of A_1B_1 (i.e. EF in fig 5.4), and so on. It is obvious that the successive increment of the

plastic deformation depth of A_0B_0, as it moves towards the pinch, is as shown in the expressions (5.1a) and (5.1b) etc.. Its total increment of plastic depth, D_T, will thus be

$$D_T = \sum_{i=0}^{n} [(A_{i+1}a_{i+1}+b_{i+1}B_{i+1}) - (A_ia_i+b_iB_i)] \qquad (5.2a)$$

The total of its infinitesimal plastic depth, at any cross section from the instant of first yield to the pinch, must be equal to the plastic depth at the pinch. If each increment of the plastic deformation is defined as dD_T in terms of its infinitesimal values, then

$$D_T = \int dD_T = \text{The plastic depth at the pinch} \qquad (5.2b)$$

(b) The effect of the counter-bending moment, W_gL_g, due to the weight of the overhanging plate before the inlet to the operative side roll (fig 5.6), gradually diminishes as a consequence of the reducing overhanging length.
- As the bent plate is transferred through the pinch gap, the weight may be significant if the plate dimensions and curvature are large (see the point (1) in section 5.3.1). The latter condition produces a counter bending moment effect in addition to the spring back, which tends to increase the radius of curvature of the bent plate.

5.3.2.2. Thin plate bending with the pre-inactive side roll operative (ref to fig 5.7)

This mechanism can be generalised as follows :

(a) The maximum plastic deformation also occurs at the pinch roll contact line. Instead of a progressively increasing

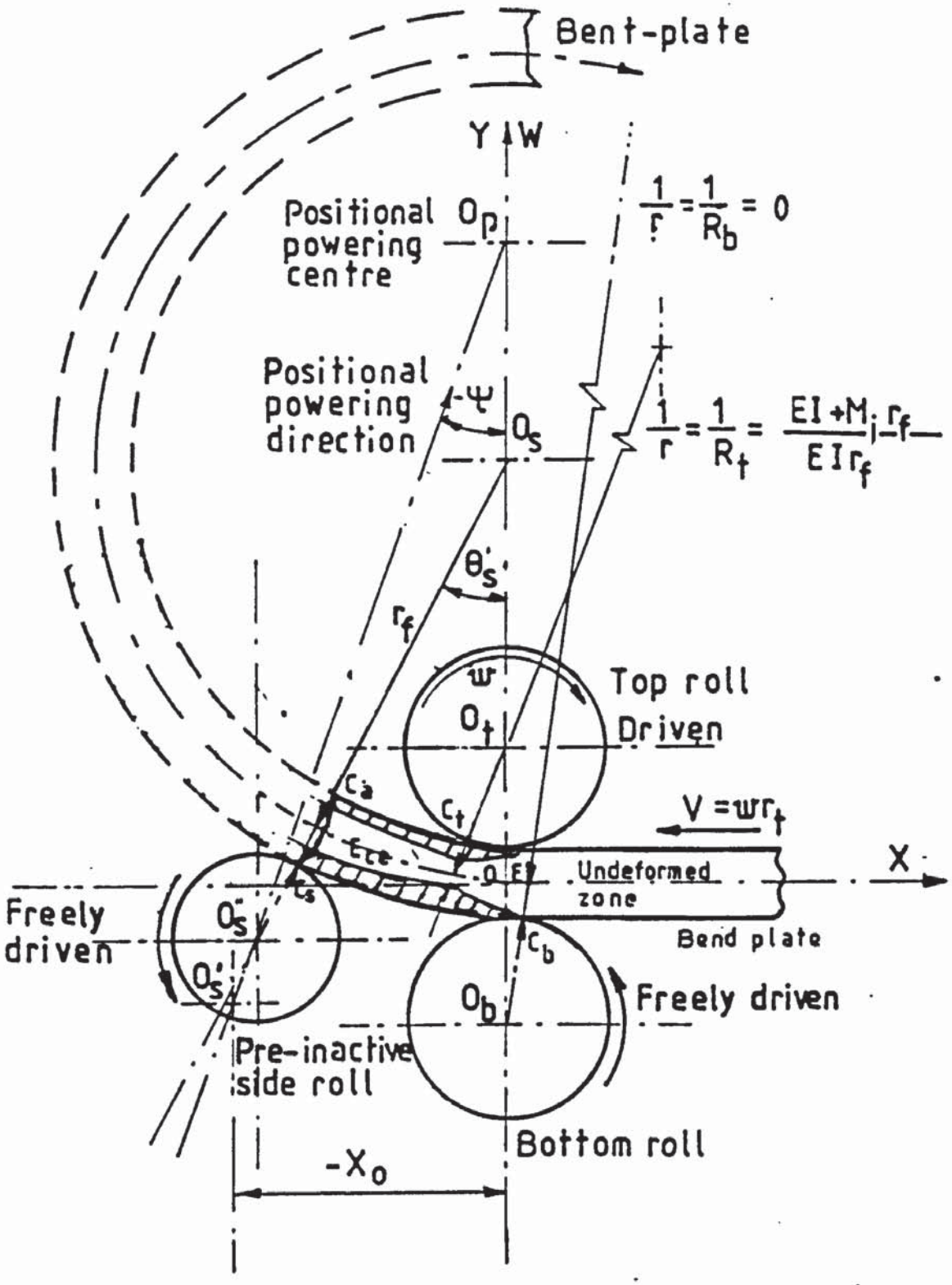

Shaded regions indicate elastoplastic / plastic deformation

E is the complate elastic deformation

E_{ce} is the elastic core in bending zone

FIG 5.7 ASSUMED DEFORMATION ZONE FOR STEADY-CONTINUOUS BENDING OF A THIN PLATE (WITH PRE-INACTIVE SIDE ROLL OPERATIVE)

deformation, the deformation before C_aC_s and past the top roll contact, C_t, (fig 5.7) is influenced by the progressive spring back of the plate, as it is being transported from the pinch roll to the inlet of the pre-inactive side roll. It is thus possible that the final position of the pre-inactive side roll may be different from that of the pre-active side roll in pre-bending, in order to accomplish uniform curvature of the bent plate.

(b) Inertia forces may possibly play a part in the plate bending process. However their contribution to the total is likely to be insignificant.

(c) Additional friction, induced at the contact surface of the plate and its supporting side roll, may oppose the movement of the bent plate out from the pinch region. This will further increase the bend in the region of $C_tC_aC_sC_b$ as shown in fig 5.7.

(d) Depending upon the centre of gravity (c.g.) of the overhanging portion relative to the pre-inactive side roll contact, the bending moment due to the overhanging c.g. may be either beneficial or detrimental to the bending process. In the case shown in figure 5.7, it may beneficially suppress the spring back in the region $C_tC_aC_sC_b$.

5.3.2.3. Thick plate bending with both side rolls operative

To bend a thick plate, both pre-active side rolls are operative. It thus has the combined effect of the last two cases for bending thin plate. Consequently it makes the contact nature more complex.

The different features of deformation, within the effective deformation, are where :

(i) at inlet to the pinch the plate is progressively deformed,

and

(ii) at exit from the pinch the plate is gradually sprung-back.

This, and the various combinations of the two side roll positions changes the roll contact, and a specific bend radius may thus be achieved by suitably positioning the two operative side rolls.

Since the two side rolls are symmetrically positioned about the pinch rolls, in the steady continuous state bending, its mechanism may be considered similar to bending a plate in a symmetrical three-roll bender.

5.3.3. The effect of surface contact and friction

Surface contact is necessary in the roller plate bending process. It enables the conveyance of the plate in and out of the pinch gap. Sufficient gripping force to prevent sliding of the plate in the pinch gap can only be produced if friction is sufficiently high. Generally, the friction between the sliding surfaces is a function of the surface texture and lubrication condition of the roller and bend plate, and the magnitude of the required pinch force. It also depends on the surface contact area. Theoretically, the estimation of the surface contact area and stress distribution in the contact region may enable the pinch force to be assessed (although this has not been done in the present analysis).

The contact friction effect on the side roll may be either beneficial or detrimental to the bending process. It may

assist in reducing the bending force required on the active side roll, but it may also contribute a proportion of torque to the drive in transporting the plate through the pinch roll.

5.4. Mathematical Modelling for roller bending of thin plate

It is difficult to achieve a single mathematical model which takes into account all the complexities of the bending process as described in section 5.3. A realistic subdivision and simplification is thus necessary.

5.4.1. Assumptions for mathematical modelling

Usually the plastic bending of a plate or beam is always accompanied with a shift of the neutral surface towards the concave surface of the bend plate [11,51]. In practice the Bauschinger effect is experienced in the strain reversal regions and this complicates the analysis by introducing an additional unknown parameter. It is assumed that there is no shift of the neutral plane in the bend plate for the present analysis.

Additionally, the following assumptions are also made.

(a) The effect on the bend radius of curvature of the plate, in the deformation zone, due to the counter-bending moment produced by the weight of the overhanging plate (before the inlet to the pre-active side roll and after the exit from the pre-inactive side roll), is negligible.

(b) There is no deflection along the width direction of a bendplate, i.e. the completed bend forms a cylindrical tube. Thus it is assumed that the contact line/region between rolls and bendplate does not vary along the width direction of the bendplate.

(c) Due to (b), it is further assumed that

(1) the geometrical interaction of the rolls and the bendplate,

and

(2) the deflection profile of the bendplate,

for thin plate bending may be approximately represented as two- dimensional systems in cartesian co-ordinates (fig 5.1, 5.8). The origin of the co-ordinates is assumed to be at the interception of the vertical plane, through the axes of the pinch rolls, and the central plane of the flat plate in the bender (see fig 5.8).

(d) The possible deflection and deformation of the rolls themselves, during the bending operation, is neglected.

(e) The high pinch force applied by each bottom roll hydraulic cylinder is such that it prevents the roll being pushed down during bending.

(f) The friction in the roll bearing is assumed negligible.

(g) There is no slip between the bendplate and the side rolls either in the pre-bending mode or in the steady continuous bending operation.

(h) As the bendplate in the steady continuous bending condition is being conveyed through the pinch region, no relative motion is assumed, i.e. sticking friction between the pinch rolls and plate. Consequently there is no friction between the contact of the bendplate and the rolls.

(i) In the pre-bending mode, the pinch force on the pinch rolls generates sufficient resistance (or friction) to prevent the plate from pulling in or out through the pinch.

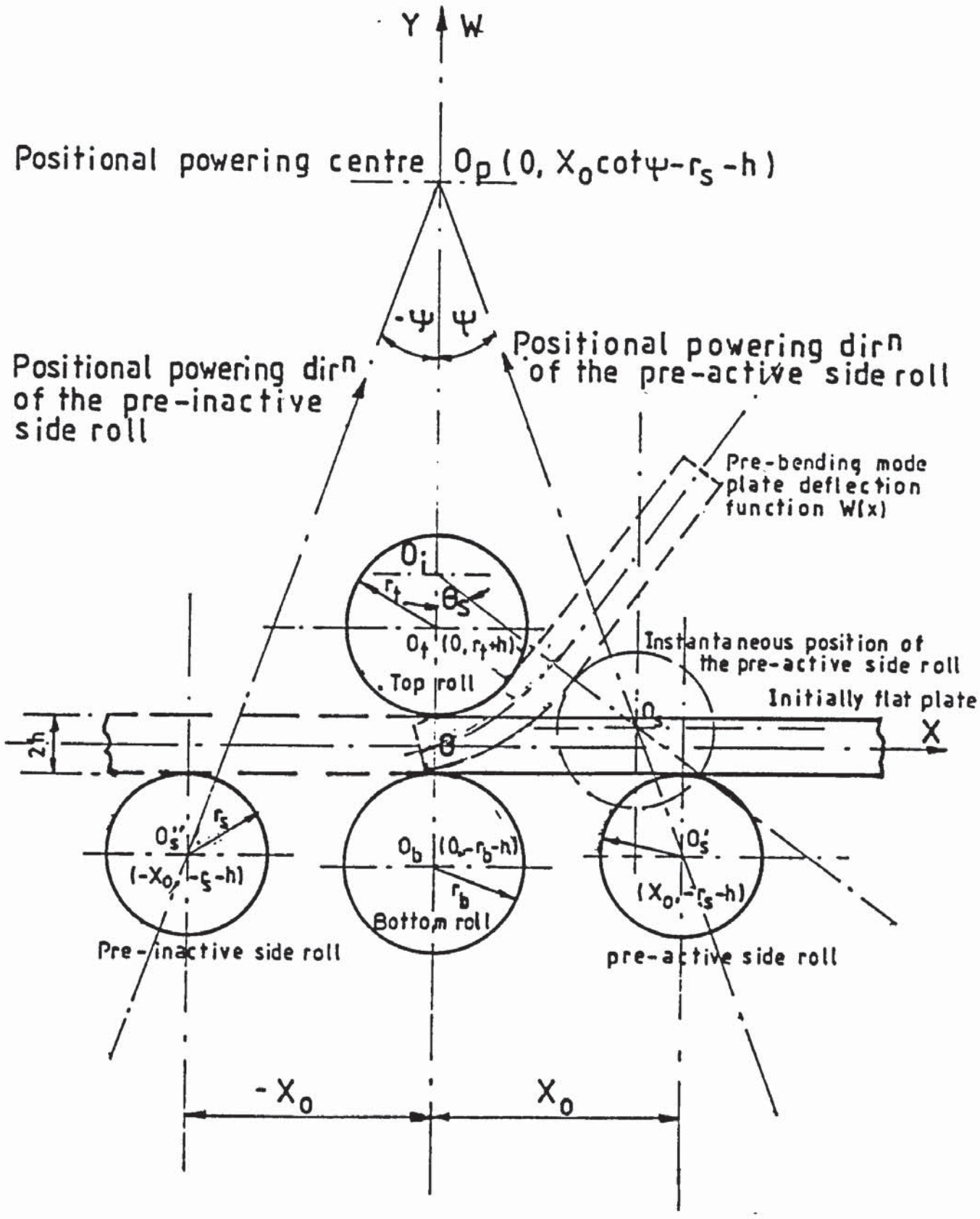

FIG 5.8 CARTESIAN CO-ORDINATE SYSTEM FOR THEORETICAL ANALYSIS OF THIN PLATE ROLLER BENDING

(j) The plate is so thin that its thickness stress, σ_z, is not significant in the analysis, a plane stress condition is thus assumed. The assumptions for the conventional plate/beam bending [105,108] analysis are also used.

(k) The bendplate is sufficiently wide to restrain the straining along its width direction in the middle of the plate. For simplification, the strains along its longitudinal edges are also assumed zero, although there is no restraint along the longitudinal edges of the plate.

(l) The bending moment distribution along the effective deformation zone is assumed as shown in fig 5.9.

(m) The plate is so thin that the edge effect (due to the assumed co-ordinate system), in this region as indicated by $C_a C_{sn} C_s C_d C_{sn} C_e$ in figure 5.10 for the stress or strain distribution is negligible.

(n) A linear longitudinal strain distribution across the thickness of the plate is assumed in the analysis as shown in figures 5.11 and 5.12. A linear distribution of the longitudinal stress across the thickness is also assumed for the elastic deformation region. For the region beyond the proportional elastic limit, an exponential function is used (fig 5.12).

(o) The longitudinal membrane strain and stress in the plate are also assumed negligible.

Other relevant simplifications will be made when required in the analysis.

5.4.2. Analytical approach

As a plate is bent from its initial condition to an

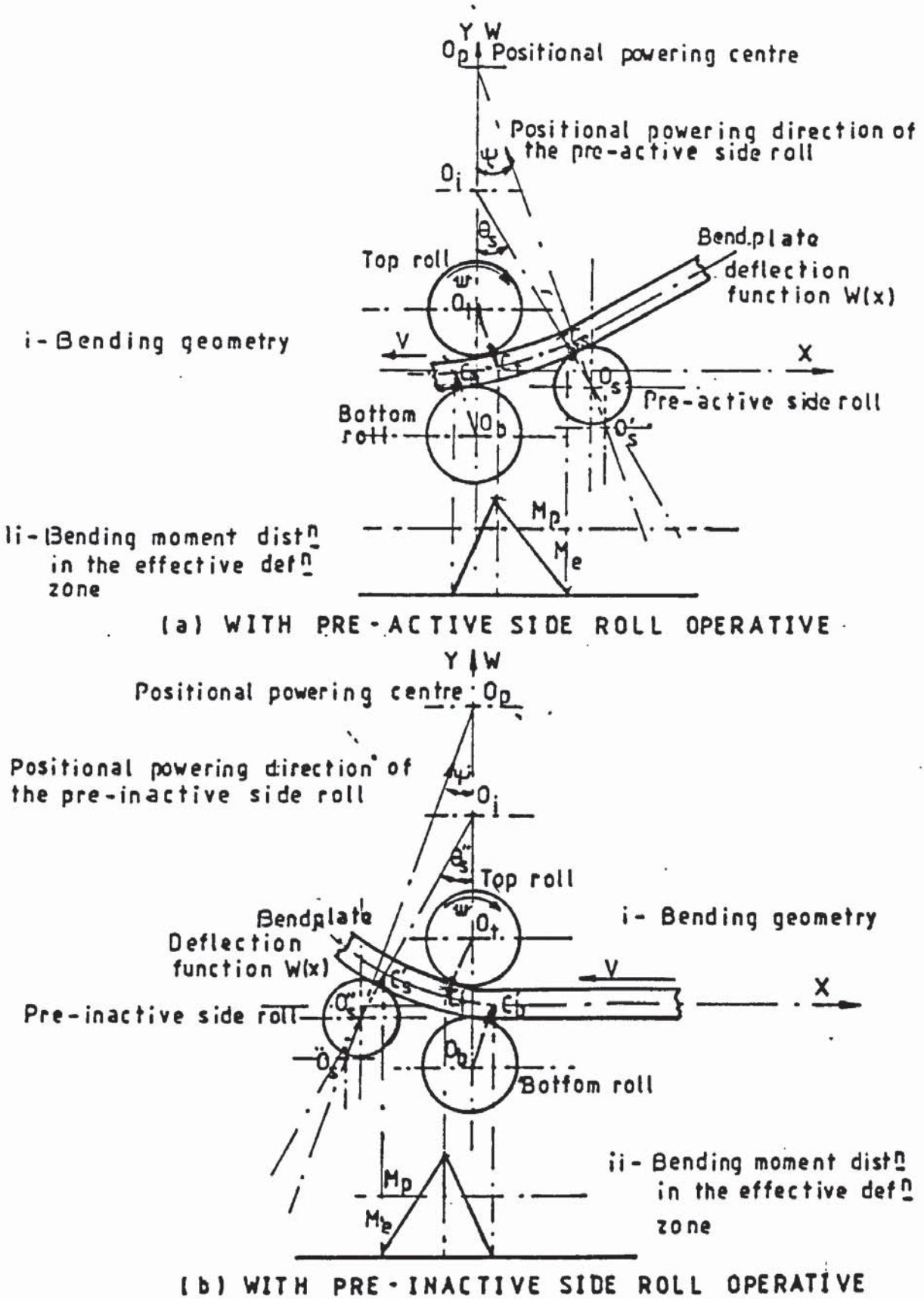

FIG 5.9 ASSUMED BENDING MOMENT DISTRIBUTION ALONG EFFECTIVE DEFORMATION ZONES

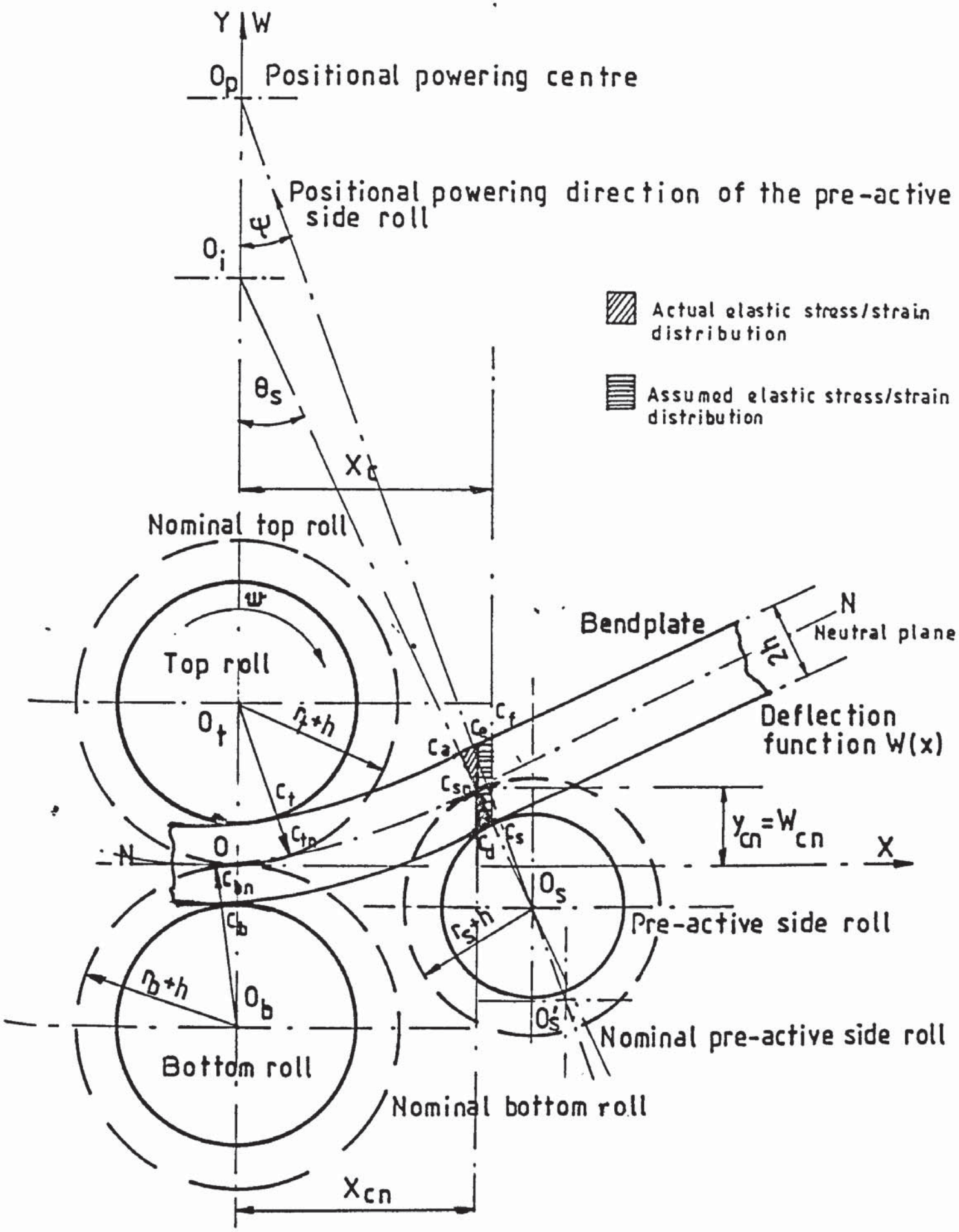

FIG 5.10 CO-ORDINATE EFFECT ON ACTUAL/ASSUMED STRESS AND STRAIN DISTRIBUTION ACROSS THICKNESS OF PLATE

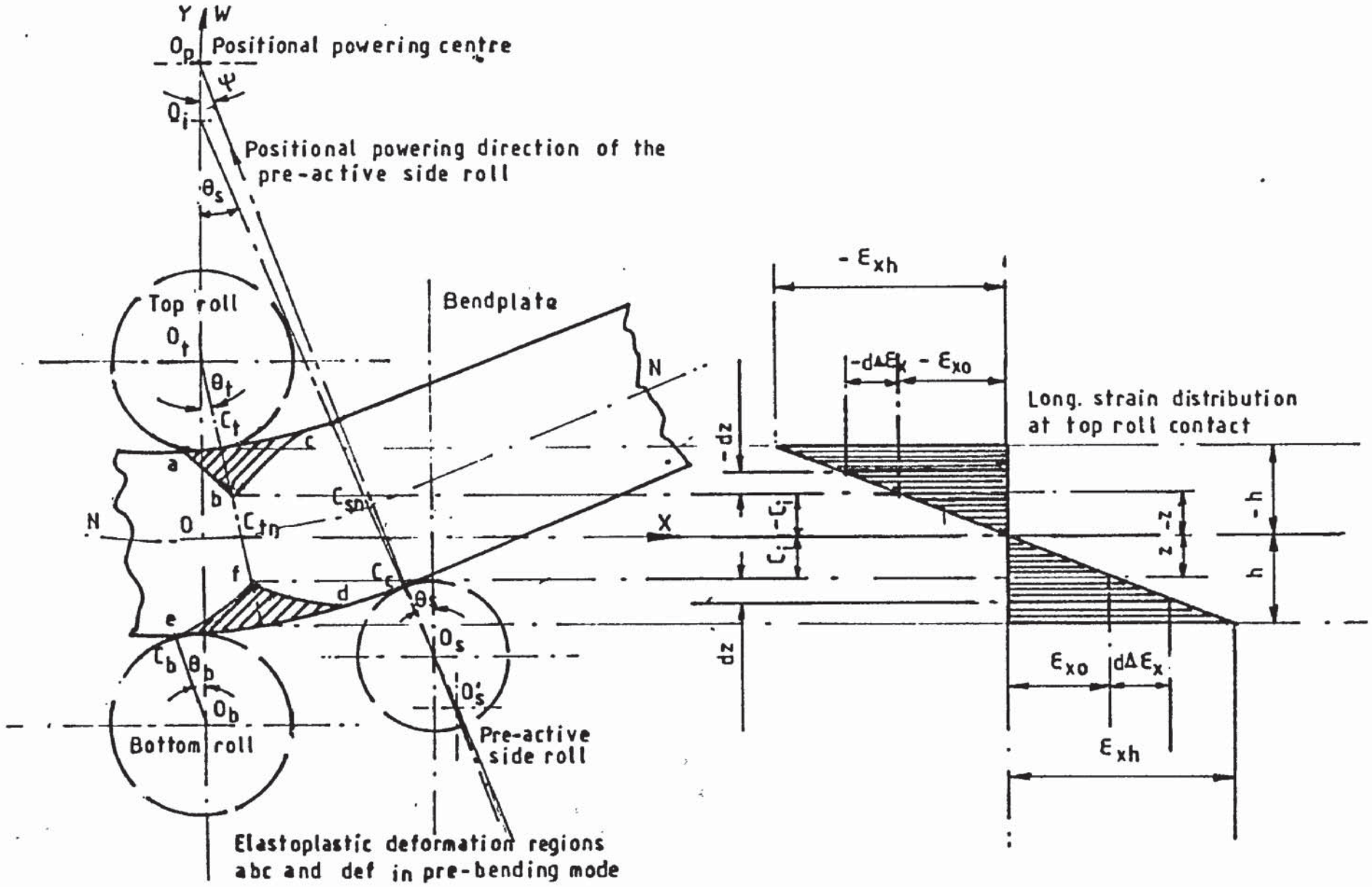

FIG 5.11 ASSUMED LONGITUDINAL STRAIN DISTRIBUTION ACROSS THICKNESS OF PLATE AT TOP ROLL CONTACT

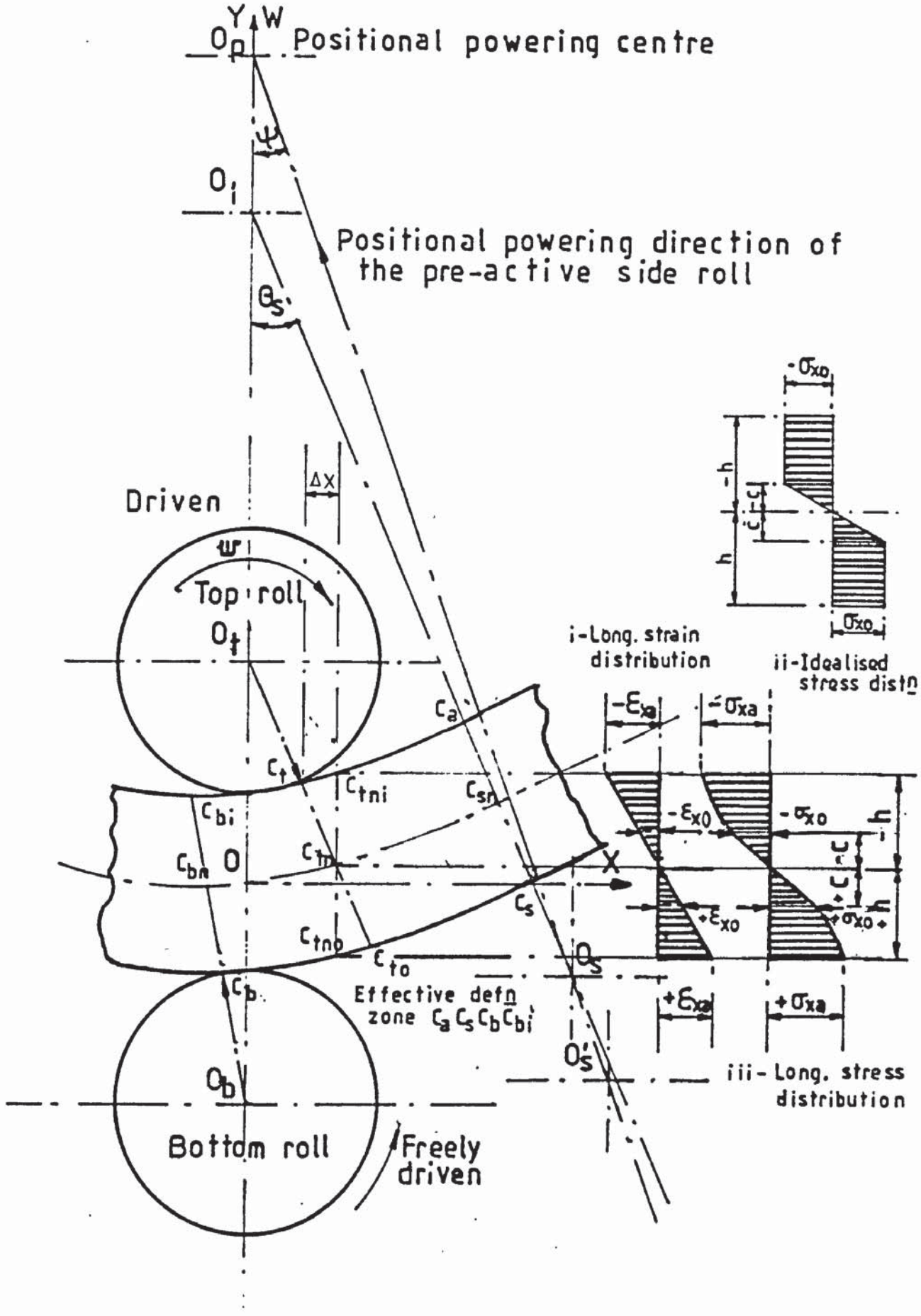

FIG 5.12 ASSUMED ELASTIC-ELASTOPLASTIC STRAIN AND STRESS DISTRIBUTIONS ACROSS THICKNESS OF PLATE AT TOP ROLL CONTACT

expected finished profile, a new static equilibrium condition will be instantaneously experienced. With this consideration and the assumption that the maximum external bending moment occurs at the top roll contact, the approach to the mathematical analysis is conceived as follows :

(1) To estimate the internal resistance of the plate, at the top roll contact, to the external bending moment about the contact line (due to the bending load applied by the operative side roll), in order to roll bend the plate to an assumed bend radius.

(2) To obtain a general deflection function, $W(X)$, in terms of a series of parameter functions, for any particular bend.

(3) To define those assumed boundary conditions for each specific operation.

(4) To obtain these parametric functions, in the general deflection function, $W(X)$, as in item (2) above, by considering
   (a) the geometrical boundary conditions as mentioned in (3),
   (b) the geometrical analysis of the deflected plate relative to the pre-set geometry of the bender,
   (c) the displacement constraints of the rolls.

(5) To relate the parametric functions in the general deflection function, $W(X)$, to the known parameters by considering the results from (1) and (4).

(6) To solve the relative bending arm from (5).

(7) To evaluate the "bending" force on the side roll by considering equilibrium analysis of the internal and external bending moment about the top roll contact.

(8) To evaluate the drive torque and power required by energy considerations.

Though the above approach is generally applicable to both thick and thin plate bending, the present analysis only concentrates on the latter. This is mainly due to the following factors.

(a) The assumed co-ordinate system (fig 5.8) reduces in accuracy as the plate thickness increases.

(b) The analysis of thick plate bending normally requires to take into account the transverse shear in the thickness of the plate.

(c) For the thick plate analysis, the normal stress in the plate thickness, σ_z, should be taken into account, thus giving a three-dimensional stress problem.

Factors (b) and (c) generate a series of non-linear partial differential equations which are difficult to solve either analytically or numerically. This is partly due to the floating boundary conditions at the contacts between rolls and bendplate (especially that between the active side roll), and also to the fact that there are too many unknown parameters in the bending process.

5.4.3. Internal resistance to the external effort about the top roll contact

For equilibrium to be satisfied for plate bending, in both pre-bending and steady continuous bending modes, the internal bending moment must equal its external counterpart. This particular section evaluates the internal bending moment at the top roll contact. The analysis assumes the material to be isotropic and work-hardening.

5.4.3.1. The internal resistance in the elastic deformation mode

A. Stress-strain relationship

At the commencement of bending, the deformation in the effective zone is completely elastic. The stress-strain relations thus obey Hooke's law.

Assuming $(\sigma_x, \sigma_y, \sigma_z)$ and (e_x, e_y, e_z) are the stress and strain system, respectively, on an infinitesimal element, equation (3.2) states

$$e_x = \varepsilon_x = [\sigma_x - \nu(\sigma_y + \sigma_z)]/E \quad \text{(a)}$$

$$e_y = \varepsilon_y = [\sigma_y - \nu(\sigma_z + \sigma_x)]/E \quad \text{(b)} \qquad (5.3)$$

$$e_z = \varepsilon_z = [\sigma_z - \nu(\sigma_x + \sigma_y)]/E \quad \text{(c)}$$

wher, e represents the engineering strains which are approximately equal to the corresponding true strain, ε, for elastic deformation.

ν is Poisson's ratio.

In plate bending, the aspect ratio of the width to thickness of the plate is relatively high, the strain in the central portion of the plate along the width direction, y (see fig 5.1 and 5.13A, it is noted that the co-ordinate for the plate itself is different to that of the bending process), can therefore be regarded as zero (due to the restraint of the materials around their vicinity). Although the strain along the longitudinal edges of the plate is not restrained, the

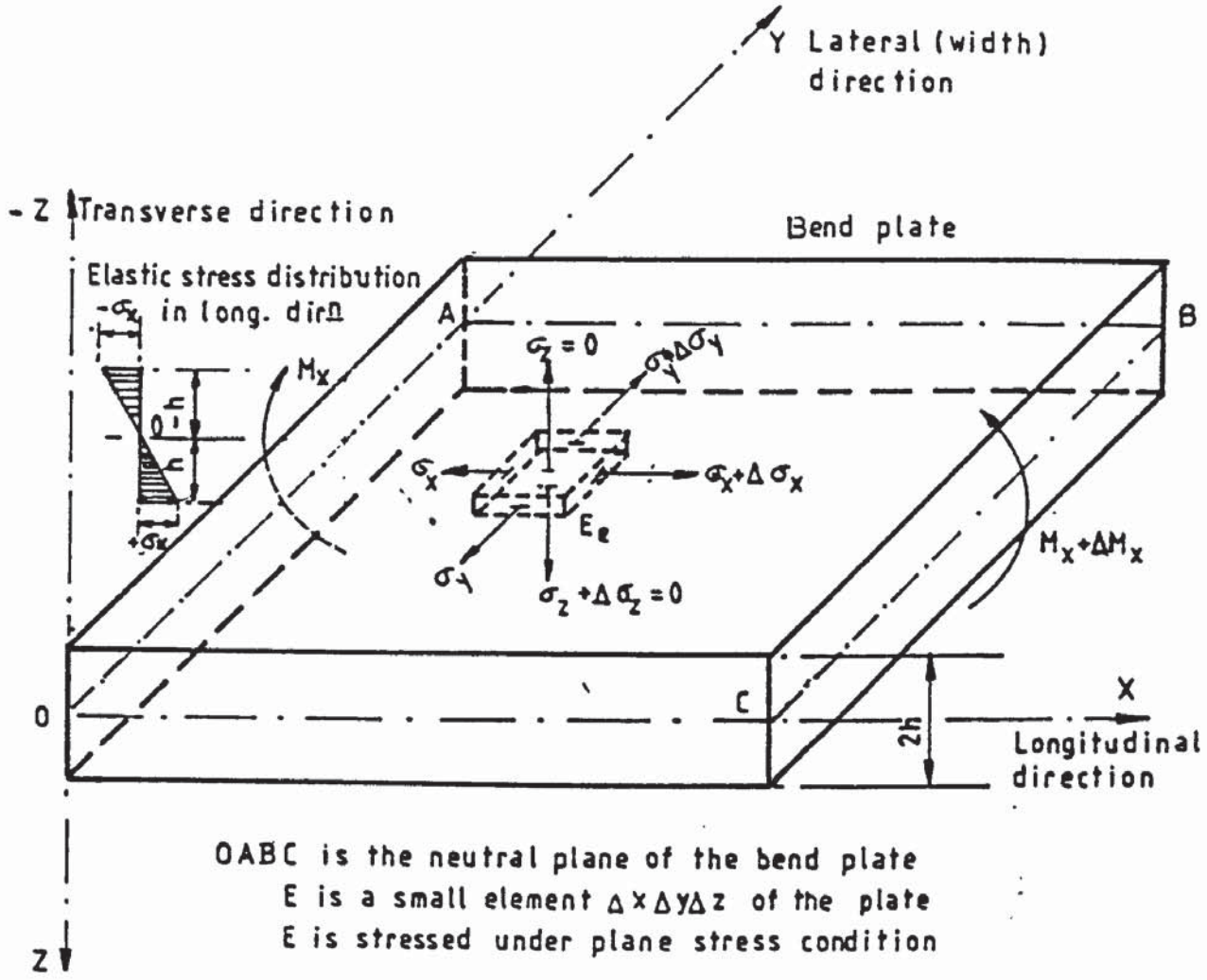

FIG 5.13A PLATE CO-ORDINATE SYSTEM AND ELASTIC STRESS DISTRIBUTION THROUGH THE PLATE THICKNESS

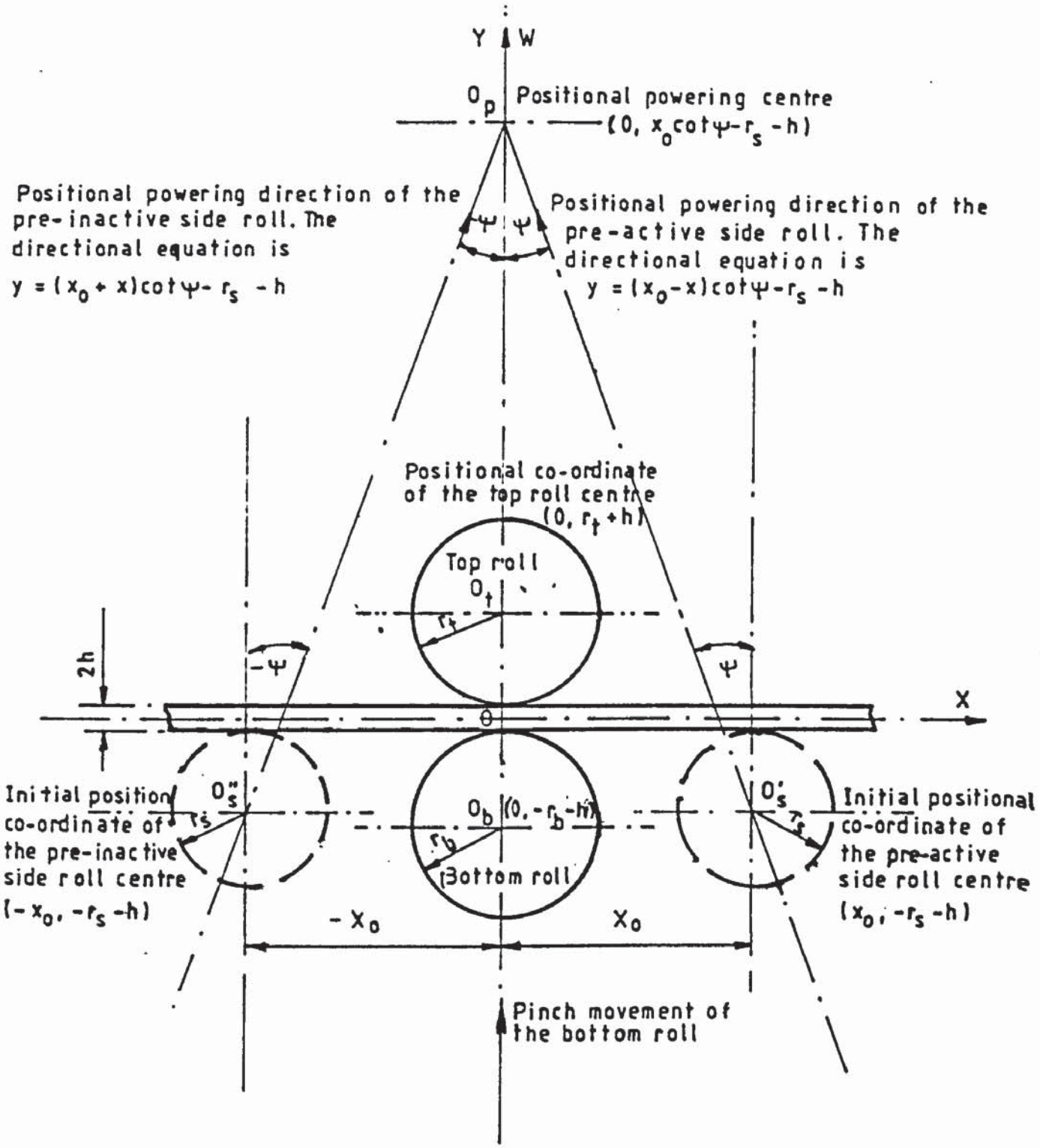

FIG 5.13B CO-ORDINATE SYSTEM AND GEOMETRICAL CONSTRAINT OF THE BENDER RELATIVE TO THE DISPLACEMENT OF THE SIDE ROLL MOVEMENT

assumption of $e_y=0$ (assumption (k) in section 5.4.1) throughout the plate simplifies the analysis. Furthermore, it is assumed that there is no roll deflection along the effective roll length. Additionally, the consideration of relatively thin plate bending leads to the assumption of $\sigma_z=0$ (see section 5.4.1). Expression (5.3b) therefore gives

$$\sigma_y = \nu \sigma_x \qquad (5.4a)$$

Substituting (5.4a) and $\sigma_z=0$ into (5.3a) gives

$$e_x = (1-\nu^2)\, \sigma_x/E \qquad (5.4b)$$

B. The effective longitudinal stress and strain at the commence of yield for single or first pass bending

The effective stress, $\bar{\sigma}$, for a three-dimensional principal stress system is expressed as follows [21].

$$\bar{\sigma} = (1/\sqrt{2})[(\sigma_x-\sigma_y)^2 + (\sigma_y-\sigma_z)^2 + (\sigma_z-\sigma_x)^2]^{1/2} \qquad (5.5)$$

Generally, the material will commence to yield if the effective stress reaches its yield value, σ_0, in the uniaxial tensile test. Consequently the substitution of $\bar{\sigma} = \sigma_0$ and $\sigma_z=0$ into equation (5.5) leads to

$$\sigma_0 = (1-\nu+\nu^2)^{1/2}\, \sigma_{x0} \qquad (5.6a)$$

which can be rearranged to give

$$\sigma_{x0} = \sigma_0/(1-\nu+\nu^2)^{1/2} \qquad (5.6b)$$

where, σ_{x0} is the magnitude of the longitudinal stress as yielding first occurs.

The corresponding longitudinal yield strain, ε_{x0}, can be obtained by substituting σ_0 for σ_{x0} into equation (5.4b), i.e.

$$\varepsilon_{x0} = [(1-\nu^2)\sigma_0]/[E(1-\nu+\nu^2)^{1/2}] \qquad (5.6c)$$

C. Pre-springback local bend radius of the bent plate at the top roll contact

Since the maximum deformation has been assumed to occur at the top roll contact, the longitudinal strain at the outer fibre layer immediately under the contact line will experience first yield. If a_0 is the corresponding pre-spring back local bend radius in the longitudinal direction of the deformed plate, at roll contact. Its curvature may be related to equation (5.6c), by the expression :

$$\varepsilon_{x0} = h/a_0 = [(1-\nu^2)\sigma_0]/[E(1-\nu+\nu^2)^{1/2}] \qquad (5.7a)$$

where, $2h=t$ is the thickness of the plate.

Expression (5.7a) can be further rearranged to give

$$1/a_0 = [(1-\nu^2)\sigma_0]/[Eh(1-\nu+\nu^2)^{1/2}] \qquad (5.7b)$$

Theoretically, a_0 can also be considered as the pre-spring

back local bend radius at the first yield line in the effective deformation zone, when the pre-spring back bend radius at the top roll contact is plastically bent to any value R.

D. Internal moment resisting the external bending moment at the first yield

The elastic stress distribution before the commencement of yield, at a particular cross section of the plate is as shown in figure 5.13A. Its total internal bending moment, M_i, can be expressed as :

$$M_i = -M_e = 2b\int_0^h \sigma_x z dz \qquad (5.8a)$$

where, b is the width of the plate, and z is the distance from the central plane of the plate.

At the condition of first yield the longitudinal stress-strain relation, for any fibre layer between the outer fibre and the neutral plane, is expressed as equation (5.4b), which may be further rewritten as

$$\sigma_x = E\varepsilon_x/(1-\nu^2) \qquad (5.4c)$$

Also the longitudinal strain of the plate is expressed as

$$\varepsilon_x = z/a_0 \qquad (5.8b)$$

which leads to

$$z=a_0\varepsilon_x \qquad (5.8c)$$

Its differential is thus

$$dz = a_0 d\varepsilon_x \qquad (5.8d)$$

From expression (5.7a) the upper integral limit can be expressed as

$$h = a_0 \varepsilon_{x0} = a_0(1-\nu^2)\sigma_0/E(1-\nu+\nu^2)^{1/2} \qquad (5.8e)$$

Substituting (5.4c), (5.8c) and (5.8d), and also the integral limit expression (5.8e) into (5.8a) gives

$$M_i = [2bEa_0^2/(1-\nu^2)] \int_0^{\varepsilon_{x0}} \varepsilon_x^2 \, d\varepsilon_x \qquad (5.8f)$$

After integration this becomes :

$$M_i = (2bEa_0^2\varepsilon_{x0}^3)/3(1-\nu^2) \qquad (5.9a)$$

Replacing the ε_{x0} by expression (5.7a) gives

$$M_i = [2ba_0^2(1-\nu^2)^2\sigma_0^3]/3E^2(1-\nu+\nu^2)^{3/2} \qquad (5.9b)$$

Further replacing

$$a_0 = [Eh(1-\nu+\nu^2)^{1/2}]/(1-\nu^2)\sigma_0$$

into (5.9b) gives

$$M_i = 2bh^2\sigma_0/3(1-\nu+\nu^2)^{1/2} \qquad (5.9c)$$

Expression (5.9c) gives the magnitude of the internal resistance in bending of the plate at the first yield

cross-section. It is also the internal bending resistance at the top roll contact if the plate contact is just at its yielding point.

5.4.3.2. Internal bending resistance in the elastoplastic deformation mode for single or first pass bending beyond the yield

Once plastic yield commences in the outer fibre layers, at the top roll contact of the bend plate, the increase of the plate curvature allows the elastoplastic deformation (fig 5.4) to penetrate into the depth of the plate and to propagate towards the effective deformation zone. As the bending proceeds, the cross section providing maximum bending resistance may consist of:

(i) a completely elastic core, which can be analysed as in section 5.4.3.1, and
(ii) two elastoplastic outer regions on the top and bottom sides the elastic core as mentioned in (i).

If the depth of the top and bottom elastoplastic region is assumed symmetrical about the neutral layers, the maximum internal bending moment can be analysed as follows.

A. Elastoplastic stress-strain relationship

The stress strain relationship in the elastoplastic region can be appropriately represented by the following Prandtl-Reuss relations.

$$\delta\varepsilon_x=\delta\lambda[\sigma_x-(\sigma_y+\sigma_z)/2] + [\delta\sigma_x-\nu(\delta\sigma_y+\delta\sigma_z)]/E \qquad (5.10a)$$

$$\delta\varepsilon_y= \delta\lambda[\sigma_y-(\sigma_z+\sigma_x)/2] + [\delta\sigma_y-\nu(\delta\sigma_z+\delta\sigma_x)]/E \qquad (5.10b)$$

$$\delta\varepsilon_z = \delta\lambda[\sigma_z-(\sigma_x+\sigma_y)/2] + [\delta\sigma_z-\nu(\delta\sigma_x+\delta\sigma_y)]/E \qquad (5.10c)$$

where $\delta\lambda$ is an instantaneous plastic constant which should be pre-determined.

In the thin plate bending plane strain problem, i.e. $\delta\varepsilon_y=\sigma_z=\delta\sigma_z=0$, (assumptions j and k in section 5.4.1), expression (5.10b) is equal to zero.

The condition to satisfy the requirement of $\delta\varepsilon_y=0$ is either one of the following two requirements.

$$\text{(i)}\quad \delta\lambda = (\delta\sigma_y-\nu\delta\sigma_x)/[E(\sigma_x-\sigma_y/2)] \qquad (5.11a)$$

$$\text{(ii)}\quad \sigma_y - \sigma_x/2 = 0 \qquad (5.11b)$$

and

$$\delta\sigma_y -\nu\delta\sigma_x = 0 \qquad (5.11c)$$

It can be seen that (ii) is a special cases of (i). Normally the consideration of (i) requires the relationship of

(a) $\delta\sigma_y$ and $\delta\sigma_x$, and

(b) σ_x and σ_y to be found.

Owing to the following factors :

(1) the present problem contains a number of floating boundary conditions,
(2) the requirement to satisfy the continuously transitional deformation modes from the elastic to elastoplastic deformation in the plate (i.e. to retain the material behaviour of equation (5.4a) and (5.4b) for the elastic

deformation),

the condition (b) is chosen. It subsequently leads to the following expressions :

$$\sigma_y = \sigma_x/2 \quad \text{for the plastic deformation} \tag{5.11c}$$

and

$$\delta\sigma_y = \nu\delta\sigma_x \quad \text{for the incremental elastic deformation} \tag{5.11d}$$

Each equation in the expressions (5.10a) to (5.10c) can therefore be split into two separate parts, i.e. $\delta\varepsilon_i^p$ (i=x,y,z) for the incremental plastic strain, and $\delta\varepsilon_i^e$ (i=x,y,z) for the incremental elastic strain. Consequently they can be re-expressed in their tensoral form as follows :

$$\delta\varepsilon_i = \delta\varepsilon_i^p + \delta\varepsilon_i^e \quad ; i=x, z. \tag{5.12}$$

in which

$$\delta\varepsilon_x^p = 3\delta\lambda\, \sigma_x/4 \tag{5.13a(1))}$$

$$\delta\varepsilon_z^p = -3\delta\lambda\, \sigma_x/4 \tag{5.13a(2))}$$

and

$$\delta\varepsilon_x^e = [(1-\nu^2)\delta\sigma_x]/E \tag{5.13b(1))}$$

$$\delta\varepsilon_z^e = [-\nu(1+\nu)\delta\sigma_x]/E \tag{5.13b(2))}$$

It is noted that the condition in expressions (5.13a) satisfies the material incompressibility in plastic deformation, whilst expressions (5.13b) clearly obey Hooke's law.

From equations (5.13b) it can be further verified that

$$\delta\varepsilon_z^e = [-\nu(1+\nu)/(1-\nu^2)]\,\delta\varepsilon_x^e$$

which can be simplified to give

$$\delta\varepsilon_z^e = [-\nu/(1-\nu)]\,\delta\varepsilon_x^e \qquad (5.13c)$$

Additionally, the integration of (5.13b) over limits of ε_{i1}^e and ε_{i2}^e leads to

$$\varepsilon_{x2}^e - \varepsilon_{x1}^e = [(1-\nu^2)(\sigma_{x2} - \sigma_{x1})]/E \qquad (5.13d(1))$$

and

$$\varepsilon_{z2}^e - \varepsilon_{z1}^e = [-\nu(1+\nu)(\sigma_{x2} - \sigma_{x1})]/E \qquad (5.13d(2))$$

With $\Delta\varepsilon_i^e = \varepsilon_{i2}^e - \varepsilon_{i1}^e$ and $\Delta\sigma_x = \sigma_{x2} - \sigma_{x1}$, the above expressions can thus be written into the following discrete forms

$$\Delta\varepsilon_x^e = [(1-\nu^2)\Delta\sigma_x]/E \qquad (5.13e(1))$$

and

$$\Delta\varepsilon_z^e = [-\nu(1+\nu)\Delta\sigma_x]/E \qquad (5.13e(2))$$

respectively.

B. Determination of the plastic parameter, $\delta\lambda$.

Since the plastic constant parameter, $\delta\lambda$, in the stress strain relation (5.13a) changes as the plastic deformation proceeds, the complete solution of the relation (5.13a) requires the function for $\delta\lambda$ to be determined. In the general

theory of plasticity [5], $\delta\lambda$ is define as follows.

$$\delta\lambda = \delta\varepsilon_p/\bar{\sigma} \qquad (5.14a)$$

where $\delta\varepsilon_p$ is an effective plastic strain,

$\bar{\sigma}$ is an effective plastic stress.

However, the respective effective plastic strain / stress is a function of the components of their corresponding directional quantities, i.e. $\delta\varepsilon_i^p/\bar{\sigma}_i$ (or they are related to the uniaxial tensile test values), respectively. Since its consideration does not facilitate the analysis, its evaluation is thus ignored in the subsequent analysis.

C. Uniaxial tensile stress-strain curve analysis for deformation beyond yield.

Consider the uniaxial tensile test curve, oab, in figure 5.14, in which og is the elastic strain at yield, i.e. ε_0, E is Young's modulus.

If a specimen is loaded from the condition o to b, it produces proportional elastic strain until it reaches the values of ε_0, beyond which permanent deformation occurs. The total strain produced by the stress beyond σ_0 to $\bar{\sigma}$ is gd, i.e. $\Delta\varepsilon_t$, which comprises of an amount of permanently plastic strain $\Delta\varepsilon^p$ and an incremental elastic strain $\Delta\varepsilon^e$. Mathematically it can be expressed as follows.

$$\Delta\varepsilon_t = \Delta\varepsilon^p + \Delta\varepsilon^e \qquad (5.16a)$$

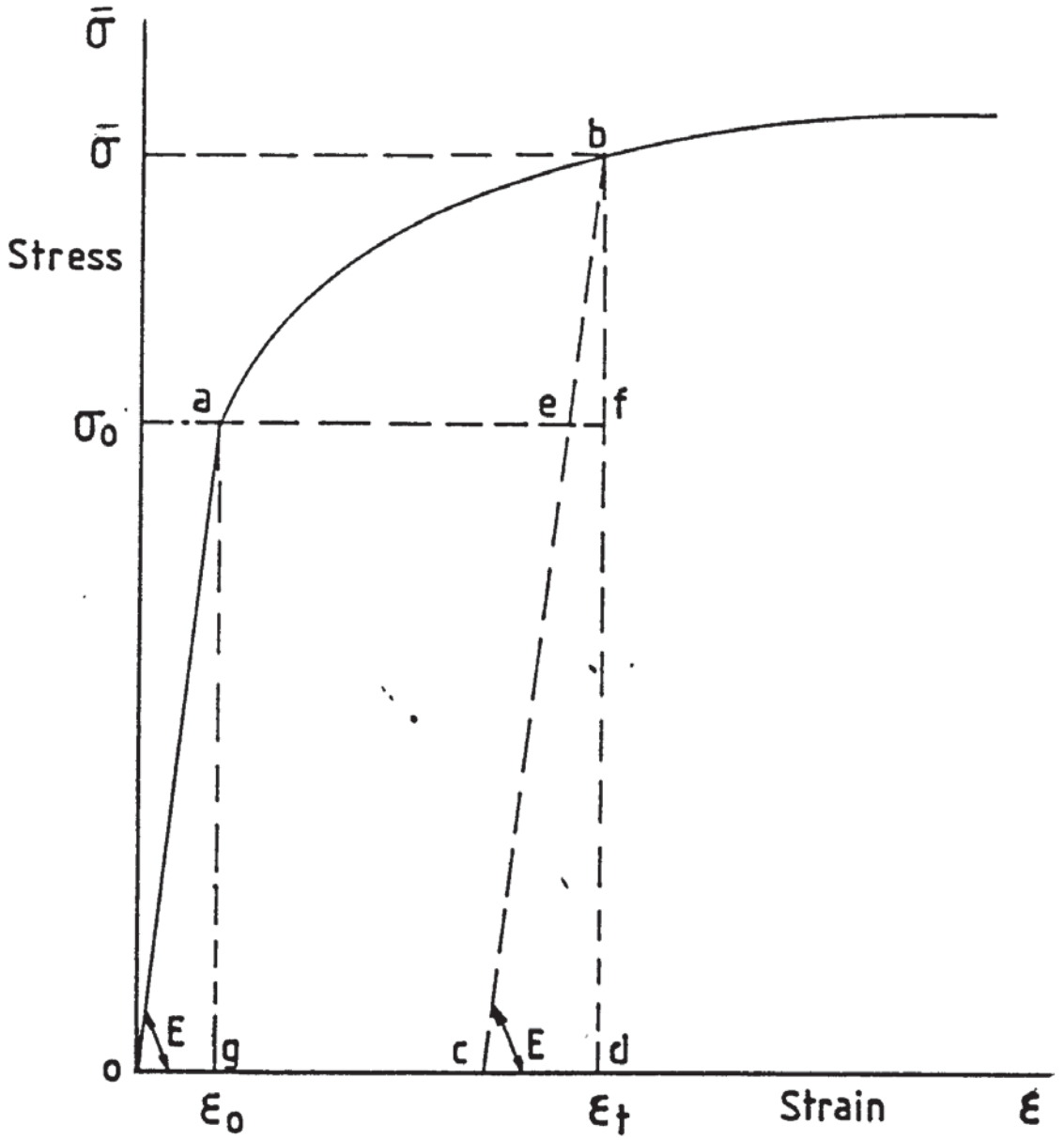

For loading from o to b

The total elastic strain $\varepsilon_e^t = cd = \varepsilon_0 + \Delta\varepsilon^e$

Elastic strain at the commencement of yield $\varepsilon_0 = \frac{\sigma_0}{E} = og$

Incremental elastic strain $\Delta\varepsilon^e = (\bar{\sigma} - \sigma_0)/E = ef$

Total incremental plastic strain $\Delta\varepsilon^p = ae = od - cd = af - ef$

As the load is released from b, the spring back strain = $cd = \varepsilon_e^t$

FIG 5.14 REPRESENTATION OF SINGLE/FIRST PASS BENDING CYCLE ON AN UNIAXIAL TENSILE STRESS-STRAIN CURVE

Furthermore, the total strain, ε_t, produced by the deformation can be written as

$$\varepsilon_t = od = og+gc+cd \qquad (5.16b)$$

which can be rewritten to give

$$\varepsilon_t = \varepsilon_0 + \Delta\varepsilon_t = \varepsilon_0 + \Delta\varepsilon^p + \Delta\varepsilon^e \qquad (5.16c)$$

The initial yield strain ε_0 can be defined as :

$$\varepsilon_0 = \sigma_0/E \qquad (5.16d)$$

The empirical uniaxial stress strain relationship beyond yield can be expressed (see Chapter Six) as

$$\Delta\bar{\sigma} = \bar{\sigma} - \sigma_0 = H\Delta\varepsilon^n \qquad (5.16c)$$

where $\Delta\varepsilon$ is the total incremental strain and equal to $\Delta\varepsilon_t$, H and n are material constants.

Consequently the total incremental elastic strain $\Delta\varepsilon^e$ can be evaluated as follows

$$\Delta\varepsilon^e = ef = \Delta\bar{\sigma}/E = H\Delta\varepsilon^n/E \qquad (5.16d)$$

or

$$\Delta\varepsilon^e = H(\Delta\varepsilon_t)^n/E = (H/E)(\Delta\varepsilon^p + \Delta\varepsilon^e)^n \qquad (5.16e)$$

Following equation (5.16a) the quantity of the permanently plastic strain, $\Delta\varepsilon^p$, can be found from the definition of the total incremental strain, $\Delta\varepsilon_t$, i.e.

$$\Delta\varepsilon^p = \Delta\varepsilon_t - \Delta\varepsilon^e = \Delta\varepsilon_t - (H/E)\Delta\varepsilon_t^n \qquad (5.17a)$$

or

$$\Delta\varepsilon^p = \Delta\varepsilon_t - \sigma_0/E - (H/E)(\Delta\varepsilon_t)^n \qquad (5.17b)$$

The above relevant expressions for $\Delta\varepsilon^p$, $\Delta\varepsilon^e$ and ε_0 are all effective strains from the uniaxial tensile test analysis. To analyse the plane strain problem for roller plate bending, it is necessary to relate the longitudinal strain to the above quantities.

D. Relating the longitudinal incremental plastic and elastic strain i.e. $\Delta\varepsilon_x^p$ and $\Delta\varepsilon_x^e$ respectively to the uniaxial tensile stress strain relationship

In figure 5.11, the total longitudinal strain at any fibre layer in the plate is assumed proportional to its distance, Z, from the plate neutral plane for any local bend radius, R, of curvature, i.e. $\varepsilon_x = z/R$. The longitudinal strain, ε_x, comprises (a) the total plastic incremental strain, $\Delta\varepsilon_x^p$, and (b) the incremental elastic strain, $\Delta\varepsilon_x^e$, components (similar characteristics are also assumed for strains of ε_y and ε_z if they exist).

Since equation (5.7) gives the magnitude of the first yield longitudinal strain in the outer fibre layer, the longitudinal strain at the interface of the purely elastic and the elastoplastic deformation modes for any bend radius R is thus given by :

$$\varepsilon_{x0} = [(1-\nu^2)\sigma_0]/E(1-\nu+\nu^2)^{1/2} \qquad (5.18a)$$

Assuming c_i is the distance of the interface from the neutral strain plane, it can be shown that

$$\varepsilon_{x0} = c_i/R = h/a_0 = [(1-\nu^2)\sigma_0]/E(1-\nu+\nu^2)^{1/2} \qquad (5.18b)$$

It therefore leads to the determination of the value c_i as follows.

$$c_i = hR/a_0 = [(1-\nu^2)R\sigma_0]/E(1-\nu+\nu^2)^{1/2} \qquad (5.18c)$$

At a layer Z away from the neutal plane, for $Z>c_i$, the work hardening effect produces a total amount of elastoplastic strain, $\Delta\varepsilon_x$ expressed as

$$\Delta\varepsilon_x = z/R - c_i/R = (z-c_i)/R = \Delta\varepsilon_x^p + \Delta\varepsilon_x^e \qquad (5.18d)$$

which can be rewritten as :

$$\Delta\varepsilon_x = z/R - [(1-\nu^2)\sigma_0]/E(1-\nu+\nu^2)^{1/2} = \Delta\varepsilon_x^p + \Delta\varepsilon_x^e \qquad (5.18e)$$

Furthermore $\Delta\varepsilon_x^e$ may be restated in term of $\Delta\varepsilon^e$ through the following procedure.

The effective elastic strain may be formulated as follows [21].

$$\Delta\varepsilon^e = (\sqrt{2}/3)[(\Delta\varepsilon_x^e-\Delta\varepsilon_y^e)^2+(\Delta\varepsilon_y^e-\Delta\varepsilon_z^e)^2+(\Delta\varepsilon_z^e-\Delta\varepsilon_x^e)^2]^{1/2} \qquad (5.19a)$$

For the plane strain problem, it has been shown that

$$\Delta\varepsilon_z^e = [-\nu/(1-\nu)]\Delta\varepsilon_x^e \qquad (5.13c)$$

and $\Delta\varepsilon_y^e=0$.

Substituting these into equation (5.19a) gives

$$\Delta\varepsilon^{e} = [2(1-\nu+\nu^2)^{1/2}\,\Delta\varepsilon_x^{e}]/3(1-\nu) \qquad (5.19b)$$

changing the independent variable above into a dependent variable, equation (5.19b) gives

$$\Delta\varepsilon_x^{e} = [3(1-\nu)\Delta\varepsilon^{e}]/2(1-\nu+\nu^2)^{1/2} \qquad (5.19c)$$

The equivalent plastic strain can also be formulated as follows [21].

$$\Delta\varepsilon^{p}=[(\sqrt{2})/3][(\Delta\varepsilon_x^{p}-\Delta\varepsilon_y^{p})^2+(\Delta\varepsilon_y^{p}-\Delta\varepsilon_z^{p})^2+(\Delta\varepsilon_z^{p}-\Delta\varepsilon_x^{p})^2]^{1/2} \qquad (5.19d)$$

For the plane strain problem as indicated in section (5.4.3.2A), equation (5.13a) gives

$\Delta\varepsilon_z^{p} = -\varepsilon_x^{p}$ and $\Delta\varepsilon_y^{p}=0.$

Substituting the above into expression (5.19d) leads to

$$\Delta\varepsilon^{p} =2\Delta\varepsilon_x^{p}/\sqrt{3} \qquad (5.19e)$$

After rearrangement this gives

$$\Delta\varepsilon_x^{p}=[(\sqrt{3})/2]\Delta\varepsilon^{p} \qquad (5.19f)$$

Equations (5.19c) and (5.19f) relate the total longitudinal incremental elastic strain, $\Delta\varepsilon_x^{e}$, and the corresponding plastic strain, $\Delta\varepsilon_x^{p}$, into the instantaneous equivalent strains. Subsequently they may be further expressed in terms of the uniaxial tensile relation.

The substitution of equations (5.19c) and (5.19f) into equation (5.18e) gives

$$z/R-[(1-\nu^2)\sigma_0]/E(1-\nu+\nu^2)^{1/2}$$
$$=(\sqrt{3})\Delta\varepsilon^{p}/2+[3(1-\nu)\Delta\varepsilon^{e}]/2(1-\nu+\nu^2)^{1/2} \qquad (5.20a)$$

after rearrangement gives

$$z/R=(\sqrt{3}/2)\Delta\varepsilon^{p}+[3(1-\nu)\Delta\varepsilon^{e}]/2(1-\nu+\nu^2)^{1/2}$$
$$+(1-\nu^2)\sigma_0/E(1-\nu+\nu^2)^{1/2} \qquad (5.20b)$$

Further substitution of equation (5.17a) and (5.16d) into equation (5.20b) for $\Delta\varepsilon^{p}$ and $\Delta\varepsilon^{e}$, respectively, and rearranging gives

$$z/R=(\sqrt{3}/2)\Delta\varepsilon+(H/E)[3(1-\nu)/2(1-\nu+\nu^2)^{1/2}-\sqrt{3}/2]\Delta\varepsilon^{n}$$
$$+(1-\nu^2)\sigma_0/E(1-\nu+\nu^2)^{1/2} \qquad (5.20c)$$

For a constant bend radius R and a particular bend cycle, in which σ_0 is considered constant, the change in Z only alters the quantity in $\Delta\varepsilon$. Subsequently, the differential form of equation (5.20c) is as follows:

$$dz=R\{\sqrt{3}/2+(nH/E)[3(1-\nu)/2(1-\nu+\nu^2)^{1/2}-\sqrt{3}/2]\Delta\varepsilon^{n-1}\}d\Delta\varepsilon$$
$$(5.20d)$$

E. Maximum cross-sectional bending resistance in the plate when subjected to an external bending moment about the top roll contact

Due to the existence of the complete elastic deformation core, sandwiched between the two elastoplastic regions, the internal bending resistance, M_I, produced by the external

bending moment, M_e, about the top roll contact can be generalised as

$$M_i = b\{\int_{elastic} \sigma_x z dz + \int_{elastoplastic} \sigma_x z dz\} \qquad (5.21)$$

In which z and dz can be conveniently replaced by

(i) $z=R\varepsilon_x$ and $dz=Rd\varepsilon_x$ for $\varepsilon_x \leq \varepsilon_{x0}$, i.e. in the elastic deformation core.

(ii) the expressions (5.20c) and (5.20d), respectively, for $\varepsilon_x > \varepsilon_{x0}$, i.e. in the elastoplastic deformation regions.

Additionally, the elastic stress, σ_x, in equation (5.21) can be expressed in term of ε_x using relationship (5.4c). However, the remaining problem is to relate the stress, σ_x, in the elastoplastic deformation regions to the empirical uniaxial tensile test relation.

Generally the equivalent stress, $\bar{\sigma}$, in plasticity is expressed as :

$$\bar{\sigma} = (1/\sqrt{2})[(\sigma_x-\sigma_y)^2+(\sigma_y-\sigma_z)^2+(\sigma_z-\sigma_x)^2]^{1/2} \qquad (5.22a)$$

Since it has been assumed that the plate is thin and the normal stress, σ_z, may be negligible (assumption (m) in section 5.4.1), equation (5.22a) can therefore be written as follows

$$\bar{\sigma} = [\sigma_x^2-\sigma_x\sigma_y+\sigma_y^2]^{1/2} \quad \text{for } \sigma_z=0 \qquad (5.22b)$$

Substituting (5.11d) into (5.22b) and after rearrangement gives :

$$\sigma_x = (2/\sqrt{3})\bar{\sigma} \qquad (5.22c)$$

Since the empirical uniaxial tensile stress-strain relation can be expressed as

$$\bar{\sigma} = \sigma_0 + H\Delta\varepsilon^{n} \qquad (5.22d)$$

the substitution of (5.22d) into (5.22c) give

$$\sigma_x = (2/\sqrt{3})\ \sigma_0 + (2H/\sqrt{3})\Delta\varepsilon^{n} \qquad (5.22e)$$

Expression (5.22e) relates the local instantaneous stress stress, σ_x, to the proportional limit, σ_0, and the total incremental strain, $\Delta\varepsilon$.

Having obtained the expression (5.22e), the integration of (5.21) can therefore be performed as follows.

Assuming $A=\int_{elastic}\sigma_x z dz$, the substitution of the relevant expression of σ_x, z and dz gives

$$A=[2R^2E/(1-\nu^2)]\int_0^{\varepsilon_{x0}}\varepsilon_x^2 d\varepsilon_x = (2R^2E\varepsilon_{xo}^3)/3(1-\nu^2)$$

Substituting expression (5.7a) into the above expression for ε_{x0} gives

$$A= [2R^2(1-\nu^2)^2\sigma_0^3]/[3E^2(1-\nu+\nu^2)^{3/2}] \qquad (5.23a)$$

Equation (5.23a) represents the bending moment per unit width within the elastic core at the top roll contact.

Let $B=\int_{\text{elastoplastic}} \sigma_x z dz$, then the substitution of (5.22e), (5.20c) and (5.20d) gives

$$B=2R^2\int_0 \{[(2/\sqrt{3})\sigma_0+(2H/\sqrt{3})\Delta\varepsilon^{n}][(\sqrt{3})\Delta\varepsilon/2 +K\Delta\varepsilon^{n}+g] [(\sqrt{3})/2 +nK\Delta\varepsilon^{n-1}]d\Delta\varepsilon\} \quad (5.23b)$$

where, $K=(H/E)\{[3(1-\nu)/2(1-\nu+\nu^2)^{1/2}] - (\sqrt{3})/2\}$,

$g=[(1-\nu^2)\sigma_0]/[E(1-\nu+\nu^2)^{1/2}]$.

In which the upper integral limit, $\Delta\varepsilon_1$, is first determined by numerically iterating equation (5.20c) for the assumed known R and Z.

After multiplication, rearrangement and integration of equation (5.23b) :

$$B=2R^2\{(2HK^2\Delta\varepsilon_1^{3n}/3\sqrt{3}) + [HK(n+1)\Delta\varepsilon_1^{2n+1}]/(2n+1) + (K/\sqrt{3})(K\sigma_0+Hg)\Delta\varepsilon_1^{2n} + (\sqrt{3}/2)H\Delta\varepsilon_1^{n+2}/2(n+2) + [K\sigma_0 + Hg/(n+1)]\Delta\varepsilon_1^{n+1} + 2K\sigma_0 g\Delta\varepsilon_1^{n}/\sqrt{3} + (\sqrt{3})\sigma_0\Delta\varepsilon_1^2/4 + g\sigma_0\Delta\varepsilon_1\} \quad (5.23d)$$

the substitution of equations (5.23a) and (5.23d) into (5.21) gives the internal bending resistance, M_i, and the corresponding external bending moment at the top roll contact. Owing to the complicated form of (5.23d), it will be retained as B in the successive analysis and the expression for M_i can thus be written as :

$$M_i = b\{[2R^2(1-\nu^2)^2\sigma_0^3]/[3E^2(1-\nu+\nu^2)^{3/2}] + B\} \quad (5.24)$$

where b is the width of the bend plate.

5.4.4. Internal bending resistance of the plate to the external effort about the top roll contact for the second and successive passes

Multipass plate bending is undertaken :

(1) to reduce the radius of a bend and to correct the uniformity of a bend,
(2) to achieve a tight-finished bend radius in bending a plate with high flexural rigidity,
(3) to optimise the working capacity of a bender in bending a thick plate.

The following analysis mainly concerns the achievement of (2).

Prior to the analysis of the multipass bending operation, it is important to visualize its mechanics and working principle.

Consider a stress-strain curve as shown in fig 5.15. If a piece of material is bent from state o to b, and then unloaded, it will follow bc to c. Subsequently a plastic strain oc will remain. If it is reloaded from c, the stressing condition will follow the curve cb elastically until it reaches b. A further plastic deformation will thus occur along the path bh. If it is re-unloaded at h, it will then follow hi to i.

From the above illustration, it is seen that multipass bending is less beneficial than the single pass bending process, since it indicates that the multipass operation accumulates work losses associated with the elastic spring-back.

The reduction of the roll forces in the multipass bending mode

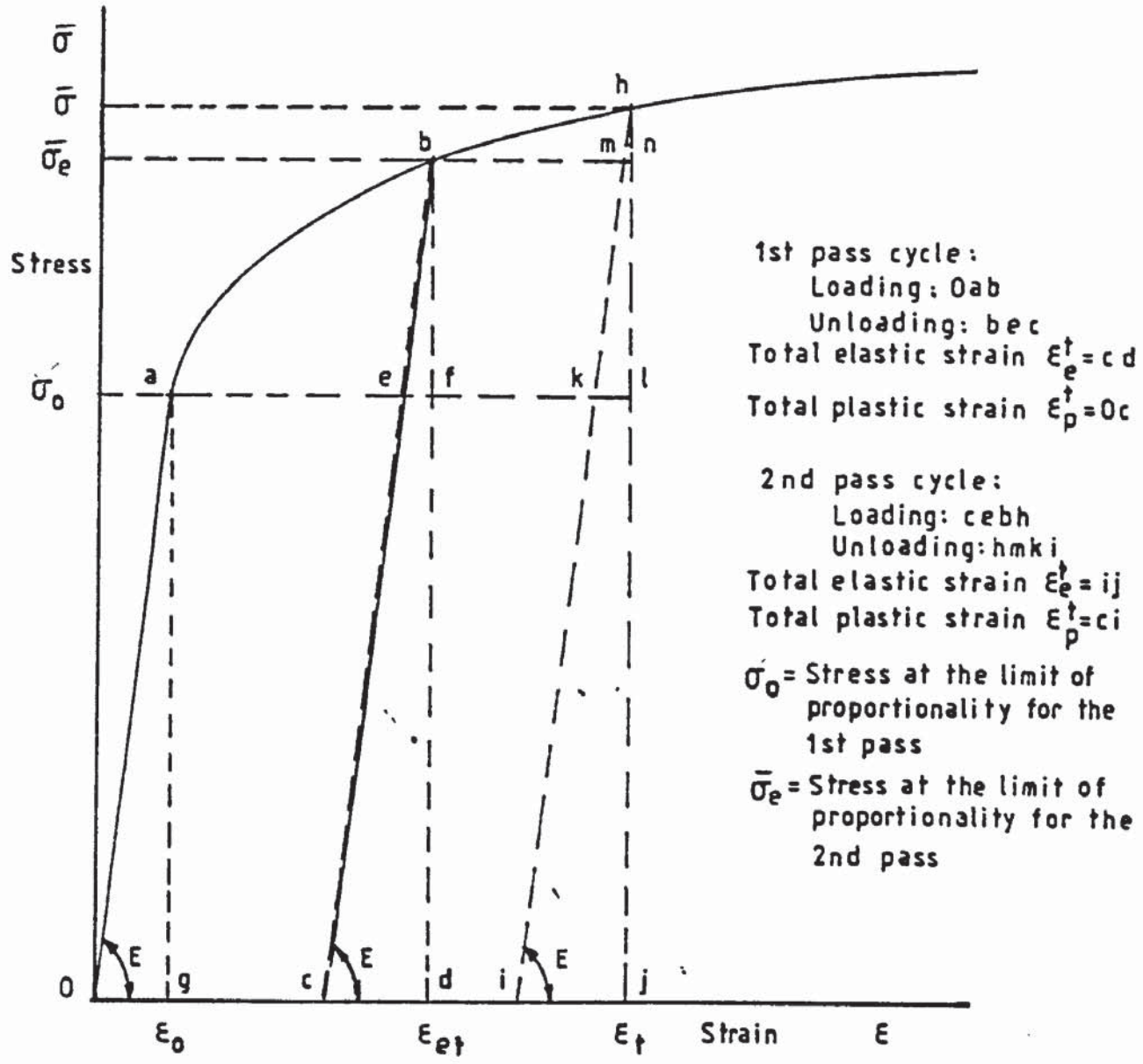

$$\varepsilon_0 = \sigma_0 / E = Og$$

1st pass: Total elastic strain $\varepsilon_e^t = cd = \varepsilon_0 + \Delta\varepsilon^e$

Incremental elastic strain beyond yield $\Delta\varepsilon^e = ef = \dfrac{\bar{\sigma}_e - \sigma_0}{E}$

Incremental plastic strain $\Delta\varepsilon^p = ae = Oc = \varepsilon_{et} - \varepsilon_e^t$

2nd pass: Total elastic strain $\varepsilon_{ei}^t = ij = \bar{\sigma} / E = \bar{\sigma}_e / E + \Delta\varepsilon_{ei}$

Incremental elastic strain $\Delta\varepsilon_{ei} = mn = (\bar{\sigma} - \bar{\sigma}_e) / E$

Incremental plastic strain $\Delta\varepsilon^p = ci = ek = bm = \varepsilon_t - \varepsilon_{et} - \Delta\varepsilon_{ei}$

FIG 5.15 REPRESENTATION OF TWO SUCCESSIVE PASS BENDING CYCLES ON AN UNIAXIAL TENSILE STRESS-STRAIN CURVE

is perhaps due to the following factors :

(a) The geometric change of the initial profile of the bend plate.
(b) The bender set-up effectively increasing the horizontal force component, whilst the vertical force component reducing relatively less as the operative side roll moves along its positional powering direction.
(c) A favourable residual stress distributions in the initial bending operation assisting the successive bending operations.
(d) The Bauschinger effect experienced in reverse bending as a result of :
    (1) the shifting of the neutral axis, and
    (2) the residual stress distribution as stated in (c) above.

Factors (b) and (d-1) also occur in the single pass bending. Consequently, they are not the major characteristics of the multipass bending.

Thus the analysis for multipass bending mainly concentrates on (a), as (c) is assumed zero throughout to simplify the analysis.

5.4.5. Equating the internal bending resistance, at the top roll contact, to the external bending moment

5.4.5.1. Stress strain relationships

A. Bending in the elastic deformation mode

With reference to fig 5.15, the plate remains in the elastic condition until point **b** is reached, with bending taking place along **cb**. Consequently Hooke's law applies and the stress-strain analysis is similar to that in section 5.4.3.1,

except that the first yield stress, σ_0, in that section is replaced by the instantaneous first yield stress, $\bar{\sigma}_e$. Normally $\bar{\sigma}_e$ corresponds to the local stress at the finished bend in the single (or previous) pass bending.

The following restates the expressions of (5.6b) and (5.6c) as :

$$\sigma_x = \bar{\sigma}_e/[(1-\nu+\nu^2)^{1/2}] \qquad (5.25a)$$

and

$$\varepsilon_x = (1-\nu^2)\bar{\sigma}_e/E(1-\nu+\nu^2)^{1/2} \qquad (5.25b)$$

where, $\bar{\sigma}_e$ is the corresponding new local yield stress at the respective fibre.

Due to the work hardening effect, those layers of fibres above the original yield, i.e. $C_i \leq Z \leq C_{io}$, will have different values of yield stresses. However the region originally in the elastic deformation mode, i.e. $Z \leq C_i$ (see section 5.4.3.2) has a local yield value of σ_0 and consequently expression (5.6b) retains its forms as

$$\sigma_x = \bar{\sigma}_e/(1-\nu+\nu^2)^{1/2} \qquad (5.25c)$$

for all the fibres in the region $Z \geq -C_i$ and $Z \leq C_i$.

Generally the further re-yield of the respective layers initially above the yield varies for each successive pass, each fibre beyond the former layer having a different yield stress. However, their corresponding effective yield characteristic will follow the uniaxial tensile yield curve

(fig 5.15) once their respective $\bar{\sigma}_e$ has been reached.

B. Equivalent strain

Following the analysis in section 5.4.3.2, each incremental strain of a fibre layer, yielded beyond its elastic limit, is the sum of (a) an incremental elastic $\Delta\varepsilon_x^e$ and (b) an incremental plastic $\Delta\varepsilon_x^p$ component. The previous analysis for the plane strain problem (section 5.4.3.2) has shown how the plastic and elastic longitudinal incremental strain component can be replaced by their corresponding equivalent strain, i.e.

$$\Delta\varepsilon_x^p = (\sqrt{3}/2)\Delta\varepsilon_e^p \qquad (5.25c)$$

and

$$\Delta\varepsilon_x^e = [3(1-\nu)\Delta\varepsilon_e^e]/2(1-\nu+\nu^2)^{1/2} \qquad (5.25d)$$

respectively.

Consideration of the uniaxial tensile stress-strain relation and the total incremental strain in the longitudinal direction of the plate (see section 5.4.3.2) leads to

$$\Delta\varepsilon_x^e = [3(1-\nu)H\Delta\varepsilon^n]/[2E(1-\nu+\nu^2)^{1/2}] \qquad (5.25e)$$

and

$$\Delta\varepsilon_x^p = \Delta\varepsilon_x - [3(1-\nu)H\Delta\varepsilon^n]/[2E(1-\nu+\nu^2)^{1/2}] \qquad (2.25f)$$

C. Relationship of the total strain to the fibre layer distance, Z, from the neutral plane of the plate

The general displacement analysis in "Mechanics of Materials" [142] for bending bars of large initial curvature

(fig 5.16) gives an expression for the longitudinal strain as follows

$$\varepsilon_x = z[(r_f/R)-1]/(r_f+z) \qquad (5.25g)$$

where, r_f is the initial radius of curvature,

R is the final radius of curvature.

(a) At the commencement of yield

The initiation of the yield at a particular fibre layer from the neutral plane of a bend plate is given by equating the local longitudinal bending strain, to equation (5.25b). This gives

$$\varepsilon_x = z[(r_f/R)-1]/(r_f+z) = [(1-\nu^2)\bar{\sigma}_e]/[E(1-\nu+\nu^2)^{1/2}] \qquad (2.25h)$$

cross-multiplication of (5.25h) and rearrangement gives

$$z = [(1-\nu^2)\bar{\sigma}_e]/\{E[(r_f/R)-1](1-\nu+\nu^2)^{1/2} - (1-\nu^2)\bar{\sigma}_e\} \qquad (2.25i)$$

Prior to the commencement of the yield, the deformation is in the elastic mode until yield first starts on the surface fibre layers, at the top roll contact. Mathematically this will occur when z in (5.25h) is replaced by h. If it is assumed that the local radius of curvature at the particular instant is r_0. The substitution of h into (5.25h) and rearranging gives the following expression for r_0 :

$$1/r_0 = [(r_f+h)(1-\nu^2)\bar{\sigma}_e/r_f Eh(1-\nu+\nu^2)^{1/2} + 1/r_f] \qquad (5.25j)$$

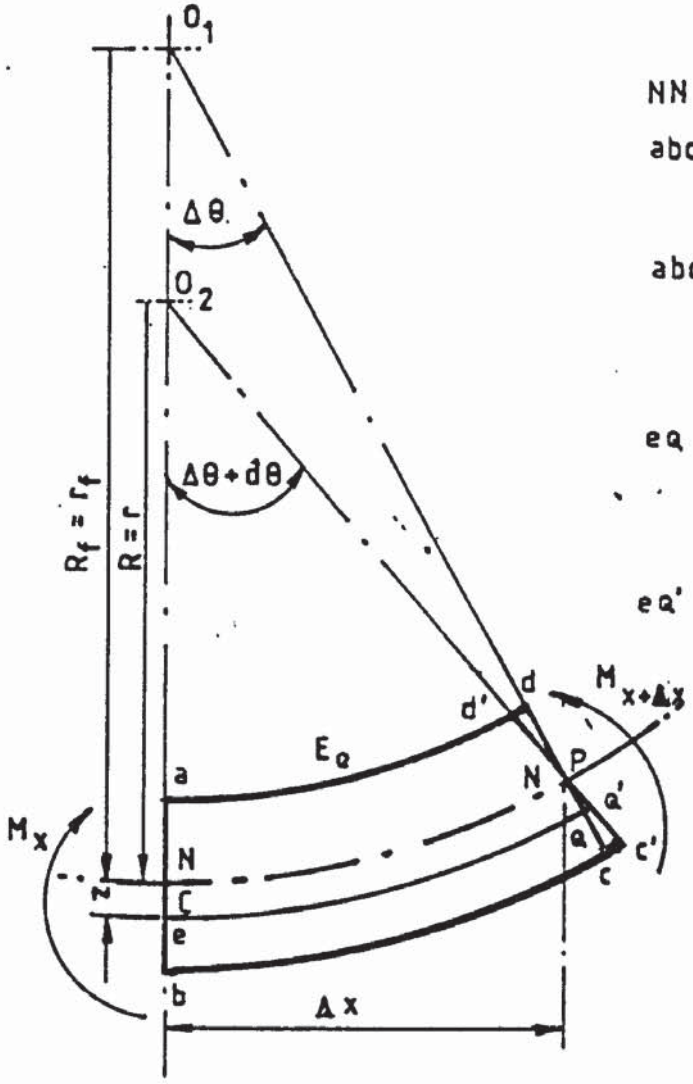

NN (neutral plane) = CP (central plane)

abcd is a sectoral element before the application of the bending moment

abc'd' is the element at equilibnium state after the application of the bending moment

eq is the initial length of the fibre layer at z from the neutral plane NN

eq' is the new length of the fibre at equilibrium condition

Longitudinal strain ε_x :—

$$\varepsilon_x = \frac{z[(R_f/R)-1]}{R_f + z}$$

FIG 5.16 LOADING GEOMETRY WHEN BENDING AN INITIALLY CURVED ELEMENT (BAR)

As the plate is further plastically deformed to a bend radius R at the top roll contact, its corresponding first yield will occur at $Z=C_{i0}$, where C_{i0} (see equation 5.18b) is greater than C_i. The position of C_{i0} can thus be determined by replacing $Z=C_{i0}$ in equation (5.25i).

Due to the fact that the core layers between $+C_i$ and $-C_i$ have originally been in the elastic deformation mode, their first yield stress still remains the value that of the first pass, σ_0. To bend the plate plastically further to the radius R, where $R<r_f$, the fibre layer at C_i will begin to yield as the bend radius $R=R_1$. R_1 can thus be evaluated from the following expression.

$$1/R_1 = \{[r_f+c_i)(1-\nu^2)\sigma_0]/[r_f E c_i(1-\nu+\nu^2)^{1/2}\} + 1/r_f \qquad (5.25k)$$

In the case of $R<R_1$, the plastic deformation will penetrate through the boundaries of $+C_i$ and $-C_i$ towards the neutral layer.

(b) Relationship of the local longitudinal incremental yield strain to the depth, Z, of the plate, from its central plane

The longitudinally local first yield strain has previously been expressed as :

$$\varepsilon_{x10} = [(1-\nu^2)\bar{\sigma}_e]/[E(1-\nu+\nu^2)^{1/2}] \qquad (2.26a)$$

where $\bar{\sigma}_e$ is the effective local first yield stress. Normally it is equal to the local final stress at the first (or preceding) pass.

Let the first yielding interface be C_{i0} from the neutral layer. Analysis has shown that :

$$C_{i0}[(r_f/R)-1]/(r_f+C_{i0}) = [(1-\nu^2)\bar{\sigma}_e]/[E(1-\nu+\nu^2)^{1/2}] \qquad (2.26b)$$

If Z is the distance from the neutral (central) layer, and is greater than C_{i0}, the incremental strain, $\Delta\varepsilon_x$, relates to the strain at C_{i0} as follows :

$$\Delta\varepsilon_x = \varepsilon_x - \varepsilon_{x10} = z\{(r_f/R)-1]/(r_f+z)-(1-\nu^2)\bar{\sigma}_e/E(1-\nu+\nu^2)^{1/2} \qquad (5.26c)$$

It has also been pointed out (see Section 5.4.3) that

$$\Delta\varepsilon_x = \Delta\varepsilon_x^p+\Delta\varepsilon_x^e \qquad (5.26d_o)$$

and

$$\Delta\varepsilon_x^p = (\sqrt{3})\Delta\varepsilon_e^p/2 = (\sqrt{3})(\Delta\varepsilon - \Delta\varepsilon_e^e)/2 \qquad (5.26e_o)$$

It can be seen from fig 5.15 that

$$\Delta\varepsilon_e^e=mn=(\bar{\sigma}-\bar{\sigma}_e)/E=H[\varepsilon_t^n- \varepsilon_{et}^n]/E \qquad (5.A0)$$

The empirical uniaxial tensile stress-strain relation (5.22d) leads to

$$\varepsilon_{et}=[(\bar{\sigma}_e-\sigma_0)/H]^{1/n} \qquad (5.A1)$$

Subsequently it gives

$$\varepsilon_{et}^{n}=(\bar{\sigma}_e-\sigma_0)/H \qquad (5.A2)$$

From fig 5.15 the following expression can be obtained

$$\varepsilon_t=\varepsilon_{et}+bn=\varepsilon_{et}+\Delta\varepsilon \qquad (5.A3)$$

it subsequently leads the incremental effective elastic strain in expression (5.A0) to

$$\Delta\varepsilon_e^{e}=(H/E)\{[(\bar{\sigma}_e-\sigma_0)/H]^{1/n}+\Delta\varepsilon\}^{n}-(\bar{\sigma}_e-\sigma_0)/E \qquad (5.A4)$$

Expression ($5.26e_o$) can therefore be re-expressed as

$$\Delta\varepsilon_x^{p}=(\sqrt{3}/2)\{\Delta\varepsilon-(H/E)\{[(\bar{\sigma}_e-\sigma_0)/H]^{1/n}+\Delta\varepsilon\}^{n}+(\bar{\sigma}_e-\sigma_0)/E\} \qquad (5.26e)$$

After suitable substitution and rearrangement the expression ($5.26d_o$) can be re-written as

$$\Delta\varepsilon_x=(\sqrt{3}/2)\Delta\varepsilon+\{(H/E)[3(1-\nu)/2(1-\nu+\nu^2)^{1/2}-(\sqrt{3}/2)]\{[(\bar{\sigma}_e-\sigma_0)/H]^{1/n}+\Delta\varepsilon\}^{n}\}+\{[3(1-\nu)/2(1-\nu+\nu^2)^{1/2}-(\sqrt{3}/2)](\bar{\sigma}_e-\sigma_0)/E\} \qquad (5.26d)$$

substitution of (5.25d), (5.26e) into (5.26c) gives

$$z[(r_f/R)-1]/(r_f+z)-(1-\nu^2)\bar{\sigma}_e/[E(1-\nu+\nu^2)^{1/2}=(\sqrt{3}/2)\Delta\varepsilon+\{(H/E)[3(1-\nu)/2(1-\nu+\nu^2)^{1/2}-(\sqrt{3}/2)]$$

$$\{[(\bar{\sigma}_e-\sigma_0)/H]^{1/n}+\Delta\varepsilon\}^n\}-\{[3(1-\nu)/2(1-\nu+\nu^2)^{1/2}-(\sqrt{3}/2)]$$

$$(\bar{\sigma}_e-\sigma_0)/E\} \qquad (5.26f)$$

After rearrangement this gives

$$z = r_f[K_1(c_0+\Delta\varepsilon)^n+a_0\Delta\varepsilon+g]/\{f_0-[K_1(c_0+\Delta\varepsilon)^n+a_0\Delta\varepsilon+g]\} \qquad (5.26g)$$

where, $K_1 = (H/E)[3(1-\nu)/2(1-\nu+\nu^2)^{1/2}-(\sqrt{3}/2)]$ (A)

$c_0 = [(\bar{\sigma}_e-\sigma_0)/H]^{1/n}$ (B)

$a_0 = (\sqrt{3})/2$ (C)

$g = [(1-\nu^2)\bar{\sigma}_e]/[E(1-\nu+\nu^2)^{1/2}]$

$-\{[3(1-\nu)/2(1-\nu+\nu^2)^{1/2}-(\sqrt{3}/2)](\bar{\sigma}_e-\sigma_0)/E\}$ (D)

$f_0=(r_f/R)-1$ (E)

In which K_1, c_0, a_0, g and f_0 are constant parameters in bending for a curved plate from r_f to R, at the top roll contact.

Let $u(\Delta\varepsilon)$ be the numerator-function and $w(\Delta\varepsilon)$ be the denominator function of (5.26g). Differentiation of (5.26g), gives :

$$dz/d\Delta\varepsilon = \{[w(\Delta\varepsilon)du(\Delta\varepsilon)/d\Delta\varepsilon] - [u(\Delta\varepsilon)dw(\Delta\varepsilon)]\}/w^2(\Delta\varepsilon) \qquad (5.26h)$$

and rearranging gives the following expression of dz :

$$dz = r_f f_0[nK_1(c_0+\Delta\varepsilon)^{n-1}+a_0]/\{f_0-[K_1(c_0+\Delta\varepsilon)^n+a_0\Delta\varepsilon+g]\}^2 d\Delta\varepsilon \qquad (5.26i)$$

Expressions (5.26g) and (5.26i) relate the distance, Z, from the neutral layer and its corresponding infinitesimal, dz, to the incremental elastoplastic strain, $\Delta\varepsilon$, of the uniaxial tensile test relation and its infinitesimal, $d\Delta\varepsilon$, respectively.

D. Relationship of the local first yield stress, $\bar{\sigma}_e$, in multipass and the distance, Z, from the neutral layer

The preceding pass imposes different degrees of the local work hardening effect in the bendplate beyond $Z=C_i$ (see section 5.4.3). Consequently, the local first yield stress for each layer, is dissimilar and the values of $\bar{\sigma}_e$ is Z dependent.

To relate the internal resistance to the external bending moment about the top roll contact effectively, it is necessary to express $\bar{\sigma}_e$ in terms of Z. Since the local $\bar{\sigma}_e$ is the effective value from its previous pass just before unloading, it can be evaluated as follows.

Equation (5.20c) and expressions (A), (B) gives :

$$z/R_{1st} = (E/H)K_1\Delta\varepsilon_1^{n} + (\sqrt{3})\Delta\varepsilon_1/2 + (1-\nu^2)\sigma_0/E(1-\nu+\nu^2)^{1/2} \qquad (5.20c)$$

where, R_{1st} is the bend radius in the preceding pass before the release of the applied load.

$\Delta\varepsilon_1$ is the corresponding equivalent local incremental strain in the preceding pass.

The empirical uniaxial tensile stress-strain relation beyond yield is expressed (Chapter Six) as

$$\bar{\sigma}_e = \sigma_0 + H\Delta\varepsilon_1^n \qquad (5.27a)$$

Suitably altering the incremental strain as a dependent variable gives :

$$\Delta\varepsilon_1 = [(\bar{\sigma}_e-\sigma_0)/H]^{1/n} \qquad (5.27b)$$

Substituting the relevant terms into (5.20c) and rearrangement gives :

$$z/R_{1st} = K_1(\bar{\sigma}_e-\sigma_0)/H + (\sqrt{3}/2)[(\bar{\sigma}_e-\sigma_0)/H]^{1/n} + (1-\nu^2)\sigma_0/E(1-\nu+\nu^2)^{1/n} \qquad (5.27c)$$

The second term on the left hand side of (5.27c) complicates the mathematical analysis. To ease the analytical approach, it can be assumed either (i) $\bar{\sigma}_e$ has a constant value or (ii) takes a mean value of $\bar{\sigma}_e$ for the elastoplastic deformation zone. On the basis that (ii) is the more reasonable assumption for the analysis, the following illustrates the approach to determine the value of $\bar{\sigma}_e$.

(a) Assume a value of Z and by iteration to obtain the corresponding value of $\Delta\varepsilon_1$ for the particular bend radius of R_{1st} using equation (5.20c).

(b) Substitute the determined value of $\Delta\varepsilon_1$ into equation (5.27a) to obtain the corresponding value of $\bar{\sigma}_e$.

(c) Use steps (a) and (b) to evaluate other values at $Z+\Delta Z$ and

so on for Z between Z_0 and Z_n (corresponding to c_{io} and h respectively).

(d) Determine the mean value, $\bar{\sigma}_{em}$, of $\bar{\sigma}_{e,i}$ using

$$\bar{\sigma}_{em} = \{\sum_{i=1}^{n} (\bar{\sigma}_{e,i}+\bar{\sigma}_{e,i-1})(z_i-z_{i-1})\}/2(z_n-z_0) \qquad (5.27d)$$

for $Z_n > Z_0$.

5.4.5.2. Determination of the internal bending resistance to the external bending moment

It has been indicated in section 5.4.3 that the internal bending resistance to the external bending moment about the top roll contact can be evaluated using the following expression.

$$M_i = b[\int_{elastic} \sigma_x z dz + \int_{elastoplastic} \sigma_x z dz] \qquad (5.28a)$$

Depending upon the bend radius, the elastic non-work hardened region may consist of (i) the initially elastic deformation core during the first or preceding pass and (ii) the work hardened elastic deformation layers on either side of the non-work hardened core (i).

For elastic deformation, the longitudinal bending stress can be evaluated using the following expression [142].

$$\sigma_x = Ez[(r_f/R)-1]/(r_f+z) \qquad (5.28b)$$

Substituting for the stress in the integral of the elastic deformation term in the equation (5.28a) gives

$$A_1 = 2\int_0^{c_{i0}} \{Ez[(r_f/R)-1]/(r_f+z)\}zdz = 2E[(r_f/R)-1]\int_0^{c_{i0}} [z^2/(r_f+z)]dz \qquad (5.28c)$$

The general integration of $A_{10}=\int_0^{c_{i0}}[z^2/(r_f+z)]dz$ can be performed by dividing its numerator by its denominator to give

$$A_{10} = \int_0^{c_{i0}}[z-r_f+r_f^2/(r_f+z)]dz$$

Completed integration, over the limits 0 and c_{i0}, gives

$$A_{10} = c_{i0}^2/2 - r_f c_{i0} + r_f^2 \ln[(r_f+c_{i0})/r_f] \qquad (5.28d)$$

Subsequently, (5.28c) becomes

$$A_1 = 2E[(r_f/R)-1]\{c_{i0}^2/2 - r_f c_{i0} + r_f^2 \ln[(r_f+c_{i0})/r_f]\} \qquad (5.28e)$$

where,

$$c_{i0}=r_f(1-v^2)\bar{\sigma}_e/\{E[(r_f/R)-1](1-v+v^2)^{1/2} - (1-v^2)\bar{\sigma}_e\} \qquad (5.28f)$$

The integral term for the elastoplastic deformation, i.e.

$$\int_{\text{elastoplastic}} \sigma_x z dz, \qquad (5.28g)$$

can be performed through the substitution of (5.26g) and (5.26i), together with the appropriate relation of σ_x and $\Delta\varepsilon$, substituted into this expression.

In section 5.4.3, it has been shown that the equivalent stress condition, assuming plane strain, allows the relation of the longitudinal stress, σ_x, and the equivalent uniaxial tensile stress, $\bar{\sigma}$, to be expressed as :

$$\sigma_x = (2/\sqrt{3})\bar{\sigma} \qquad (5.28h)$$

As mentioned in the sub-section 5.4.4.1, the empirical stress strain relation for the test has the following form :

$$\bar{\sigma} = \bar{\sigma}_e + H\Delta\varepsilon^n \qquad (5.28i)$$

The replacement of $\bar{\sigma}$ in (5.28h) by (5.28i) gives :

$$\sigma_x = (2/\sqrt{3})(\bar{\sigma}_e + H\Delta\varepsilon^n) \qquad (5.28j)$$

Subsequently,

$$A_2 = \int_{\text{elastoplastic}} \sigma_x z dz = 2\int_{c_{i0}}^{h} (2/\sqrt{3})(\bar{\sigma}_e + H\Delta\varepsilon^n) z dz \qquad (5.28k)$$

The substitution for z and dz in terms of the corresponding incremental function gives

$$A_2 = (4/\sqrt{3}) r_f^2 \int_0^{\Delta\varepsilon_2} \{(\bar{\sigma}_e + H\Delta\varepsilon^n) f_0 (K_1(c_0+\Delta\varepsilon)^n + a_0\Delta\varepsilon + g)$$

$$[nK_1(c_0+\Delta\varepsilon)^{n-1} + a_0] / \{f_0 - [K_1(c_0+\Delta\varepsilon)^n + a_0\Delta\varepsilon + g]\}^3\} d\Delta\varepsilon \qquad (5.29a)$$

Integrating (5.29a), successively using the combined methods of (i) integration by reduction, (ii) integration by part, (iii) integration by substitution, i.e. with $\sin^2 D = [K_1(c_0+\Delta\varepsilon)^n + a_0\Delta\varepsilon + g]$, gives

$$A_2 = (r_f^2/a_0)\left\{\left([\sigma_0 + H(c_0+\Delta\varepsilon_2)^n]([K_1(c_0+\Delta\varepsilon_2)^n + a_0\Delta\varepsilon_2 + g]/\right.\right.$$

$$\{f_0 - [K_1(c_0+\Delta\varepsilon_2)^n + a_0\Delta\varepsilon_2 + g]\})^2 - (\sigma_0 + Hc_0^n)[K_1 c_0^n + g/(f_0 - K_1 c_0^n - g)]^2\Big)$$

$$-(Hf_0/K_1)\left\{\left([K_1(c_0+\Delta\varepsilon_2)^n + a_0\Delta\varepsilon_2 + g]/\{f_0 - [K_1(c_0+\Delta\varepsilon_2)^n + a_0\Delta\varepsilon_2 + g]\}\right.\right.$$

$$\left.\left. - [K_1 c_0^n + g/(f_0 - K_1 c_0^n - g)]\right) + 2\ln\left(\{1 - [K_1(c_0+\Delta\varepsilon_2)^n + a_0\Delta\varepsilon_2 + g]/f_0\}/\right.\right.$$

$$\left.\left.[1 - (K_1 c_0^n + g)/f_0]\right) + \left([K_1(c_0+\Delta\varepsilon_2)^n + a_0\Delta\varepsilon_2 - K_1 c_0^n]/f_0\right) - (a_0/f_0)\int_0^{\Delta\varepsilon_2}$$

$$\left[\left(\left[K_1(c_0+\Delta\varepsilon)^n+a_0\Delta\varepsilon+g\right]/\left\{f_0-\left[K_1(c_0+\Delta\varepsilon)^n+a_0\Delta\varepsilon+g\right]\right\}\right)^2 d\Delta\varepsilon\right]\Big\}\Big\} \qquad (5.29b)$$

where $\Delta\varepsilon_2$ is the upper limit of the integral for the second and subsequent pass bending operation.

The integral term remaining in (5.29b) is difficult to solve analytically. However, a numerical solution is possible.

For convenience the expression (5.28a) relating the internal bending resistance, M_i, to the external effort about the top roll contact, is restated as follows :

$$M_i = b(A_1+A_2) \qquad (5.29c)$$

5.4.6. Further theoretical analysis on the mechanics of four-roll thin plate bending process

Subsequent mathematical modelling for the mechanics of this process is presented in Appendix 5.1.

In Appendix 5.1 the derivation of the general mathematical expressions is presented for :

(i) the bending force on the rollers,

(ii) the driving torque in conveying the bendplate in continuous bending mode,

and

(iii) the power required for bending the plate in continuous bending mode,

both for single and multipass bending mode However, this section serves to describe briefly the approach of the analysis.

The mathematical modelling was derived by considering the force and moment equilibrium at any particular operating condition and the energy required to continue the deformation in the deformation zone and in the progression of the springback deformation zone (refer to fig 5.17 to fig 5.27).

The approach can be generalised as follows :

(a) To define the co-ordinates of the roller nominal contacts with the bendplate, with reference to figs 5.17, 5.22 and 5.23.

(b) To derive the bending force expressions on the rollers by considering the internal and external moment equilibrium about the top roll nominal contact (with reference to fig. 5.18 and 5.19), and force equilibrium.

(c) To obtain the mathematical expressions for the geometrical constraint of the roller bender (with reference to fig. 5.3, 5.5 and 5.13B).

(d) To obtain the general deflection functions, $W(X)$, of a plate in the bender, for both single and multipass bending modes utilising the biharmonic plate equations for (i) an initially flat plate [108] and (ii) an initially curved plate [104,108].

(e) To derive mathematical expressions for the top roll driving torque and the power required for the continuous bending mode by energy consideration (with reference to fig. 5.3, 5.4, 5.18, 5.19, and 5.20 to 5.27).

The mathematical expressions derived by the above considerations are left in terms of :

(1) the respective unknown co-ordinates of the nominal contacts between the bendplate and the rollers, and

(2) the unknown parametric functions of **a**, **b**, **c** and **d** in the

respective deflection function.

Solution for a specific mode of bending requires firstly the quantification of the above unknowns. Relations to establish them with the known and anticipated geometrical parameters of the bender and bent plate, respectively, are thus derived by

(A) establishing the positional equations of the rollers, in the bender co-ordinate system, during bending,
(B) obtaining the first derivative of the positional equations in (A),
(C) anticipating the geometrical boundary conditions,
(D) relating the unknown parametric functions, **a**, **b**, **c** and **d** to the equations obtained in (A), (B) and (C), and finally,
(E) further establishing the particular mathematical relations among the nominal contact co-ordinate quantities by the remaining anticipated boundary conditions in (C).

The complete solution of the derived equations, in Appendix 5.1, demands the appropriate values for the nominal contacts in (E) to be firstly iterated. Owing to their multi-variable non-linearity, the iterative technique requires special attention and a sophisticated computer algorithm. Consequently, theoretical predictions at the present stage only concentrate on the results for solving the model in sections 5.4.3 to 5.4.5.

5.5. Theoretical prediction

As a result of the present research, a mathematical model to predict the *mechanics of four-roll thin plate bending has* been evolved. However, computation was only performed to predict

(i) the plate internal resistance to external bending moment about the top roll contact,
(ii) the local bend radius at the top roll contact,
(iii) the distance, from plate central (neutral) plane, of

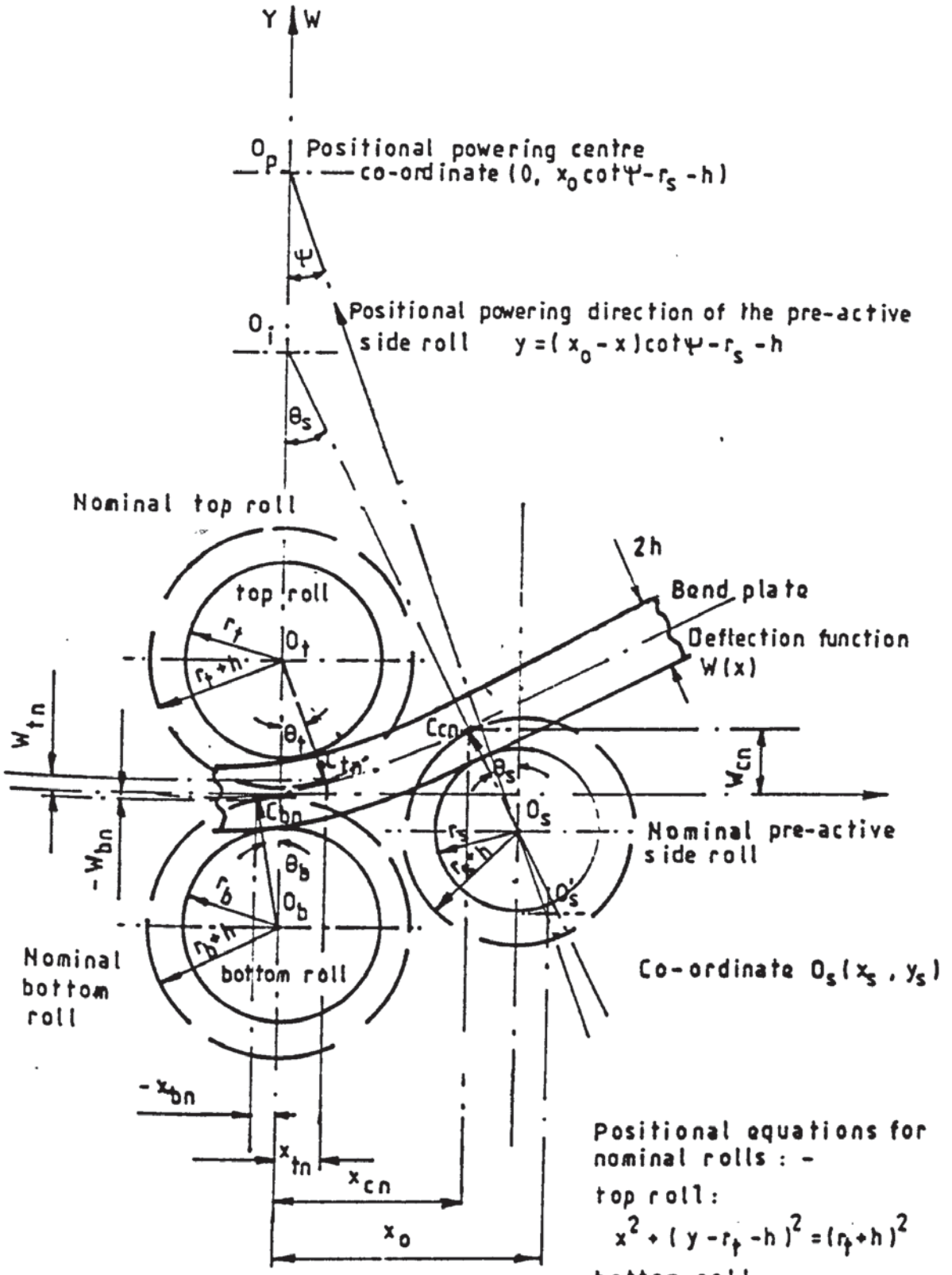

FIG 5.17 MODEL BENDER GEOMETRY FOR SINGLE/FIRST PASS PRE-BENDING MODE

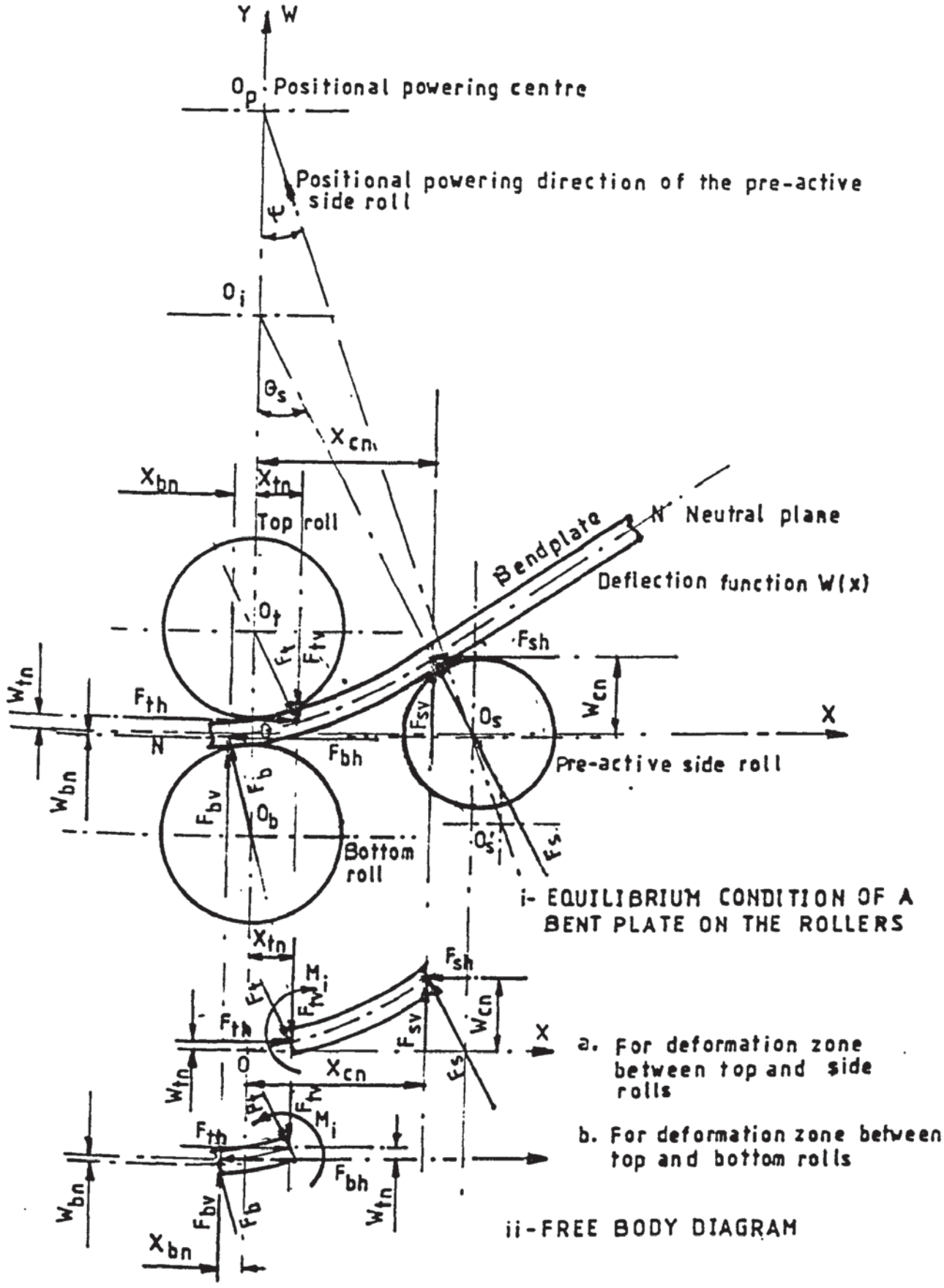

FIG 5.18 LOADING CONDITION WITH PRE-ACTIVE SIDE ROLL OPERATIVE

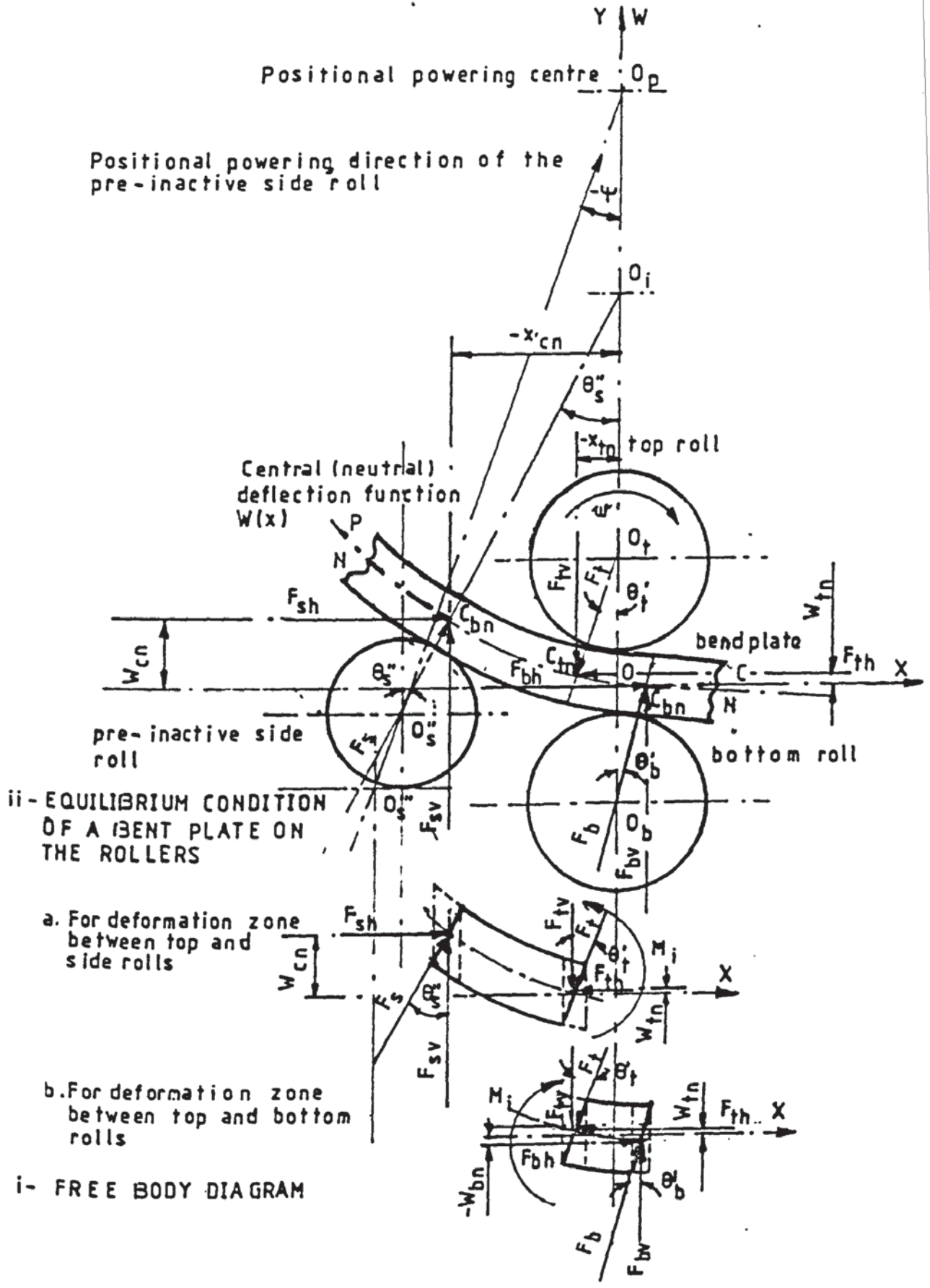

FIG 5.19 LOADING CONDITION WITH PRE - INACTIVE SIDE ROLL OPERATIVE

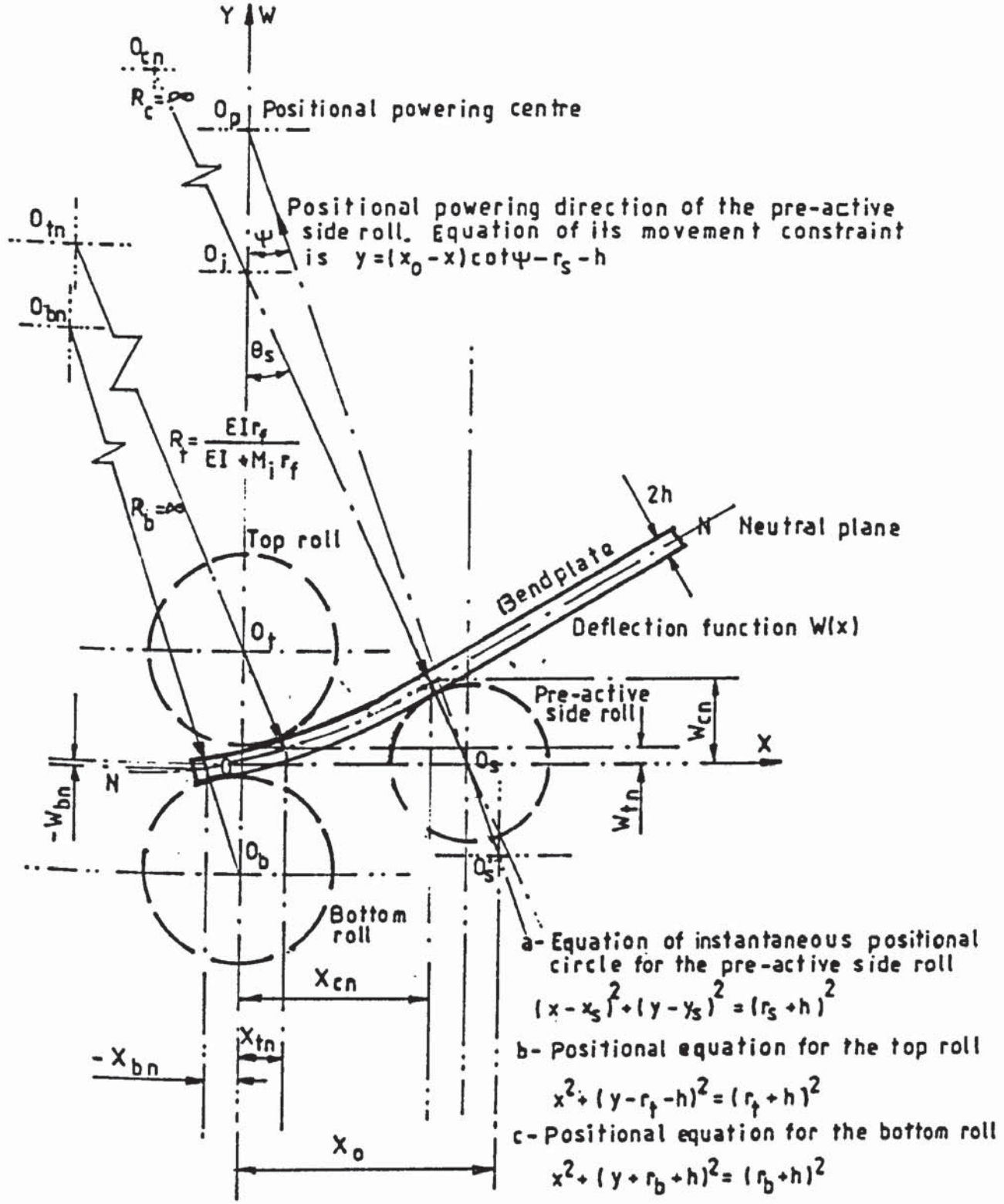

FIG 5.20 GEOMETRICAL CONDITIONS FOR SINGLE/FIRST PASS PRE-BENDING MODE AND AT THE INITIATION OF THE CONTINUOUS BENDING MODE

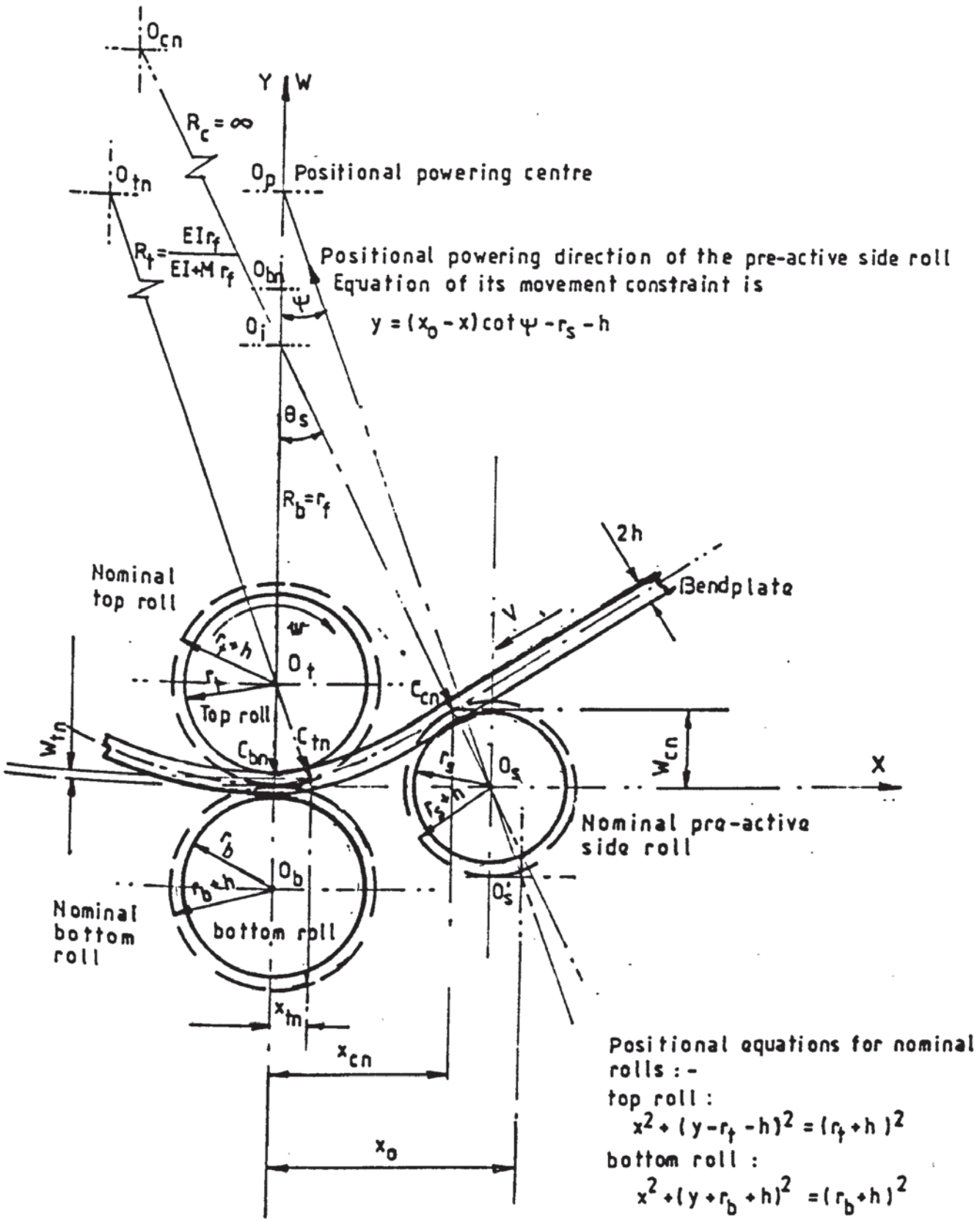

Positional equations for nominal rolls :-

top roll :

$$x^2 + (y - r_t - h)^2 = (r_t + h)^2$$

bottom roll :

$$x^2 + (y + r_b + h)^2 = (r_b + h)^2$$

pre-active side roll :

$$(x - x_s)^2 + (y - y_s)^2 = (r_s + h)^2$$

FIG 5.21 GEOMETRICAL CONDITION FOR SINGLE/FIRST PASS STEADY CONTINUOUS BENDING MODE WITH THE PRE-ACTIVE SIDE ROLL OPERATING

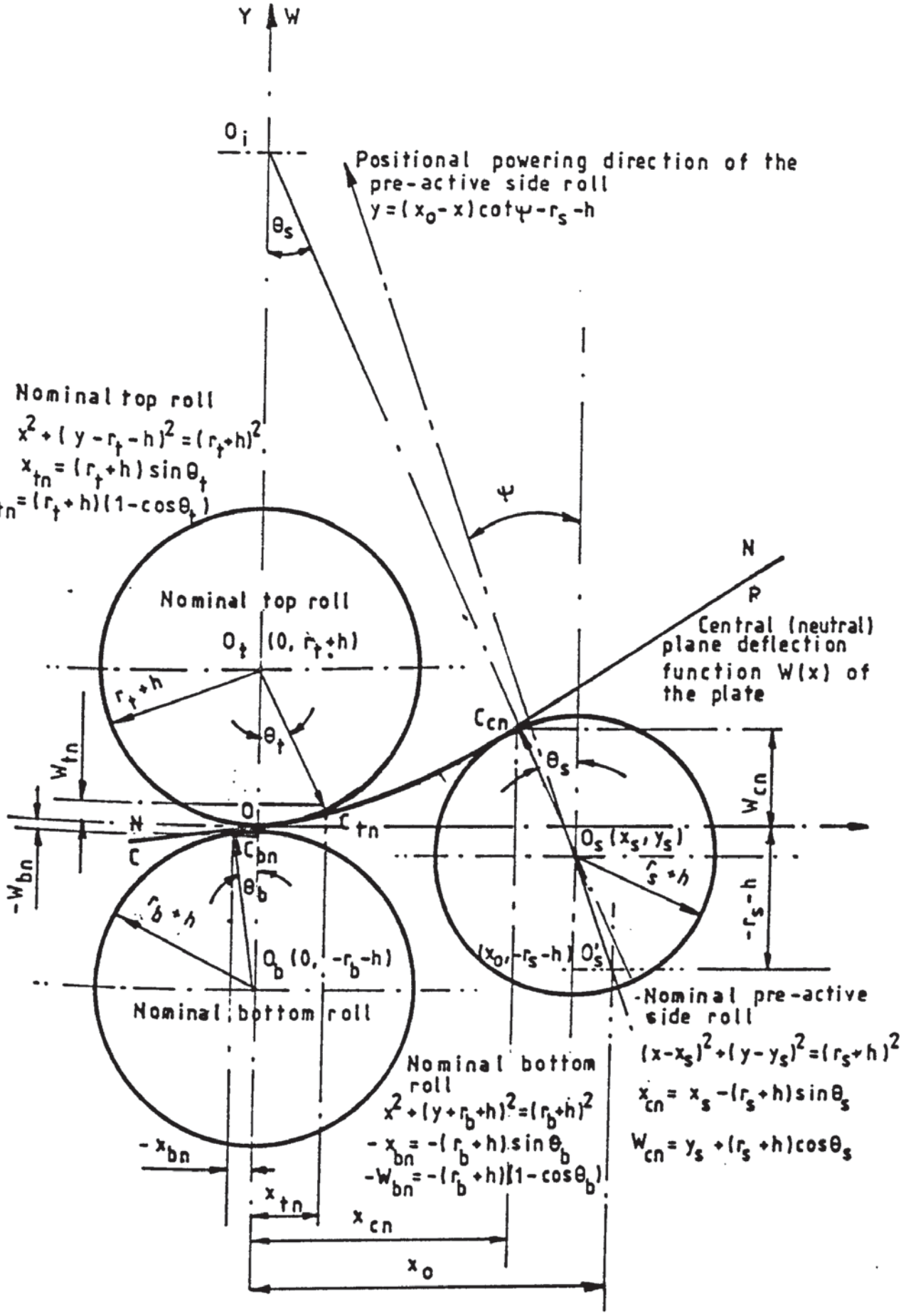

FIG 5.22 NOMINAL CONTACTS OF ROLLERS WITH CENTRAL PLANE OF A BEND PLATE DURING BENDING

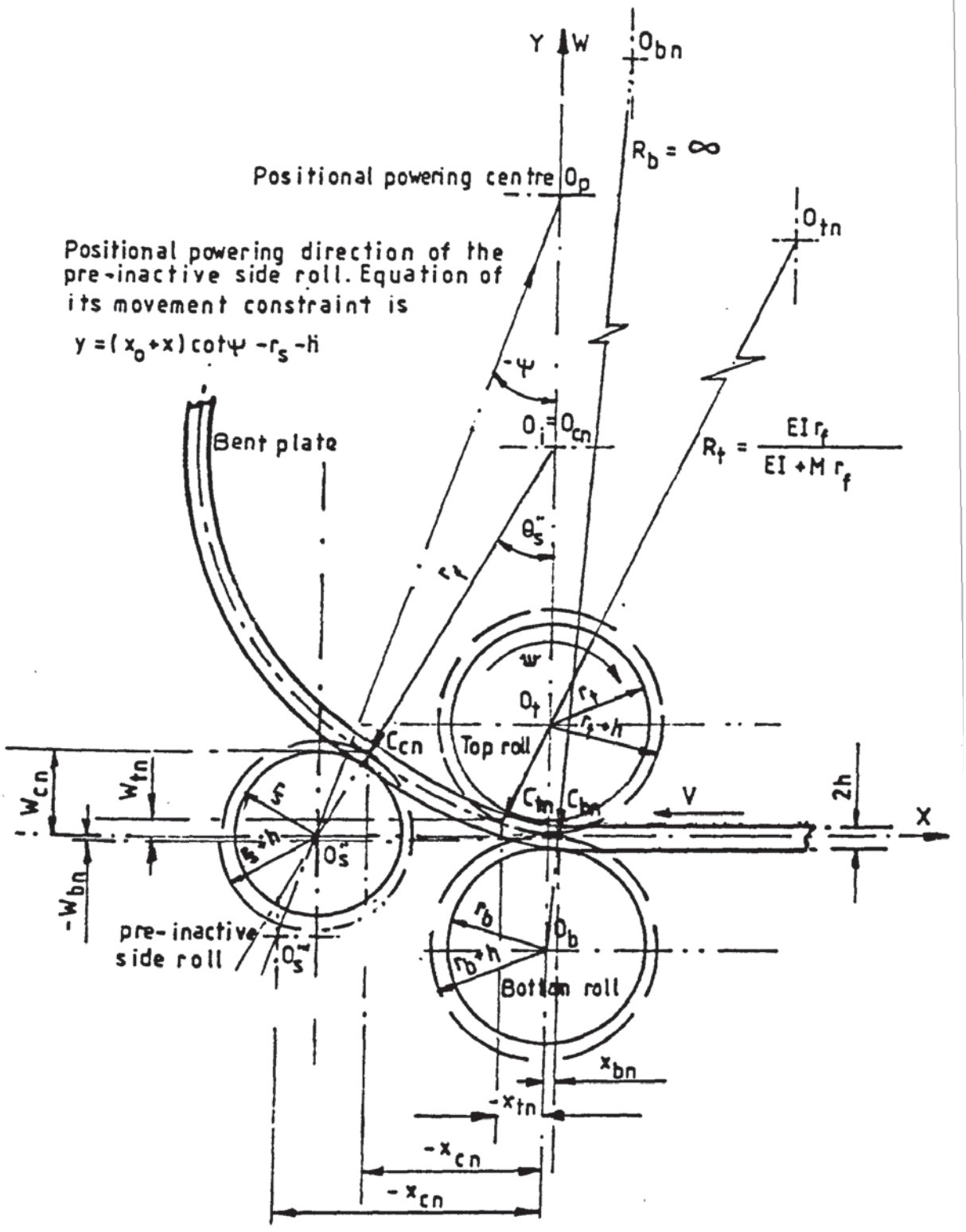

Positional equations for nominal rolls :-

top roll $\quad x^2 + (y - r_t - h)^2 = (r_t + h)^2$

Bottom roll $\quad x^2 + (y + r_b + h)^2 = (r_b + h)^2$

Pre-inactive side roll $\quad (x - x_s)^2 + (y - y_s)^2 = (r_s + h)^2$

FIG 5.23 GEOMETRICAL CONDITION FOR SINGLE/FIRST PASS STEADY CONTINUOUS BENDING MODE WITH THE PRE-INACTIVE SIDE ROLL OPERATING

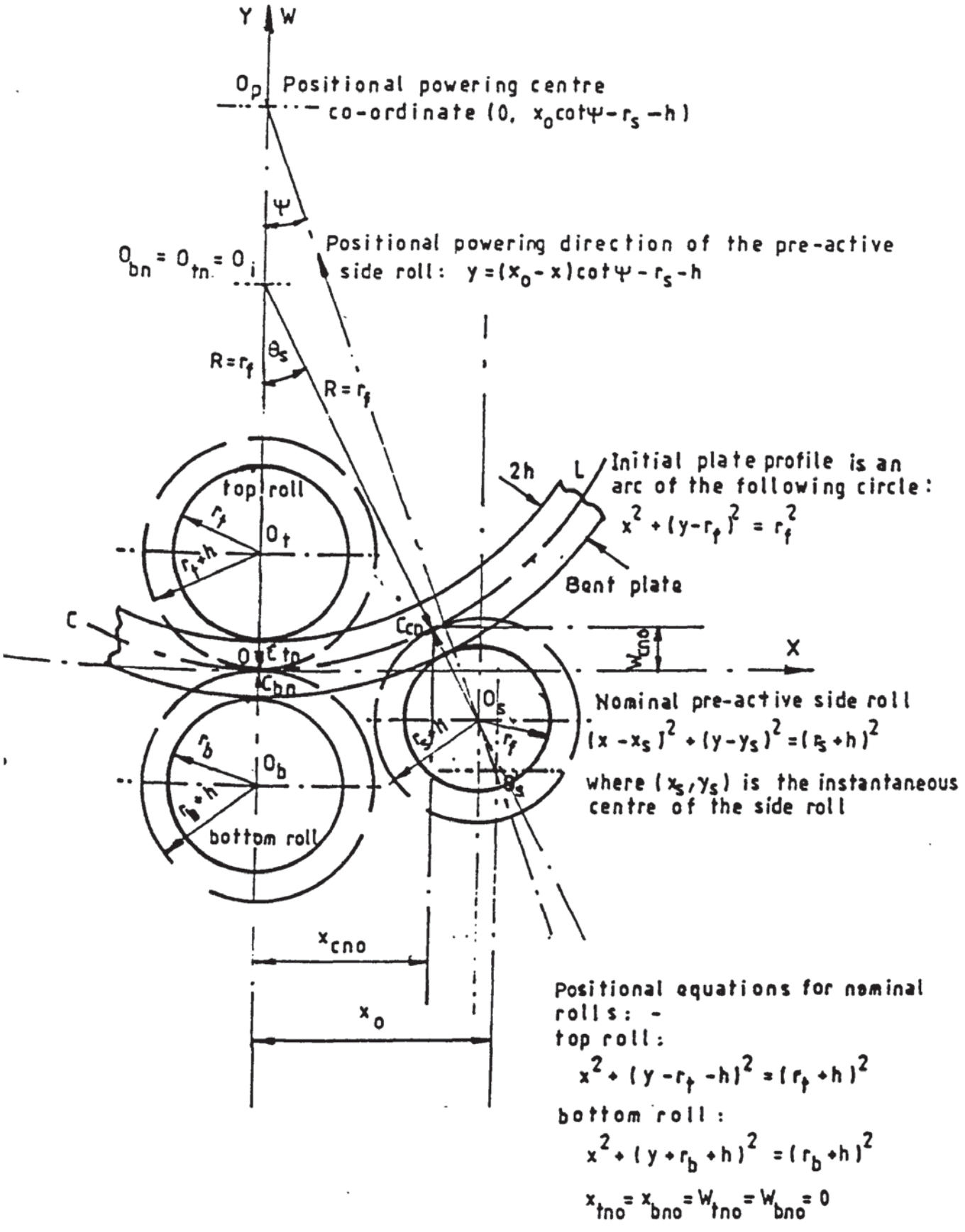

FIG 5.24 INITIAL OPERATIVE SIDE ROLL CONTACT GEOMETRY BEFORE SECOND/SUBSEQUENT PRE-BENDING PASS

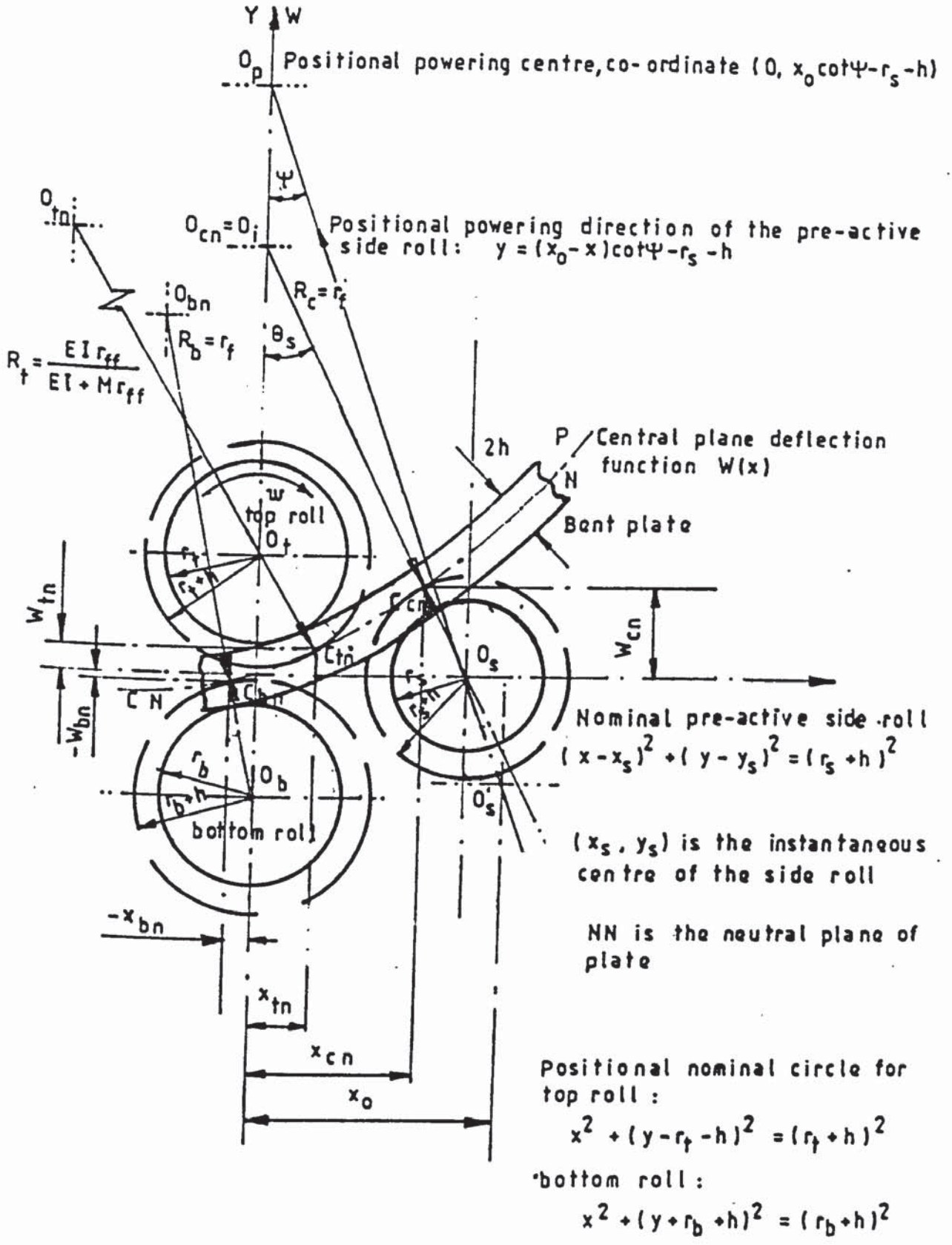

FIG 5.25 GEOMETRICAL CONDITIONS FOR EITHER MULTIPASS PRE-BENDING OR AT THE INITIATION OF CONTINUOUS BENDING FOR THE PRE-ACTIVE SIDE ROLL OPERATIVE MODE

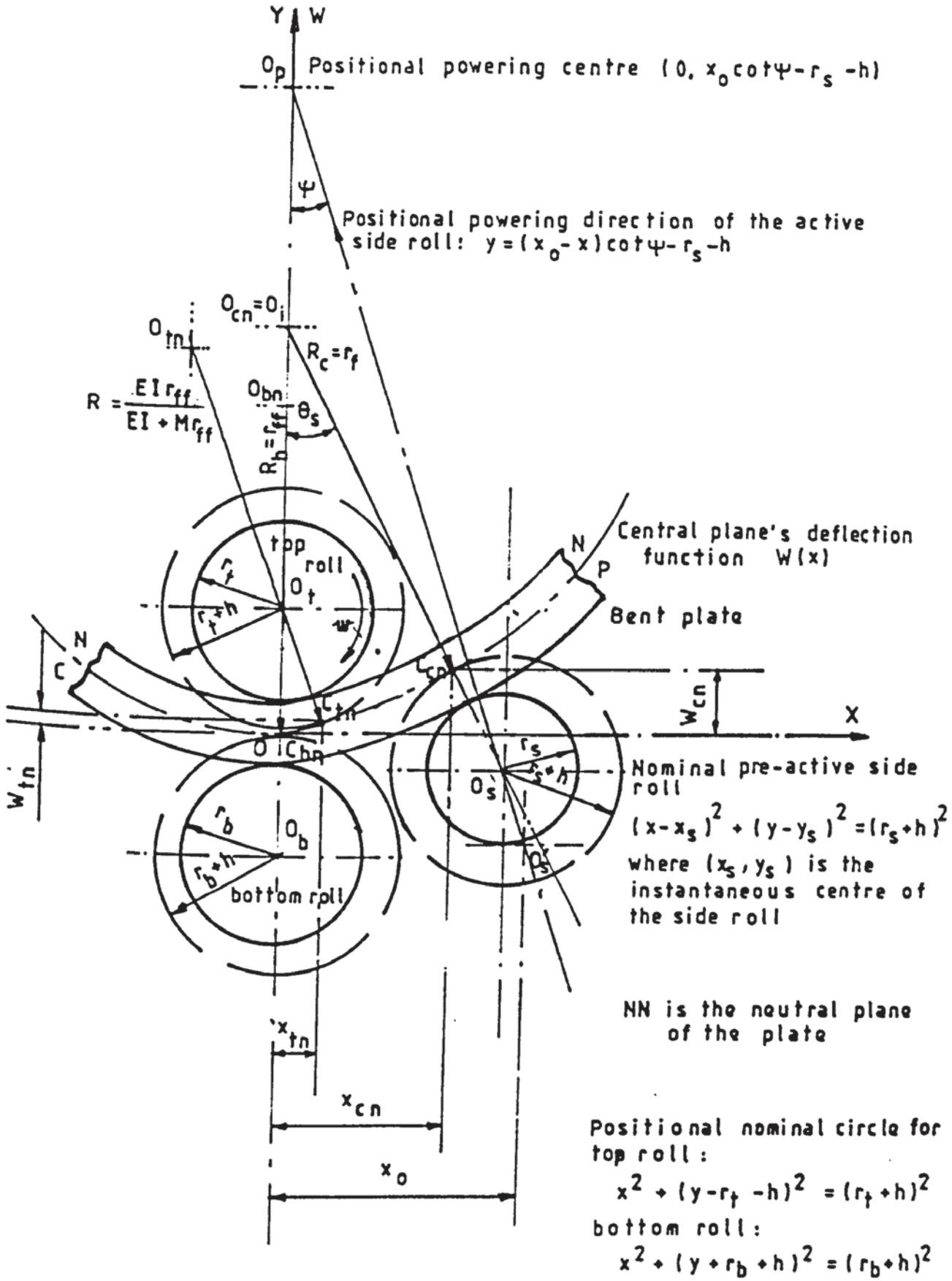

FIG 5.26 MULTIPASS STEADY-CONTINUOUS BENDING MODE GEOMETRY WITH THE PRE-ACTIVE SIDE ROLL OPERATING

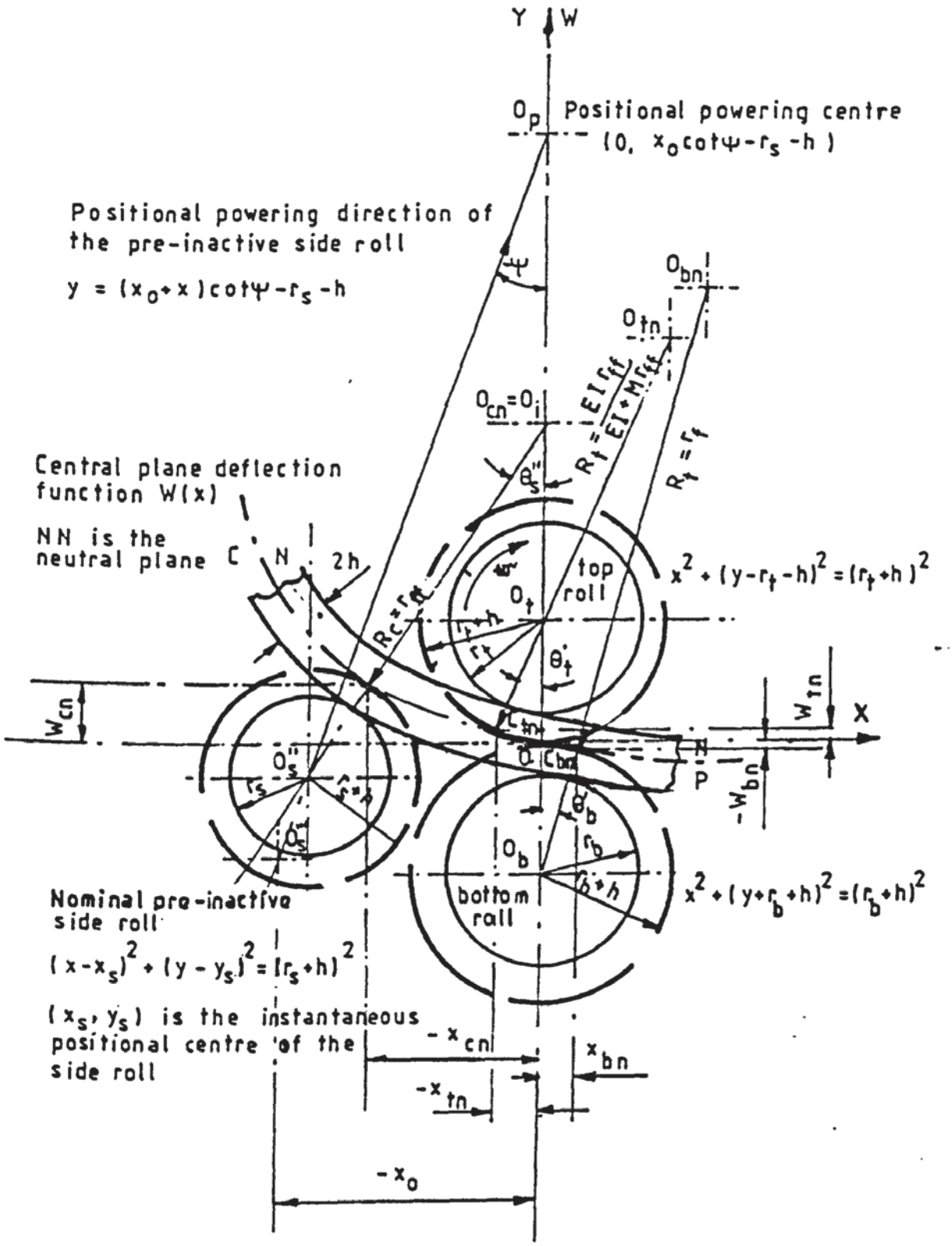

FIG 5.27 MULTIPASS STEADY-CONTINUOUS BENDING MODE GEOMETRY WITH THE PRE-INACTIVE SIDE ROLL OPERATING

the elastic-elastoplastic interface at the top roll contact,

and

(iv) the relative springback curvature from the local bend radius at top roll contact to the finished plate bent radius.

All the aforementioned results are relative to an anticipated finished bend radius. The predictions were conducted for both single and multipass bending modes (see Sections 5.4.3 to 5.4.5).

5.5.1 Computer programmes

To accomplish the theoretical predictions, appropriate expressions in sections (5.4.3.1) to (5.4.5.2) were put into two separate programmes : one for the single pass bending mode and another for the multipass bending mode.

The programmes were written in BASIC language for the Hewlett Packard microcomputer. The programme listings are shown in Appendix 5.2.

The iterative technique used in the programmes is the combination of

(i) the conventional step progressive iteration

and

(ii) the modified bisection iteration.

The following describes briefly the computation procedure in each programme.

5.5.1.1. Computer programme for single pass bending mode

The application of the adopted iterative technique in this programme can be identified as follows :

(a) To determine the maximum bend radius, a_0, at the top roll

nominal contact using expression (5.7b).

(b) To initiate the upper limit for the value of local bend radius, R, at the top roll contact

-if the anticipated finished bend radius, r_f, is smaller than a_0, R in expression (5.20c) is assumed to be r_f, otherwise R is taken as $0.99a_0$.

(c) To iterate for the value of $\Delta\varepsilon_1$ in expression (5.20c) with $z=h$ using the adopted iterative technique.

(d) To determine the value of B in expression (5.23d) with the already iterated value of $\Delta\varepsilon_1$ from (c) and the particular value of R.

(e) To estimate the plate internal resistance, M_i, to the external bending moment about the top roll contact using expressions (5.23d) and (5.24).

(f) To check whether the determined value of M_i satisfies the following condition

$$1/r_f+M_i/EI-1/R=0 \qquad (5.29d)$$

(g) To check whether the absolute magnitude on the left hand side of the expression (5.29d) is within a specified iterative tolerance, Tol, if the condition in (5.29d) is not satisfied.

(h) To repeat (c), (d), (f) and (g) with a large step decrement in R [if neither condition in (f) nor (g) is satisfied and the left hand side in expression (5.29d) is negative] until the left hand side in (5.29d) gives a positive value. Thereafter (h) is replaced by (i) in the subsequent iteration for the particular iterative loop.

(i) To bisect the value of R with the previously stored value of R, which was given a negative or a positive value on

the left hand side of (5.29d), and the latest value of R which gives a positive or negative value on the left hand side of (5.29d).

(j) To repeat (c), (d), (f) and (g) with the new value of R obtained in (i) until either condition in (f) or (g) is satisfied.

-The latest iterated values of R and $\Delta\varepsilon_1$ are taken as the solution of (5.20c). The corresponding calculated values of M_i and M_f/EI are taken as the estimated internal resistance and the spring back curvature.

(k) To compute the distance of elastic-elastoplastic interface from plate central plane using expression (5.18c).

(l) To repeat the procedure (c) to (k) if computation for other values of r_f are expected for the same bendplate.

-the continuation of the programmes requires that the new r_f is smaller than its previous value. In this case the upper limit of R as in (b) is updated by the value obtained by (i). For r_f larger than that of the previous one, restarting the programme is necessary.

5.5.1.2. Computer programme for multipass bending mode

The first pass in this programme was written almost exactly similarly to the procedures (a) to (k) in the programme for the single pass bending mode. Additional procedures for the second and subsequent pass bending programme are as follows :

(l) To evaluate the subsequent first yield stresses, $\bar{\sigma}_e$, for respective fibre layers in the elastoplastic deformation band, using expressions (5.20c) and (5.27a), and then estimate the corresponding mean yield stress, $\bar{\sigma}_{em}$, using expression (5.27d).

(m) To evaluate the local bend radius, r_0, which commences the first yield on the outer plate surface, using (5.25j).

(n) To initiate the upper limit of R for iteration.

-If the anticipated finished bend radius, r_{ff}, is less than r_0, R is assumed to be r_{ff}, otherwise R is taken as $0.99r_0$.

(o) To iterate for the corresponding value of $\Delta\varepsilon$ (i.e. for $\Delta\varepsilon_2$) in expression (5.26g), at the given R and $z=h$, using firstly the step decrement iteration and then the modified bisection iteration.

(p) To determine the respective distance z of the elastic-elastoplastic interface, c_{i0}, from the plate central plane using expression (5.28f).

(q) To compute A_1 in expression (5.28e) with $\bar{\sigma}_e=\bar{\sigma}_{em}$.

(r) To integrate numerically the integral term in (5.29b) using Simpson's method and the iterated value of $\Delta\varepsilon_2$ from (o) above.

(s) To compute the plate internal bending moment resistance, M_i, in expression (5.29c).

(t) To check whether the evaluated M_i satisfies the following condition

$$1/r_{ff}+M_i/EI-1/R=0 \qquad (5.29e)$$

(u) To check whether the absolute magnitude in the left hand side of the expression (5.29e) is within a specified iterative tolerance, Tol, if the condition in (5.29e) is not satisfied.

(v) To repeat (o) to (u) with a large step decrement in R [if neither condition in (t) nor (u) is satisfied and the left hand side in expression (5.29e) is negative] until the left hand side in (5.29e) gives a positive value. Thereafter (v) is replaced by (w) in the subsequent

iteration for the particular iterative loop.

(w) To bisect the value of R with the previously stored value of R, which was given a negative or positive value on the left hand side of (5.29e), and the latest value of R which gives a positive or negative value on the left hand side of (5.29e).

(x) To repeat (o) to (u) with the new value of R obtained in (w) until either condition in (t) or (u) is satisfied. -The latest iterated values of R and $\Delta\varepsilon_2$ are taken as the solution of (5.26f). The corresponding calculated values of M_i and M_i/EI are taken as the estimated internal resistance and the springback curvature.

(y) To compute the distance of elastic-elastoplastic interface, c_{i0}, from the plate central plane, corresponding to the iterated R using expression (5.28f).

(z_0) To evaluate the new mean yield stress in the elastoplastic deformation band.

(z) Firstly to replace the value of r_f by r_{ff} and repeat procedures (m) to (Z_0), and then repeat the procedures (n) to (z) if a further bending pass is expected.

5.5.2. Numerical prediction and graphical results

Numerical prediction was conducted for the HP30 aluminium plates (See Section 5.5) with the value for Poisson's ratio, ν, taken as 0.34.

5.5.2.1. Single pass bending mode

Computative prediction for bending HP30 aluminium plate specimens of thicknesses : 8.1 mm, 10.2 mm, 12.07 mm and 14.67 mm by widths : 80.5 mm, 120 mm and 214 mm (with the respective mechanical properties determined by uniaxial tensile test as described in Chapter six) to accomplish finished bend radii between 2500 mm and 40 mm were performed. The obtained graphical results are shown in figs 5.28 to 5.31.

The respective maximum local bend radius, at the top roll contact, as plastic deformation just occurs on the plate outer fibre layers are listed in Table 5.1.

5.5.2.2. Multipass bending mode

At least five sets of computative results for bending HP30 aluminium plate specimens of 8.1mm thick by 80.5 mm wide to successive finished bend radii in range of 2700 mm to 500 mm were performed. Each set of the results constituted more than two successive passes. Details of the relevant number of passes and the magnitude of the successive pass anticipated bend radius in each pass are listed in Table 5.2. The relevant graphical results are shown in figs 5.32 to 5.36 for studying the successive finished bend radius effect in the multipass bending mode.

Additional prediction to bend three HP30 aluminium plate specimens : 8.1 mm thick by 80.5 mm wide, 10.2 mm thick by 80.5 mm wide, and 12.07 mm thick by 80.5 mm wide HP30, were also carried out. The successive finished bend radius for each pass in the prediction ranged between 2500 mm and 500 mm in step decrement of 400 mm. The prediction assumed that the plate condition was initially flat. Its results were then plotted in figs 5.37 to 5.41 for comparing the thickness effect in the multipass bending mode.

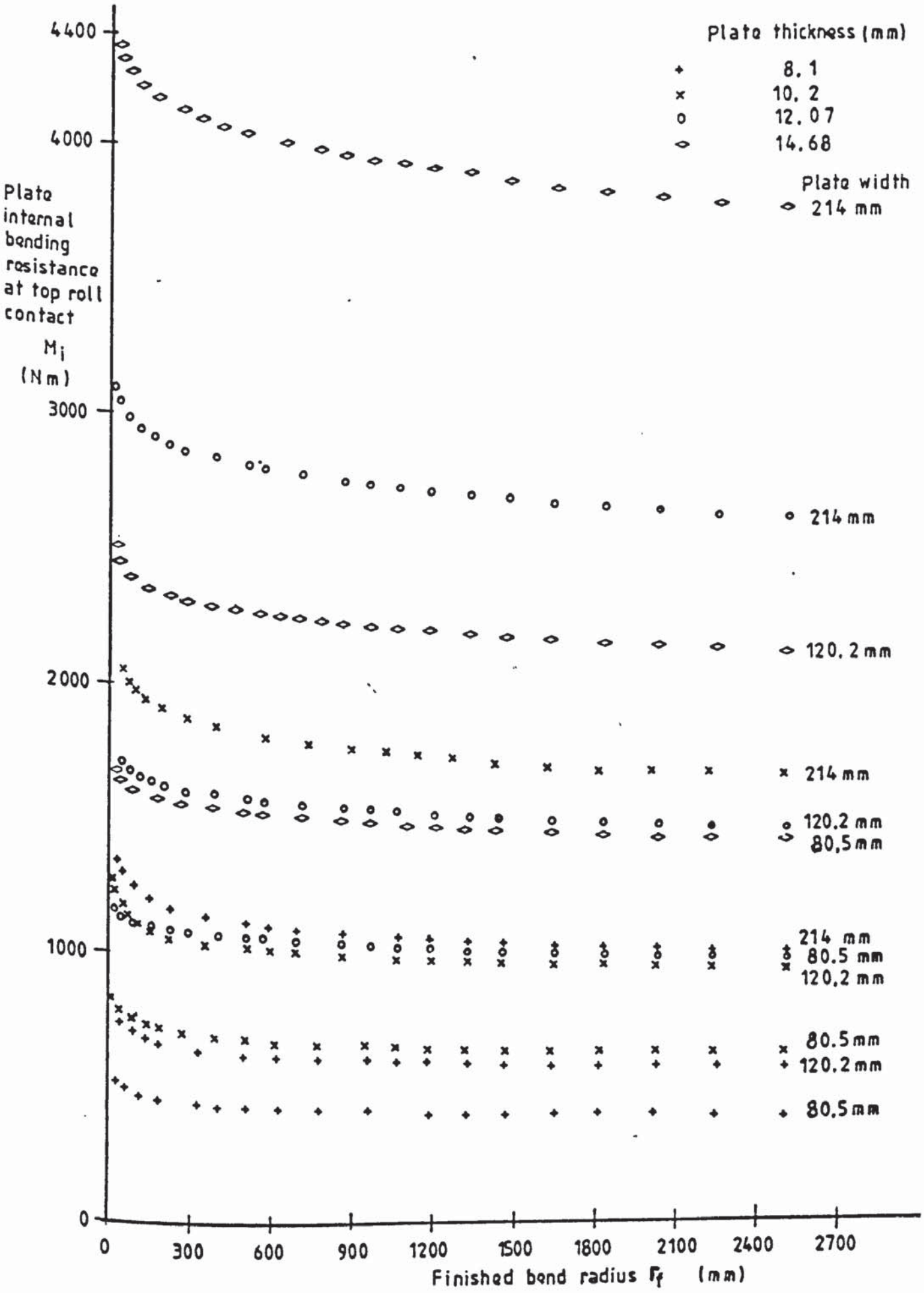

FIG 5.28 THEORETICAL PREDICTION FOR PLATE INTERNAL BENDING RESISTANCE AT TOP ROLL CONTACT (SINGLE/FIRST PASS BENDING OF FLAT HP30 ALUMINIUM PLATE SPECIMENS)

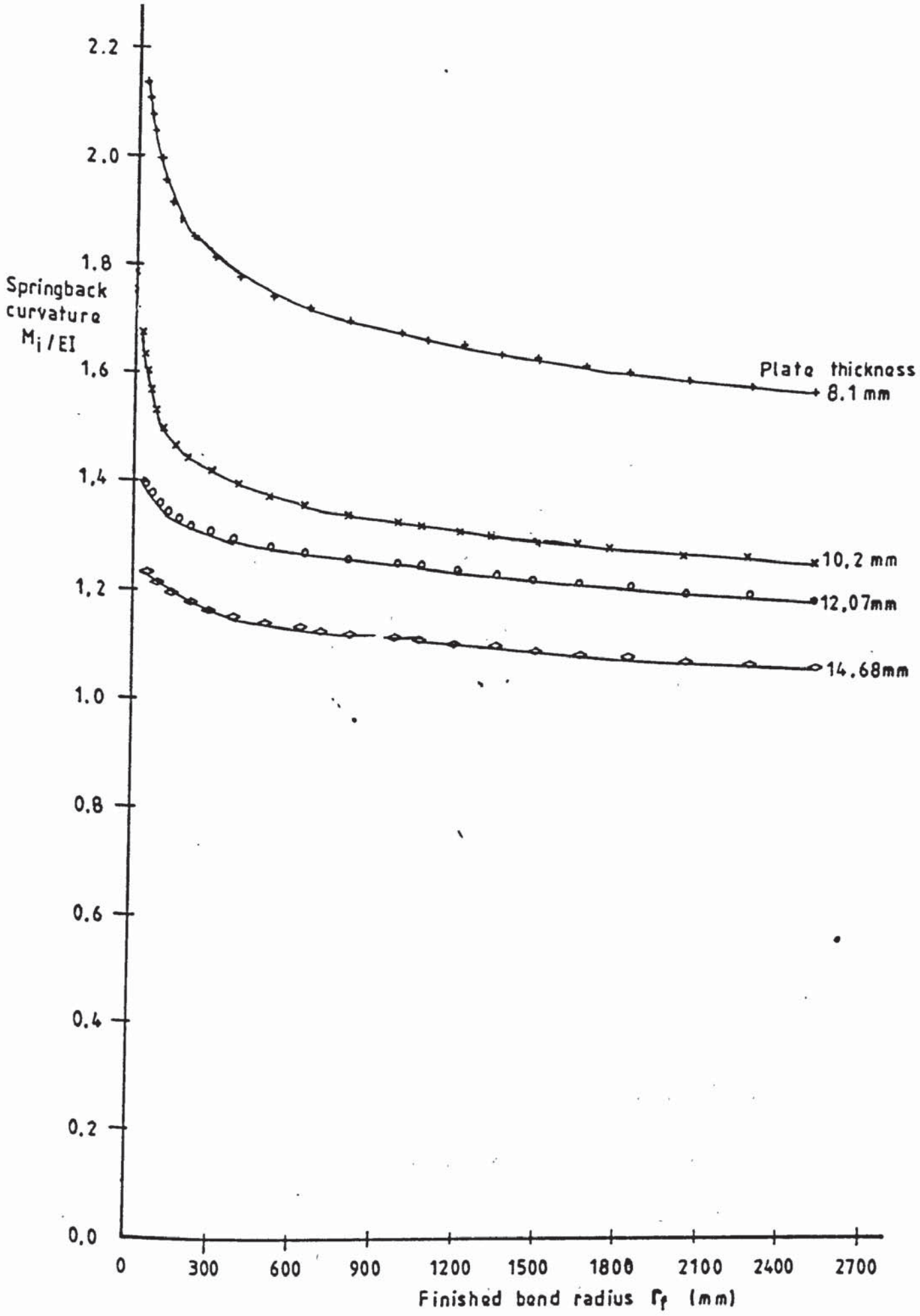

FIG 5.29 THEORETICAL PREDICTION FOR SPRINGBACK CURVATURE IN SINGLE/FIRST PASS BENDING OF FLAT HP30 ALUMINIUM PLATE SPECIMENS

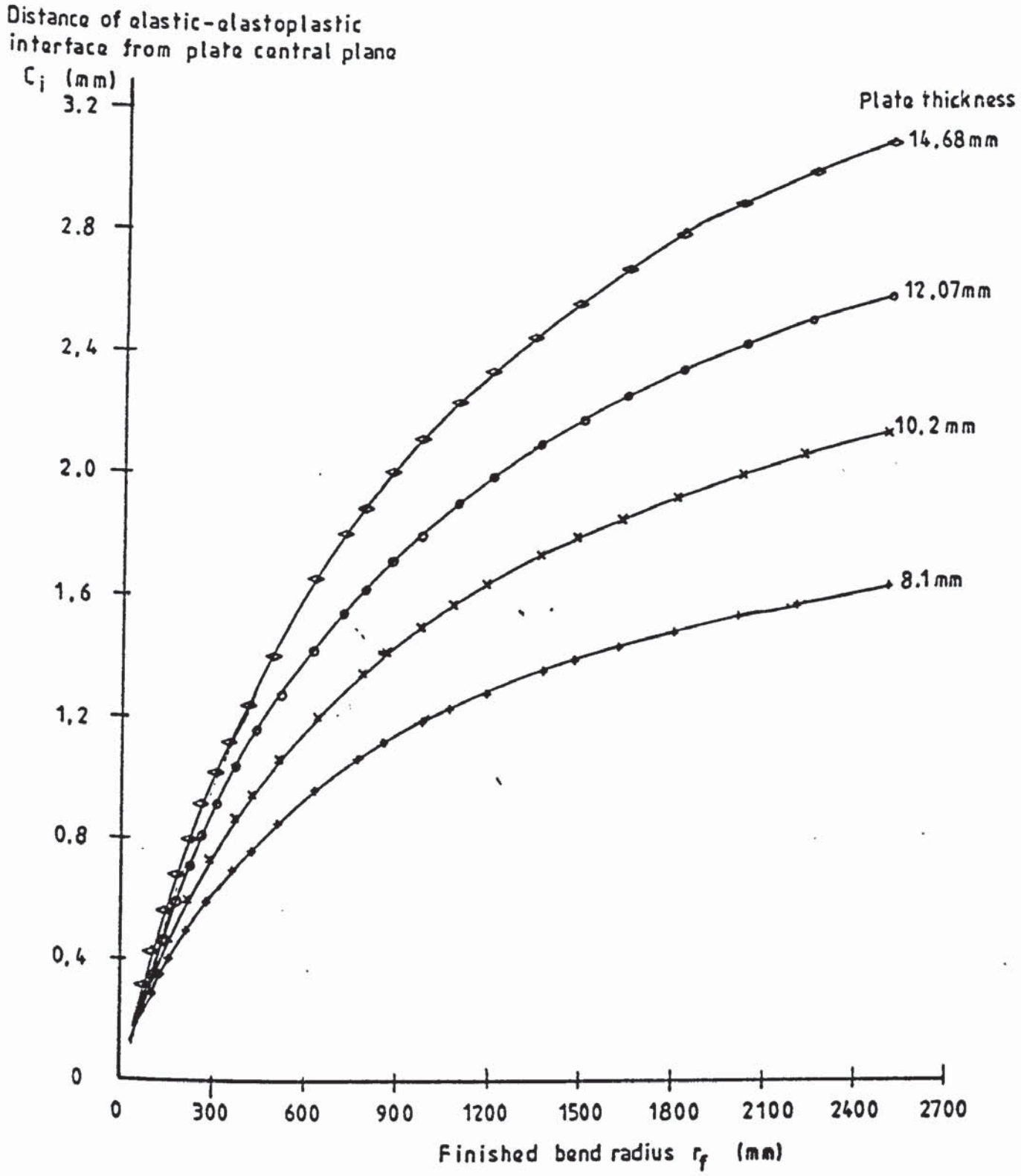

FIG 5.30 THEORETICAL PREDICTION FOR DISTANCE OF ELASTIC-ELASTOPLASTIC INTERFACE (FROM PLATE CENTRAL PLANE) IN SINGLE/FIRST PASS BENDING OF FLAT HP30 ALUMINIUM PLATE SPECIMENS

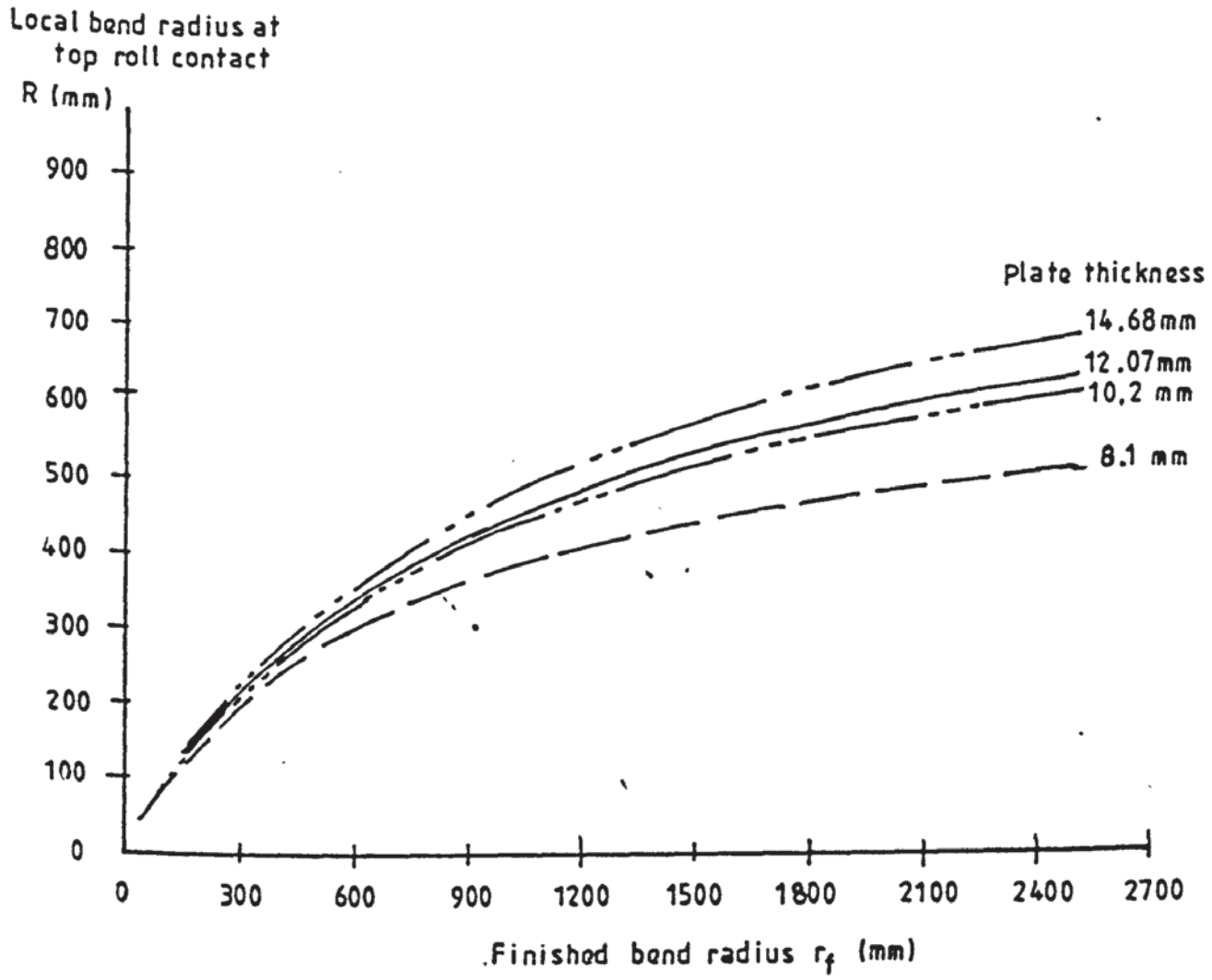

FIG 5.31 THEORETICAL PREDICTION FOR LOCAL BEND RADIUS AT TOP ROLL CONTACT IN SINGLE/FIRST PASS BENDING OF FLAT HP30 ALUMINIUM PLATE SPECIMENS

Table 5.1 Predicted Maximum Local Yield Bend Radius at Top Roll Contact For the HP30 Aluminium Plate Specimens

Plate thickness of the sample specimens (mm)	Yield stress, σ_0, (N/mm^2)	Young's modulus E (kN/mm^2)	Maximum local yield bend radius at top roll contact (mm)
8.1	215.	67.188	1260
10.2	244.	69.714	1451
12.07	285.	69.512	1467
14.68	282.	62.667	1624

Table 5.2 Number of Bending Passes of HP30 Aluminium Plate Specimens for Theoretical Prediction

Dimensions of plate specimens (mm) [thickness by width]	Spec. Label (figs 5.32 - 5.36)	No of passes	The intermediate finished bend radius (mm)
8.1 X 80.5	A	6	2500, 2100, 1700, 1300, 900, 500
	B	12	2500, 2300, 2100, 1900, 1700, 1500, 1300, 1100, 900, 700, 500, 300.
	C	6	2300, 1800, 1300, 1200, 800, 300.
	D	7	2700, 2500, 2300, 2100, 1900, 1500, 700.
	E	3	2500, 1500, 700.
	F	4	2000, 1700, 1000, 700.
	G	2	2500, 700.
8.1 X 80.5		6	2500, 2100, 1700, 1300, 900, 500.
10.2 X 80.5			
12.07 X 80.5			

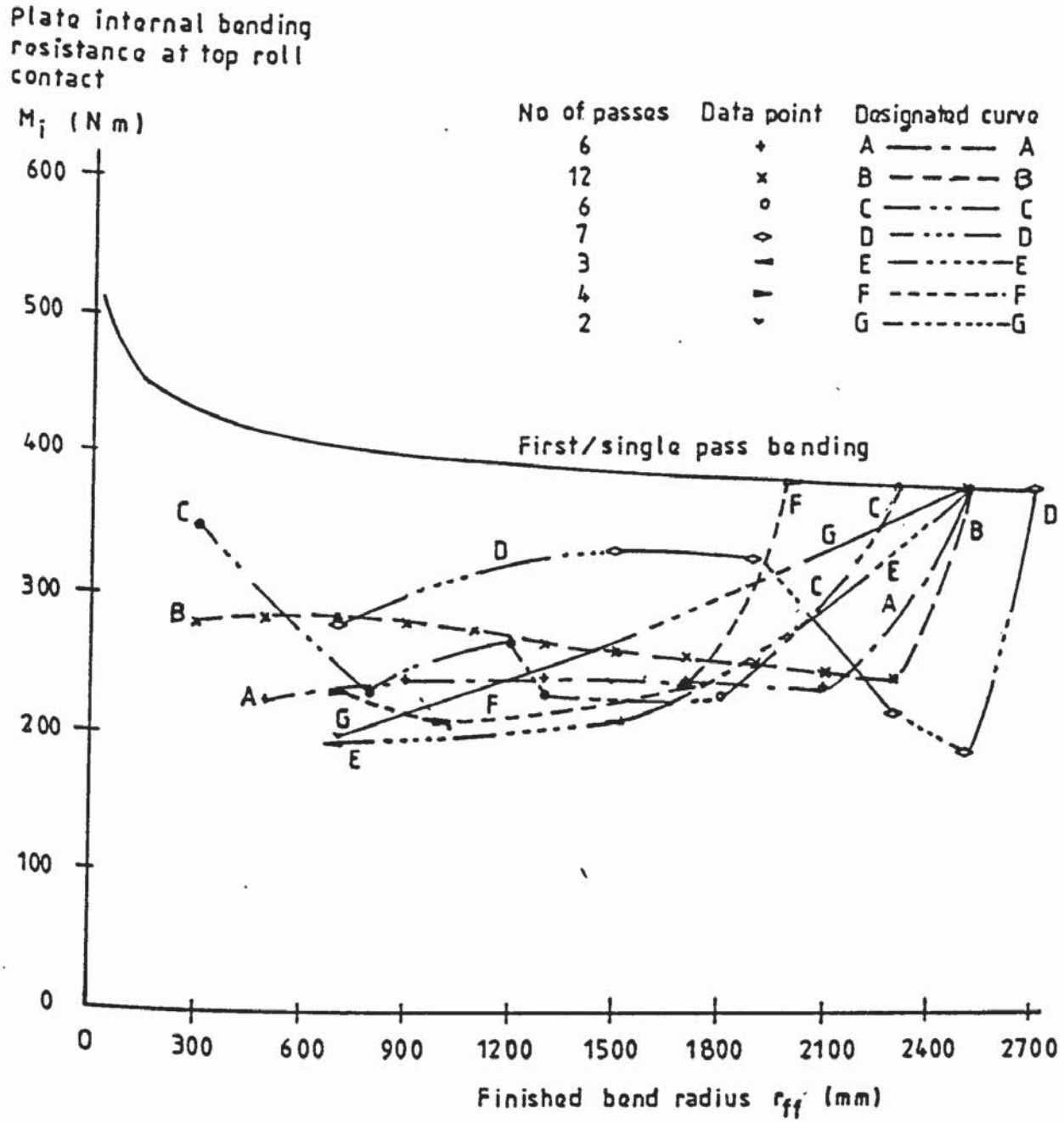

FIG 5.32 THEORETICAL PREDICTION FOR PLATE INTERNAL BENDING RESISTANCE AT TOP ROLL CONTACT IN MULTIPASS BENDING OF 8.1mm THICK × 80.5 mm WIDE HP30 ALUMINIUM PLATE

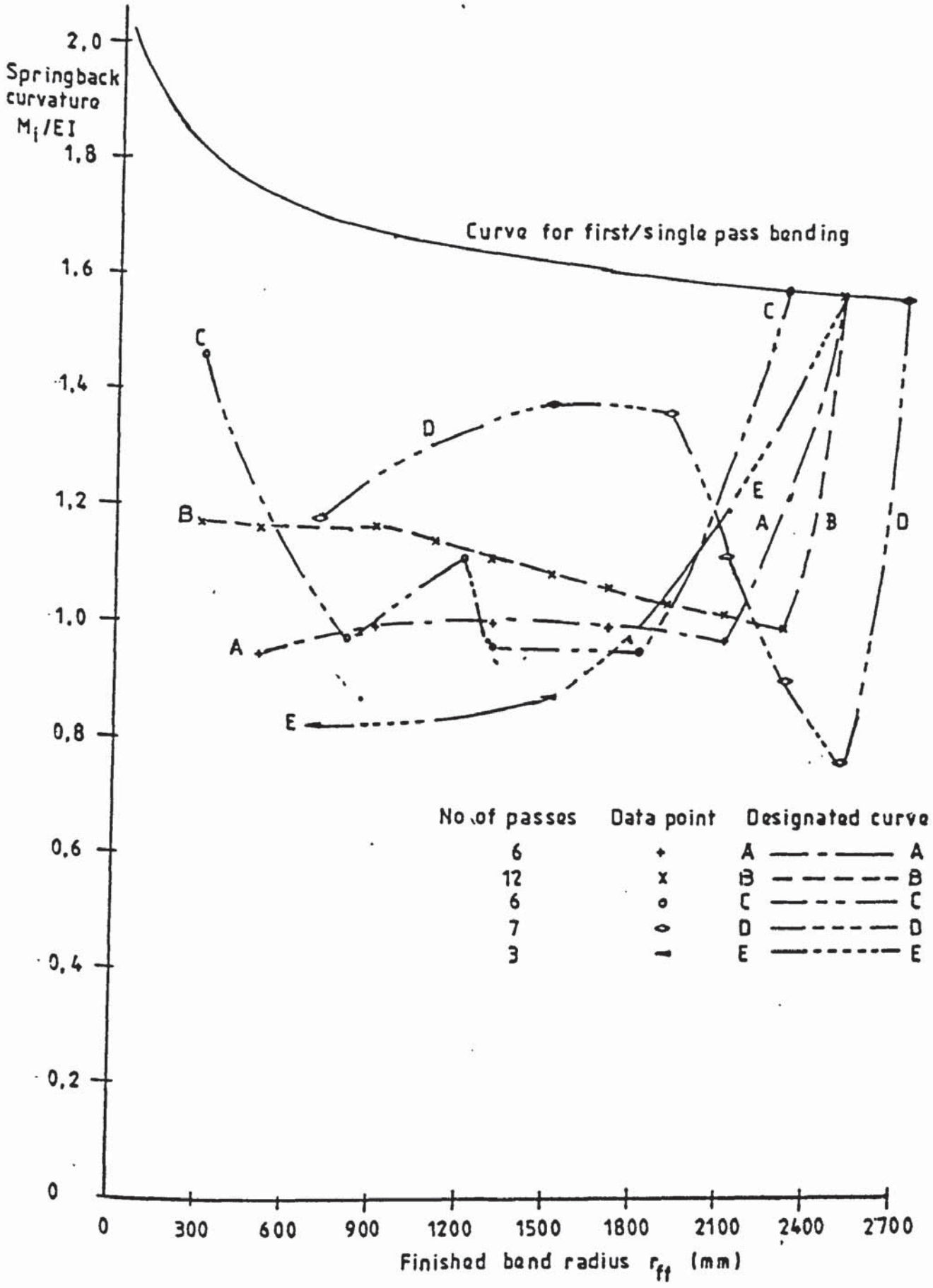

FIG 5.33 THEORETICAL PREDICTION FOR SPRINGBACK CURVATURE IN MULTIPASS BENDING OF 8.1mm THICK × 80.5mm WIDE HP30 ALUMINIUM PLATE

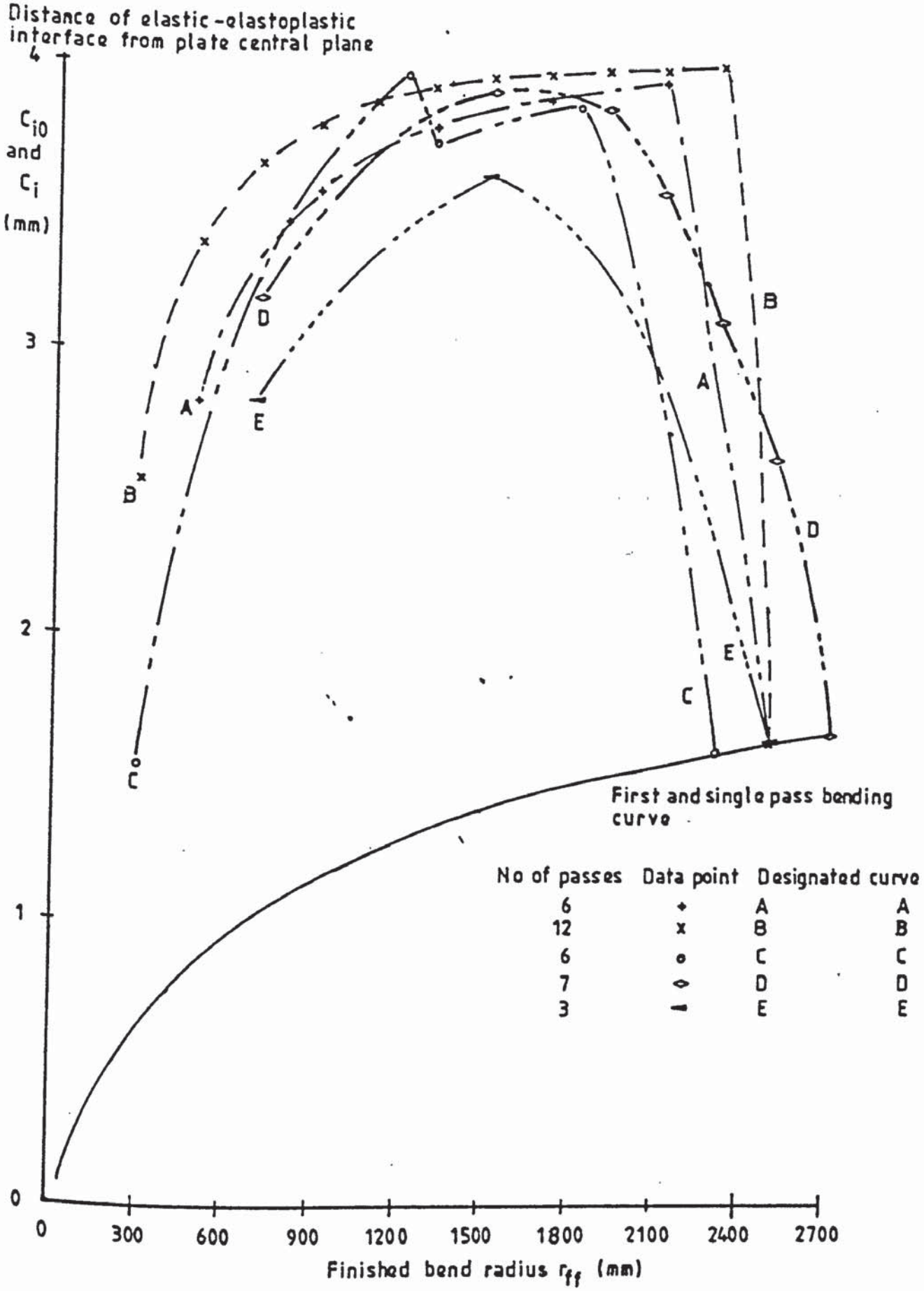

FIG 5.34 THEORETICAL PREDICTION FOR DISTANCE OF ELASTIC-ELASTOPLASTIC INTERFACE (FROM PLATE CENTRAL PLANE) IN MULTIPASS BENDING OF 8.1mm THICK × 80.5mm WIDE ALUMINIUM PLATE

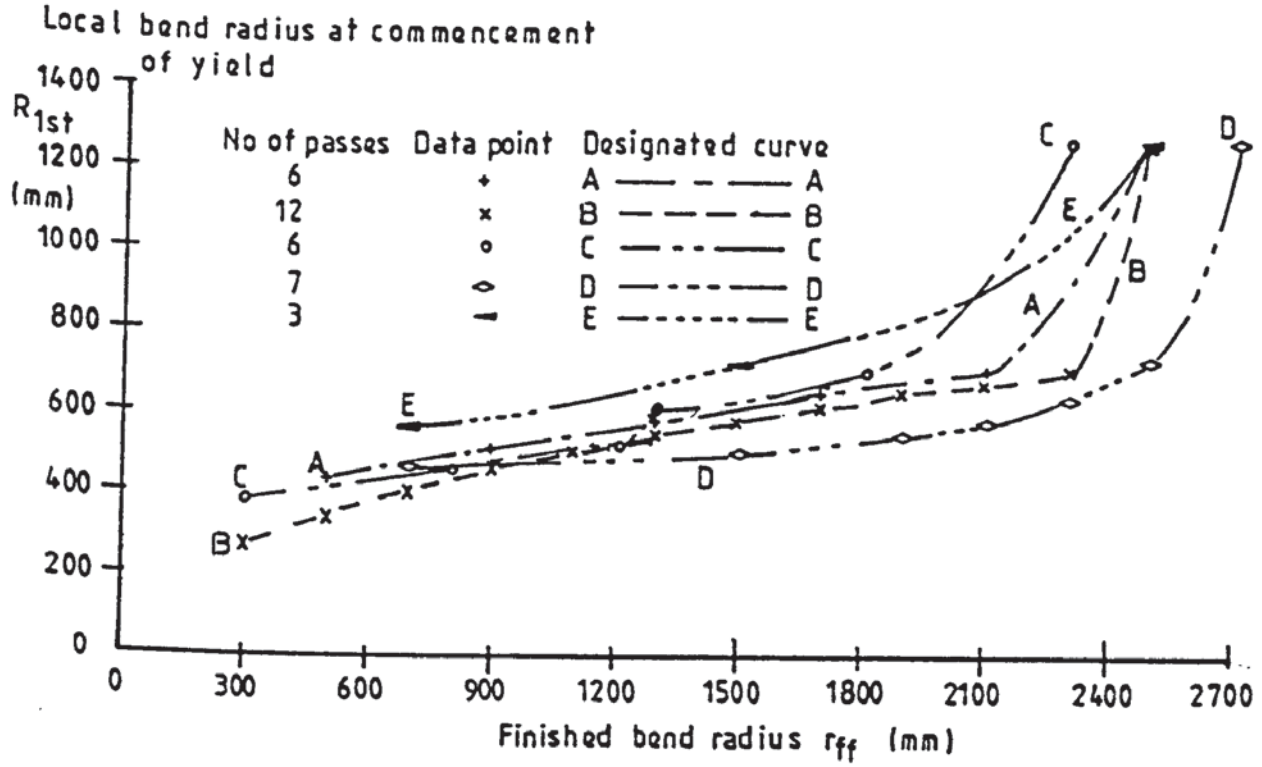

FIG 5.35 THEORETICAL PREDICTION FOR FIRST YIELDING LOCAL BEND RADIUS AT TOP ROLL CONTACT IN MULTIPASS BENDING OF 8,1 mm THICK × 80,5 mm WIDE HP30 ALUMINIUM PLATE

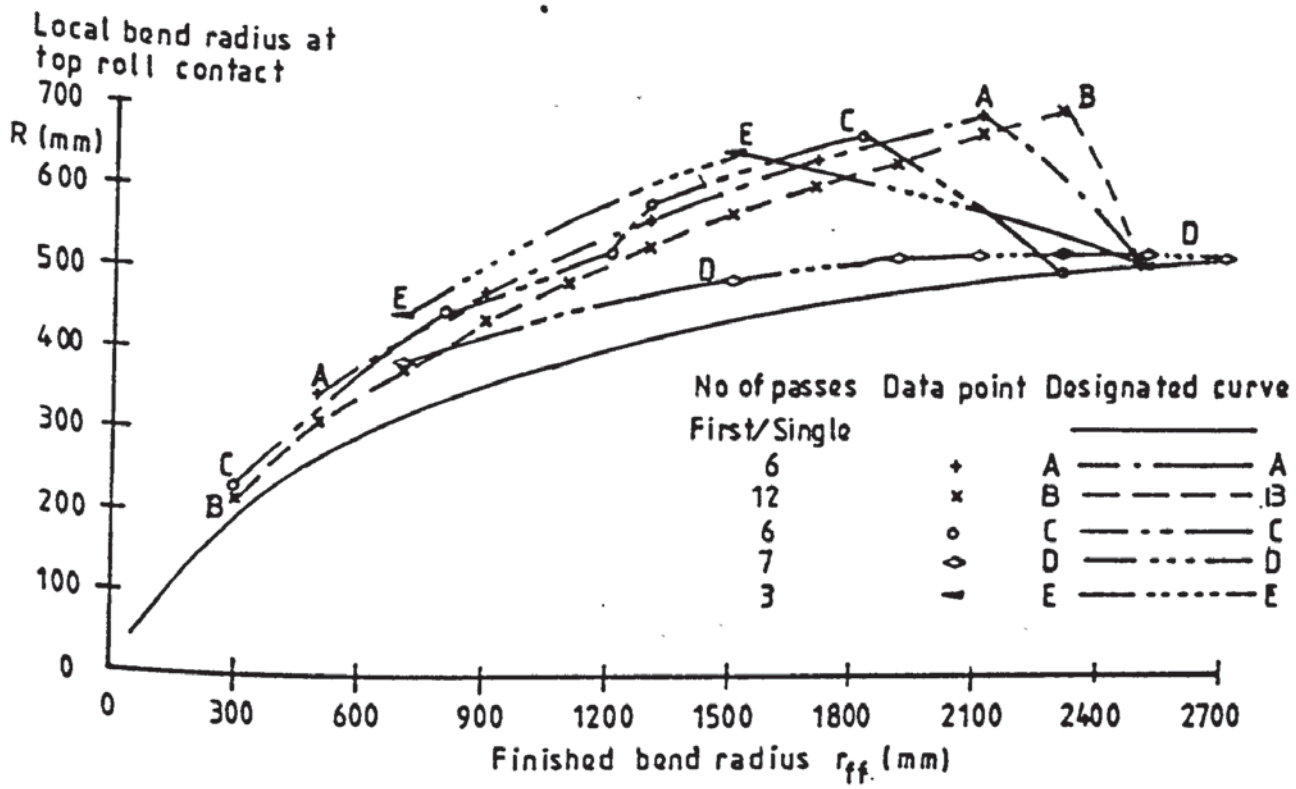

FIG 5.36 THEORETICAL PREDICTION FOR LOCAL BEND RADIUS AT TOP ROLL CONTACT IN MULTIPASS BENDING OF 8,1 mm THICK × 80,5 mm WIDE HP30 ALUMINIUM PLATE

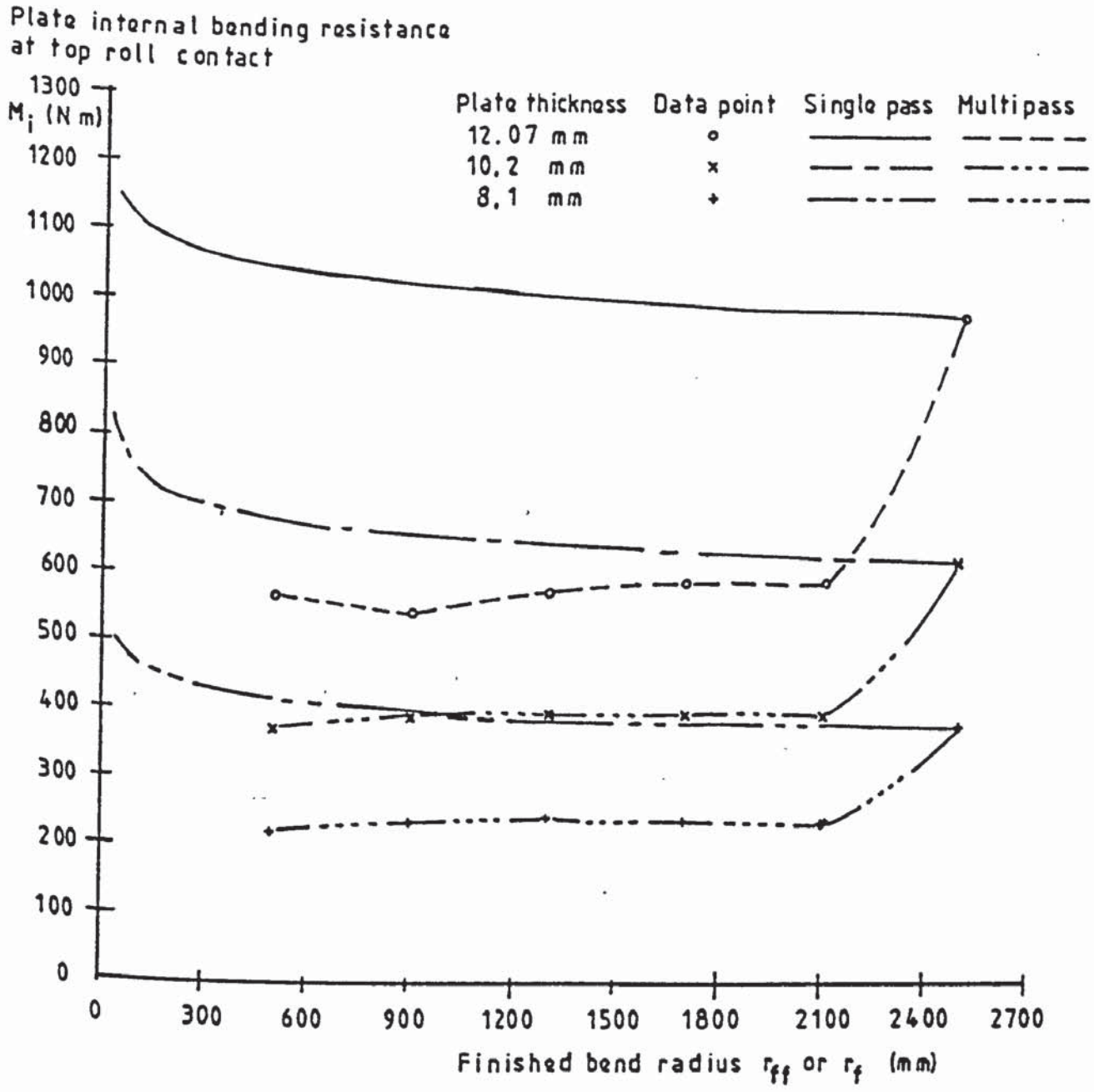

FIG 5.37 THICKNESS EFFECT ON THEORETICAL RESULTS FOR PLATE INTERNAL BENDING RESISTANCE AT TOP ROLL CONTACT (MULTIPASS BENDING OF 80,5 mm WIDE HP30 ALUMINIUM PLATE)

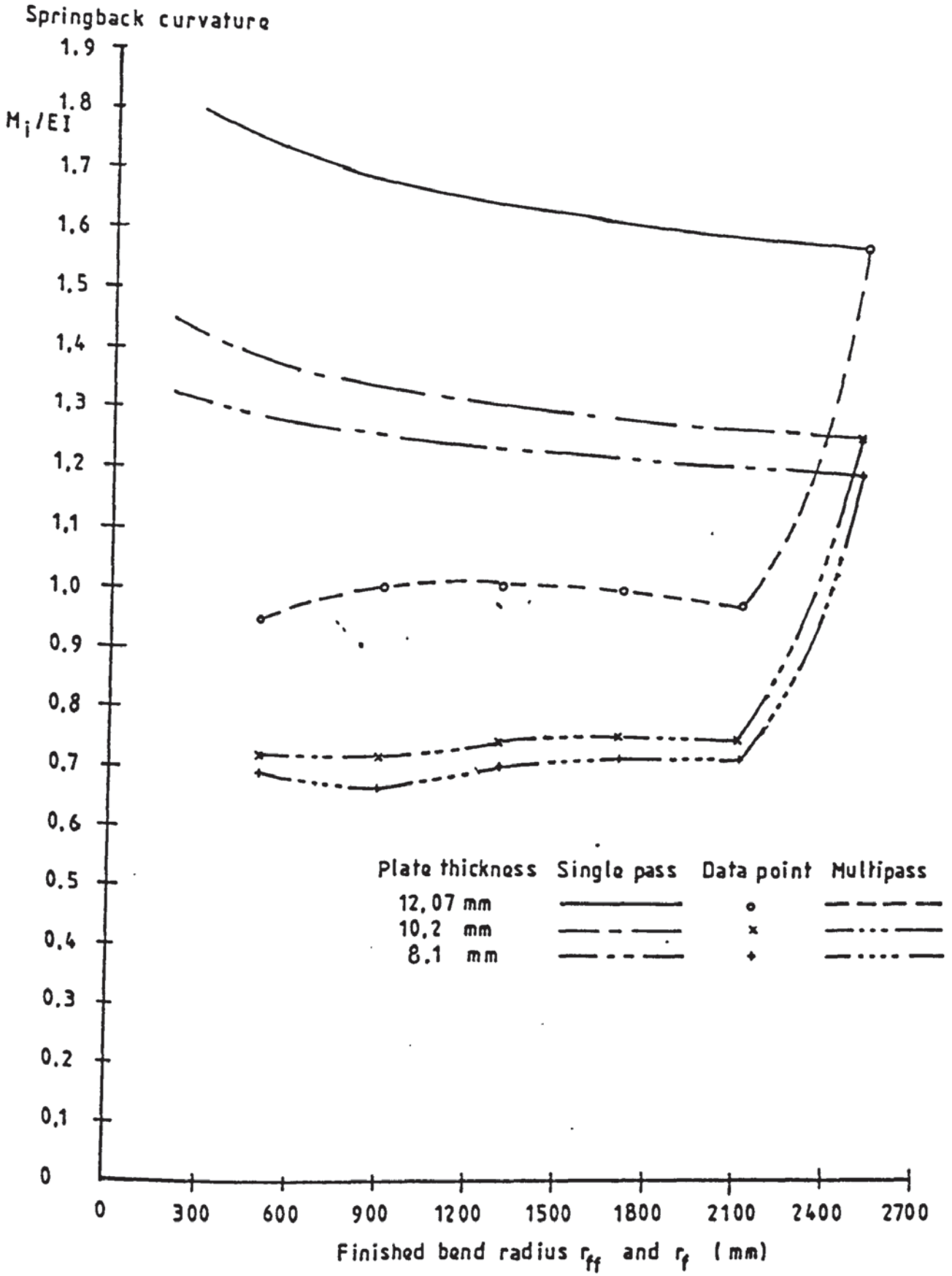

FIG 5.38 THICKNESS EFFECT ON THEORETICAL RESULTS FOR SPRINGBACK CURVATURE IN MULTIPASS BENDING OF 80,5 mm WIDE HP30 ALUMINIUM PLATE

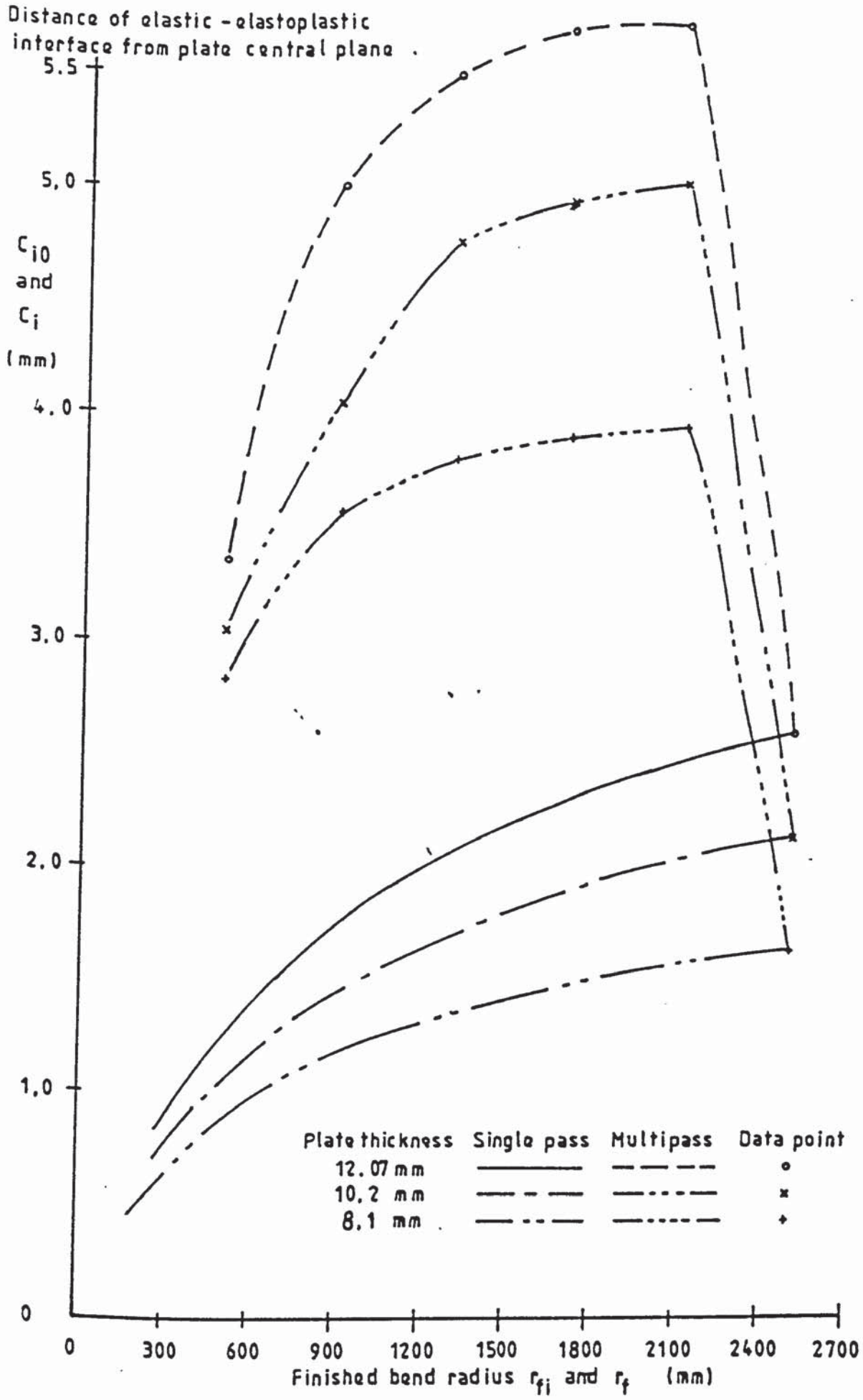

FIG 5.39 THICKNESS EFFECT ON THEORETICAL RESULTS FOR DISTANCE OF ELASTIC-ELASTOPLASTIC INTERFACE, FROM PLATE CENTRAL PLANE (MULTIPASS BENDING OF 80,5mm WIDE HP30 ALUMINIUM PLATE)

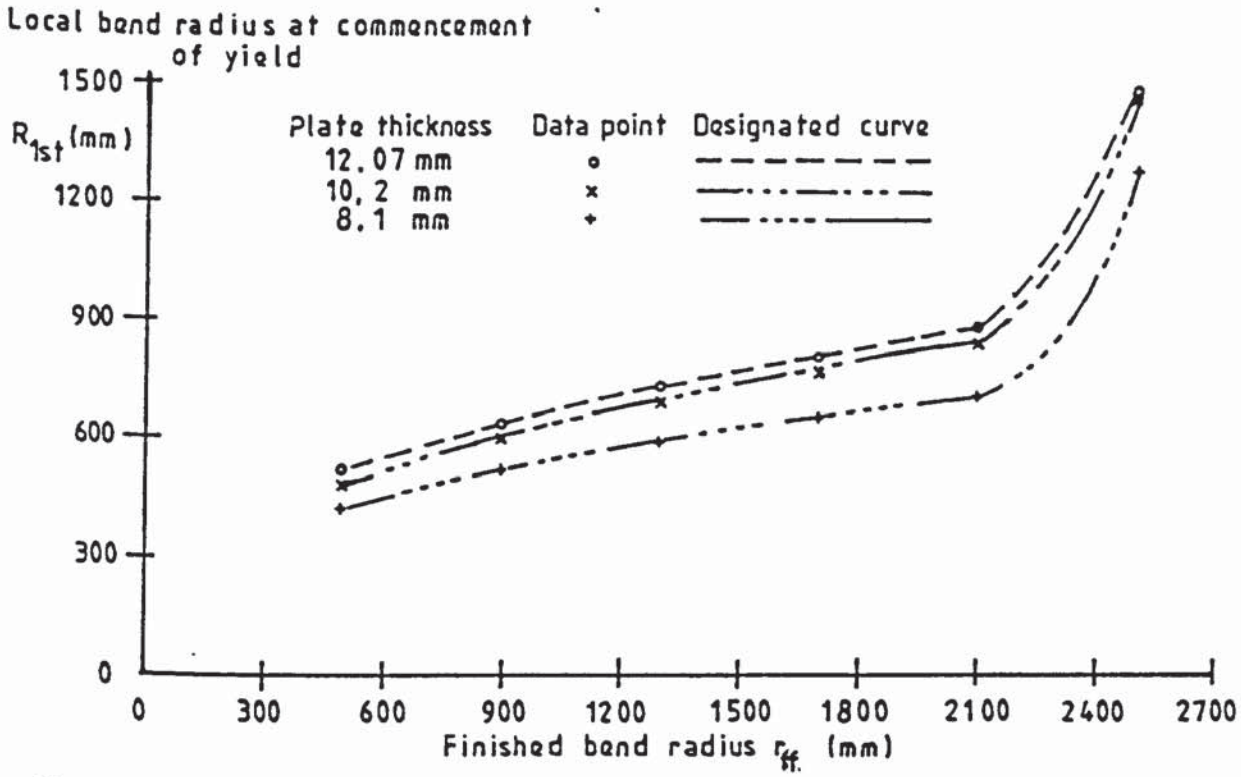

FIG 5.40 THICKNESS EFFECT ON THEORETICAL RESULTS FOR FIRST YIELDING LOCAL BEND RADIUS AT TOP ROLL CONTACT (MULTIPASS BENDING OF 80.5mm WIDE HP30 ALUMINIUM PLATE)

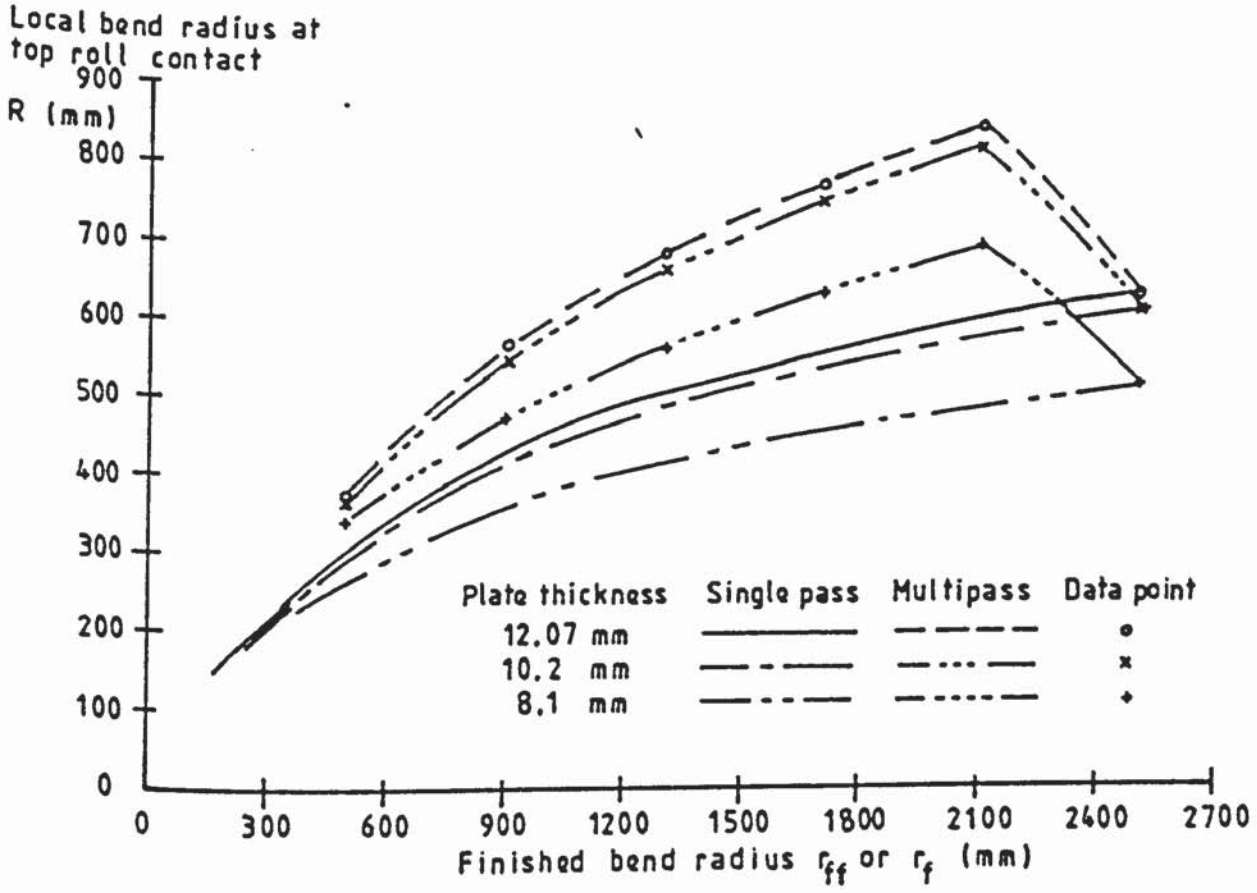

FIG 5.41 THICKNESS EFFECT ON THEORETICAL RESULTS FOR LOCAL BEND RADIUS AT TOP ROLL CONTACT (MULTIPASS BENDING OF 80.5 mm WIDE HP30 ALUMINIUM PLATE)

CHAPTER SIX

MATERIAL PROPERTIES AND PERIPHERIAL INVESTIGATION

6.1 Introduction

Metal-working is undertaken when a metal is plastically deformed. Consequently, the investigation of the mechanics of plastic forming of material demands a knowledge and determination of the material properties, such as the stress-strain relation, strain rate etc..

Throughout the last few decades, materials scientists and engineers have been attempting to correlate the mechanical properties of various materials into a single analytical relationship. Because the behaviour of a material is influenced by the different degrees of working and heat treatment conditions, the material structures and chemical constituents etc., it is impossible, from the available analytical techniques, to fulfil this objective. The technique which is commonly used in engineering applications to evaluate the mechanical properties of a material is through either one or a combination of the following tests.

a. Uniaxial tensile
b. Compressive
c. Torsional
d. Bending.

From either one of the above tests, a mechanical property curve can then be obtained. An empirical mathematical function can also be derived which will form part of the theory relevant to the forming process.

6.2. The experimental specimens

The experimental specimens used in this study were HP30 aluminium plates. According to the supplier, their chemical composition was as follows :

Si	0.7-1.3 %
Fe	0.5 %
Cu	0.1 %
Mn	0.4-1.0 %
Mg	0.6-1.2 %
Cr	0.2 %
Zn	0.2 %
Ti	0.1 %

and the strength of the plates, at proof strain of 0.2 %, was quoted as 240-295 N/mm^2.

The plates were cast and rolled to the required thicknesses of 8 mm, 10.4 mm, 12.3 mm and 14.7 mm, respectively, and then annealed.

In order to ensure that the specimens for each thickness had the same mechanical properties, the following special requests were made to the supplier :

a. All the specimens of different thickness should be cut from the same parent plate.
b. The longitudinal direction of each specimen should be properly aligned with the rolling direction of the parent plate.
c. All edges of the specimens should be cut at a slow speed. Each pair of the parallel edges of a specimen should also be milled at a slow speed and parallelism must be ensured. These requirements minimise the possible tempering or annealling effect of the material at the cut edges.

The dimensions of all the specimens were carefully checked to ensure that they conformed to the specifications.

6.3. Tensile tests

6.3.1. Introduction:

In the roller plate bending process, the manner of deformation at any cross-section varies along the plate. Generally a considerable length of the deformation zone retains its elastic state. It is essential to account for this length in the analysis to satisfactorily predict the bending mechanics of the process. Furthermore the transitional state from an elastic deformation to a plastic deformation required a suitable evaluation of an effective stress or strain, at any particular instance. The indentation compressive technique, for deriving the stress strain relationship, is a test not normally carried out in Industry. The tensile test however can easily be performed to derive the stress-strain relation for moderate strains. Therefore it was decided to implement the tensile test to complement the indentation compression tests.

6.3.2. Tensile test specimen preparation :

Bearing in mind the possible variation in the mechanical properties between the four different thicknesses of aluminium specimens, as a result of probable dissimilar degrees of working and heat treatment conditions, a test specimen (fig 6.1) was thus machined from each individual plate thickness according to the specifications quoted in BS18:Part 1-1970.

The test specimens were then prepared with their gauge length orientated to the rolling direction of their parent plates. The homogeneity of the plate was also considered by specifically preparing specimens with their test direction orthogonal to the rolling direction of the parent plate. All specimens were made to an aspect ratio (width/thickness) of 4 in their axial length.

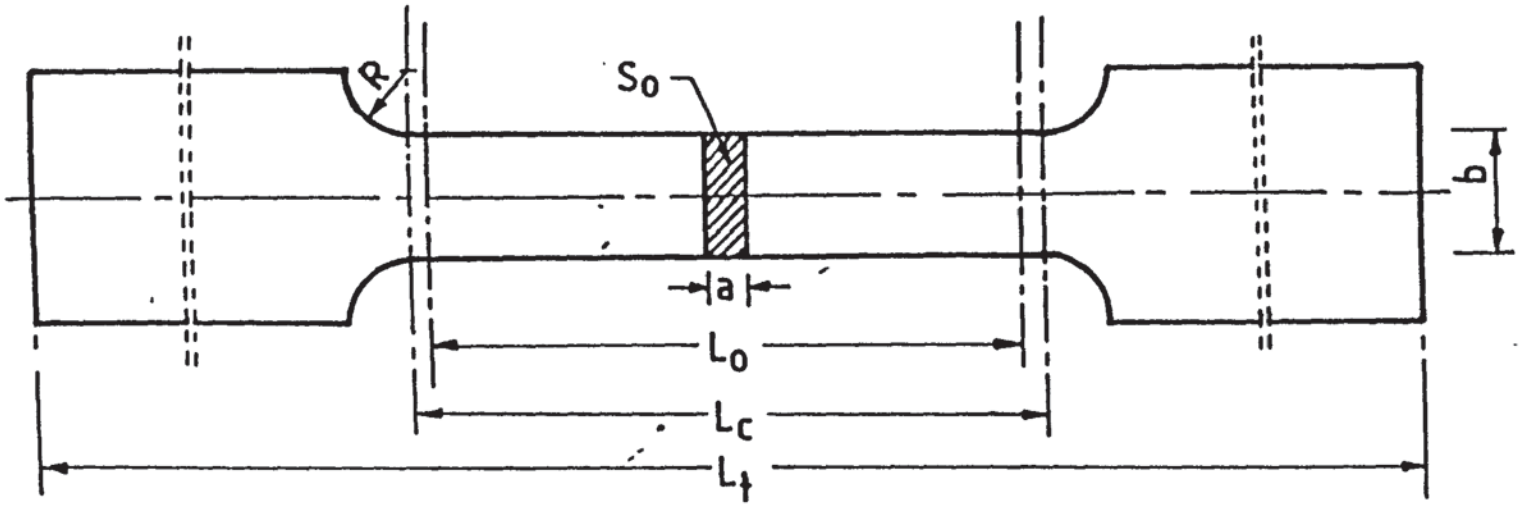

a = Thickness of the specimen

b = Width of the specimen

L_c = Parallel length

L_o = Gauge length

L_t = Total length

R = Transition radius

S = Gauge length original cross-sectional area

FIG 6.1 UNIAXIAL TENSILE TEST SPECIMENS

6.3.3. Tensile tests and results

The tensile tests were carried out using a certified Avery-Denison testing machine. The machine was capable of performing the tests either at constant strain rate or constant rate of incremental loading.

Prior to each test, the machine was allowed to stabilise and the approximate yield load of each specimen was estimated. The full scale of the loading axis in the recording chart of the machine was then set to its closest appropriate range, so as to reduce the induced error in the transpolation of measurements.

For the tensile tests, the full scale of the extension on the recording chart was set at 5 mm while the full scale of the loading was set at 120 kN for 8 mm thick specimen and 300 kN for 10.44 mm, 12.09 mm and 14.68 mm thick specimens.

The plots of the true stress versus true strain are shown in figs 6.2 to 6.5. Fig 6.6 compares the traces of the relations for each specimen thickness. The comparative plots clearly illustrate the variation due to the work and heat treatment conditions of the specimens.

6.3.4. Empirical stress strain relationship

Since the stress-strain curve for each plate thickness consists of a linear relation and a non-linear relation (see fig 6.2 to 6.5), the stress strain relation below the proportionality limit, at σ_0 and ε_0, is thus expressed as $\bar{\sigma}=E\varepsilon$, while the relation above the limit is approximated as

$$\bar{\sigma}= \sigma_0+\Delta\bar{\sigma} \qquad (6.1)$$

where, $\Delta\bar{\sigma}=H(\varepsilon - \varepsilon_0)^n$,

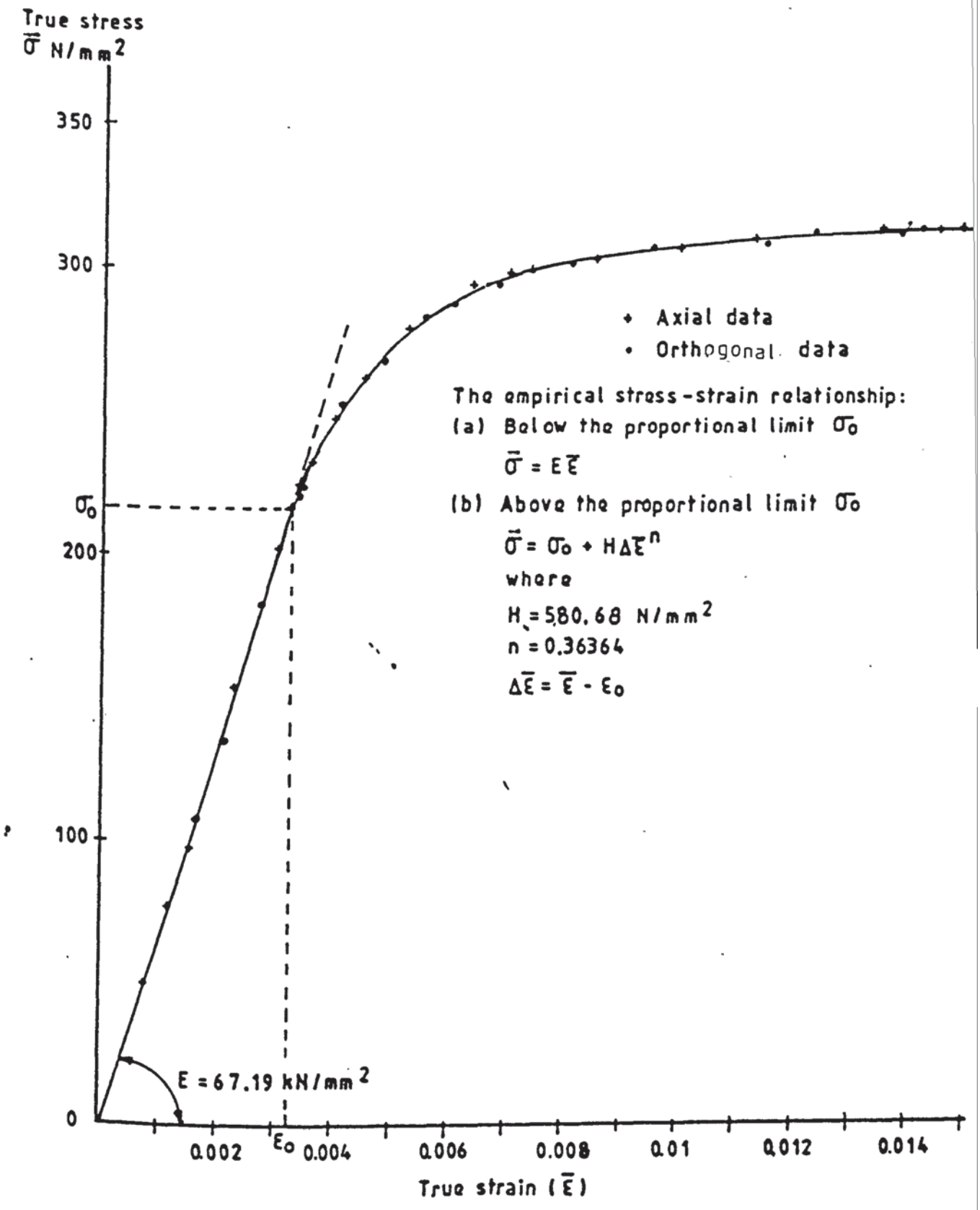

FIG 6.2 UNIAXIAL TENSILE STRESS-STRAIN RELATIONSHIP FOR HP30 ALUMINIUM PLATE (8.10 mm THICK)

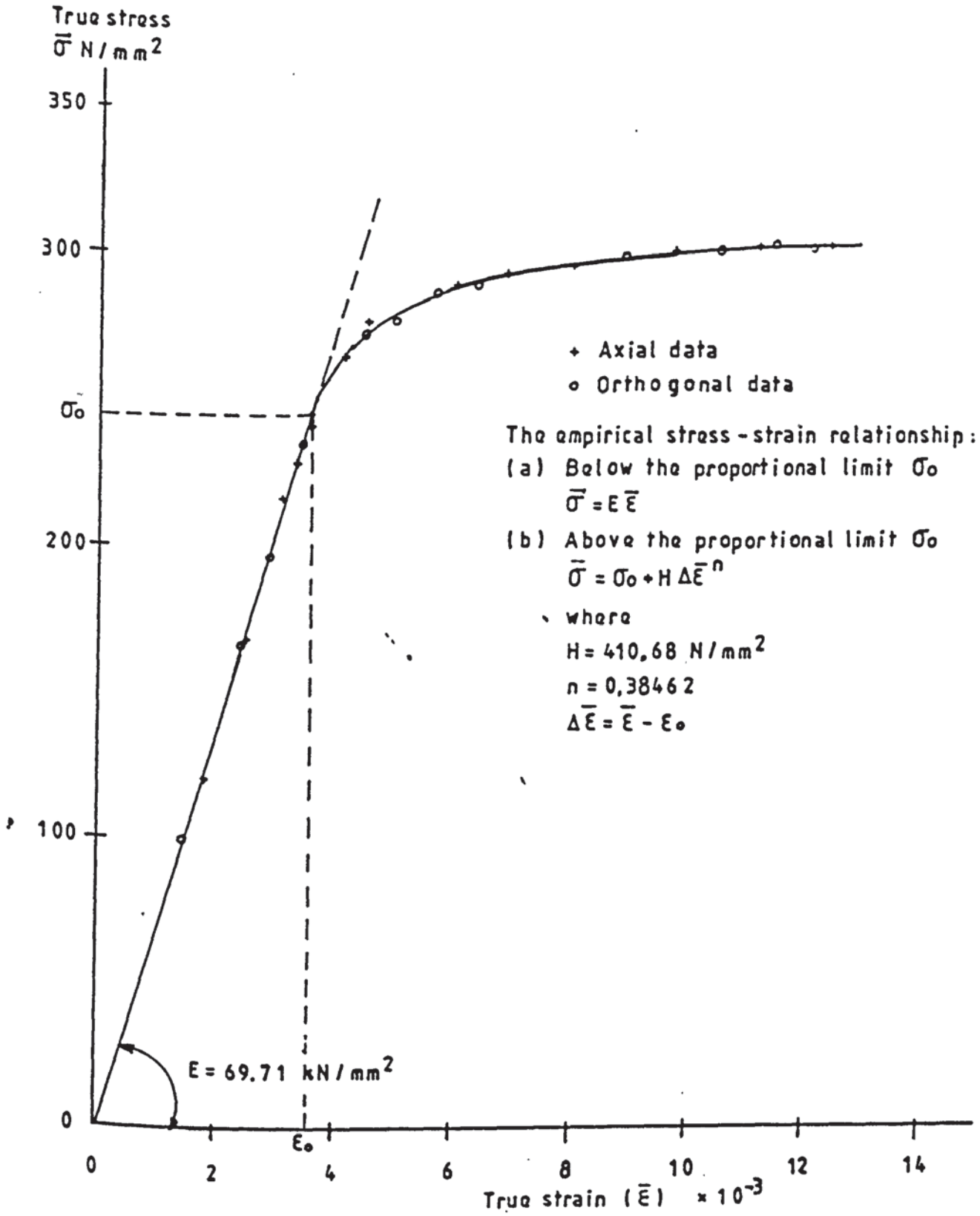

FIG 6.3 UNIAXIAL TENSILE STRESS-STRAIN RELATIONSHIP FOR HP30 ALUMINIUM PLATE (10.44 mm THICK)

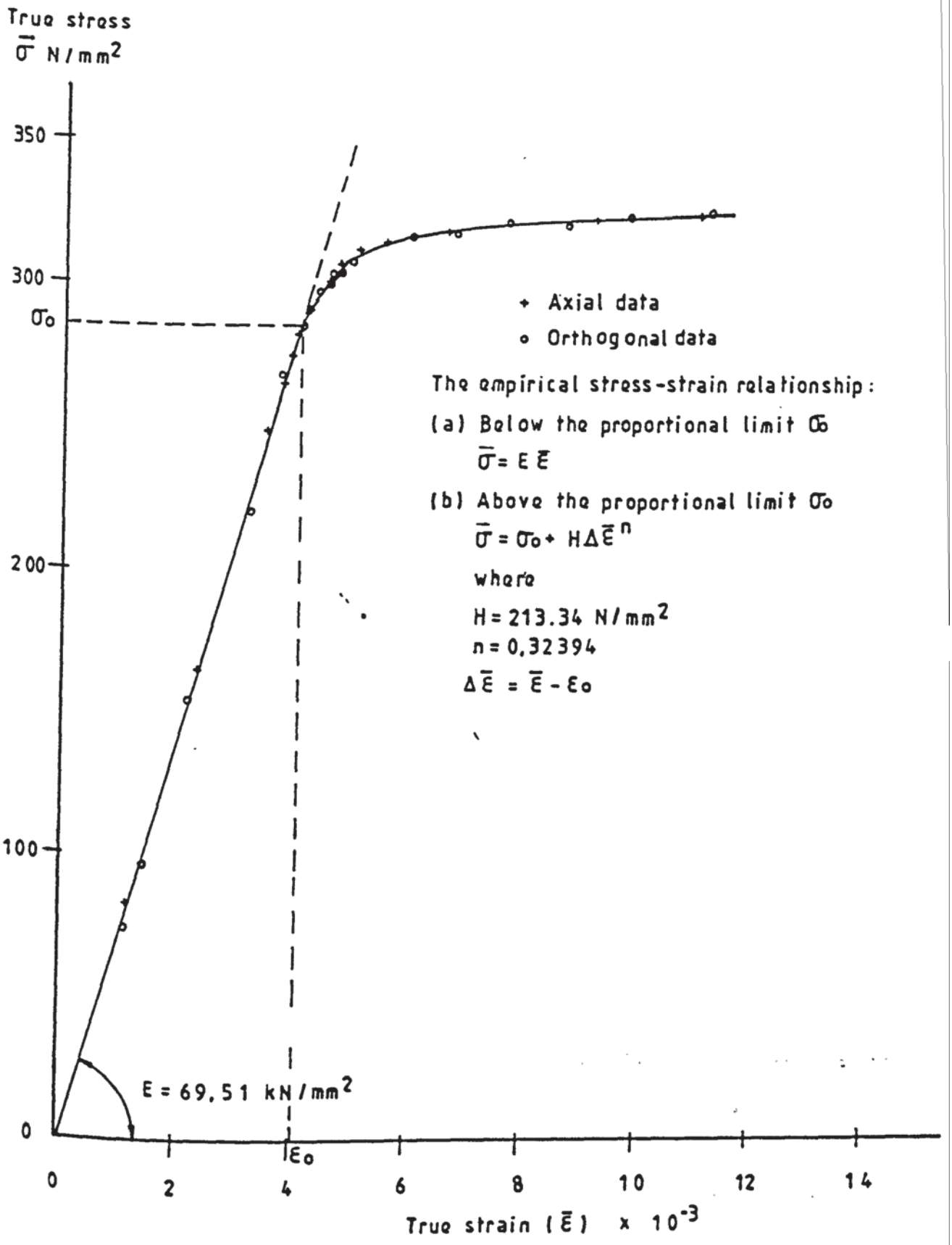

FIG 6.4 UNIAXIAL TENSILE STRESS-STRAIN RELATIONSHIP FOR HP30 ALUMINIUM PLATE (12.09 mm THICK)

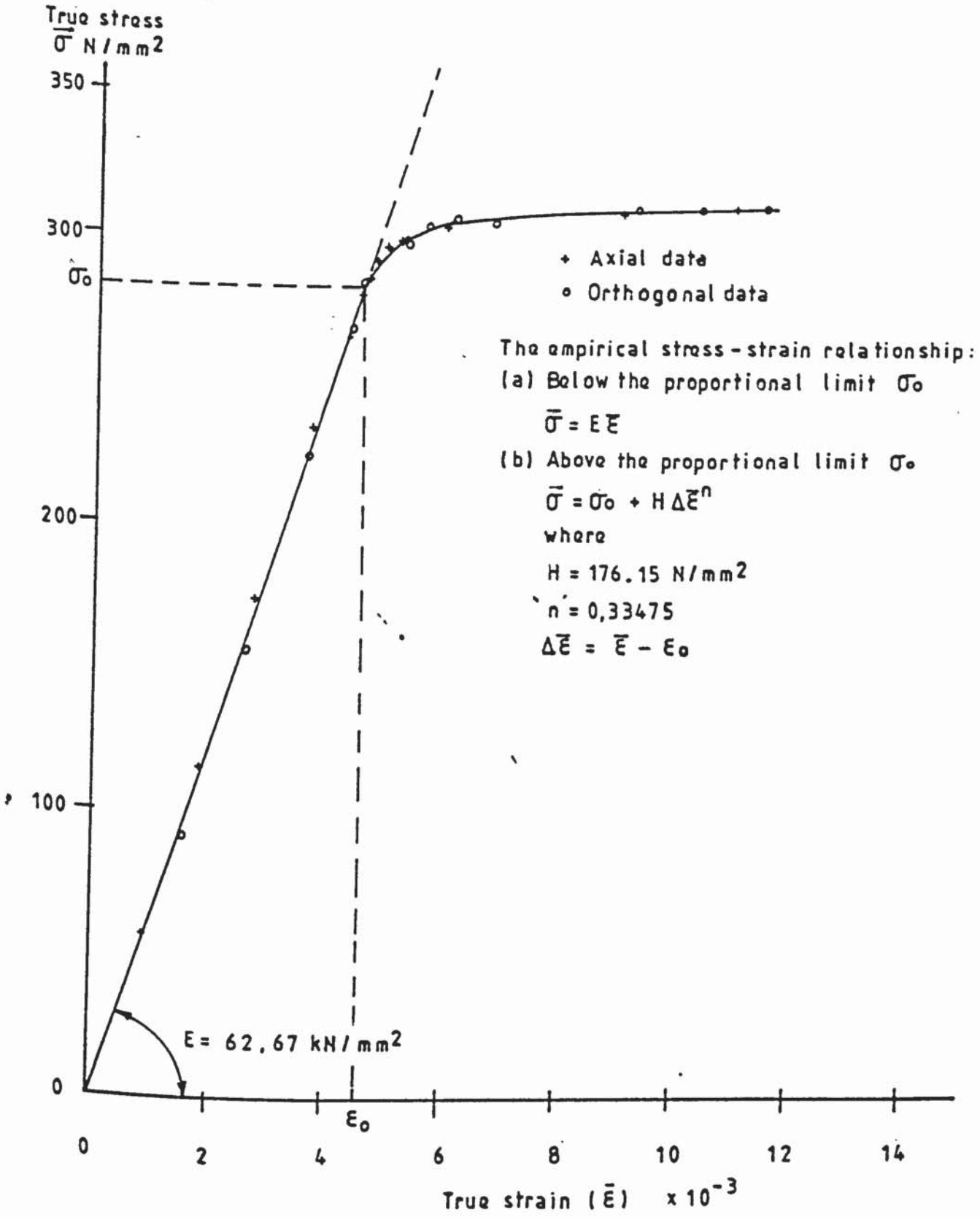

FIG 6.5 UNIAXIAL TENSILE STRESS-STRAIN RELATIONSHIP FOR HP30 ALUMINIUM PLATE (14.68 mm THICK)

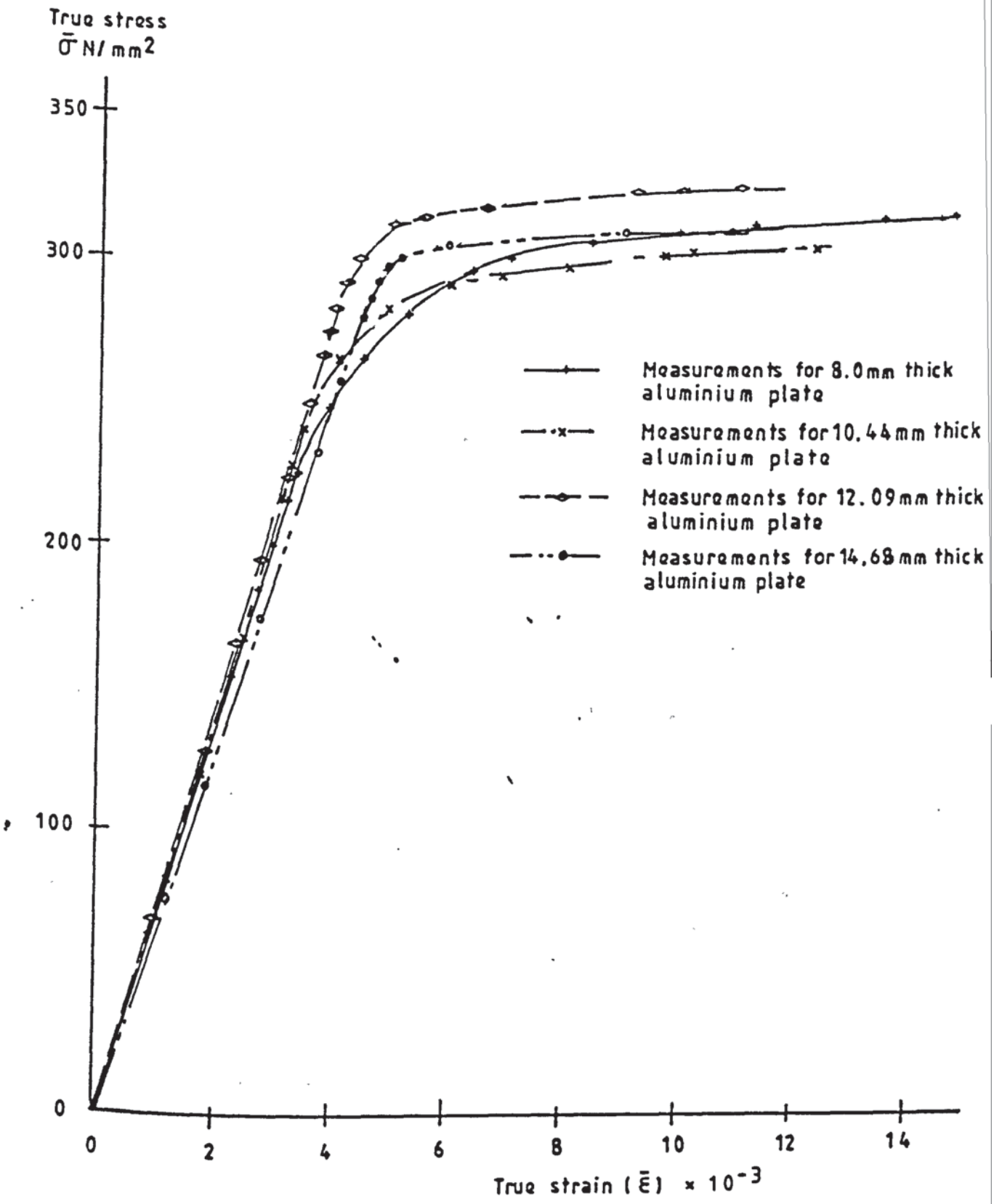

FIG 6.6 COMPARISON OF UNIAXIAL TENSILE STRESS-STRAIN RELATIONS FOR HP30 ALUMINIUM SPECIMENS

H and n are specimen hardening constants,

$\Delta\bar{\sigma}$ is the stress increment above σ_0,

$\varepsilon_0 = \sigma_0/E$ is the limit of the proportional strain,

E is the derived Young's modulus of the specimen.

The corresponding values of the above parameters for each thickness of the plates are evaluated and indicated as follows:

Thickness	Proportional limits		Young's modulus	Material constants	
t (mm)	σ_0 (N/mm^2)	ε_0	E (N/mm^2)	H (N/mm^2)	n
8.1	215	0.0032	67187.5	580.68	0.36364
10.44	244	0.0035	69714.4	410.68	0.38462
12.09	285	0.0041	69512.2	213.34	0.32394
14.68	282	0.0045	62667.	176.15	0.33475

The comparison of the stress values from the graph in the non-linear region with the derived empirical formula, for the stresses at strains of 4.6×10^{-3} and 110×10^{-3} respectively, gives

Thickness	Stress at strain of 4.6×10^{-3}			Stress at strain of 110×10^{-3}		
t (mm)	$\bar{\sigma}$ (N/mm^2)		Discrepancy	$\bar{\sigma}$ (N/mm^2)		Discrepancy
	Empirical	Graph	%	Empirical	Graph	%
8.1	266.8	264	1.06	314.4	310	1.4
10.44	273.9	274	-0.04	306.6	302	1.48
12.09	303.3	301	0.72	327.6	324	1.09
14.68	290.1	284.5	1.92	314.6	310	1.48

The above shows that the derived empirical expressions correlate satisfactorily to the transpolated measurements.

6.4. Homogeneity of the specimens

Homogeneity of a material is an indication of the degree of material isotropy. In the study of plasticity, the normal yield criteria, such as Tresca, von Mises and Rankine etc., are only applicable to isotropic material. For anisotropic material, Hill [9] has proposed a yield criterion for metal forming, which is as follows :

$$2f(\sigma_{ij})=F(\sigma_x-\sigma_y)^2+G(\sigma_y-\sigma_z)^2+H(\sigma_z-\sigma_x)^2+2(L\,\tau_{xy}^2+M\,\tau_{yz}^2+N\,\tau_{xz}^2)=1 \qquad (6.2)$$

where F, G, H, L, M, N are parametric characteristics of the current state of anisotropy.

The account of the anisotropy in expression (6.2) complicates the mathematical issue. Wherever it is possible, isotropic assumption is usually made in most engineering plastic analysis.

Embracing the idea of verifying the validity of the isotropy assumption for the bending material, it is necessary to justify the degree of the material homogeneity. To achieve this objective, tensile tests of the specimens stressing orthogonally to the rolling direction were also performed. In addition to the tensile test, indentation compression tests in both orthogonal directions were also carried out. The results obtained are also plotted in figs 6.2 to 6.5 for the tensile test, and figs 6.8 to 6.11 for the compression test. The sets of results and the estimated percentages of deviation indicate that they were within 2 % of each other. The evaluation of the probable maximum error band in the interpolation of the measurements, for the tensile test, gave a maximum error of 1.12 %, which was almost the same order as the deviation in the homogeneity test. It therefore justifies the neglecting of the material anisotropy.

It should be pointed out that the scattering of the results in figs 6.8 to 6.11 may be attributed to the induced inaccuracy in the measurements.

6.5. Indentation tests

6.5.1. Introduction :

Many metal forming processes can be considered as plane strain deformation. It is generally recognised that a stress strain relationship for the plane strain condition can be readily derived for such processes. In his study of plasticity, Nadai [146] mentioned the arrangement of the indentation compressive test. Orowan [148] further suggested that it was appropriate to use it for the determination of the yield stress characteristics of materials for the cold rolling process. Ford [144] then experimentally applied the test. In a series of investigations into the technique, Watts and Ford [148,149] established its accuracy, relative to the effects of various geometric parameters of die breadths, specimen thicknesses and strip widths etc., for the true yield stress in compression. They also compared the basic stress strain curves obtained by the technique with those obtained by the tensile and normal compressive test etc.. The work of Watts and Ford confirmed the applicability of the indentation compressive technique in determining the material stress-strain curves for the plane strain condition.

It was anticipated that the bending behaviour of the plate, in the roller bender, could be regarded as a plane strain problem. Consequently this leads to the adoption of the technique to obtain a relative stress-strain curve for each specimen thickness, t.

6.5.2. Test specimen preparation

6.5.2.1. Consideration of the specimen dimensions :

The technique of indentation test to evaluate the stress-strain relationship for plane strain condition has been well established by numerous investigators. Specifications of the ratios of the specimen thickness to the platen breadth, b, and to the specimen width, W, respectively, for producing reliable results have been widely published. According to Rowe [147], tests with, $1/4 \leq t/b \leq 1/2$, and $b/w = 1/5$, are recommended in order to produce an acceptable set of results.

The original plan to bend 30 mm thick lead specimens, to simulate the hot roll bending of mild steel, demanded a subpress capable of accommodating a 300 mm wide lead specimen. It was impossible to achieve this with the subpress available, as it only had a maximum width of 178 mm. The design and manufacture of a new subpress was not viable in the prevailing circumstances.

In order to ensure that the width of each test specimen was within the allowable subpress width, the following possible solutions were considered.

a. To machine the specimen to the thickness which conformed to the specification of the indentation tests [147].

b. To choose a new ratio of t/b which would reliably give the testing values - this would involve the design of new platens.

Alternative (a) was not favoured because the specimen surface would need to be carefully machined. Improper machining of the specimens could alter the metallurgical properties and consequently would deviate from the objective of the tests.

The other alternative, i.e. (b), was not to conform to the specified ratio of the specimen breadth and platen width. In this case, it was essential to assess the degree of accuracy of each measured yield stress relative to its true value in any particular initial b/w ratio. It was also essential to assess the accuracy of the value for the subsequent yield stresses as the test was progressivly carried out. A careful study of Watts and Ford [148,149] data indicated that, if the initial ratio of $b/w=1$, a maximum deviation of 0.7 % for $t/b=1$ would possibly occur. Also, if t/b was initially taken as 1, the maximum deviation from the true stress would be 3.8 % at $t/b=0.6$. Generally, it gave $1.02 \leq Y/2K \leq 1.038$ (where Y is the uniaxial yield stress and k is the shear yield value) in the range of $0.76 \geq t/b \geq 0.6$, and the rest of the values of $Y/2k$ were less than 1.02. Watts' data also showed that the maximum deviation was 2% when $t/b \leq 0.4$ [refer to fig 33 of ref 148].

This suggests that the maximum deviation obtained, as a result of a reducing ratio of strip thickness and die breadth , t/b, with an initial ratio of $t/b=1$, is only within 3.8 % from the true stress. This is adequate for the present purpose of determining the plane stress- strain curves.

The conclusions drawn from the above study substantiate the possible choice of $t/b=1$ for the commencing test. Finally, the evaluation of all the specimen widths (W) with a chosen ratio of $b/w=5$ gave values which were well within the limit of the subpress width.

6.5.2.2. Machining the indentation specimens

Since the bending specimens for a particular thickness were cut off from the same parent plate, it was envisaged that an indentation specimen from any similar thickness of plate would produce a representative result for the specimens of that particular thickness. The test specimens for each thickness were carefully cut off, from the appropriate specimen to be bent. They were then finely edge-milled to their correct dimensions. This minimised the tempering effect of the material during the rolling process.

The majority of test specimens were prepared with their width orientation parallel to the rolling direction of their parent plate. There were, however, some specimens cut with their widths orthogonal to the rolling direction. The latter specimens were to be used for investigating the degree of material isotropy or anisotropy.

The dimensions of these prepared specimens are stated in figs 6.8 to 6.12.

6.5.2.3. Platen design

To carry out the tests, new platens were designed and made. The newly designed platens are shown in fig 6.7.

It should be pointed out that some of the platens were also designed to test mild steel and lead specimens.

6.5.3. Test apparatus and procedures

The test were carried out using a 1000 kN Avery compression testing machine and the platens shown in fig 6.7.

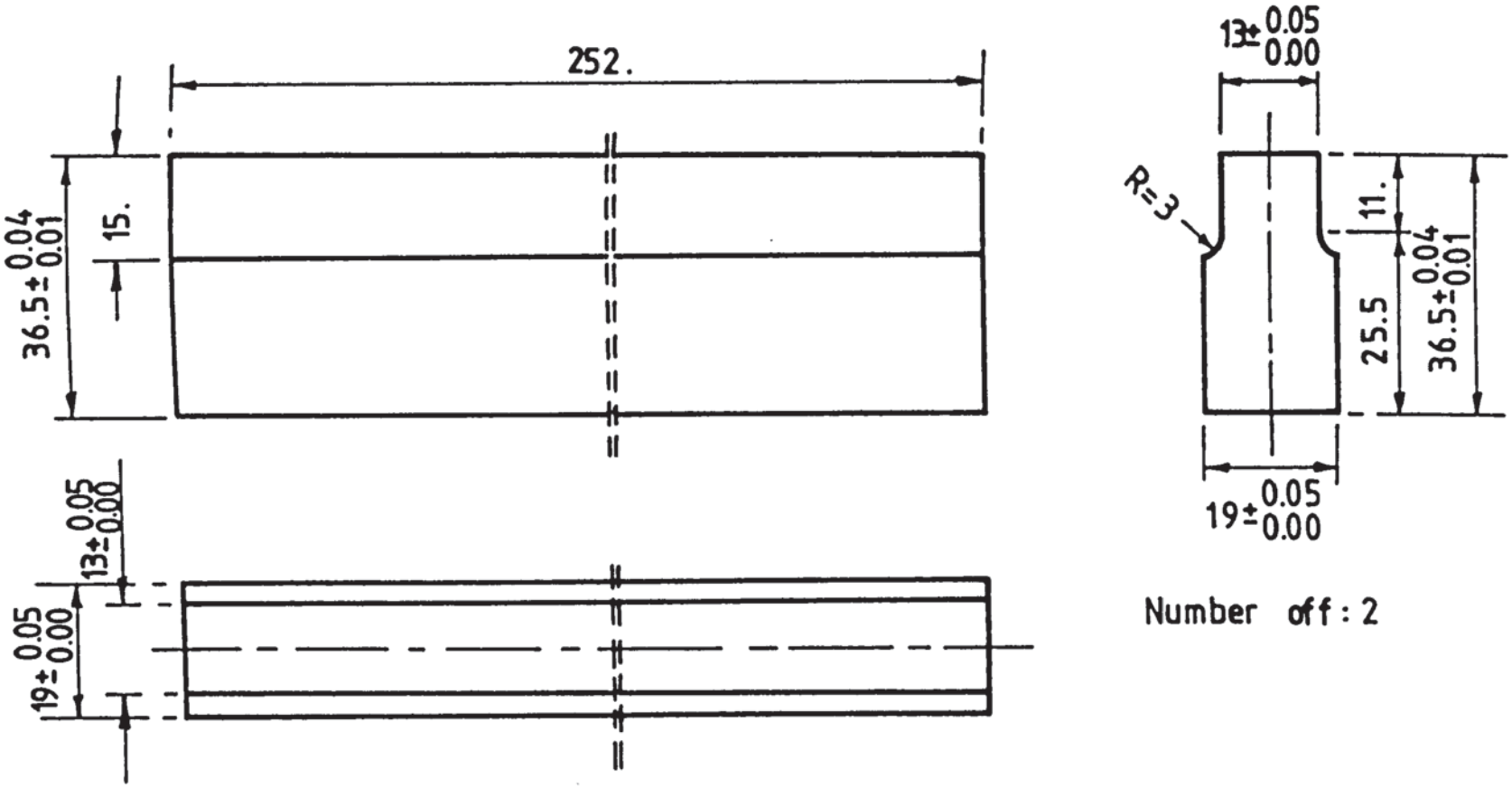

Number off : 2

Material: Tool steel
Hardness no: RC 58-60.

All surfaces, except the ends are ground
All dimensions are in mm

FIG 6.7 DESIGN OF INDENTATION TEST PLATENS (1)

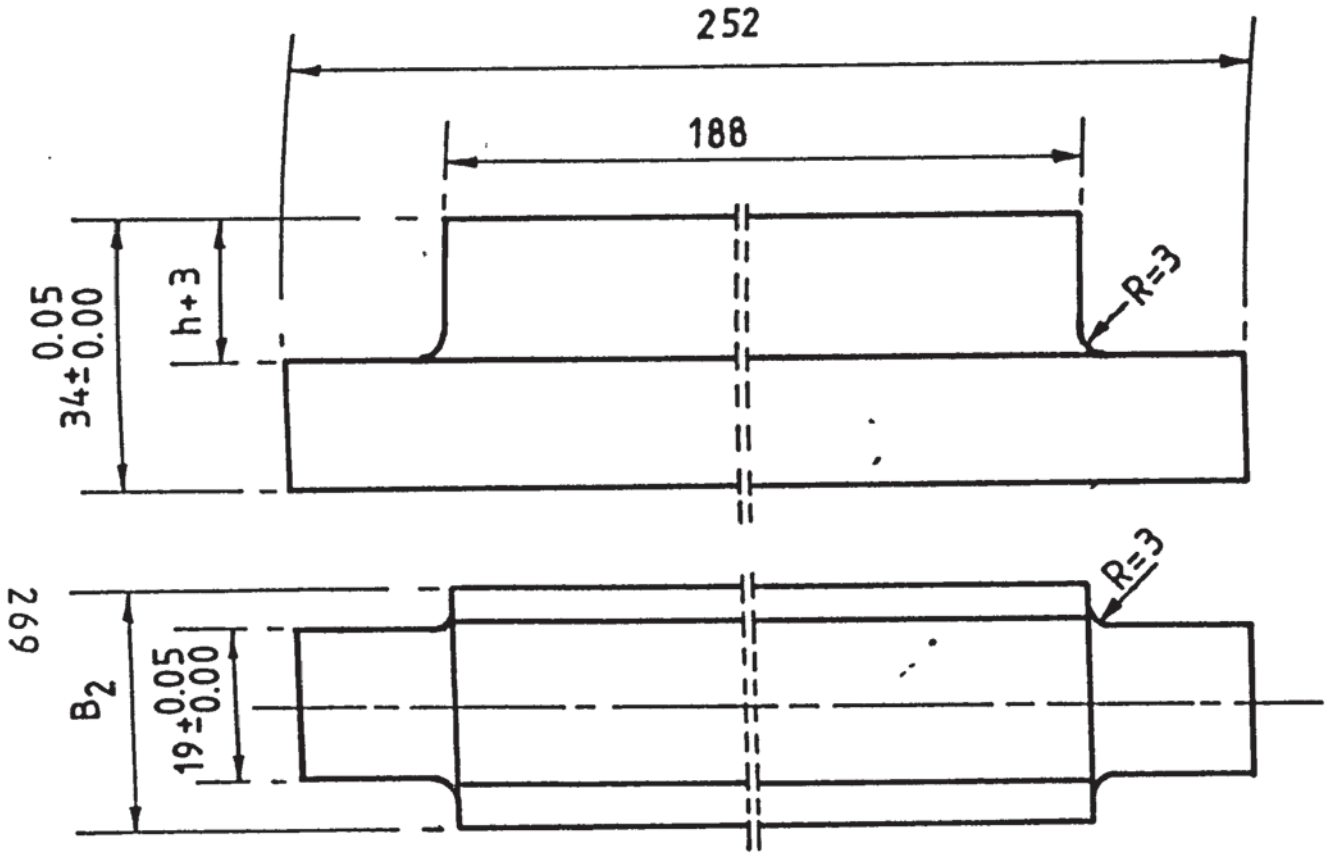

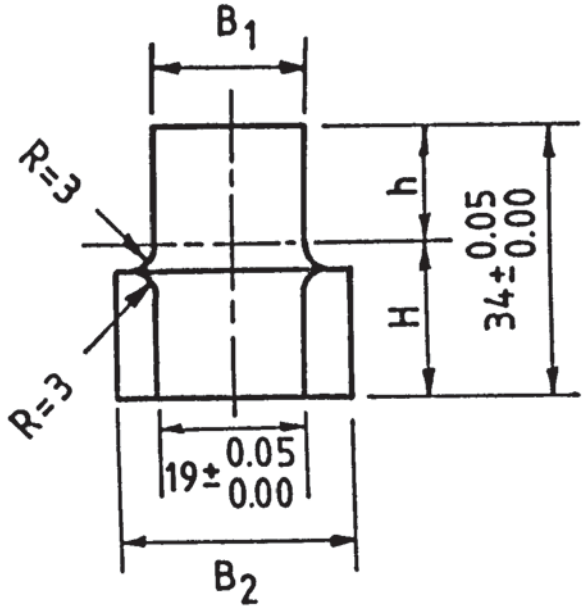

Material: Tool steel
Hardness no: RC 56-58
All dimensions are in mm
All surfaces, except the ends, are ground.

Dimensions				No. off
B_1 = 16	B_2 = 25	h=13	H=21	2
=18	= 25	=15	=19	2
=20	= 30	=15	=19	2

FIG 6.7 DESIGN OF INDENTATION TEST PLATENS (2)

Prior to the test, the dimensions of each specimen were carefully measured. A pencil line, parallel to the width direction, was drawn at the mid-span of each specimen. Two other straight lines were drawn at either side of the first line ; the distance of each line from the former line was equivalent to half the platen breadth. The latter lines enveloped the indentation platen contact surface. Around the indentation platen and either face of the specimen, a thin graphite film was dispersed to act as a lubricant.

Particular attention was paid to the correct alignment of the two outer-marked lines with the longitudinal edges of the platen. Whenever a test was carried out, the platen was located at the mid-span of the specimen. All the above precautions were taken to ensure uniform straining in the specimen width. This achieved the plane strain condition.

At the commencement of the test, the load required to produce 2-5 % reduction in the specimen thickness was estimated. Subsequently, the incremental loading was in steps of 10 kN. When the total reduction in the thickness wass above 0.5 %, the incremental loading was reduced to either 3 or 5 kN.

Between each successive indentations, the instantaneous thickness and the width of the specimen were measured. Alignment and lubrication were continuously monitored throughout the test. It should be noted that each set of tests, for each thickness of the plate, was performed using the same pair of platens.

6.5.4. Results

The results are plotted as true stess versus true strain in figs 6.8 to 6.11. The comparison of the mechanical properties for the four thicknesses of the plate is in fig

6.12. The plot in fig 6.12 clearly indicates the different degree of hardening of each thickness of plates. It also shows that the annealling condition after rolling has not fully restored the original properties. This may be caused by the different thickness or other factors.

6.5.4.1. Empirical relationship

Since the true stress-strain relationship from the tests is primarily for the plastic condition, it is thus expressed empirically in the following form.

$$\sigma = H \varepsilon^{n} \qquad (6.3)$$

where, H and n are the material constants.

The logarithm plot of the test measurements for each thickness of the plates gave the magnitudes of the material constants in equation (6.3). These magnitudes are :

Thickness of plates t (mm)	Material constants in equation (6.2) H N/mm^2	n
8.	469.13	0.0541.
10.44	444.43	0.0476
12.09	482.43	0.0519
14.68	435.45	0.0368

6.5.4.2. Effect of the specimen width

The tests were performed partly to further confirm the homogeneity of the test specimens and partly to give an insight into the effects of the specimen width. The various specimens were cut off from the same parent plate.

The graphical representation of the results are shown in

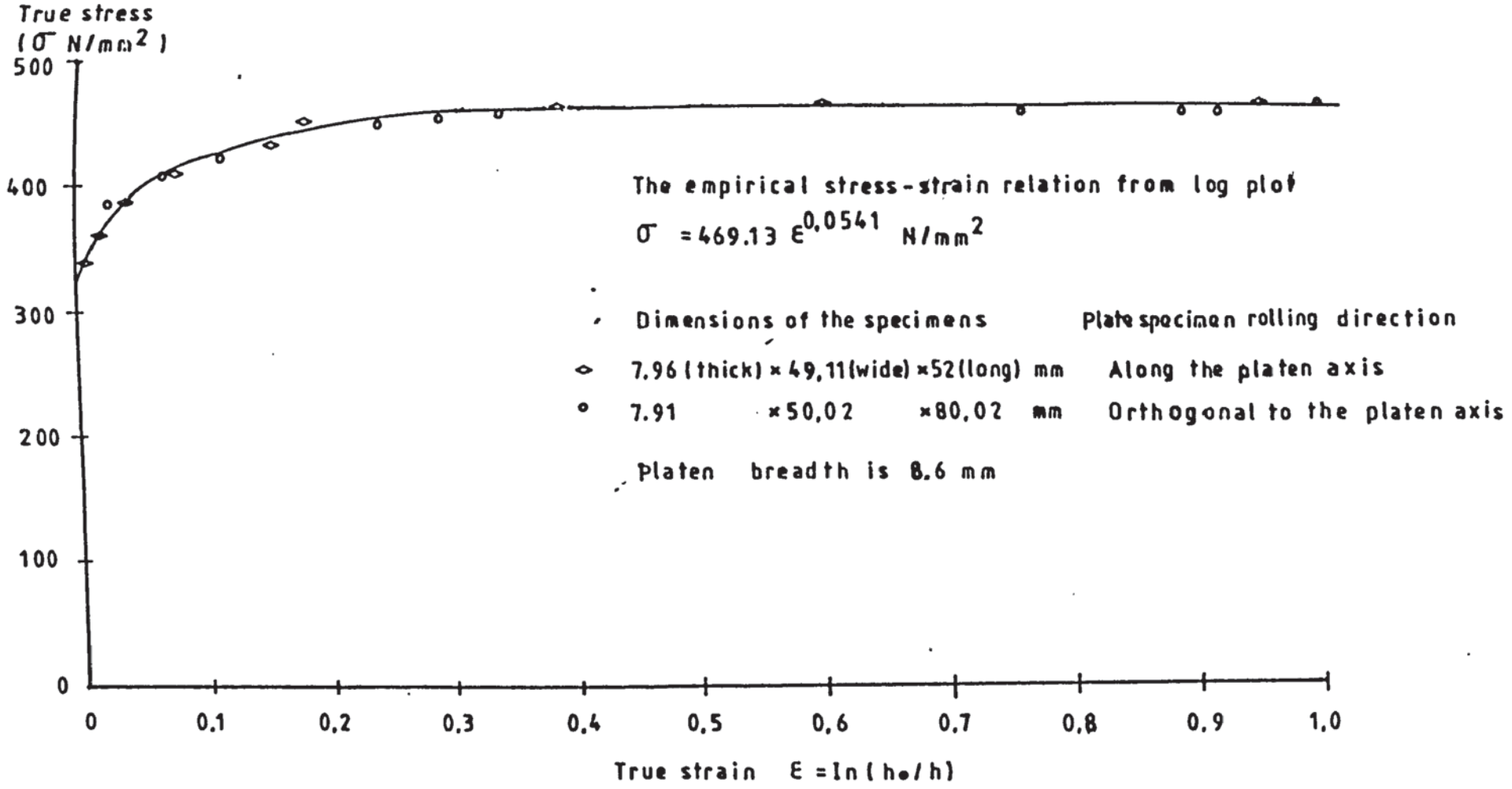

FIG 6.8 THE STRESS-STRAIN RELATION FROM PLANE STRAIN COMPRESSION TESTS ON HP30 ALUMINIUM PLATE OF 8.0 mm THICKNESS

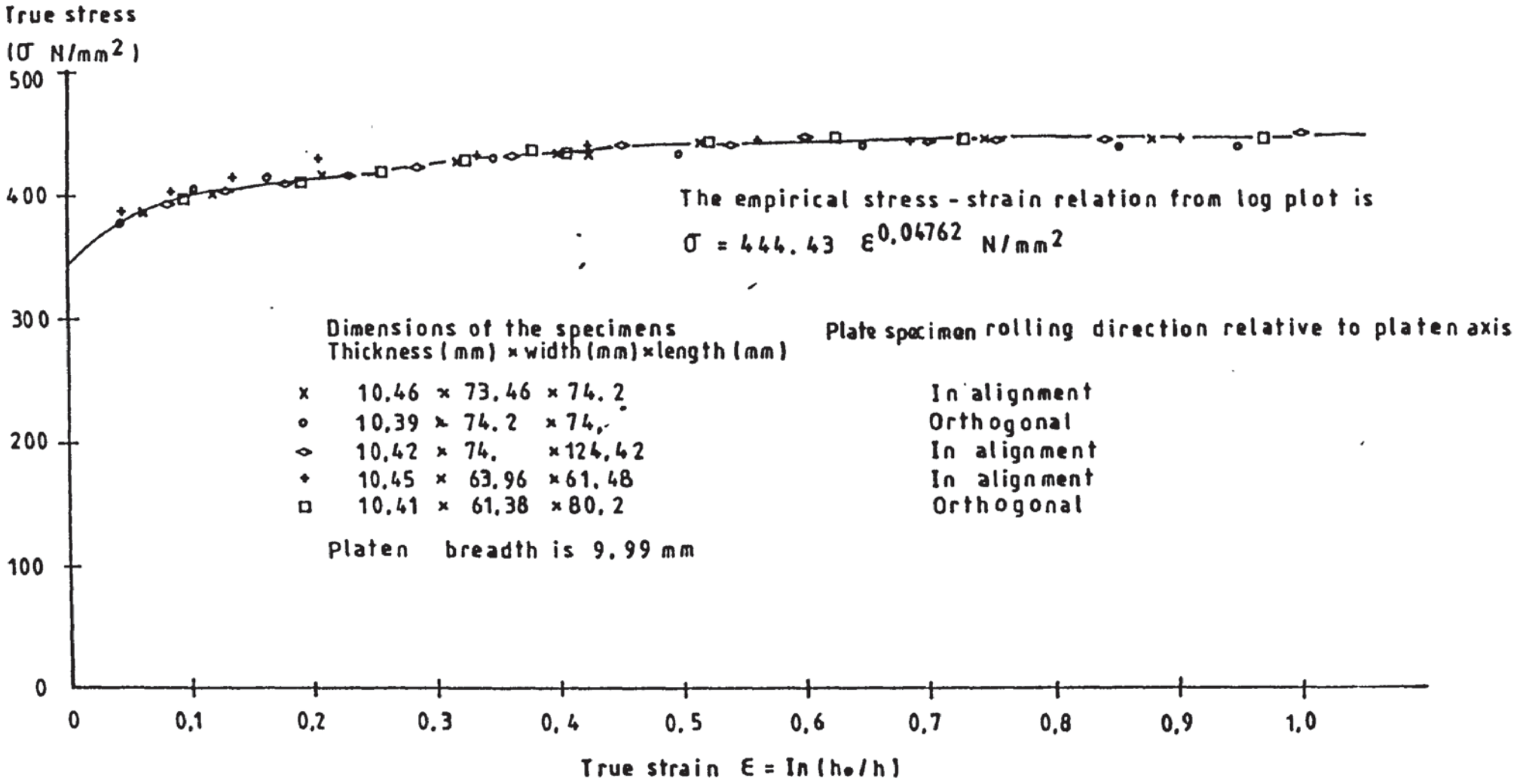

FIG 6.9 THE STRESS-STRAIN RELATION FROM PLANE STRAIN COMPRESSION TESTS ON HP30 ALUMINIUM PLATE OF 10,44 mm THICKNESS

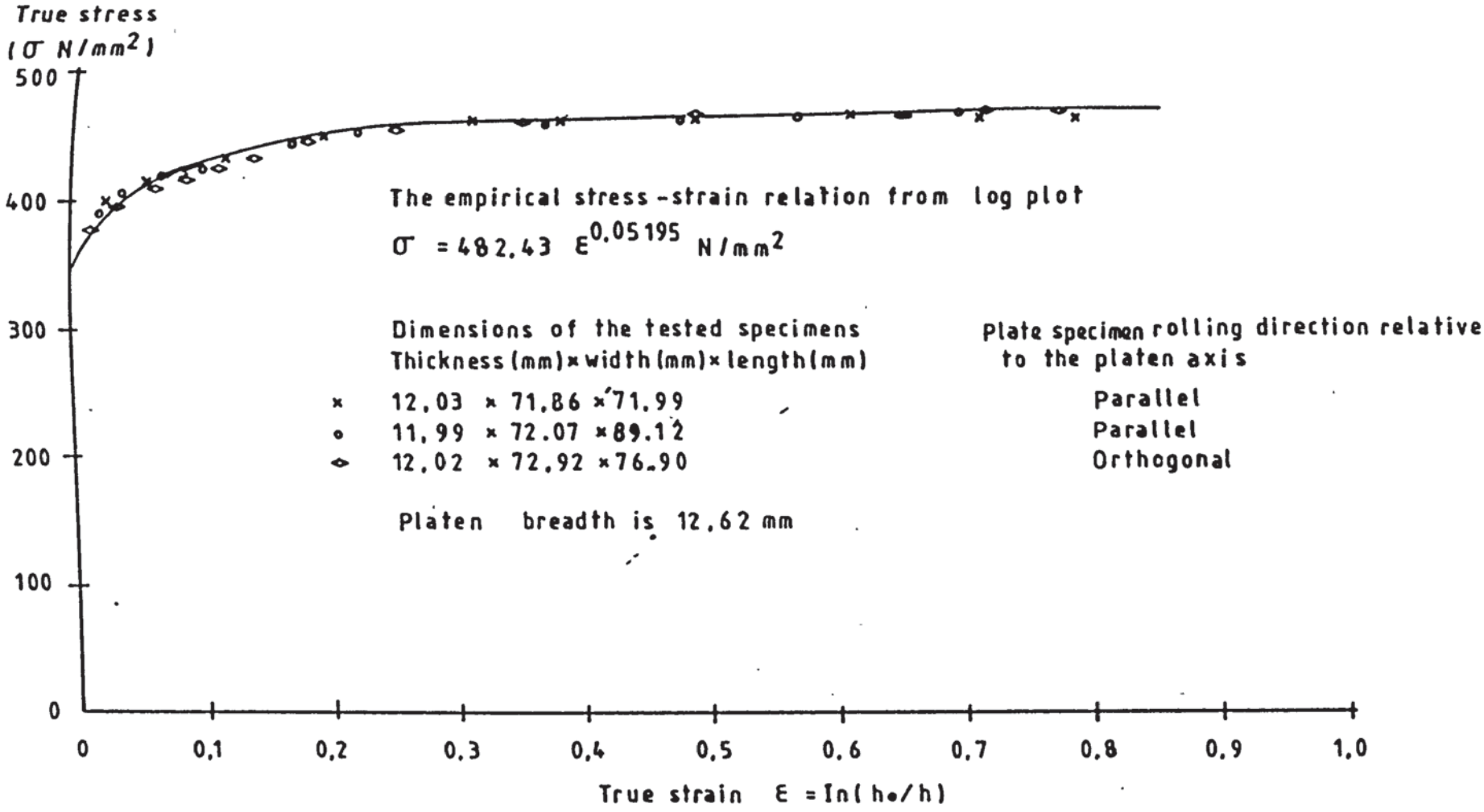

FIG 6.10 THE STRESS-STRAIN RELATION FROM PLANE STRAIN COMPRESSION TESTS ON HP30 ALUMINIUM PLATE OF 12.09 mm THICKNESS

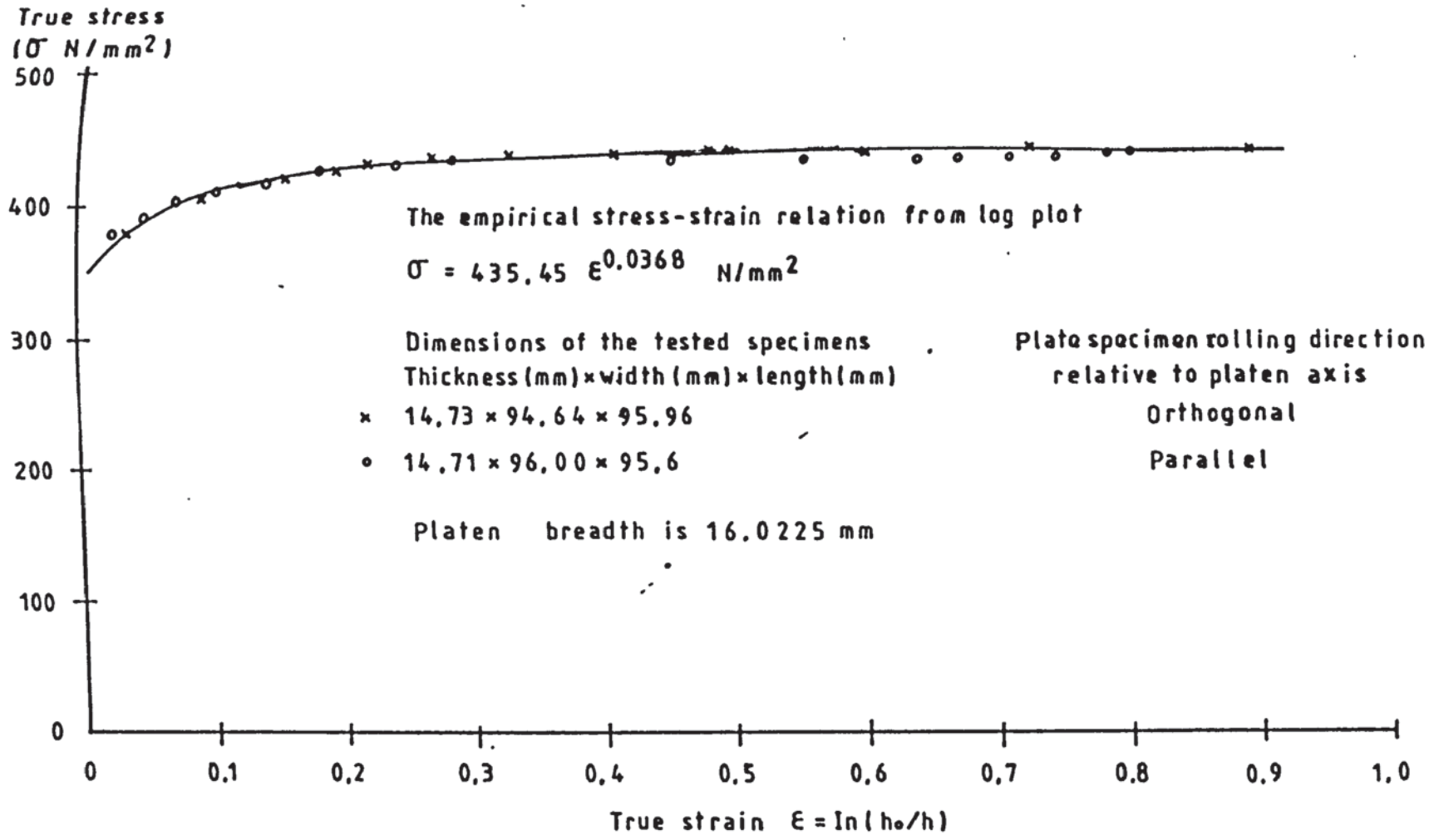

FIG 6.11 THE STRESS - STRAIN RELATION FROM PLANE STRAIN COMPRESSION TESTS ON HP30 ALUMINIUM PLATE OF 14.68 mm THICKNESS

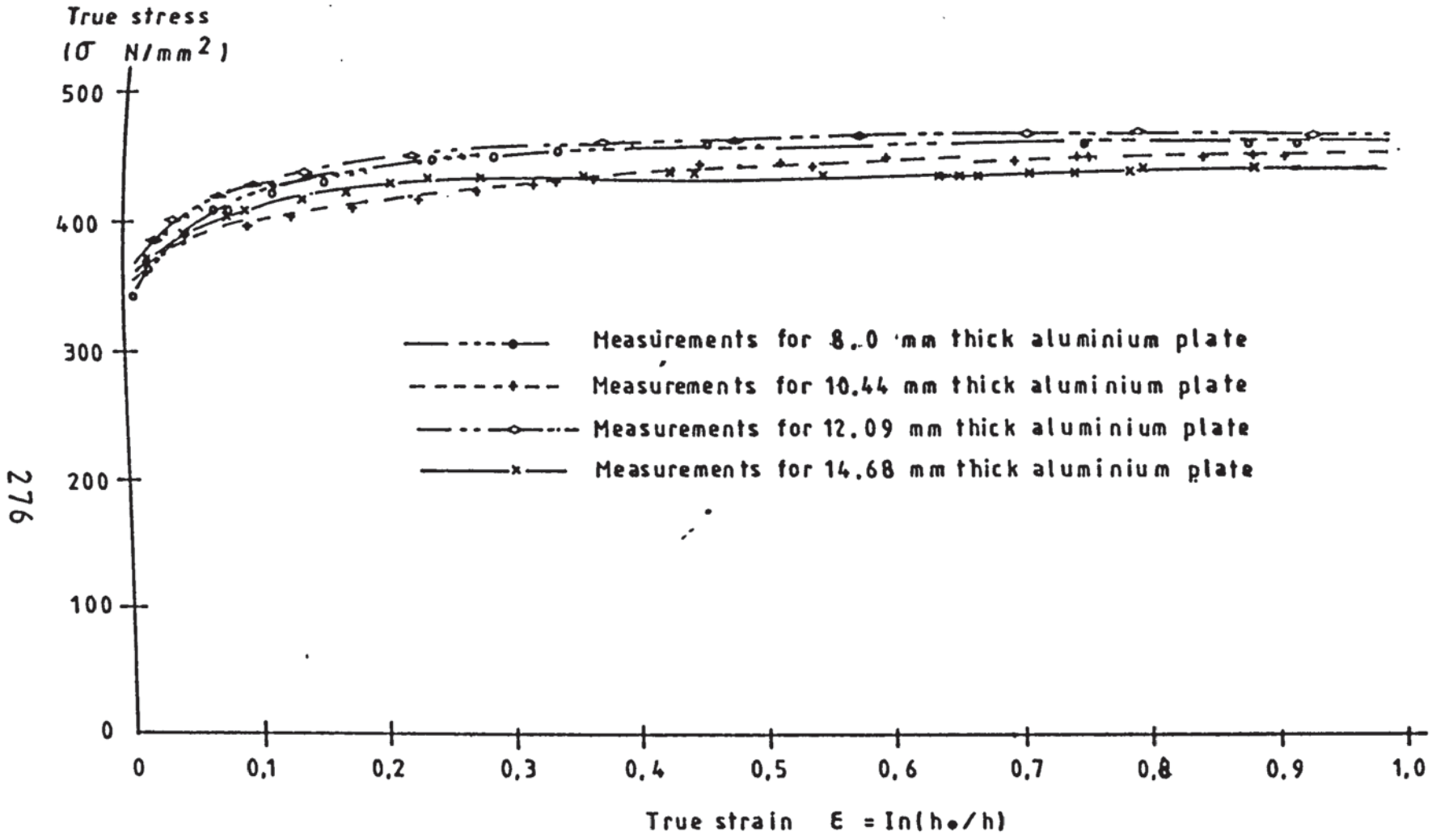

FIG 6,12 COMPARISON OF THE STRESS - STRAIN RELATIONS FROM PLANE STRAIN TESTS ON HP30 ALUMINIUM PLATE SPECIMENS

figs 6.8 to 6.11. The comparison of the results with the other tests revealed little difference. This was sufficient to prove that the widths of the specimens, for the tests in section 6.5.4.1, produced accurate test results.

6.5.4.3. Effect of the specimen length

The effect of the specimen lengths was also tested, as part of the indentation tests. The results for 12.09 mm thick specimens are shown in fig 6.10. The plot indicates that the effect is negligible. It thus shows that the length/width ratios of the test specimens sufficiently restricts the spread in the direction of the platen breadth.

6.6. Conclusions of the tensile and indentation tests

The correlation of the results for the tensile tests with those for the indentation tests has not been carried out. This was because the indentation tests produced the plastic stress strain relation, whereas the tensile test results consisted of the elastic and plastic components. Also the overlapped region of the tests were small (cf. fig 6.2-6.5 and 6.8-6.11).

However, both tests have clearly shown the different degree of hardening for the different thicknesses of bending specimens. They also indicate that the degree of tempering/annealing are also different. The uniaxial tensile tests have also proved that the quoted strength (Section 6.2) of the specimens did not exactly conform to the test results, which gave the proportional limit of the specimens in the range of 245 N/mm^2 to 294N/mm^2.

6.7 Hardness tests

6.7.1. Introduction

Hardness is the property which indicates the resistance of the metal to surface indentation. In the roller plate bending process, sufficient pinch pressure has to be applied in order to grip the plate properly. This is necessary so that the plate will not be easily pulled or pushed away from or through the top and bottom rolls.

It is obvious that the pinch pressure along the pinch contact area also provides the necessary transportation of the plate being bent, through the pinch region in the steady state bending condition. It is very important to ensure that there will be no impression left on the finished bent plate. Consequently it would be beneficial if a knowledge of the specimen hardness was known and recorded.

6.7.2. The tests

Only Brinell hardness tests were carried out in this study. The test procedure closely followed the specifications of British standard BS240:Part 1:1962. All the specimens were prepared to conform to the BS specifications. Throughout the series of tests, a 10 mm diameter indenter was used, and the applied load was "1000kgf".

In each test, five hardness readings were taken at different locations on the surface of each specimen. Mean values of the measured hardness numbers were then calculated for the individual specimen.

All the measurements and the estimated hardness are tabulated in Table 6.1.

6.8 Other peripheral investigation

For reference purpose, surface finish measurements for both rollers and bend plate specimens were also conducted. Appendix

6.1 gives the reason for conducting the measurements. The results are tabulated in Tables A6.1 and A6.2 respectively.

Table 6.1 Hardness Measurements of The HP30 Aluminium Plate Specimens

The following table shows the results of the Brinell hardness number measurements. The measurements were taken using a 10mm ball with a loading of "1000Kgf".

Specimen thickness (mm)	Diameter of impressions (mm)		Brinell hardness Numbers (Kgf/mm^2)	
	Readings	Average	Readings	Average
8.0	3.4 3.5 3.45 3.5 3.5	3.47	107. 101. 104. 101. 101.	102.8
10.44	3.5 3.65 3.5 3.5 3.5	3.55	101. 92.3 101. 101. 95.	98.06
12.09	3.5 3.5 3.5 3.5 3.5	3.5	101. 101. 101. 101. 101.	101.
14.68	3.4 3.5 3.5 3.5 3.5	3.48	107. 101. 101. 101. 101.	102.5

CHAPTER SEVEN

EXPERIMENTAL PROCEDURE AND RESULTS

7.1. Introduction

Prior to the experimental study of the mechanics of the continuous roller bending of plates, it was important to clearly define the relevant parameters which were necessary to achieve the ultimate objectives of the research. Furthermore, it was essential to identify how the necessary parameters were to be obtained.

The objective of the present research has already been described in section 1.2. The measurement of the force on the rolls during bending was performed by using loadcells (sections 4.2, 4.3, 4.6 and 4.7). The torque on the top driving rolls was measured by the torqumeters (sections 4.4 and 4.8). This Chapter will be devoted to describing the experimental procedures and the presentation of the results.

7.2. Experimental procedure

7.2.1. Experimental specimens

In the present investigation only HP30 aluminium specimens were tested.

The aluminium specimens were 8 mm and 10.09 mm thick. Their widths were 80 mm, 120 mm and 240 mm, respectively. The experiments were performed mainly in the multipass bending modes, however the single pass bending mode for 8 mm thick and 80 mm wide aluminium plate specimens was also conducted.

Table 7.1 shows the dimensions of the experimental specimens and their corresponding number of bending passes.

Table 7.1 HP30 Aluminium Plate Specimens For Bending Tests

The following HP30 aluminium plate specimens have been bent in the study of the mechanics of the continuous roller bending plates.

Indicated are the multipass bendings which have been progressively carried out.

Specimen dimensions (mm)			Number of bending passes	Item specified in Table A6.2 for surface measurements
Thickness	Width	Length		
8.02	80.2	346	6	I
8.1	80.5	397	1	A
8.1	80.5	692	1	B
8.04	120.2	346	6	K
8.1	120.2	692	1	D
8.1	120.2	1823	1	E
8.02	214	692	4	C
10.2	80.4	346	6	F
10.4	80.2	692	4	H
10.2	120.3	346	5	G

7.2.2 Geometrical set-up of the experimental rig

7.2.2.1. Rig setting

Since the research commenced with the initial objective of exploring the bending mechanics of a four-roll Verrina bender at HWT, the geometrical setting of the model bender was made to simulate the Verrina bender.

Referring to fig 3.4, the experimental setting of the model was as follows.

a- The positional powering angle, ψ, of the side rolls was set at 20 degrees.

b- The initial positional bending arm, $X=X_0$, was set to 186 mm, which was 1/10 of the value for the Verrina bender. The pinch gap was 36 mm. The bending arm was measured from the centre of the bottom pinch roll to the centre of the side roll.

The front view of the experimental rig so set-up is shown in fig 7.1.

7.2.2.2 Setting precaution

Since the side roll had more than two degrees of adjustment freedom with respect to its centre of positional powering direction, O_p, above the centre of the top roll (fig 7.2), its accurate setting was important and required special attention.

The procedure for setting up the rig (refer to fig 7.2) to simulate the Verrina bender was thus derived as follows :

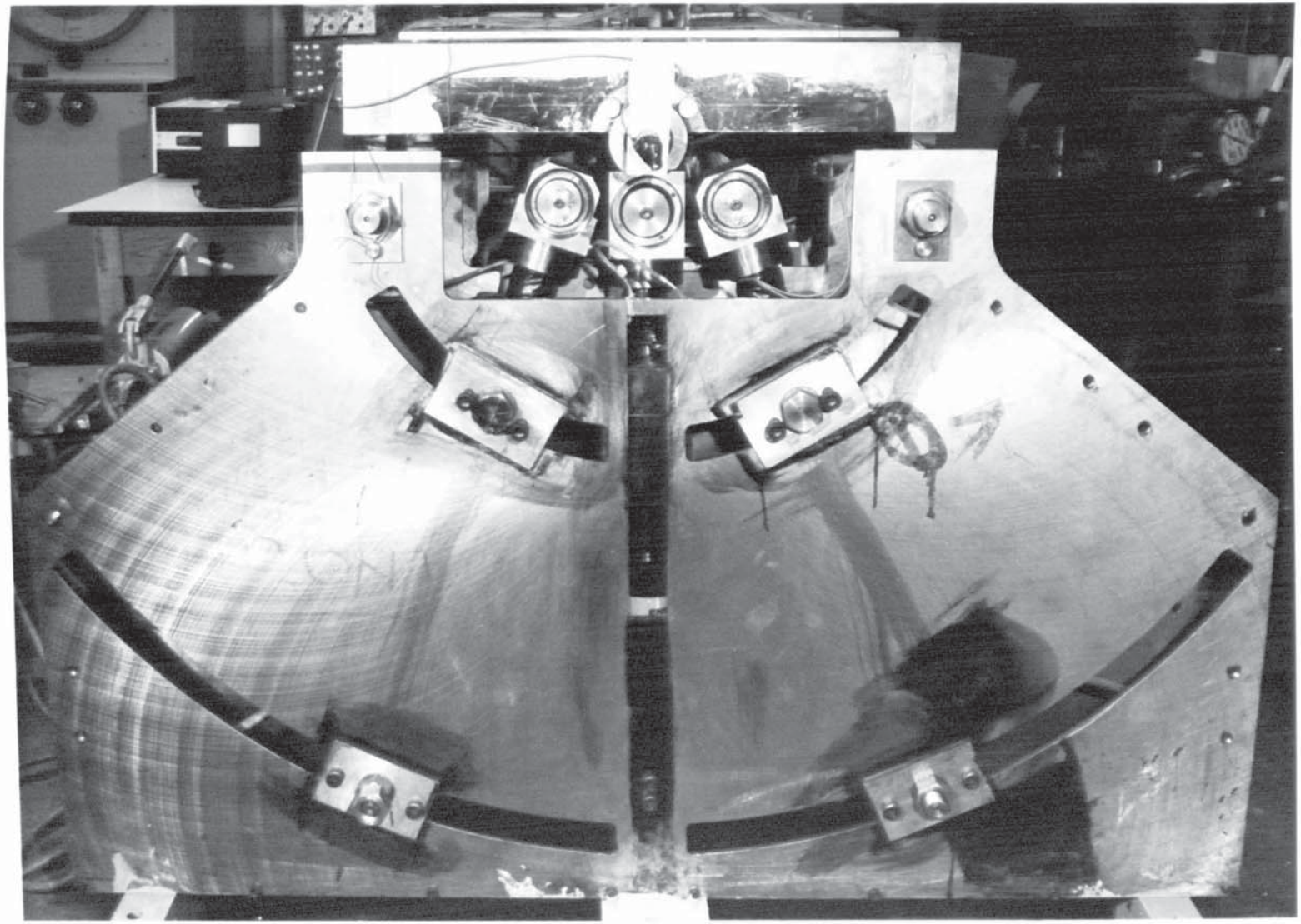

FIG 7.1 FRONT VIEW OF THE MODEL BENDER

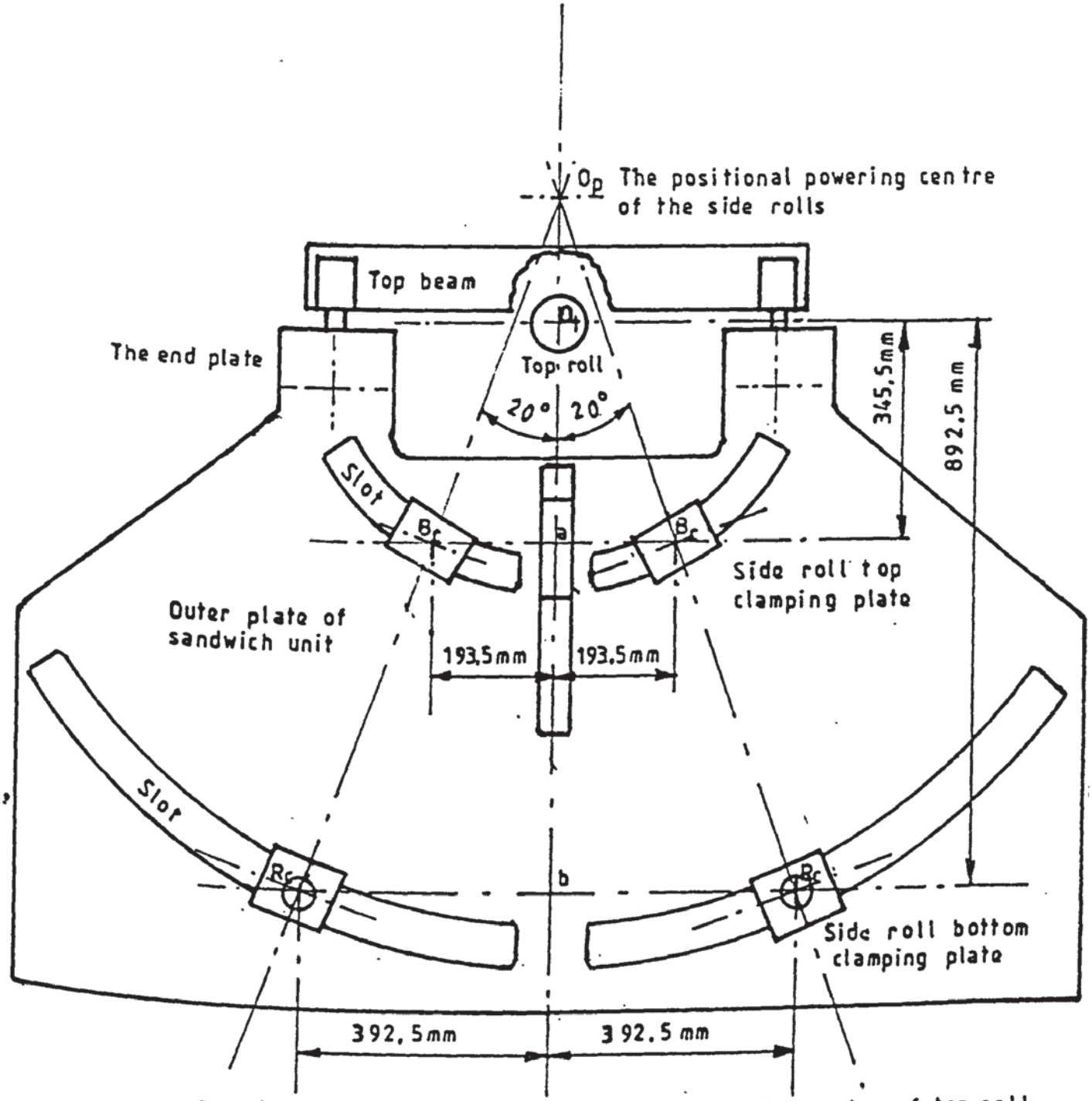

FIG 7.2 THE SIDE ROLL SETTING OF THE MODEL BENDER FOR SIMULATING THE VERRINA BENDER

a- Using the centre of the top pinch roll as the datum, a vertical central line through the top and bottom pinch rolls and horizontal lines at distances of 345.5 mm and 892.5 mm, respectively, were scribed on the surface of the outer plates of the sandwich unit; thus giving two points of intersection.

b- The inclination of the positional powering leg of each side roll was adjusted until the centres of the top bolts, and the bottom clamping rod (i.e. B_c and R_c respectively in fig 7.2) were 193.5 mm and 392.5 mm, horizontally away from the top and bottom points of intersection, as mentioned in (i).
- In order to ensure that the clamping bolts and the rods on the inner plates of the sandwiching unit were properly aligned to those on the outer plates of the bending unit, each pair of legs was set and secured using a straight edge bar.

c- Finally, the angle of the activating direction of the powering hydraulic piston was checked using a spirit level. The relevant measurements of the setting were then confirmed.

7.2.3. Area of investigation

To understand fully the continuous roller bending of plates process, extensive studies were planned during the initial rig design stage.

To explore the general mechanics of the roller bending processes, primarily in the four roll bending mode, a detailed experimental programme was provisionally drawn up as shown in Table 7.2 [150]. The original experimental schedule examined the following :

Table 7.2 The Initially Proposed Experimental Investigations in Four-Roll Plate Bending Process (see ref 150)

The following are some of the symbols used in the table :

Combination of rolls :-

cr1 - Dimension of	top roll	= 90 mm
	bottom roll	= 90 mm
	side roll	= 75 mm
cr2 - Dimension of	top roll	= 90 mm
	bottom roll	= 90 mm
	side roll	=100 mm
cr3 - Dimension of	top roll	= 90 mm
	bottom roll	=117 mm
	side roll	= 75 mm
cr4 - Dimension of	top roll	= 90 mm
	bottom roll	=117 mm
	side roll	=100 mm

Surface roughness :-

s0	- As supplied
s1	- Finest
s2	- Rough
s3	- Roughest

Number of passes :-

n1	- 1 pass
n2	- 2 passes
n3	- 3 passes
n4	- 4 passes

£ - Both slip and non-slip effects to be investigated.

Positional powering angle of the side rolls :-

ß1-21.5°, ß2-45°, ß3-70°, ß4-80°

Table 7.2 The Initially Proposed Experimental Investigations in Four-Roll Plate Bending Process

Plate Specimen thickness (mm)	BENDING TESTS			
	ROLL LENGTH OF THE PLATE SPECIMENS (mm)			
	80	120	214	305
(i) ALUMINIUM PLATE SPECIMENS				
8	s0+cr1+n1+ß3			
10	s0+cr1+n1+ß3 £ s0+cr3+n1+ß3			
			s0+cr2+n1+ß3 s0+cr4+n1+ß3	
				s1+cr1+n1+ß3 £ s2+cr1+n1+ß3 £ s3+cr1+n1+ß3 £ s0+cr1+n1+ß1 s0+cr1+n1+ß2 s0+cr1+n1+ß4
13	s0+cr1+n1+ß3 £			
				s0+cr1+n2+ß3 s0+cr1+n3+ß3
16	s0+cr1+n1+ß3 £			
				s0+cr1+n2+ß3 s0+cr1+n3+ß3 s0+cr1+n4+ß3

Table 7.2 The Initially Proposed Experimental Investigations in Four-Roll Plate Bending Process (Cont)

Plate Specimen thickness (mm)	BENDING TESTS			
	ROLL LENGTH OF THE PLATE SPECIMENS (mm)			
	80	120	214	305
	(ii) LEAD PLATE SPECIMENS			
13	s0+cr1+n1+ß3 £			
16				s0+cr1+n1+ß3 £ s0+cr1+n2+ß3 s0+cr1+n3+ß3 s1+cr1+n1+ß3 £ s2+cr1+n1+ß3 £ s3+cr1+n1+ß3 £ s0+cr3+n1+ß3 s0+cr1+n1+ß1
18				s0+cr1+n1+ß3 s0+cr1+n2+ß3 s0+cr1+n3+ß3 s0+cr1+n4+ß3
20	s0+cr1+n1+ß3			
				s0+cr1+n2+ß3 s0+cr1+n3+ß3 s0+cr1+n4+ß3

Table 7.2 The Initially Proposed Experimental Investigations in Four-Roll Plate Bending Process (Cont)

Plate Specimen thickness (mm)	BENDING TESTS			
	ROLL LENGTH OF THE PLATE SPECIMENS (mm)			
	80	120	214	305
(iii) MILD STEEL PLATE SPECIMENS				
4	s0+cr1+n1+ß3			
6	s0+cr1+n1+ß3 £			
				s0+cr1+n2+ß3
				s0+cr2+n1+ß3
				s0+cr3+n1+ß3 £
				s0+cr4+n1+ß3
				s1+cr1+n1+ß3 £
				s2+cr1+n1+ß3 £
				s3+cr1+n1+ß3 £
				s0+cr1+n1+ß1
				s0+cr1+n1+ß2
				s0+cr1+n1+ß4
8				s0+cr1+n1+ß3 £
				s0+cr1+n2+ß3
				s0+cr1+n3+ß3
10	s0+cr1+n1+ß3			
				s0+cr1+n2+ß3
				s0+cr1+n3+ß3
				s0+cr1+n4+ß3

1. The effect of geometrical set-up of the roller bender.
2. Slip effect between the bend-plate and the side rolls with respect to the deformation zone.
3. Frictional effect due to the surface texture condition of the bend plate specimens and the rollers.
4. Roll size effect of the top and bottom pinch rolls.

The experimental schedule would pay particular attention to the force and torque in bending various thicknesses and widths of plates to different bend radii. Dissimilar plate materials, i.e. aluminium, mild steel and lead would also be considered.

Unfortunately, due to lack of financial support, the complete experimental study was not performed as had been originally planned. Furthermore, this situation considerably extended the allocated time for the construction of the bender. A modified experimental programme was thus required. Noting that the prime objective of the research was to produce a mathematical theory to predict the force and torque in the bending process, with the experimental work being used only to verify the reliability of the theoretical model, a significant reduction of the experimental work was possible.

The actual area of the experimental investigation was therefore limited to bending 8 mm and 10.09 mm thick aluminium plates of the widths shown in Table 7.1. The number of bending passes for each specimens bent is also indicated in the Table. In addition, the edge setting of each bend was also investigated.

The bending was carried out with two side rolls of diameter 75 mm, and a diameter of 90 mm for both top and bottom pinch rolls. The geometrical set-up of the bender is shown in fig 7.2.

7.2.4. Measurement procedure

To achieve meaningful signals from the loadcells and the torquemeter, a series of supplementary measurements were also required. The supplementary measurements were as follows :

a- thickness and width of the plate to be bent.
b- finished bend radius of the bent plate.
c- vertical and horizontal displacements, at the beginning and completion of each bend, of the side roll relative to the bottom pinch roll and the top beam.
d- rotational speed of the top roll.
e- length of the straight end for each bent plate.

A description of the relevant physical measurements is presented in the following sections.

7.2.4.1. Preparation for commencing each test

All the rollers and the bend plate to be bent were carefully cleaned before the starting of the experiment. Both sides of the bend plate at the pinch end were coated with engineers blue, which was used to obtain the trace of indentation on each side of the plate during pre-bending.

A. The instruments

Prior to the starting of the experiment, the power supply to the u.v. recorders, the amplifier circuitries (see Chapter Four), all the respective strain gauge bridges and all the other supplementary instruments were switched on. At least half an hour was allowed to elapse so that stable conditions were achieved.

B. Setting of the gap and rollers

Pre-setting the gap was performed by using slip gauges. Two blocks of slip gauges were built such that they were equal to

the thickness of the plate. Each slip gauge block was placed at either end of the designed roll length of the top and bottom pinch rolls (fig 7.3(a)). The parallelism of the top and bottom pinch rolls was ensured by checking various positions along the gap using the slip gauges. Normally, the gap was set at approximately 0.1 mm over the thickness of the plate to be bent.

After setting the gap, a flat plate was then passed through it. This plate was allowed to hang over the nominated pre-bending operative side roll (it will be named the pre-active side roll in the following context) and a spirit level was placed on the mid-span of the plate (fig 7.3(b-i)). The pre-active side roll was then slowly "pumped up" until the spirit level indicated that the pre-active side roll was level with the bottom pinch roll. The levelling was carefully checked, along several positions in the roller roll length direction (fig 7.3(b-ii)), using the levelling plate and the spirit level.

The measurements were then taken for the following quantities :

a- The distances from the top of the bottom pinch roll bearing housings to the bottom face of the top beams.
b- The horizontal distances between the centres of the bottom pinch roll and the pre-active side roll for each end of the rolls.
c- The distances from the centres of the pre-active side roll to the bottom face of the top beam.

The measurements were used as the initial datum points for determining the displacements of the corresponding rolls in the subsequent bending tests.

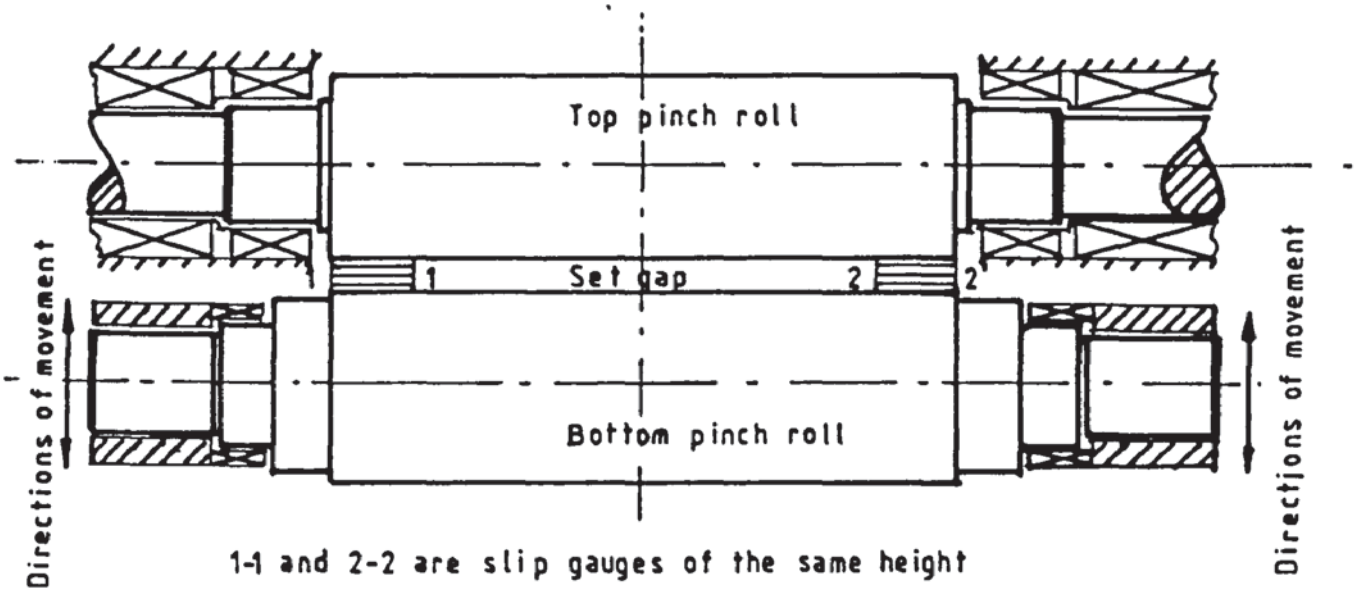

1-1 and 2-2 are slip gauges of the same height

(a) Pre-setting the roll gap, for roll-bending a specific thickness of plate specimen, using slip gauges

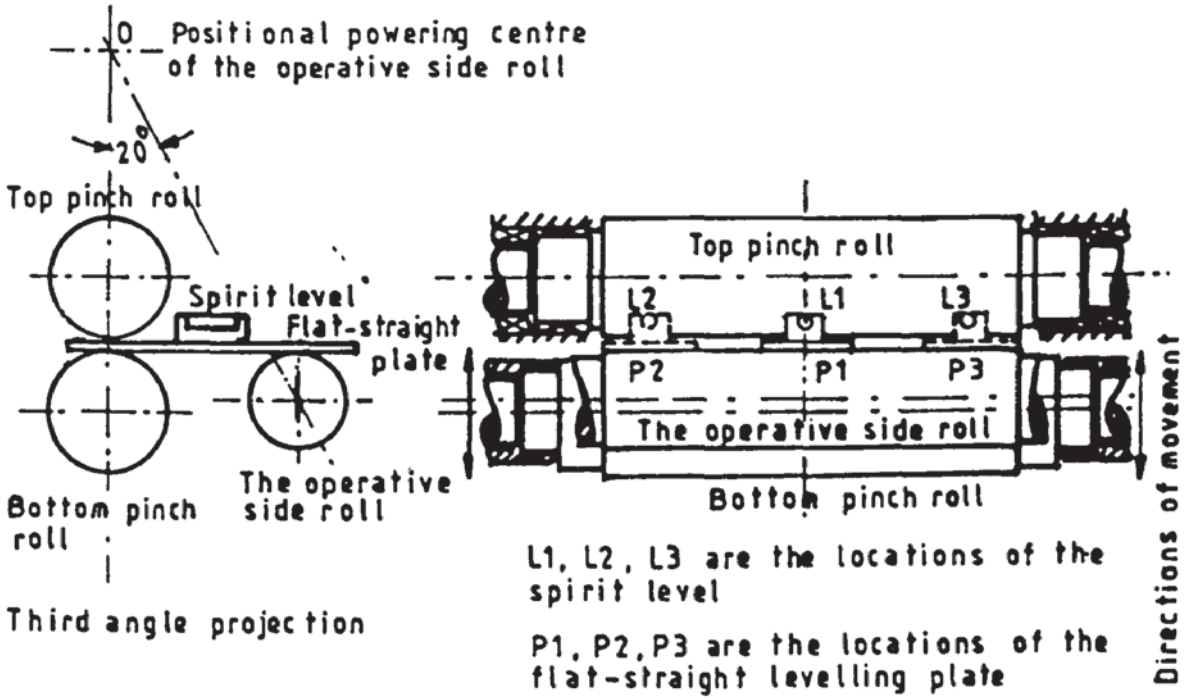

i - The end view

ii- The side view

(b) Technique for levelling the bottom pinch roll and the operative side roll prior to the setting of bending specimen

FIG 7.3 TECHNIQUES FOR PRE-SETTING THE ROLL GAP AND LEVELLING THE BOTTOM PINCH ROLL AND THE OPERATIVE SIDE ROLL PRIOR TO THE SETTING OF BENDING SPECIMEN

C. Plate locating

To ensure that the bend plate was centrally located in the rolls, thus preventing the offset problem, the centre of the width of each roll was carefully marked. Two parallel lines, each one half-width of the plate from the central were marked on the pre-active side roll. The two latter lines were mainly used as a guide for locating the plate.

In locating the bend-plate in the pinch gap, a long machine tool packing bar was used to square the lateral edge of the plate through the pinch. The bend plate was then adjusted square until the two longitudinal edges of the plate were in line with the two previously marked lines. Re-checking of the plate level was again performed.

D. Circuit lead of the torquemeter

Since the bridge circuit lead of the torquemeter was designed to wrap round the propshaft (see section 4.12), the lead length was limited. Care was particularly taken to ensure that there was a sufficient lead length available to complete the plate bend. It was therefore necessary to make sure that the driving direction of the top roll was such as to allow the release of the lead for wrapping around the shaft during subsequent bending.

7.2.4.2. Bending procedure and measurements

Each channel circuit was electrically zeroed and the mechanical position of the output for each galvonometer on the u.v. charts were further identified and noted.

The following stages in the test procedure were then carried out :

(a) The plate was gripped by "pumping up" the bottom pinch roll.

- The levelling of the bottom pinch roll was checked by measuring the distance from the top face of its bearing housings to the bottom face of the top beams. The adjustment was repeated until equalisation at either end of the bottom roll was achieved with a sufficient grip force in the pinch gap.

(b) The setting was rechecked to ensure that the pre-active side roll was just touching the bottom face of the bend-plate.

- To bend an initially flat plate, this preparatory setting did not necessitate any further adjustment. For an initially curved bend plate, re-adjustment was usually required.

(c) The following measurements were then taken at either end of each effective roll.

1- distance from the top of the bottom pinch roll bearing housing to the bottom face of the top beam,

2- horizontal distance from the centre of the bottom pinch roll to the centre of the pre-active side roll,

3- vertical distance from the centre of the pre-active side roll to the bottom face of the top beam.

(d) The pre-active side roll was then positioned at an assumed vertical distance from the bottom faces of the top beams to the centres of the pre-active side roll.

(e) The locking of all the hydraulic valves was then checked.

(f) Items c-2 and c-3 were then repeated.

(g) The plate was then conveyed through the pinch until a sufficient length of the bend had covered the distance

from the pinch to the pre-inactive side roll.

(h) The pre-active side roll was then lowered until the plate was free.

(i) The pre-active side roll was then positioned to touch the curved surface of the bent section of the plate. Measurements of items c-2 and c-3 were then repeated. In this case the pre-active side roll was replaced by the pre-inactive side roll.

(j) Next the pre-inactive side roll was positioned to the measured distance as stated in item (f) above.

(k) The plate was then rolled to complete the bend.

(l) Finally the position of the galvanometer output, from each bridge, on the u.v. charts was checked.

Since there were eighteen galvanometer outputs on the SE and four on the Southern Instrument u.v. recorders, continuous tracing of the signal during the bending process was considered. However, to minimise the lengths of the u.v. charts produced by the bending intermissions in (b), (c), (e), (f) and (j), an alternative discrete recording technique was adopted. The discrete tracing method started and stopped the recording before and after the performance of procedures (a), (d), (g), (h), (i), (k) and (l), respectively. It thus gave a tracible chart as the other procedures did not affect the traces.

These experimental procedures are relevant to thin plate bending only. For thick plate bending, which was not performed in this study, modification of the above procedure is needed.

7.2.4.3. Post bending measurements

A. Bend radii

The finished bend radius of the plate (after the release of the load) was measured by a designed radius measurement device (section 4.10). Several bend radius measurements were taken along various positions of the bend. Fig 4.26 illustrates the operation of the radius measurement device. Its operational feature was to set the longitudinal edge parallel to the circumference of the bend by means of a set-square.

B. Minimum straight edge of the bend

The linear length remaining in each bend (for the pre-bending mode) was evaluated by measuring the difference of the lengths of the contact bends, on the concave and the convex surfaces of the bend, from the set transverse edge of the plate. The above measurements were obtained by painting engineering blue on either surface of the plate.

7.3. Experimental data analysis

It is important that the measurements obtained are properly analysed and systematically presented. Great care was taken to follow the correct trace for each bridge output so as to obtain the appropriate parameters. Described below is the analysis of the experimental data.

7.3.1. Parameters of the bending mechanics

For the present study, the relevant parameters were :

a- bending forces on the pinch rolls and the side rolls required to bend a plate to the required bend radius for single or multipass bendings.
b- power required to bend a plate to the expected radius for a single or multipass bendings.

c- maximum torque required to bend a plate from the pre-bending to the continuous steady state bending mode.

d- optimum setting edge required for the pre-bending mode.

The above parameters, both before and after the release of the applied loads, are expected to provide an insight into the mechanics of bending. Although only the latter parameters were investigated in this study, a relevant semi-empirical mathematical model for investigating the former parameters is presented in Appendix 7.1.

7.3.2. Determination of the experimental torque on each roll

The force on each roll (for the bottom pinch roll and the two side rolls) was measured by two separate loadcells ; each at either end of the roll. For the top roll, there were four loadcells. Each pair was used to support a top beam, to which was mounted the top roll (see fig 3.5). Each loadcell measured the axial force, F_a, and bending force, F_b. The signal from each loadcell was converted to a force quantity by using the appropriate calibration equations in Table 4.1. The resultant force, F, on each side roll was then determined as follows.

$$F=[(\sum_{i=1}^{n} F_{a_i})^2+(\sum_{i=1}^{n} F_{b_i})^2]^{1/2} \qquad (7.1)$$

where, $n=2$ for the bottom pinch roll and each of the side rolls.

$n=4$ for the top roll.

The loading (or contact) angle, θ, of either the bottom or top pinch roll, may be evaluated using the following expression (if required).

$$\theta = \tan^{-1}\left[\left(\sum_{i=1}^{n} F_{b_i}\right)/\left(\sum_{i=1}^{n} F_{a_i}\right)\right] \qquad (7.2)$$

Since each side roll has a positional powering angle of ψ, the components of the vertical force, F_v, and the horizontal force, F_h, can be expressed as follows.

$$F_v = \left(\sum_{i=1}^{n} F_{b_i}\right)\sin\psi + \left(\sum_{i=1}^{n} F_{a_i}\right)\cos\psi \qquad (7.3a)$$

and,

$$F_h = \left(\sum_{i=1}^{n} F_{b_i}\right)\cos\psi + \left(\sum_{i=1}^{n} F_{a_i}\right)\sin\psi \qquad (7.3b)$$

7.3.3. Evaluation of the experimental torque

Since the present experiment was performed under the bending conditions, which simulated the Verrina bender, the two side rolls were thus free to rotate. The lubricated bearing of each side roll indicated that there would not be any slip between the bend plate and the side roll. The only torque existing in the experiment was therefore the torque on the top roll.

The torque input on the top roll was measured by a calibrated torquemeter (section 4.8). The output signal was traced on a SE u.v. recorder. The measured torques were (i) the mean torque, T_m, and (ii) the maximum torque, T_{max}.

In determining the mean torque, it was noticed that its trace on the u.v. chart was oscillating within a small band

width. The mean torque, T_m, was thus evaluated from the difference on the u.v. chart between the mean chart value, T_r, of the oscillation and the initially set reference chart value, T_0, as the continuously steady state was reached., i.e.

$$T_m=a(T_r-T_0)+b \qquad (7.4)$$

where a,b are the calibration constants as shown in Table 4.1.

T_r, T_0 are the measured chart width of the trace in mm.

The maximum torque was defined as the highest torque experienced in each continuous bending mode. It was evaluated by replacing the reference quantities of T_m and T_r by T_{max} and T_i, respectively, in the calibrative equation (7.4). In this case T_i was the chart width measurement in mm at the transitional state.

7.3.4. Determination of the speed of the top roll

The rotational speed of the top roll was measured by a tachometer mounted at the free end of the top roll (fig 4.28). It was evaluated by the difference of the u.v. chart readings of the corresponding trace at the instant of steady rotation and its initial datum by the following equation :

$$N=c(\omega_r-\omega_0)+d \qquad (7.5)$$

where N is the rotational speed in r.ov/min.

ω_r, ω_0 are the measurements, in mm, from the chart and denotes the steady rotation and the initial datum respectively.

c,d are the calibrative constants from Table 4.1.

7.3.5. Determination of the experimental power

The mean power, P_m, of the drive in each bend was determined according to the following equation.

$$P_m=2NT_m/60 \qquad (7.6)$$

where N is the number of rotations in rev/min.

7.3.6. Evaluation of the experimental work done (if required)

The total work done, W_d, to complete a bend in the continuous roller bending process can be evaluated from the traces of the u.v. chart using the following equation :

$$W_d=(2NT_m/60V_c)(L_a/2+L_s+L_d/2) \qquad (7.7)$$

where, V_c is the chart speed of the u.v. recorder.

L_a, L_s and L_d are the length of the u.v. traces during acceleration, steady driving and deceleration, respectively. These lengths are in relation to the torque on the top roll during bending.

7.3.7. The inner bend radius

This can be measured by using the bend radius measuring device (section 4.10) and equation 4.8.

7.3.8. Displacement of the nominated active side roll

Referring to section 7.2.4, The horizontal

displacement, Δx_s, of the nominated active side roll is established by

$$\Delta x_s = x_{0i} - x_i \qquad (7.9)$$

where, x_{0i} is the horizontal distance between the centres of the bottom pinch roll and the nominated active side roll prior to the bending.

x_i is the corresponding distance of the above after or at any instance of bending.

The vertical displacement, Δy_s, of the nominated active side roll can be calculated using following statement.

$$\Delta y_s = y_{0i} - y_i \qquad (7.10)$$

where, y_{0i} is the vertical distance from the centre of the nominated active side roll to the bottom face of the top beam prior to the bending.

y_i is the corresponding distance of the above after or at any instant of bending.

The evaluation of the displacements are useful for the experimental investigation of the springback analysis in bending a thin plate, as described in Appendix 7.1.

7.4. Graphical presentation of the experimental results

Some expressions, described in section 7.3, for the data-analysis were only relevant to the empirical study of the specific parameters (section 7.3.1) before the release of the bending loads. In the present research, the experimental investigation of springback was not analysed. Consequently,

the following only presents the graphical results relevant to those after the release of the bending loads.

All the relevant graphical results are presented in figs 7.4 to 7.23.

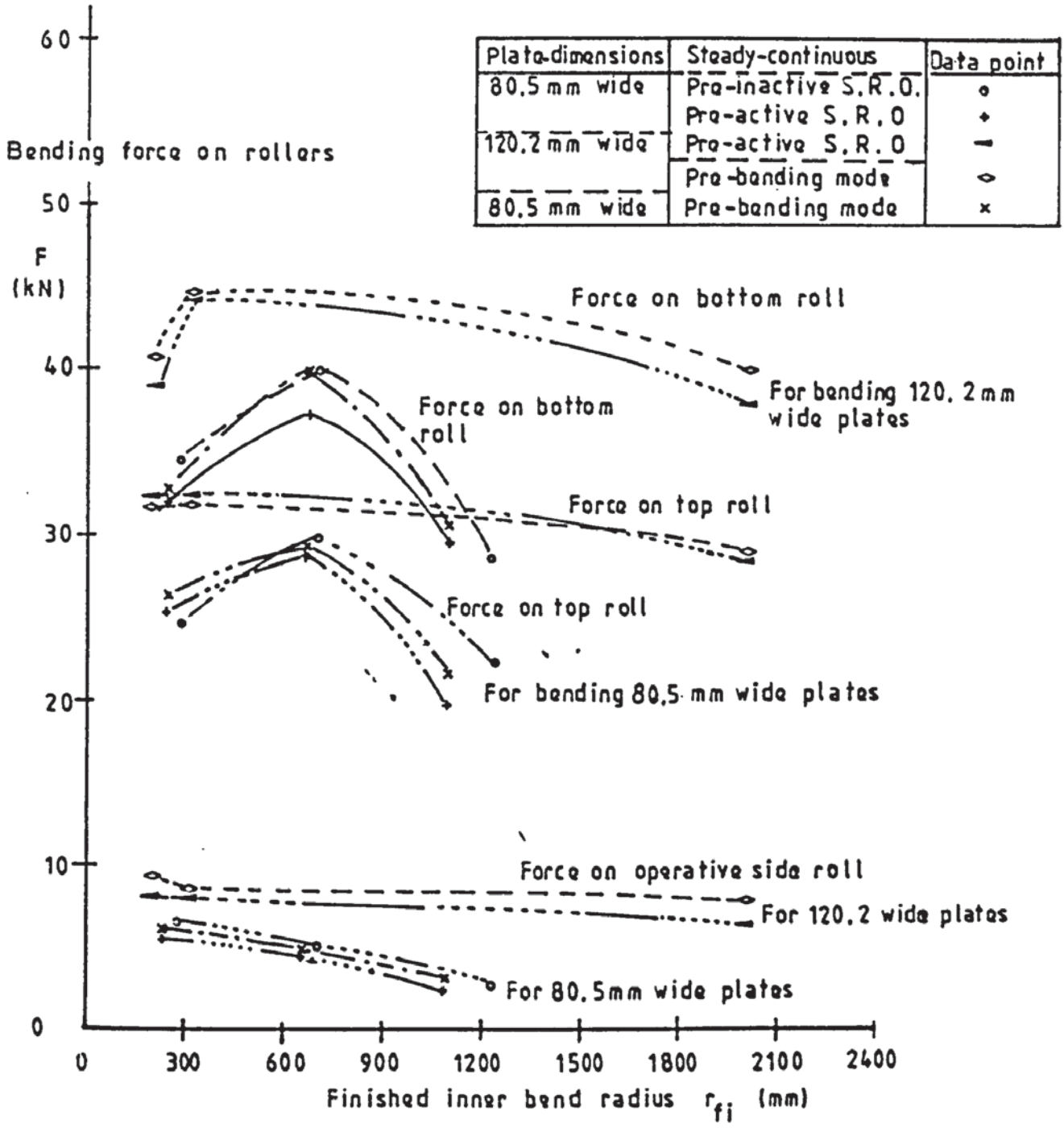

FIG 7.4 CHARACTERISTICS OF BENDING FORCE ON ROLLERS FOR SINGLE/FIRST PASS BENDING OF HP30 ALUMINIUM PLATES (8.mm THICK BY 80.5mm AND 120.2mm WIDE)

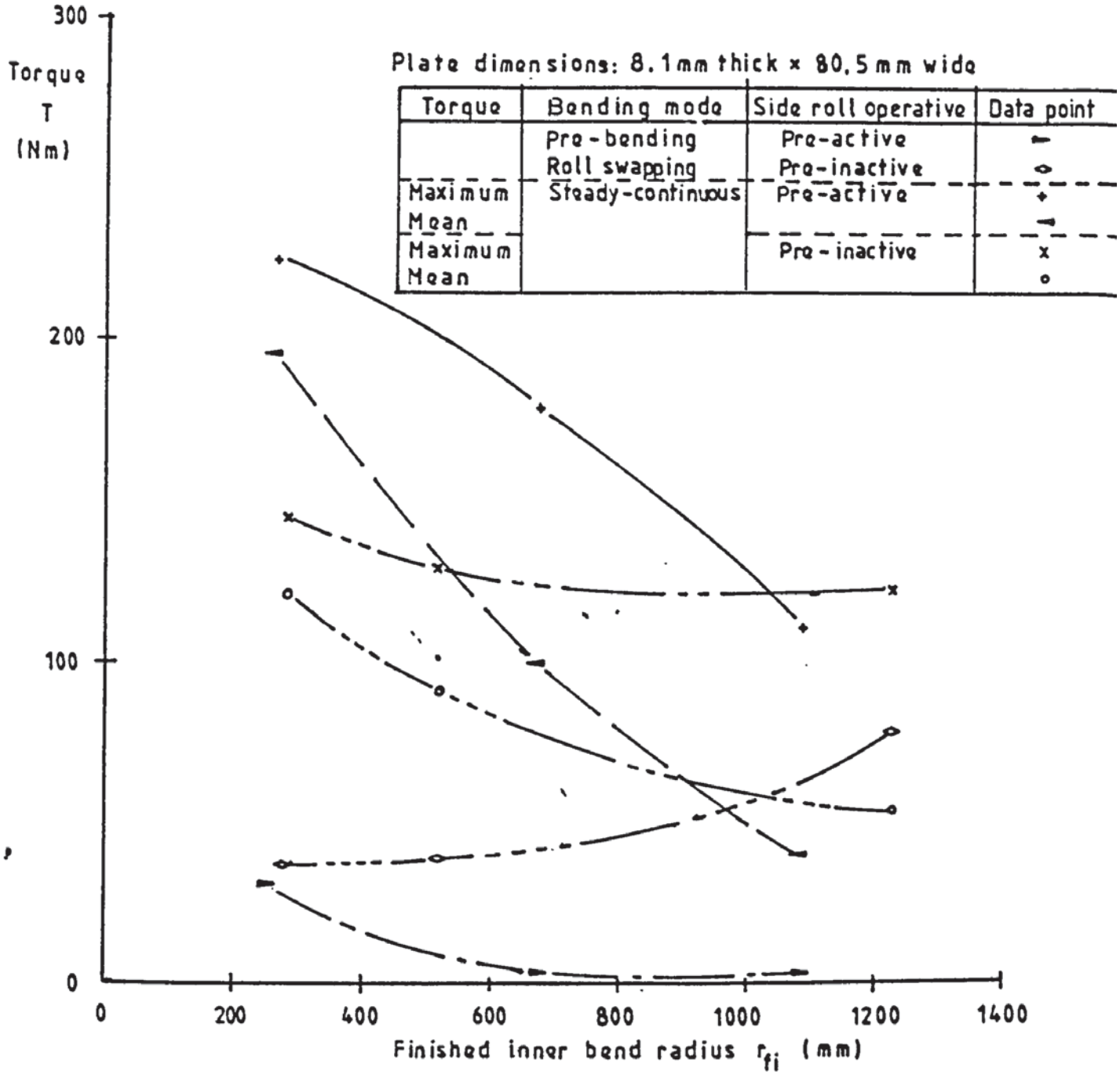

FIG 7.5 EXPERIMENTAL TORQUE CHARACTERISTICS FOR SINGLE/FIRST PASS BENDING OF HP30 ALUMINIUM PLATE (8.1mm THICK BY 80.5 mm WIDE)

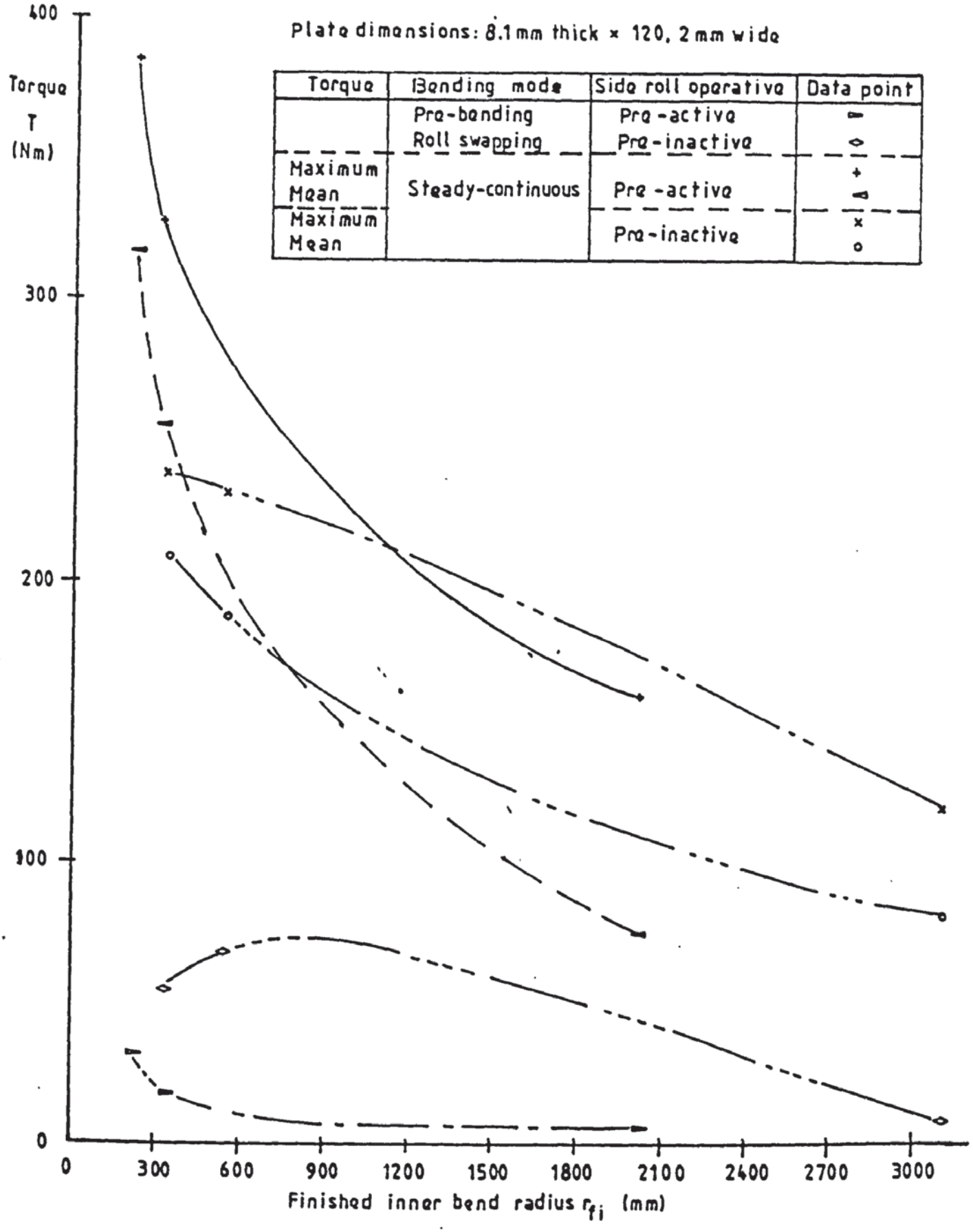

FIG 7.6 EXPERIMENTAL TORQUE CHARACTERISTICS FOR SINGLE/FIRST PASS BENDING OF HP30 ALUMINIUM PLATE (8.1 mm THICK BY 120.2 mm WIDE)

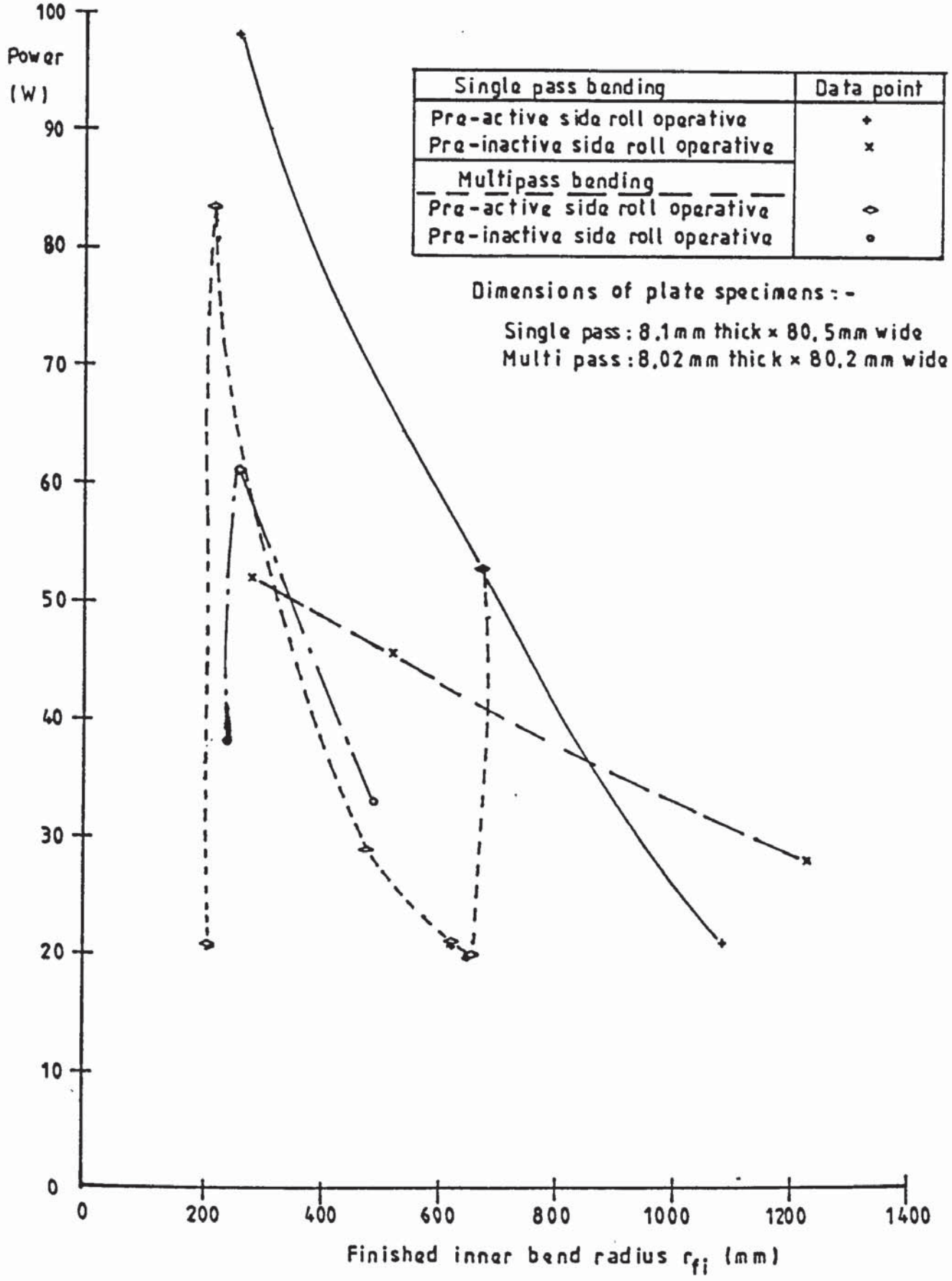

FIG 7.7 EXPERIMENTAL POWER CHARACTERISTICS (AT MEAN TORQUE) FOR SINGLE AND MULTI PASS BENDING OF 8,1 mm THICK × 80,5 mm WIDE HP30 ALUMINIUM PLATE

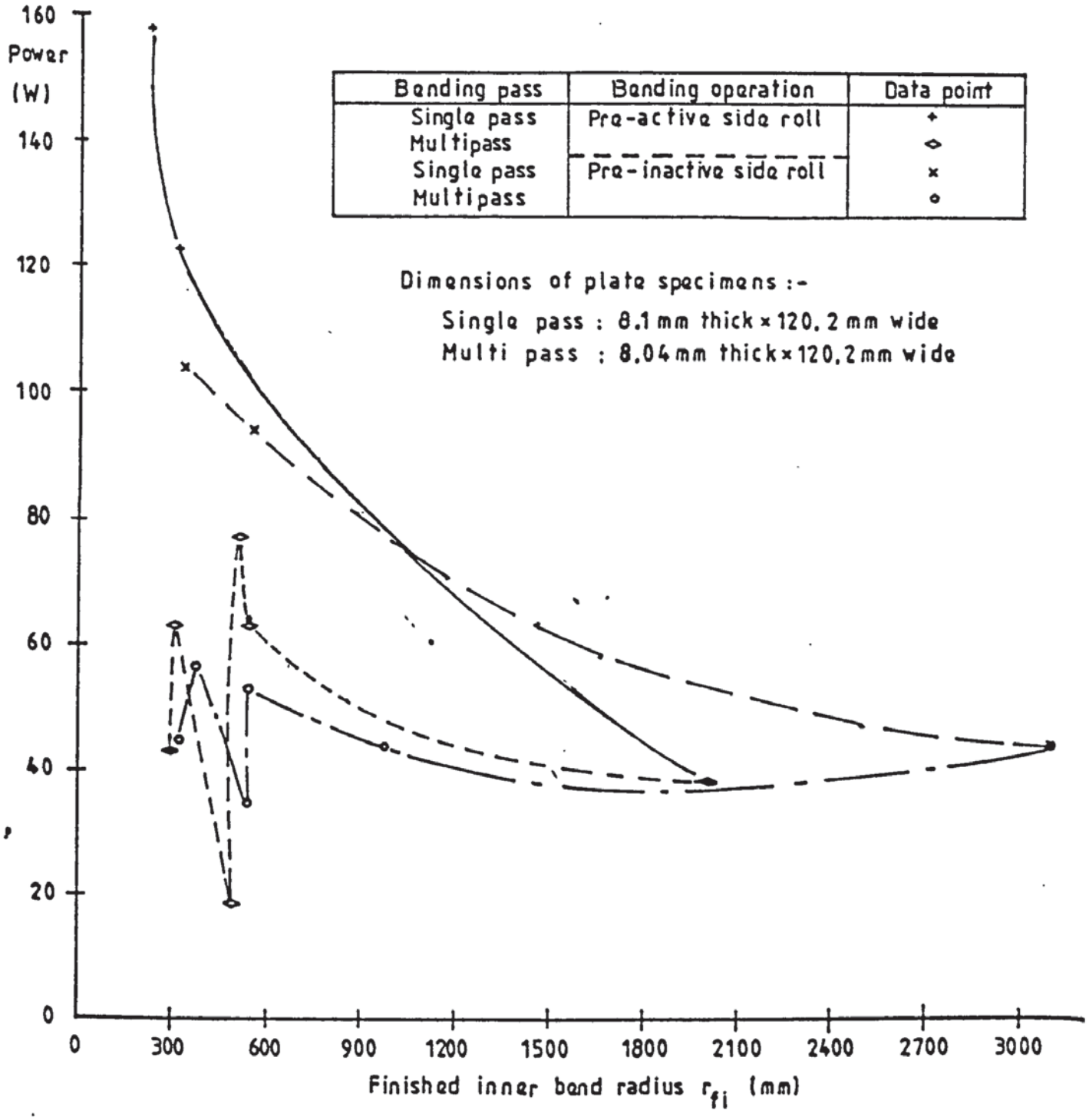

FIG 7.8 EXPERIMENTAL POWER CHARACTERISTICS (AT MEAN TORQUE) FOR SINGLE AND MULTI PASS BENDING OF 8.1 mm THICK × 120.2 mm WIDE HP30 ALUMINIUM PLATE

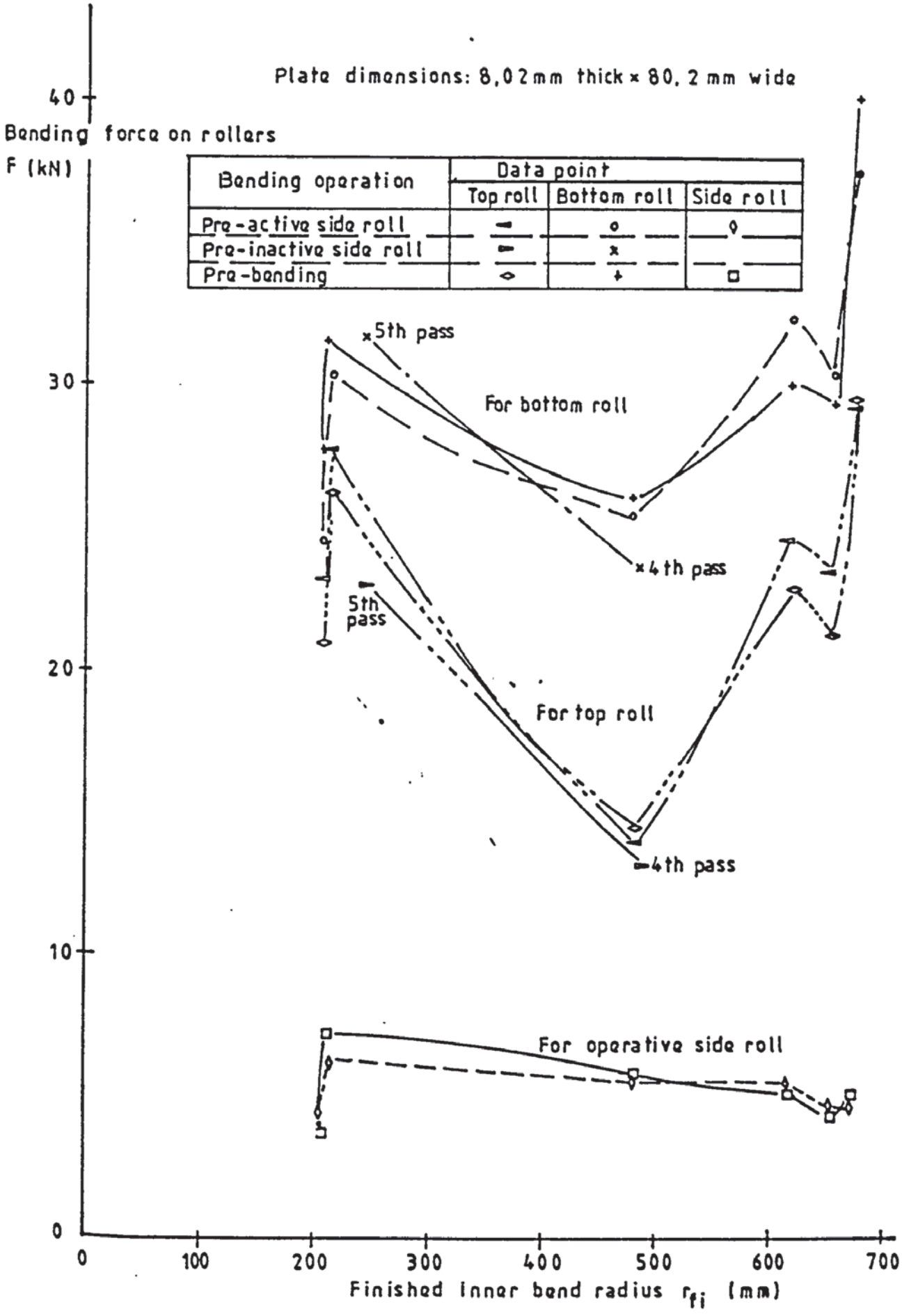

FIG 7.9 EXPERIMENTAL FORCE CHARACTERISTICS FOR MULTIPASS BENDING OF 8,02 mm THICK × 80,2 mm WIDE HP30 ALUMINIUM PLATE

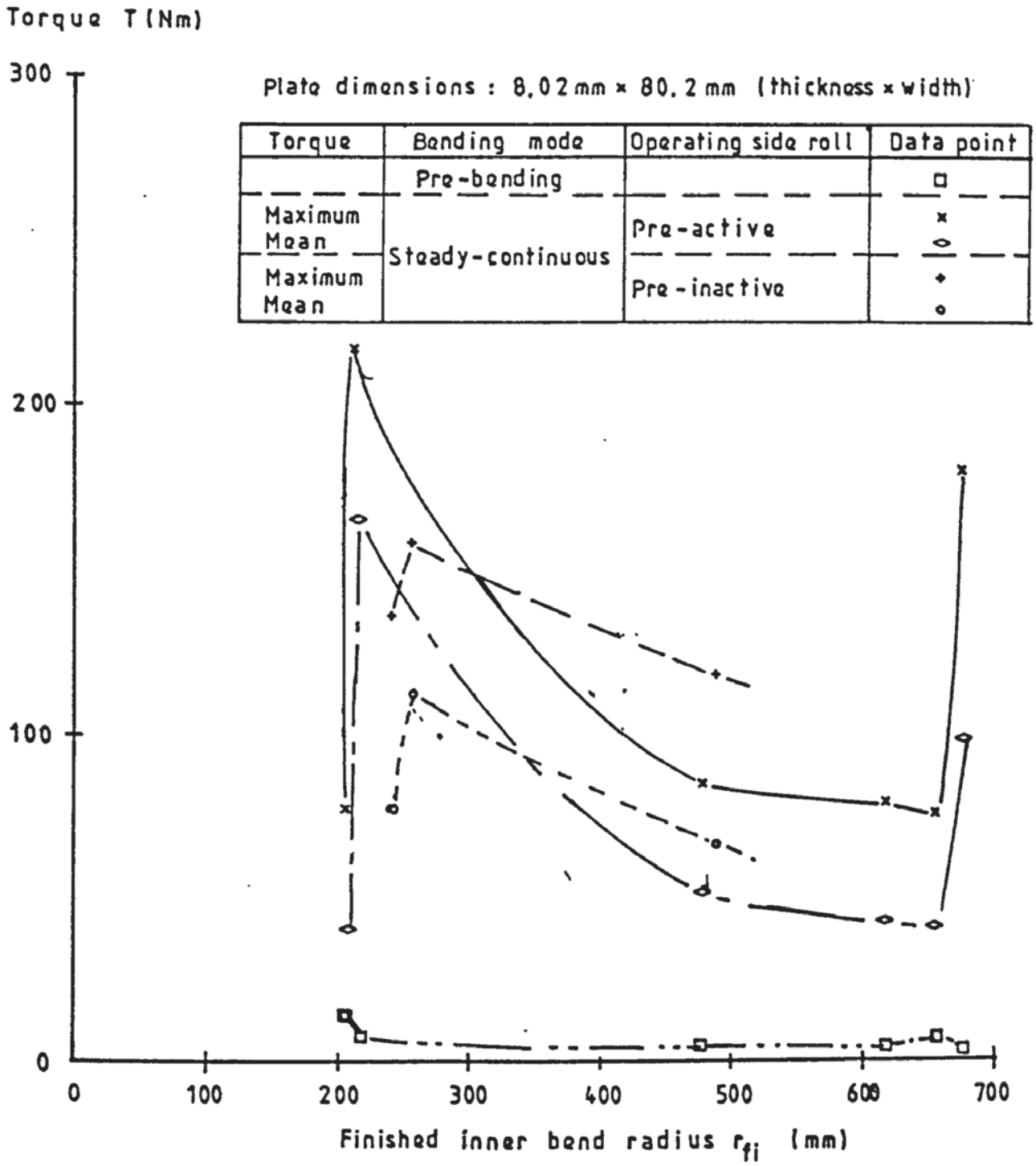

FIG 7,10 EXPERIMENTAL TORQUE CHARACTERISTICS FOR MULTIPASS BENDING OF 8,02 mm THICK × 80,2 mm WIDE HP30 ALUMINIUM PLATE

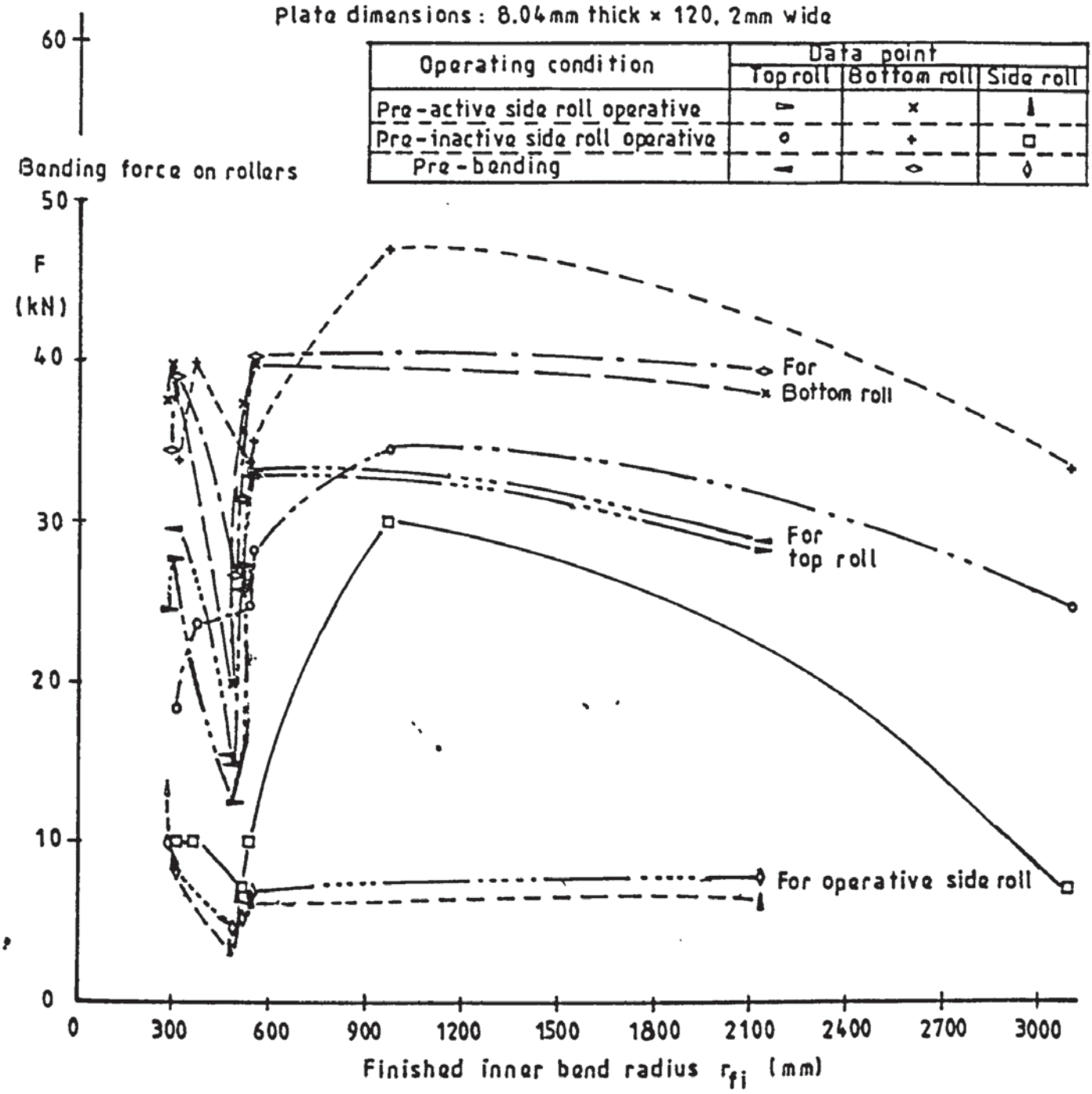

FIG 7.11 EXPERIMENTAL FORCE CHARACTERISTICS FOR MULTIPASS BENDING OF 8.04 mm THICK × 120. 2 mm WIDE HP30 ALUMINIUM PLATE

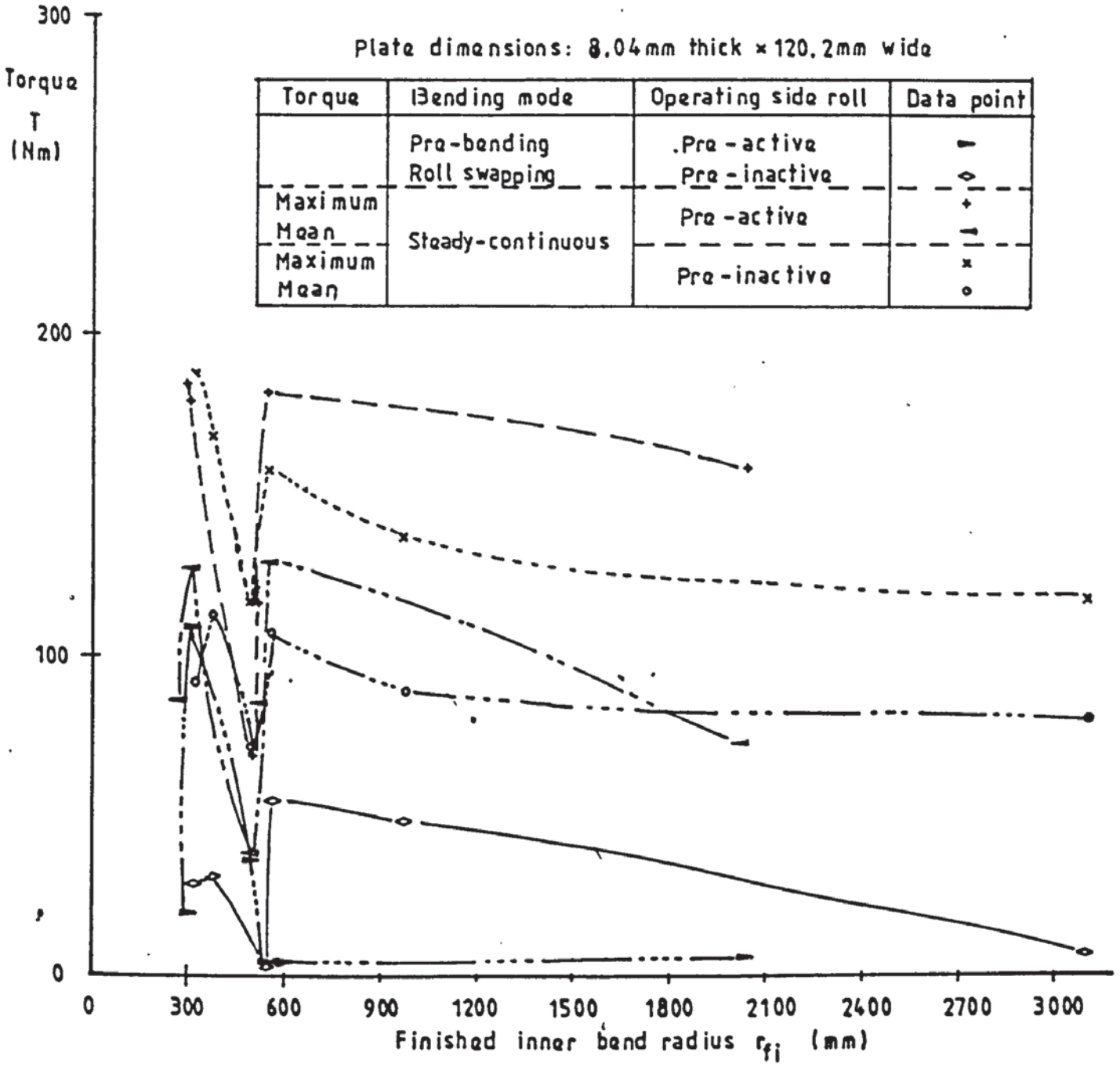

FIG 7.12 EXPERIMENTAL TORQUE CHARACTERISTICS FOR MULTIPASS BENDING OF 8.04 mm THICK × 120.2 mm WIDE HP30 ALUMINIUM PLATE

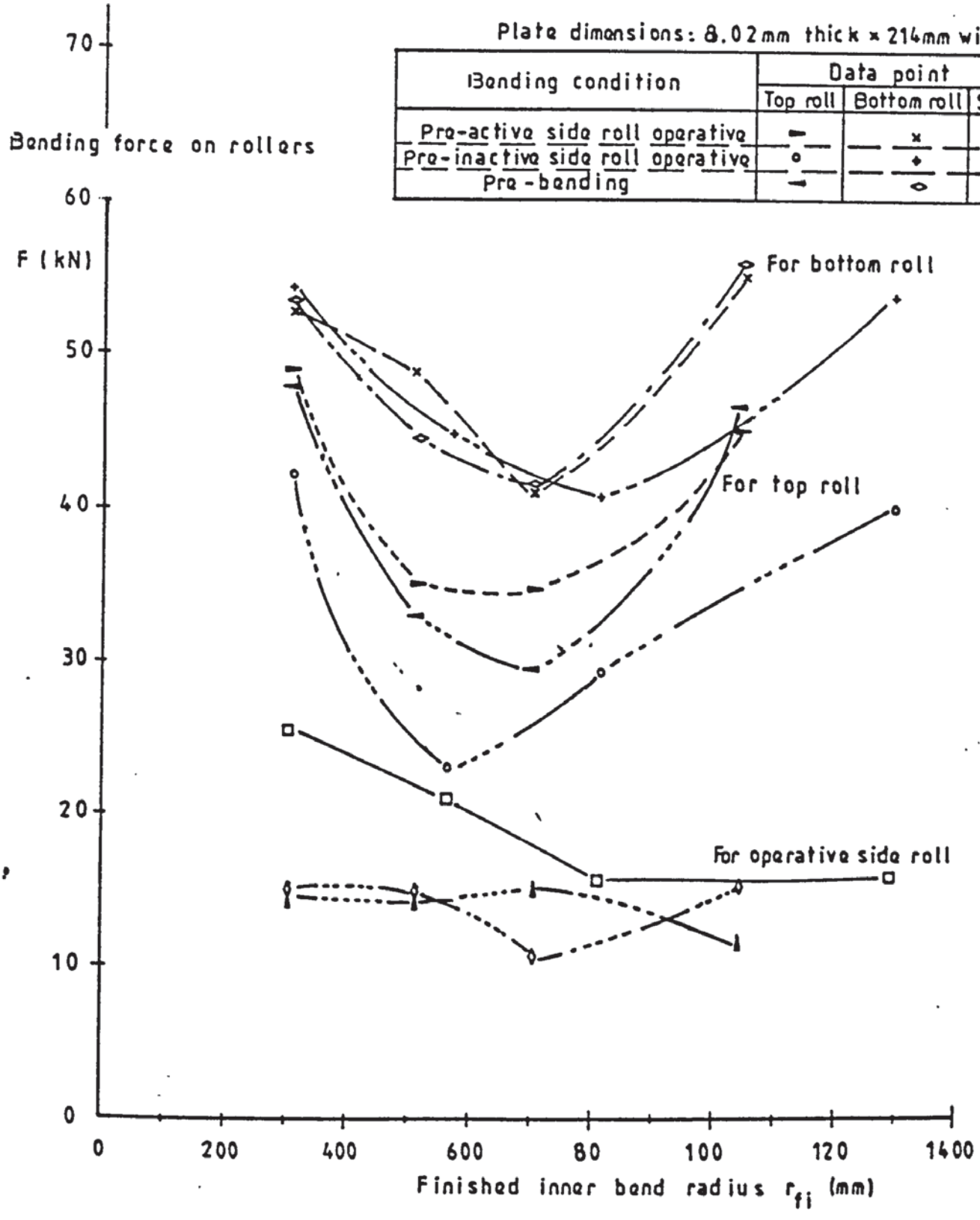

FIG 7.13 EXPERIMENTAL FORCE CHARACTERISTICS FOR MULTIPASS BENDING OF 8,02 mm THICK × 214 mm WIDE HP30 ALUMINIUM PLATE

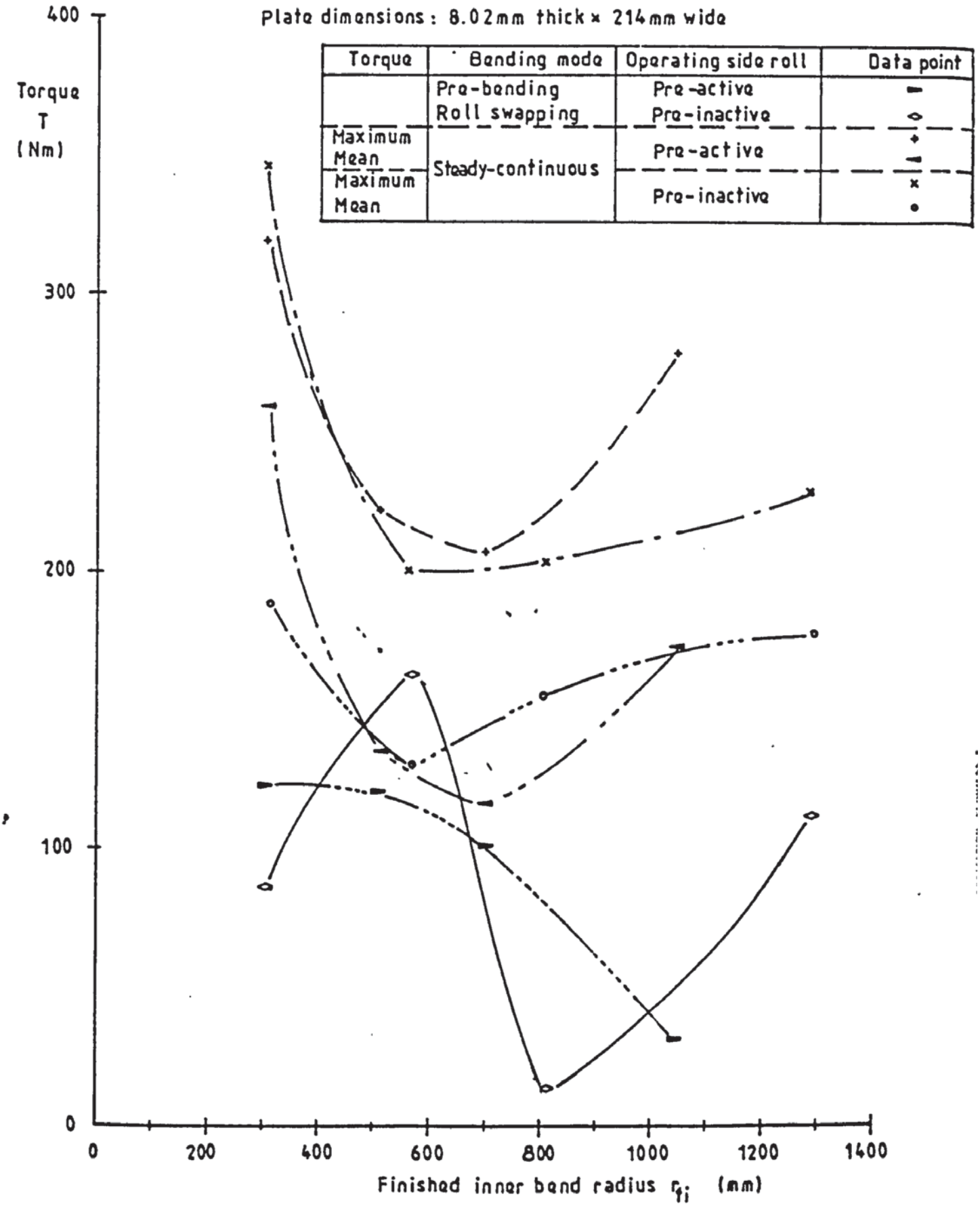

FIG 7.14 EXPERIMENTAL TORQUE CHARACTERISTICS FOR MULTIPASS BENDING OF 8.02 mm THICK × 214 mm WIDE HP30 ALUMINIUM PLATE

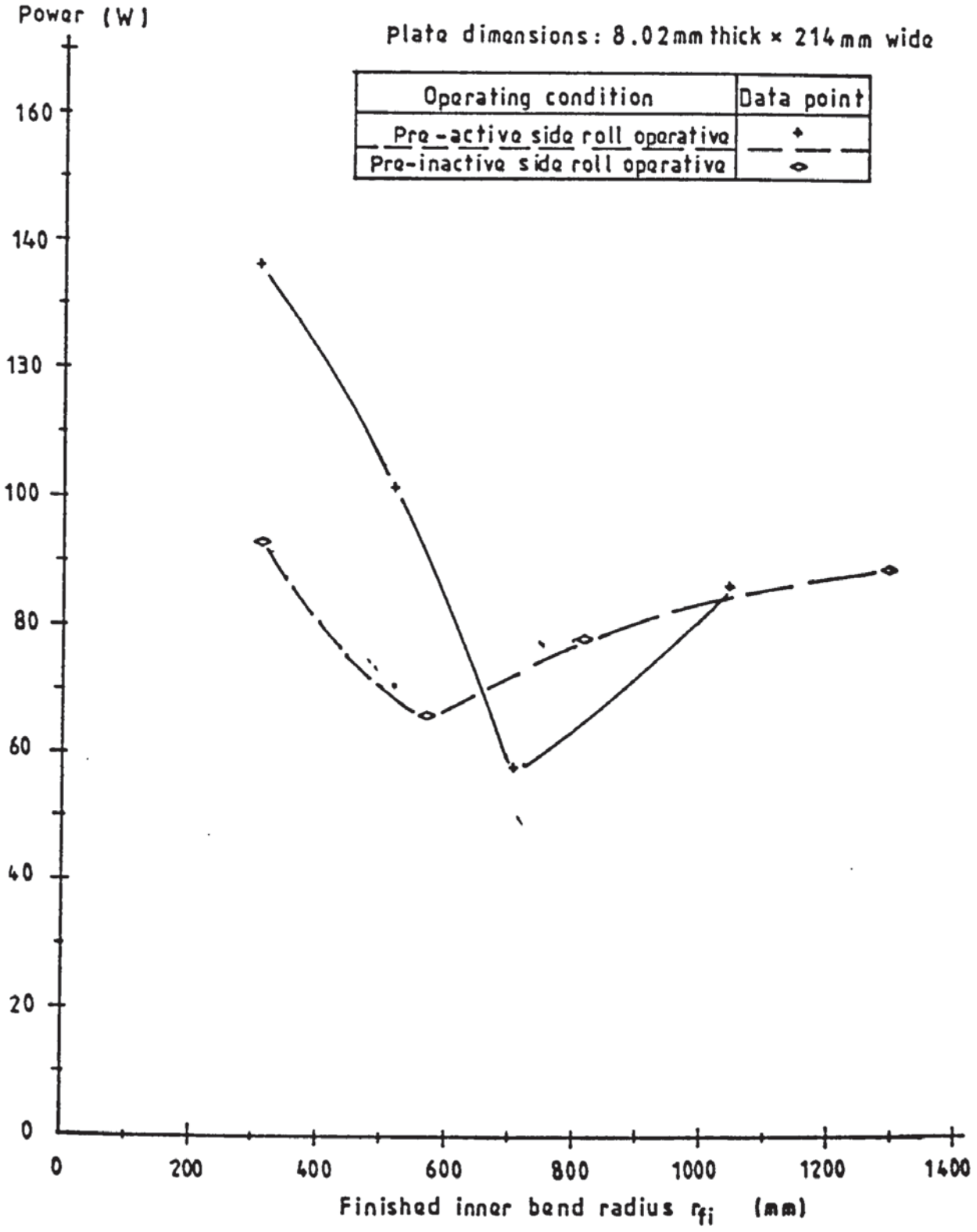

FIG 7.15 EXPERIMENTAL POWER CHARACTERISTICS (AT MEAN TORQUE) FOR MULTIPASS BENDING OF 8.02 mm THICK × 214 mm WIDE HP30 ALUMINIUM PLATE

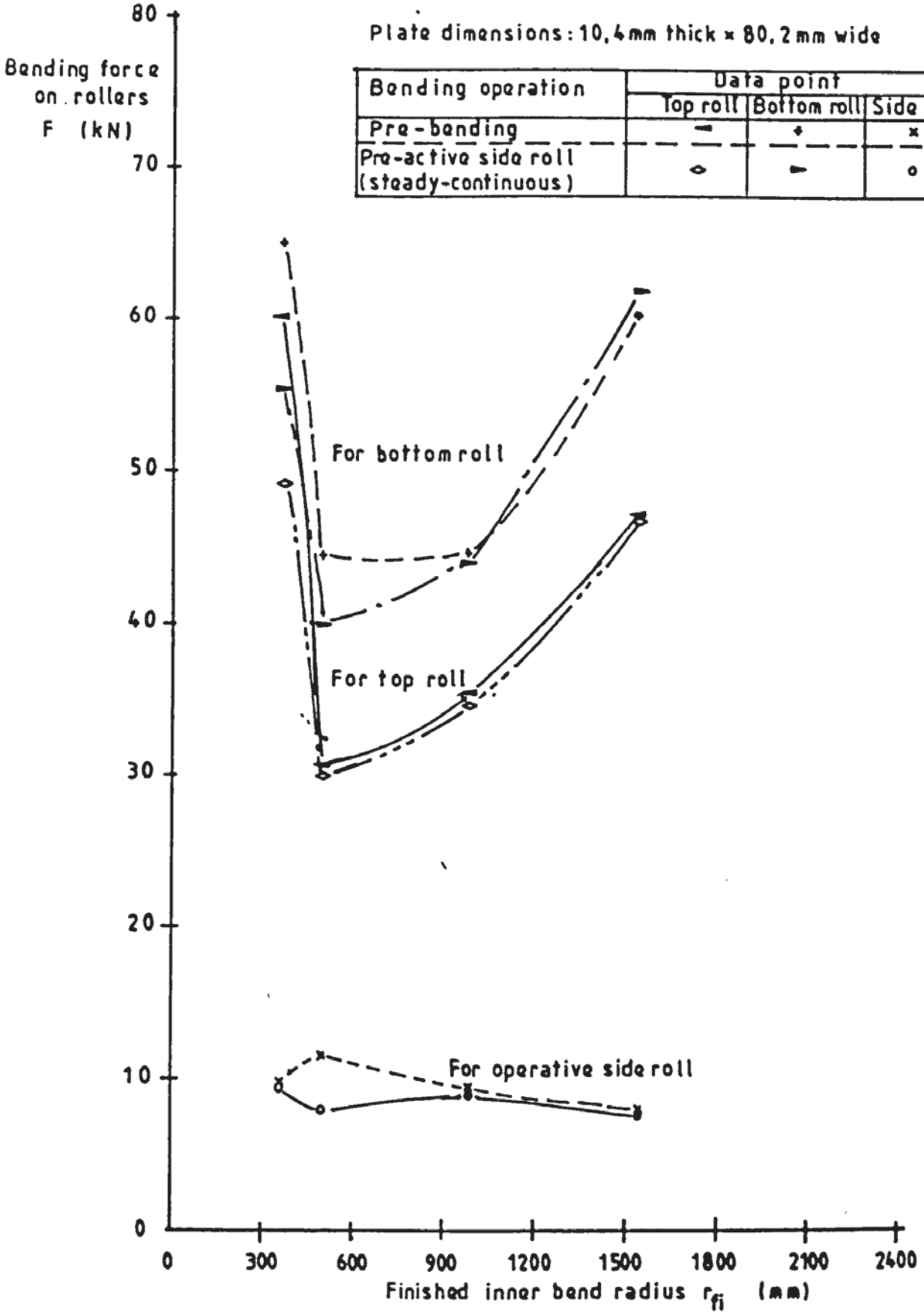

FIG 7.16 EXPERIMENTAL FORCE CHARACTERISTICS FOR MULTIPASS BENDING OF 10.4 mm THICK × 80.2 mm WIDE HP30 ALUMINIUM PLATE

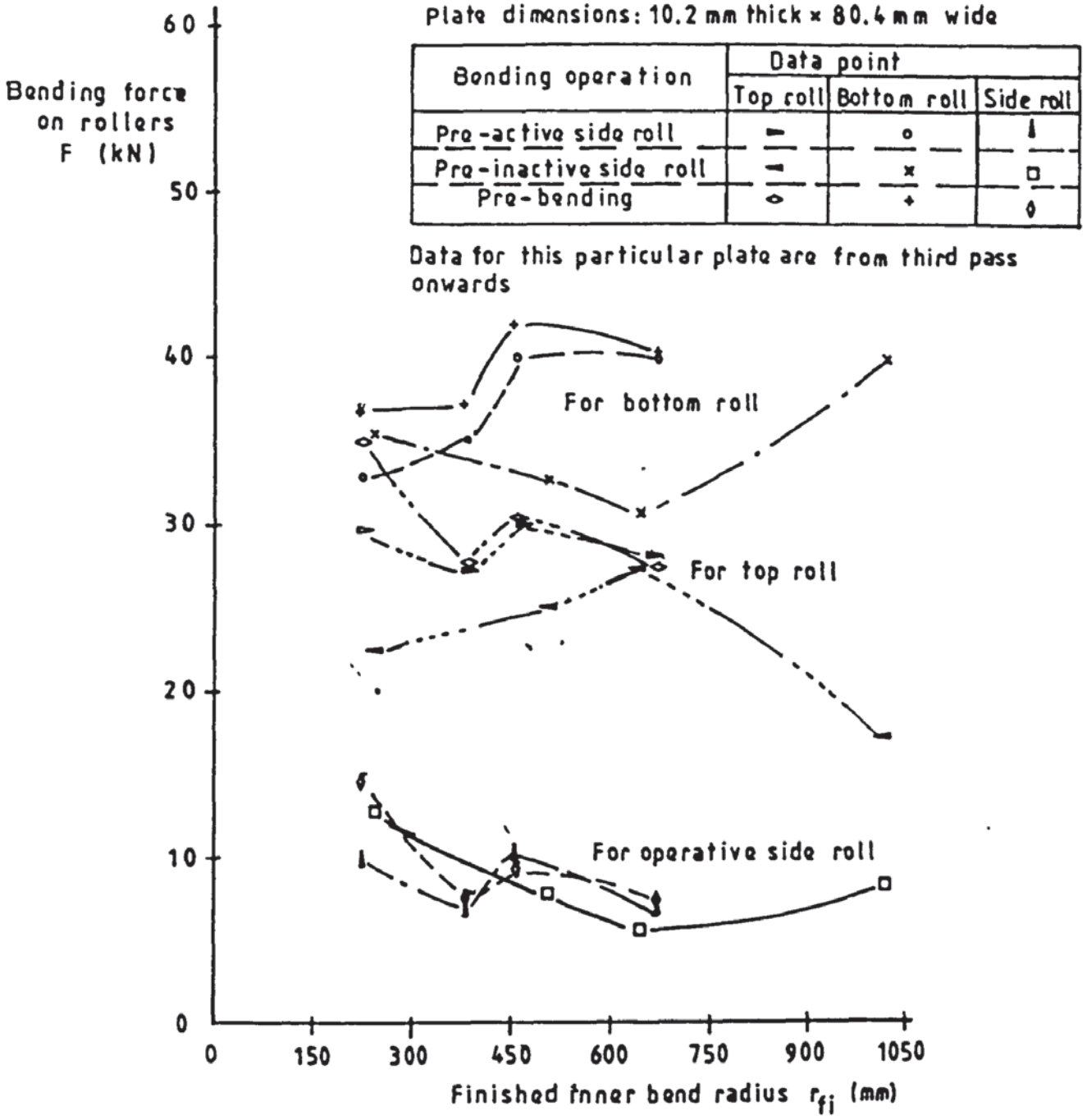

FIG 7.17 EXPERIMENTAL FORCE CHARACTERISTICS FOR MULTIPASS BENDING OF 10.2 mm THICK × 80.4 mm WIDE HP30 ALUMINIUM PLATE

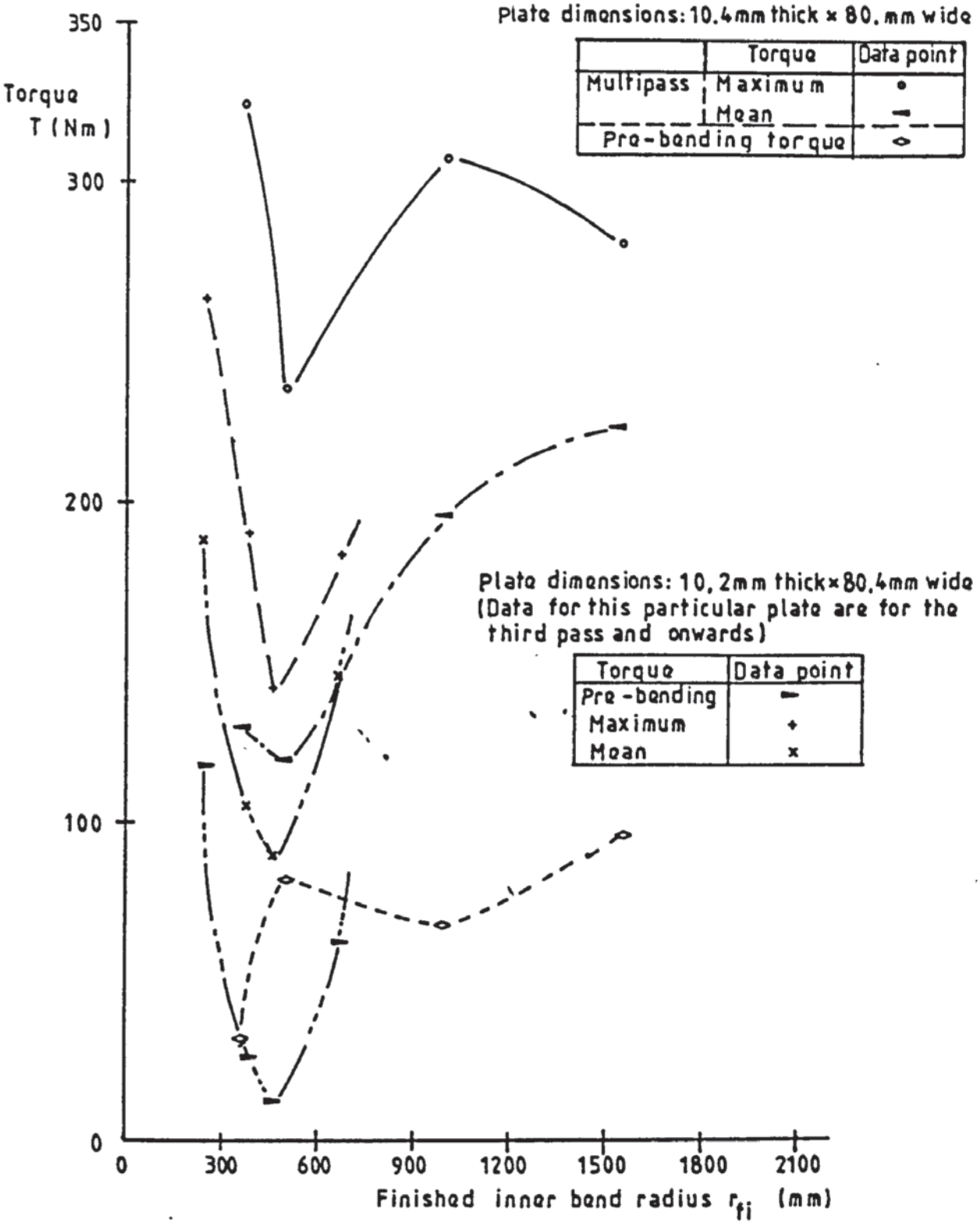

FIG 7.18 EXPERIMENTAL TORQUE CHARACTERISTIC FOR MULTIPASS BENDING OF 10,4 mm THICK × 80, mm WIDE AND 10, 2 mm THICK × 80,4 mm WIDE HP30 ALUMINIUM PLATES

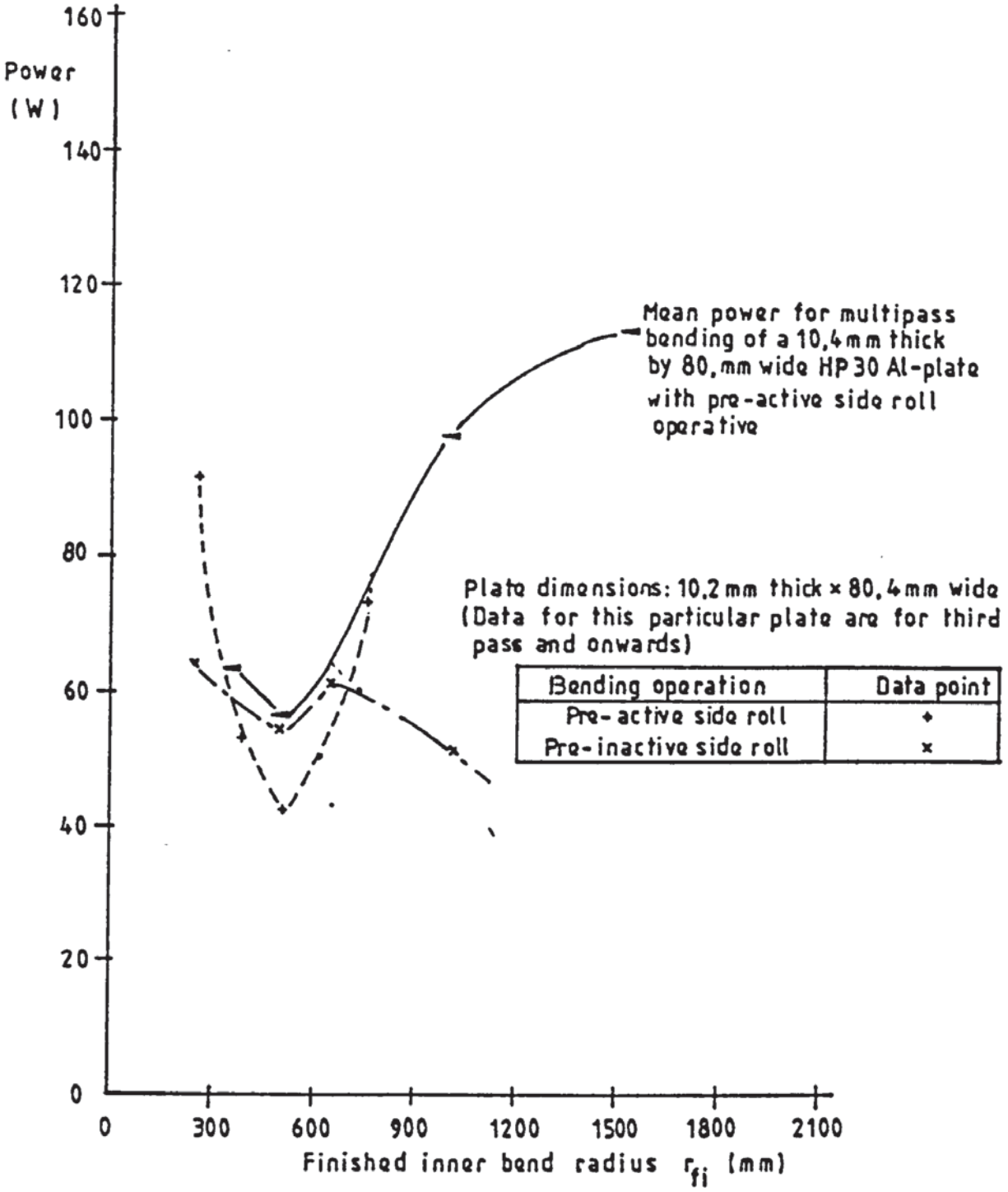

FIG 7.19 EXPERIMENTAL POWER CHARACTERISTICS (AT MEAN TORQUE) FOR MULTIPASS BENDING OF 10,4 mm THICK × 80, mm WIDE AND 10,2 mm THICK × 80,4 mm WIDE HP30 ALUMINIUM PLATES

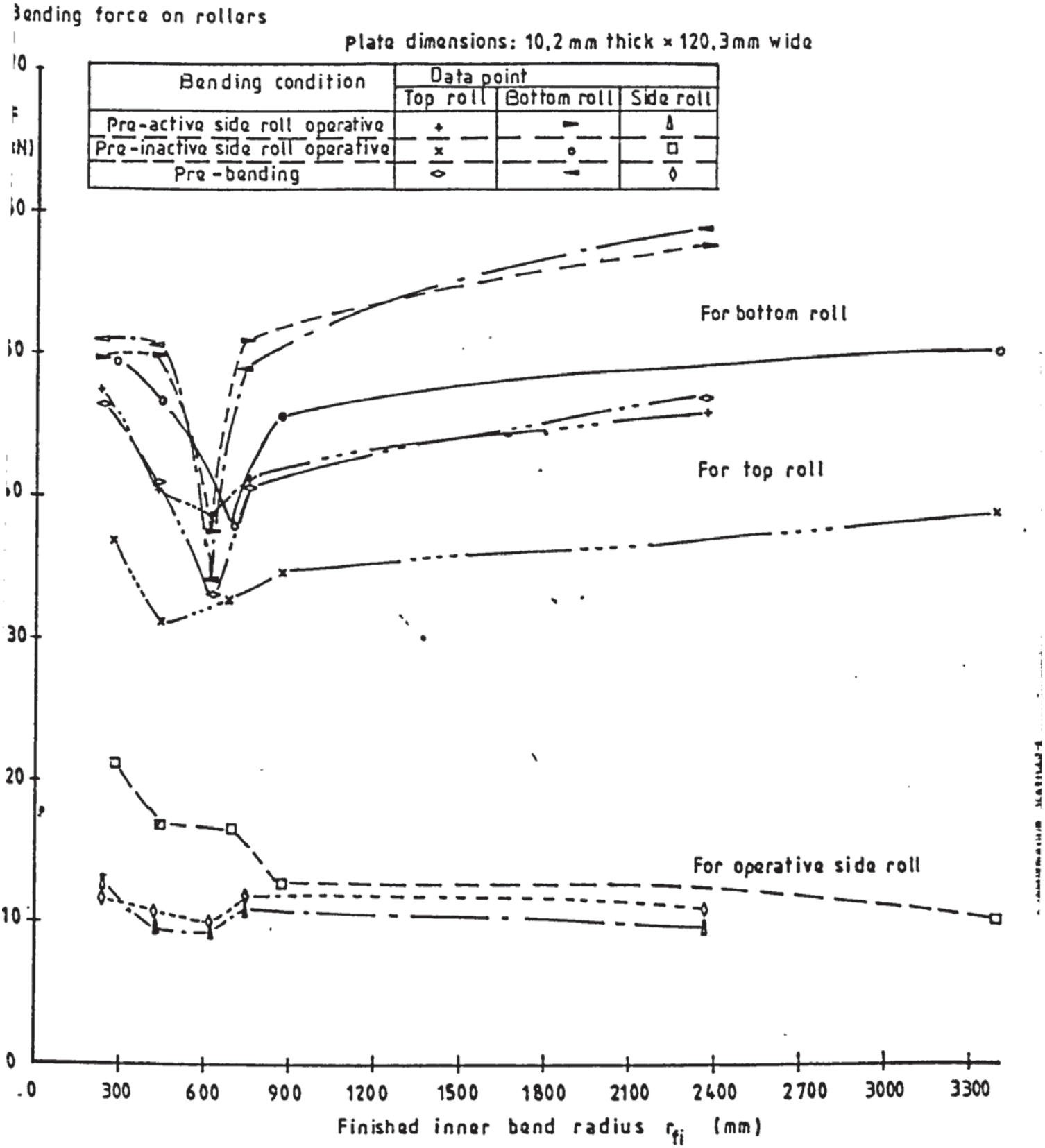

FIG 7.20 EXPERIMENTAL FORCE CHARACTERISTICS FOR MULTIPASS BENDING OF 10.2 mm THICK × 120.3mm WIDE HP30 ALUMINIUM PLATE

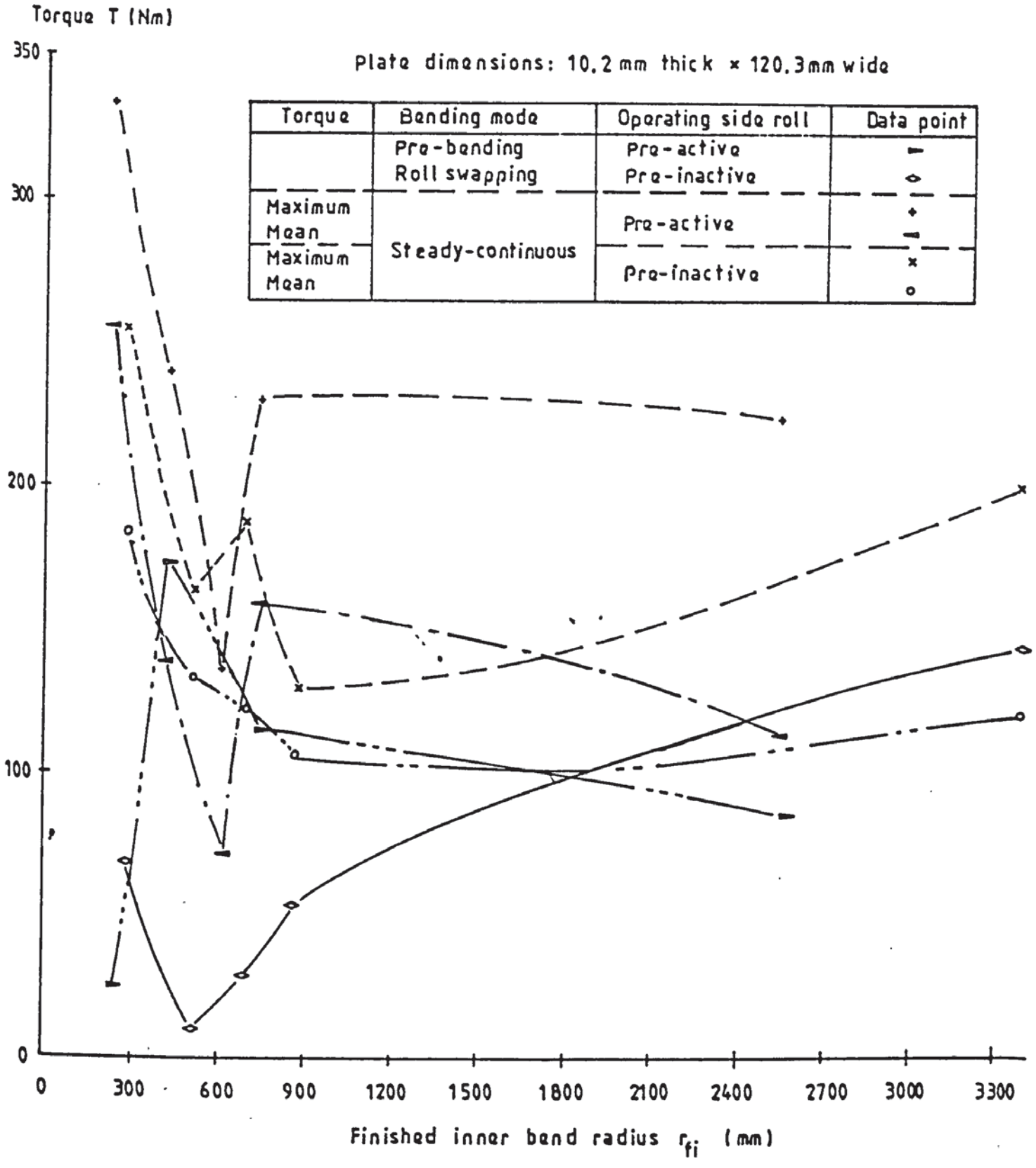

FIG 7.21 EXPERIMENTAL TORQUE CHARACTERISTICS FOR MULTIPASS BENDING OF 10.2 mm THICK × 120.3 mm WIDE HP30 ALUMINIUM PLATE

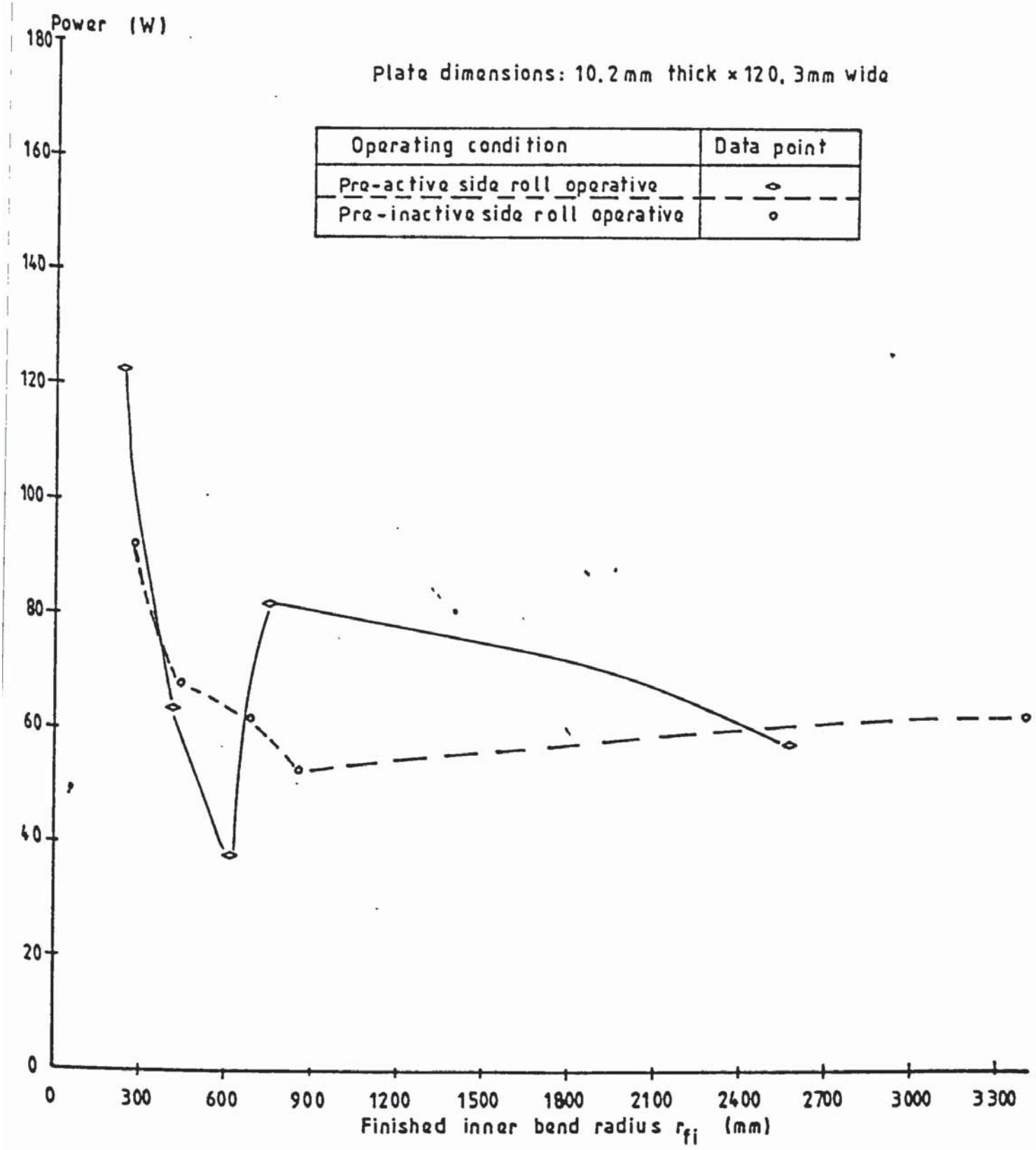

FIG 7.22 EXPERIMENTAL POWER CHARACTERISTICS (AT MEAN TORQUE) FOR MULTIPASS BENDING OF 10.2 mm THICK ×120.3 mm WIDE HP30 ALUMINIUM PLATE

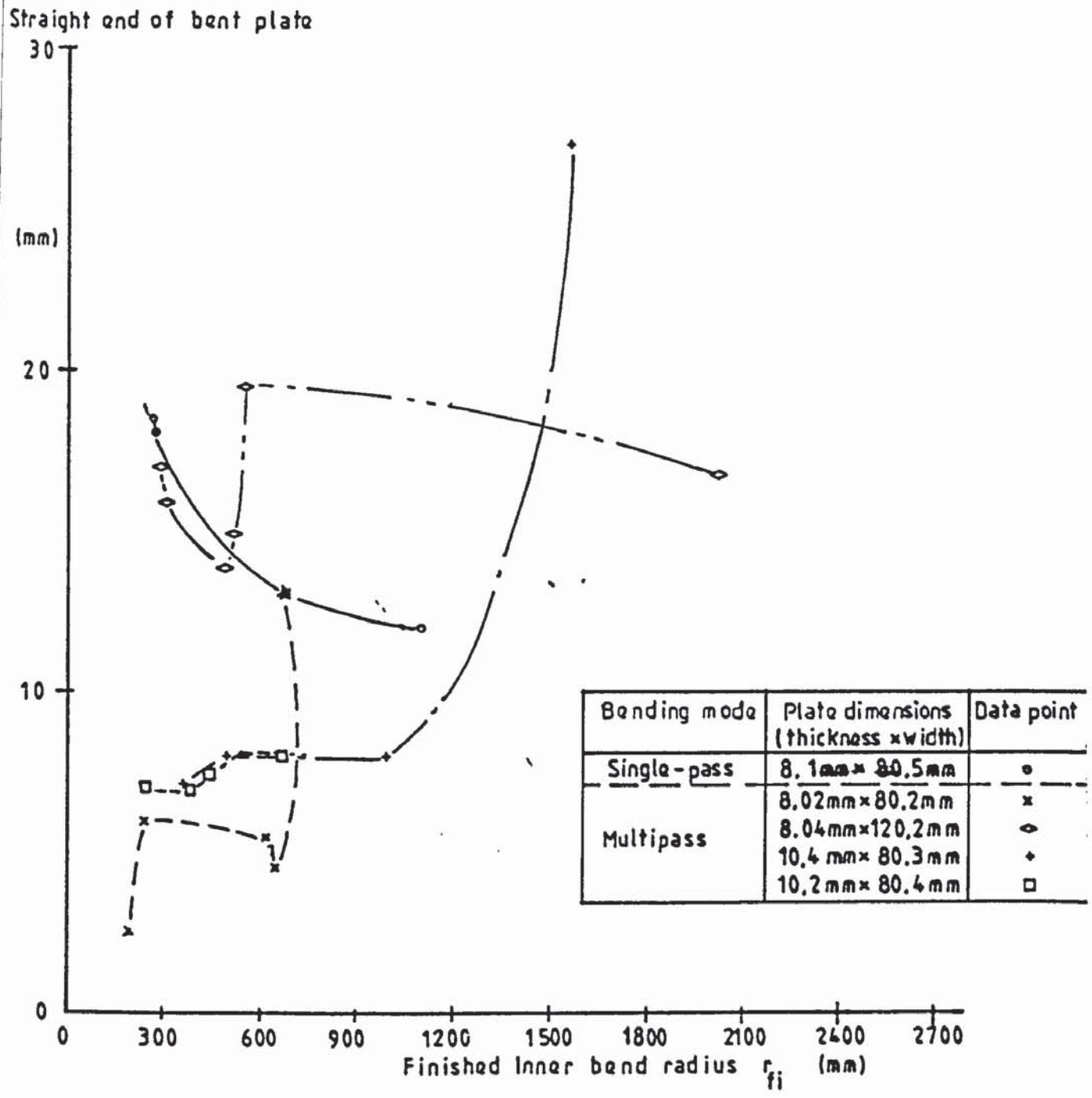

FIG 7.23 MEASURED REMAINING "STRAIGHT END" CHARACTERISTICS FOR BENDING OF HP30 ALUMINIUM PLATE SPECIMENS

CHAPTER EIGHT

OBSERVATION AND DISCUSSION

8.1. Properties of the HP30 aluminium plate specimens

Uniaxial tensile and indentation tests indicated that the anisotropy of the HP30 aluminium bendplate specimens was negligible (fig. 6.2 to 6.5 and fig. 6.8 to 6.11). However, both tests showed the various degrees of hardening, tempering and annealing for different thicknesses of the specimens. These can be identified by studying the slopes of the curves for each particular thickness of plate specimens in figs 6.6 and 6.12.

It was observed that the material hardening constant, H, for thinner specimens was higher than those of the thicker ones (see fig. 6.6 and section 6.3.4). This meant that the thinner plate was more susceptible to work hardening.

8.2. On the mechanics of roller plate bending

Most mechanisms involved in the roller plate bending have been discussed in section 5.3, i.e. prior to the evolution of the present mathematical model (Chapter five and Appendix 5.1). Experimental studies to evaluate the bending forces on the rollers, torque and power required on the top roll, in bending HP30 aluminium plates to its finished bend radius, were conducted (figs 7.4 to 7.23 in Chapter seven). Theoretical predictions to determine the internal bending resistance at the top roll contact for bending the corresponding aluminium plates were also performed (Chapter five, figs 5.28 to 5.41). The following discusses certain aspects of the mechanics of the process which were observed from the theoretical prediction, as well as the experimental study.

8.2.1. Discussion on the theoretical prediction

8.2.1.1. For single pass bending

A. Predicted maximum local yield bend radius at the top roll contact

Table 5.1 shows the predicted maximum local yield bend radius at the top roll contact for bending HP30 aluminium plate specimens having four different thickneses : 8.1 mm, 10.2 mm, 12.07 mm and 14.68 mm. It can be seen that the respective local bend radius for the yield commencing in the two outer fibre layers of the plate, at the top roll contact, increases with thicker plate specimens. This is obvious from a consideration of equation (5.7b), which was used to determine this radius. Since equation (5.7b), i.e.

$$a_0 = [Eh(1-\nu+\nu^2)^{1/2}]/[(1-\nu^2)\sigma_0] \qquad (8.1a),$$

was derived by assuming that the plate deformation is a plane strain problem (see Section 5.4.3.1), its value is thus independent of plate width, b, and only varies with Eh/σ_0 (For a constant Poisson's ratio, ν). When E and σ_0 are constants, a_0 is markedly dependent upon the plate thickness, $t=2h$. This was proved by running the single pass bending computer programme for the four plate thicknesses with the assumed plate mechanical properties as : $E=67.188$ kN/mm^2 and $\sigma_0=215$ N/mm^2.

The obtained values of a_0 are listed as follows :

Plate specimen thickness (mm)	Value of predicted a_0 (mm)
8.1	1260.3
10.2	1624.2
12.07	1878.0
14.68	2284.1

Comparing these values listed with those in Table 5.1, it is seen that the above values for specimen thicknesses from 10.2 mm upwards are generally higher than the corresponding values in Table 5.1. The lower value of a_0, in Table 5.1, is mainly due to the variation of the measured values E and σ_0. The variation of the latter values is a result of different degree of work hardening and heat treatment of the plate specimens as discussed in section 8.1. It is also observed from Table 5.1 that a_0 for the 10.2 mm thick plate is 1451 mm, which is rather close to 1466.8 mm for the 12.07 mm plate. This may be merely due to the fact that the ratios of Eh/σ_0 for the two plate specimens are very close to each other.

B. Plate internal bending resistance at top roll contact (fig 5.28)

Fig 5.28 shows the theoretical prediction of the plate internal resistance to external bending moment about the top roll nominal contact for bending HP30 aluminium plates of

thicknesses : 8.1 mm, 10.2 mm, 12.07 mm and 14.68 mm
with widths : 80.5 mm, 120.2 mm and 214 mm,

to accomplish a finished bend radius of between 2500 mm and 40 mm.

Comparison of the plate dimension effect to the particular plate internal bending resistance at the contact indicates that :

1) In bending plates of 12.07 mm thick x 120.2 mm wide and 14.68mm thick x 80.4 mm wide, the internal bending resistance is 3.3 % higher for the former than the latter

plate at a finished bend radius, r_f, of 2500 mm. It is also 4. % higher at r_f=600 mm.

2) In bending HP30 aluminium plates of 8.1 mm thick x 214 mm wide, 12.07 mm thick x 80.5 mm wide and 10.2 mm thick x 120.2 mm wide, the first specimen needs 3.1 % higher internal bending resistance than the second specimen, and 7.8 % higher than the third specimen for the finished bend radius of 2500 mm. At the finished bend radius of 600 mm, the corresponding values for the first specimen is 5.3 % higher than the second and 9.9 % higher than the third specimen.

3) In bending HP30 aluminium plates of 10.2 mm x 80.5 mm wide and 8.1 mm thick x120.2 mm wide, the first specimen is 10.7 % higher than the second one at r_f=2500 mm and 10.7 % higher than the second one at r_f=600 mm.

4) In bending all the HP30 aluminium specimens, the 14.68 mm thick x 214 mm wide specimen has the greatest bending resistance, at the top roll contact. The others, in decreasing order of internal bending resistance are :

12.07 mm thick x 214 mm wide, 14.68 mm thick x 120.2 mm wide,
10.20 mm thick x 214 mm wide, 12.07 mm thick x 120.2 mm wide,
14.68 mm thick x 80.4 mm wide, 8.1 mm thick x 214 mm wide,
12.07 mm thick x80.5 mm wide, 10.2 mm thick x 120.2 mm wide,
10.20 mm thick x 80.5 mm wide, 8.1 mm thick x 120.2 mm wide,
and 8.1 mm thick x 80.5 mm wide.

The difference of the internal bending resistance, between any two successive plates, is largest for the first four plate specimens.

The above and the graphical results indicate that the plate internal bending resistance at the top roll contact, for each

group of the plate dimensions specified in (1), (2) and (3), are rather close. They are within the order of 11%. An attempt was made to normalise the above specific bending characteristics with each respective perfect plastic bending moment, i.e. $M_p=bh^2\sigma_0$, fully through the depth of the plate at the top roll contact, at r_f=2500 mm. The attempt to correlate them into a single relationship failed (See Table 8.1). Further study of figs 5.29 and 5.30 tends to suggest that this was primarily a result of the different nature of springback and the penetration depth of the elastic-elastoplastic interfaces (See sub-sections C and D in this section for further discussion). These in turn were a function of the mechanical properties of each individual thickness specimen. However correlation for individual thickness of plate specimens, by itself, seemed to be possible. This was verified by the characteristics in figs 5.29 and 5.31 in which M_i/EI, c_i and R are correlated to each individual curve for each thickness of plates, respectively. In addition, the normalised values of M_i, i.e. M_i/M_p, for each particular plate thickness in Table 8.1 further supports this arguement. Item (4) above and the characteristics in fig 5.28 suggest that the plate internal bending resistance at the top roll contact for each individual plate thickness is a direct function of its width (see Equation 5.24).

Other plate internal bending resistance characteristics at the top roll contact observed from fig 5.28 are as follows :

a) $|dM_i/dr_f|$ increases with both bendplate thickness and width.

b) $|dM_i/dr_f|$ increases rapidly as the finished bend radius, r_f, reaches the value of 400 mm and below.

c) In bending a plate specimen for r_f beyond 400 mm, especially for 8.1 mm thick HP30 aluminium plate, a smaller $|dM_i/dr_f|$ is obtained.

d) The trend of $|dM_i/dr_f|$ tends to show an asymptotical charateristics as r_f reaches values around and below 100 mm. This is clearly illustrated from the curve for the 10.2 mm thick x 120.2 mm wide specimen, which is approximately asymptotic at r_f equal to 20 mm.

Among all the specimens, the 8.1 mm thick x 80.5 mm wide plate gives the smallest values of $|dM_i/dr_f|$, especially for $r_f \geq 600$ mm, and a rather smooth M_i-r_f curve. This suggests that in practice, particular attention should be paid to properly and accurately controlling the bending of the plate. This is necessary to ensure that values of r_f beyond 600 mm can be precisely achieved. In fact it was observed during the bending experiment that a small difference in the vertical and horizontal displacement of the operative side roll generated a large difference of the finished r_f; i.e. when bending two initially flat plates, with the same dimensions. Generally the greater the $|dM_i/dr_f|$ along a curve, the easier it was to control the process in order to accomplish the anticipated finished r_f during the bending operation.

The characteristic mentioned in item (a) and the normalised value of M_i/M_p in Table 8.1 illustrate that M_i at the top roll contact is a direct function of the plate thickness and width. The observed features in items (b) and (d) may partly be attributed to the higher rate of springback, $|d(M_i/EI)/dr_f|$ (fig 5.29), and the higher penetrating rate of the elastic-elastoplastic interface, $|dc_i/dr_f|$, towards the neutral surface of the plate (fig 5.30) within the particular range of r_f. Other reasons which give rise to the characteristics of the bending mechanics await further investigations.

C. Relative springback characteristics of the bentplates at top roll contact and finished bending condition (fig 5.29)

Fig 5.29 shows the relative springback characteristics for the bent plates between the condition at the top roll contact and the completion of bending. Due to the assumption of plane strain, the springback is independent of plate width and shows a good correlation for each particular individual plate thickness. Comparison of the springback characteristics for the four specific plate thicknesses shows that the thinner plate specimen gives higher levels of springback. The specimens, in decreasing order of springback, are listed below :

(i) 8.1 mm thick plate.
(ii) 10.2 mm thick plate.
(iii) 12.07 mm thick plate.

and,

(iv) 14.68 mm thick plate.

The marked difference in magnitudes between the curve for 8.1 mm thick plate and that for 10.2mm thick plate, as shown in

Table 8.1 Normalised value of the plate internal bending resistance at the top roll contact

Dimensions of Plate Specimens (thickness x width) (mm)	Fully plastic bending moment $M_p=bh^2\sigma_0$ (N m)	Estimated plate internal resistance M_i at r_f=2500 mm (N m) [see fig 5.28]	M_i/M_p at r_f=2500 mm
8.1 x 80.5	1135.55	378.84	0.3314
8.1 x 120.2	1695.56	565.68	0.3314
8.1 x 214.	3018.72	1007.11	0.3314
10.2 x 80.5	2041.02	620.18	0.3039
10.2 x 120.2	3053.91	927.95	0.3039
10.2 x 214.	5432.55	1650.73	0.3039
12.07 x 80.5	3342.38	974.65	0.2916
12.07 x 120.2	4990.73	1455.32	0.2916
12.07 x 214.	8885.32	2600.11	0.2916
14.68 x 80.5	4886.04	1409.49	0.2885
14.68 x 120.2	7304.76	2107.22	0.2885
14.68 x 214.	13005.14	3751.63	0.2885

fig 5.29, may be partly due to the magnitude of h^3 in I, partly due to the difference in the value of Young's modulus, E, and partly due to the relatively high work hardening constant, H, of the former plate (cf. the slope for the tensile test curve of the respective plate in fig. 6.6). The effect of the last two conditions is illustrated in fig 8.1 and explained in sub-section D.

In contrast to the plate internal bending resistance (at top roll contact) characteristics (See fig 5.28), fig 5.29 shows that the magnitude of $|d(M_i/EI)/dr_f|$ for the thinner plate is greater than that for the thicker plates. The similarity between the springback and the plate internal bending resistance characteristics is that both have a sharp increase of $|d(M_i/EI)/dr_f|$ when r_f is approximately equal to or less than 400 mm, i.e. $r_f \leq 400$ mm. Also, both possess the asymptotic characteristics at or near $r_f \leq 20$ mm. This is obvious because the quantity of springback is also a direct function of M_i at the top roll contact.

D. Characteristics of the distance of the elastic-elastoplastic interface from the plate neutral plane at the top roll contact (fig. 5.30)

Fig 5.30 is the graphical representation of the characteristics of the distance of the elastic-elastoplastic deformation interface, c_i, from the neutral plane of the plate at the top roll contact, relative to the plate finished bend radius r_f. It can be observed from the figure that the curves for the four plate thicknesses tend to converge, from r_f=2500

mm towards r_f=20 mm. This indicates that the rate of the elastic-elastoplastic deformation interface, $|dc_i/dr_f|$, penetrating towards the neutral plane of the plate at the top roll contact, is greater for the thicker plate specimens than that for the thinner ones. It can also be observed from the graphs that all the curves for the different plate thickness almost overlap each other when r_f is approximately equal to 80 mm. The overlapping and the converging of the curves for c_i suggest that the effective plastic deformation rate through the plate thickness at the contact is relatively higher for the thicker plate than for the thinner ones. This subsequently suppresses the springback more efficiently. However the deformation nature of a particular plate is always related to its material properties. An explanation of the springback characteristics by considering the material properties will be illustrated in sub-section F.

E. Characteristics of the local bend radius (R) of a plate, at the top roll contact, relative to the plate finished bend radius (r_f) (fig 5.31)

Fig 5.31 represents the graphical results of the predicted plate local bend radius, R, at the top roll contact, in relation to the anticipated finished bend radius, r_f. The general characteristics are similar to those of c_i versus r_f, as shown in (fig 5.30), except that the spacing between the curves is smaller in comparison with fig 5.30. It is also observed that the curves almost coincide when r_f is approximately equal to or less than 200 mm. In additional, the

ratio of R/r_f increases from its minimum value of 0.2 at r_f=2500 mm (ref to curve for 8.1 mm thick plate) to 0.75 at r_f=200 mm.

F. Consideration of springback from uniaxial tensile relation

In order to illustrate theoretically the effect of material properties, i.e. Young's modulus E and material hardening constant H, on the relative amount of springback for the plates, the uniaxial tensile stress-strain relationship for plates of 8.1 mm thick and 10.2 mm thick, respectively, are re-plotted in fig 8.1. Detailed comparison will now be made as follows.

Referring to fig 8.1, if oab represents the loading curve in bending the 10.2 mm thick plate from o to b, it thus produces a total effective strain of ε_t=od. The release of bending forces on the plate at point b allows it to follow bc to c (bc is parallel to oa). It subsequently gives a total effective plastic strain equal to $oc=\Delta\varepsilon_t^p$ and the total recoverable effective elastic strain of $cd=\Delta\varepsilon_t^e$. In bending the 8.1 mm thick plate to give an equivalent total effective strain of ε_t, the respective loading point, for the 8.1mm thick plate, on the uniaxial tensile stress-strain curve is at b'. The unloading line from b' for the 8.1 mm thick plate is thus b'c', which is parallel to oa'. In this case the total effective plastic strain is oc' and the recoverable total effective elastic strain is c'd. Since dc'>dc, the higher slope of the

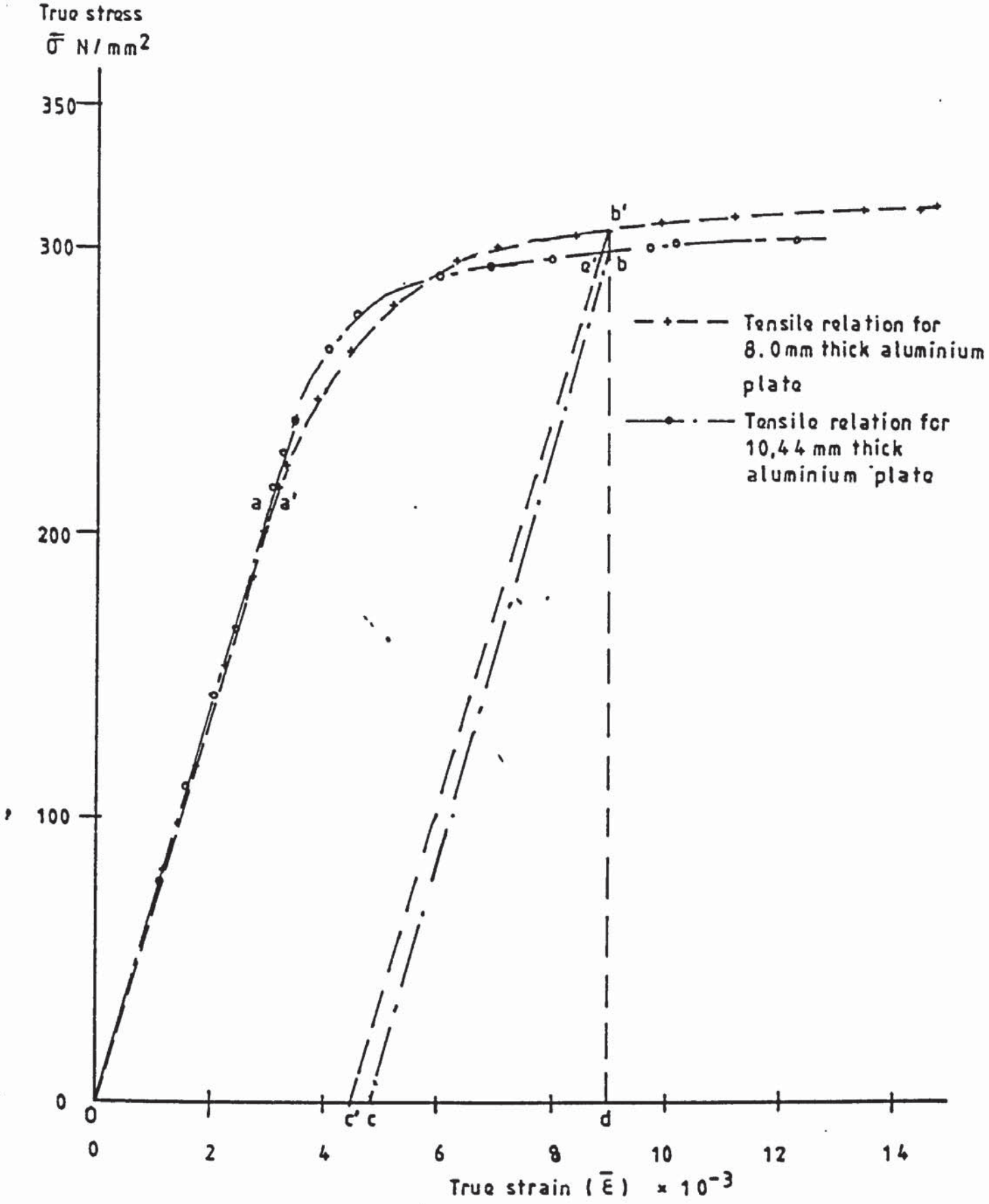

FIG 8.1 CONSIDERATION OF SPRINGBACK FROM UNIAXIAL TENSILE STRESS-STRAIN RELATION

strain hardening section of the uniaxial tensile stress strain curve and the relatively lower value of E for the latter plate will lead to higher springback quantity.

G. Practical application of the predicted results

The above predicted results can be applied to the industrial production environment by referring to the following procedure :

1) Decide on the anticipated finished bend radius of the bendplate.
2) Determine, from fig 5.31, the corresponding local bend radius, R, at the top roll contact.
3) Check whether any geometrical blockage is likely to occur in the bender by considering :
   (i) the positional powering direction of the side roll,
   (ii) the size of the top roll to see whether the roll is larger than the respective local bend radius. If the roll is larger the operation will fail.
4) Evaluate, from fig 5.28, the plate internal bending resistance for bending the finished bend radius.
5) Estimate the corresponding horizontal and vertical bending component of the bending force on the side roll by gradually adjusting the side roll position in the bender. This can be done either graphically or numerically. The side roll adjustment will be repeating until the plate curvature boundary condition at the top roll is equal to $1/R$ and at the side roll is equal to zero.
6) Evaluate the bending force on the side roll by equating the external bending moment due to the side roll bending force (with the corresponding bending arms estimated from step (5) above) about the top roll contact with the plate and the respective internal bending resistance evaluated from step (4) above.

The above procedure only gives an approximate estimation of the side roll bending force, F_s. An accurate evaluation of F_s requires the solution of the mathematical model presented in Appendix 5.1 (after M_i and R have been determined).

8.2.1.2. For multipass bending

The theoretical prediction for multipass bending of HP30 aluminium plate specimens is presented in figs 5.32 to 5.41. Figs 5.32 to 5.36 compare the effect of the bending pass on the plate internal bending resistance, local bend radius, the distance of the elastic-elastoplastic interface from central plane, at the top roll contact, and the springback. Figs 5.37 to 5.41 compare the thickness effect to these parameters.

A. Bending pass effect

It is observed from fig 5.32 that the multipass bending, within the prediction range, generally gives lower plate internal bending resistance, M_i, at the top roll contact, compared with the single pass bending. As can be seen from fig 5.32, the random distribution of the curves, for each series of the predicted bending operation, suggests that M_i for multipass bending is not only dependent upon the number of bending passes, but is also dependent upon the step interval of any two intermediate successive finished bend radii. Studying the characteristics of these curves, it can be concluded that there is no particular single curve which can correlate all the data for the different number of bending passes and the various step intervals between any two intermediate finished bend radii. Comparison of the characteristics of the curves of A, C and D seems to suggest

that the magnitude of the intermediate bend radius for the first pass may also affect the subsequent values of M_i, in any particular series of bending operations. Furthermore, curves A, B and E indicate that there is a specific combination of

(i) number of bending passes,

and,

(ii) step intervals of the intermediate finished bend radii,

which will maintain the lowest M_i throughout a particular bending series. However, this aspect will require further verification through theoretical and experimental investigation.

Fig 5.33 shows that the respective characteristics of the springback are basically similar to that for M_i. This is because the springback is a direct function of M_i, and the material properties and plate dimensions are the same.

The predictions for the distance of the elastic-elastoplastic interface, C_{i0}, are shown in fig 5.34, which shows that C_{i0}, for each particular series of multipass operations, also varies from the other series of multipass operations, with a different number of bending passes and step intervals of successive intermediate r_{ff}. Nevertheless, all the values of C_{i0}, within the predicted range, are higher than C_i for the single/first pass bending. This indicates that the depth of the two elastoplastic bands which sandwich the fully elastic deformation core, is relatively smaller in comparison with that of the single/first pass bending. (It should be noted that the theoretical values of C_{i0} were obtained by

assuming an initially fully elastic condition in the plate before its subsequent pass bending). It is observed that most values of C_{i0} for all the multipass operations, except the one designated by the letter D, commences with a higher value of C_{i0} for the second pass bending. The subsequent passes give lower values of C_{i0} for the predicted results. The second pass for the multipass operation with the curve designated by the letter D has a lower value of C_{i0} compared with its subsequent four passes.

Fig 5.35 shows the corresponding first yield local bend radius at the top roll contact for each series of multipass operation in bending the plate specimen. It can be observed that the trace for each particular series of multipass operation is also different to that for the others. Its variation is mainly dependent upon the initial and anticipated plate geometry for each successive bending pass.

Observations from fig 5.36 (Characteristics of the local bend radius at the top roll relative to the finished bend radius) also indicate its complex characteristics. Generally, the local bend radius varies with the number of bending passes and the step interval for each successive intermediate finished bend radius, as well as the initial plate geometry.

Correlating the characteristics observed from figs 5.32 to 5.36, it can be concluded that the mechanics for multipass bending is very complicated. This results from the variation in the springback, the depth of elastic-elastoplastic interface, the respective first yield local bend radius and the local bend radius. All these depend upon the multipass bending route required to accomplish the anticipated finished bend radius. In any subsequent bending pass, the plate initial

geometry is also an essential factor which affects the above parameters, since it varies the magnitude of the first yield local bend radius, R_{1st} (fig 5.35), and M_i, c_{i0} etc..

B. Plate thickness effect

The plate thickness effect in multipass roller bending was also investigated theoretically. Comparison of the predicted results for bending 80.5 mm wide HP30 aluminium plates with thicknesses of 8.1 mm, 10.2 mm and 12.07 mm, to accomplish a finished bend radius of 500 mm within six passes in same step decrement for r_f, can be seen in figs 5.37 to 5.41. The following generalises some of the observed characteristics derived from the comparison.

Fig 5.37 compares the values of M_i for the multipass bending of the three different plate thicknesses, and also with the single pass bending. It can be seen that values of M_i for multipass bending, within the predicted range of r_{ff} (or r_f for single pass bending), are generally lower than those for the single pass bending. Observation of the spacing between the curves for single and multipass bending of the plates seems to indicate that the multipass would be more advantageous for bending the two thicker plates, especially for the 12.07 mm thickness, which is the thickest plate. Estimation of the percentage of reduction in M_i due to multipass bending, relative to that of the single pass bending, gave the following values :

(i) 39.2 %, 41.1 % and 40. % for plate specimen thickness of 8.1 mm, 10.2 mm and 12.07 mm,

respectively, at r_f=2100 mm,

and

(ii) 45.8 %, 47.9 % and 46.1 % for plate thickness of 8.1 mm, 10.2 mm and 12.07 mm, respectively, at r_f=500 mm.

The above relative percentages do not suggest that multipass bending is superior in bending thicker plates. However, multipass bending could be recommended for a production environment as it may optimise bender capacity. This is because it has a higher difference in the absolute values of M_i.

In attempting to explain the larger difference in the absolute values of M_i for bending thicker plate, the springback characteristics (fig 5.38) were examined. The trend and spacing between the curves, for single and multipass bending, for each plate thickness, suggests that the absolute magnitude for the suppression of springback in multipass is higher for thinner plate. This tends to indicate that the suppression of springback might not be the reason for the lower absolute values of M_i for bending the thicker plate. Additionally, the calculation of the percentage of springback suppression relative to M_i/EI values for single pass bending, gives the following values :

(i) 38.2 %, 37.5 % and 46.8 % for plate thickness of 8.1 mm, 10.2 mm and 12.07 mm, respectively, at r_f=2100 mm,

and,

(ii) 46.2 %, 44.9 % and 45.9 % for plate thickness of 8.1 mm, 10.2 mm and 12.07 mm, respectively, at r_f=500 mm.

The above percentages do not contradict the previous statement.

Comparing the characteristics for the distance of the elastic-elastoplastic interface (i.e. C_{i0} for multipass bending and C_i for single pass bending) in fig 5.39, it is observed that the respective spacing difference, $\Delta C_{i0}=C_{i0}-C_i$, between the curves of the single and multipass bending for each individual thickness, for the thicker plate is relatively higher (i.e. ΔC_{i0} for 12.07 mm plate is 3.24 mm while for 10.2 mm and 8.1 mm plates is 2.97 mm and 2.36 mm, respectively, at r_f=2100 mm). This means that the effective depth of the plastic deformation band is reduced relatively greater for thicker plate than for the thinner. Furthermore, the first yield local bend radius, R_{1st}, characteristics (fig 5.40) tend to indicate that the value of R_{1st} for the thicker plate in each pass, is greater than that for the thinner ones. In addition, for the bending route of the thicker plates, the characteristics of the local bend radius, R, relative to the finished bend radius, r_{ff}, for the multipass bendings (fig 5.41), generally have a higher radius increment compared to that for single pass bending. All these suggest that the greater reduction in the absolute value of M_i, within the predicted range of the multipass bending, for the thicker plates, may be due to the following factors :

(1) The initial external bending moment about the top roll contact, needed to overcome the elastic work done necessary in generating the first yield is less for bending thicker plate than for bending thinner ones. Subsequently higher values of R_{1st} are obtained, as can be seen in fig 5.40.

(2) The relatively higher reduction in plastic deformation depth, Δc_{j0} (fig 5.39), to accomplish the anticipated r_{ff}, indicates that a relatively smaller plastic work is required.

(3) The relatively higher increment of the values in R (fig 5.41) means that the work required to accomplish the deformation of ΔR is reduced.

However, the consideration of the material properties from fig 6.6 also suggests that it may partly be a result of the instantaneous material stress-strain behaviour (relationship), i.e. the effect of the respective values of the material hardening constant, H.

8.2.2. Discussion on the experimental results

Since there were a total of sixteen u.v. galvanometer signals on the SE recorder, some of the output signals were enmeshed together and were difficult to separate. Therefore only those results which were distinguishable from the u.v. chart are presented in the text. The respective measurements were subsequently presented for the following two operative conditions :

(1) the pre-bending active (pre-active) side roll operative and,

(2) the pre-bending inactive (pre-inactive) side roll operative.

All the data were taken from the u.v. chart at the steady equilibrium operating conditions. The corresponding data for the maximum torque were presented on the basis that the top roll drive experienced the required torque, otherwise, the continuous bending operation would subsequently fail.

8.2.2.1. General observation from the experimental data

The bending force on the rollers for the single and multipass bendings are shown in figs 7.4, 7.9, 7.11, 7.13, 7.16 and 7.17. From the figures it is observed that the measured force on the top roll is lower than that on the bottom roll. This contradicts the expected results : Generally, it was expected that the top roll would exert a higher force than the bottom roll. Initially, it was thought that these results were due to the fact that the top roll load cells were mounted so as to give a "portal frame" structure within the bending unit (see fig 3.5) of the model bender. The additive vertical force components from the operative side roll and the bottom roll would thus generate twisting moments in the top beam and the load cell interfaces. Consequently the induced twisting moments would oppose and cancel the expected bending signal, thus affecting the accuracy of the measured load on the top roll. In order to establish this assumption, an estimation of the magnitude of induced twisting moments was carried out with a load of 250 kN vertically applied at the midspan of each top beam (Item 1 in fig 3.5b). This, in total, gave a maximum induced bending force on the top loadcells within an estimated 12 % of the total applied load. Observation from fig 7.4 indicates that the top roll bending force is 34 % lower than that of the bottom roll at r_{fi}=711 mm, for single pass bending of 8 mm thick x 80 mm wide HP30 aluminium plates. This gives at least 20 % difference from the estimated value of 12 % (Taking account for the side roll bending force, the difference would be even higher than 20 %). Consequently this analysis seems to suggest that the observed characteristics for the top roll (see fig 7.4) could be an inherent bending mechanism of the process. However the understanding of the cause and the nature of this mechanism would need further investigation.

8.2.2.2. For single pass bending

Due to the reason mentioned at the beginning of section 8.2.2, i.e. difficulty in interpreting some of the u.v. traces, and the limited data points collected, the single pass results were limited to the bending of three 8.04 mm thick x 80.2 mm wide and three 8.04 mm thick x 120.2 mm wide HP30 aluminium plates.

A. Bending force characteristics

Fig 7.4 shows the respective bending force on the operative side roll, and the top and bottom pinch rolls. It is observed from the figure that the bending forces, for either pre-bending or pre-active and pre-inactive side roll operative conditions, in bending the 80.2 mm wide plates, gradually increases as the finished inner radius, r_{fi}, decreases from 1230 mm to 270 mm. The curves indicate that the bending force on the operative side roll varies with the bending operational modes, i.e. (i) pre-bending and (ii) steady continuous bending for (a) pre-active side roll and (b) pre-inactive side roll operation. The trace shows that for a particular plate dimension, continuous bending gives slightly lower forces on the side roll relative to the pre-bending mode. It also shows that the force experienced in the pre-inactive side roll bending condition is relatively higher than that in the pre-bending condition. The above characteristics are theoretically possible as a result of the different anticipated boundary conditions of the plate geometry within the bender (see fig 5.7, 5.20, 5.21 and 5.23). This subsequently alters the contacts of the bendplate and the rollers, i.e. the alteration in magnitude of X_{cn}, X_{tn}, X_{bn}, W_{cn}, W_{tn}, W_{bn} respectively. It, in turn, changes the value of the bending arms (i.e. ΔX_{ct}, ΔX_{tb}, ΔW_{ct} and ΔW_{tb}) and the effective force components (i.e. F_{sv}, F_{sh}, F_{tv}, F_{th}, F_{bv} and F_{bh}) (See sections

5.3 and 5.4). The change of the geometrical boundary conditions generally leads to a different deformation distribution in the effective deformation zones. The distinguishable deformation natures for each of the three operation modes are as follows :

(1) In pre-bending, the deformation zones between the operative side roll and the top roll contacts, and between the top and bottom roll contacts are progressively deformed.

(2) In the steady continuous bending, with the pre-active side roll operative, the plate between the top and bottom roll contacts is progressively sprungback, and between the operative side roll and top roll contacts the plate is progressively deformed. Furthermore, a certain longitudinal length of the plate in the latter zone has been deformed in the pre-bending mode prior to the resumption of continuous bending.

(3) In the steady continuous bending with the pre-inactive side roll operative, the plate in between the top and bottom roll contacts is progressively deformed while that in between the operative side roll and the top roll contacts is progressively sprung back.

The deformative mechanism which occurs in operation mode (1) generally requires a higher bending force on the roll than that in operation mode (2). Due to the physical constraint of the bottom roll position during bending, the initial flat geometry of the plate as it enters the pinch region, and also the deformation nature in (3),it is necessary to shift the top roll contact downstream towards the pre-inactive side roll so as to achieve the finished bend radius, r_{ff} and also to extend the effective bending arms, ΔW_{tb} and ΔX_{tb}, of the bending force on the bottom roll. Furthermore, the pre-inactive side roll needs to be positioned higher (see Section 8.6 for

explanation). The latter leads to shorter bending arms, ΔW_{st} and ΔX_{st}, of the bending force components on the side roll. These subsequently give rise to higher bending forces required by the particular bending mode.

The above mechanisms generally take place in both single and multipass bendings. This statement is supported by all the figures appertaining to the characteristics of the bending forces (figs 7.4, 7.9, 7.11, 7.13, 7.16 and 7.17).

Observing the characteristics in fig 7.4, it suggests that in bending the 80.2 mm wide plates, both the top and bottom rolls experience similar loading characteristics. The bending force firstly increases to a maximum value at a certain value of r_{fi} and then gradually decreases (the plotted curve resumes a parabolic shape).

However, the top roll loading for bending the 120.2 mm wide plate seems to lie between those of the bottom roll and the operative pre-active side roll. It is observed that after a certain value of r_{fi}, this decreasing characteristic also appears on the bottom roll loading curve. It is acknowledged however that the data points seem to be insufficient for correctly representing the loading characteristic ; especially where this wide gap between the first and second data points. However, the larger rigidity of the 120.2 mm plate does, to a certain extent, affect the position of the operative side roll and its contact. It subsequently affects the top and bottom roll contacts and the magnitude and characteristic of the bending forces on the rolls. Nevertheless, it is felt that further experimental data are needed in order to confirm this particular assertion. This assertion is based on the theoretical prediction (in sub-section 8.2.1.1 above) as well

as on the analysis of Table 8.1, which have indicated that the plate internal bending resistance, at the top roll contact, in bending a particular plate thickness specimens, may be correlated into one curve (See fig 5.29 to 5.31 for springback, depth of elastoplastic deformation and local bend radius).

The higher bending force on the rollers for the steady-continuous bending mode with pre-inactive side roll operative, in comparison with that for pre-bending mode, indicates that the former bending force may be a main factor for evaluating the actual bender capacity.

B. Torque characteristics

The pre-bending, mean and maximum torques experienced on the top roll during bending each single pass bending operation are presented in fig 7.5 (for 80.2 mm wide plates) and fig 7.6 (for 120.2 mm wide plates). The plotted trends from the limited results available indicate the following torque characteristics :

(1) The pre-bending torque on the top roll steadily increases from 3.2 N m at r_{fi}=1087 mm to 31.4 N m at r_{fi}=255 mm for the 80.2 mm wide plate. For the 120.2 mm wide plate, it increases from 5.2 N m at r_{fi}=2021 mm to 32.2 N m at r_{fi}=214 mm.

- The measured pre-bending torque on the top roll suggests the existence of a tangential force, F_{sh}, which is transmitted to the pinch region and subsequently to the top roll. It also indicates that the reversely driven top roll in pre-bending, as envisaged in item (g) of section 5.3.1, may reduce the overall resultant pinch force.

(2) The applied torque on the top roll, in the pre-continuous

(i.e. roll swapping) bending with the inactive side roll operative, shows a trend of higher values than those of the pre-bending operation. This may be due to the fact that a higher position of the operative side roll is required to achieve the anticipated r_{fi}. This leads to an increase in the contact angle, θ_s' (see fig 5.7), between the plate and the pre-inactive side roll. The bender geometry is such that it may also give a higher value of the effective horizontal force component, $F_s'\cos\beta'$, as a consequence of increasing the contact angle, θ_s' (this is identical to the result of increasing θ_s, See fig 5.5). From the available data, the trend of the plotted curve (fig 7.5) for bending 80.5mm wide plate shows a steadily decreasing torque from 77.2 N m at r_{fi}=1250 mm to 38.1 N m at r_{fi}=281 mm. In contrast, the trend for the curve (fig 7.6) of 120.2 mm wide plate shows an initial increase of torque from 7.1 N m at r_{fi}=3051 mm to a maximum at a value of certain r_{fi} and then decrease to 53.5 N m at r_{fi}=341 mm. The above characteristics may be due to the variation of the top roll contact, which alters the loading nature of $F_s'\cos\beta'$ relative to the top roll itself. It may also be due to the effect of the relative rigidity of the plate.

(3) Both maximum and mean torques on the top roll for the steady continuous bending, with the pre-active side roll operative, increase steadily (fig 7.5 and 7.6). However the curve for the former has a convex trend (with respect to the origin of the co-ordinate) while that for the latter has a concave trend for bending the 80.5 mm wide

plate (fig 7.5). Both curves for bending the 120.2 mm wide plate have a concave characteristic (fig 7.6). It is observed that the two curves for both torques, in bending either plate width, showed a wider spacing between them at high values of r_{fi}. The spacing becomes narrower as r_{fi} decreases.

(4) The maximum and mean torques on the top roll for bending the two plate widths, with the pre-inactive side roll operative, are also plotted on figs 7.5 and 7.6. The trend of the curves for the wider plate shows convex shape for the former torque and a concave shape for the latter one (fig 7.6), while the trend for the curves of the narrower plate has a concave shape for both torques (fig 7.5). The convergency of the magnitude of both torques at lower r_{fi} is also observed for curves of either plate width.

(5) Comparing the trend of the curves for either maximum or mean torque of the two plate widths, in both pre-active and pre-inactive side roll bending modes, it can be seen that the value of torque for the latter bending mode commences with a higher one (at high r_{fi}) and finishes at a lower value (at smaller r_{fi}) than the former operational mode.

The characteristics observed in (3), (4) and (5), from the limited data, are probably as a result of altering the loading conditions relative to the top roll and changes in the nature of the plate-roll contacts and plate deformation during bending.

C. Power characteristics at mean torque

The power characteristics (at mean torque) in bending the specimens of the two plate widths are shown in fig 7.7 (for 80.5 mm wide plates) and fig 7.8 (for 120.2 mm wide plates). Since it was evaluated by using equation (7.6), it is a direct function of the mean torque, T_m. Its characteristics for either the pre-active and pre-inactive side roll bending modes have the same trend as that mentioned in items (3) to (5) for the mean torques under both bending modes. These can be seen by comparing figs 7.5 and 7.7, and figs 7.6 and 7.8, respectively.

8.2.2.3. For multipass bending

The measured parameters for multipass bending of HP30 aluminium plates are shown in the following figures :

(i) Bending force characteristics on the rollers : figs 7.9, 7.11, 7.13, 7.16, 7.17 and 7.20.

(ii) Torque characteristics on the top roll : figs 7.10, 7.12, 7.14, 7.18 and 7.21.

and

(iii) Power characteristics on the top roll drive : figs 7.7, 7.8, 7.15, 7.19 and 7.22.

The figures show that the bending characteristics not only varies with the plate dimensions, but it also varies with the bending route and number of passes, the magnitude of the intermediate interval of any two successively anticipated bend radii and the plate geometry before subsequent bending is undertaken. This is so even in bending specimens of the same plate thickness and width. The irregularity of the trend for these characteristics agrees with the theoretical prediction for the internal bending resistance of the plate at the top roll (see figs 5.32 and 5.37). It is therefore concluded that the irregularity of the trend is a consequence of the

different degree of springback, the depth of elastoplastic deformation interface in the plate, and the penetration of the plastic deformation into the effective deformation zones between the top roll and operative side roll contacts (see Section 8.2.1.2). For bending the specimens of different plate thicknesses, it should also be noted that the dissimilar material properties (See fig 6.6) may also be a major contribution to the mechanics of bending (see sub-section F in section 8.2.1 for example).

As a check of the irregularity of the bending force curves for multipass bending, an inspection on the instruments' circuitries and the respective loadcell alignment was performed, and correct working conditions and the alignment of the related sensing components confirmed. Further analysis on the torque and power characteristics for the multipass data indicated the same trend of irregularity (for example, See fig 7.10, 7.12, 7.15 and 7.19 etc.) as a result of different bending routes. In addition, theoretical predictions of the internal bending moment of the plate for 8.1 mm thick x 80.5 mm wide HP30 aluminium plates (figs 5.32 to 5.36) also show the irregular characteristics for multipass bending. It subsequently leads to the conclusion that the observed bending characteristics are due to the different nature of the material deformation and the bender/plate geometry as bending proceeds.

Comparison of the driving power at mean torque for 8.1mm thick x 80.5mm wide (fig 7.7) and 8.1mm x 120.2mm wide (fig 7.8) plates, tends to suggest that, for the particular bending routes indicated in figs 7.7 and 7.8, multipass bending requires less torque and power to achieve a tighter bend radius than those for single pass operation. However the overall power accumulated from each individual successive pass (i.e. overall work done in bending the plate) may be higher than that of the single pass bending. This is partly due to

the accumulated loss from the recoverable elastic springback in each successive pass for the former operation (see Section 5.4.4), and partly as a result of the fact that the multipass bending mode takes a longer operational time.

8.2.2.4. For the straight end remaining in the bent plates

Fig 7.23 shows some characteristics of the straight end remaining in the bent plates for single pass bending of 8.04 mm thick x 80.4 mm wide HP30 aluminium plates, and multipass bending of a 8.04 mm thick x 80.2 mm wide, a 8.04 mm thick x 120.2 mm wide and a 10.4 mm thick x 80. mm wide HP30 aluminium plates. The measured straight ends are merely for the pre-bending operation only (the straight end remaining at the completion of the continuous stage for pre-inactive side roll operation was not measured). The trend of the curves also shows the same irregular characteristics as for multipass bending mode. However it indicates that the straight end remaining after the first bending is greater for the plates having a higher flexural rigidity. The second and subsequent passes normally gave a shorter straight end compared with the first pass. Studying the curve of the remaining straight end for the single pass bending of the 8.02 mm thick x 80. mm wide plate in comparison with its multipass bending counterpart, it can be seen that the straight end remaining in the bentplate is higher for the tighter bend radius in the former bending mode while that for the latter bending mode is subsequently reduced. This suggests that multipass bending mode may be advantageous in reducing the magnitude of the straight end left in the plate. Consequently, it reduces the cost of machining off the straight end in order to form a complete tubular section. Also material wastage is reduced.

8.3. Discussion on the mathematical model

8.3.1. On the choice of the co-ordinate system

The curvilinear co-ordinate system [5] was originally chosen for the roller plate bending problem. However, the floating boundary conditions made the solution for the co-ordinate system very difficult. The cartesian co-ordinate was therefore used instead. There are certain shortcomings of this system. They can be generalised as follows :

(1) The use of the biharmonic equation for plate bending in cartesian form, with no attempt to modify it by further considering its local thickness gives $C_{tni}C_{tno}$ (fig 5.12) as

$$C_{tni}C_{tno} \doteq [(C_tC_{t0}/2)^2 + \Delta X^2]^{1/2} \times 2$$

where $C_tC_{t0}=t$, i.e. the thickness of the plate.

(2) Due to (1), the accuracy may reduce when
(i) a thicker plate was bent,
and,
(ii) a tighter bend-radius was anticipated.

Consequently, the chosen co-ordinate system was only valid in bending thin plate. It was also valid in pre-bending a thick plate to a large bend-radius.

(3) Since the nominal contacts of the rolls in the analysis were taken along the central plane, the value of x at any section was taken along the central plane of the plate. Referring to fig 5.10, it can be seen that the lines through the contact and centre of the rolls, e.g. $O_sC_sC_{sn}C_a$ through the plate depth, is different from that of the analytical line C_eC_d. Nevertheless, the extra area $C_eC_{sn}C_aC_e$, covered by the analytical line C_eC_d, can be

corrected by the uncovered area $C_d C_{sn} C_s C_d$. Consequently, the analysis of the work done, required to bend the plate, in the effective deformation zones, can be considered accurate. This is true only when $C_e C_{sn} C_a C_e$ is closely equal to $C_d C_{sn} C_s C_d$ in thin plate bending.

(4) Since the deflection profile of the bendplate was taken along the central plane and the plate is relatively thin, the deflection function in the co-ordinate system approximately represents the actual deflection profile (provided the iterated values for the expected/assumed boundary conditions are of the same order).

8.3.2. On the application of biharmonic plate equation for small deflection bending

Plastic deformation must occur in forming processes [5,17]. Prescott [89] has clearly pointed out that the plate bending problem had to be considered as a large deflection problem once the deflection itself is equal to or greater than the plate thickness. Based on the small deflection equation of plate (i.e. equation 2.1), von Karman [108] and Prescott [89] have derived a large deflection equation for plate (i.e. equation 2.3). The latter equation has been widely applied in the analysis of large elastic deflection plate problem. In roller plate bending, deflection is always large, but an analysis employing the modified biharmonic equation for plate generated non-linear partial differential equations that were difficult to solve. Consequently, this approach was abandoned.

8.3.3. On the surface contact

Since the surface contact is a necessary feature of the continuous roller plate bending process (see Section 5.3), the

determination of the apportion of the surface contacts between the top and bottom rolls with the bendplate may provide a means of accurately evaluating the forces on the top and bottom roll.

8.4. Discussions on the design of model bender

To initiate the investigation of the mechanics of the four roller bending of plates, a fully instrumented four-roll model bender has been designed and constructed. The model bender was initially designed to simulate a four-roll Verrina bender at Head Wrightson Teesdale (HWT) Ltd.. A rudimental theory was first derived to estimate the design capacity of the model bender. It was necessary to ensure that the designed model was capable of simulating the Verrina bender well. Calculations for the bender prototype and the model using the derived rudimental theory in Chapter three indicated that this was achieved (see section 3.4.1).

The designed model bender also embraces most of the features of the three-roll benders. Hence, by suitable adjustments, it can be used as a three-roll bender. It thus facilitates the experimental study of the mechanics of the roller plate bending, either for three- or four- roll operating modes. In addition, the model has motor drives for the side roll and therefore provides a means of investigating the slip effect on the mechanics of the four-roll plate bending.

The instrumentation includes ten loadcells (each has two strain gauge bridges), three torquemeters and tachometer. This, together with the mathematical analysis in Appendix 7.1, enabled the empirical assessment of the quantity of springback in the bending operation; and the determination of the form radius at the top roll contact of a bending plate before springback.

The derived rudimental theory (i.e. equations 3.19 and 3.31 etc.) shows that the force on the top and bottom roll is inversely proportional to the coefficient of friction, μ, between the bendplate and the rollers in the pre-bending stage. Physically, this is possible because of the following reasons :

1) The pinch force applied by the bottom roll is partly to deform the plate at the plate's straight edge section and partly to grip the plate so as to prevent it from being retracted or pushed through the pinch.

2) Due to (1), the higher coefficient of friction, μ, means a greater resistance to both plate retraction and push-through in the pinch. Subsequently it reduces part of the necessary normal pinch force.

The aforementioned possibility had to be properly proved by a series of planned experimental investigations. An obvious example is to study experimentally the bending mechanics with different surface finishes of either the bendplate or the rollers. Although this has been envisaged at the initial research planning stage [150] (see Table 7.2), it is regretted that the tests concerned could not be performed in the present research due to time and cost constraints.

8.4.1. Bender capacity

Before the research was initiated, the roller bender capacity was considered to be dependent upon the following factors.

a) The flexural rigidity of the rollers
   - the rollers have to deform the plate to the required

bend radius. Failure to do so would means that the rollers would either fail elastically or produce a large deflection which would reduce the quality of the bent plate. Thus this is a important factor of the bender capacity.

b) The capacity of the bearings and the rigidity of the mounting components.

c) The capacity of the bending and power supply to the bottom pinch and the side rolls
- This means that the capacity of the hydraulic cylinders should generate sufficient power.

d) The capacity of the motor drive to commence / perform the continuous bending
- This is a crucial factor to estimate whether an anticipated sectorial or tubular bentplate can be achieved by the roller bender.

Hardly any theoretical analysis on the mechanics of four-roll bender is available in the current literature [17]. Furthermore due to

(i) the complex interactive nature of the rollers and the plate being bent (see section 5.3),

and

(ii) the complicated mechanism involved in the multipass bending mode (see theoretical and experimental results),

roll bending charts supplied by bender manufacturer to the users are not reliable. It thus jeopardizes their commercial competitiveness. The present theoretical analysis gives a means of understanding the mechanics of a four roll plate bender in bending a plate to any finished bend radius. It thus provides a means for determining the bender capacity for a

given task. The latter can be achieved as follows .

(1) Firstly, calculate the corresponding forces on the rollers and the driving torque necessary on the top roll, for the critical bending conditions.
- The conditions are :
a) when the movement of the operative side roll is prevented by either of the pinch roll (Normally the top roll -see fig 3.2)
b) at the initiation of bending an initially flat plate in pre-bending stage (see fig. 3.3).

(2) Secondly, compare the respective calculated values with
a) the roll flexural rigidity to see whether they can sustain the loading.
b) the power in the hydraulic cylinders for the bottom pinch roll and the side rolls to see whether the power is capable of doing the work.
c) the driving torque and the power of the top roll motor drive to see whether they are sufficient.

(3) Thirdly, perform a thorough stress-strain analysis, for all the mounted components and the frame work of the bender, to see whether they can sustain the loads.

8.4.2. Critical operational conditions of the bender

In the roller plate bending process, the critical operational conditions of a bender mainly depends on the following factors :

a) the required bending forces and driving torques for a particular bending operation,
and,
b) the allowable displacement of either the operative side roll or the bottom pinch roll.

The geometric conditions shown in fig 3.2 and fig 3.3 can be considered as examples of the critical operation, (b) above, for the designed model bender (see Chapter three).

8.5 Discussion on the experimental techniques

The experimental technique / procedure used in Chapter seven only gave valid data for equilibrium conditions. The data for the intermediate stages, from initiation of the bending to the chosen equilibrium condition were difficult to analyse. This was because each end of the operative side roll was pumped up using different hydraulic cylinders which were powered by a single hydraulic pump.

In the process of the experiment neither pair of the control valves (i.e. V1 and V4, or V2 and V3, respectively, in fig 3.6) in the hydraulic powering line were suitably adjusted to achieve equal movement of both ends of the operative side roll. The bending was thus carried out by firstly raising up the side roll and then levelling the ends of the side roll. Consequently, the actual bending mode is one of twisting pre-bending. The deformation nature in the effective deformation zone for the initiation of bending to the end of pre-bending is thus difficult to assess. This is because it varies with the differential displacement of one end relative to the other (i.e. it varies with the degree of plate twisting). Also there is no adequate instrumentation to detect its instantaneous relative displacement.

Due to :

1) the above mentioned end differential displacement of the operative side roll,

and,

2) the differential of the the applied pressure line along

the operative side roll,

the plane strain assumption in the theoretical analysis for the effective deformation zone does not seem to be fully justified. The proposed theory may not be applicable at any intermediate equilibrium condition during the pre-bending operation. However the equilibrium condition at the final stage of the pre-bending, with level ends of the side roll, may be appropriate to the theory.

It should be noted that in the practical production environment, the steady-continuous bending operation for roller bending of tubular section is operated with both ends levelled. The operation is therefore a uniform edge-loaded bending problem (if the deflection of the roller is neglected).

To reduce the twisting bending effect, it is suggested that the operative side roll should be raised level and very slowly.

8.6 Discussion on the position of the side rolls in continuous bending for the pre-active or pre-inactive side roll operative mode

Item (a) in section 5.3.2.1 and item (a) in section 5.3.2.2 mentioned that the different deformation mechanisms occur in the effective deformation zone between the operative side roll and top roll contacts, when

(1) the pre-bending active side roll is operative,

and when

(2) the pre-bending inactive side roll is operative.

The former is identified as one of progressive deformation while the latter as one of progressive springback. It can be envisaged that the effective bending deformation of the latter

occurs from the inlet of the bottom roll contact to the outlet of the top roll contact band. Since :

a) the top roll is permanently fixed,
b) the change of the vertical position of the bottom roll, during bending, may be assumed small (It was assumed zero in the theoretical analysis), and its sideways movement is rigidly constrained,

and,

c) the axis of both the top and bottom pinch rolls is in the same vertical plane.

The variation of the plate distance from the inlet at the bottom roll contact to the outlet at the top roll contact band may be negligible, assuming that the position of the pre-inactive side roll is constant. Normal practice in carrying out the continuous roller bending mode is to maintain the powering condition in the bottom roll hydraulic cylinders, in the same manner as that at the end of the pre-active side roll operative mode. Detailed comparison of the two operations allows the following particulars to be observed.

A) The change in the expected geometrical boundary conditions (ref to figs 5.21 and 5.23) related to the plate geometry condition in the steady-continuous bending are as follows.
   i- For bending an initially flat plate with the pre-inactive side roll operative, the boundary condition at the bottom pinch roll has zero curvature while the curvature, at the outlet from the pre-inactive side roll, is $1/r_f$ (see fig 5.23).
   ii- For bending an intially flat plate with the pre-active side roll operative, there is a zero curvature at the pre-active side roll and $1/r_f$ at the bottom roll contact (see fig 5.21).

B) The change in the expected magnitude of the plate curvature at the top roll contact to that of the bottom roll contact (see fig. 5.21 and 5.23) is as follows.

i- It is M_f/EI alone for the pre-active side roll operative mode,

and,

ii- It is $1/r_f+M_f/EI$ for the pre-inactive side roll operative mode, an additional change of $1/r_f$ in comparison with that in (i).

C) There is no additional power supply added to the hydraulic cylinders of the bottom pinch roll from the hand pump for the pre-inactive side roll operative mode (i.e. it remains as that of the pre-active side roll operation). Additionally the optimal vertical position of the bottom pinch roll is pre-restrained by the plate thickness.

In view of item (B) to accomplish the additional change of curvature $1/r_f$ for the pre-inactive side roll operation requires an extra power supply to raise up the bottom roll hydraulic cylinders. Due to item (C), this cannot be achieved. The alternative is to alter the top roll contact band (i.e. to move it downstream closer to the pre-inactive side roll) by moving up the pre-inactive side roll. Subsequently, a higher position of the pre-inactive side roll, compared that with the pre-active side roll, is required. Certainly it can also be argued that the higher position is a consequence of the final curvature of the bendplate from the exit of the pre-inactive side roll.

The different position of the operative side roll in both operative bending modes has been experimentally confirmed : It

was found that the steady continuous bending mode with the pre-inactive side roll set to the same height as that for the pre-active side roll, generated a smaller bend curvature of the plate for the same bending condition.

8.7 Comments on the straight edge produced at the end of the steady continuous bending

Noting the higher position of the pre-inactive side roll compared with that of the pre-active side roll in steady continuous bending mode, it can be envisaged that there must be a straight edge section remaining at the end of the bent plate at the completing stage of bending. Certainly its magnitude depends upon the following factors.

a) The achieving of the finished bend radius of a bent plate.
b) The initial geometry of the bendplate.
c) The initial positional distance, X_0, of the operative side roll.
d) The positional powering direction (i.e. the positional powering angle, ψ) of the operative side roll.
c) The size of the top and bottom pinch rollers.

The principle for shifting the top roll contact away from the bottom roll in the pre-inactive side roll operative mode compensates the effectiveness of the bending force on the latter roll. To achieve this, either one or a combination of the following methods can be considered.

i) Increase the magnitude of the vertical bending arm, $\Delta W=\Delta y$, at a constant value of X.
   - For a particular bender configuration, this can be achieved by introducing a smaller diameter top pinch roll (to give a more rapid change of curvature).

ii) Reduce the bottom roll curvature, i.e. a larger

diameter roll, so as to increase its effective contact/ horizontal bending arm, ΔX, of its initial bending force component.

iii) The combination of (i) and (ii).

iv) The appropriate choice of the positional powering angle, ψ, of the operative side roll.

However, the choice of (i) substantially weakens the rigidity of the top roll. It subsequently reduces the bender capacity and the finished bent plate quality (It is noted that the latter effect may be due to the roll deflection itself). Its design would require complementary back-up rolls, for example, like the design of the "cluster" rolling mill. Nevertheless, this may increase the design and manufacturing cost of the bender itself. Additionally, a careful analysis / investigation would be required in order to optimise the geometrical interaction of the roller movement.

8.8. Discussions on the roller plate bender design

An understanding of the bending mechanism of the four roll bender will effectively improve its design. Although the present research firstly initiates the investigation in the particular bending process, the consideration of the possible mechanism involved in section 5.2 and the experimental results in figs 7.4 to 7.23 provide certain suggestions for future four-roll bender design. The following specifies these aspects.

8.8.1. Elimination of the counter-bending effect in the pre-bending mode (refer to fig 5.3 and fig 5.6)

Though the effect of the counter-bending moment, due to the overhanging plate end before the inlet to the operative side

in pre-bending, has not been assessed experimentally, its existence will certainly increase the bending load on the operative rolls. This is mainly due to the following reasons :

a) The counter-bending monent reduces the effective plate curvatures along the effective deformation zone, between the operative side roll and the top roll contacts. It therefore decreases the penetration length of the plastic deformation zone in the effective deformation zone (hereafter termed EDZ).
-Normally its existence alters the distribution of the external bending moment along the EDZ. Technically the counter bending moment beyond the operative side roll may superimpose the bending moment before top roll contact and generate a bending moment diagram as shown in fig 8.2. It therefore , significantly diminishes the magnitude of the effective bending moment (in the EDZ), created by the identical bending load on the operative side roll when the counter-bending moment is not present.

b) The counter bending moment generates negative curvature near the operative side roll. It may also produce a large surface contact band. Consequently it magnifies the friction effect against the plate transportation in the continuous bending mode, if the operative side roll is not completely free to rotate. It thus further smoothens the curvature in the EDZ and increases the driving torque on the top pinch roll.

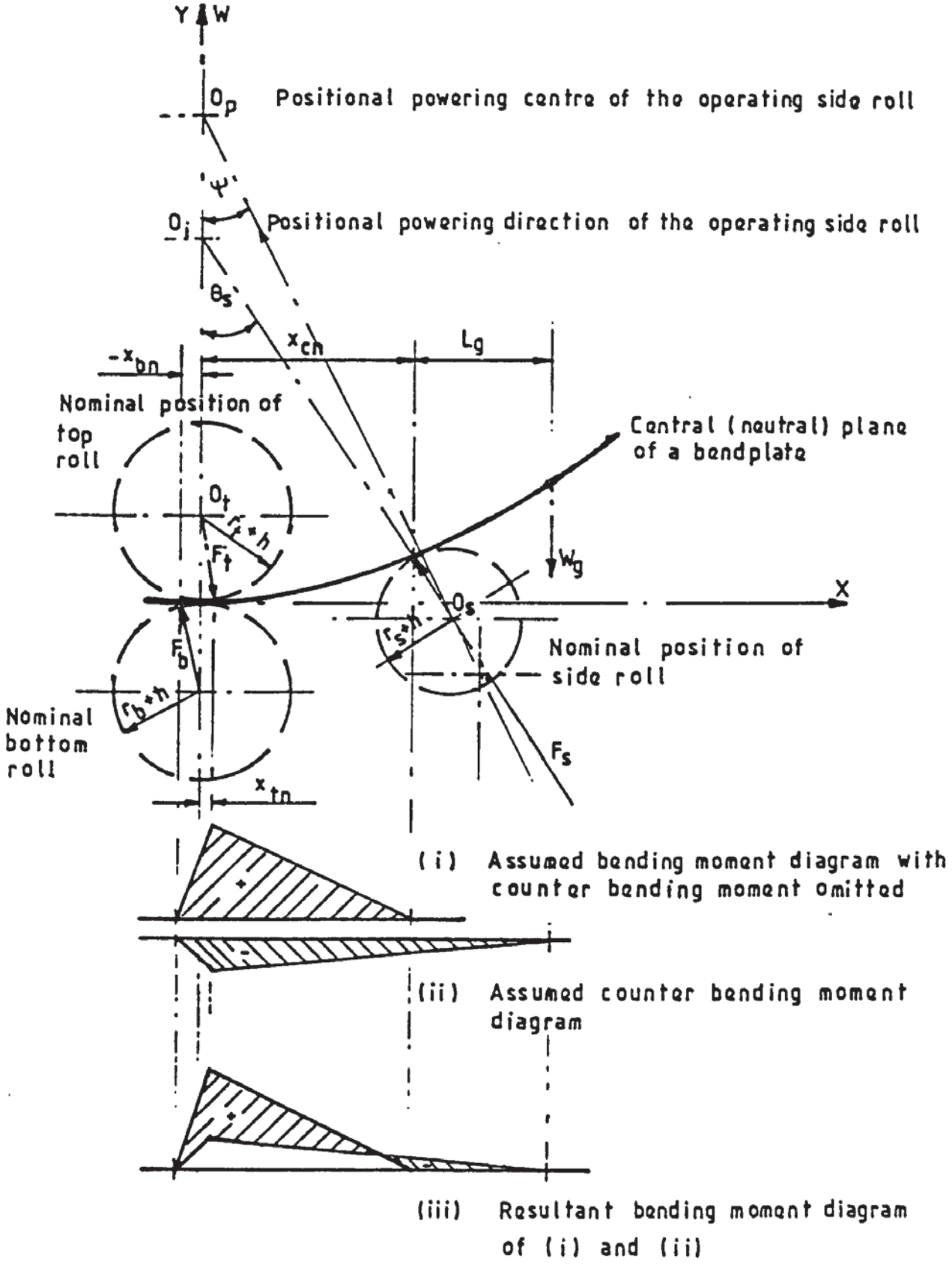

FIG 8.2 EFFECT OF COUNTER BENDING MOMENT ON THE BENDING MOMENT DISTRIBUTION IN THE EFFECTIVE DEFORMATION ZONE

c) The counter bending moment tends to stretch the plate section in the EDZ against the bending direction. It thus changes the stress and strain distribution across the plate thickness as shown in fig 8.3. The shifting of the neutral axis inward toward the bent plate concave surface indicates that the tensile strain on the convex side increases. This may subsequently cause a thinning effect.

d) The stretching effect tends to pull the bendplate out from the pinch region. To counter it a higher pinch pressure is required. This results in higher pinch forces on both pinch rolls.

To eliminate the counter bending effect, modifications may have to be made to the four roll bender design. Possible solution may be as follows :

1) To implement a rail support system for the overhanging plate before inlet to the operative side roll.

2) To introduce a supporting side roll at the instantaneous centre of gravity of the overhanging part of the plate.

3) To design a vertical bender instead of a horizontal bender.

It is observed that the solutions (1) and (3) have in fact been utilised. Other effective modification awaits further study.

8.8.2. The magnitude of the initial bending arm, X_0, i.e. the initial position of the side roll (refer to fig 3.3)

A model bender designed geometry which has been considered

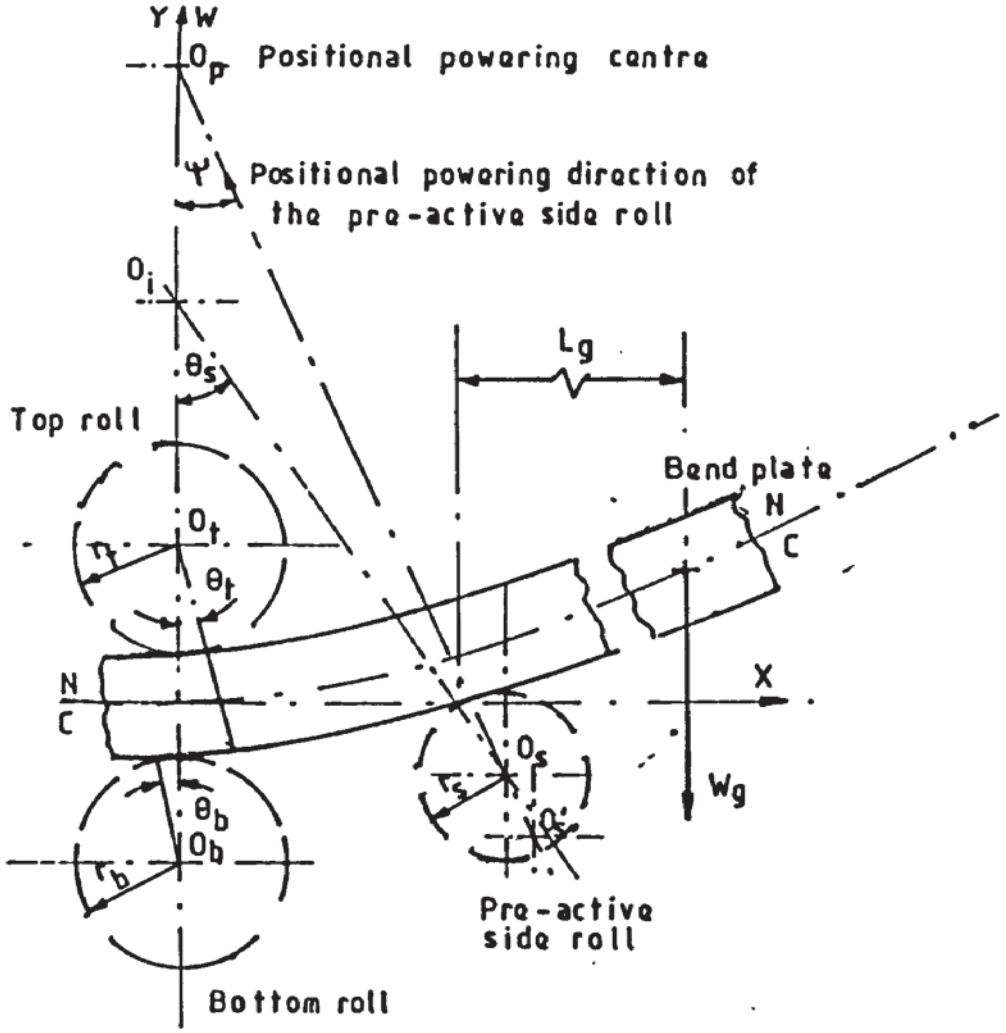

a - Bending geomtry of a bend plate

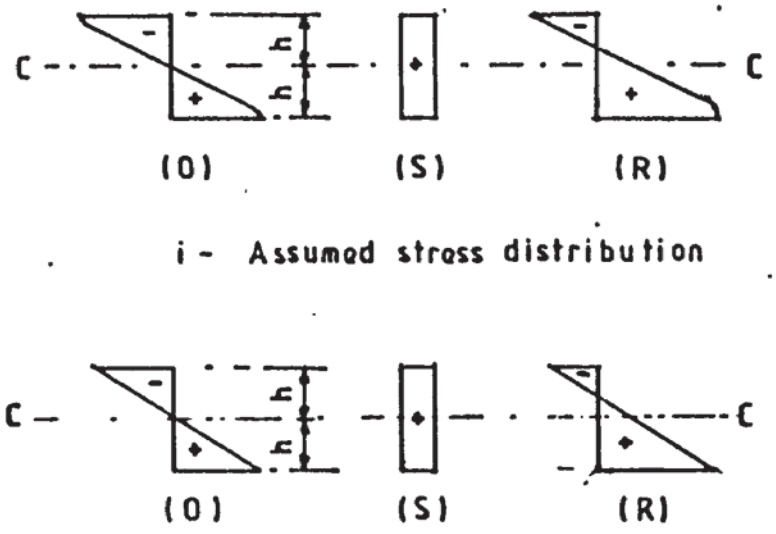

i - Assumed stress distribution

ii - Assumed strain distribution

CC = Contral plane of bend plate
(O) = With Wg omitted
(S) = Due to the indued stretching of Wg alone
(R) = Resultant distribution of (O) and (S)

b - Longitudinal stress-strain distribution through plate depth in the effective deformation zone

FIG 8.3 EFFECT OF COUNTER BENDING MOMENT ON STRESS-STRAIN DISTRIBUTION IN THE EFFECTIVE DEFORMATION ZONE

in Chapter three is shown in fig 3.3. It was taken as a critical operation because the magnitude of the effective bending force on the operative side roll primarily depends upon the value of the initial bending arm, X_0, (see figs 3.3 and 5.8). Generally the larger the X_0, the smaller will be the operative side roll bending force, F_s, required to initiate the bending. This seems to be an attractive choice for a design study. Consideration of the four-roll bender process suggests that the value of X_0 limits the range of the finished bend radius that can be achieved from the bending process.

Referring to fig 5.2, it can be seen that the continuity of the bending operation (after the completion of pre-bending) demands that the bent plate (emerging from the pinch region) be suitably bridged over the pinch and the pre-bending inactive side roll. To accomplish a tight bend radius means that a particular value of X_0 is required, otherwise the operation may fail due to a longer "straight end" remaining in the bent plate. This indicates that its chosen magnitude must give the following characteristics.

a) Produces an acceptable initial bending force
   -Generally a higher initiating bending force on the side roll implies that a high flexual rigidity is necessary for the operative side roll. It also means a higher powering pressure in the side roll hydraulic cylinder. Consequently its size and installation will substantially increase the bender design and manufacturing cost.

b) Produces finished tubular sections with a wide range of bend radii, thus optimising the bender capability.

8.8.3. Choice of the positional powering angle, ψ, of the operative side roll

The appropriate choice of the positional powering angle, ψ, for the operative side roll is critical. This is because its geometry determines the effective bending displacements, i.e. the relative bending arms (ΔW and ΔX), of the side roll for the force vectors (F_{sv} and F_{sh}) respectively, as bending proceeds. A properly designed roller bender must have a positional powering angle, ψ, which significantly increases the effective vertical displacement, ΔW, but only slightly reduces its corresponding horizontal displacement, ΔX. It should also give

(1) a high initial vertical bending force, $P_v = F_{sv}$, from the hydraulic cylinder so as to effectively initiate the bending,

and,

(2) an acceptable position of the operative side roll to achieve a tight bend radius.

Generally the selection of ψ is dependent on the choice of X_0.

8.8.4. Choice of roll size

The dimension of a bender roller determines its rigidity and deflection in the roller bending process. Although a large diameter roller can sustain a higher bending force, it creates additional mounting problems. It also reduces the versatility of the bender to bend the plate to a smaller radius of curvature.

The geometry of a finished product is dependent on the top roll diameter, the relative material properties of the rollers

and bendplate, and the bender capacity. The larger top roll indicates the larger the finished bend radius It is therefore a major factor to be identified in the design stage. Nevertheless, a larger size of bottom roll may be beneficial in reducing the remaining straight ends due to the initial pre-bending stage and the completion of each continuous bending mode. This is possibly a consequence of increasing the effective surface contact between the plate and the bottom pinch roll. The plate retraction from the pinch region is also affected by the diameter of the bottom pinch roll. This is as a result of modifying the surface friction in the contact area and possible constrictions imposed by the geometry of the pinch roll gap.

CHAPTER NINE

CONCLUSIONS

9.1 Conclusions

A major part of this research was the design and construction of an experimental model bender. Its design and instrumentation allowed the mechanics of most three- and four-roll plate bending processes for both single and multipass modes to be studied.

A semi-empirical mathematical analysis was also proposed for four roll bending of thin plates. The analysis could be used to study experimentally the springback and the local bend radius, before springback, at the top roll contact.

A rudimentary analysis, which considered the three critical bending operations of the four-roll pre-bending process, was presented. The analysis gave an assessment of the four-roll bending capacity. The analysis indicated that an increase in the coefficient of friction, in the contact region of the pinch rolls and the plate, would reduce the pinch resultant force required to bend a plate to a particular bend radius.

The mechanisms involved in the four roll continuous roller plate bending of plates were detailed. It was concluded that the plate deformation in the effective deformation zones (EDZ) between the contacts for (a) the top and the pre-active side rolls and (b) the top and the bottom rolls were :

(i) both progressively deformed for the pre-bending operation,

(ii) progressively deformed in zone (a), and progressively sprungback in zone (b) for the steady-continuous bending mode with the pre-active side roll in operation.

For steady-continuous bending mode with pre-inactive side roll in operation, the EDZ in (b) was progressively deformed while the EDZ between the contacts of the top and the pre-inactive side roll was a progressively sprungback. In addition, the

contacts between the rollers and the bendplate varied as the bending proceeded in the pre-bending mode. It consequently varied the effective bending arms of the force components on the operating side roll, and consequently their magnitude.

A mathematical model to determine the bending mechanics (i.e. force, torque, power, depth of plastic deformation, springback) for single/multi pass of four-roll thin plate bending was constructed. The model was derived from the elastic-elastoplastic deformation through the plate thickness, the force (moment) equilibrium conditions, and the geometry for the appropriate boundary conditions.

Computer programmes for evaluating internal bending resistance, for single and multipass bending modes of the plate, were developed. Theoretical prediction of the respective bending modes in bending HP30 aluminium specimens were conducted.

Theoretical prediction for single pass bending of HP 30 aluminium plates (of thickness: 8.1 mm, 10.2 mm, 12.07 mm and 14.68 mm) indicates that it is not possible to correlate the plate bending internal bending moment (M_I), for all the specimens with different plate thicknesses, into a single relationship. This is mainly as a result of different amounts of springback, and the penetration depth of the elastoplastic deformation band (due to the effects of various material properties and plate flexural rigidity). However the normalisation of the internal bending moment (M_I) for plates with a particular thickness plate seemed promising. Generally, bending a thicker plate gave a higher first yielding bend radius (R_{1st}) and local bend radius (R), at top roll contact, in comparison with bending a thinner one. The internal bending

resistance of the plate (M_i) at the top roll was shown to be a direct function of the plate dimensions.

It was concluded that in multipass bending, the internal bending resistance of the plate (M_i) varied with the bending route, the number of bending passes undertaken and the bendplate initial geometry. The absolute magnitude of M_i, within the predicted range and bending route, was lower than its corresponding value for the accomplishment of a particular bent radius in single pass bending. Its reduction was greater in multipass roller bending a thicker plate. Nevertheless, the correlation of the values of M_i into a single relationship for multipass roller bending was not possible since different bending routes had been considered.

From the experimental investigation, it can be concluded that the rollers generally exert the highest bending force in the steady-continuous bending mode with the pre-inactive side roll in operation. In the pre-bending mode a higher bending force is normally required on the rollers than the steady-continuous bending mode with the pre-active side roll in operation. For the single pass bending mode, the bending force on the operative side roll, the torque and the power characteristics steadily increase as the bent radius r_f decreases. For the multipass roller bending operation, all the above characteristics and the measured "straight end" remaining in the bent plate are irregular and depend upon the bending route and the number of passes.

The theoretical and experimental results from the present research lead to the conclusion that the mechanics involved in four roll plate bending are very complex. The fact that the multipass roller bending of plates generates different

parametric characteristics, as a result of the different bending routes, suggests a possible reason why most of the rolling charts supplied by bender manufacturers are not fully reliable.

CHAPTER TEN

SUGGESTIONS FOR FURTHER WORK

10.1. Introduction

The roller bending of plates is a rather complicated, yet effective production process. A full understanding of the mechanics of the process will provide a means of further improving the process and optimising its productivity. Subsequently, it will reduce the unit cost of the products and increase its competitiveness. It will also provide a foundation to furnish data for the new design of the roller and the methodology in producing various bend products. This should then lead to the automation of the manufacturing process in order to keep up with the development of modern technology.

The work that has been done in the present research is intended to provide an initiation into the understanding of the working mechanism of the process. To achieve the full potential of the process, further research on the roller bending of plates is required.

10.2. Further work to extend the understanding of the continuous roller bending process

10.2.1. Experimental aspects

10.2.1.1. Bending specimens

The experimental results in the present research were limited to bending HP30 aluminium plates of thickness, 8 mm and 10.09 mm, with widths as shown in Table 7.1. The results show the different characteristics of single and multipass bending, and the complexity of multipass bending. However, more experimental data, for bending aluminium plates of the same and other combinations of thicknesses, widths and number of passes should be obtained ; especially for single pass

bending. Furthermore, extension of the bending tests to include mild steel, brass and lead (to simulate the hot roll bending of mild steel) specimens would be beneficial. This will provide of experimental data useful to four-roll plate bender (especially the Verrina bender) operators.

Since the present experimental work has only been carried out on thin plate, a complete understanding of the mechanics of roller plate bending demands that thick plate experiments be also carried out.

10.2.1.2. Geometrical layout of the rollers in the bender

Since the present experiment was performed with the geometrical setting of the model bender simulating the Verrina bender, which had an angle of 20° for the positional powering direction of the side rolls, the results would only be adequate to this specific setting.

The geometrical set-up of the side rolls affects the combination of the horizontal and vertical components of the bending force and the bending efficiency. Consequently, it is suggested that tests for various geometrical settings of the roller model bender should be carried out.

10.2.1.3. Residual strain (stress) measurements

It is possible to study the residual strain (stress) distributions in the outer fibres of a bent plate by noting the displacements of scribed grid-meshes on either side of its surface. The transverse strain distribution profile on the plate edges may also be investigated by the same technique. This work will develop further the understanding of the mechanism of the process, and is suggested as part of a programme of further studies.

10.2.1.4. Roll size effect

The roll size of a roller plate bender will affect the path contour of the contact region between the bent plate and the roll as bending proceeds. It can be envisaged that the size of the bottom pinch roll may affect the length of the straight end required in pre-bending, i.e. a larger roll diameter may possibly reduce the length of the straight end (or vice versa). The actual physical effects of the bending characteristics can only be investigated through a systematic experimental study.

10.2.1.5. Slip effect

Friction tends to resist the slip between bodies in contact, producing a straining effect on the contact area. Depending upon the slip vector, its effect may be beneficial or detrimental to the process of the roller bending of plates. Such a study of the slip effect on the side roll and on the bottom pinch roll will give an insight into the mechanism involved in the bending process.

10.2.1.6. Surface texture (friction) effect

Surface texture determines the magnitude of the frictional traction, which is a means by which the plate is conveyed through the pinch region in the steady state of continuous roller bending. This friction also prevents the slipping of the plate in the pre-bending stage. Like the slip effect, its effect may ultimately assist in increasing or decreasing the plate curvature during bending.

For the above reasons, the contribution of the surface texture effect to bending, together with a knowledge of the slip effect, will enable the mechanics of the roller bending

of the plates to be more easily evaluated.

10.2.1.7. Rotational drive on the top roll while pre-bending takes place

In pre-bending, the bending force on the nominated active side roll has a horizontal force component, which tends to push or pull the plate through the pinch contact gap. This component is mainly resisted by the frictional traction present in the pinch gap. It is thought that this push or pull effect may be overcome by the reverse rotation of the top roll, although this may prove difficult. This situation also creates uncertainty as to whether the rotation will further push or pull the plate out of the pinch gap. A suitable investigation into this aspect should be considered.

10.2.2. Metallurgical aspect

Permanent deformation of metal always involves changes in the metallurgical structure within the metal itself. It is suggested that by relating the alteration of the grain structures before and after bending, it should be possible to gain an insight into the stress-strain condition of the bent plate specimens.

10.2.3. Theoretical analysis

10.2.3.1. Theoretical analyses for thick and thin plate bending

The theoretical analysis undertaken in this research merely considers the thin plate bending mode. The thick plate bending mode in four-roll bender requires a consideration of the transverse shear through the plate thickness. Although the governing partial differential equations and functions relevant to large plate deflection may be derived, their

nonlinearity and the floating boundary condition of the bending geometry limits the possibility of obtaining a solution to the equations. It is felt that further work should be undertaken to solve such governing equations, in order to obtain a general solution for the roller plate bending process.

In addition, further improvement of the present developed theory may be achieved by using the curvilinear co-ordinate system [5], large plate deflection theory [89] and surface contact problem [117 to 141].

10.2.3.2. Deflection of rollers

The theory produced in Chapter five, assumes a uniformly distributed pressure on each individual roller during bending. This implies that there is no deflection of the rolls. However, in the plate bending process, roll deflection is always present. For this reason, the applied bending loads are no longer uniformly distributed. Thus, modification of the theory may have to be made, in order to predict the mechanics of the bending process adequately.

Since both ends of each nominated active side roll are sometimes balanced individually, twisting of the plate is experienced. The analysis will therefore be more complete if account is taken of this possibility.

10.2.3.3. Bauschinger effect

Normally, plastic bending of plate involves the shifting of the neutral axis inward towards the concave surface. Consequently, the Bauschinger effect may be experienced in the region which has changed from a state of tension to one of compression. It may be interesting to consider this effect in theory.

10.3. Improvement of the model bender

10.3.1. improvement in instrumentation

Since there are eighteen output signals on the SE u.v. recorder and four output signals on the Southern Instruments u.v. recorder, the output chart traces tend to become enmeshed. It makes the analysis of the data difficult, and time-consuming. It is thus recommended that a computer data logging system be utilised to process the signals. Another alternative is to split the output signals to other u.v. recorders.

Another problem with the instrumentation is that in bending the aluminium specimens the bending signals from the side roll load cells are too small. Further amplification of these signals is advisable.

10.3.2. Modification of the model bender

By mounting the ends of the top roll to the top beams and to the associated loadcells at either end of each beam, a "rigid portal frame structure" is formed (fig. 3.5). The vertical bending load component tends to create a twisting moment which is sensed by the top loadcells. The resultant moment makes the bending signals from the top loadcells unreliable. Appropriate modification should eliminate this effect.

In addition, the top corner edges of the pair of inner end plates (fig 3.5) are too high. They can thus prevent the transportation of the widest plate of width ,305 mm, through the bending unit. The recommended modifications are as follows.

a) To cut off the plate corners and to reinforce the plates, by either welding or rivetting the reinforcement strips onto them, thus avoiding shear failure of the metal above the corner hole (see Item drawing no.1, Appendix 3.1) : For alignment purposes, each pair of the holding rods should be inserted during welding.
b) To re-design higher top loadcells, so as to place the top roll in a higher position.
   - this also requires the re-design of the side and bottom roll loadcells in order to allow the necessary strokes of their respective hydraulic cylinders.

Another drawback in the design of the model bender is that there are four holding rods which locate the bottom clamping blocks of the side roll to the end plates. It has been found that aligning each pair of holding rods is laborious. For convenience and accuracy, it is recommended that only two long holding rods should be designed and installed.

10.4. Possibility of automating the process

The model bender has been designed to hydraulically power the bottom pinch roll and the side rolls. This facilitates the possible investigation into automating the process, either by dynamic or kinematic control. It is clear that the application of CNC to the roller bending of plate is possible using the present model bender, once an interface control circuit is built and complementary facilities are designed.

APPENDIX 1.1

GLOSSARY

GLOSSARY

The following describes some glossaries used in this thesis.

Bendplate (bend plate) - The plate, which is either (1) at its initial geometry condition before bending or (2) being bent in a roller bender, is intended to be bent in accomplishing an anticipated bend radius.

Bentplate (bent plate) - The plate which has been bent to the final anticipated bend radius after the release of bending load of the rollers.

Positional powering angle, ψ, of the side roll

- The angle between the axis of the side roll hydraulic cylinder and the vertical plane through the axes of the top and bottom pinch rolls

Positional powering centre of the side roll

- The intercept-point/line where the axis of the side roll hydraulic cylinder crosses the vertical plane through both the axis of the top and the bottom pinch roll.

Positional powering direction of the side roll

- The direction in which the axis of the side roll hydraulic cylinder is being moved along.

Pre-active side roll

- The operative side roll which is employed to perform the initial pre-bending procedure (3), figs 5.2(i), for thick plate bending and (2),5.2(ii), for thin plate bending, in the roller plate bending process.

Pre-bending operation

- It is defined, in most places of this thesis, as the bending operation to perform the procedure (3), figs 5.2(i), for thick plate bending and (2),5.2(ii), for thin plate bending.

Pre-inactive side roll

- The operative side roll which is not employed to perform the initial pre-bending procedure (3), figs 5.2(i), for thick plate bending and (2),5.2(ii), for thin plate bending.
  (Note : The choice of the pre-active side roll and the pre-inactive side roll, in figs 5.1 and 5.3 - 5.27, is arbitary, it depends upon the inlet-direction of the bendplate to the bender. For example, if the bendplate inlets from the l.h.s. of the bender, fig 5.1, the pre-inactive side roll will become the pre-active side roll)

Continuous bending with the pre-active side roll operative (or operating)

- The continuous roller thin plate bending mode when the pre-active side roll is performing the bending, e.g. the procedure (3),fig. 5.2(ii), if the bendplate enters the bender at the operating side roll in

(2), fig 5.2(ii).

Continuous bending with the pre-inactive side roll operative (or operating)

- The continuous roller thin plate bending mode when the pre-inactive side roll continues the bending process in order to complete the bending (i.e. procedures (5) - (6), fig 5.2(ii), if the bendplate enters the bender as in (1) - (3), fig 5.2(ii)).

Roll swapping bending mode

- The intermediate bending stage when the loading on the pre-active side roll is completely released and the pre-inactive side roll is raised up to the anticipated position, before proceeding the continuous bending mode with the pre-inactive side roll operative mode. The bending has been performed to replace the proceduce (4), fig 5.2(ii), during experiment.

APPENDIX 2.1

LITERATION SURVEY ON PLASTICITY

A2.1. Plasticity

The development of the science of plasticity has been significantly enhanced through the combined efforts of numerous researchers, such as : Levy, Tresca, von Mises, Mohr, Von Karman, Prandtl, Reuss, Hencky, Nadai, Lode, Prager, Hodge, Drucker, Hill, Johnson etc., throughout the last century.

Publications in plasticity are so numerous that it is difficult to review them extensively in this Appendix. The following review only briefly points out some of the concepts and developments in this field of study.

Basically the study of plasticity concentrates on the behaviour of material after yield has occurred. The fact that many materials behave differently beyond the first yield complicates the theoretical analysis. The production of a unified mathematical theory which embraces most of the physical plastic deformation phenomena, such as : creep, fatigue, strain rate effect, material anisotropy, fracture, Bauschinger and hardening effects etc., has proved to be rather difficult. Nevertheless a number of researchers have been consistently working towards this direction [1 to 31].

Since real materials are often reasonably isotropic in their unstrained state, plasticity is developed by assuming that materials are homogeneous. Except for the perfect plastic material, the homogeneous state of stress (i.e. pure tension, compression or pure shear) beyond the elastic limit of a solid normally produces strain, which is partly elastic and partly plastic. Tests indicate that the curve $\sigma=f(\varepsilon)$ for unloading and loading will not generally coincide after yielding occurs. In most polycrystalline metallic materials, strain hardening effect usually increases the yield stress σ_Y required to

produce a new permanent strain ε. Materials will achieve a stable condition of yielding only if $(d\sigma/d\varepsilon)>0$.

In a brief review of the theories of strength in applied mechanics, Nadai [23] discussed the various possibilities under which general failure is observed in engineering materials. He considered in detail the mechanical conditions under which, (i), engineering materials start to deform permanently, and (ii), rupture or visible separation of parts of a surface within a member of a structure occurs. He pointed out that the speed of deformation had an influence on the magnitude of the yield stress, σ_Y, producing a given strain ε. Accordingly, at normal temperature the yield stress σ_Y for a ductile metal increases with the strain rate $(d\varepsilon/dt)$ in the following logarithmic function.

$$\sigma_Y = \sigma_1 + \sigma_2 \log(V/V_0) \qquad \text{(A2.1)}$$

where σ_1, σ_2 and V_0 are material constants, V is defined as $(d\varepsilon/dt)$.

A2.1.1. Yield criteria

The principal objective in the development of plasticity theory is to determine the history of the state of stress and strain at all points in a partially or totally plastic body when the history of the boundary loadings and displacement are specified. Most practical problems, applying the plasticity theories, are analysed through the considerations of equilibrium, compatibility, boundary conditions, stress-strain relations and yield condition (or flow potential).

The yield condition establishes a mathematical criterion which describes the yielding of a multi- dimensionally

stressed or strain material in relation to its uni- axial stress/strain relation. Several existing yield criteria are available. They are as follows :

(1) Rankine maximum stress theory
(2) Saint Venant maximum strain theory
(3) Tresca (or Coulomb) maximum shear theory
(4) Beltrami maximum strain energy theory
(5) Huber (Hencky)-von Mises distortion energy theory
(6) Mohr yielding theory
(7) Internal friction theory

The above yielding theories are revelant mainly for isotropic materials. Their respective deformation and mathematical formulation can be found in most texts on plasticity [5,11,17,21].

Several other yield criteria for anisotropic materials have been proposed in the literature. Hill [9], in 1947, extended the Huber- Mises criterion for isotropic materials to anisotropic material. He formulated the criterion in the following form

$$2f = F(\sigma_{yy}-\sigma_{zz})^2+G(\sigma_{zz}-\sigma_{xx})^2+H(\sigma_{xx}-\sigma_{yy})^2+2L(\tau_{yz})^2+2M(\tau_{zx})^2 +2N(\tau_{xy})^2 =1 \qquad \text{(A2.2)}$$

where f is a potential function. F, G, H, L, M, N are constants characteristic of the current rate of anisotropic, and are related to each other as $N=F+2H=G+2H$, $L=M$.

The criterion ignores the Bauschinger effect and the influence of hydrostatic pressure on yielding.

Marin [20] has also proposed a yield criterion for anisotropic materials with different yields in tension and compression. The expression of Marin's criterion can be found

in reference 17.

The mathematical derivation of a strain hardening yield criterion for isotropic material normally initiates from a yield surface which is a monotonically increasing function of the plastic work. In tensor form it is expressed as

$$W = \int \sigma_{ij}\, d\varepsilon_{ij} \qquad \text{(A2.3)}$$

that is

$$\sigma_Y = f\left(\int \sigma_{ij}\, d\varepsilon_{ij}\right) \qquad \text{(A2.4)}$$

Derivation of this expression can be seen in referances 11 and 21.

It is well known that the rheological behaviour of a metal is often dependent upon the current state of the stress and the deformation history. A common example is to be found following uniaxial plastic straining where the elastic limit is often higher for subsequent loading in the same direction. This type of directional behaviour is termed as the Bauschinger effect [29]. Dubey and Hillier [3] took into account the ideal strain hardening solid having principal axes of anisotrpy and a significant Bauschinger effect. They thus proposed a general yield criterion and flow rule based on the invariant principle.

The Dubey and Hillier criterion is considered as a modified Hill theory of anisotropy [9]. They used the third invariant of stresses σ_{ij} to obtain the following linear combination for the generalised yield stress

$$\sigma_Y = A\sigma_{kk} + [(1/2)C_{ijkl}\sigma_{ij}\sigma_{kl}]^{1/2} + [(1/3)D_{ijklmn}\sigma_{ij}\sigma_{kl}\sigma_{mn}]^{1/3} \qquad \text{(A2.5)}$$

where σ_Y is a positive and real quantity.

In applying the general yield equation (A2.5), the following

particulars should be considered.

(1) Only the real root of the second bracket is considered

(2) The coefficient A must be identically zero if yield is independent of the hydrostatic stress

(3) The symmetry of the stress tensor requires that

$$C_{ijkl} = C_{jikl} = C_{ijlk}$$

and also $D_{ijklmn} = D_{jiklmn} = D_{ijlkmn} = D_{ijklnm}$

(4) On the basis of the flow rule $d\varepsilon_{ij}=d\lambda(\partial f/\partial\sigma_{ij})$ and the incompressibility condition, $d\varepsilon_{ij}=0$, the anisotropic coefficients are restricted as follows

$D_{ijklmn}=D_{klijmn}=D_{ijmnkl}=D_{mnklij}$, and

$D_{ii1111}=D_{ii2222}=D_{ii3333}=D_{ii1122}=D_{ii2233}=D_{ii3311}$

(5) The postulate of principal axes of anisotropy requires that

$C_{ii11}=C_{ii22}=C_{ii33}=0$

are satisfied .

Dubey and Hillier [3] also illustrated the technique in determining the coefficients of anisotropy for their general yield equation (2.5).

A2.1.2 Stress-strain relations

A2.1.2.1. Incremental relation

Owing to the complex non-linear material behaviour after yield, which is a consequence of various degree of pre-working, chemical constitutes in a material, material microstructure orientation and heat treatment etc., the widely applicable stress strain relation of Hooke's law in elasticity does not apply to plastic analysis. However, Saint Venant in

1870 first proposed that the principal axes of strain increment coincided with the axes of principal stress. Levy in 1871 and von Mises in 1913 independently generalized a relationship between strain increment and the reduced stress.

Levy-Mises relation is generally expressed in the following form.

$$d\varepsilon_{ij}=\sigma'_{ij}d\lambda \qquad \text{(A2.6)}$$

where $d\lambda$ is an instantaneous non-negative constant of proportionality, which may vary throughout a strain process

σ'_{ij} is the tensor of the current deviatoric stress

$d\varepsilon_{ij}$ is the tensorial incremental strain

The Levy-Mises equation is normally used for rigid perfectly plastic solid, in which the elastic strain may often be neglected.

The stress-strain relations for an elastic-plastic solid were first proposed by Prandtl in 1924 for the case of plane strain deformation. It was then generalised by Reuss in 1930 as in the following form.

$$d\varepsilon^{p}_{ij} = \sigma'_{ij}\, d\lambda \qquad \text{(A2.7)}$$

where $d\varepsilon^{p}_{ij}$ indicates the plastic strain increment.

Normally the total strain increment, $d\varepsilon_{ij}$, in the elastic-plastic material is expressed as the sum of the elastic strain increment $d\varepsilon^{e}_{ij}$ and the plastic strain increment $d\varepsilon^{p}_{ij}$, i.e.

$$d\varepsilon_{ij} = d\varepsilon^{p}_{ij} + d\varepsilon^{e}_{ij} \qquad \text{(A2.8a)}$$

which can further be expressed as follows

$$d\varepsilon_{ij} = \sigma'_{ij}\, d\lambda + (d\sigma'_{ij}/2G)+[(1-2\nu)/E]\delta_{ij}\, d\sigma_{m} \qquad \text{(A2.8b)}$$

where, G is the shear modulus, δ_{ij} is the Kronecker delta and $d\sigma_m$ is the incremental hydrostatic stress.

Based on the Levy-Mises and Prandtl-Reuss stress strain relations, other relations considering the work hardening, plastic potential flow rate and total strain etc., have subsequently been developed [5,11,17,21].

A2.1.2.2. Deformation stress-strain relation

Hencky in 1924 attempted to extend the total strain theory to plasticity. He proposed that the total plastic strain ε^p_{ij} is proportional to the deviatoric stress σ'_{ij}. Hencky's plastic relation may be expressed as follows

$$\varepsilon^p_{ij} = \Phi\sigma'_{ij} \qquad \text{(A2.9a)}$$

For the total strain, it is expressed as follows

$$\varepsilon'_{ij} = [\Phi+(1/2G)]\ \sigma'_{ij} \qquad \text{(A2.9b)}$$

$$\varepsilon_{ij} = [(1-2\nu)\sigma_{ij}]/E \qquad \text{(A2.9c)}$$

where Φ is a positive scalar quantity during loading and zero on unloading.

Deformation theories of plasticity for work hardening materials postulate that the state of stress determines the state of strain uniquely as long as plastic deformation continues. For isotropic materials, the axes of principal stress and strain coincide. By assuming isotropy, plastic incompressibility and the absence of influence of the hydrostatic pressure, Prager [27] gave the most general form of deformation theory as follows.

$$\varepsilon^p_{ij} = P(J_2,J_3)\sigma'_{ij} + Q(J_2, J_3)\ t_{ij} \qquad \text{(A2.10)}$$

where $t_{ij} = \sigma'_{ik}\sigma'_{kj} - (2/3)(J_2\delta_{ij})$, which is the derivation of

the stress.

P, Q are the functions of J_2 and J_3 in general.

J_2, J_3 are the function of the second and third invariants, respectively.

Such a mathematical theory of plasticity could be usable for general stress history only if it is explicitly stated that a function $f(J_2, J_3)$ is the criterion of loading or further deformation. It is noted that the foregoing description of $f(J_2, J_3)$ applies strictly to a single loading which may be followed by one elastic unloading.

A2.1.3. Verification and modification of plasticity theories

Any mathematical theory must be based on the physical facts common to most plastic metals. A proposed plasticity theory will only be acceptable if it agrees with the experimental data. Throughout the last few decades, tests with metallic materials have been performed to justify the validity of the proposed mathematical theories.

Prager [28] in 1948 examined the conditions of continuity and uniqueness which the stress strain laws of flow and deformation types must fulfill in order to make sense physically. He concluded that the deformation expression (i.e. Hencky's) types can easily be constructed to give the continuity in either condition . He also identified that the uniqueness mainly depends on each individual stress strain law under consideration. Defining the boundary values is normally the basic problem.

Prager (28) also specifically discussed the alternative

forms of some of these laws, such as Nadai's formulation of the deformation type [22] and Lanning's formulation of the flow type [26]. He found that the conditions of the continuity and uniqueness of the above laws were also identical to their own type as previously stated. In his attempt to generalise a unified stress-strain law, Prager [6] established a general law of deformation type which fitted the test results of Lode [19] and Taylor and Quinney [30]. It is generally recognized that Prager's generalisation is too complex for most engineering applications [17]. Nevertheless, Prager [28] realised that the existing intricate mathematical theories in plasticity only gave exact solutions to a small number of special cases, and stressed the development of the approximate, i.e. the methods of integration- variational principle of stress analysis in the plastic range.

In his examination of several mathematical theories of plasticity, Drucker [2] correlated Osgood's experimental data [25] employing the following relationships.

(1) maximum shear stress τ_{max} versus maximum shear strain $\gamma_{max.}$

(2) Octahedral shear stress τ_{oct} versus octahedral shear stress γ_{oct}.

(3) equivalent shear stress τ_{eq} versus octahedral shear strain γ_{oct}.

He noted that the equivalent shear stress expression as a function of the second and third invariants, J_2 and J_3 respectively, improved the correlation of many of the results. He thus proposed a correlation relationship in the following form :

$$\tau_{eq} = \tau_{oct} (1-2.25J_3^2/J_2^2)^{1/6} \qquad \text{(A2.11)}$$

In response to Prager's deformation theory of equation (A2.10), which does not fully describe the continuity of loading and unloading, Drucker [2] indicated that modifications were required for a more general stress history and for material with an initial elastic range.

The incremental theory results from the assumption that once a given value of f is reached, no further plastic deformation will occur until a higher value is attained, and that the increment in permanent strain is proportional to the increment in f. Many essential features of the incremental theory can be illustrated by the most elementay form $f=f(J_2)$. If it is expressed in tensorial form, the incremental strain reduces to the following form :

$$d\varepsilon^{p}_{ij} = P(J_2)\, \sigma'_{ij}\, dJ_2 \qquad \text{(A2.12)}$$

It is obvious that there will be no change in any component of plastic strain if $dJ_2=0$.

The general desire for formulating a more general mathematical theory of plasticity led Handelman et al [6] to propose the following expression for the incremental strain.

$$d\varepsilon^{p}_{ij}=[P(J_2,J_3)\sigma'_{ij}+Q(J_2,J_3)t_{ij}]df(J_2,J_3) \qquad \text{(A2.13)}$$

To which the following elastic strain increment $d\varepsilon^{e}_{ij}$, i.e.

$$d\varepsilon^{e}_{ij}=[(1+\nu)d\sigma'_{ij}]/E + [(1-2\nu)d\sigma_{ij}\delta_{ij}]/E \qquad \text{(A2.14)}$$

is added to obtain a total strain increment $d\varepsilon_{ij}$.

For an anisotropic material, Drucker [2] introduced an

elementary strain stress relation as follows :

$$d\varepsilon_{ij} = g_{ij}\, d\sigma_{ij} \qquad \text{(A2.15)}$$

where g_{ij} is the function of the state of stress and includes elastic and plastic behaviour.

Employing the plastic potential expression (A2.2) and the von Mises stress-strain relation of $d\varepsilon_{ij}=(\partial f/\partial\sigma_{ij})d\lambda$, Hill [9] derived the following relations between stress and strain increments, which he expressed as follows, for anisotropic materials.

$$d\varepsilon_{xx}=d\lambda[H(\sigma_{xx}-\sigma_{yy})+G(\sigma_{xx}-\sigma_{zz})],\quad d\varepsilon_{yz}=d\lambda L\,\sigma_{yz}$$
$$d\varepsilon_{yy}=d\lambda[F(\sigma_{yy}-\sigma_{zz})+H(\sigma_{yy}-\sigma_{xx})],\quad d\varepsilon_{zx}=d\lambda M\,\sigma_{zx} \qquad \text{(A2.16)}$$
$$d\varepsilon_{zz}=d\lambda[G(\sigma_{zz}-\sigma_{xx})+F(\sigma_{zz}-\sigma_{yy})],\quad d\varepsilon_{xy}=d\lambda N\,\sigma_{xy}$$

in which $d\varepsilon_{ii}=0$ is applied as for all stress systems.

A2.1.4. Experimental techniques to verify the plasticity theories

Lode (19) pioneered the verification of the Prandtl-Reuss relation of the stress strain increment. He introduced the variables of μ and V, which are defined as follows :

$$\mu=(2\sigma_2-\sigma_1-\sigma_3)/(\sigma_1-\sigma_2)=(2\sigma'_2-\sigma'_1-\sigma'_3)/(\sigma'_1-\sigma'_2) \qquad \text{(A2.17)}$$

$$v=(2d\varepsilon_2-d\varepsilon_1-d\varepsilon_3)/(d\varepsilon_1-d\varepsilon_2) \qquad \text{(A2.18)}$$

On the basis of equation (A2.6) and the analysis of the stress strain Mohr circle, Lode and Nadai [23] noticed that μ should be equal to V if the Prandtl-Reuss relation of stress strain increment held. Lode thus measured the parameters by

using circular thin walled tubes (of steel, copper and nickle) subjected to internal pressure and axial load. Following Lode's experiment, Taylor and Quinney [30] performed a number of carefully planned tests to evaluated Lode's variables. The latter experiment was carried out by stressing thin walled tubes of aluminium, copper and mild steel in combined tension and torsion.

Both Lode, and Taylor and Quinney's test data showed a clearly observable deviation of the curves $V=f(\mu)$ from the straight line $\mu=V$. However, it was generally recognised that the relation of $V=\mu$ was sufficiently accurate to apply the Prandtl-Reuss flow theory, to the first approximation, for ductile metals to describe the simple mechanics of the plastic state.

If the absolute isotropy of the thin walled tubes might not be applicable, Hill [13] developed an experimental technique which would exercise a greater control on the degree of material anisotropy. Hill's apparatus is simple and depends on the testing, in simple tension, of a thin, uniform rectangular strip, in which a groove/notch has been cut. Hundy and Green [16] adopted Hill's technique to determine the plastic stress strain relations. Their data have a good agreement with Levy-Mises relation.

A2.1.5. Experiments to verify yield criteria

Tests with isotropic metallic materials by Ludwik [22] have shown that if a system of principal stresses $\sigma_1, \sigma_2, \sigma_3$ is at a limit of plasticity , then the addition or substraction of a three axial uniform tensile stress or of a hydrostatic compression σ_m $[=(\sigma_1+\sigma_2+\sigma_3)/3=\sigma_{ii}/3]$, produce a stress system

$\sigma_{ii} - \sigma_m$ which is also at the limit of plasticity. It is therefore concluded that yielding is independent of the hydrostatic pressure provided that σ_m is not too large. It also indicates that the yield only depends on the principal stress differences of $\sigma_1 - \sigma_2$, $\sigma_2 - \sigma_3$ and $\sigma_3 - \sigma_1$.

Through a series of tests, Lode [23], and Taylor and Quinney [30] verified that the Huber-von Mises yield criterion :

$$(\sigma_1 - \sigma_2)^2 + (\sigma_2 - \sigma_3)^2 + (\sigma_3 - \sigma_1)^2 = 2\sigma^2 = \text{constant} \qquad \text{(A2.19)}$$

was in close agreement (within 3 %) with experimental data for ductile materials.

Since the principal shear stresses can be related to the principal stress differences as follows :

$$\tau_1 = (\sigma_2 - \sigma_3)/2, \quad \tau_2 = (\sigma_3 - \sigma_1)/2, \quad \tau_3 = (\sigma_1 - \sigma_2)/2 \qquad \text{(A2.20)}$$

The Huber-Mises yield equation can therefore be alternatively expressed in the form [23]

$$\tau_1^2 + \tau_2^2 + \tau_3^2 = 2k^2 = \text{constant} \qquad \text{(A2.21)}$$

where the maximum shear stress k is equal to $\sigma_Y/2$.

Using Mohr's representation of stresses by means of the three principal stress and strain circles, Nadai [23] concluded that the first and second invariants of stress tensors have a significance for the laws of the yielding of perfectly plastic materials : The first invariant, $J_1 = \sigma_m = \sigma_{ii}/3$, determines the origin M (fig A2.1) for the three principal stress circles, while the second invariant expressed the Huber-Mises condition of yielding for ductile metals.

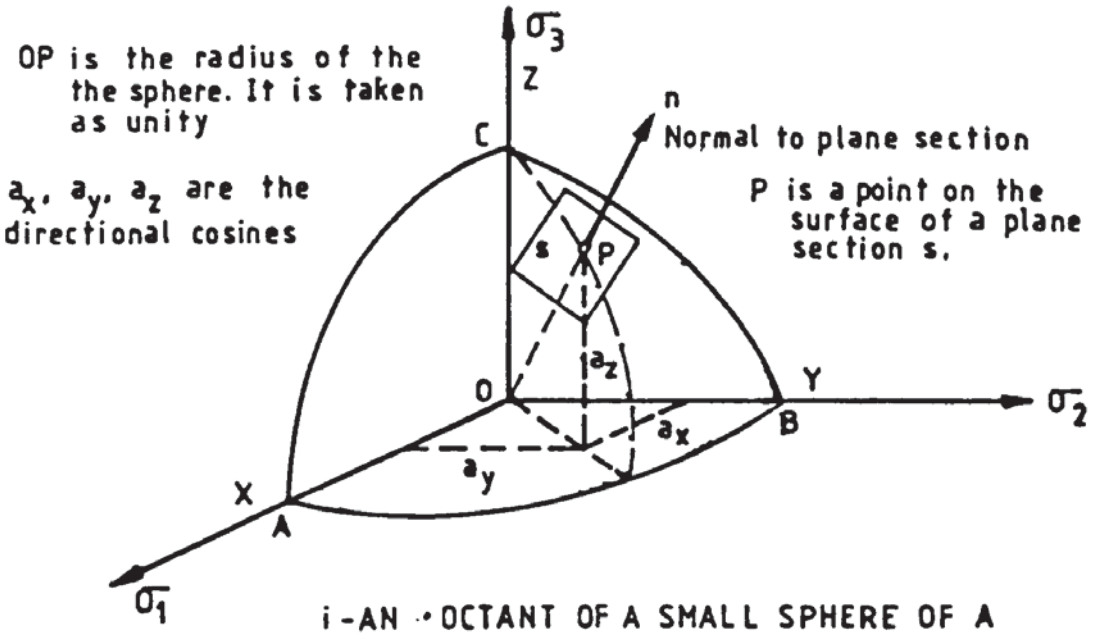

i - AN OCTANT OF A SMALL SPHERE OF A STRESSED MATERIAL

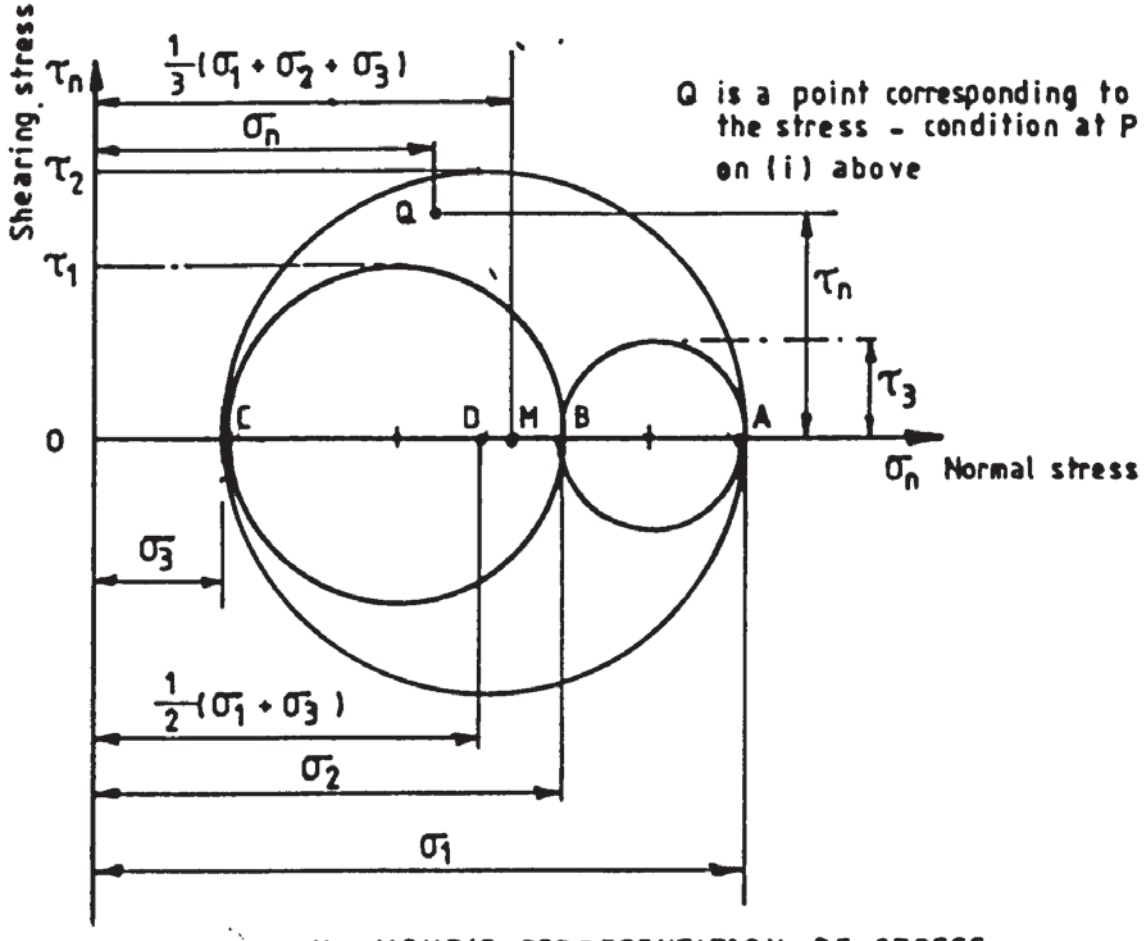

ii - MOHR'S REPRESENTATION OF STRESS

FIG A2,1 MOHR'S CIRCLE REPRESENTATION OF 3-D PRINCIPAL STRESSES AND MEAN STRESS M (AFTER REF 23)

To account for the experimental fact that the hydrostatic pressure has some influence on the yield of the less compact polycrystalline metals, Schleicher [23] suggested that the total elastic strain energy could be assumed as a function of the mean pressure σ_m, such as :

$$\sigma_1^2+\sigma_2^2+\sigma_3^2-(2/\nu)(\sigma_2\sigma_3+\sigma_3\sigma_1+\sigma_1\sigma_2)=f(\sigma_m) \qquad \text{(A2.22)}$$

Lode and Burzynski [23] suggested that this more general kind of yielding could be accommodated by assuming that the energy of distortion is a function of σ_m.

A2.1.6. Physical explanation of plasticity

Hencky [7], in his review of the knowledge of inelastic behaviour of metals up to 1934, attempted to present a coherent physical picture. He extended the scope of the basic laws by earlier experiment, in such a manner that the later experiments could be accounted for by a theory flexible enough to represent all phenomena of practical importance. He pointed out that the value of a mathematical theory is to furnish an analysis, against which the true behaviour of a specimen can be distinguished and measured.

Hencky also emphasised that in developing any mathematical theory, the following physical facts of plastic metals should be carefully considered

(1) All metals are polycrystalline substance
- the measured stress and strain are only the average of microstresses and strains of thousands of crystal grains in the particle.

(2) The two causes of the permanent set in a material are :
   (a) thermal plasticity - a finite change in the molecules distance between points in materials due to heat movement of molecules.
   (b) athermal plasticity - the finite deformations undergone through sliding along a certain planes in each individual crystal grain.

(3) Plasticity in polycrystalline metals is always a mixture of thermal and athermal plasticity.

(4) At elevated temperature the loaded material does not reach static equilibrium, but shows a permanent creep.

(5) In any elastic plastic system, the loading and unloading phases must be clearly distinguished.

In view of (5), it is noted that in practice only the loading phase of a system can plastically occur, which is normally defined as $df/dt \geq 0$, while the unloading condition is defined as $df/dt < 0$. In which the microstress potential f is expressed as

$$f=[(\sigma_1-\sigma_m)^2+(\sigma_2-\sigma_m)^2+(\sigma_3-\sigma_m)^2]^{1/2} \qquad \text{(A2.23)}$$

and t is time.

An adequate mathematical theory should embody all the above points and be capable of solving the problem of creep for small strain.

A2.1.7. Rupture

In reviewing the theory of strength, Nadai [23] also briefly discussed the occurrence of material fracture due to tensile stress, in relation to the octahedral shear stress τ_{oct}, i.e.

$$\tau_{oct}=(2/3)[\tau_1^2+\tau_2^2+\tau_3^2]^{1/2}=f(\sigma_m) \qquad (A2.24)$$

He pointed out that the yielding surface in the form of expression (A2.24) could not be extended beyond the region where one of the three principal stresses was a tensile stress and had at least reached the tensile strength of rupture. The rupture surface was thus expressed as $H(\sigma_1, \sigma_2, \sigma_3)=0$ for points stressed in the system of rectangular co-ordinates σ_1, σ_2 and σ_3. The surface consists of the three mutually perpendicular planes :

$$\sigma_1=C, \quad \sigma_2=C, \quad \sigma_3=C$$

where C is an positive stress, i.e. the tensile strength in pure tension.

For sliding fracture, the rupture surface is a plane inclined at a certain angle to one of the principal stress planes, and Nadai [23] noticed that Mohr's theory might be sufficient to predict its generation of fracture and orientation.

In the case of the fracture of ductile materials, Nadai pointed out that the complex nature of the cause of rupture made the application of general yield relation to predict its initiation rather difficult.

A2.1.8. Methods of integration - variational

principles in plasticity

Most plasticity problems are rather complex, it is only possible to obtain exact solutions for a few practical problems. Approximate techniques are thus sought.

In 1909, Haar and von Karman [4] stipulated a variational principle as the basis of the theory of plasticity. The Haar-Karman principle is an extension of the principle of least work to elastic plastic bodies. Accordingly, the principle is not suitable for a generic elastic-plastic body but only for the bodies with special stress strain relation, e.g. Hencky relation. Finzi [4] extended Haar and von Karman's principle to problems of plasticity. He pointed out that his formulation was valid for completely statically determinate problems regardless of stress strain relation and yield criterion.

After reviewing the classical equation of Levy-Mises and Prandtl-Reuss for an ideally plastic material, Hill [8] showed that the Levy-Mises relation corresponds to maximum platic work in a prescribed strain increment subject to the Huber-Mises yield criterion. This relation can be shown to correspond to the stationary work principle, by using Reuss' geometrical representation of stress and strain increment, and the Huber-Mises circle. Hill then established a maximum principle for an element in free flow obeying (a) the Huber-Mises yield criterion , i.e. $\sigma'_{ij}\sigma'_{ij}=2k^2$, and (b) Levy-Mises relations, i.e. $d\varepsilon_{ij}=\sigma'_{ij}d\lambda$.

By considering a plastic mass in quasi-state equilibrium under a stress system σ_{ij} and supposing the mass had a flow velocity u_i on its boundary surface, Hill showed that the

general principle of variational displacement could be expressed as follows :

$$\int (\bar{\sigma}_{ij} - \sigma_{ij}) u_i \eta_j dS = -(1/2)\int \lambda (\bar{\sigma}'_{ij} - \sigma'_{ij})(\bar{\sigma}'_{ij} - \sigma'_{ij}) dV \geq 0 \qquad \text{(A2.25)}$$

where $\bar{\sigma}_{ij}$ is a corresponding equilibrium stress system to produce a flow velocity u_i.

η_j is a directional consine of the outward normal.

The consideration of uniqueness leads equation (A2.25) equal to zero.

Through the supposition of the two sets of quantities σ_{ij} and u_j which are related by :

$$(1/2)(\partial u_i/\partial x_j + \partial u_j/\partial x_i) - \alpha \sigma'_{ij} + \beta \sigma_m \delta_{ij} \qquad \text{(A2.26)}$$

where α, β may be variable but are positive, and

$\sigma_m = \sigma_{ij}/3$,

σ_{ij} satisfies the equations of equilibrium $\partial \sigma_{ij}/\partial x_j = 0$.

Hill demonstrated [8] that the two variational principles : the maximum work principle and the energy theorem in elasticity are a special case of the same, more general theorem.

In applying equation (A2.26), the velocities over the whole or part of the surfaces are usually prescribed. The principle was also used by Hill [8] in determining the stress distribution in a prismatic uniform cross-section, plastically deformed by certain forces and couples applied to the end. It was found that it produces identical results with other methods.

Hill's derivation is also applicable to work hardening materials under the condition that the elastic strain increments are neglected. The application of the principle to work hardening materials requires that $\bar{\sigma}'_{ij}\bar{\sigma}'_{ij}$ are not constant to the given values of $\sigma'_{ij}\sigma'_{ij}$ at each point at the moment under consideration.

Hodge and Prager [15] modified the differential stress-strain relations of Handelman et al [6] by including function $f(J_2,J_3^2)$ of a material. The modified general relation is expressed as follows.

$$d\varepsilon_{ij}=(1+\nu)d\,\sigma'_{ij}+(1-2\nu)d\,\sigma_m\delta_{ij}+(1/2)[P\,\sigma'_{ij}+QJ_3t_{ij}][df+|df|] \qquad (A2.27)$$

where P, Q, f are functions of J_2 and J_3,

$$t_{ij}=\sigma'_{ik}\,\sigma'_{kj}-(2/3)J_2\delta_{ij}$$

δ_{ij} is the Kronecker delta

Equation (A2.27) is valid for the conditions of both loading, i.e. $df\geq 0$, and unloading, i.e. $df\leq 0$. This is a relation of the flow type.

From the basis of equation (A2.27) and the theorems of integration, reciprocity, and the principle of virtual displacements, Hodge and Prager [15] established a minimum principle for plastic materials with strain hardening for all cases :

$$\int \dot{\sigma}_{ij}\,\dot{\varepsilon}_{ij}\,dV\leq \int_V \dot{\sigma}'_{ij}\dot{\varepsilon}'_{ij}\,dV+\int_{V_{12}} F\dot{f}\dot{f}'dV-\int_{V_{21}} F\dot{f}\dot{f}'dV \qquad (A2.28)$$

in which the dot on each variable indicates the change of

rate, and $\dot{\sigma}'_{ij}$ and $\dot{\varepsilon}'_{ij}$ denote the artificial stress and strain rate. F is a positive function of $\partial f/\partial\sigma_{ij}$, V_{12} and V_{21} are the parts of a body V.

Hodge and Prager's [15] procedure to derive the minimum (upper bound) principle can also be used for the mixed boundary problem, where the stresses are given throughout the interior of the body, the stress rates on a part of the surface, S_β, and the velocities (u_i) on the remainder of the surface, S_A, are known. Under the above system if

$$\bar{\Psi} = (1/2)\int_V \dot{\sigma}_{ij}\,\dot{\varepsilon}_{ij}\,dV - \int_{S_A} \dot{T}_i u_i\,dS_A \qquad \text{(A2.29)}$$

where $\dot{T}_i$ is traction rate on S_A,

It can be shown that $\bar{\Psi}$ is less for the actual stress rates than for any system of artificial stress rates.

Hill [12] examined the factors governing the distortion of stress in a plastic rigid body at the yield point. He drew particular attention to some of the properties which are intimately related to certain extremum theorems for a plastic-rigid body, namely, the principle of maximum plastic work and its complementary minimum principle. The principles refer to the rate of working of forces on the surface of a plastic zone, at all points at which deformation is occurring. Since any equilibrium system of the forces acting on a rigid zone does no work, Hill identified that the extremum principles applied also to the work of the forces on a body which was only partly plastic. He was also able to show that the extremum theorems provide a means of obtaining approximations, to the actual rate of work, and also to the yield points themselves.

The development and advance of the application of variational principle in plasticity have continued throughout the last few decades. A complete study in the principles is given by Washizu [31]. A comprehensive application of the techniques to metal forming has also been made by Avitzur [1].

A2.1.9. Application of plasticity theory to metal forming

The practical application of plasticity theory to a number of deformation processes are generalised in texts by Ford and Alexander [5], Hill [9], Mendelson [21] etc..

Realising, at the time, that the analyses of metal forming processes were generally based on an over-simplification of the deformation pattern, Hill [13] in 1963 proposed a rigorous method of analysis for these working processes (after a series of studies in heterogeneous compression, bar drawing and forging). Hill claimed that his method was applicable to any plastic material and could accommodate all conditions of friction, tool geometry, and kinematics. His method can be generalised as follows :

(1) It begins by choosing a class of velocity fields from which the best approximation will eventually be taken
- the chosen velocity fields must satisfy all kinematic conditions.

(2) The associated stress is either determined using the material constitutive law, or to within a certain value of the hydrostatic pressure if the material is incompressible
- Generally the associated distribution of stress in the deformation zone of a chosen velocity field will not satisfy all the statical requirements.

(3) In selecting the considered class of velocity fields which most nearly satisfies the statical requirements, the converse of the virtual work rate principle for a continuum demands that a sufficient sub-class of virtual orthorgonalising motion W_j satisfies the following equation

$$\int \sigma_{ij}(\partial w_j/\partial x_i)dV = \int \tau_j w_j dS_I - \pi\int n_j w_j dS_F + \int [(n_i\tau_i)n_j + mKL_j]w_j dS_c$$

(A2.30)

where S_c is the surface adjoining a tool or container, S_F is the unconstrained surface, S_I is the junction with the rigid zone, τ_j denotes the surface traction computed from the considered approximation fields σ_{ij}, π is a uniform fluid pressure on the surface S_F (if there is any), mK is a constant frictional stress over surface S_C, K is the shear yield stress of deforming body, n_j is the local unit outward normal, and L_j is a unit tangent vector opposed in sense to the relative velocity of slip in the approximation field.

(4) The orthogonalising family W_j to be selected must be sufficiently wide and should be just extensive enough to select a simple approximating velocity field from the particular class constructed to satisfy the kinematic conditions

- If the class were defined by equations involving an unknown function of just one position variable, then W_j must also involve an arbitrary function of one variable.

(5) Applying the calculus of variational technique to equation

(A2.30), treating W_j as a variable, once the family is chosen.

(6) From (5) a system of equilibrium equations and boundary conditions, suited to the particular approximating class and uniquely determining its best member, are obtained.

Lahoti and Kobayashi [18] applied Hill's method to analyse the ring compression with barrelling, spread in Steckel rolling, and thickness change in tube sinking. They compared the results with other existing theories and with experiments. The comparison indicated that the Hill's method was valid and yielded improvement in values calculable by other methods. They subsequently concluded that the method would play an important role in the applications to the problems of metal forming.

APPENDIX 3.1

PART DETAIL DESCRIPTIONS AND ITEM DRAWINGS OF THE MODEL BENDER UNIT

The model bender description is presented in order of the operational function of each composite item.

A3.1. Part components for the hydraulic power line of the side and pinch roll

A3.1.1. The connecting blocks (Item drawing No.13 and 22)

The connecting blocks were made from Sanderson Kayser KE805 steel. They were machined to the dimensions specified in the drawings 13 and 22 respectively, and heat-treated to achieve Rockwell Hardness number C41-46.

A3.1.1.1. Connecting block for the bottom pinch roll (Item drawing No.13)

The connecting block was a square column block of 220 mm long x 185 mm high x 120 mm wide. The ISO threads (M80x2-6H) x 90 mm deep hole located the loadcell. The hole of 2.375 in dia (with 2-$11^1/2$ NPT threads) x 18 mm deep located the Enerpac hydraulic cylinder (EHC) adaptor No.A28, which attached the EHC No.R256 to the connecting block. The rectangular tongue 20 mm deep x 50 mm wide x 180 mm high at either end of the block slides along the middle slots of the end supporting plates (item 1). It thus gave lateral rigidity to the bottom pinch roll to counter the side thrust produced during the bending operation.

A3.1.1.2. Connecting block for the side roll (Item drawing No.22)

This was a circular block 100 mm dia x 180 mm height with a ISO M80x2-6H thread x 100 mm deep hole for screwing into the upper face of the loadcell (Item 29). At the lower face there was a 1.656 in dia (with $1^1/4$-$11^1/2$ NPT threads) x 180 mm deep

hole for attaching the fixing EHC adaptor No.13, which connects to the EHC No.RC1010. The circular block in a bronze bush bearing (item 32) facilitated axial movement and was securely fixed in the top clamping block (Item 20) of the side rolls.

A3.1.2. Loadcells for the bottom pinch and side rolls (Item drawing No.29)

The loadcells were made of Sanderson Kayser KE805 steel. They were machined to the dimensions specified in drawing item 29 and heat treated to Rockwell hardness No.C49-53.

Each loadcell consists of :

(a) a M80x2-6g thread x 40 mm long section at the top which was screwed to the bearing housing (item 12 for the bottom pinch roll, or item 19 for the side roll).

(b) strain gauge bridges for sensing the bending and axial loads were bonded to the central ground section of 58 mm dia x 80 mm long.

(c) a M80x2-6g thread x 100 mm long section at the bottom, which was attached to the connecting block (Item 13 for the bottom pinch roll, or Item 22 for the side roll).

Owing to the necessity to maintain the rigidity of the model, the loadcells were designed to produce an allowable bending deflection of 0.85 mm and 0.767 mm for the respective bottom and side roll (see section 4.2). Subsequently, the estimated strains were considerably less than the normally accepted strain of 0.1 %.

A3.1.3. Bearing housings (Item drawing No.12 and 22)

These were also made of Sanderson Keyser KE805 steel and heat treated to Rockwell hardness No.C41-46.

A3.1.3.1. Bearing housing for side roll (Item drawing No.22)

The detail of the design is shown in drawing item 22. It can be seen that there is an open section 28.34 mm long, which will free the tilting blockage of the roller in the bearing housing bore. Adjacent to it is a bearing shoulder neck of diameter 65 mm x 10 mm long. The bore section, of diameter 71.4 mm x 33.32 mm long, accommodates a Torrington spherical bearing No.17SF28. The bearing was secured by a raceway locking ring (item 28), having successive sections of 76 mm dia x 3 mm long and an ISO M80x2-6g thread x 10 mm long respectively.

The rear part of the housing bore, of length 25.34 mm had a radius of 44 mm at the upper half and a radius of 46 mm at the lower half. This also allowed tilting of the roller ends.

The holes of ISO M80x2-6H thread x 40 mm deep at the bottom of the housing accommodates the top of the loadcell (item22). The 7 mm deep steps, on either side of the upper part of the side walls with chamfers at either side of the top of the housing provides movement within the bottom pinch roll bearing housing.

A3.1.3.2. Bearing housing for bottom pinch roll (Item drawing No.12)

The detail of the design is as shown in drawing item 123. As for the side rolls, the open section of length 25.95 mm at the front of the bearing housing bore prevents tilting of the bottom roll. Adjacent is the bearing housing bore which has a shoulder neck section of 73 mm dia x 10 mm long. The bore

section of dia 80.91 mm x length 38.10 mm accommodates the Torrington spherical bearing No.20SF32. There is also a section of dia 80.91 mm x length 3 mm and a section threaded ISO M95x2-6H x length 10 mm respectively for the bearing locking ring (item 16). The partial bore of radius 54 mm at the rear prevents any interference when tilting the bottom pinch roll.

A hole, threaded ISO M80x2-6H x length 40 mm, at the bottom of the housing accepts the top section of the load cell (item 29).

A3.1.4. End supporting plates (Item drawing No.1)

Rigidity is the prime design requirement of the end supporting plates. It was envisaged that a sandwich structure for the plates would meet this requirement and the final design for the end supporting plates is shown in drawing item 1.

The peripheral shape of the plates were cut from a mild steel plate of 10 mm thick x 1060 mm high x 1700 mm wide. The chamfer at the top corner of each side plate facilitated adjustments of the units sandwiched between the plates.

The two clearance holes of dia 36 mm in the two outer plates and of dia 42 mm in the two inner plates, provided access to the holding pins for the top roll loadcells (item 8). The two M12 threaded holes below these two clearance holes enabled the top loadcells to be securely located. The 525 mm square section x 121 mm thickness, provided access to the drives and movement of the bottom and side rolls. The vertical slot 50 mm wide x 317 mm long along the centre line of the plates located the bottom pinch connecting block (item 13), allowing vertical movement within the slot. The two M16 holes along the central line located the holding blocks (item 15) of

the bottom roll hydraulic cylinder to the top of the base blocks (item 14). The arcuate slots of inner radius 371 mm and outer radius 421 mm with respect to the centre (which was the centre of the top roll) 10 mm above the top edge and in the central line of the plate, located the top clamping blocks (item 20) of the side roll. The arcuate slots of inner radius 950 mm and outer radius 1000 mm located the bottom clamping blocks of the side roll (item 24). There were twelve M12 holes along the edges of the plate which fastened the holding strips (item 4) and the cross holding strip (item 5) to the end supporting plates. The eight screwed holes along the base line were for attaching the end supporting plates to the bottom holding plates (item 7).

A3.1.5. Hydraulic cylinder base-blocks for the side roll (Item drawing No.23)

These were made from Sanderson Kayser KE805 steel. The finishing blocks were heat treated to Rockwell hardness No.C41-46.

The circular bore, of dia 57 mm x 60 mm deep, in the 77 mm square lug x 70 mm thick at the top of the block, located the EHC No.RC1010 unit. On one side of each base block was a screwed split yoke which retained the EHC no.RC1010. The hole of diameter 22 mm in the plate allowed access for connecting the hose to the hydraulic hand pump. The semi-disc lug of dia 120 mm gave support to the bottom clamping block (item 24) of the side roll and direction adjustment. The side roll the hole of dia 45 mm provided access for the locking rod (item 25). It also acted as the centre for the positional adjustment of the side roll.

A3.1.6. Bottom clamping blocks for the side roll hydraulic cylinder (Item drawing No.24)

The blocks were made from mild steel and the design detail is shown in drawing item 24. The hollow triangular section of height 60 mm x base 120 mm, sustained the down thrust of the side roll by supporting the disc lug of the hydraulic base block (item 23).

The arcuate ends of the length 9 mm; inner radius 950 mm and outer radius 1000 mm transferred the downward thrust of the side roll to the end supporting plate (item 1). The block was fixed in the corresponding slot on the end supporting plate, and securely clamped the framework by the locking rod (item 25), through the hole of dia. 30 mm in the block and the locking plates (item 26) at either end. The four threaded holes for GKN M16 cap-screws reinforced the clamping effect of the end supporting plate onto the framework.

A3.1.7 Top clamping block of side roll hydraulic cylinder (Item drawing No.20)

The block was made from Sanderson Kayer KE805 steel and heat treated to Rockwell hardness No.C41-46. It absorbed the bending force on the side roll.

Each block contained :

(a) A retaining base, 75 mm deep x 160 mm wide x 240 mm long, with a hole of diameter 105 mm which located the hollow cylindrical column.

(b) A threaded hole ISO M33x2-6g of length 60 mm on each end face, through which screws clamped the block onto the end supporting plate of the framework together with the top clamping position blocks (item 21) of the side roll.

(c) A hollow cylindrical column, of outside diameter 140 mm x length 225 mm, with a neck shoulder of diameter 102.5 mm x

length 3 mm, retained the bronze bush (item 32) in at the top. The internal bore of diameter 105 mm located the bronze bush (item 32), which controlled the movement of the attached connecting block (item 22). At the bottom of the central surface, there was an ISO M140x2-6g threaded section for screwing the bronze bush retaining ring (item 30). The column was welded to the retaining block as stated in (a). The length 60 mm of the column (discussed in (b)), above the retaining block reinforced the bending rigidity of the connecting block (item 22). It also optimized the maximum movement of the side rolls. The square-end faces facilitated the setting up of the positional angle of the side roll.

A3.1.8. Torrington 17SF28 bearing locking rings (Item drawing No.27)

These were made from mild steel and locked the outer raceway of the 17SF28 bearing in the bearing housing (item 19). The rings were designed to allow sufficient space in the housing for the tilting of the end of the side roll. The shoulder neck, outside diameter 76 mm by length 4 mm, contacted the end of the bearing raceway. The ISO M80x2-6g threaded section of 11 mm long screwed into the bearing housing (item 19). The 10 mm wide slot at the rear allowed the bearing to be tightened in the housing.

A3.1.9. Locking ring for the free end of the side roll (Item drawing No.28)

The rings which were positioned on the inner raceway of the spherical bearing were machined from mild steel rods, and are shown in the item drawing 28. The hole in the cap located the free end of the side roll. The 20 mm outside diameter of the reduced neck was designed to provide sufficient space for tilting the end of the roller in the housing (item 19). The hole on the back of the cap provided access for the M8 GKN cap

screw to the free end of the roll.

The purpose of the locking ring was to eliminate the side thrust of the side roll as it is tilted, and subsequently to ensure the alignment of the effective length of the rollers.

A3.1.10. Locking rings for the driven end of the side roll (Item drawing No.31)

The rings which were positioned on the inner raceway of the spherical bearing, were also made from mild steel.

Referring to item drawing 31, the 60 mm diameter shoulder in the end face tightened the ring against the inner raceway of the Torrington 17SF28 bearing. Its outside diameter gave minimum interference to the tilting movement of the side roll. The 1.75 in diameter by 20 mm deep bore at the front locked the sliding bearing. The 50 mm outside diameter by 15.11 mm long section also allowed free movement of the roll. The 15 mm deep M39x2-6H threaded section enabled the locking ring to be screwed onto the corresponding section on the side roll as it passed through the ring.

A3.1.11. Locking rods for the bottom clamping block (side roll hydraulic cylinder) (Item drawing No.25)

The rods were made of Kayser KE805 steel and heat treated to Rockwell hardness No.C41-46.

Each rod passed through the bottom clamping block (item 24) and the hydraulic cylinder base block (item 23). It thus clamped the two blocks onto the end-supporting plates by the action of locking plates (item 26) and nuts. Each rod had an outer diameter of 30 mm and length 392 mm. At either end of the rod, there was a 68 mm long section threaded with ISO M30

threads to clamp and locate the bottom clamping block (item 24) onto the bending unit framework.

A3.1.12. Locking plates for the top clamping block of the side roll (Item drawing No. 21 and 33)

Items 21 and 33 were machined from 100 mm wide x 160 mm long x 22 mm thick mild steel plates. On one side of the plate the 15 mm high annular sector of inner radius 371 mm and outer radius 421 mm, located the plates in the corresponding arcuate slots in the end supporting plates (item 1). It thus gave the required rigidity in clamping the top block of the side roll (item 20). The 33 mm diameter hole in the middle of each plate provided access to the clamping block (item 20). The two M16 threaded holes, 40 mm from either side of the 33 mm hole, located pressure screws to reinforce the clamping effect of the top clamping block (item 20), and so produced the necessary rigidity for the side roll.

A3.1.13. Bush locking ring (item drawing No.30)

Drawing item 30 shows the ISO M40x2 threaded x 15 mm long bore for screwing the mild steel ring to the top clamping block of the side roll (item 20). The 102.5 mm diameter bore gave access to the connecting block (item 22). The head shoulder at the bottom held the bronze bush (item 33) in the top clamping block. The overall dimensions were as follows :

(1) outer diameter 150 mm,

(2) the depth 20 mm.

A3.1.14. Base block for the bottom roll of the hydraulic cylinder (Item drawing No.14)

The details of the mild steel block is shown in the drawing item No.14. It was 86 mm wide x 140 mm high x 86 mm thick, with a recess of 20mm deep x 12mm wide on either side face.

The recess provided the clamping action for the hydraulic cylinder retaining block of the bottom roll (item 15).

A3.1.15. Retaining block for the bottom roll hydraulic cylinder (Item drawing No.15)

The mild steel block had overall dimensions 70 mm wide x 87 mm long x 70 mm high. The recess arcuate section of radius 43 mm x 55 mm thick clamped the bottom of the EHC.No.526 to the top of the base block (item 14). The two threaded M6 holes located the cap screws which attached the block onto the corresponding hole in the end supporting plates (item 1).

A3.1.16. Locking ring for the pinch roll (Item drawing No.16)

The basic design was similar to that of the locking ring for the free end of the side roll (item 28).

The ring was cap screwed at the end of the bottom pinch roll and located the spherical bearing which prevented any side movement of the roll.

A3.1.17. Torrington 20SF32 bearing housing locking ring (Item drawing No.17)

The ring locked the outer raceway of the 20SF32 bearing in its housing (item 12) and so eliminated any possible movement of the bearing and gave sufficient space for the tilting of the end of the roll. Its dimensions are shown in drawing item 17. The four equally spaced M5 holes on the ring provide access for the adjustment and tightening tool.

A3.2. The framework of the bending unit

A3.2.1. Bottom plates for the framework (Item drawing

No.7)

In order to allow the end supporting plates (item 1) to be properly screwed onto the edges of the mild steel plate, all edges around each bottom plate were machined. Along the longer edges the sixteen threaded holes for the cap screws attached the end supporting plates.

A3.2.2. Cross holding stiffeners (Item drawing No.5)

The mild steel stiffeners supported the two pairs of end supporting plates (item 1). Each stiffener was 150 mm wide x 187.5 mm long x 10 mm thick. Welded to each end of the stiffeners were additional stiffeners 50 mm high x 150 mm thick. These stiffeners were welded square to one another. The M16 holes on the additional stiffener fastened the two pairs of end plates together.

Attention was paid to ensure the squareness of the finished channel section.

A3.2.3. Bridge stiffeners for end supporting plates (Item drawing No.4)

The design was similar to item 5 except that the bride stiffener was 240 mm long x 50 mm wide x 10 mm thick, with the leg piece being 50 mm high x 10 mm wide x 10 mm thick. Each pair of end supporting plates were fastened by one M16 hole on each leg piece.

The stiffening plates together with the base plates of item 7 were used to secure each pair of end supporting plates. It thus formed a sandwich unit within which the relevant components of the powering unit of the bottom and side roll were located.

A3.2.4. Locking pins for the loadcells of the top roll (Item drawing No.8)

The pins were made from Sanderson Kayser KE805 steel and heat treated to a Rockwell hardness No.C41-46. They locked the top loadcells (item 3) between each pair of end plates forming the sandwich unit (see fig 3.5). The overall length of each pin was 405 mm. There are two sections along each pin : one was a 273 mm long section of 36 mm diameter with its end section 72 mm long being threaded with a ISO M36x2 thread. The other section 130 mm long with an end section 81 mm long was threaded with a ISO M42x2 thread.

The reduction from diameter 42 mm to diameter 36 mm, on each pin, was added to apply full pressure on the loadcell (item) towards the outer end supporting plate when clamped within the rigid sandwich unit.

In assembling the loadcell and the pin, the 36 mm diameter screwed end was tightened first.

A3.2.5. Clamping plates for the top loadcells (Item drawing No.9)

The mild steel clamping plates were used as washes for the locking pin (item 8). The threaded hole on each plate accommodated a M12 cap screw to reinforce the rigidity of the top load cell location. The plate with the 36 mm diameter hole was used for clamping on the outer end supporting plate, whilst that with the 42 mm diameter hole clamped the inner end supporting plate of each sandwich unit.

A3.2.6. Loadcells for the top roll (Item drawing No.3)

The load cells were made from Sanderson Kayser KE805 steel and heat treated to a Rockwell hardness No.C49-53. They were

primarily used as sensing components to detect the axial and bending forces experienced by the top roll during bending of the plate. They also contributed to the framework of the bender.

To achieve the required rigidity for the loadcells a strain lower than the accepted strain of 0.1 % was utilised in the design calculations. The design parameters are as described in Chapter four.

The upper section, 195 mm wide x 96 mm high x 40 mm thick, had a central through hole of diameter 32 mm to accommodate the slots at either end of the bottom face of the top beam (item 2). This hole also enabled the load cell to be screwed into the top beam.

The strain gauge bridges were bonded to the central ground section, 185 mm wide x 60 mm high x 30 mm thick, of the cell.

The lower loadcell section, 240 mm wide x 96 mm high x 70 mm thick, was secured by the sandwich unit (see fig 3.5) formed by the two end supporting plates (item 1). The stepped hole, of dia. 42 mm x 43 mm long, in the right hand section enabled the locking pin (item 8) to locate the loadcell onto the outer end supporting plate. This effect combined with the bolt pressure at either end of the pin (item 8) secured the loadcell in the sandwich unit. The 43 mm long central hole with M12 threads at each end complete with cap screws and washers further ensured the complete rigidity of the load cell within the framework.

The middle and upper waisted section at the right hand side of the cells, allowed the widest plate (i.e. 305 mm) to be conveyed through the bender.

A3.2.7. The top cross beams (Item drawing No.2)

Each mild steel beam had overall dimensions of 110 mm deep x 194 mm wide x 780 mm long. At a position 20 mm from each end of the bottom beam, there was a slot, 96 mm deep x 194 mm wide x 40 mm thick, which accommodated the upper section of the top loadcell (item 3). A 105 mm deep M32 hole was drilled in the position shown. This enabled the top loadcells to be screwed securely to the slots in the top beams.

At the centre of the bottom face, there was an arcuate recess, of radius 50 mm, over the whole width from the beam. This located the bearing housing of the top roll (item 6) with the centre line 10 mm away from the bottom face. Another arcuate recess of radius 75 mm x 15 mm deep had the same centre. There were three 25mm long M15 tapped holes at a pcd of 62.5 mm on the face of this latter recess. The latter recess was mainly for locating the flanges of the top roll bearing housing (item 6). The screw holes allowed the detachment of the top roll bearing housing from the beam. It therefore facilitated the removal of the top roll in order to release the bent workpiece if required.

Under operational conditions the top cross beams had a maximum deflection of 0.32 mm at its full load of 250 kN.

A3.2.8. Bearing housings of the top roll (Item drawing No.6)

The mild steel housings were located in the recesses provided on the lower face of the top beam. This provided a convenient attachment to the beam, and thus facilitated the release of the bent workpiece from the top roll. For this reason, they were designed as shown in drawing item 6.

Referring to the item drawing, it can be seen that each 15 mm thick sectorial flange of outside radius 75 mm and inner

radius 50 mm, with three M15 holes on pcd=62.5 mm at either end of the housing, was mounted onto the top beam. The outer diameter of the bearing was selected to clear the bottom and side roll bearing housings, as shown in the drawing.

The front section of the housing bore had a diameter 2.999 in x 1.947 in for housing the Torrington bearing no.HJ364828. The bearing was held in position by a shoulder neck of diameter 2.688 in x 3 mm wide, and by a circlip groove of dia 3.097 in x 0.104 in as shown. Beyond this shoulder neck, there was another shoulder neck of 2.25 in diameter x 4 mm wide for insertion of the four Torrington bearings No.HJ303920 in the remaining bore, i.e. section of diameter 2.436 in x 186 mm long. The four HJ303920 bearings were then locked in position by a circlip in a groove of diameter 2.594 in x 0.085 in at 19.391 in from the rear face of the bore of diameter 2.436 in (or 183.45 mm from the front of the through bore).

The inner faces of the two flanges were accurately machined to produce a sliding fit in the top beam (item 2).

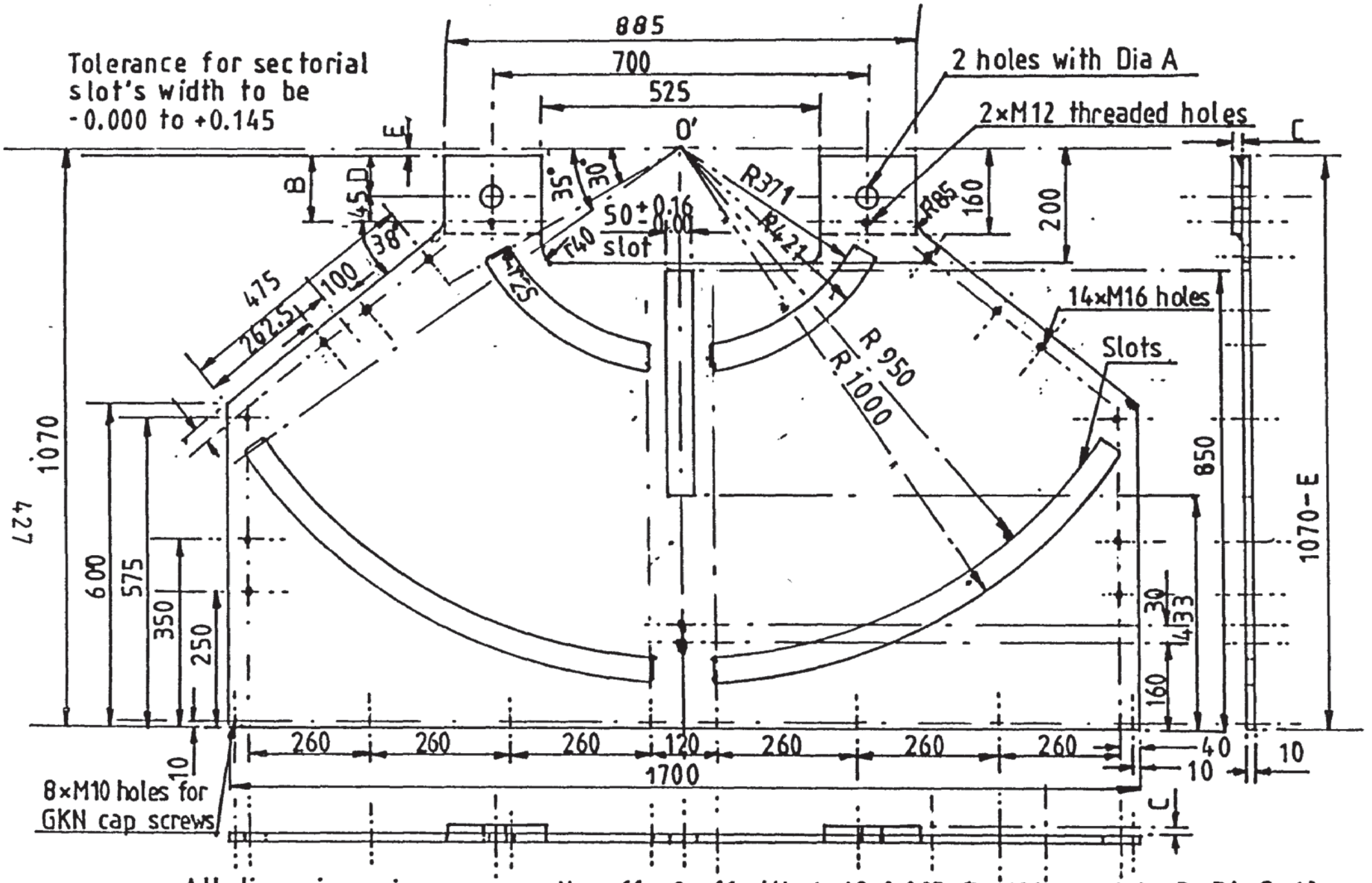

All dimensions in mm
Material : Steel plates
Scale : 1 to 10

No off : 2 off with A=42+0.025 B=121 C=0.0 D=76 E=10
2 off with A=36+0.025 B=81 C=30 D=36 E=50

ITEM DRAWING NO 1 SUPPORTING PLATES

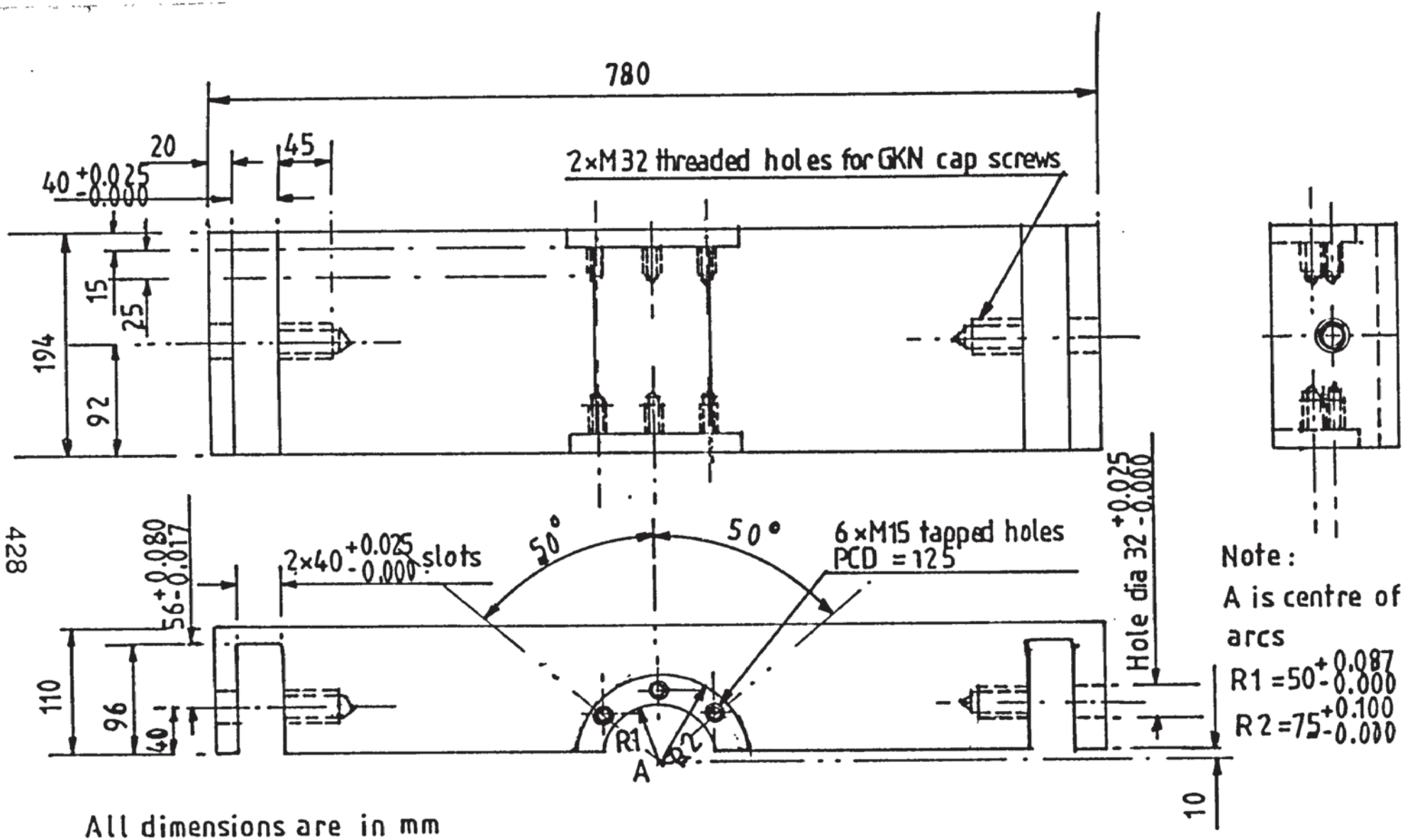

All dimensions are in mm

Material : M/S

Scale : 1 to 5

No off: 2

ITEM DRAWING NO 2 TOP CROSS BEAM

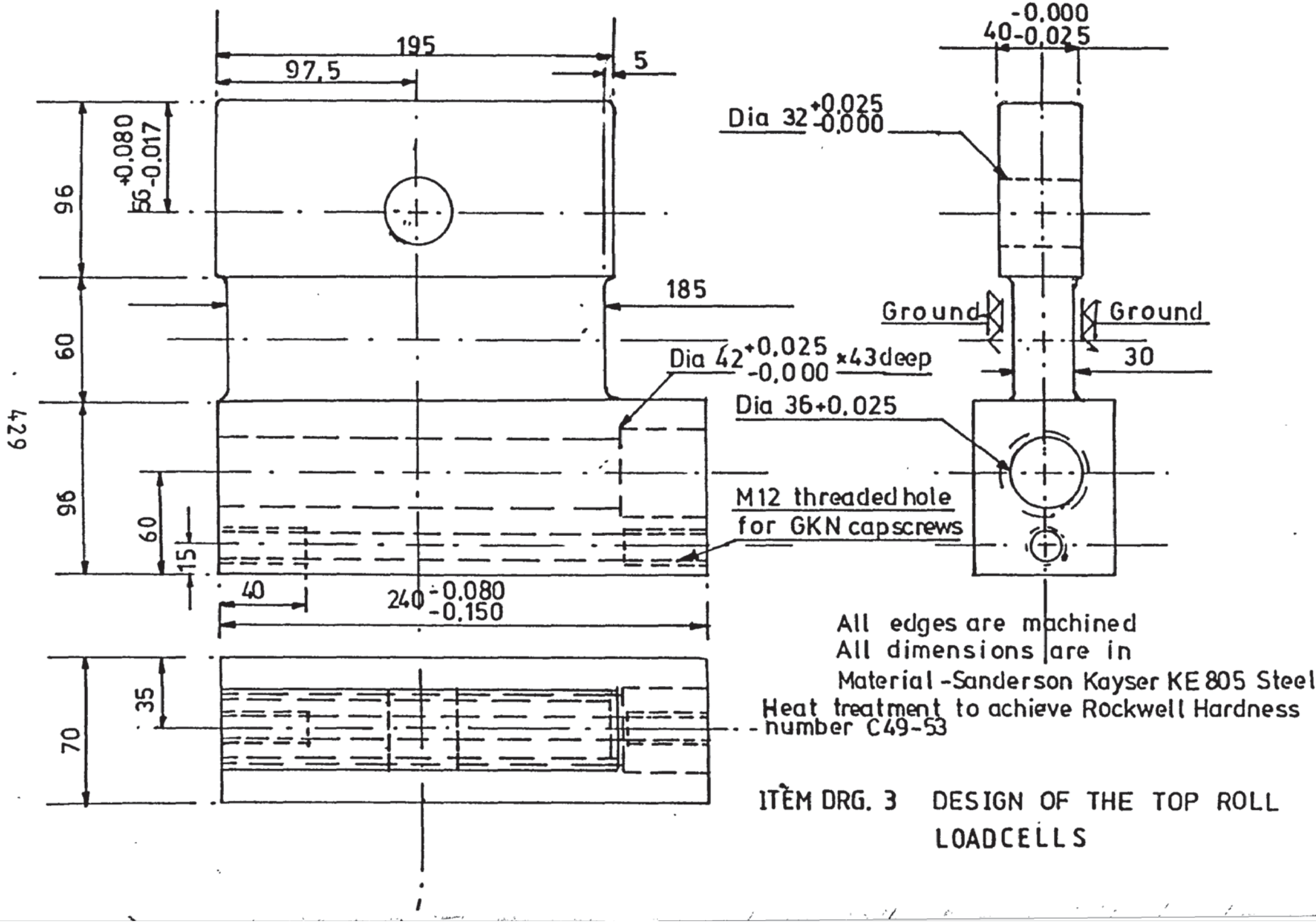

ITEM DRG. 3 DESIGN OF THE TOP ROLL LOADCELLS

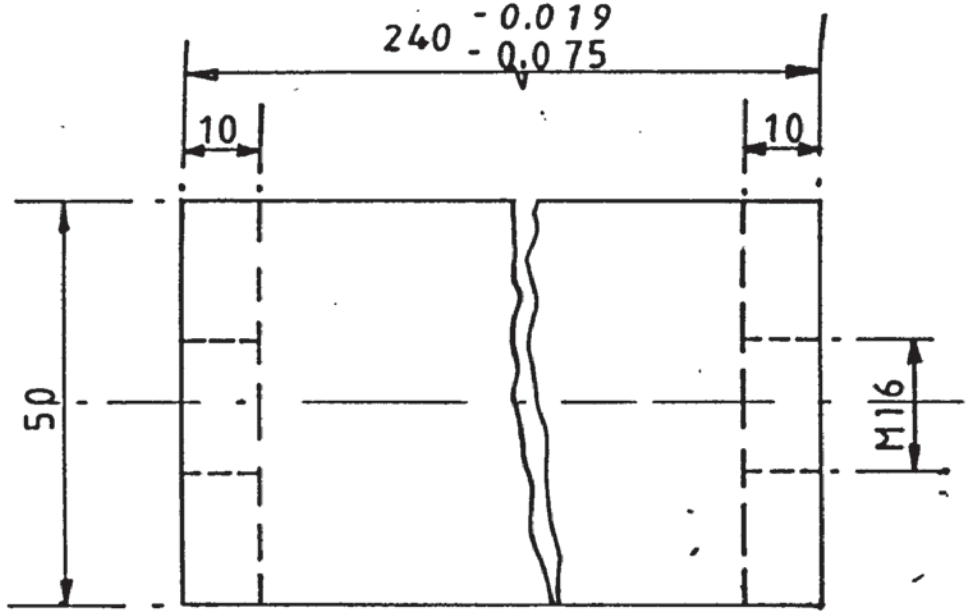

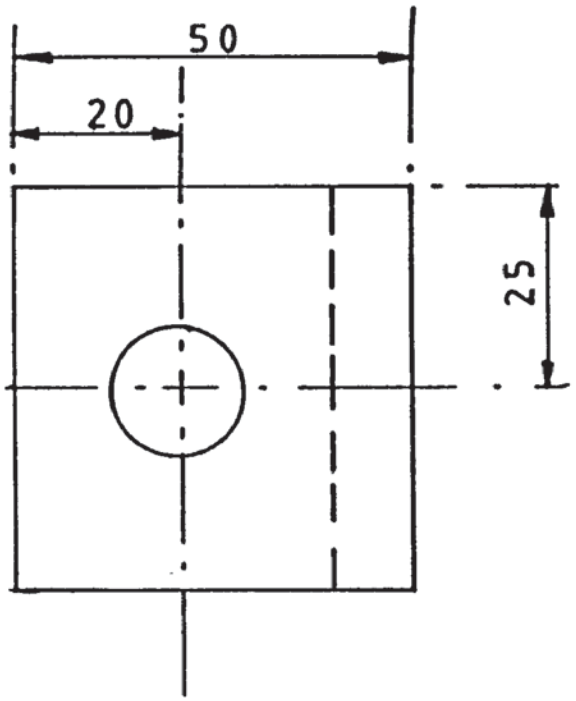

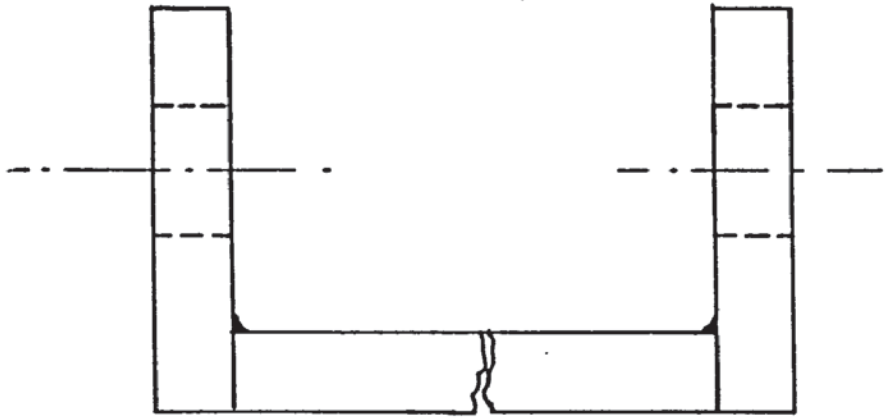

All dimensions are in mm

Material ;Steel strips

No off : 8

Scale : Full

ITEM DRAWING NO 4 HOLDING STRIPS FOR THE END SUPPORTING PLATES

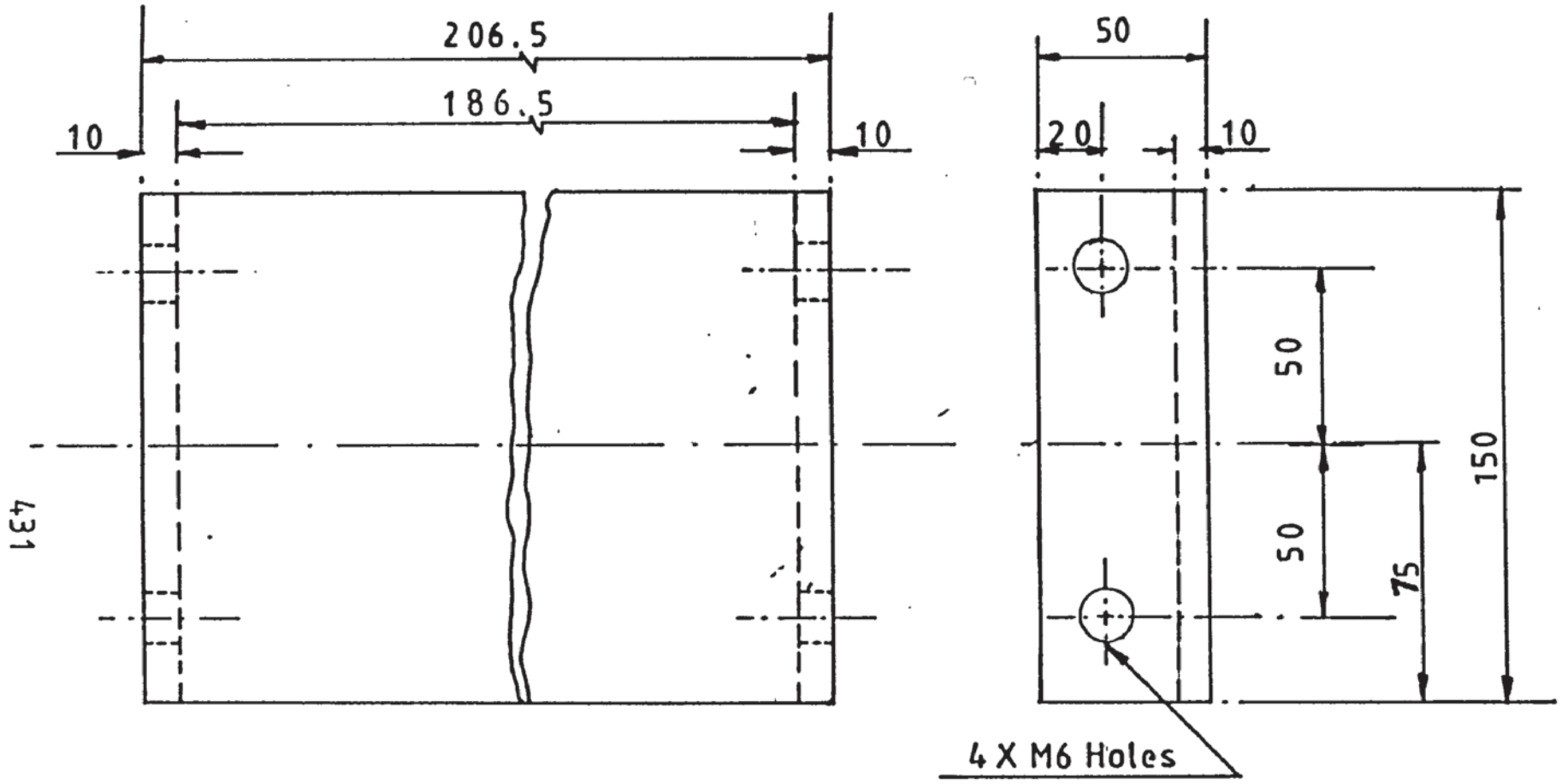

All dimensions are in mm

Material: M/S

No off: 8

DRAWING FOR ITEM NO 5

CROSS HOLDING STRIPS

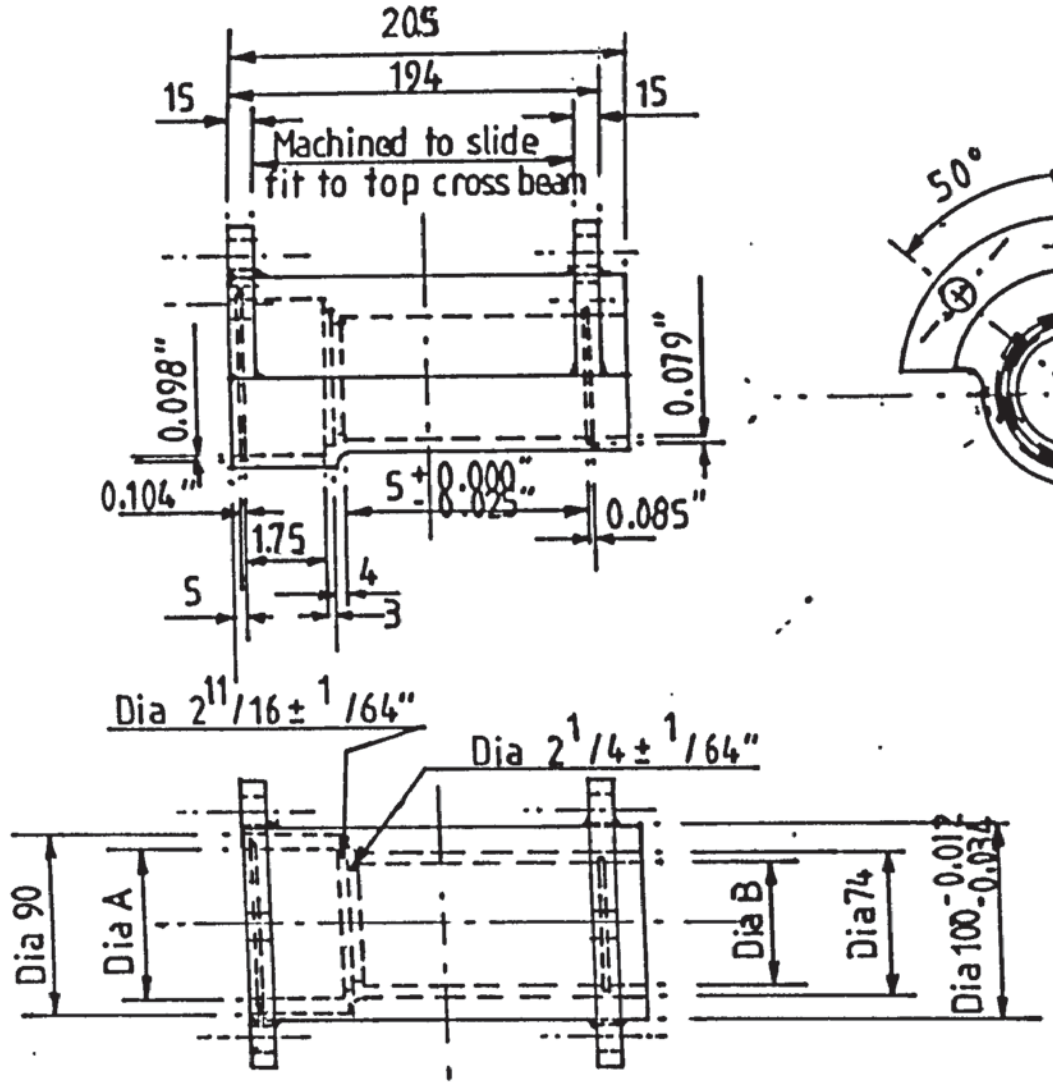

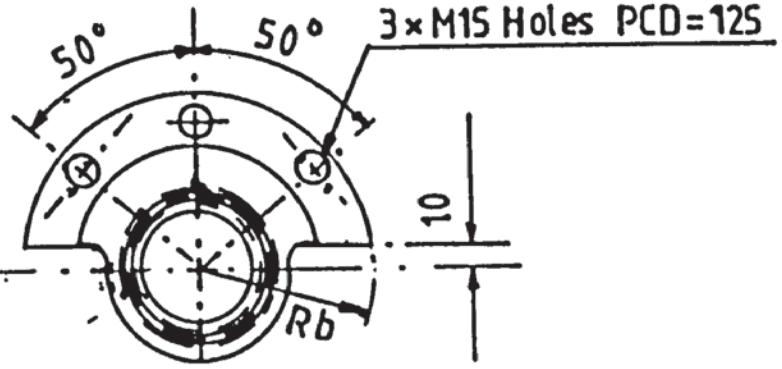

$Rb = R75^{-0.0075}_{-0.0220}$

$A = 2.9985^{+0.0011"}_{-0.0000"}$

$B = 2.436^{+0.0012"}_{-0.0000"}$

All dimensions are in mm unless specified

Material : M/S

No off: 2

Scale: 1 to 4

ITEM DRAWING NO 6 BEARING HOUSING OF THE TOP ROLL

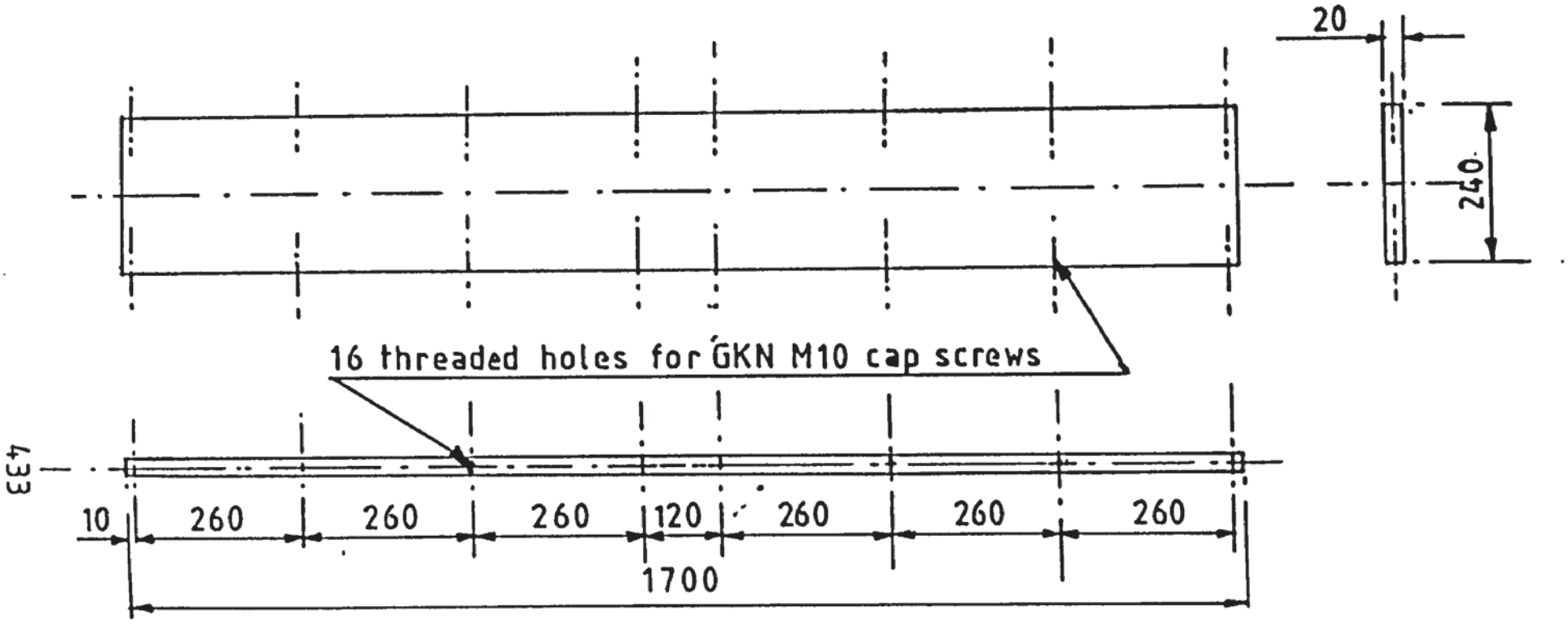

All dimensions are in mm
All edges are machined
Material : M/S bright drawn
No off : 2

ITEM DRAWING NO 7 BOTTOM HOLDING PLATES FOR THE BENDING UNIT

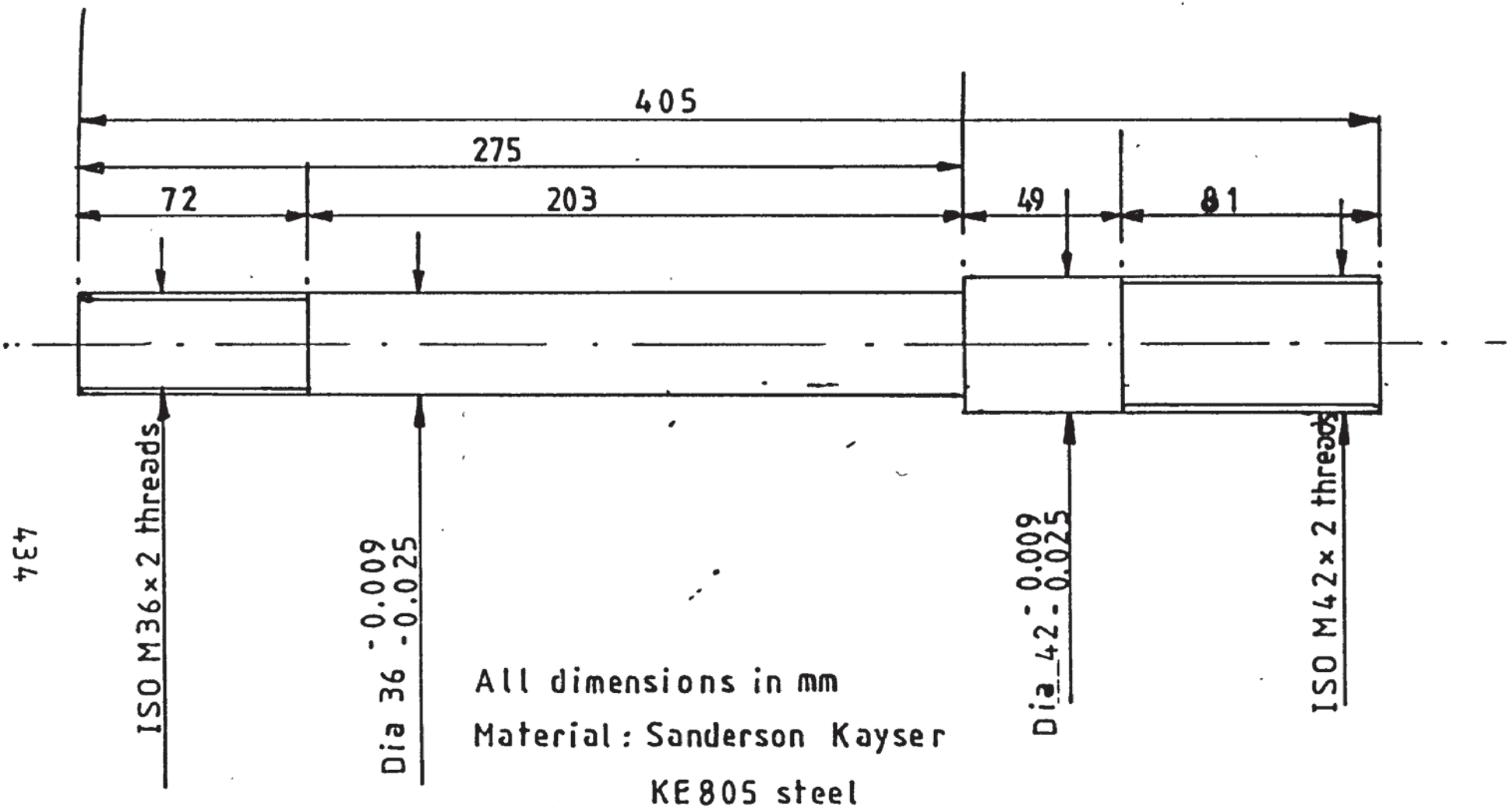

All dimensions in mm

Material : Sanderson Kayser
KE805 steel

No off : 4

Scale : 1 to 2

Heat treatment to Rockwell hardness no C41 - 46

ITEM DRAWING NO 8 LOCKING PINS FOR THE TOP ROLL LOAD CELLS

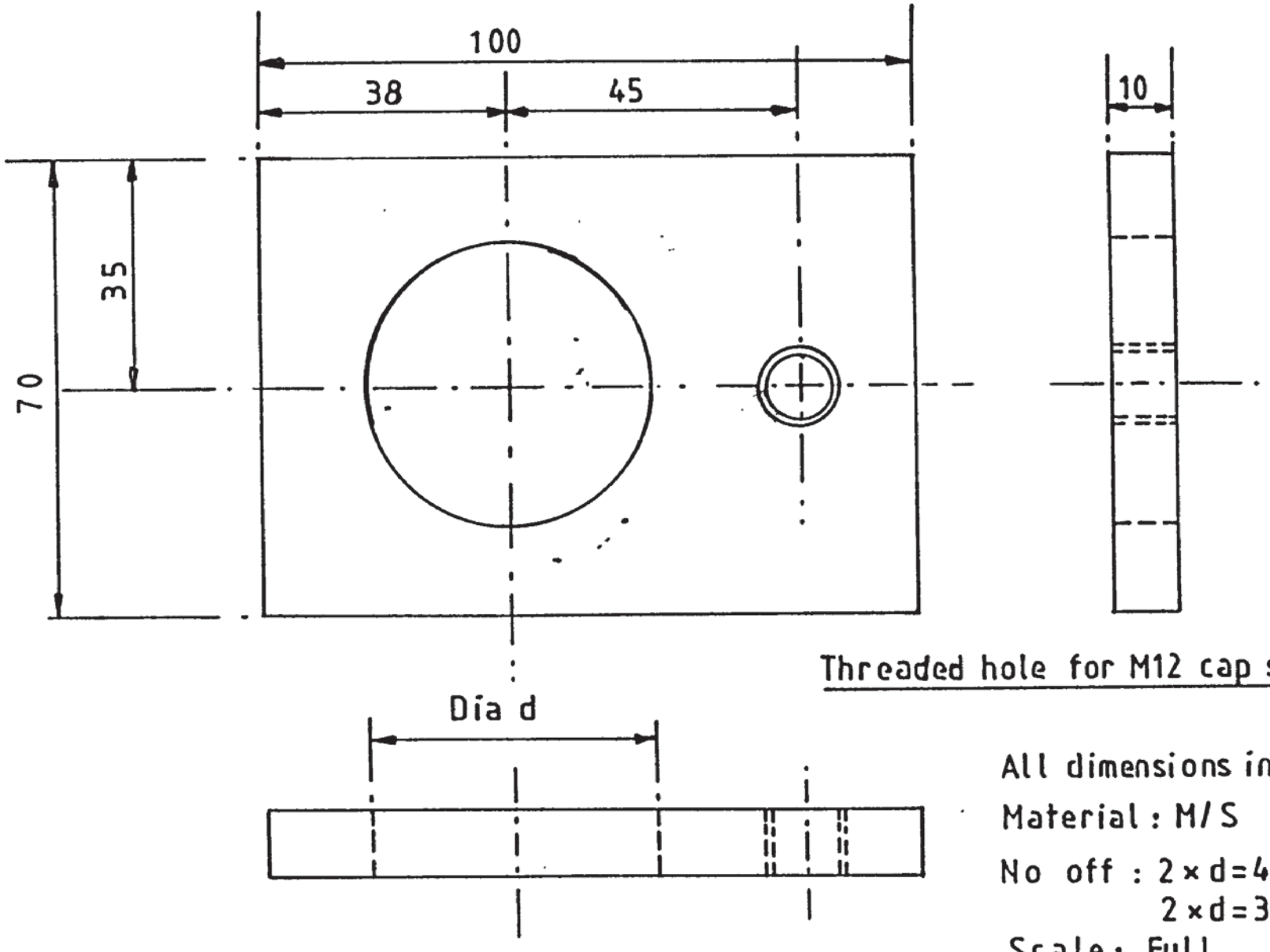

Threaded hole for M12 cap screws

All dimensions in mm

Material : M/S

No off : $2 \times d = 42^{+0.025}$

$2 \times d = 36^{+0.025}$

Scale: Full

ITEM DRAWING NO 9 CLAMPING PLATES FOR THE TOP BEAM LOADCELLS

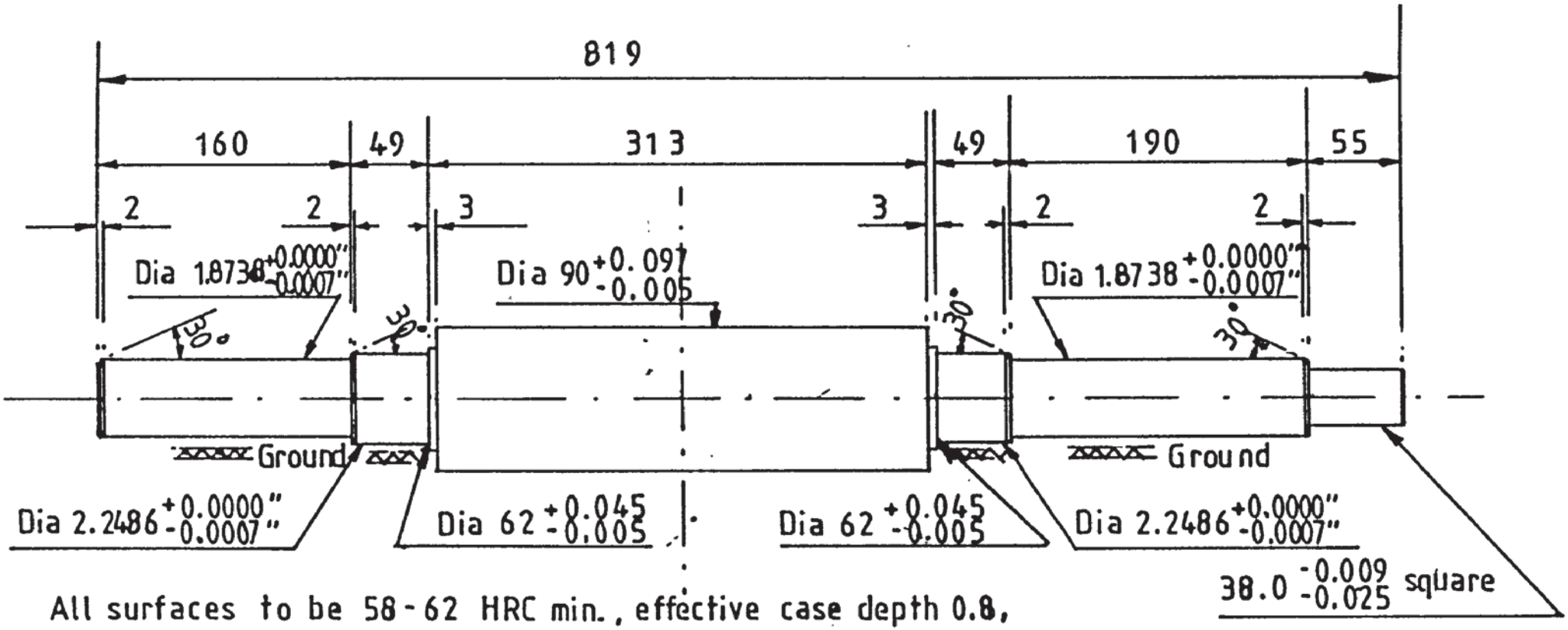

436

All surfaces to be 58 - 62 HRC min., effective case depth 0.8,
straighness 0.008/45, roundness 0.0025 max, surface finish 0.4 max.

All dimensions in mm unless specified
Material : UDDEHOLM tool steel UHB Arne
No off: 1
Scale : 1 to 4

ITEM DRAWING NO 10 THE TOP ROLL

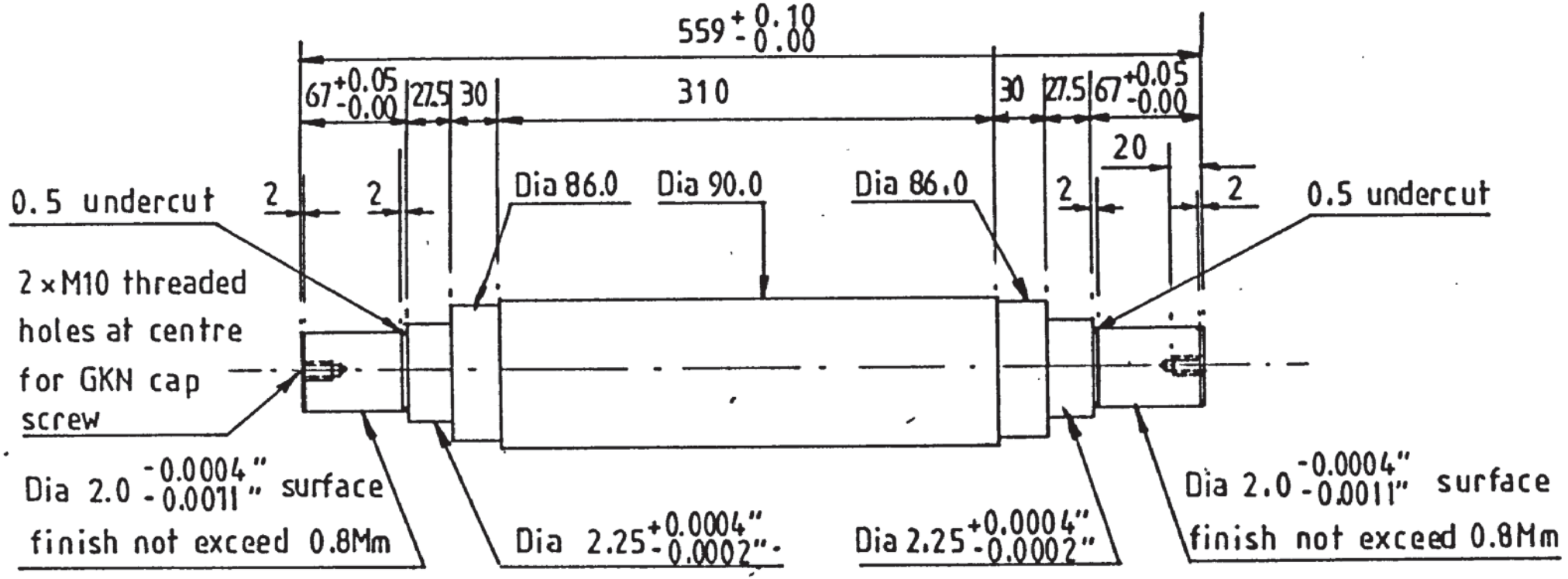

437

Surface hardness to be 58 - 62 HRC, case depth 5 mm

Surface straightness 0.008 mm/45 mm

All dimensions in mm unless specified

Material : UDDEHOLM tool steel UHB Arne

No off : 1

Scale : 1 to 4

ITEM DRAWING NO 11 THE BOTTOM PINCH ROLL

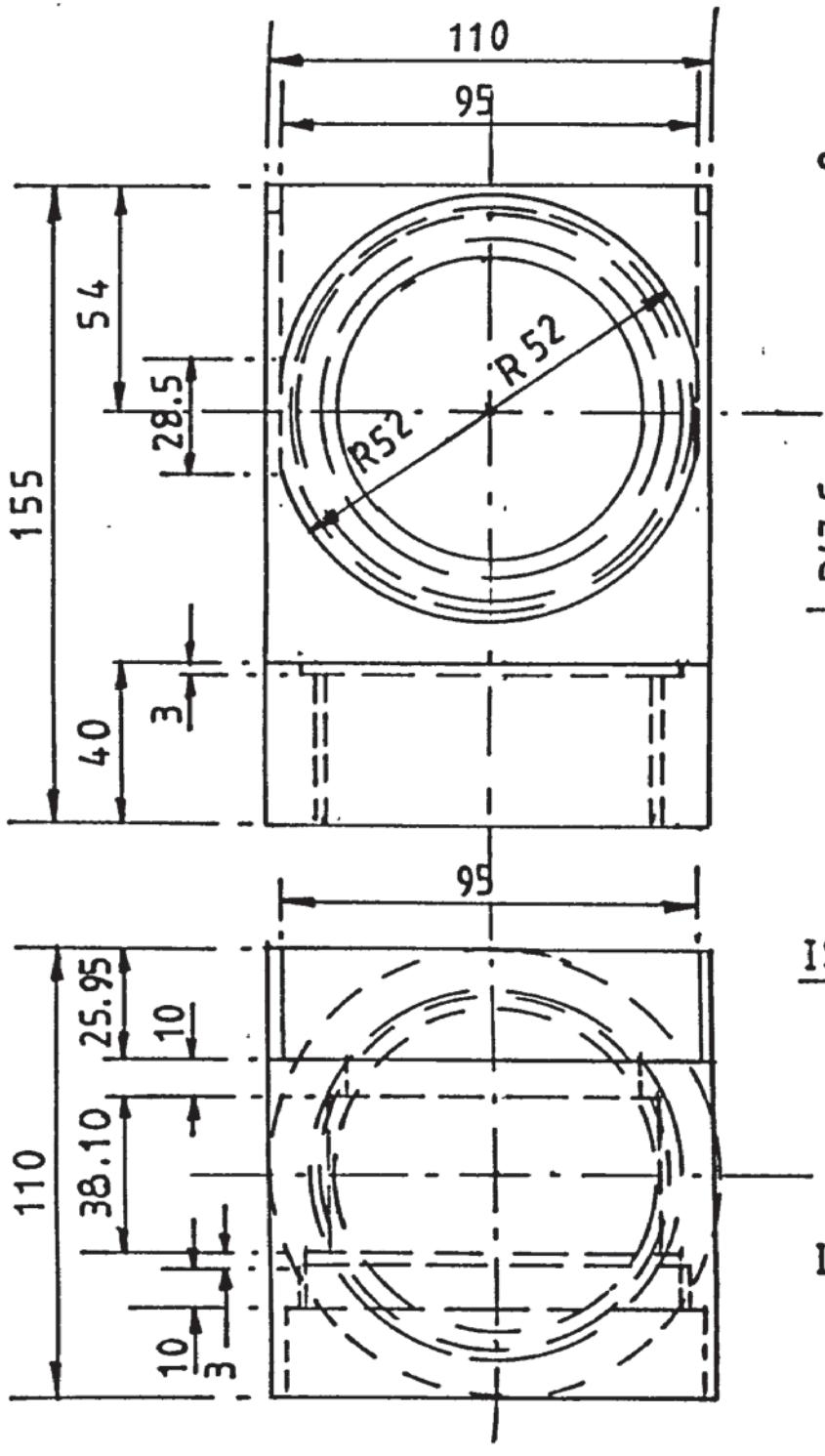

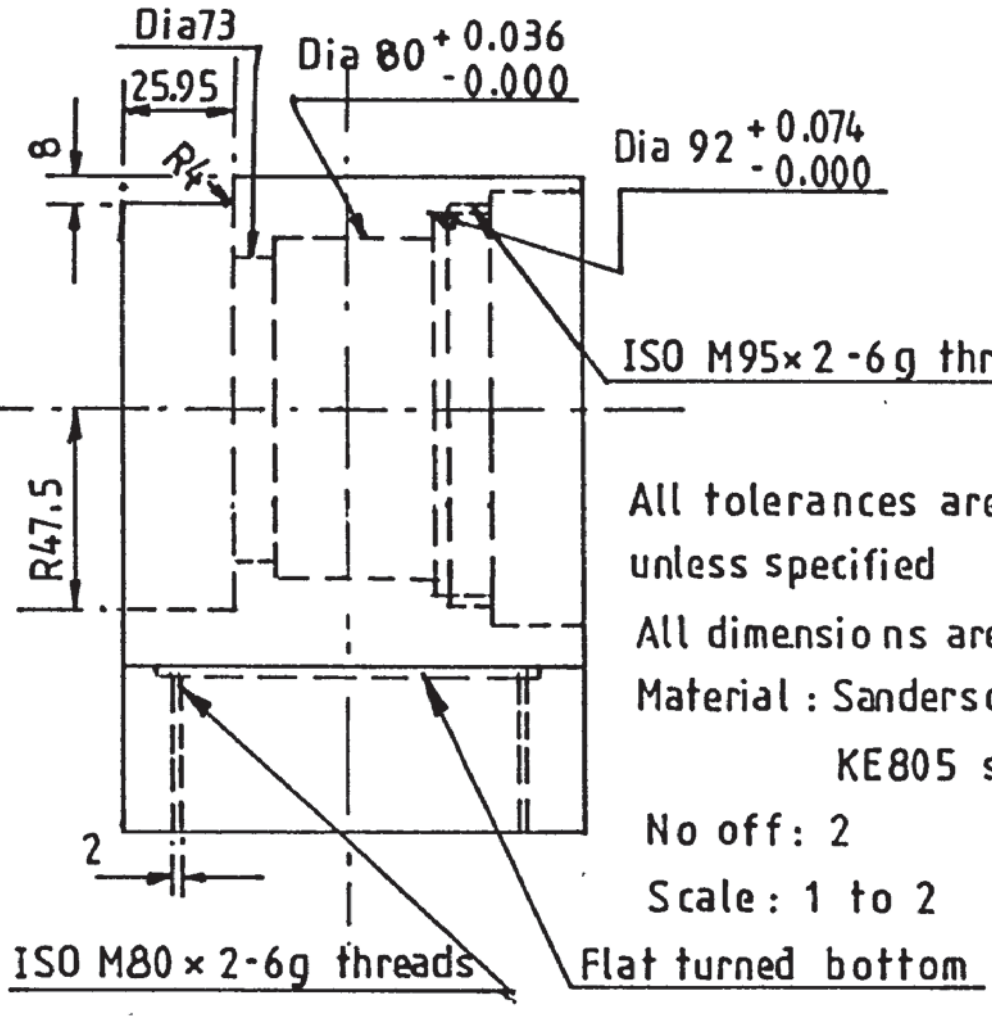

All tolerances are H9 unless specified

All dimensions are in mm

Material : Sanderson Kayser KE805 steel

No off: 2

Scale: 1 to 2

Heat treatment to Rockwell hardness no C41-46

ITEM DRAWING NO 12

BEARING HOUSING OF THE BOTTOM ROLL

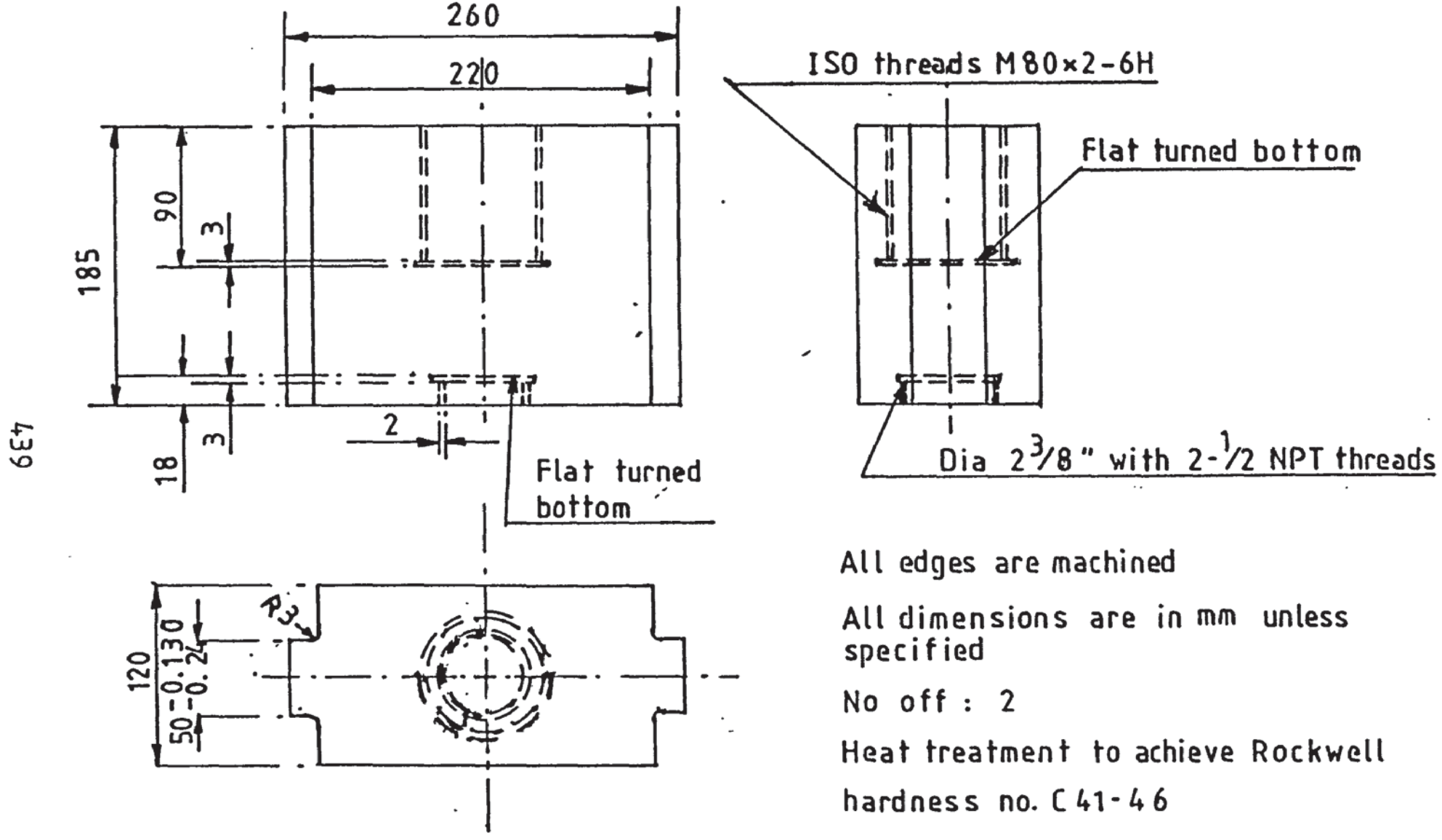

All edges are machined

All dimensions are in mm unless specified

No off : 2

Heat treatment to achieve Rockwell hardness no. C 41-46

ITEM DRAWING NO 13 CONNECTING BLOCK OF THE BOTTOM ROLL

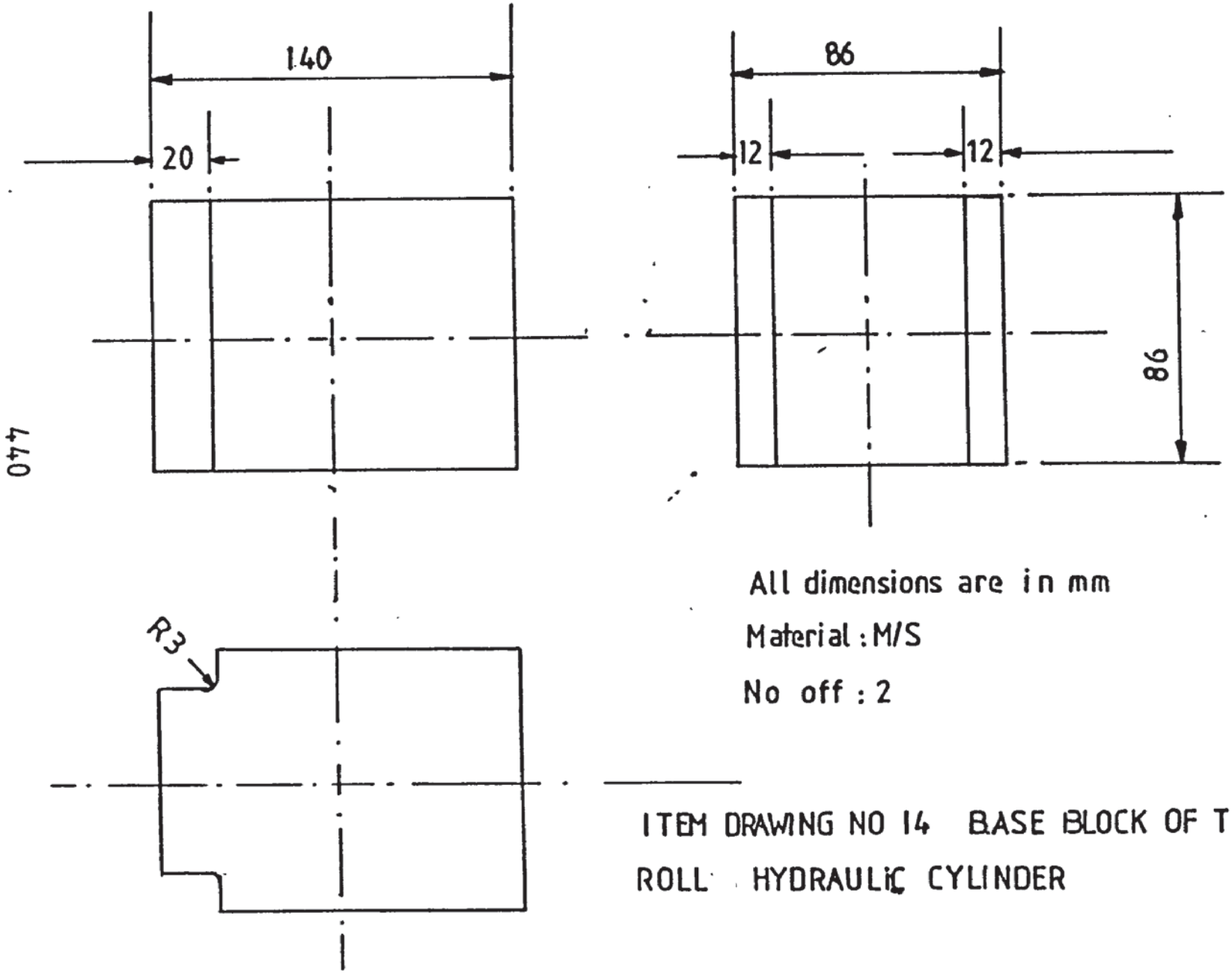

All dimensions are in mm

Material : M/S

No off : 2

ITEM DRAWING NO 14 BASE BLOCK OF THE BOTTOM ROLL HYDRAULIC CYLINDER

All dimensions are in mm
Material : M/S
No off : 2

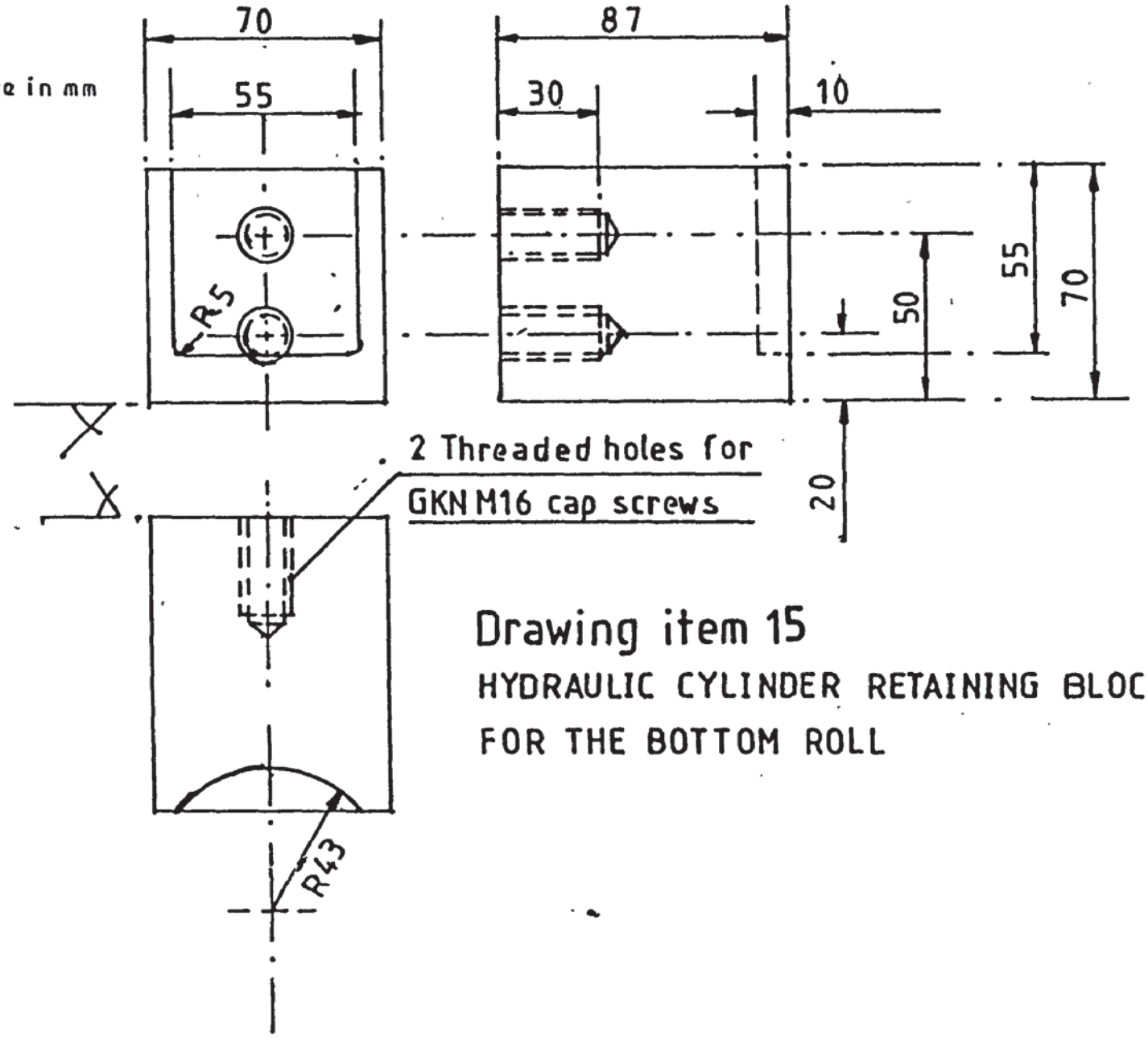

Drawing item 15

HYDRAULIC CYLINDER RETAINING BLOCK FOR THE BOTTOM ROLL

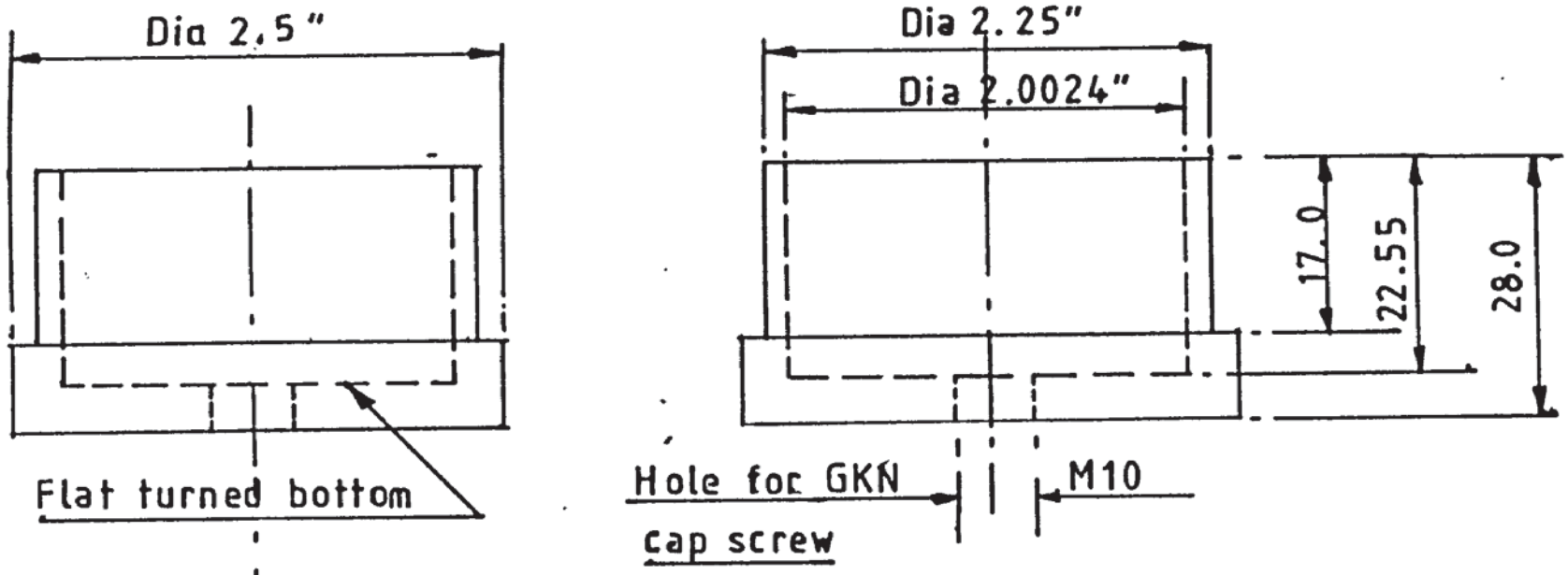

All dimensions are in mm unless specified

Material.: M / S

No off : 2

Scale: Full

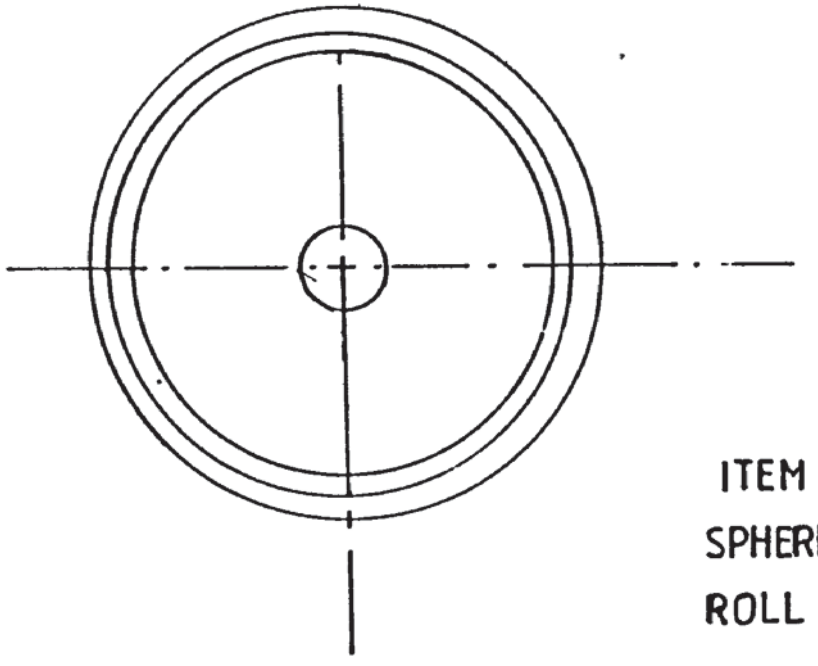

ITEM DRAWING NO 16 LOCKING RING FOR THE SPHERICAL BEARING'S INNER RACEWAY OF THE BOTTOM ROLL

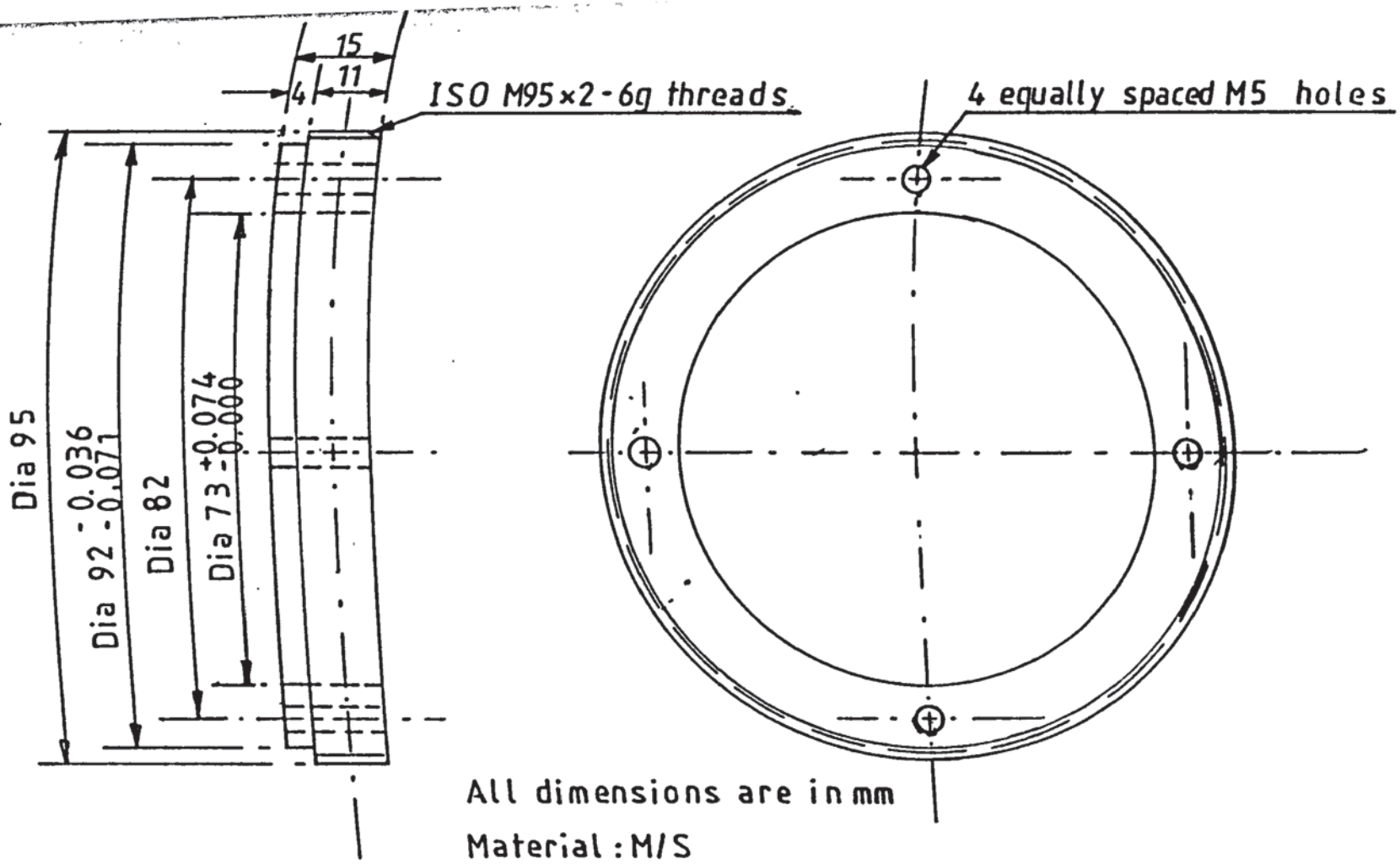

All dimensions are in mm

Material : M/S

No off : 2

Scale : Full

ITEM DRAWING NO 17 TORRINGTON 20SF32 BEARING HOUSING LOCKING RINGS

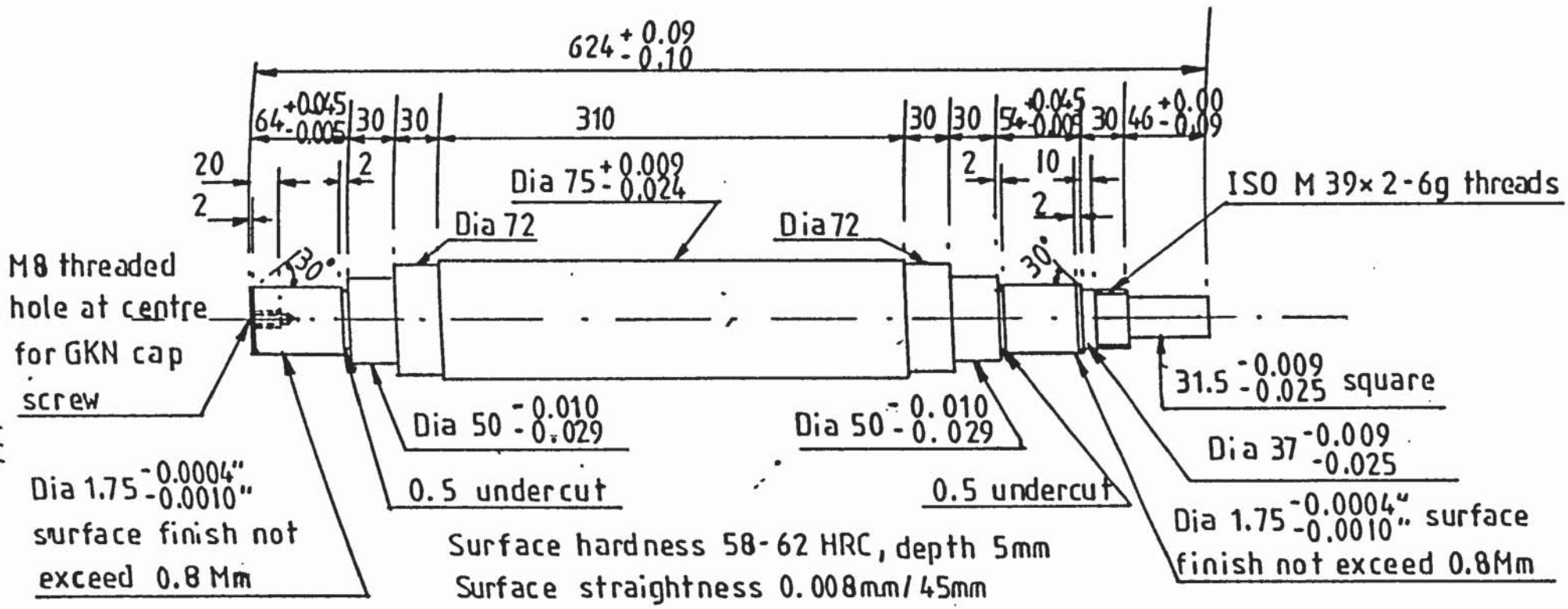

All dimensions in mm unless specified

Material: UDDEHOLM tool steel UHB Arne

No off : 2

Scale : 1 to 4

ITEM DRAWING NO 18 THE SIDE ROLL

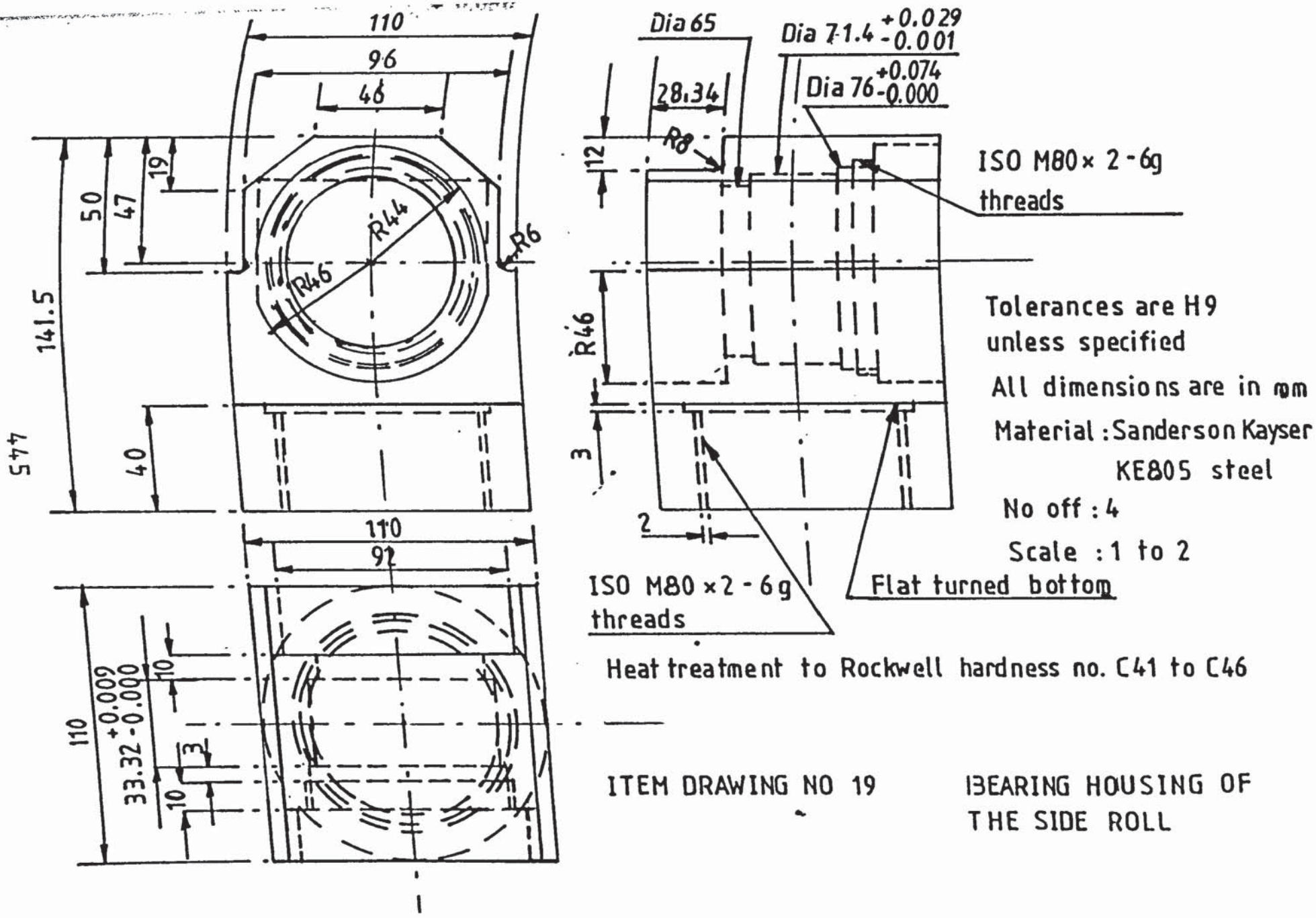

Tolerances are H9 unless specified

All dimensions are in mm

Material : Sanderson Kayser KE805 steel

No off : 4

Scale : 1 to 2

Heat treatment to Rockwell hardness no. C41 to C46

ITEM DRAWING NO 19

BEARING HOUSING OF THE SIDE ROLL

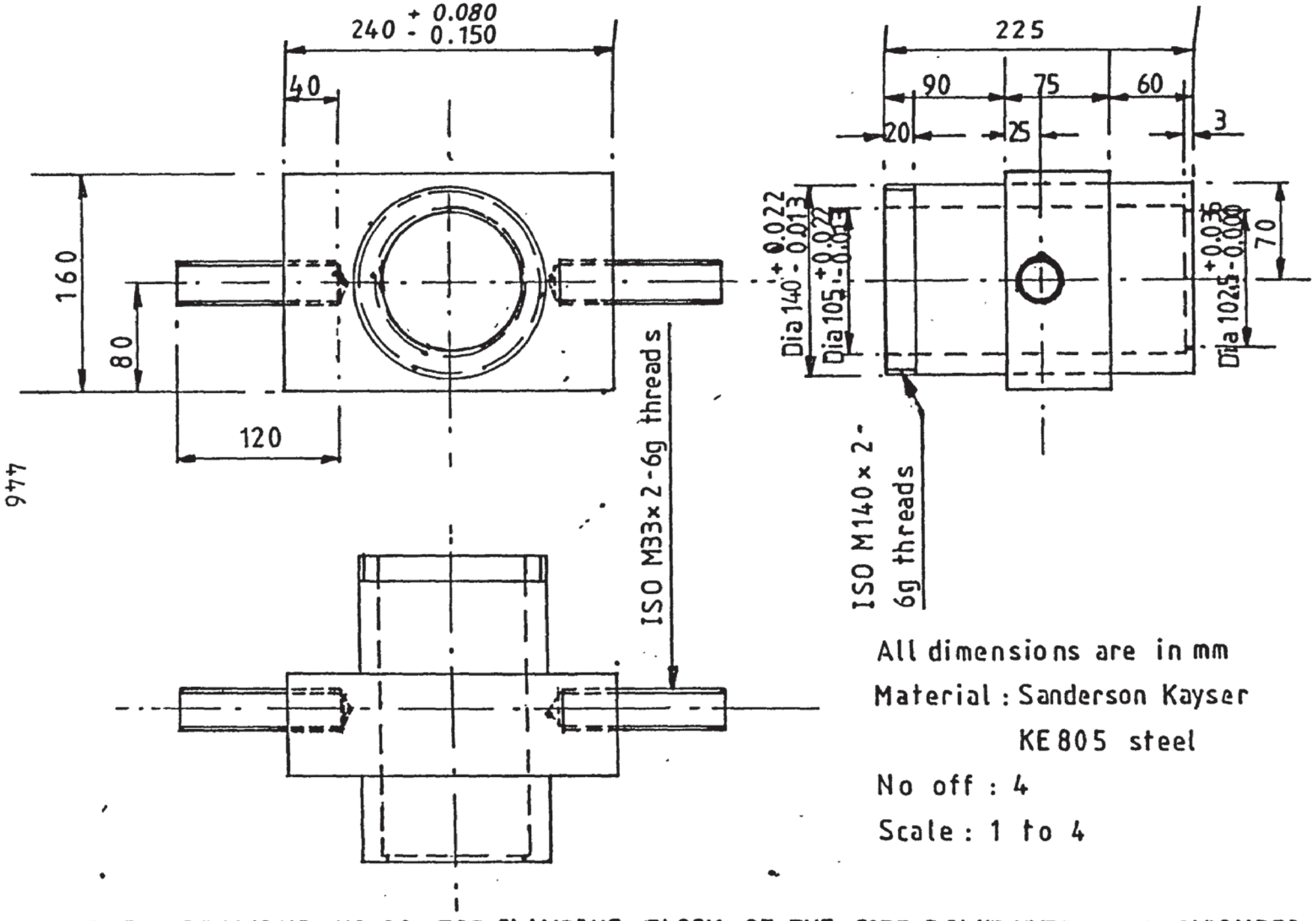

All dimensions are in mm

Material : Sanderson Kayser KE 805 steel

No off : 4

Scale : 1 to 4

ITEM DRAWING NO 20 TOP CLAMPING BLOCK OF THE SIDE ROLL'S HYDRAULIC CYLINDER

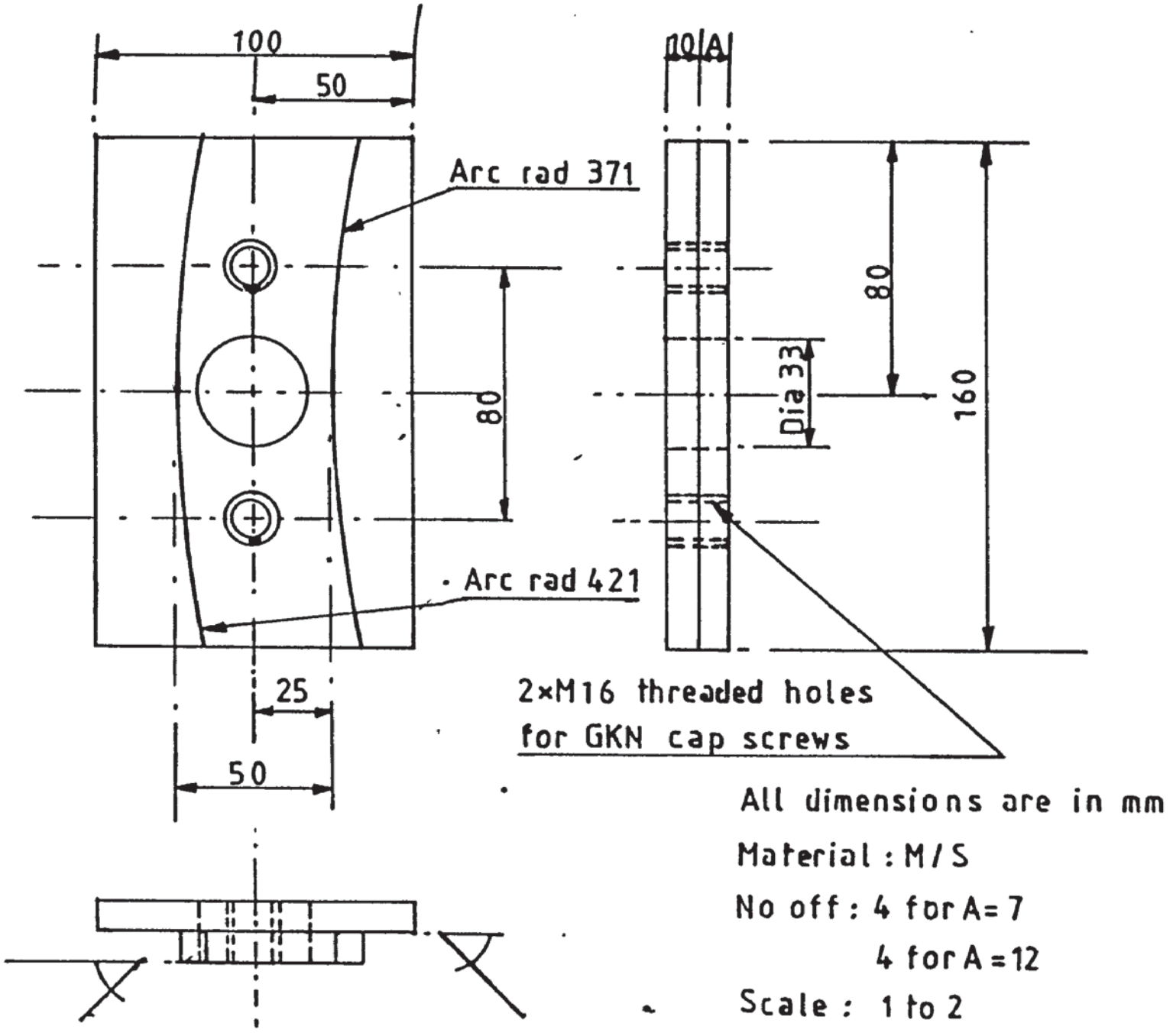

ITEM DRAWING NO 21 LOCKING PLATE FOR THE SIDE ROLL TOP CLAMPING BLOCK

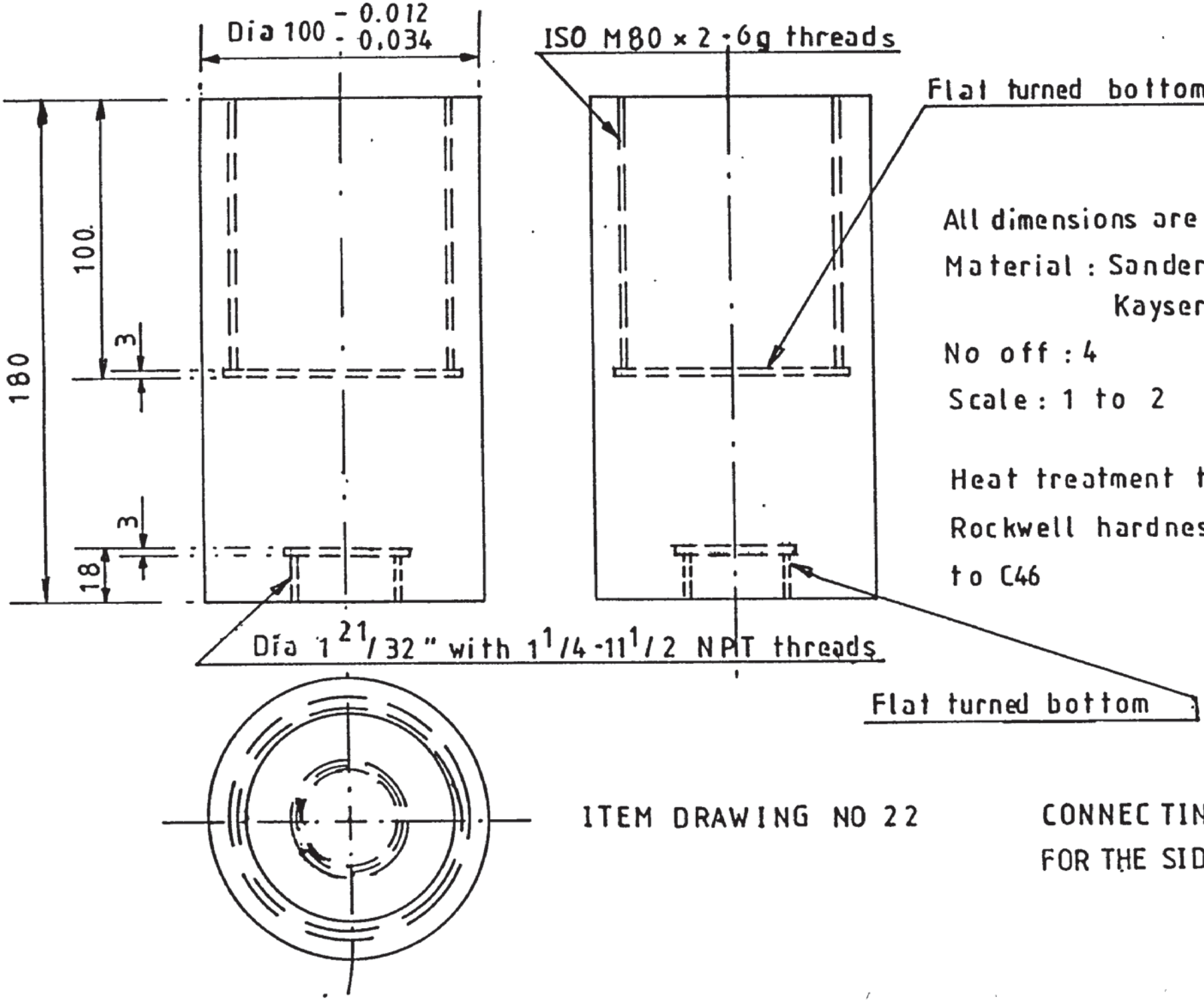

All dimensions are in mm

Material : Sanderson Kayser steel

No off : 4

Scale : 1 to 2

Heat treatment to achieve Rockwell hardness no C41 to C46

ITEM DRAWING NO 22

CONNECTING BLOCK FOR THE SIDE ROLL

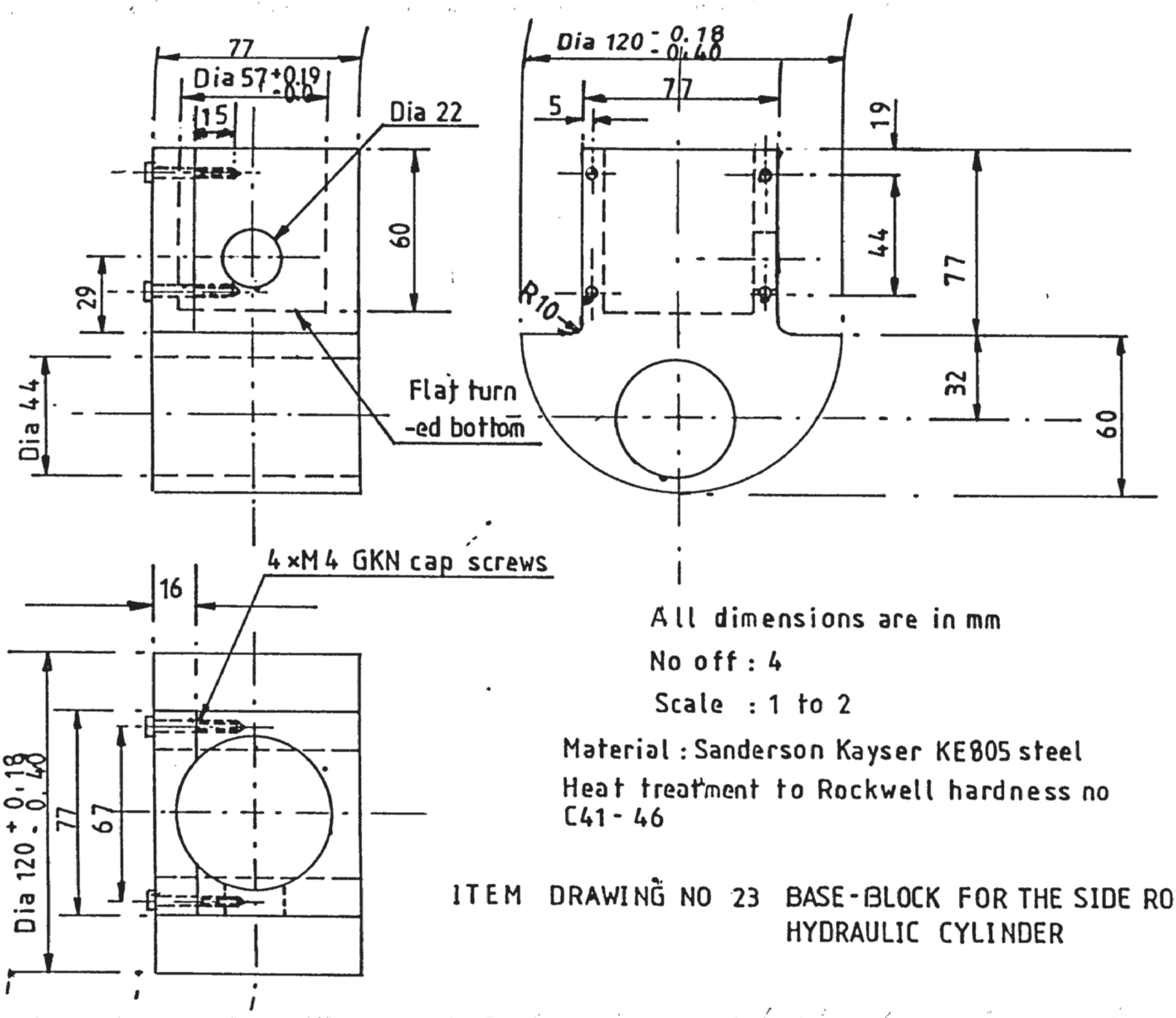

All dimensions are in mm

No off : 4

Scale : 1 to 2

Material : Sanderson Kayser KE805 steel

Heat treatment to Rockwell hardness no C41 - 46

ITEM DRAWING NO 23 BASE-BLOCK FOR THE SIDE ROLL HYDRAULIC CYLINDER

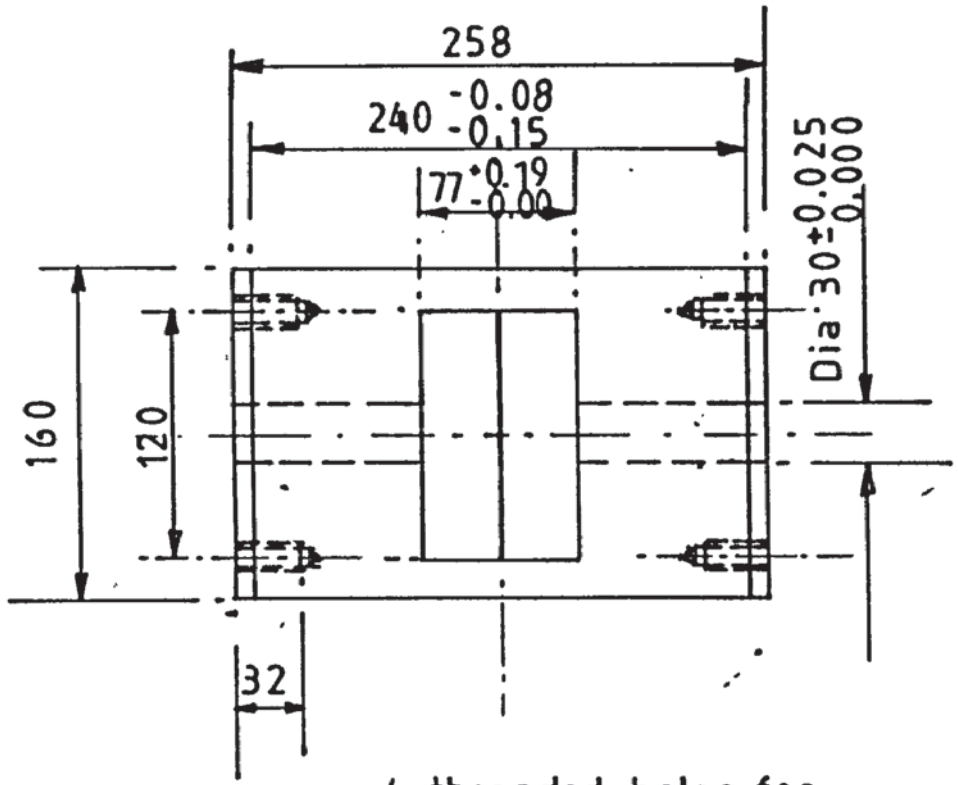

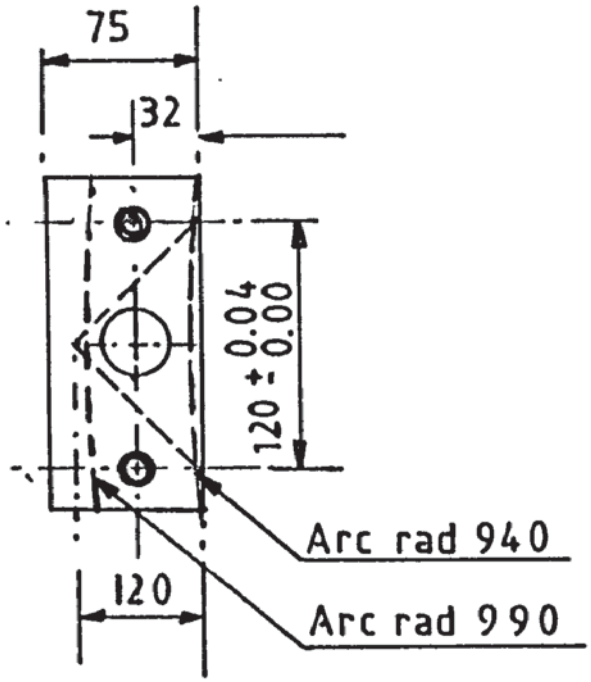

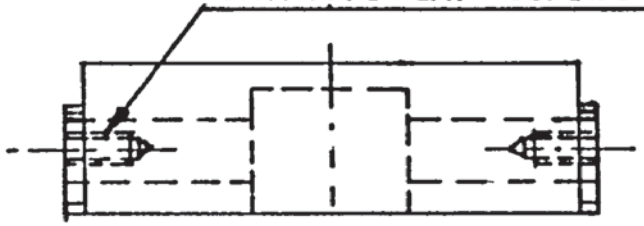

All edges are machined

All dimensions are in mm

Material : M/S

No off: 4

Scale : 1 to 4

ITEM DRAWING NO 24 BOTTOM CLAMPING BLOCK FOR THE SIDE ROLL HYDRAULIC CYLINDER

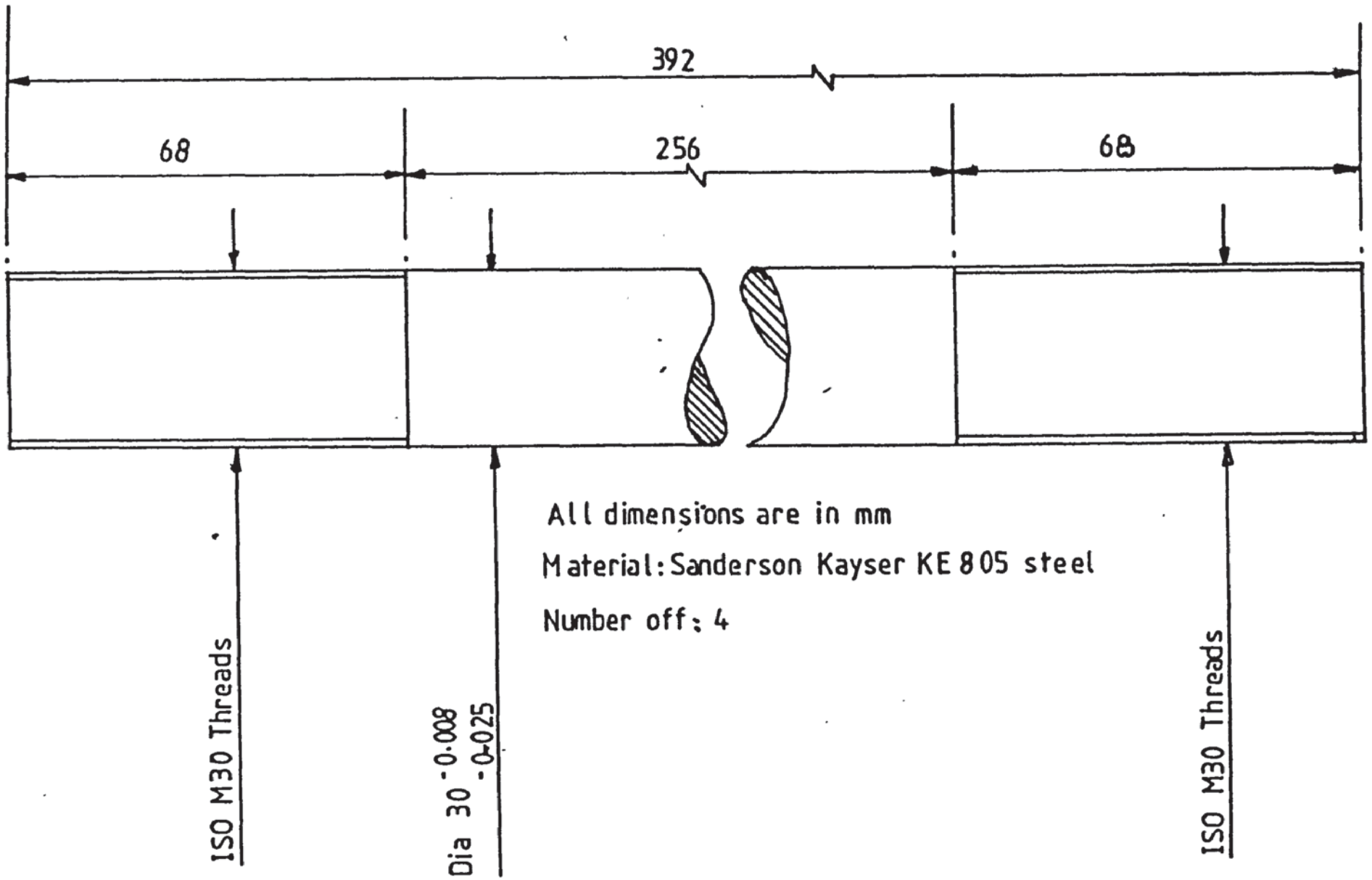

ITEM DRAWING NO 25 LOCKING ROD FOR THE BOTTOM CLAMPING BLOCK OF THE SIDE ROLL HYDRAULIC CYLINDER

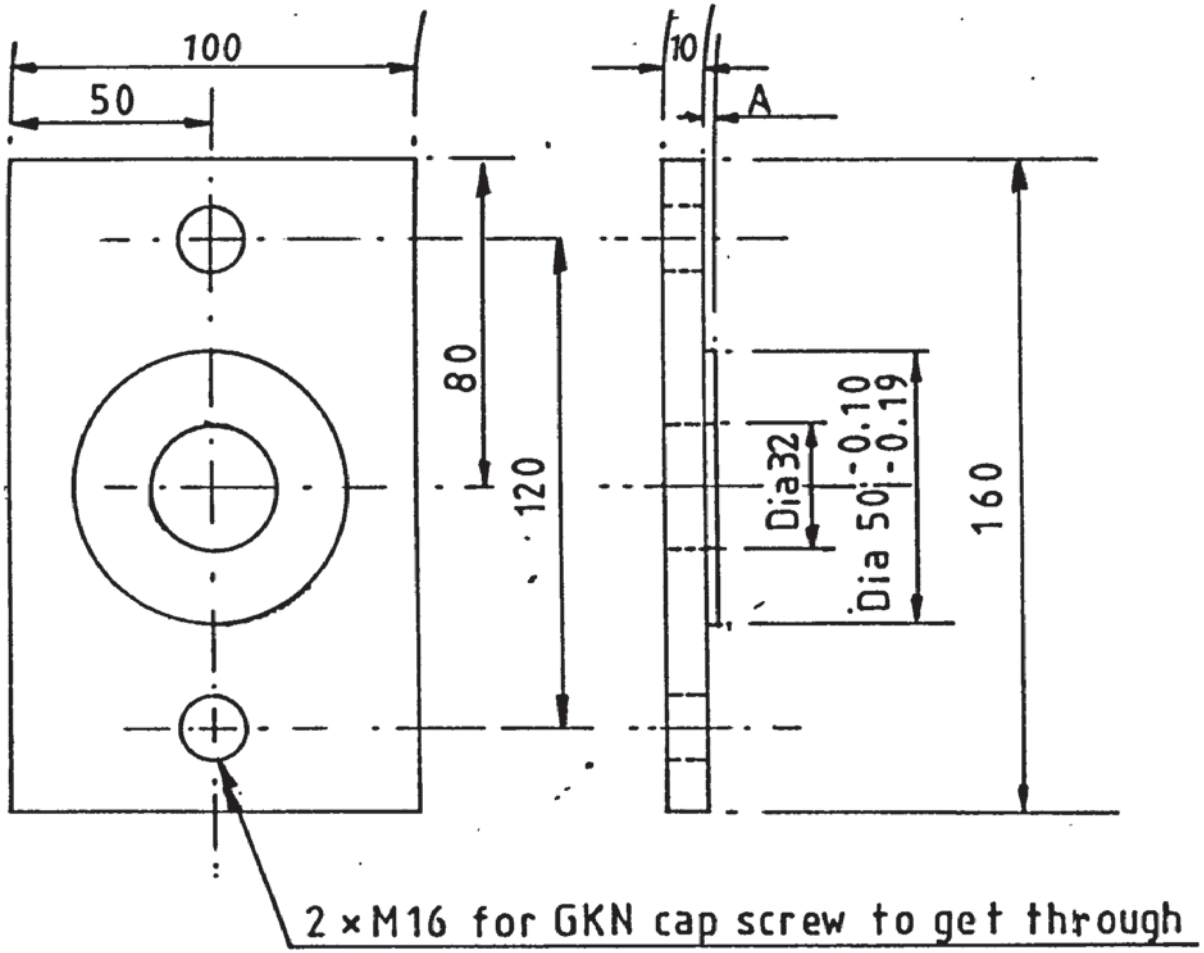

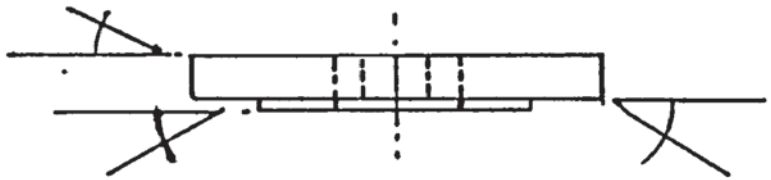

All dimensions are in mm

Material : M/S

No off : 4 for A = 2

4 for A = 1.5

Scale : 1 to 2

ITEM DRAWING NO 26 LOCKING PLATE FOR THE SIDE ROLL BOTTOM CLAMPING BLOCK

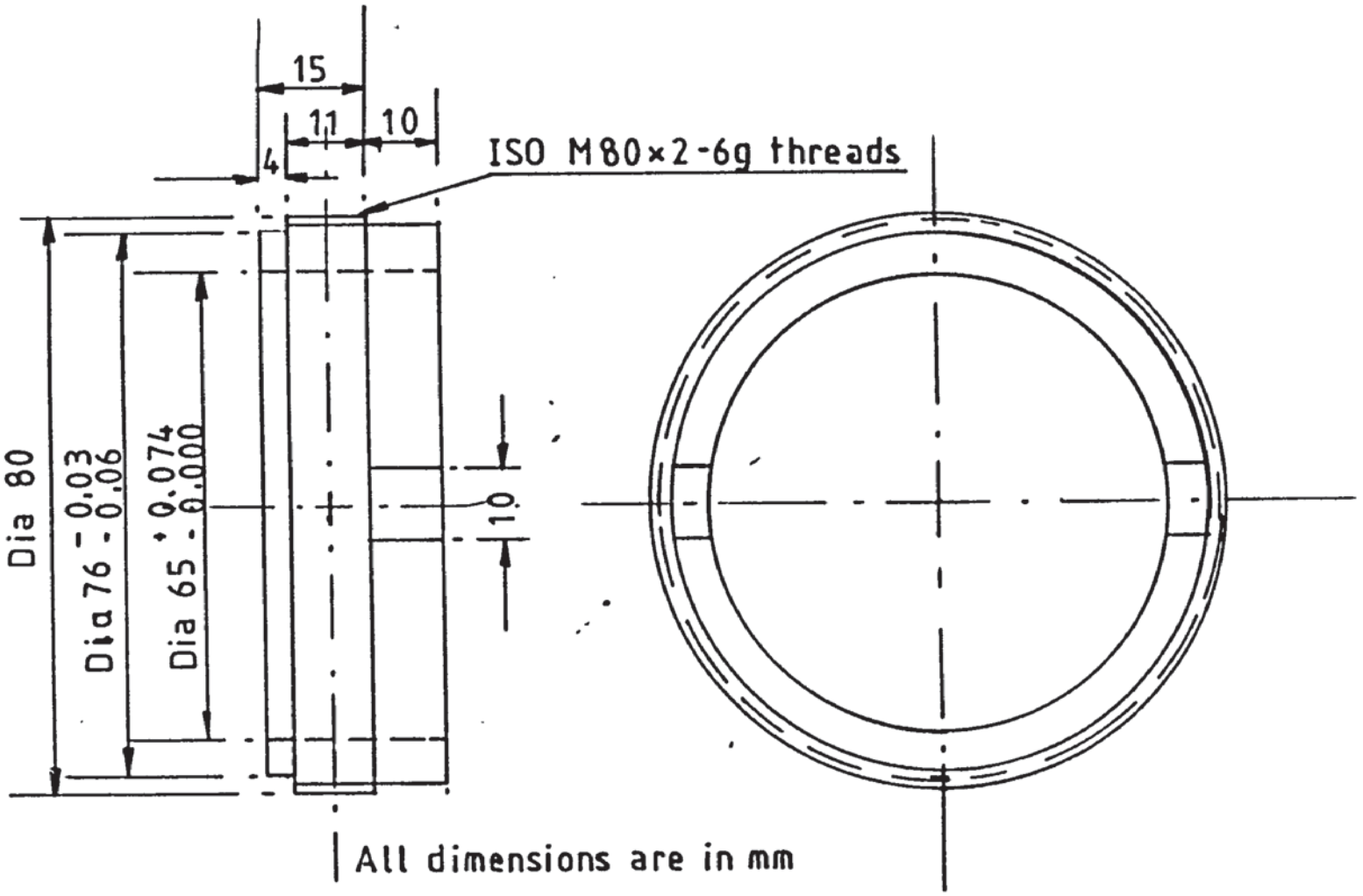

All dimensions are in mm

Material : M/S

No off : 4

Scale : Full

ITEM DRAWING NO 27 TORRINGTON 17SF28 BEARING HOUSING LOCKING RING

ES7

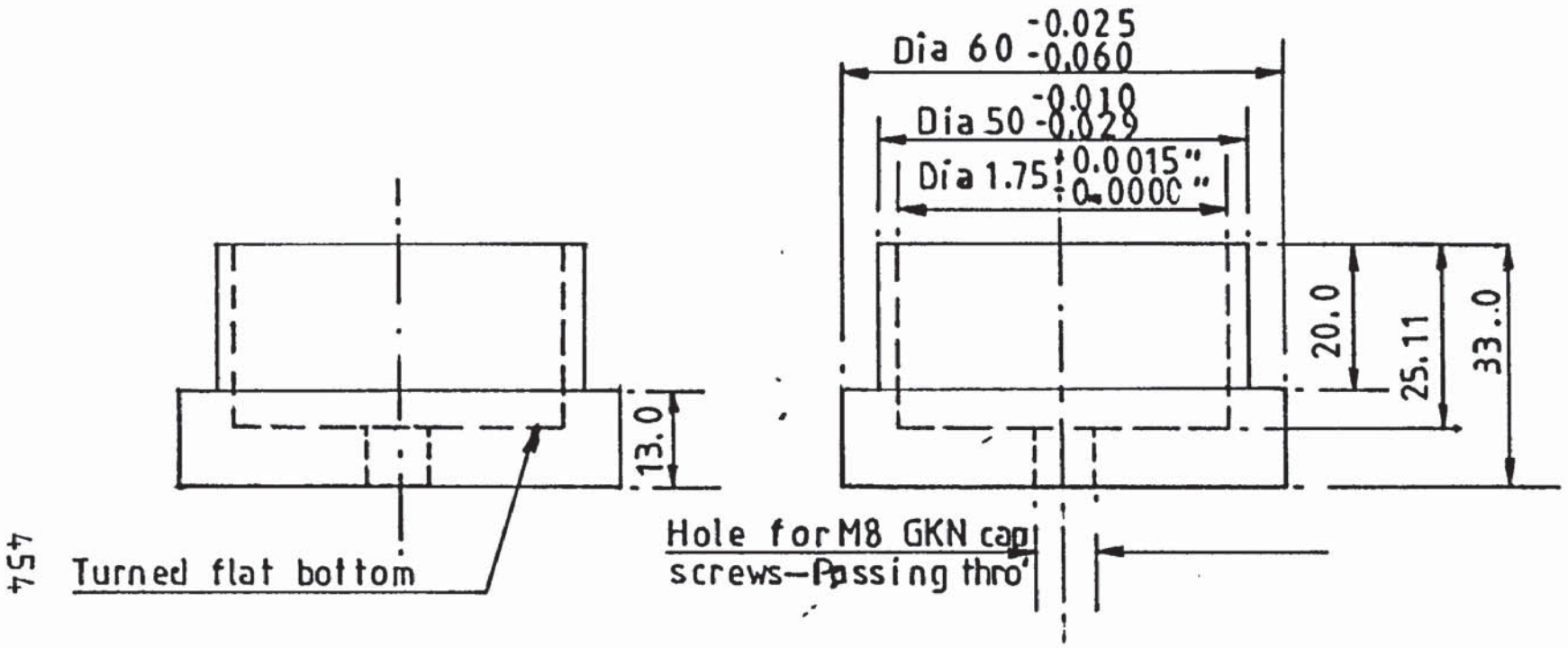

All dimensions in mm unless specified

Material : M/S

No off : 2

Scale : Full

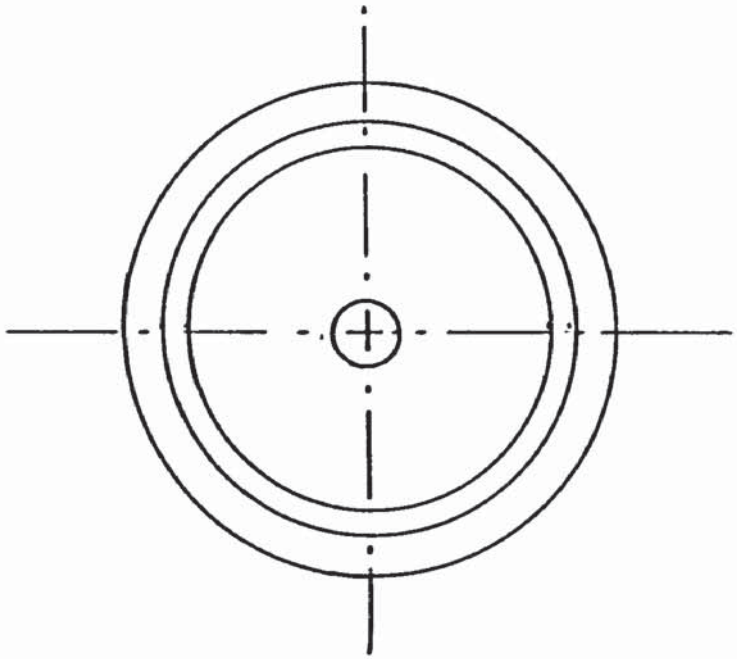

ITEM DRAWING NO 28 THE LOCKING RING FOR THE SIDE ROLL SPHERICAL BEARING (INNER RACEWAY, FREE END SIDE)

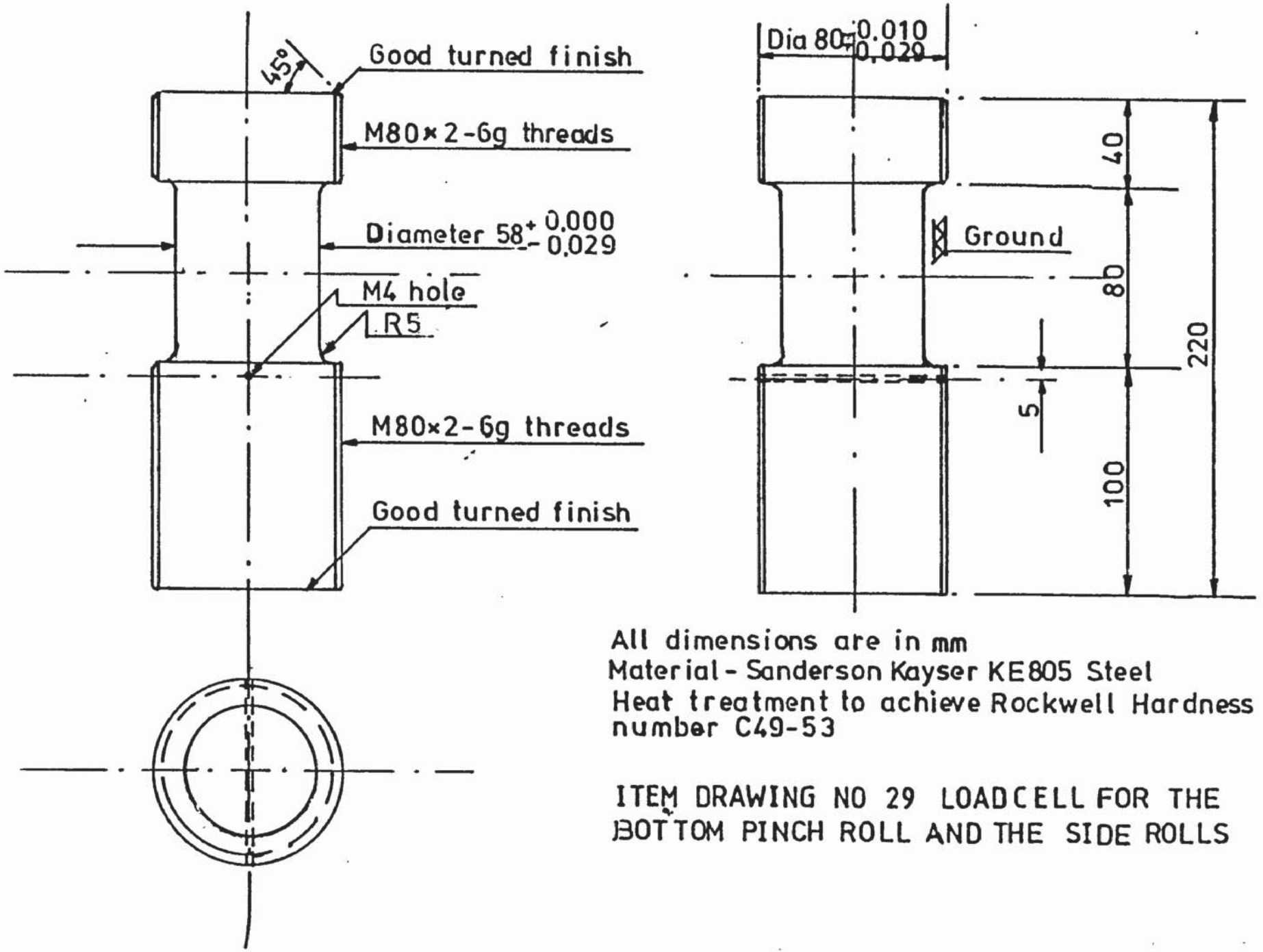

554

All dimensions are in mm
Material - Sanderson Kayser KE805 Steel
Heat treatment to achieve Rockwell Hardness number C49-53

ITEM DRAWING NO 29 LOADCELL FOR THE BOTTOM PINCH ROLL AND THE SIDE ROLLS

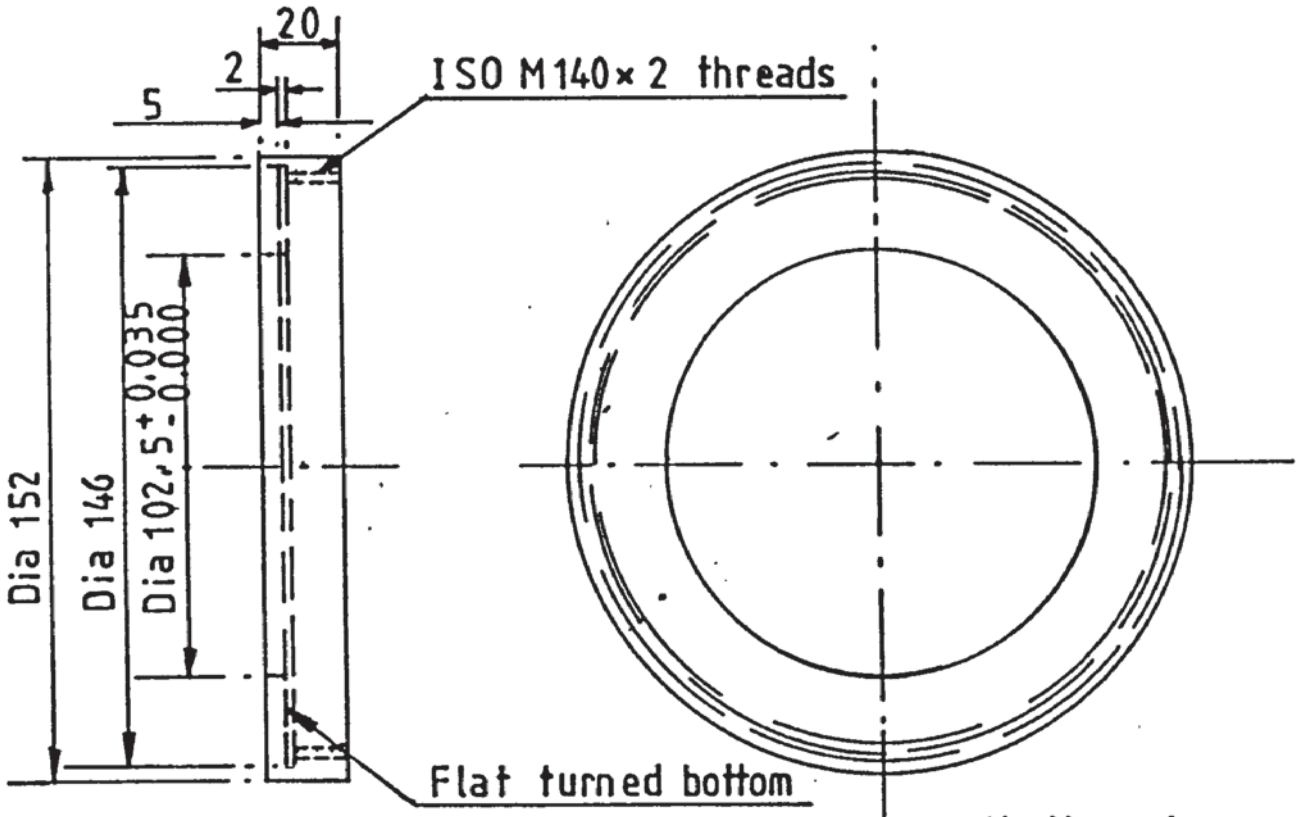

All dimensions are in mm

Material: M/S

No off: 4

Scale: 1 to 2

ITEM DRAWING NO 30 GLACIER MB100DU BEARING LOCKING RING

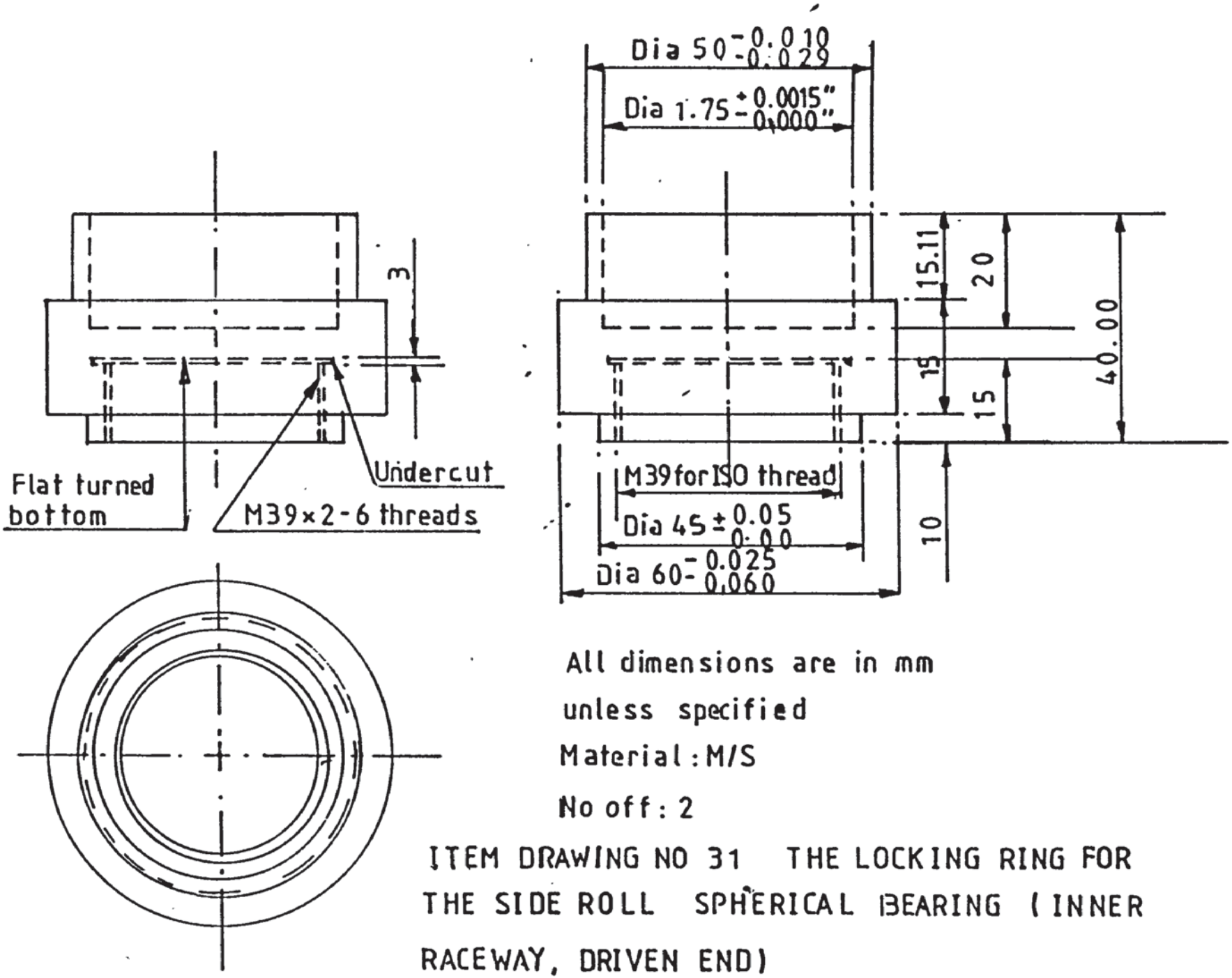

457

All dimensions are in mm
unless specified
Material : M/S
No off : 2

ITEM DRAWING NO 31 THE LOCKING RING FOR THE SIDE ROLL SPHERICAL BEARING (INNER RACEWAY, DRIVEN END)

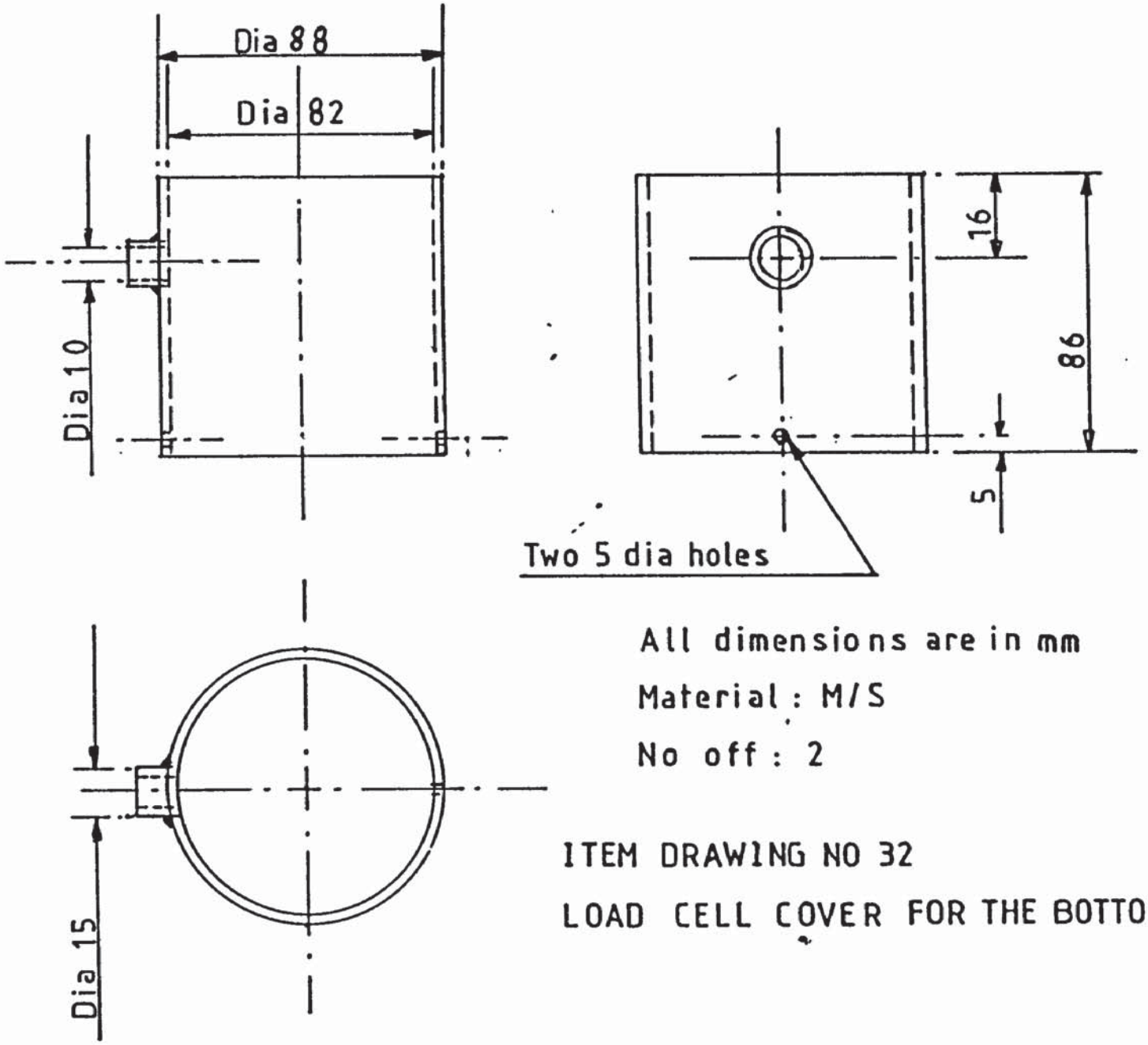

All dimensions are in mm

Material : M/S

No off : 2

ITEM DRAWING NO 32

LOAD CELL COVER FOR THE BOTTOM ROLL

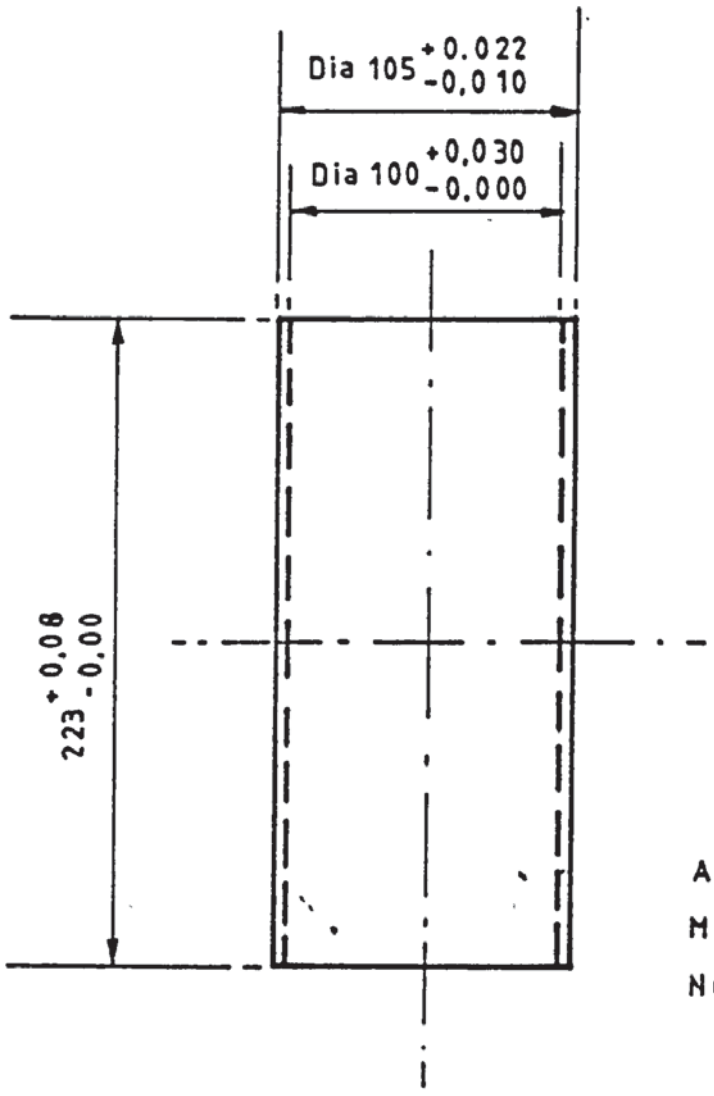

All dimensions in mm

Material ; Bronze

No off: 4

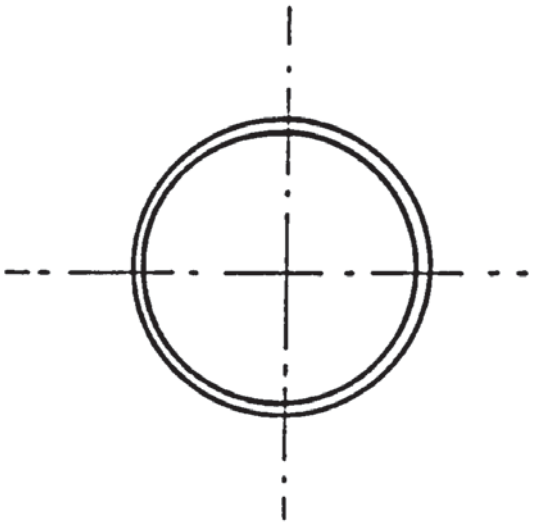

ITEM DRAWING NO 33 BUSH BEARINGS FOR THE SIDE ROLL CONNECTING BLOCK

APPENDIX 4.1

DERIVATION OF THE BENT PLATE INNER RADIUS EXPRESSION (4.8)

A4.1 DERIVATION OF THE BENT PLATE INNER RADIUS EXPRESSION (4.8)

The following mathematical theory formed the basic principle for the design of a device to measure the inner radius of curvature of a bent plate.

Consider a circle as shown in fig A4.1, in which ACB is any sector of the circle and AB is the base of the sector having a length L. Line CEOD bisects the sector base AB through the centre of the circle O. Thus AE=EB=L/2, AB is perpendicular to CD and DC is the diameter, d, of the circle.

Considering now ΔACD, in which

$$(AD)^2=(DC)^2-(AC)^2 \qquad (A4.1)$$

From ΔAED, we have

$$(AD)^2=(AE)^2+(DE)^2 \qquad (A4.2)$$

Also from ΔACE

$$(AC)^2=(AE)^2+(EC)^2 \qquad (A4.3)$$

Substituting (A4.2) and (A4.3) into (A4.1) gives

$$(AE)^2+(DE)^2=(DC)^2-(AE)^2-(EC)^2$$

After appropriate manupulation and rearrangement this leads to

$$DC=[(AE)^2+(EC)^2]/EC \qquad (A4.4)$$

The substitution of DC=d, AE=L/2 and EC=h gives the expression (4.8) as :

$$d=[(L^2/4)+h^2]/h \qquad (4.8).$$

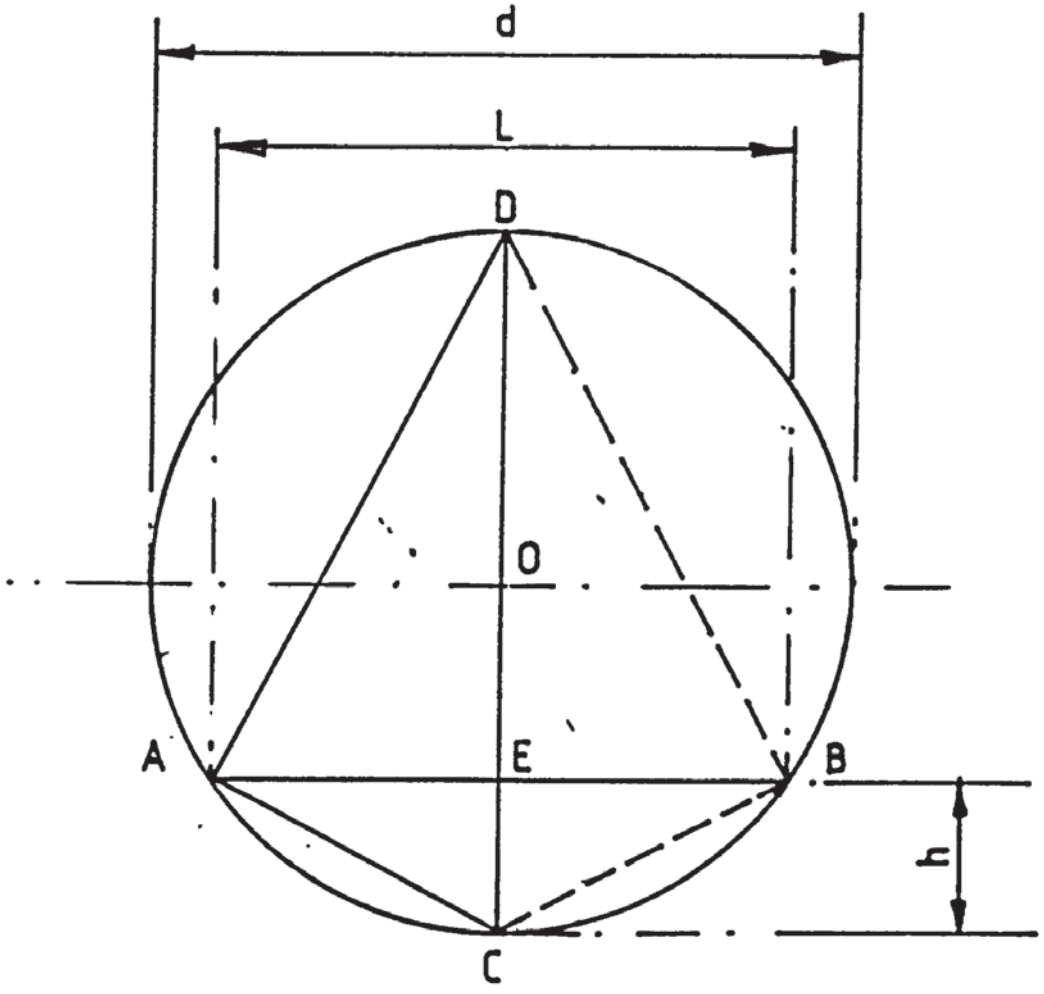

FIG A4.1 THE DESIGN PRINCIPLE OF THE DEVICE TO MEASURE THE INNER BEND RADIUS OF CURVATURE

APPENDIX 5.1

FURTHER THEORETICAL ANALYSIS ON THE MECHANICS OF FOUR ROLL THIN PLATE BENDING PROCESS

This appendix continues the theoretical analysis in Chapter five; it completes the mathematical modelling on the mechanics of the four-roll thin plate bending process. Consequently the equation and section numbers follow section 5.4.5 in Chapter five.

5.4.6. Determination of the forces on the bending rollers

Following the evaluation of the internal bending moment, in the plate, at the top roll contact, the bending forces on the working rollers can thus be determined by consideration of equilibrium. Since equilibrium occurs in any deflection condition of the plate, the subsequent analysis is applicable to both single or multipass bending.

The co-ordinates of the roller contacts with the bendplate, before spring back takes place, with reference to figs 5.22 and 5.23, are as follows :

i. with the pre-active side roll in operation (fig 5.22)

(a) For the operative side roll : co-ordinate $(x_{cn}, y_{cn}=w_{cn})$
contact angle θ_s.

(b) For the top roll : co-ordinate $(x_{tn}, y_{tn}=w_{tn})$
contact angle θ_t.

(c) For the bottom roll : co-ordinate $(-x_{bn}, -y_{bn}=-w_{bn})$
contact angle θ_b.

ii. With the pre-inactive side roll in operative (fig 5.23)

(a) For the operative side roll : co-ordinate $(-x_{cn}, y_{cn}=w_{cn})$ contact angle θ_s".

(b) For the top roll : co-ordinate $(-x_{tn}, y_{tn}=w_{tn}$ contact angle θ_t".

(c) For the bottom roll : co-ordinate $(x_{bn}, -y_{bn}=-w_{bn})$ contact angle θ_b".

5.4.6.1. With pre-active side roll operative

A. Evaluation of the bending force, F_s, on the pre-active side roll

Normally, equilibrium only occurs as the external bending moment, M_e, about the top roll contact, is equal to the corresponding internal bending resistance of the plate. Referring to figs 5.18 and 5.19, the external bending moment about the top roll contact can be expressed as follows :

$$M_e = F_s \cos\beta \{(w_{cn}-w_{tn})\sin\theta_s + (x_{cn}-x_{tn})\cos\theta_s\} \qquad (5.30a)$$

In which the angle β (fig 5.5) represents :

(1) $\beta = \psi - \theta_s$ when $\psi > \theta_s$,

(2) $\beta = 0$ when $\psi = \theta_s$,

and

(3) $\beta = \theta_s - \psi$ when $\psi < \theta_s$,

respectively.

Equating expression (5.30a) to its respective internal bending resistance, at top roll contact, for the single pass (equation 5.24) and the multipass (equation 5.29c) gives the following expressions.

(i) for single pass bending :

$$F_s = b\left\{\left[\left([2R^2(1-\nu^2)^2\sigma_0{}^3]/[3E^2(1-\nu+\nu^2)^{3/2}]\right)+B\right]/\left(\cos\beta[\right.\right.$$

$$\left.\left.(w_{cn}-w_{tn})\sin\theta_s+(x_{cn}-x_{tn})\cos\theta_s\right]\right)\right\} \qquad (5.30b)$$

where B represents the expression of (5.23d).

(ii) For multipass bending :

$$F_s = b(A_1+A_2)/\{\cos\beta\,[(w_{cn}-w_{tn})\sin\theta_s + (x_{cn}-x_{tn})\cos\theta_s]\} \qquad (5.30c)$$

where A_1 and A_2 represent the expressions of (5.28h) and (5.29a) respectively.

B. Force, F_b, on the bottom pinch roll

The force, F_b, on the bottom pinch roll can also be found by considering equilibrium about the top roll, because :

The external bending moment due to the bending force on the bottom pinch roll about the top roll contact is equal to the internal bending resistance to the external bending moment about the top roll

Mathematically, it can be expressed as

$$F_b[(w_{tn}+w_{bn})\sin\theta_b+(x_{tn}+x_{bn})\cos\theta_b]$$

$$= b\left\{\left([2R^2(1-\nu^2)^2\sigma_0{}^3]/[3E^2(1-\nu+\nu^2)^{3/2}]\right)+B\right\}$$

which leads to

$$F_b=\left\{b\left[2R^2(1-\nu^2)^2\sigma_0{}^3/3E^2(1-\nu+\nu^2)^{3/2}+B\right]\right\}/\left[(w_{tn}+w_{bn})\sin\theta_b + (x_{tn}+x_{bn})\cos\theta_b\right] \quad (5.30d)$$

for the single or first pass bending, and

$$F_b=\left[b(A_1+A_2)\right]/\left[(w_{tn}+w_{bn})\sin\theta_b+(x_{tn}+x_{bn})\cos\theta_b\right] \quad (5.30e)$$

for the second and subsequent pass bending.

c. Force, F_t, on the top roll

Once the forces on the pre-active side roll and the bottom pinch roll have been found, the pinch force on the top roll can then be obtained through an equilibrium consideration. Its evaluation assumes line contacts, instead of a contact band, between the rolls and workpiece.

From fig 5.18, the equilibrium condition gives the vertical force components on the top roll contact as follows.

$$F_t\cos\theta_t = F_s\cos\theta_s + F_b\cos\theta_b \quad (5.30f)$$

and the horizontal force component on the top roll contact as :

$$F_t\sin\theta_t = F_s\sin\theta_s + F_b\sin\theta_b \quad (5.30g)$$

Subsequently, the top roll force can thus be obtained either by (5.30f) or by (5.30g). If (5.30f) is used, it leads to

$$F_t = (F_s\cos\theta_s+F_b\cos\theta_b)/\cos\theta_t \quad (5.30h)$$

Substituting the expressions for the bending forces on the pre-active side roll and the bottom roll, for both single and multi-pass modes, the following expressions are abtained.

$$F_t=(b/\cos\theta_t)\Big\{[2(1-\nu^2)^2R^2\sigma_0{}^3/E^2(1-\nu+\nu^2)^{3/2}] + B\Big\}\Big\{$$

$$(1/\cos\beta[(w_{cn}-w_{tn})\tan\theta_s+(x_{cn}-x_{tn})])+(1/[(w_{tn}+w_{bn})\tan\theta_b$$

$$+(x_{tn}+x_{bn})])\Big\} \qquad (5.30i)$$

for the single pass bending, and

$$F_t=[b(A_1+A_2)]/\cos\theta_t]\Big\{(1/\cos\beta[(w_{cn}-w_{tn})\tan\theta_s+(x_{cn}-x_{tn})])+$$

$$(1/[(w_{tn}+w_{bn})\tan\theta_b+(x_{tn}+x_{bn})])\Big\} \qquad (5.30j)$$

for the second and subsequent pass bending.

5.4.6.2. With the pre-inactive side roll in operative (fig 5.19)

Basically expressions (5.30b), (5.30c), (5.30d), (5.30f), (5.30i) and (5.30j) are still applicable for the operation mode, the only difference is to replace : θ_s, θ_b and θ_t by $\theta_s"$, $\theta_b"$ and $\theta_t"$, respectively.

5.4.7. Geometrical constraint of the roller bender setting

Though the positional contact of the pre-active side roll, and the pre-inactive side roll, varies in the co-ordinate system (fig 5.5) as the bending proceeds, its instantaneous position is constrained by the geometrical setting of the bender.

Figs 5.13B and 5.23 assume that the positional co-ordinates of the centre of the pre-active side roll and the pre-inactive side roll are $(x_0, -r_s-h)$ and $(-x_0, -r_s-h)$, where r_s is the side roll radius and h is half of the plate thickness, respectively, at the following conditions :

(a) when the initial flat plate is gripped horizontally, and
(b) when the surface of the side rolls is just touching the bottom face of the initially flat plate, which is as condition (a).

If ψ and ψ'' (or $-\psi$) are the positional powering angle of the pre-active side roll and the pre-inactive side roll respectively, it can be shown that the positional powering centre , O_p, is at the co-ordinate of $(0, x_0\cot\psi-r_s-h)$. Consequently, the positional powering direction of each side roll hydraulic cylinder is constrained to the following positional straight lines on the co-ordinate system, as adopted in the present analysis.

(1) $y=(x_0-x)\cot\psi-r_s-h$ (5.31a)

where, h is half of the bendplate thickness,

r_s is the radius of the operative side roll.

for the pre-active side roll movement.

(2) $y=(x_0+x)\cot\psi'-r_s-h$ (5.31b)

for the pre-inactive side roll movement.

5.4.8. The general deflection function, W or W(x), of a plate for single and first pass bending

The deflection function of a plate being bent is important

in determining the contacts of the rolls with the bendplate. Subsequently, it provides a means to evaluate the bending arms about the top roll contact, and the force components applied by the nominated operative side roll.

The appropriate approach to determine the deflection function of a plate is to use the relevant modified governing equation (expression 2.3 in Chapter two) for large deflections [89,105,108]. However, the use of (2.3) generates partial differential equations which are difficult to solve, and it is therefore assumed that the normal biharmonic equation for plate bending will represent the deflection profile of the present case.

The biharmonic equation for the deflection of a thin plate in two dimensional bending, uniformly loaded over its upper surface, is as follows [108].

$$\partial^4 w/\partial x^4 + 2\partial^4 w/\partial x^2 \partial y^2 + \partial^4 w/\partial y^4 = -q/D \qquad (5.32a)$$

where, W is the deflection function normal to the plate.

q is the load per unit area on the plate.

D is the flexural rigidity of the plate.

x is in the longitudinal direction of the plate.

y is in the width direction of the plate.

Since there is no load on the plate surface from the top roll contact to the side roll contacts, the r.h.s. of equation (5.32a) is therefore zero . Additionally, since the finished product from the roller bending process is cylindrical, it is therefore assumed that there is no deflection along the plate width, i.e. W is independent of y. Equation (5.32a) can thus be simplified as follows.

$$d^4 w(x)/dx^4 = 0 \qquad (5.32b)$$

The expressions of the first, second, third and fourth

integrations of (5.32a) are

$$d^3w(x)/dx^3 = a \qquad (5.32c)$$

$$d^2w(x)/dx^2 = ax + b \qquad (5.32d)$$

$$dw(x)/dx = ax^2/2 + bx + c \qquad (5.32e)$$

and

$$w(x) = ax^3/6 + bx^2/2 + cx + d \qquad (5.32f)$$

In (5.32f), **a**, **b**, **c** and **d** are certain parametric functions which can be determined by various assumed geometrical boundary conditions in the roller plate bending process.

The respective parametric functions in (5.32f) vary, depending upon the operative modes, as described in section 5.2, and their relative anticipated boundary conditions for thin plate bending.

5.4.9. General deflection function of a plate for second and subsequent pass (multipass) bending

The multipass operation greatly complicates the mathematical analysis (section 5.4.5). However, the fundamental analysis for their deflection function is similar to the first pass operation. One difference is the initial geometric function of the bender prior to the execution of the bending operation (fig 5.24). Another difference is the anticipated geometrical boundary conditions, at the nominal contacts, of the plate (comparing figs 5.20 and 5.23 with figs 5.25 and 5.27, respectively).

5.4.9.1. Initial geometrical function of the bendplate

After the first pass bending, the bendplate, excluding its straight end, has an initial radius of curvature r_f. When the bendplate is gripped in the bender, its initial deflection

profile is that of the previous pass and, with respect to the defined co-ordinate (Note that in fig 5.24 - y in the figure is replaced by W in the following analysis) forms a sector defined by :

$$x^2+(w-r_f)^2 = r_f^2 \qquad (5.33a)$$

It can be re-arranged to give

$$w= r_f-\sqrt{(r_f^2-x^2)} \qquad (5.33b)$$

for $w \leq r_f$

and

$$w= r_f+\sqrt{(r_f^2-x^2)} \qquad (5.33c)$$

for $w > r_f$

respectively.

The initial deflection function of the bendplate is required for obtaining :
(1) The deflection function of the bendplate as bending proceeds, so as to evaluate the nominal roller contacts with the central plane of the plate, and subsequently to determine the bending forces, torques and powers etc.,
(2) the initial nominal contact of the operative side roll prior to the bending operation.

The nominal roll contact of a plate depends upon the initial setting of :

(a) the initial bending arms, i.e. X_0 and $-X_0$ in figs 5.1 and 5.13B,

and

(b) the positional powering angle, ψ and $-\psi$ ($=\psi''$) in figs 5.1 and 5.13B, of the operative side roll,

for a particular four-roll bender. However, the value of W

(or y) is less than the positional co-ordinate of O_i (see fig 5.24) for most bending operations. Consequently, (5.33b) is taken as the initial deflection profile of the plate.

If the initial deflection profile of the plate is W_0, i.e. $W=W_0$, (5.33b) can be written as :

$$W_0 = r_f-\sqrt{(r_f^2-x^2)} \qquad (5.33d)$$

5.4.9.2. General deflection function for the multipass bending mode

To analyse the multipass deflection of a plate, it may be assumed that the following biharmonic equation [104,108] for an initially curved plate is also applicable to the problem.

$$\partial^4(w-w_0)/\partial x^4+2\partial^4(w-w_0)/\partial x^2\partial y^2+\partial^4(w-w_0)/\partial y^4= -q/D \qquad (5.34a)$$

where, q is load per unit area on the plate.

y is along the width of a plate for a specific plate co-ordinate system.

X is along the longitudinal direction of a plate for a specific plate co-ordinate system.

w is the final deflection function of a plate in the bender.

W_0 is initial deflection function of the plate.

This co-ordinate system (X,y,Z) for the plate is different from that used for the co-ordinate system relative to the bender itself.

As mentioned previously, the profile of the anticipated plate product is independent of its width direction. Additionally, there is no load on the plate. It therefore

leads to the simplification of the biharmonic equation (5.34a) giving the following expression.

$$\partial^4(w-w_0)/\partial x^4=0 \qquad (5.34b)$$

Since the general solution of (5.34b) is in the following form,

$$w-w_0=ax^3/6+bx^2/2+cx+d \qquad (5.34c)$$

the substitution of (5.33d) into (5.34c) gives

$$w=ax^3/6+bx^2/2+cx+d+r_f-\sqrt{(r_f^2-x^2)} \qquad (5.34d)$$

The expression (5.34d) is the general deflection function for the multipass bending mode, and **a**, **b**, **c** and **d** are its respective parametric functions. Like the first and single pass bending operation, its parametric function is different for each operational condition, and each is normally evaluated by considering the anticipated boundary conditions for each operation. These will be illustrated in section 5.6.

5.4.10. Summary of the above analyses

The analysis so far is applicable to both pre-bending and continuous bending operations, especially those in sections 5.4.3 to 5.4.7. Though the general deflection functions derived in sections 5.4.8 and 5.4.9 are also applicable to both bending operations, their corresponding parametric functions are different for each operational boundary condition and for either bending operation.

5.4.11 Determination of the torques and powers required for continuous bending

Continuous bending is performed upon completion of pre-bending. Normally, continuous bending modes can be carried out either utilizing the pre-bending active side roll (henceforth referred to as pre-active side roll) or the

pre-inactive side roll, to continue the bending after the pre-bending mode. Nevertheless, either case requires the pre-inactive side roll to complete the bend (section 5.2).

The following section analyses the driving torque and the power required for the continuous bending modes.

5.4.11.1. Continuous bending with the pre-active side roll operative

Continuous bending may also be considered as part of the pre-bending operation when it is required to achieve a uniform bent length (to cover a longitudinal distance), from the vertical plane through the axes of the side roll, i.e. $C_t'C_s'$ in figure 5.9(b). In the following analysis, this is classified as "continuous bending with the pre-active side roll operating mode".

Initially the transportation of the plate through the pinch is carried out under the load system as analysed in section 5.4.6. Here, as the plate is being transported through the pinch, until the end of the straight edge is at the original bottom roll contact, its contact begins to shift due to the changing curvature of the rolled plate.

Generally, at any particular instant, the deformed plate at the outlet of the bottom roll contact is expected to retain a radius of curvature, r_f (which is the previous pass finished bend radius), neglecting the gravitational effect (see section 5.3 in Chapter five).

In order to analyse the problem, it is necessary to clarify the bending stages as follows :

(1) The commencement of the transportation of the plate.

(2) The continuation of the transportation of the plate whilst

the bending process of the initial straight edge is being completed.

(3) The steady continuous bending of the plate after the bending of the straight end edge has been completed.

Normally, in these first two stages there is a detectable shift of the plate of the bottom contact, although the position of the pre-active side roll remains in its initial pre-bending state. It is envisaged that the steady continuous state will only be achieved once stage (3) is reached.

Due to the transitional operation in stages (1) and (2), a complete physical mechanism for the bending process appears to be rather complicated. Detailed analysis of the problem is difficult. Various approaches to the analysis are thus simplified as follows.

(a) To evaluate the transitional torque required for starting continuous bending, i,e, stage (1).

(b) To evaluate the torque required in the continuous bending as it reaches a steady state, i.e. stage (3).

Stage (2) above will be ignored for the present analysis because it involves a complicated transient analysis. However it is assumed that the corresponding values for the particular stage lie between those in stages (1) and (3).

A. General expressions for the driving torque and power for the various bending modes

Since the plate deflection functions can be suitably generalised by expressions (5.32f) (for the first and single pass bending) and (5.34d) (for the second and subsequent pass bending) for either stage, the relevant driving torque and power can also be expressed in general form as derived in the following sub-sections.

B. General expression for the external bending moment about any cross-section X away from the origin in the effective deformation zone

The assumed simplification that the external bending moment (see figs 5.18 and 5.19) in the effective deformation zone is a linear distribution (see fig 5.9) facilitates the evaluation of its value, M_x, at any cross section $X=X_{xn}$ from the origin. Referring to figs 5.9, 5.18 and 5.19, at equilibrium M_x can be expressed as follows :

$$M_x=F_s\cos\beta\{(w_{cn}-w_{xn})\sin\theta_s+(x_{cn}-x_{xn})\cos\theta_s\} \qquad (5.35a)$$

at any cross-section between the top roll contact and the bottom roll contact.

and

$$M_x=F_b\{(w_{xn}+w_{bn})\sin\theta_b+(x_{xn}+x_{bn})\cos\theta_b\} \qquad (5.35b)$$

at any cross section between the top roll contact and the bottom roll contact.

In the above two expressions, W_{xn} is the deflection along the plate's central surface at $X=X_{xn}$.

The substitution of the relevant expressions for F_s and F_b from section 5.4.6. in this appendix gives :

(i) For the effective deformation zone between operative side roll and top roll contacts.

$$M_x=\left\{\left(b([2R^2(1-\nu^2)^2\sigma_0{}^3/3E^2(1-\nu+\nu^2)^{3/2}]+B)\cos\beta\right)/[(w_{cn}-w_{tn})\theta_s\right.$$

$$\left.+(x_{cn}-x_{tn})]\right\}\left((w_{cn}-w_{xn})\tan\theta_s+(x_{cn}-x_{xn})\right) \qquad (5.35c)$$

for the single and first pass bending mode.

and

$$M_x=\{[b(A_1+A_2)\cos\beta]/[(w_{cn}-w_{tn})\tan\theta_s+(x_{cn}-x_{tn})]\}\{(w_{cn}-w_{xn})\tan\theta_s+(x_{cn}-x_{xn})\} \quad (5.35d)$$

for the second and subsequent pass bending mode.

(ii) For the cross-section between the top roll and bottom roll contacts :-

$$M_x=\left\{b([2R^2(1-\nu^2)^2\sigma_0{}^3/3E^2(1-\nu+\nu^2)^{3/2}]+B)/[(w_{tn}+w_{bn})\tan\theta_b+(x_{tn}+x_{bn})]\right\}\left((w_{xn}+w_{bn})\tan\theta_b+(x_{xn}+x_{bn})\right) \quad (5.35e)$$

for the single and first pass bending mode.

and

$$M_x=\{[b(A_1+A_2)]/[(w_{tn}+w_{bn})\tan\theta_b+(x_{tn}+x_{bn})]\}\{(w_{xn}+w_{bn})\tan\theta_b+(x_{xn}+x_{bn})\} \quad (5.35f)$$

for the second and subsequent pass bending mode.

C. The work done, W, required to start the transportation of plate

Noting that the deformation mechanism in conveying the plate is as shown in item (1) in section 5.2 (fig 5.4), the initiation of the plate movement through the pinch, at any instant, requires an amount of work done equal to the work to produce the effective deformation zone, i.e. $C_tC_aC_sC_bC_t$ (fig 5.4).

The work done, W, to deform the effective zone (between the

top roll and operative side roll contacts) may be expressed as follows.

$$W = \int_{\theta} M_x d\theta \qquad (5.36a)$$

where, $d\theta$ is the change of the rotational angle of the plate in bending.

Basically, $d\theta$ can be rewritten as

(1) dx/R for the single and first pass bending mode, and

(2) $[(1/R)-(1/r_f)]dx$ for the second and subsequent pass bending mode.

where R is the instantaneous local bend radius of curvature, r_f is the initial radius of curvature of the plate, dx is the longitudinal length of an element (i.e. E_e in fig 5.13A and 5.16). Consequently, the expression (5.36a) can be re-expressed as follows :

$$W = \int_{x} M_x dx/R \qquad (5.36b)$$

for the single and first pass bending mode.

and

$$W = \int_{x} M_x[(1/R)-(1/r_f)]dx \qquad (5.36c)$$

for the second and subsequent pass bending mode.

Mathematically, the instantaneous local bend radius R can be related to the respective deflection function, $W=W(X)$, of (5.32f) and (5.34d) as follows.

$$1/R = d^2w(x)/dx^2 \qquad (5.36d)$$

The initial plate radius r_f can be related to the initial

deflection function, $W_0(x)$, as follows.

$$1/r_f = d^2w_0(x)/dx^2 \qquad (5.36e)$$

The relationship between the expression (5.32f), (5.34d) and (5.36b) to (5.36e), and in addition to the respective bending moment expressions, enables the following expressions to replace (5.36b) and (5.36c).

$$W = A\int_x (ax+b)G(x)dx \qquad (5.36f)$$

where,

$$A=\left\{b\left([2R^2(1-\nu^2)^2\sigma_0{}^3/3E^2(1-\nu+\nu^2)^{3/2}]+B\right)\cos\beta\right\}/[(W_{cn}-W_{tn})\tan\theta_s + (x_{cn}-x_{tb})] \qquad (5.36g)$$

and

$$G(x)=[w_{cn}-(ax^3/6+bx^2/2+cx+d)]\tan\theta_s+(x_{cn}-x) \qquad (5.36h)$$

for the single and first pass bending mode.

and,

$$A=b(A_1+A_2)\cos\beta/[(w_{cn}-w_{tn})\tan\theta_s+(x_{cn}-x_{tn})] \qquad (5.36i)$$

and

$$G(x)=\{w_{cn}-[ax^3/6+bx^2/2+cx+d+r_f-(r_f^2-x^2)^{1/2}]\}\tan\theta_s+(x_{cn}-x) \qquad (5.36j)$$

for the second and subsequent pass bending mode, respectively.

Subsequently, the integral in expression (5.36f) generates the following results.

$$W=A\{(a/6)[\tan\theta_s(-ax^5/5-bx^4-2(c+1)x^3+3(w_{cn}-d+x_{cn})x^2)-2x^3+3x_{cn}]$$

$$+(b/6)[\tan\theta_s(-bx^3-3(c+1)x^2+6(w_{cn}-d-x_{cn})x)-3x^2+6x_{cn}]+B_a\}$$

(5.37a)

where B_a is a constant,

for the single and first pass bending mode.
and,

$$W=A\{(a/6)[\tan\theta_s(-ax^5/5-bx^4-2(c+1)x^3+3(x_{cn}+w_{cn}-d-r_f)x^2$$
$$-2r_f^3[1-(x/r_f)^2]^{3/2})-2x^3+3x_{cn}x^2]+(b/6)[\tan\theta_s(-bx^3-3(c+1)x^2$$
$$+3r_f^2[\sin^{-1}(x/r_f)+(x/r_f)[1-(x/r_f)^2]^{1/2}])+6(w_{cn}+x_{cn}-d-r_f)x]\}$$
$$+B_b \qquad (5.37b)$$

where B_b is an integral constant,

for the second and subsequent pass (multipass) bending mode, respectively.

(5.37a) and (5.37b) are the general expressions for the respective bending mode. Any particular operation for each individual bending mode only alters the parametric functions of **a**, **b**, **c** and **d**, which can normally be evaluated by considering the anticipated boundary conditions of the operation.

D. The general expressions for the relative driving torque

If N is the rotational speed of the top roll and T is the driving torque, the power required to drive the plate is :

Driving power (P) = Driving torque (T) x Conveying speed (V)

that is :

$$P=2\pi NT/60 \qquad (5.38a)$$

where N is the number of rotations of the top roll per

minute.

If the total effective bending length of the bendplate is l_b, the total energy E_{ab} absorbed in bending may be expressed as :

$$E_{ab} = W l_b \qquad (5.38b)$$

Since the power, P, required to drive the plate can be formulated as :

P= [Total work done to deform a plate length (l_b)] / [Time (t) taken to bend a plate length (l_b)]

$$= E_{ab}/t \qquad (5.38c)$$

The time, t, for bending can be found from the equation (5.38d)

t = Bent length transported (l_b) /Transporting velocity (V)

(5.38d)

Assuming there is no slip between the top roll and the bendplate during the transportation of the plate through the pinch, V is therefore equal to the surface velocity of the top roll. Subsequently, the velocity can be stated as :

$$V = 2\pi r_t N/60 \qquad (5.38e)$$

Substituting (5.38e) into (5.38d) leads to

$$t = (60) l_b / 2\pi r_t N \qquad (5.38f)$$

The power required to deform a plate over a length l_b, i.e. (5.38c), can therefore be re-expressed as :

$$P = 2\pi r_t N W l_b / (60) l_b = 2\pi r_t N W/60 \qquad (5.38g)$$

Equating (5.38g) with (5.38a) leads to the driving torque, T, given by:

$$T = W r_t \qquad (5.38h)$$

The appropriate substitution of expressions (5.36g) and (5.37a), and (5.36i) and (5.37b) into (5.38h) gives the corresponding driving torque for the single/first pass bending mode, and for the second/subsequent pass bending mode, respectively.

5.4.11.2. Continuous bending with the pre-inactive side roll operative

Generally, the approach of the analysis is similar to that in sub-section 5.4.11.1. The only difference is in the denominator of the bending moment in the expressions (5.35c) to (5.35f), (5.36g), (5.36i), (5.37a) and (5.37b). However, the general form of the other expressions still holds for the operative mode. The following sub-sections details them.

A. The external bending moment about any cross section between the bottom and operative side roll contacts

The assumed effective deformation occurs in the region between the bottom and top roll contacts and allows the following general expression to be obtained.

$$M_x=F_b[(w_{tn}-w_{xn})\sin\theta_b'+(x_{tn}+x_{xn})\cos\theta_b'] \qquad (5.39a)$$

for the particular progressively deformed deformation zone. and

$$M_x=F_s\cos\beta[(w_{cn}-w_{xn})\sin\theta_s'+(x_{cn}+x_{xn})\cos\theta_s'] \qquad (5.39b)$$

for the spring back deformation zone between the top and operative side roll contacts.

Generally, the specific co-ordinate system gives a negative value for x_{xn}.

The substitution of the relevant expressions for the

bending forces on either the bottom and the operative side roll gives :

(i) The moment for the effective deformation zone between the bottom and top roll contacts-

$$M_x=\{b([2R^2(1-\nu^2)^2\sigma_0{}^3/3E^2(1-\nu+\nu^2)^{3/2}]+B)/[(w_{tn}+w_{bn})\tan\theta_b' +(x_{tn}+x_{bn})]\}[(w_{tn}-w_{xn})\tan\theta_b'+(x_{tn}+x_{xn})] \quad (5.39c)$$

for the single and first pass bending mode.

and

$$M_x=\{b(A_1+A_2)/[(w_{tn}+w_{bn})\tan\theta_b'+(x_{tn}+x_{bn})]\}/[(w_{tn}-w_{xn})\tan\theta_b' +(x_{tn}+x_{xn})] \quad (5.39d)$$

for the second and subsequent pass bending mode.

(ii) The moment for the progressive spring back region between the top and operative side roll contacts -

$$M_x=\{b([2R^2(1-\nu^2)^2\sigma_0{}^3/3E^2(1-\nu+\nu^2)^{3/2}]+B)'\cos\beta/[(w_{cn}-w_{tn})\tan\theta_s' +(x_{cn}-x_{tn})]\}[(w_{cn}-w_{xn})\tan\theta_s'+(x_{cn}+x_{xn})] \quad (5.39e)$$

for the single and first pass bending mode.

and

$$M_x=\{b(A_1+A_2)\cos\beta/[(w_{cn}-w_{tn})\tan\theta_s'+(x_{cn}-x_{tn})]\}[(w_{cn}-w_{xn})\tan\theta_s' +(x_{cn}+x_{xn})] \quad (5.39f)$$

for the second and subsequent pass bending mode.

B. Work done, W, required to commence continuous bending of the plate

Let

$$A=\{b[2R^2(1-\nu^2)^2\sigma_0{}^3/3E^2(1-\nu+\nu^2)^{3/2}]+B\}/[(w_{tn}+w_{bn})\tan\theta s +(x_{tn}+x_{bn})] \quad (5.40a)$$

and

$$G(x)=(ax^3/6+bx^2/2+cx+d-w_{tn})\tan\theta_b+(x-x_{tn}) \quad (5.40b)$$

for the single and first pass bending mode in the progressively deformed deformation zone.

and,

$$A=b(A_1+A_2)/[(w_{tn}+w_{bn})\tan\theta_b+(x_{tn}+x_{bn})] \quad (5.40c)$$

and

$$G(x)=[ax^3/6+bx^2/2+cx+d+r_f-(r_f^2-x^2)^{1/2}-w_{tn}]\tan\theta_b+(x-x_{tn}) \quad (5.40d)$$

for the second and subsequent pass bending mode in the progressively deformed deformation zone, between the bottom and top roll contacts.

It therefore leads to the following expression for the deformation work, W_0, as :

$$W_0=A\{(a/6)(\tan\theta_b[ax^5/5+bx^4+2cx^3+3(d-w_{tn})x^2]+2x^3-3x_{tn}x^2) +(b/6)(\tan\theta_b[bx^3+3cx^2+6(d-w_{tn})x]+3x^2-6x_{tn}x)\}+B_c \quad (5.40e)$$

for the single and first pass bending mode.

and

$$W_0=(A/6)\{a(\tan\theta_b[ax^5/5+bx^4+2cx^3+3(d+r_f-w_{tn})x^2+2r_f^3[1-(x/r_f)^2]^{3/2}] +2x^3-3x_{tn}x^2)+b(\tan\theta_b[bx^3+3cx^2-3r_f^2\{\sin^{-1}(x/r_f)+(x/r_f)[1-(x/r_f)^2]^{1/2}+ 6(d+r_f-w_{tn})x\}-3x^2-6x_{tn}x)\}+B_d \quad (5.40f)$$

for the second and subsequent pass bending mode.

In which B_c and B_d are integral constants.

The total deformed energy, W_s, remaining in the

progressively sprung back deformation zone can be obtained as follows.

Let

$$A_0=\{b([2R^2(1-\nu^2)^2\sigma_0{}^3/3E^2(1-\nu+\nu^2)^{3/2}]+B)\cos\beta/[(w_{tn}-w_{cn})\tan\theta_s" +(x_{tn}-x_{cn})] \quad (5.40g)$$

and

$$G_0(x)=[ax^3/6+bx^2/2+cx+d-w_{cn}]\tan\theta_s"+(x-x_{cn}) \quad (5.40h)$$

for the single and first pass bending mode.

and

$$A_0=b(A_1+A_2)\cos\beta/[(w_{tn}-w_{cn})\tan\theta_s"+(x_{tn}-x_{cn})] \quad (5.40i)$$

and

$$G_0(x)=[ax^3/6+bx^2/2+cx+d+r_f-(r_f^2-x^2)^{1/2}-w_{cn}]\tan\theta_s"+(x-x_{cn}) \quad (5.40j)$$

for the second and subsequent pass bending mode.

The result of the following integral

$$W_s=A_0\int [(1/R_x)-(1/r_f)]G_0(x)dx=A_0\int (ax+b)G_0(x)dx \quad (5.40k)$$

gives the general expressions for the total retained plastic deformation work (or energy), in the progressive spring back deformation zone, similar to those of (5.40e) and (5.40f) respectively. It is necessary to replace A, w_{tn}, x_{tn} and the integral constants by A_0, w_{cn}, x_{cn} and B_e (and B_f) respectively. Subsequently, the total energy, W_t, contained in the two effective deformation zones can be represented by :

$$W_t=W_0+W_s \quad (5.40l)$$

In which W_0 is taken over the contact surface between the

bottom and top rolls, and W_s is taken over the contact surface between the top and pre-inactive side rolls.

C. Driving torque and power on the top roll

The general expressions, i.e. (5.38g) and (5.38h), apply to the bending modes by suitably substituting the expression (5.401) evaluated for each bending mode.

5.4.11.3. Summary of the analyses

The above analysis gives the general approach. To quantitate a particular bending mode requires determining the respective parametric functions, i.e. **a**, **b**, **c** and **d**, in the corresponding general deflection function. The deflection function can normally be established by appropriately considering the anticipated boundary conditions of a bendplate, under its equilibrium loading boundary condition. Examples for these will be summarised in the following section (section 5.4.13).

5.4.12. Determination of the general deflection function and the nominal contacts between the rolls and the plate central plane

Prior to the determination of the respective parametric functions, i.e. **a**, **b**, **c** and **d**, it is useful to define the co-ordinate circles of each roll in the adopted co-ordinate system of the bender.

5.4.12.1. Positional circle equations of the rolls

As previously mentioned (section 5.4.3), the prime concern of the present research is to understand the mechanics of the roller bending of plates. Due to the geometry of the finished

products, it is possible to assume the the bending is independent of the plate width. It thus simplifies the theorectical analysis, and the co-ordinates of the rollers can suitably be represented by the circle equations as shown in the following sub-sections.

A. Positional circle equation of the top roll

Since the translational movement of the top roll is permanently prevented, its nominal positional circle (see fig 5.22) is expressed as follows

$$x^2+(w-r_t-h)^2=(r_t+h)^2$$

(5.41a(i))

Which can be written as :

$$x^2+w^2-2(r_t+h)w=0$$

(5.41a(ii))

Its first derivative is in the following form :

$$dw/dx= -x/(w-r_t-h) \qquad (5.41b(i))$$

From (5.41a(i)), the value of W can be expressed as :

$$w=(r_t+h) \pm [(r_t+h)^2-x^2]^{1/2} \qquad (5.41b(ii))$$

Normally, the top roll contact occurs around the bottom half of the top roll, i.e. W is generally less than (r_t+h), consequently the negative root of the second term at the r.h.s. is taken, giving expression (5.41b(i)) as :

$$dw/dx=x/[(r_t+h)^2-x^2]^{1/2} \qquad (5.41b(iii))$$

B. Positional circle equation of the bottom pinch roll

The nominal circle (see fig 5.22) equation of the pinch roll, relative to the origin of the chosen co-ordinate system (fig 5.13B), with the X-axis along the central plane of the initially flat plate as it is being gripped by the bender, can

be expressed as follows :

(i) For no displacement of the centre of the roll

$$x^2+(w+r_b+h)^2=(r_b+h)^2 \qquad (5.41c(i))$$

which can be further written as :

$$x^2+w^2+2(r_b+h)w=0 \qquad (5.41c(ii))$$

Its first derivative is :

$$dw/dx= -x/(w+r_b+h) \qquad (5.41c(iii))$$

Also (5.41c(i)) gives

$$w= [(r_b+h)^2-x^2]^{1/2}-r_b-h \qquad (5.41c(iv))$$

Since the bottom roll contact is on its top half surface, the positive root of the first term at the r.h.s. is thus taken. It therefore leads (5.41(iii)) to be expressed as

$$dw/dx= -x/[(r_b+h)^2-x^2]^{1/2} \qquad (5.41c(v))$$

(ii) For displacement of W_d of the centre for the bottom roll

$$x^2+(w+w_d+r_b+h)^2=(r_b+h)^2 \qquad (5.41d(i))$$

which can be re-written as

$$x^2+(w+w_d)^2+2(r_b+h)(w+w_d)=0 \qquad (5.41d(ii))$$

Its first derivative is

$$dw/dx= -x/(w+w_d+r_d+h) \qquad (5.41d(iii))$$

Since there is no displacement of the centre of the bottom roll, the substitution of the appropriate root for W gives

$$dw/dx= -x/[(r_b+h)^2-x^2]^{1/2} \qquad (5.41d(iv))$$

which is identical to (5.41c(v)).

C. Positional equation of the operative side rolls

Since the operative (i.e. either the pre-active or the

pre-inactive) side roll is floating as pre-bending proceeds, the positional circle equations can not be clearly defined. However, their instantaneous positional circle can be obtained as follows.

Let (X_s,W_s) be the instantaneous centre of the operative side roll (see figs 5.17, 5.22 and 5.27), this therefore leads to the following positional circle to be written as :

$$(x-x_s)^2+(w-w_s)^2=(r_s+h)^2 \qquad (5.41e(i))$$

Its first derivative is

$$dw/dx= (x_s-x)/(w-w_s) \qquad (5.41e(ii))$$

Since contact with the operative side roll is mostly on the top half of the roller, W can thus be expressed as :

$$w=w_s+[(r_s+h)^2-(x-x_s)^2]^{1/2} \qquad (5.41e(iii))$$

Subsequently, (5.41e(ii)) becomes

$$dw/dx=(x_s-x)/[(r_s+h)^2-(x-x_s)^2]^{1/2} \qquad (5.41e(iv))$$

5.4.12.2. Determination of the parametric functions in the general deflection functions

The general assumed geometrical boundary conditions for each particular operation are shown in figs 5.20 to 5.27. It can be observed that assumed boundary conditions are common for at least several operations. In order to shorten the presentation of the text, the parametric functions are obtained by considering only the more common geometrical boundary conditions.

A. The more complete general deflection function of a plate during first and single pass bending

(a) General function for the pre-active side roll

operative mode

(1) The common general geometrical boundary conditions

Referring to figs 5.20 (for pre-bending mode) and figures 5.21(for the continuous bending mode), the following common boundary conditions can be generalized.

(i) At the nominal contact of the pre-active side roll, i.e. $X=X_{cn}$, the bending curvature, $1/R_c$, and the deflection of the bendplate are given by :

$$1/R_c=d^2w/dx^2=0 \qquad (5.41f)$$

and

$$w=w_{cn}=y_{cn} \qquad (5.41g)$$

respectively.

(ii) At the nominal contact of the top pinch roll, i.e. $X=X_{tn}$, the bending curvature, $1/R_t$, and the respective tangent of the bent plate are

$$1/R_t=d^2w/dx^2=1/r_f+M_i/EI \qquad (5.41h)$$

and

$$\tan\theta_t=dw/dx= x_t/[(r_t+h)^2-x_{tn}^2]^{1/2} \qquad (5.41i)$$

respectively.

The slope expression (5.41i) has been obtained by considering that the tangent of the deflected plate has to equal that of the nominal circle of the top roll (refer to expression (5.41b(iii)) at contact.

(2) Parametric functions

The consideration of expressions (5.32d) and the boundary

conditions of (5.41f) and (5.41h) gives the general parametric functions of **a** and **b** expressed as :

$$\mathbf{a}= 1/[r_t(x_{tn}-x_{cn})] \qquad (5.42a)$$

and

$$\mathbf{b}= -x_{cn}/[R_t(x_{tn}-x_{cn})] \qquad (5.42b)$$

respectively.

The consideration of (5.32e) and the boundary condition of (5.41i) gives:

$$\mathbf{c}= x_{tn}/[(r_t+h)^2-x_{tn}^2]^{1/2}-ax_{tn}(x_{tn}-2x_{cn})/2 \qquad (5.42c)$$

The consideration of (5.32f) and the boundary condition of (5.41g) gives :

$$\mathbf{d}=w_{cn}+(ax_{cn}/6)[2x_{cn}^2+3x_{tn}(x_{tn}-2x_{cn})]-x_{tn}x_{cn}/[(r_t+h)^2-x_{tn}^2)]^{1/2} \qquad (5.42d)$$

(3) The common general deflection function for the bending mode

Substituting the above parametric functions, **a**, **b**, **c** and **d** into the general deflection function (5.32f) and re-arranging gives, for the particular operational mode, the common deflection function :

$$w=[1/6R_t(x_{tn}-x_{cn})]\{x^3-x_{cn}(3x^2-2x_{cn}^2)-3x_{tn}(x_{tn}-2x_{cn})(x-x_{cn})\}$$
$$+x_{tn}(x-x_{cn})/[(r_{tn}+h)^2-x_{tn}^2]^{1/2}+w_{cn} \qquad (5.43)$$

(b) The general function for the pre-inactive side roll operative

(1) The common general geometrical boundary conditions

Referring to fig 5.23, the following common boundary conditions can be generalized.

(i) At the nominal contact of the pre-active side roll, i.e. $X=-X_{cn}$, the bending curvature, $1/R_c$, and the deflection of the bendplate are related by :

$$1/R_c= d^2w/dx^2=1/r_f \qquad (5.44a)$$

and

$$W=W_{cn}=y_{cn} \qquad (5.44b)$$

respectively.

(ii) At the nominal contact of the top pinch roll, i.e. $X=-X_{tn}$, the bending curvature, $1/R_t$, and the respective tangent of the bendplate are related by :

$$1/R_t=d^2w/dx^2=1/r_f+M_i/EI \qquad (5.44c)$$

and

$$\tan\theta_t=dw/dx= -x_{tn}/[(r_t+h)^2-x_{tn}^2]^{1/2} \qquad (5.44d)$$

respectively.

(2) The common parametric function

Consideration of the expression (5.32d) and the boundary conditions of (5.44a) and (5.44c) gives :

$$a= [1/(x_{cn}-x_{tn})][(1/R_t)-(1/r_f)] \qquad (5.44e)$$

and

$$b=[1/(x_{cn}-x_{tn})](x_{cn}/R_t-x_{tn}/r_f) \qquad (5.44f)$$

Likewise the expression (5.32e) and the boundary condition of (5.44d) gives :

$$c=[1/(x_{cn}-x_{tn})]\{(x_{cn}/R_t-x_{tn}/r_f)-(1/R_t-1/r_f)(x_{tn}^2/2)\}$$
$$-x_{tn}/[(r_t+h)^2-x_{tn}^2]^{1/2} \qquad (5.44g)$$

and the expression (5.32f) and boundary condition of (5.44b) gives :

$$d=w_{cn}+[1/(x_{cn}-x_{tn})][(x_{cn}/6)(x_{cn}^2+x_{tn}^2)(1/R_t-1/r_f) -(x_{cn}/2)(x_{cn}+2x_{tn})(x_{cn}/R_t-x_{tn}/r_f)]-x_{tn}/[(r_t+h)^2-x_{tn}^2]^{1/2} \quad (5.44h)$$

(3) The general complete deflection function

After the evaluation of the relevant parametric function, a more common complete deflection function for the operational mode can be obtained by substituting (5.44e) to (5.44h) into (5.32f). The following gives the function after appropriate re-arrangement.

$$w=[1/(x_{cn}-x_{tn})]\{(1/R_t-1/r_f)[x^3/6-x_{tn}^2x/2+(x_{cn}/6)(x_{cn}^2+3x_{tn}^2)] +(x_{cn}/R_t-x_{tn}/r_f)[x^2/2+x_{tn}x-(x_{cn}/2)(x_{cn}+2x_{tn})]\} +x_{tn}(x_{cn}-x)/[(r_t+h)^2-x_{tn}^2]^{1/2}+w_{cn} \quad (5.45)$$

B. The more complete general deflection function of an plate for second and subsequent pass bending (multipass bending)

(a) The general function for the pre-active side roll operative mode

(1) The common general geometrical boundary conditions

Referring to figs 5.25 and 5.26, the following common boundary conditions can be expected.

(i) At the nominal contact of the pre-active side roll, i.e. $X=X_{cn}$, the bending curvature, $1/R_c$, and the deflection of the bendplate are related by :

$$1/R_c=d^2w/dx^2=1/r_f \qquad (5.46a)$$

where, r_f is the finished bend radius of the previous bend of the bendplate.

and

$$w=w_{cn}=y_{cn} \qquad (5.46b)$$

respectively.

(ii) At the nominal contact of the top pinch roll, i.e. $x=x_{tn}$, the bending curvature, $1/R_t$, and the respective tangent of the bendplate are related by :

$$1/R_t=d^2w/dx^2=1/r_{ff}+M_i/EI \qquad (5.46c)$$

where, r_{ff} is the expected finished bend radius of the bendplate after the completion of the bending pass.

and

$$\tan\theta_t=dw/dx= x_{tn}/[(r_t+h)^2-x_{tn}^2]^{1/2} \qquad (5.46d)$$

respectively.

(2) The general parametric functions within the deflection function

Consideration of the second derivative of (5.34d) and the boundary conditions of (5.46a) abd (5,46c) gives :

$$a=[1/(x_{cn}-x_{tn})][(1/r_f-1/R_t)-x_{cn}^2/(r_f^2-x_{cn}^2)^{3/2}+x_{tn}^2/(r_f^2-x_{tn}^2)^{3/2} -1/(r_f^2-x_{cn}^2)^{1/2}+1/(r_f^2-x_{tn}^2)^{1/2}] \qquad (5.47a)$$

and

$$b=[1/(x_{cn}-x_{tn})][x_{cn}/R_t-x_{tn}/r_f-x_{cn}^2x_{tn}/(r_f^2-x_{cn}^2)^{3/2} +x_{cn}x_{tn}^2/(r_f^2-x_{tn}^2)^{3/2}-x_{tn}/(r_f^2-x_{cn}^2)^{1/2}+x_{cn}/(r_f^2-x_{tn}^2)^{1/2}]$$

(5.47b)

Likewise the first derivative of (5.34d) and the boundary condition of (5.46d) gives **c** in terms of **a** and **b** etc. as follows.

$$\mathbf{c}= -\mathbf{a}x_{tn}^2/2-\mathbf{b}x_{tn} \qquad (5.47c)$$

Also the first derivative of (5.34d) and the boundary condition of (5.46c) gives an expression, for **d** in terms of **a** and **b** etc., as follows.

$$\mathbf{d}=w_{cn}-(\mathbf{a}x_{cn}/6)(x_{cn}^2-3x_{tn}^2)-(\mathbf{b}x_{cn}/2)(x_{cn}-2x_{tn})-r_f+(r_f^2-x_{cn}^2)^{1/2} \qquad (5.47d)$$

(3) The common general deflection function for the operation

The substitution of (5.47a) to (5.47d) into (5.34d) will give, as before, the common deflection function. It is simplified, in terms of **a** and **b** etc., as follows :

$$w=(a/6)[x^3-3x_{tn}^2x-x_{cn}(x_{cn}^2-3x_{tn}^2)]+(b/2)[x^2-2x_{tn}x-x_{cn}(x_{cn}-2x_{tn})]$$
$$+w_{cn}-(r_f^2-x^2)^{1/2}+(r_f^2-x_{cn}^2)^{1/2} \qquad (5.48)$$

Further substitution for **a** and **b** gives the complete common deflection function for the particular operation.

(b) The general function for the pre-inactive side roll operative mode

(1) The common general geometrical boundary conditions

Referring to fig 5.27, the following common boundary conditions can be generalized.

(i) At the nominal contact of the pre-inactive side roll, i.e. $X=-X_{cn}$, the bending curvature, $1/R_c$, and the deflection of the bendplate are related by :

$$1/R_c=d^2w/dx^2=1/r_{ff} \qquad (5.49a)$$

and

$$w=w_{cn}=y_{cn} \qquad (5.49b)$$

respectively.

(ii) At the contact of the top pinch roll, i.e. $X=-X_{tn}$, the bending curvature, $1/R_t$, and the respective tangent of the bent plate are related by :

$$1/R_t=d^2w/dx^2=1/r_{ff}+M_i/EI \qquad (5.49c)$$

and

$$\tan\theta_t=dw/dx= -x_{tn}/[(r_t+h)^2-x_{tn}^2]^{1/2} \qquad (5.49d)$$

respectively.

(2) The general parametric functions within the deflection function

Consideration of the second derivative of (5.34d) and the boundary conditions of (5.49a) and (5.49c) gives :

$$a=[1/(x_{cn}-x_{tn})]\{(1/R_t-1/r_f)+x_{cn}^2/(r_f^2-x_{cn}^2)^{3/2}+1/(r_f^2-x_{cn}^2)^{1/2} -x_{tn}^2/(r_f^2-x_{tn}^2)^{3/2}-1/(r_f^2-x_{tn}^2)^{1/2}\} \qquad (5.50a)$$

and,

$$b=[1/(x_{cn}-x_{tn})]\{x_{cn}/R_t-x_{tn}/r_f+x_{cn}^2x_{tn}/(r_f^2-x_{cn}^2)^{3/2}+x_{tn}/(r_f^2-x_{cn}^2)^{1/2} -x_{cn}x_{tn}^2/(r_f^2-x_{tn}^2)^{3/2}-x_{cn}/(r_f^2-x_{tn}^2)^{1/2}\} \qquad (5.50b)$$

Likewise the first derivative of (5.34d) and the boundary condition of (5.49d) gives an expression for **c**, it terms of **a** and **b** as follows :

$$c = -ax_{tn}^2/2 + bx_{tn} \qquad (5.50c)$$

and (5.34d) and the boundary condition of (5.49b) gives an expression for **d**, in terms of **a** and **b** etc., as follows :

$$d = w_{cn} + (ax_{cn}/6)(x_{cn}^2 - 3x_{tn}^2) - (bx_{cn}/2)(x_{cn} - 2x_{tn}) - r_f + (r_f^2 - x_{cn}^2)^{1/2} \qquad (5.50d)$$

(3) The deflection function for the particular operation

Substituting the respective parametric function into (5.34d) gives the complete common deflection function of the bent plate. However, the following deflection function is only expressed in terms of **a** and **b** etc..

$$w = (a/6)\{x^3 - 3x_{tn}^2 x + x_{cn}(x_{cn}^2 - 3x_{tn}^2)\} + (b/2)\{x^2 + 2x_{tn}x - x_{cn}(x_{cn} - 2x_{tn})\}$$
$$+ (r_f^2 - x_{cn}^2)^{1/2} - (r_f^2 - x^2)^{1/2} + w_{cn} \qquad (5.50d)$$

A more complete deflection function can be obtained by suitable substitution of the expressions for **a** and **b** respectively.

5.4.13. Relationship of the relevant co-ordinates of the roller contacts and the known parameters of the bender

Since the nominal contacts of the rollers with the central plane of a bendplate are preliminarily assumed, the application of the above expressions requires their evaluation before the bending mechanics can be assessed. This can be done by further consideration of the other remaining geometrical boundary conditions (ref to figs 5.20 - 5.27) and the condition of tangency of the bendplate and the positional circles of the rollers, at the nominal contacts. The procedure to obtain the relations is rather tedious and therefore the

relevant relations and boundary conditions are tabulated in Table A5.1 for the following bending operations :

5.4.13.1. First and single pass bending mode

1- With the pre-bending active side roll operative for :
   (a) the pre-bending mode,
   (b) the transitional operation from the pre-bending to the continuous bending mode,
   (c) the steady-continuous bending mode.

2- With the pre-bending inactive side roll operative for :
   (a) the transitional operation to initiate the continuous bending mode,
   (b) the steady-continuous bending mode.

5.4.13.2. Second and subsequent pass bending modes

1- With the pre-bending active side roll operative for :
   (a) the pre-bending mode,
   (b) the transitional operation to initiate the continuous bending mode,
   (c) the steady-continuous bending mode.

2- With the pre-bending inactive side roll operative for :
   (a) the transitional operation to initiate the continuous bending mode,
   (b) the steady-continuous bending mode.

respectively.

For the present analysis, the determination of the co-ordinates of the nominal contacts should be performed by suitably iterating the relations specified in Table A5.1 for the particular operation. The evaluated values are then substituted into the relevant plate deflection function, the expressions for bending forces on the rollers, the expressions

for the top roll driving torque and the relative expression for the driving power etc., to complete the analysis.

Table A5.1 Relationship for the Relevant Co-ordinates Of The Roller Contacts to the known Parameters of Bender Geometry

SINGLE/FIRST PASS BENDING OPERATIONS

A. Pre-active side roll operating mode

1. Common general deflection function for the bending mode

$$w=[1/6R_t(x_{tn}-x_{cn})]\{x^3-x_{cn}(3x^2-2x_{cn}^2)-3x_{tn}(x_{tn}-2x_{cn})(x-x_{cn})\} +x_{tn}(x-x_{cn})/[(r_t+h)^2-x_{tn}^2]^{1/2}+w_{cn} \quad (5.43)$$

and,

$$dw/dx = [1/2R_t(x_{tn}-x_{cn})]\{x^2-2x_{cn}x-x_{tn}(x_{tn}-2x_{cn})\} +x_{tn}/[(r_t+h)^2-x_{tn}^2]^{1/2} \quad (5.43a)$$

$$d^2w/dx^2 = [1/R_t(x_{tn}-x_{cn})](x-x_{cn}) \quad (5.43b)$$

2. Common general relationship (figs 5.20 and 5.21)

Additional common general boundary conditions :

a) ***At top roll nominal contact***

i. $x=x_{tn}$, $w=w_{tn}$

From equations (5.41b(ii)) and (5.43), it gives

$$w_{tn}=(r_t+h)-[(r_t+h)^2-x_{tn}^2]^{1/2} =[1/6R_t(x_{tn}-x_{cn})]\{x_{tn}^3-x_{cn}(3x_{tn}^2-2x_{cn}^2)-3x_{tn}(x_{tn}-2x_{cn})(x_{tn}-x_{cn})\} +x_{tn}(x_{tn}-x_{cn})/[(r_t+h)^2-x_{tn}^2]^{1/2}+w_{cn} \quad (5.43c)$$

in which $1/R_t=1/r_f+M_i/EI$

b) ***At nominal contact of the operative side roll***

i. $x=x_{cn}$, $(dw/dx)_{roller}=(dw/dx)_{plate}$
From equations (5.41e(iv)) and (5.43a), it gives

$$(x_s-x_{cn})/[(r_s+h)^2-(x_{cn}-x_s)^2]^{1/2} = [1/2R_t(x_{tn}-x_{cn})]\{-x_{cn}^2-x_{tn}(x_{tn}-2x_{cn})\}+x_{tn}/[(r_t+h)^2-x_{tn}^2]^{1/2} \quad (5.43d)$$

ii. From equations (5.31a) and (5.41e(iii)), it leads to

$$w_{cn}=y_{cn}=(x_0-x_s)\cot\psi-r_s-h+[(r_s+h)^2-(x_{cn}-x_s)^2]^{1/2} \quad (5.43e)$$

c) ***At bottom roll nominal contact*** (for x_{bn} and w_{bn} are not equal to zero)

i. $x=-x_{bn}$, $w=-w_{bn}$
From equations (5.41c(iv)) and (5.43), it gives

$$-w_{bn}=-y_{bn}= r_b+h-[(r_b+h)^2-x_{bn}^2]^{1/2}$$
$$=[1/6R_t(x_{tn}-x_{cn})]\{-x_{bn}^3-x_{cn}(3x_{bn}^2-2x_{cn}^2)+3x_{tn}(x_{tn}-2x_{cn})(x_{bn}+x_{cn})\} - x_{tn}(x_{bn}+x_{cn})/[(r_t+h)^2-x_{tn}^2]^{1/2}+w_{cn} \quad (5.43f)$$

ii. $x=-x_{bn}$, $(dw/dx)_{roller}=(dw/dx)_{plate}$
From equations (5.41c(v)) and (5.43a), it gives

$$x_{bn}/[(r_b+h)^2-x_{bn}^2]^{1/2} = [1/2R_t(x_{tn}-x_{cn})]\{x_{bn}^2+2x_{cn}x_{bn}-x_{tn}(x_{tn}-2x_{cn})\} + x_{tn}/[(r_t+h)^2-x_{tn}^2]^{1/2} \quad (5.43g)$$

d) ***At bottom roll nominal contact*** (for x_{bn} and w_{bn} are equal to zero - fig 5.21)

i. $x=x_{bn}=0$, $w=-w_{bn}=0$
From equations (5.41c(iv)) and (5.43), it gives

$$w=-w_{bn}=-y_{bn}=0$$
$$0=[1/6R_t(x_{tn}-x_{cn})]\{2x_{cn}^3+3x_{tn}(x_{tn}-2x_{cn})x_{cn}\}$$
$$-x_{tn}x_{cn}/[(r_t+h)^2-x_{tn}^2]^{1/2}+w_{cn} \qquad (5.43h)$$

ii. $x=x_{bn}=0$, $(dw/dx)_{roller}=(dw/dx)_{plate}$
From equations (5.41c(v)) and (5.43a), it gives

$$0=[1/2R_t(x_{tn}-x_{cn})]\{-x_{tn}(x_{tn}-2x_{cn})\}+x_{tn}/[(r_t+h)^2-x_{tn}^2]^{1/2} \qquad (5.43i)$$

3. Specific relationship for particular bending operations

Additional specific boundary conditions for "pre-bending" operational mode:

At bottom roll nominal contact

$x=-x_{bn}$, $1/R_b=(d^2w/dx^2)_{plate}=0$.
From equation (5.43b), it gives

$$(d^2w/dx^2)_{plate}=[1/R_t(x_{tn}-x_{cn})](-x_{bn}-x_{cn})=0 \qquad (5.43j)$$

Additional specific boundary conditions for "steady continuous bending" operational mode :

At bottom roll nominal contact

i. For $x=-x_{bn}$ and $w=-w_{bn}$, $1/R_b=(d^2w/dx^2)_{plate}=1/r_f$.
In this case, equation (5.43b) becomes

$$(d^2w/dx^2)_{plate}=[1/R_t(x_{tn}-x_{cn})](-x_{bn}-x_{cn})=1/r_f \qquad (5.43k)$$

ii. For $x=-x_{bn}=0$ and $w=-w_{bn}=0$, $1/R_b=(d^2w/dx^2)_{plate}=1/r_f$.
In this case, the relevant values for x_{bn} and w_{bn}, in equations (5.43f) and (5.43k), are zero.

A. Pre-inactive side roll operating mode

1. Common general deflection function for the bending mode

$$w=[1/(x_{cn}-x_{tn})]\{(1/R_t-1/r_f)[x^3/6-x_{tn}^2x/2+(x_{cn}/6)(x_{cn}^2+3x_{tn}^2)] +(x_{cn}/R_t-x_{tn}/r_f)[x^2/2+x_{tn}x-(x_{cn}/2)(x_{cn}+2x_{tn})]\} +x_{tn}(x_{cn}-x)/[(r_t+h)^2-x_{tn}^2]^{1/2}+w_{cn} \qquad (5.45)$$

and,

$$dw/dx=[1/(x_{cn}-x_{tn})]\{(1/R_t-1/r_f)[x^2/2-x_{tn}^2/2] +(x_{cn}/R_t-x_{tn}/r_f)[x+x_{tn}]\}-x_{tn}/[(r_t+h)^2-x_{tn}^2]^{1/2} \qquad (5.45a)$$

$$d^2w/dx^2=[1/(x_{cn}-x_{tn})]\{(1/R_t-1/r_f)x+(x_{cn}/R_t-x_{tn}/r_f)\} \qquad (5.45b)$$

2. Common general relationship (fig 5.23)

Additional common general boundary conditions :

a) ***At top roll nominal contact***

i. $x=-x_{tn}$, $w=w_{tn}$

From equations (5.41b(ii)) and (5.45), it gives

$$w_{tn}=(r_t+h)-[(r_t+h)^2-x_{tn}^2]^{1/2}$$
$$= [1/(x_{cn}-x_{tn})]\{(1/R_t-1/r_f)[x_{tn}^3/3+(x_{cn}/6)(x_{cn}^2+3x_{tn}^2)]$$
$$+(x_{cn}/R_t-x_{tn}/r_f)[-x_{tn}^2/2-(x_{cn}/2)(x_{cn}+2x_{tn})]\}$$
$$+x_{tn}(x_{cn}+x_{tn})/[(r_t+h)^2-x_{tn}^2]^{1/2}+w_{cn} \qquad (5.45c)$$

in which $1/R_t=1/r_f+M_i/EI= (EI+M_i r_f)/EIr_f$

b) ***At nominal contact of the operative side roll***

i. $x=-x_{cn}$, $(dw/dx)_{roller}=(dw/dx)_{plate}$

From equations (5.41e(iv)) and (5.45a), it gives

$$(x_s+x_{cn}) /[(r_s+h)^2-(-x_{cn}-x_s)^2]^{1/2}$$
$$= [1/(x_{cn}-x_{tn})]\{(x_{cn}/R_t-x_{tn}/r_f)[-x_{cn}+x_{tn}]\}-x_{tn}/[(r_t+h)^2-x_{tn}^2]^{1/2} \qquad (5.45d)$$

ii. From equations (5.31b) and (5.41e(iii)), it leads to

$$w_{cn}=y_{cn}=(x_0+x_s)\cot\psi'-r_s-h+[(r_s+h)^2-(-x_{cn}-x_s)^2]^{1/2} \qquad (5.45e)$$

c) ***At bottom roll nominal contact*** (for x_{bn} and w_{bn} are not equal to zero)

i. $x=x_{bn}$, $w=-w_{bn}$

From equations(5.41c(iv)) and (5.45), it gives

$$-w_{bn}=-y_{bn}=r_b+h-[(r_b+h)^2-x_{bn}^2]^{1/2}$$
$$=[1/(x_{cn}-x_{tn})]\{(1/R_t-1/r_f)[x_{bn}^3/6-x_{tn}^2x_{bn}/2+(x_{cn}/6)(x_{cn}^2+3x_{tn}^2)]$$
$$+(x_{cn}/R_t-x_{tn}/r_f)[x_{bn}^2/2+x_{tn}x_{bn}-(x_{cn}/2)(x_{cn}+2x_{tn})]\}$$
$$+x_{tn}(x_{cn}-x_{bn})/[(r_t+h)^2-x_{tn}^2]^{1/2}+w_{cn} \qquad (5.45f)$$

ii. $x=x_{bn}$, $(dw/dx)_{roller}=(dw/dx)_{plate}$

From equations (5.41c(v)) and (5.43a), it gives

$$-x_{bn}/[(r_b+h)^2-x_{bn}^2]^{1/2}$$
$$=[1/(x_{cn}-x_{tn})]\{(1/R_t-1/r_f)[x_{bn}^2/2-x_{tn}^2/2]$$
$$+(x_{cn}/R_t-x_{tn}/r_f)[x_{bn}+x_{tn}]\}-x_{tn}/[(r_t+h)^2-x_{tn}^2]^{1/2}$$

(5.45g)

3. Specific relationship for particular bending operations

Additional specific boundary conditions for transitional "roll swapping bending" operation

At bottom roll nominal contact

$x=x_{bn}$, $1/R_b=(d^2w/dx^2)_{plate}=1/r_f$

From equation (5.45b), it gives

$$(d^2w/dx^2)_{plate}=1/r_f=[1/(x_{cn}-x_{tn})]\{(1/R_t-1/r_f)\,x_{bn}+(x_{cn}/R_t-x_{tn}/r_f)\}$$

(5.45h)

Additional specific boundary conditions for "steady continuous bending" mode

At bottom roll nominal contact (Ref to Fig 5.23)

$x=x_{bn}$, $1/R_b=(d^2w/dx^2)_{plate}=0$
From equation (5.45b), it gives

$$(d^2w/dx^2)_{plate}= 0 =[1/(x_{cn}-x_{tn})]\{(1/R_t-1/r_f)\, x_{bn}+(x_{cn}/R_t-x_{tn}/r_f)\} \quad (5.45i)$$

SECOND/SUBSEQUENT (MULTI) PASS BENDING OPERATIONS

A. Pre-active side roll operating mode

1. Common general deflection function for the bending mode

$$w=(a/6)[x^3-3x_{tn}^2x-x_{cn}(x_{cn}^2-3x_{tn}^2)]+(b/2)[x^2-2x_{tn}x-x_{cn}(x_{cn}-2x_{tn})] +w_{cn}-(r_f^2-x^2)^{1/2}+(r_f^2-x_{cn}^2)^{1/2} \quad (5.48)$$

and,

$$dw/dx=(a/2)[x^2-x_{tn}^2]+ b[x-x_{tn}]+ [x/(r_f^2-x^2)^{1/2}] \quad (5.48a)$$

$$d^2w/dx^2= ax+ b+ [1/(r_f^2-x^2)^{1/2}] +[x^2/(r_f^2-x^2)^{3/2}] \quad (5.48b)$$

in which **a**, **b**, **c** and **d** are the common general parametric functions as defined in equations (5.47a), (5.47b), (5.47c) and (5.47d), respectively.

The plate local radius of curvature, $1/R_t$, at the top roll nominal contact is expressed as follows :

$$1/R_t=(d^2w/dx^2)_{plate}=1/r_{ff}+M_i/EI=(EI+M_ir_{ff})/EIr_{ff}$$

2. Common general relationship (figs 5.25 and 5.26)

Additional common general boundary conditions :

a) ***At top roll nominal contact***

i. $x=x_{tn}$, $w=w_{tn}$
From equations (5.41b(ii)) and (5.48), it gives

$$w_{tn}=(r_t+h)-[(r_t+h)^2-x_{tn}^2]^{1/2}$$
$$=(a/6)[-2x_{tn}^3-x_{cn}(x_{cn}^2-3x_{tn}^2)]+(b/2)[-x_{tn}^2-x_{cn}(x_{cn}-2x_{tn})]$$
$$+w_{cn}-(r_f^2-x_{tn}^2)^{1/2}+(r_f^2-x_{cn}^2)^{1/2} \qquad (5.48c)$$

b) ***At nominal contact of the operative side roll***

i. $x=x_{cn}$, $(dw/dx)_{roller}=(dw/dx)_{plate}$
From equations (5.41e(iv)) and (5.48a), it gives

$$(x_s-x_{cn})/[(r_s+h)^2-(x_{cn}-x_s)^2]^{1/2}$$
$$= (a/2)[x_{cn}^2-x_{tn}^2]+ b[x_{cn}-x_{tn}]+ [x_{cn}/(r_f^2-x_{cn}^2)^{1/2}] \qquad (5.48d)$$

ii. From equations (5.31a) and (5.41e(iii)), it leads to

$$w_{cn}=y_{cn}=(x_0-x_s)\cot\psi-r_s-h+[(r_s+h)^2-(x_{cn}-x_s)^2]^{1/2} \qquad (5.48e)$$

c) ***At bottom roll nominal contact*** (for x_{bn} and w_{bn} are not equal to zero)

i. $x=-x_{bn}$, $w=-w_{bn}$
From equations (5.41c(iv)) and (5.48), it gives

$$-w_{bn}=-y_{bn}=r_b+h-[(r_b+h)^2-x_{bn}^2]^{1/2}$$
$$=(a/6)[-x_{bn}^3+3x_{tn}^2x_{bn}-x_{cn}(x_{cn}^2-3x_{tn}^2)]+(b/2)[x_{bn}^2+2x_{tn}x_{bn}$$
$$-x_{cn}(x_{cn}-2x_{tn})]+w_{cn}-(r_f^2-x_{bn}^2)^{1/2}+(r_f^2-x_{cn}^2)^{1/2}$$
$$(5.48f)$$

ii. $x=-x_{bn}$, $(dw/dx)_{roller}=(dw/dx)_{plate}$
From equations (5.41c(v)) and (5.48a), it gives

$$x_{bn}/[(r_b+h)^2-x_{bn}^2]^{1/2} = (a/2)[x_{bn}^2-x_{tn}^2]- b[x_{bn}+x_{tn}]- [x_{bn}/(r_f^2-x_{bn}^2)^{1/2}] \quad (5.48g)$$

d) ***At bottom roll nominal contact*** (for x_{bn} and w_{bn} are equal to zero - fig 5.26)

i. $x=x_{bn}=0$, $w=w_{bn}=0$
From equations (5.41c(iv)) and (5.48), it gives

$$w=w_{bn}=y_{bn}=0$$
$$0=(a/6)[-x_{cn}(x_{cn}^2-3x_{tn}^2)]-(b/2)[x_{cn}(x_{cn}-2x_{tn})]+w_{cn}-r_f+(r_f^2-x_{cn}^2)^{1/2} \quad (5.48h)$$

ii. $x=x_{bn}=0$, $(dw/dx)_{roller}=(dw/dx)_{plate}$
From equations (5.41c(v)) and (5.48a), it gives

$$0=-(a/2)x_{tn}- b \quad (5.48i)$$

3. Specific relationship for particular bending operations

Additional specific boundary conditions for "pre-bending" operational mode

a) ***At bottom toll nominal contact***

i. For $x=-x_{bn}$ and $w=-w_{bn}$, $1/R_b=(d^2w/dx^2)_{plate}=1/r_f$
From equation (5.48b), it gives

$$1/r_f= -ax_{bn}+ b+ [1/(r_f^2-x_{bn}^2)^{1/2}] +[x_{bn}^2/(r_f^2-x_{bn}^2)^{3/2}] \quad (5.48j)$$

ii. For $x=x_{bn}=0$ and $w=w_{bn}=0$, $1/R_b=(d^2w/dx^2)_{plate}=1/r_f$
From equation (5.48b), it gives

$$0= \mathbf{b} \qquad (5.48k)$$

Additional specific boundary conditions for "steady continuous bending" operational mode

a) ***At bottom roll nominal contact***

i. For $x=-x_{bn}$ and $w=-w_{bn}$, $1/R_b=(d^2w/dx^2)_{plate}=1/r_{ff}$
In this case, equation (5.43b) becomes

$$1/r_{ff}=-\mathbf{a}x_{bn}+ \mathbf{b}+ [1/(r_f^2-x_{bn}^2)^{1/2}] +[x_{bn}^2/(r_f^2-x_{bn}^2)^{3/2}] \qquad (5.48l)$$

ii. For $x=-x_{bn}=0$ and $w=-w_{bn}=0$, $1/R_b=(d^2w/dx^2)_{plate}=1/r_{ff}$
In this case, equation (5.43b) becomes

$$1/r_{ff} =\mathbf{b}+ [1/r_f] \qquad (5.48m)$$

B. Pre-inactive side roll operating mode

1. Common general deflection function for the bending mode

$$w=(\mathbf{a}/6)\{x^3-3x_{tn}^2x+x_{cn}(x_{cn}^2-3x_{tn}^2)\}+(\mathbf{b}/2)\{x^2+2x_{tn}x-x_{cn}(x_{cn}-2x_{tn})\} +(r_f^2-x_{cn}^2)^{1/2}-(r_f^2-x^2)^{1/2}+w_{cn} \qquad (5.51)$$

and,

$$dw/dx= (a/2)\{x^2-x_{tn}^2\}+b\{x+x_{tn}\}+[x/(r_f^2-x^2)^{1/2}] \quad (5.51a)$$

$$d^2w/dx^2= ax+b+[1/(r_f^2-x^2)^{1/2}] +[x^2/(r_f^2-x^2)^{3/2}] \quad (5.51b)$$

in which **a**, **b**, **c** and **d** are the common general parametric functions as defined in equations (5.50a), (5.50b), (5.50c) and (5.50d), respectively.

The plate local radius of curvature, $1/R_t$, at the top roll nominal contact is expressed as follows :

$$1/R_t=(d^2w/dx^2)_{plate}=1/r_{ff}+M_i/EI=(EI+M_ir_{ff})/EIr_{ff}$$

2. Common general relationship (fig 5.27)

Additional general boundary conditions :

a) ***At top roll nominal contact***

i. $x=-x_{tn}$, $w=w_{tn}$

From equations (5.41b(ii)) and (5.51), it gives

$$w_{tn}=(r_t+h)-[(r_t+h)^2-x_{tn}^2]^{1/2}$$
$$=(a/6)\{2x_{tn}^3+x_{cn}(x_{cn}^2-3x_{tn}^2)\}+(b/2)\{-x_{tn}^2-x_{cn}(x_{cn}-2x_{tn})\}$$
$$+(r_f^2-x_{cn}^2)^{1/2}-(r_f^2-x_{tn}^2)^{1/2}+w_{cn} \quad (5.51c)$$

b) ***At nominal contact of the operative side roll***

i. $x=-x_{cn}$, $(dw/dx)_{roller}=(dw/dx)_{plate}$
From equations (5.41c(iv)) and (5.51a), it gives

$$(x_s+x_{cn})/[(r_s+h)^2-(-x_{cn}-x_s)^2]^{1/2}$$
$$= (a/2)\{x_{cn}^2-x_{tn}^2\}+b\{-x_{cn}+x_{tn}\}-[x_{cn}/(r_f^2-x_{cn}^2)^{1/2}] \quad (5.51d)$$

ii. From equations (5.31b) and (5.41e(iii)), it leads to
$$w_{cn}=y_{cn}=(x_0+x_s)\cot\psi"-r_s-h+[(r_s+h)^2-(-x_{cn}-x_s)^2]^{1/2} \quad (5.51e)$$

c) ***At bottom roll nominal contact***

i. $x=x_{bn}$, $w=-w_{bn}$
From equations (5.41c(iv)) and (5.51), it gives

$$-w_{bn}=-y_{bn}=r_b+h-[(r_b+h)^2-x_{bn}^2]^{1/2}$$
$$=(a/6)\{x_{bn}^3-3x_{tn}^2x_{bn}+x_{cn}(x_{cn}^2-3x_{tn}^2)\}+(b/2)\{x_{bn}^2+2x_{tn}x_{bn}$$
$$-x_{cn}(x_{cn}-2x_{tn})\}+(r_f^2-x_{cn}^2)^{1/2}-(r_f^2-x_{bn}^2)^{1/2}+w_{cn} \quad (5.51f)$$

ii. $x=x_{bn}$, $(dw/dx)_{roller}=(dw/dx)_{plate}$
From equations (5.41c(v) and (5.51a), it gives

$$-x_{bn}/[(r_b+h)^2-x_{bn}^2]^{1/2}$$
$$= (a/2)\{x_{bn}^2-x_{tn}^2\}+b\{x_{bn}+x_{tn}\}+[x_{bn}/(r_f^2-x_{bn}^2)^{1/2}] \quad (5.51g)$$

3. Specific relationship for particular operations

Additional specific boundary conditions for "transitional roll swapping" bending mode

a) ***At bottom roll nominal contact***

$x=x_{bn}$, $(d^2w/dx^2)_{plate}=1/r_{ff}$

In this case, equation (5.51a) gives

$$1/r_{ff} = ax_{bn}+b +[1/(r_f^2-x_{bn}^2)^{1/2}] +[x_{bn}^2/(r_f^2-x_{bn}^2)^{3/2}] \qquad (5.51h)$$

Additional specific boundary conditions for "steady continuous bending" operational mode

a) ***At bottom roll nominal contact***

$x=x_{bn}$, $(d^2w/dx^2)_{plate}=1/r_f$

In this case, equation (5.51a) gives

$$1/r_f = ax_{bn} +b +[1/(r_f^2-x_{bn}^2)^{1/2}] +[x_{bn}^2/(r_f^2-x_{bn}^2)^{3/2}] \qquad (5.51i)$$

APPENDIX 5.2

LISTING OF COMPUTER PROGRAMMES

```
10 ! * M/1STPASS * TO EVALUATE THE BENDING MOMENT AND LOCAL BEND RADIUS AT THE
20 ! * --------- * TOP ROLL NOMINAL CONTACT IN ORDER TO ROLL-BEND A PLATE TO A
30 ! FILE: M1B   * RADIUS OF Rfinish ****************************************
40 ! *-------------------------------------------------------------------*
50 !      *-----------------------------------*
60 ! ****** THE FIRST AND SINGLE PASS BENDING MODE ********
70 !      *-----------------------------------*
80 ! *  ££ INPUT DATA ££ *
90 ! *  ---------------- *
100  ! 1- Material properties:-
110  !       E       = Young's modulus
120  !       H       = Material hardness constant
130 !        n       = Material hardness index
140 !        Sigma0  = The first yield stress of the bend plate
150 !        v       = Poisson's ratio of the bend material
160 !
170 ! 2- Dimensions of the bend plate:-
180 !        h       = Half of the plate's thickness
190 !        Rfinish= Expected bend radius of the plate at its completion of bend
200 !        b       = Width of the bend-plate
210 !        z       = The distance of an interested fibre layer, of a plate, from
220 !                  its neutral layer
230 !
240 ! 3- Other information
250 !       Accuracy  = Iterative accuracy for the total incremental strain
260 !                   relative to the uniaxial tensile stress/strain relation
270 !       RAccuracy = Iterative accuracy for the local bend-radius, of the
280 !                   plate, at the top roll nominal contact
290 !       N         = An input integer for deciding whether the BISECTION
300 !                   ITERATIVE METHOD is used in iterating the local bend
310 !                   radius,R, of the top roll nominal contact. N=1 for
320 !                   using the METHOD otherwise N=0.
330 !       Nreq      = The number of consecutive finished bend radius,Rfinsih
340 !                   interested for estimating the theorectical data
350 !
360 ! *-------------------------------------------------------------------*
370 !
380    CLEAR
390 !
400 ! ***** Data input:-
410 !
420    DISP "Please key in the following data accordingly!"
430 !
440    DISP "Material properties of the bend plate : "
450 !
460     DISP "1. Young's Modulus, 2. Material hardness constant"
470             INPUT E,H
480 !
490     DISP "3. Material hardness index, 4. First yield stress of material"
500             INPUT n,Sigma0
510 !
520     DISP "5. The Poisson's Ratio of the bend plate"
530             INPUT v
540 !
550 CLEAR
560 !
570     DISP "Dimensions of the bend plate :"
580     DISP "1. Half of the plate's thickness, 2. Finished bend radius"
590             INPUT h,Rfinish
```

```
600 !
610     DISP "3. Width of the bend plate, 4. Fibre distance from neutral axis"
620             INPUT b,z
630 !
640 CLEAR
650 !
660     DISP "Other informations :"
670     DISP "Iterative Accuracy (1) for incremental strain, (2) for local bend
radius"
680             INPUT Accuracy,RAccuracy
690 !
700 !   DISP "3. Key in 1 for using BISECTION ITERATION to evaluate the local"
710 !   DISP "   bend radius at top roll contact, OTHERWISE key in 0"
720 !           INPUT N
721         N=0
730 !
740     DISP "PLEASE KEY-IN the number of consecutive estimations for the"
750     DISP "finished bend radius,Rfinish, iterested"
760             INPUT Nreq
770 !
780 ! ------------------------------------------------------------------------
790 !     *-----------------------------------*
800 ! ***** To calculate the common parameters *****
810 !     *-----------------------------------*
820         c1=1-v^2 @ c2=SQR (1-v+v^2) @ Nrad=0
830         a1=E*c1 @ a2=c1*Sigma0 @ a3=SQR (3)/2
840         a4=1-v @ a5=1-v+v^2
850         A1=H*(3*a4/(2*c2)-a3)/E @ A2=a2/(E*c2)
860         d1=n+1 @ K=H*(3*a4/(2*c2)-a3)/E @ d2=E*K+a4/c2
870 !
880         I=b*(2*h)^3/12 ! The second moment of the bend plate cross
890 !                        sectional area
900 !
910         EI=E*I @ n2=n+2 @ n3n=3*n @ np2=2*n+1
920         G=c1*Sigma0/(E*c2)
930 !
940 !     *-------------------------------------------------------------------*
950 ! ***** To initiate the determination of the incremental strain relative **
960 ! ***** to the uniaxial tensile stress/strain relation and the local bend**
970 ! ***** radius at the top roll nominal contact                          **
980 !     *-------------------------------------------------------------------*
990 !
1000 !
1010        EpsilonDiff0=0 ! The assumed initial incremental strain limit
1020 !                        for the iteration. It means to start the
1030 !                        iteration from the elastic-elastoplastic
1040 !                        interface
1050        EpsilonX0=A2 ! The strain on the elastic-elastoplastic interface
1060        a0=A2/h @ a0=1/a0 ! The maximum radius of curvature at the top
1070                          ! roll instantaneous nominal contact, beyond
1080                          ! which completely elastic deformation occurs
1090 !
1100         PRINT "The maximum radius,a0, of curvature at the top roll nominal"

1110         PRINT "contact, beyond which only the elastic deformation occurs"
1120         PRINT "a0= ";a0;"(m). SUBSEQUENTLY, its local bend radius,R, must"
1130         PRINT "be smaller than a0 = ";a0;"  m, in order to have plastic"
1140         PRINT "deformation for the finished bend plate"
1150         PRINT "                                                "
1160 !
1170         PRINT "                                                "
1180         PRINT "*** THE INPUT DATA FOR THE RESPECTIVE SINGLE PASS BENDING"
1190         PRINT "     ARE AS FOLLOWS ***"
1200         PRINT "                                                 "
1210         PRINT "E       =";E,"Rfinish =";Rfinish
1220         PRINT "n       =";n,"Sigma0  =";Sigma0
```

```
1230          PRINT "H        =";H,"v        =";v
1240          PRINT "b        =";b,"z        =";z
1250          PRINT "N        =";N
1251          PRINT "Accuracy=";Accuracy
1252          PRINT "RAccuracy=";RAccuracy
1260          PRINT "                          "
1270 !
1280         IF N=0 THEN GOTO 1310
1290         IF Rfinish<a0 THEN Ra1=Rfinish ELSE Ra1=.99*a0
1300         Ra2=.1*Rfinish @ GOTO 1330
1310         IF Rfinish<a0 THEN R=Rfinish ELSE R=.99*a0
1320 !
1330         GOSUB CURVATURE  ! To evaluate the relative strain and bend radius
1331         PRINT "**** The accuracies of the iterative function ****"
1332         PRINT "DelEpsilon1=";DelEpsilon1,"DelEpsilon2=";DelEpsilon2
1333         PRINT "RTest1      =";RTest1,"RTest2      =";RTest2
1334         PRINT "                                "
1340 !
1350         R=(Ra1+Ra2)/2
1360 IF Vepsilon1>Vepsilon2 THEN EpsilonDiff0=Vepsilon2 ELSE EpsilonDiff0=Vepsil
on1
1370         GOSUB STRAIN
1380 !
1390         Ci=R*A2 ! The elastic-elastoplastic interface
1400         Vepsilon=(EpsilonDiff0+EpsilonDiff)/2 ! The estimated delta strain
1410         GOSUB B1VALUE
1420         Mi=2*b*R^2*(c1*Sigma0^2*G/(3*E*a5)+B1)
1430         MiEI=Mi/EI
1431         Faccuracy=1/R-MiEI-1/Rfinish
1440 !
1450         PRINT "                                          "
1460         PRINT "THE FOLLOWING ARE THE THEORETICAL RESULTS FOR SINGLE/FIRST"
1470         PRINT "PASS BENDING TO ACHIEVE Rfinish=";Rfinish;" (METRES)"
1480         PRINT "-------------------------------------------------------"
1490         PRINT "The expected bend radius,Rfinish, of the bending   = ";Rfinis
h
1500         PRINT "The local bend radius at top roll contact,R,       = ";R
1510         PRINT "The elastic-elastoplastic interface,Ci,            = ";Ci
1520         PRINT "The incremental strain on the surface,Vepsilon,    = ";Vepsil
on
1530         PRINT "The resistant moment at the top roll contact,Mi,     =";Mi
1540         PRINT "The spring back curvature,MiEI, at top roll contact =";MiEI
1541         PRINT "The accuracy for the iterated radius, i.e. Faccuracy=";Faccur
acy
1542         PRINT "                                                 "
1543         PRINT "                                                 "
1550 !
1560         Nrad=Nrad+1
1570         IF Nrad=Nreq THEN GOTO 1670
1580 IF Vepsilon2>Vepsilon1 THEN EpsilonDiff0=Vepsilon1 ELSE EpsilonDiff0=Vepsil
on2
1590         Rret=Rfinish
1600         Rfinish=.9*Rfinish @ Rrat=(Rret-Rfinish)/Rret
1610 !
1620 BEEP
1630 !
1640         IF N=0 THEN GOTO 1050
1650         Ra1=R @ Ra2=Rrat*R @ GOTO 1050
1660 !
1670 BEEP 40,250
1671 BEEP
1672 BEEP
1680 PRINT "                                          "
1690 PRINT "----------------END OF THE PROGRAM----------------"
1700 DISP "----------------END OF THE PROGRAM----------------"
1710 !
```

```
1720        END
1730 !
1740 ! ++++++++++++++++++++++++++++++++++++++++++++++++++++++++++++++++++++++++++++++
1750 STRAIN: ! ***** STRAIN SUBROUTINE for iterating incremental strain *****
1760 ! ---------------- To define a function as a condition to end the iteration

1770    DEF FNF(x,b1) = a3*x+A1*x^n+A2-b1
1780 !
1790 b1=z/R ! The longitudinal strain for the fibre layer z away from NA
1800 Epsilonh=h/R ! The longitudinal strain for the outer fibre layer
1810 EpsilonDiff=Epsilonh-EpsilonX0 ! The upper incremental strain limit
1820 !                                The lower incremental strain limit is
1830 !                                EpsilonDiff0
1840 ! **** To initiate the iteration *************
1850 !      -------------------------
1860        DelEpsilon1=FNF(EpsilonDiff0,b1)
1870 !
1880        IF DelEpsilon1>0 THEN EpsilonDiff0=.99*EpsilonDiff0 ELSE GOTO 1920
1890        DelEpsilon1=FNF(EpsilonDiff0,b1)
1900        GOTO 1880
1910 !
1920        DelEpsilon2=FNF(EpsilonDiff,b1)
1930 !
1940        IF DelEpsilon2<0 THEN EpsilonDiff=1.02*EpsilonDiff ELSE GOTO 1990
1950        DelEpsilon2=FNF(EpsilonDiff,b1)
1960        GOTO 1940
1970 !
1980 !
1990        ProFunction=DelEpsilon1*DelEpsilon2
2000 !
2010 ! **** To commence the iteration *********
2020 !      --------------------------
2030   IF ProFunction=0 THEN GOTO 2220
2040   IF ProFunction>0 THEN GOTO 2130
2050 !
2060         IF ABS (DelEpsilon1)>ABS (DelEpsilon2) THEN GOTO 2140
2070 !
2080        EpsilonDiff=(EpsilonDiff0+EpsilonDiff)/2
2090        DelEpsilon2=FNF(EpsilonDiff,b1)
2100        Vepsilon=EpsilonDiff
2110   GOTO 2180
2120 !
2130         IF ABS (DelEpsilon2)>ABS (DelEpsilon1) THEN GOTO 2080
2140         EpsilonDiff0=(EpsilonDiff0+EpsilonDiff)/2
2150         DelEpsilon1=FNF(EpsilonDiff0,b1)
2160         Vepsilon=EpsilonDiff0
2170 !
2180   aA=ABS (DelEpsilon1) @ aA3=ABS (DelEpsilon2)
2190   IF ABS (aA-aA3)<= Accuracy THEN GOTO 2230
2200   GOTO 1990
2210 !
2220 IF ABS (DelEpsilon1)=0 THEN Vepsilon=EpsilonDiff0 ELSE Vepsilon=EpsilonDiff

2230 ! PRINT "                    "
2240 ! PRINT "EpsilonDiff0 =";EpsilonDiff0,"EpsilonDiff =";EpsilonDiff
2250 ! PRINT "DelEpsilon1  =";DelEpsilon1,"DelEpsilon2 =";DelEpsilon2
2260 ! PRINT "Vepsilon     =";Vepsilon,"R            =";R
2270 ! PRINT "                                  "
2280 !
2290 RETURN
2300 ! ++++++++++++++++++++++++++++++++++++++++++++++++++++++++++++++++++++++++++++++

2310 CURVATURE: ! ***** CURVATURE SUBROUTINE for iterating the local bend radius

2320 !            ***** at the top roll nominal contact ************************
```

```
2330 ! -THE ITERATION USES THE EXISTING "SIMPLE BISECTION METHOD"-
2340 ! ***** To define a test function to end the iteration *****
2350 ! ***** ---------------------------------------- *****
2360       DEF FNR(R,Rfinish,MiEI) = 1/R-MiEI-1/Rfinish ! The defined function
2370 !    **--------------------------------------**
2380 !
2390 !     The function for the internal resistance to external bending momemt
2400 !
2410       DEF FNM(R,Sigma0) = 2*b*R^2*(c1*Sigma0^2*G/(3*E*a5)+B1)
2420 !   **-----------------------------------------------------------**
2430 ! ** To decide whether the BISECTION METHOD being used for evaluating the
2440 !    local curvature at the top roll nominal contact. For N is equal to any

2450 !    value, other than 0, the BISECTION METHOD is being executed.
2460 !
2470       IF N=0 THEN GOTO 3150
2480 !
2490 ! - To commence the iteration using the Bisection Method:-
2500 !
2510 !
2520    FOR L=1 TO 2
2530       IF L=1 THEN R=Ra1 ELSE R=Ra2
2540       GOSUB STRAIN
2550       GOSUB B1VALUE
2560 !
2570 ! - Internal resistance to the external bending moment:-
2580 !
2590       Mi=FNM(R,Sigma0)
2600       MiEI=Mi/EI ! The spring back curvature
2610 !
2620       IF L=1 THEN GOTO 2660
2630 !
2640       Mi2=Mi @ MiEI2=MiEI @ Vepsilon2=Vepsilon @ Ra2=R @ GOTO 2700
2650 !
2660       Mi1=Mi @ MiEI1=MiEI @ Vepsilon1=Vepsilon @ Ra1=R
2670 !
2680    NEXT L
2690 !
2700       RTest1=FNR(Ra1,Rfinish,MiEI1)
2710       RTest2=FNR(Ra2,Rfinish,MiEI2)
2720    PRTest=RTest1*RTest2
2730 !
2740    IF PRTest=0 THEN GOTO 3080
2750    IF PRTest>0 THEN GOTO 2900
2760 !
2770       IF ABS (RTest1)>ABS (RTest2) THEN GOTO 2920
2780 !
2790       Ra2=(Ra1+Ra2)/2 @ R=Ra2
2800       GOSUB STRAIN
2810       GOSUB B1VALUE
2820       Mi=FNM(R,Sigma0)
2830       MiEI=Mi/EI
2840 !
2850       RTest2=FNR(R,Rfinish,MiEI)
2860       VR=R @ Ra2=R
2870       Vepsilon2=Vepsilon
2880       GOTO 3020
2890 !
2900     IF ABS (RTest2)>ABS (RTest1) THEN GOTO 2790
2910 !
2920      Ra1=(Ra1+Ra2)/2 @ R=Ra1
2930      GOSUB STRAIN
2940      GOSUB B1VALUE
2950      Mi=FNM(R,Sigma0)
2960      MiEI=Mi/EI
2970      RTest1=FNR(R,Rfinish,MiEI)
```

```
2980      VR=R @ Ra1=R
2990      Vepsilon1=Vepsilon
3000 !
3010 !
3020      bsA=ABS (Ra1) @ bsA5=ABS (Ra2)
3030      IF ABS (bsA-bsA5)<= RAccuracy THEN GOTO 3340
3040 !
3041 ! PRINT "                                        "
3042 ! PRINT "Mi          =";Mi,"MiEI          =";MiEI
3043 ! PRINT "RTest1      =";RTest1,"RTest2        =";RTest2
3044 ! PRINT "B1          =";B1,"R             =";R
3045 ! PRINT "Ra1         =";Ra1,"Ra2           =";Ra2
3046 ! PRINT "VR          =";VR,"Rfinish        =";Rfinish
3047 ! PRINT "                                        "
3048 !
3050      GOTO 2720
3060 !
3070 !
3080    IF ABS (RTest1)=0 THEN VR=Ra1 ELSE VR=Ra2
3090 !
3100      R=VR @ GOTO 3340
3110 ! *****-------------------------------------------------------------------***
3120 ! ***** FOR Bisection Iterative Method IS NOT USED IN THE SUBROUTINE ***
3130 ! *****-------------------------------------------------------------------***
3140 !
3150 !
3160 !
3170          GOSUB STRAIN
3180          GOSUB B1VALUE
3190          Mi=FNM(R,Sigma0)
3200          MiEI=Mi/EI
3210 !
3220          RTest=FNR(R,Rfinish,MiEI)
3221 !
3222          IF RTest=0 THEN Ra2=R ELSE GOTO 3230
3223          RTest2=0 @ GOTO 3330
3224 !
3230          IF RTest>0 THEN Ra2=R ELSE GOTO 3260
3240          RTest2=RTest @ GOTO 2720
3250 !
3260          NewCurve=(1+1.29)*(1/R) ! The new expected curvature at top
3270 !                                  roll nominal contact
3280          Ra1=R @ RTest1=RTest @ Ra2=0 @ RTest2=0 @ VR=0
3290 !
3300          R=1/NewCurve
3310          EpsilonDiff0=Vepsilon
3311 !
3312 ! PRINT "                                        "
3313 ! PRINT "Mi          =";Mi,"MiEI          =";MiEI
3314 ! PRINT "RTest1      =";RTest1,"RTest2        =";RTest2
3315 ! PRINT "B1          =";B1,"R             =";R
3316 ! PRINT "Ra1         =";Ra1,"Ra2           =";Ra2
3317 ! PRINT "VR          =";VR,"Rfinish        =";Rfinish
3318 !
3320          GOTO 3170 ! To continue iteration for R
3330 !
3340 ! PRINT "                                        "
3350 ! PRINT "Mi          =";Mi,"MiEI          =";MiEI
3360 ! PRINT "RTest1      =";RTest1,"RTest2        =";RTest2
3370 ! PRINT "B1          =";B1,"R             =";R
3380 ! PRINT "Ra1         =";Ra1,"Ra2           =";Ra2
3390 ! PRINT "VR          =";VR,"Rfinish        =";Rfinish
3400 ! PRINT "                                        "
3410 !
3420 RETURN
3430 ! ++++++++++++++++++++++++++++++++++++++++++++++++++++++++++++++++++++++++++
```

```
3440 B1VALUE: ! ***** B1VALUE SUBROUTINE for calculating the bending moment in
3450 !          ***** the elastoplastic deformation zone **********************
3460 !
3470      D1=H*K^2*Vepsilon^n3n/(3*a3)
3480      D2=d1*H*K*Vepsilon^np2/np2
3490      D3=K/SQR (3)*(K*Sigma0+H*G)*Vepsilon^(2*n)
3500      D4=a3*H*Vepsilon^n2/(2*n2)
3510      D5=(K*Sigma0+H*G/d1)*Vepsilon^d1
3520      D6=G*Sigma0*K*Vepsilon^n/a3
3530      D7=Sigma0*Vepsilon^2*a3/2
3540      D8=G*Sigma0*Vepsilon
3550 !
3560  B1=D1+D2+D3+D4+D5+D6+D7+D8
3570 !
3580 ! PRINT "B1            =";B1
3590 !
3600  RETURN
3610 ! ++++++++++++++++++++++END OF THE PROGRAM++++++++++++++++++++++++++++++++++
```

```
10 ! * M/2NDPASS * TO EVALUATE THE BENDING MOMENT AND LOCAL BEND RADIUS AT THE
20 ! * ---------- * TOP ROLL NOMINAL CONTACT IN ORDER TO ROLL-BEND A PLATE TO A
30 ! FILE: MULTI * RADIUS OF RRfinish FROM ITS INITIALLY CURVED CONDITION****
40 ! *-------------------------------------------------------------------------*
50 !      *-----------------------------------------*
60 ! ****** THE SECOND AND SUBSEQUENT PASS BENDING MODE ******
70 !      *-----------------------------------------*
80 !
90 !  DIMENSIONING ARRAY OF SigmaE, Z, And Rbent. String variables: Lunit,
100 ! Punit
110       DIM SigmaE(50),Z(50),Rbent(50),Lunit$(10),Punit$(3),UN$(2)
120       DIM Vde(50)
130 !
140 !    *-----------------------------------------------------------------*
150 ! *** A. TO EVALUATE THE MEAN FIRST YIELD STRESS FOR THE SECOND AND ***
160 ! ***    SUBSEQUENT PASS BENDING FROM ITS PRECEDING BENDING          ***
170 !    *-----------------------------------------------------------------*
180 !
190    PRINTER IS 701
200 !
210 ! *  ff INPUT DATA ff *
220 ! *  ---------------- *
230  ! 1- Material properties:-
240        PRINT "
250  !     E     = Young's modulus
260  !     H     = Material hardness constant
270 !      n     = Material hardness index
280 !      Sigma0 = The first yield stress of the bend plate
290 !      v     = Poisson's ratio of the bend material
300 !
310 ! 2- Dimensions of the bend plate:-
320 !      h     = Half of the plate's thickness
330 !      Rfinish= The bend radius of the plate at the completion of first
340 !               bend
350 !      b     = Width of the bend-plate
360 !      z     = The distance of an interested fibre layer, of a plate, from
370 !              its neutral layer
380 !    Rbent(I)= Expected bend radii of the plate at each completion of bend
390 !
400 ! 3- Other information
410 !      Accuracy  = Iterative accuracy for the total incremental strain
420 !                  relative to the uniaxial tensile stress/strain relation
430 !      RAccuracy = Iterative accuracy for the local bend-radius, of the
440 !                  plate, at the top roll nominal contact
450 !      N         = An input integer for deciding whether the BISECTION
460 !                  ITERATIVE METHOD is used in iterating the local bend
470 !                  radius,R, of the top roll nominal contact. N=1 for
480 !                  using the METHOD otherwise N=0.
490 !      Npass     = The number of bending passes anticipated
500 !
510 ! *-------------------------------------------------------------------------*
520 !
530    CLEAR
540 !
550 ! ***** Data input:-
560 !
570     DISP "PLEASE KEY-IN the unit for Young's modulus, stresses"
580           INPUT Lunit$
590     DISP "PLEASE kEY-IN the unit for the plate dimensions and bend-radius!"
600           INPUT Punit$
610 !
```

```
620     DISP "Please key in the following data accordingly!"
630     DISP "                                    "
640 !
650     DISP "Material properties of the bend plate : "
660 !
670      DISP "1. Young's Modulus, 2. Material hardness constant"
680              INPUT E,H
690 !
700      DISP "3. Material hardness index, 4. First yield stress of material"
710              INPUT n,Sigma0
720 !
730      DISP "5. The Poisson's Ratio of the bend plate"
740              INPUT v
750 !
760      DISP "Dimensions of the bend plate :"
770      DISP "1. Half of the plate's thickness, 2. Initial bend radius"
780              INPUT h,Rfinish
790 !
800      DISP "3. Width of the bend plate, 4. Fibre distance from neutral axis"
810              INPUT b,z
820 !
830      DISP "Other informations :"
840      DISP "Iterative Accuracy (1) for incremental strain, (2) for local bend
radius"
850              INPUT Accuracy,RAccuracy
860 !
870              N=0
880 !
890      DISP "4. Key in the number of bending passes anticipated after the first
pass bending"
900              INPUT Npass
910 !
920 CLEAR
930      DISP "THE Anticipated Bend Radii at the COMPLETION of each bending pass"

940      DISP "after the FIRST BENDING."
950      DISP "***** PLEASE key in the anticipated bend radii in sequence ! ***"
960 !
970              FOR Li=1 TO Npass STEP 1
980              INPUT Rbent(Li)
990              NEXT Li
1000 !
1010 ! ------------------------------------------------------------------------
1020 !     *-----------------------------------*
1030 ! ***** To calculate the common parameters *****
1040 !     *-----------------------------------*
1050          c1=1-v^2 @ c2=SQR (1-v+v^2)
1060          a1=E*c1 @ a2=c1*Sigma0 @ a3=SQR (3)/2
1070          a4=1-v @ a5=1-v+v^2
1080          A1=H*(3*a4/(2*c2)-a3)/E @ A2=a2/(E*c2)
1090          d1=n+1 @ K=H*(3*a4/(2*c2)-a3)/E @ d2=E*K+a4/c2
1100 !
1110          I=b*(2*h)^3/12 ! The second moment of the bend plate cross
1120 !                         sectional area
1130 !
1140          EI=E*I @ n2=n+2 @ n3n=3*n @ np2=2*n+1
1150          G=(1-v^2)*Sigma0/(E*c2)
1160 !
1170 !     *-------------------------------------------------------------------*
1180 !  **** To initiate the determination of the incremental strain relative *
1190 ! **** to the uniaxial tensile stress/strain relation and the local bend*
1200 ! **** radius at the top roll nominal contact                            *
1210 !    *-------------------------------------------------------------------*
1220 !
1230 !
1240        EpsilonDiff0=0 ! The assumed initial incremental strain limit
```

```
1250 !                        for the iteration. It means to start the
1260 !                        iteration from the elastic-elastoplastic
1270 !                        interface
1280        EpsilonX0=A2 ! The strain on the elastic-elastoplastic interface
1290 !
1300        a0=A2/h @ a0=1/a0 ! The maximum radius of curvature, at the top
1310                          ! roll instantaneous nominal contact, beyond
1320                          ! which completely elastic deformation occurs
1330        PRINT "                                  "
1340        PRINT "The maximum radius of curvature at the top roll nominal"
1350        PRINT "contact, a0 = ";a0;Punit$;"Subsequently, its local bend"
1360        PRINT "radius,R, must be smaller than a0 = ";a0;"  ";Punit$
1370 !
1380  PRINT "                                    "
1390  PRINT "E      = ";E,"H      = ";H
1400  PRINT "n      = ";n,"Sigma0 = ";Sigma0
1410  PRINT "v      = ";v,"h      = ";h
1420  PRINT "Rfinish= ";Rfinish
1430  PRINT "b      = ";b,"z      = ";z
1440  PRINT "N      = ";N
1450  PRINT "Accuracy =";Accuracy
1460  PRINT "RAccuracy=";RAccuracy
1470  PRINT "                                      "
1480 !
1490 !
1500 PRINT "THE CORRESPONDING UNIT for (1) Young's modulus is     ";Lunit$
1510 PRINT "                           (2) dimensions of plate is ";Punit$
1520 PRINT "                                      "
1530 !
1540        IF N=0 THEN GOTO 1570
1550        IF Rfinish<a0 THEN Ra1=Rfinish ELSE Ra1=.99*a0
1560        Ra2=.1*Rfinish @ GOTO 1590
1570        IF Rfinish<a0 THEN R=Rfinish ELSE R=.99*a0
1580 !
1590        GOSUB CURVATURE  ! To evaluate the relative strain and bend radius
1600 !
1610        PRINT "**** **** THE FIRST PASS BENDING **** ****"
1620        PRINT "          ----------------------"
1630        PRINT "**** The accuracies of the iterative functions"
1640        PRINT "DelEpsilon1=";DelEpsilon1,"DelEpsilon2=";DelEpsilon2
1650        PRINT "RTest1     =";RTest1,"RTest2      =";RTest2
1660        PRINT "                                          "
1670 !
1680        R=(Ra1+Ra2)/2
1690 IF Vepsilon1>Vepsilon2 THEN EpsilonDiff0=Vepsilon2 ELSE EpsilonDiff0=Vepsil
on1
1700 !
1710        GOSUB STRAIN
1720 !
1730        Ci=R*EpsilonX0 ! The elastic-elastoplastic interface
1740        Vepsilon=(EpsilonDiff0+EpsilonDiff)/2
1750        GOSUB B1VALUE
1760        Mi=2*b*R^2*(c1*Sigma0^2*G/(3*E*a5)+B1)
1770        MiEI=Mi/EI
1780        Faccuracy=1/R-MiEI-1/Rfinish
1790 !
1800 PRINT "                              "
1810 PRINT "                              "
1820 PRINT "THE FOLLOWING ARE THE THEORETICAL RESULTS FOR THE SINGLE/FIRST PASS
BENDING"
1830 PRINT "-------------------------------------------------------------------
-------"
1840 PRINT "The resistance to extenal bending moment at top roll contact = ";Mi
1850 PRINT "The radius of curvature at top roll contact,MiEI ,           = ";MiE
I
1860 PRINT "The local bend radius at the top roll contact,R,             = ";R
```

```
1870 PRINT "The finished bend radius of the bend-plate,Rfinish,          = ";Rfi
nish
1880 PRINT "The maximum local yield bend radius at top roll contact,a0,  = ";a0
1890 PRINT "The fibre layer for the elastic-elatoplastic inerface,Ci,    = ";Ci
1900 PRINT "The total incremental-equivalent strain on outer fibre,VdelE = ";Vep
silon
1910 PRINT "The accuracy of the iterated local bend radius,Faccuracy     = ";Fac
curacy
1920 PRINT "                                                 "
1930 PRINT "                                                 "
1940 !
1950 !      *-----------------------------------------------------------*
1960 ! ***** To evaluate the mean first yield stress for the second pass *****
1970 !      *-----------------------------------------------------------*
1980 !
1990         Ndz=6
2000         Tol=.001
2010 !
2020 CLEAR
2030 !
2040         dz0=h-Ci @ dZn=dz0/Ndz @ SigmaEm=0
2050         SigmaE(1)=Sigma0 @ Vde(1)=0 @ Z(1)=Ci @ Z(Ndz+1)=h
2060         SigmaE(Ndz+1)=Sigma0+H*Vepsilon^n @ Vde(Ndz+1)=Vepsilon
2070 !
2080         EpsilonDiff0=0
2090 !
2100       FOR Li=2 TO Ndz STEP 1
2110         Z(Li)=Z(Li-1)+dZn
2120         z=Z(Li)
2130         GOSUB STRAIN
2140         Vde(Li)=Vepsilon
2150         SigmaE(Li)=Sigma0+H*Vepsilon^n
2160         EpsilonDiff0=Vepsilon
2170         Ai1=(SigmaE(Li)+SigmaE(Li-1))*(Z(Li)-Z(Li-1))
2180         SigmaEm=SigmaEm+Ai1
2190       NEXT Li
2200 !
2210         SigmaEm=SigmaEm+(SigmaE(Ndz)+SigmaE(Ndz+1))*(Z(Ndz+1)-Z(Ndz))
2220         SigmaEm=.5*SigmaEm/dz0 ! The mean first yield stress in the
2230 !                                 elastoplastic deformation zone after
2240 !                                 the first pass bending
2250 !
2260         PRINT "                                 "
2270         PRINT "The determined mean first yield stress,SigmaEm, = ";SigmaEm
2280         PRINT "The elastic-elastoplastic interface is at Ci    = ";Ci
2290         PRINT "The local bend radius at top roll,R             = ";R
2300         PRINT "                                 "
2310 PRINT "The number of intervals for the integration of the elastoplastic zon
e "
2320 PRINT "            "
2330 PRINT "            "
2340 !
2350 !
2360       PRINT "                                 "
2370       PRINT "**** The local incremental stress/strain on each fibre layer"
2380       PRINT "     ------------------------------------------------------"
2390 !
2400     FOR Li=1 TO Ndz+1 STEP 1
2410       PRINT "The layer distance,Z(";Li;")                    = ";Z(Li)
2420       PRINT "The incremental strain on the layer,Vde(";Li;")= ";Vde(Li)
2430       PRINT "The local first yield stress,SigmaE(";Li;")     = ";SigmaE(Li)
2440       PRINT "                                 "
2450     NEXT Li
2460 !
2470 !      *-----------------------------------------------------------*
2480 ! ***** TO ITERATE THE LOCAL BEND RADIUS AT THE TOP ROLL NOMINAL *****
```

```
2490 !. ***** CONTACT IN THE SECOND/SUBSEQUENT PASS BENDING            *****
2500 !      *-----------------------------------------------------*
2510 !
2520        Ncpass=1 @ RRfinish=Rbent(1)
2530 !
2540 ! To determine the local bend radius at the top roll contact for the first
2550 ! yield condition
2560        G2=c1*SigmaEm/(E*c2)
2570        R1st=G2*(Rfinish+h)/(h*Rfinish)+1/Rfinish
2580        R1st=1/R1st ! The bend radius for the 1st yield
2590 !
2600        IF Ncpass=1 THEN UN$="ND"
2610        IF Ncpass=2 THEN UN$="RD"
2620        IF Ncpass>2 THEN UN$="TH"
2630        NA=Ncpass+1
2640 !
2650        PRINT "                                              "
2660        PRINT "                                              "
2670        PRINT "           *--------------------------*"
2680        PRINT "  ********* THE";NA;UN$;"-PASS BENDING *********  "
2690        PRINT "           *--------------------------*"
2700        PRINT "                                "
2710  PRINT "The first yield local bend radius at top roll contact,R1st = ";R1st

2720        PRINT "                                "
2730 !
2740 ! To initiate the iteration
2750        IF N=0 THEN GOTO 2780
2760        IF RRfinish<R1st THEN Ra1=RRfinish ELSE Ra1=.99*R1st
2770        Ra2=.1*RRfinish @ GOTO 2820
2780        IF RRfinish<R1st THEN R=RRfinish ELSE R=.99*R1st
2790        Ci=c1*Rfinish*Sigma0/(E*(Rfinish/R-1)*c2-c1*Sigma0)
2800        EpsilonX0=Ci*(Rfinish/R-1)/(Ci+Rfinish)
2810 !
2820        z=h
2830        Co=((SigmaE-Sigma0)/H)^(1/n)
2840        F1=c1*SigmaEm/(E*c2)-K/H*(SigmaE-Sigma0)
2850        G1=K
2860 !
2870        GOSUB MCURVAT  ! A subroutine to iterate for the local bend radius
2880 !                      at the top roll nominal contact in multipass
2601 !                      bending mode
2890 !
2900        PRINT "                                "
2910        PRINT "The iterative accuracies for the functions are:-"
2920        PRINT "DelEpsilon1 =";DelEpsilon1,"DelEpsilon2 =";DelEpsilon2
2930        PRINT "RTest1      =";RTest1,"RTest2        =";RTest2
2940 !
2950        PRINT "                                "
2960        PRINT "The iterated local bend radius at top roll contact,R, = ";R
2970        PRINT "The iterated incremental strain on the outer layer     = ";Veps
ilon
2980        PRINT "The bending moment at the top nominal contact,Mi,      = ";Mi
2990        PRINT "The initial radius,Rfinish, of the plate               = ";Rfin
ish
3000        PRINT "The bend radius,RRfinish, at its complete stage        = ";RRfi
nish
3010 !
3020         PRINT "                               "
3030         PRINT "                               "
3040        R=(Ra1+Ra2)/2
3050 IF Vepsilon1>Vepsilon2 THEN EpsilonDiff0=Vepsilon2 ELSE EpsilonDiff0=Vepsil
on1
3060        GOSUB MSTRAIN
3070        Vepsilon=(EpsilonDiff0+EpsilonDiff)/2
3080        GOSUB Am1VALUE
```

```
3090        GOSUB Am2VALUE
3100        Mi=2*b*(Am1+Am2) @ MiEI=Mi/EI
3110        Faccuacy=1/R-MiEI-1/RRfinish
3120        C0em=c1*Rfinish*SigmaEm/(E*f3*c2-c1*SigmaEm)
3130 !
3140 PRINT "THE FOLLOWING ARE THE THEORETICAL RESULTS FOR THE ";NA;UN$;" PASS BE
NDING"
3150 PRINT "-----------------------------------------------------------------
-"
3160         PRINT "The expected previous pass bend radius,Rfinish= ";Rfinish
3170         PRINT "The local bend radius at top roll contact,R  = ";R
3180         PRINT "The elastic-elastoplastic interface,C0em     = ";C0em
3190         PRINT "The incremental strain on the surface        = ";Vepsilon
3200         PRINT "The resistant moment at the top roll contact = ";Mi
3210         PRINT "The finished bend radius of the bending      = ";RRfinish
3220         PRINT "The radius of curvature at top roll contact  = ";MiEI
3230         PRINT "The iterative accuracy for R, i.e. Faccuracy = ";Faccuracy
3240         PRINT "The iterative accuracies for (i) DelEpsilon1 = ";DelEpsilon1
3250         PRINT "                             (ii) DelEpsilon2 = ";DelEpsilon2
3260         PRINT "                                              "
3270 !
3280 ! * To evaluate the local incremental stress/strain on the fibre layers*
3290 ! * in the elastoplastic deformation region at the top roll contact    *
3300 ! *-------------------------------------------------------------------*
3310 !
3320         dz0=h-C0em @ dZn=dz0/Ndz @ SigmaEa=SigmaEm @ SigmaEm=0
3330         SigmaE(1)=SigmaEa @ Vde(1)=0 @ Z(1)=C0em @ Z(Ndz+1)=h
3340         SigmaE(Ndz+1)=SigmaEa+H*Vepsilon^n @ Vde(Ndz+1)=Vepsilon
3350 !
3360         EpsilonDiff0=0
3370 !
3380        FOR Li=2 TO Ndz STEP 1
3390         Z(Li)=Z(Li-1)+dZn @ z=Z(Li)
3400         GOSUB MSTRAIN
3410         Vde(Li)=Vepsilon @ SigmaE(Li)=SigmaEa+H*Vepsilon^n
3420         EpsilonDiff0=Vepsilon
3430         Aia=(SigmaE(Li)+SigmaE(Li-1))*(Z(Li)-Z(Li-1))
3440         SigmaEm=SigmaEm+Aia
3450        NEXT Li
3460         SigmaEm=SigmaEm+(SigmaE(Ndz)+SigmaE(Ndz+1))*(Z(Ndz+1)-Z(Ndz))
3470         SigmaEm=.5*SigmaEm/dz0 ! The mean yield stress for the particular
3480                                ! pass in the bending
3490 !
3500 PRINT "                                "
3510 PRINT "**** The local incremental stress/strain on each layer in elastoplas
tic zone"
3520 PRINT "-----------------------------------------------------------------
--------"
3530        FOR Li=1 TO Ndz+1 STEP 1
3540         PRINT "The fibre distance,Z(";Li;"), from neutral layer   =";Z(Li)
3550         PRINT "The incremental strain on the layer,Vde(";Li;")    =";Vde(Li)

3560         PRINT "The local instantaneous yield stress,SigmaE(";Li;")=";SigmaE(
Li)
3570         PRINT "                                    "
3580        NEXT Li
3590 !
3600 PRINT "The determined mean yield stress for the pass,SigmaEm =";SigmaEm
3610 PRINT "The estimated elastic-elastoplastic interface is at    ";C0em
3620 PRINT "The corresponding local bend radius at top roll contact=";R
3630 PRINT "                                    "
3640 PRINT "                                    "
3650 PRINT "                                    "
3660 !
3670 BEEP
3680 BEEP
```

```
3690 BEEP
3700        IF Ncpass=Npass THEN GOTO 3730
3710        Ncpass=Ncpass+1 @ Rfinish=RRfinish @ RRfinish=Rbent(Ncpass)
3720        GOTO 2560
3730 END
3740 ! ++++++++++++++++++++++++++++++++++++++++++++++++++++++++++++++++++++++++++++++

3750 STRAIN: ! ***** STRAIN SUBROUTINE for iterating incremental strain *****
3760 ! ---------------- To define a function as a condition to end the iteration

3770     DEF FNF(x,b1) = a3*x+A1*x^n+A2-b1
3780 !
3790 b1=z/R ! The longitudinal strain for the fibre layer z away from NA
3800 Epsilonh=h/R ! The longitudinal strain for the outer fibre layer
3810 EpsilonDiff=Epsilonh-EpsilonX0 ! The upper incremental strain limit
3820 !                                  The lower incremental strain limit is
3830 !                                  EpsilonDiff0
3840 !
3850         IF EpsilonDiff>= 0 THEN GOTO 3930
3860         PRINT "The bending is completely elastic at the top roll contact"
3870         PRINT "with the assumed bend radius at its contact! PLEASE STOP"
3880         PRINT "the program AND RE-RUN it with re-adjusted input data!"
3890         GOTO 730
3900 !
3910 ! **** To initiate the iteration *************
3920 !       ------------------------
3930         DelEpsilon1=FNF(EpsilonDiff0,b1)
3940 !
3950         IF DelEpsilon1>0 THEN EpsilonDiff0=.99*EpsilonDiff0 ELSE GOTO 3990
3960         DelEpsilon1=FNF(EpsilonDiff0,b1)
3970         GOTO 3950
3980 !
3990         DelEpsilon2=FNF(EpsilonDiff,b1)
4000 !
4010          IF DelEpsilon2<0 THEN EpsilonDiff=1.02*EpsilonDiff ELSE GOTO 4060
4020          DelEpsilon2=FNF(EpsilonDiff,b1)
4030          GOTO 4010
4040 !
4050 !
4060         ProFunction=DelEpsilon1*DelEpsilon2
4070 !
4080 ! **** To commence the iteration *********
4090 !       --------------------------
4100   IF ProFunction=0 THEN GOTO 4310
4110   IF ProFunction>0 THEN GOTO 4210
4120 !
4130          IF ABS (DelEpsilon1)>ABS (DelEpsilon2) THEN GOTO 4220
4140 !
4150         EpsilonDiff=(EpsilonDiff0+EpsilonDiff)/2
4160         DelEpsilon2=FNF(EpsilonDiff,b1)
4170         Vepsilon=EpsilonDiff
4180 !
4190   GOTO 4260
4200 !
4210          IF ABS (DelEpsilon2)>ABS (DelEpsilon1) THEN GOTO 4150
4220          EpsilonDiff0=(EpsilonDiff0+EpsilonDiff)/2
4230          DelEpsilon1=FNF(EpsilonDiff0,b1)
4240          Vepsilon=EpsilonDiff0
4250 !
4260   aA=ABS (DelEpsilon1) @ aA3=ABS (DelEpsilon2)
4270   IF ABS (aA-aA3)<= Accuracy THEN GOTO 4330
4280 !
4290   GOTO 4060
4300 !
4310 IF ABS (DelEpsilon1)=0 THEN Vepsilon=EpsilonDiff0 ELSE Vepsilon=EpsilonDiff
```

```
4320 !
4330 RETURN
4340 ! ++++++++++++++++++++++++++++++++++++++++++++++++++++++++++++++++++++++++++++++

4350 CURVATURE: ! ***** CURVATURE SUBROUTINE for iterating the local bend radius

4360 !             ***** at the top roll nominal contact ************************

4370 ! -THE ITERATION USES THE EXISTING "SIMPLE BISECTION METHOD"-
4380 ! ***** To define a test function to end the iteration *****
4390 ! ***** ------------------------------------------- *****
4400        DEF FNR(R,Rfinish,MiEI) = 1/R-MiEI-1/Rfinish ! The defined function
4410 !    **---------------------------------------**
4420 !
4430 !     The function for the internal resistance to external bending momemt
4440 !
4450        DEF FNM(R,Sigma0) = 2*b*R^2*(c1*Sigma0^2*G/(3*E*a5)+B1)
4460 !   **-----------------------------------------------------------**
4470 ! ** To decide whether the BISECTION METHOD being used for evaluating the
4480 !    local curvature at the top roll nominal contact. For N is equal to any

4490 !    value, other than 0, the BISECTION METHOD is being executed.
4500 !
4510       IF N=0 THEN GOTO 5210
4520 !
4530 ! - To commence the iteration using the Bisection Method:-
4540 !
4550 !
4560   FOR L=1 TO 2
4570       IF L=1 THEN R=Ra1 ELSE R=Ra2
4580       A0=0
4590       GOSUB STRAIN
4600       GOSUB B1VALUE
4610 !
4620 ! - Internal resistance to the external bending moment:-
4630 !
4640       Mi=FNM(R,Sigma0)
4650       MiEI=Mi/EI ! The spring back curvature
4660 !
4670       IF L=1 THEN GOTO 4710
4680 !
4690       Mi2=Mi @ MiEI2=MiEI @ Vepsilon2=Vepsilon @ Ra2=R @ GOTO 4750
4700 !
4710       Mi1=Mi @ MiEI1=MiEI @ Vepsilon1=Vepsilon @ Ra1=R
4720 !
4730   NEXT L
4740 !
4750       RTest1=FNR(Ra1,Rfinish,MiEI1)
4760       RTest2=FNR(Ra2,Rfinish,MiEI2)
4770 !
4780   PRTest=RTest1*RTest2
4790 !
4800   IF PRTest=0 THEN GOTO 5140
4810   IF PRTest>0 THEN GOTO 4970
4820 !
4830       IF ABS (RTest1)>ABS (RTest2) THEN GOTO 4990
4840 !
4850       Ra2=(Ra1+Ra2)/2 @ R=Ra2
4860       GOSUB STRAIN
4870       GOSUB B1VALUE
4880       Mi=FNM(R,Sigma0)
4890       MiEI=Mi/EI
4900 !
4910       RTest2=FNR(R,Rfinish,MiEI)
4920       VR=R @ Ra2=R
4930       Vepsilon2=Vepsilon ! @ A5=RTest2
```

```
4940       GOTO 5090
4950 !
4960 !
4970      IF ABS (RTest2)>ABS (RTest1) THEN GOTO 4850
4980 !
4990      Ra1=(Ra1+Ra2)/2 @ R=Ra1
5000      GOSUB STRAIN
5010      GOSUB B1VALUE
5020      Mi=FNM(R,Sigma0)
5030      MiEI=Mi/EI
5040      RTest1=FNR(R,Rfinish,MiEI)
5050      VR=R @ Ra1=R
5060      Vepsilon1=Vepsilon ! @ A5=RTest1
5070 !
5080 !
5090     sA4=ABS (Ra1) @ sA5=ABS (Ra2)
5100    IF ABS (sA4-sA5)<= RAccuracy THEN GOTO 5420
5110 !
5120      GOTO 4780
5130 !
5140    IF ABS (RTest1)=0 THEN VR=Ra1 ELSE VR=Ra2
5150 !
5160      R=VR @ GOTO 5420
5170 ! *****-------------------------------------------------------------------***
5180 ! ***** FOR Bisection Iterative Method IS NOT USED IN THE SUBROUTINE ***
5190 ! *****-------------------------------------------------------------------***
5200 !
5210         GOSUB STRAIN
5220         GOSUB B1VALUE
5230         Mi=FNM(R,Sigma0)
5240         MiEI=Mi/EI
5250 !       deltaR=ABS (MiEI-MiEI0)
5260 !
5270         RTest=FNR(R,Rfinish,MiEI)
5280 !
5290         IF RTest>0 THEN Ra2=R ELSE GOTO 5330
5300         RTest2=RTest
5310         GOTO 4780
5320 !
5330         NewCurve=(1+1.25)*(1/R) ! The new expected curvature at top
5340 !                                  roll nominal contact
5350 !
5360         Ra1=R @ RTest1=RTest
5370 !
5380         R=1/NewCurve
5390         EpsilonDiff0=Vepsilon
5400 !
5410         GOTO 5210 ! To continue iteration for R
5420 !
5430 RETURN
5440 ! ++++++++++++++++++++++++++++++++++++++++++++++++++++++++++++++++++++++++++

5450 B1VALUE: ! ***** B1VALUE SUBROUTINE for calculating the bending moment in
5460 !          ***** the elastoplastic deformation zone **********************
5470 !
5480      D1=H*K^2*Vepsilon^n3n/(3*a3)
5490      D2=d1*H*K*Vepsilon^np2/np2
5500      D3=K/SQR (3)*(K*Sigma0+H*G)*Vepsilon^(2*n)
5510      D4=a3*H*Vepsilon^n2/(2*n2)
5520      D5=(K*Sigma0+H*G/d1)*Vepsilon^d1
5530      D6=G*Sigma0*K*Vepsilon^n/a3
5540      D7=Sigma0*Vepsilon^2*a3/2
5550      D8=G*Sigma0*Vepsilon
5560 !
5570  B1=D1+D2+D3+D4+D5+D6+D7+D8
5580 !
```

```
5590  RETURN
5600 ! ++++++++++++++++++++++++++++++++++++++++++++++++++++++++++++++++++++++++++++++
5610 !                *-------------------------------------------------------------*
5620 MSTRAIN: ! **** MSTRAIN SUBROUTINE for iterating the incremental strain **
5630 ! ----------**** relative to the uniaxial tensile stress/strain relation **

5640 !                *-------------------------------------------------------------*
5650 !             **** THE SUBROUTINE IS MAINLY FOR THE MULTIPASS BENDING MODE **
5660 !                *-------------------------------------------------------------*
5670 !
5680 !     *-----------------------------------------------------------*
5690 ! **** To define function as a condition for ending the iteration*
5700 !     *-----------------------------------------------------------*
5710 !
5720         DEF FNMR(x,f1,R) = f1*(a3*x+G1*x^n+F1)+1/Rfinish-1/R
5730 !
5740      f1=(Rfinish+z)/(z*Rfinish)
5750      Epsilonh=h*(Rfinish/R-1)/(Rfinish+h) ! Strain on outer fibre
5760      EpsilonDiff=Epsilonh-EpsilonX0 ! The upper incremental strain limit
5770 ! Note:=============== The lower incremental strain limit is EpsilonDiff0
5780 !
5790 ! ***** To initiate the iteration *****
5800 !      *--------------------------*
5810 !
5820         DelEpsilon1=FNMR(EpsilonDiff0,f1,R)
5830 !
5840        IF DelEpsilon1>0 THEN EpsilonDiff0=.99*EpsilonDiff0 ELSE GOTO 5880
5850        DelEpsilon1=FNMR(EpsilonDiff0,f1,R)
5860        GOTO 5840
5870 !
5880         DelEpsilon2=FNMR(EpsilonDiff,f1,R)
5890 !
5900        IF DelEpsilon2<0 THEN EpsilonDiff=1.1*EpsilonDiff ELSE GOTO 5950
5910        DelEpsilon2=FNMR(EpsilonDiff,f1,R)
5920        GOTO 5900
5930 !
5940 !
5950         ProFunction=DelEpsilon1*DelEpsilon2
5960 !
5970 ! ***** To commence the iteration *****
5980 !      *--------------------------*
5990    IF ProFunction=0 THEN GOTO 6230
6000    IF ProFunction>0 THEN GOTO 6120
6010 !
6020 !
6030        IF ABS (DelEpsilon1)>ABS (DelEpsilon2) THEN GOTO 6140
6040 !
6050        EpsilonDiff=(EpsilonDiff0+EpsilonDiff)/2
6060        DelEpsilon2=FNMR(EpsilonDiff,f1,R)
6070        Vepsilon=EpsilonDiff
6080 !      A3=DelEpsilon2
6090    GOTO 6180
6100 !
6110 !
6120        IF ABS (DelEpsilon2)>ABS (DelEpsilon1) THEN GOTO 6050
6130 !
6140        EpsilonDiff0=(EpsilonDiff0+EpsilonDiff)/2
6150        DelEpsilon1=FNMR(EpsilonDiff0,f1,R)
6160        Vepsilon=EpsilonDiff0
6170 !
6180        aA0=ABS (DelEpsilon1) @ aA3=ABS (DelEpsilon2)
6190        IF ABS (aA0-aA3)<= Accuracy THEN GOTO 6250
6200 !
6210    GOTO 5950
6220 !
6230 IF ABS (DelEpsilon1)=0 THEN Vepsilon=EpsilonDiff0 ELSE Vepsilon=EpsilonDiff
```

```
6240 !
6250  RETURN
6260 ! ++++++++++++++++++++++++++++++++++++++++++++++++++++++++++++++++++++++++++++++
6270            !    *-------------------------------------------------*
6280            !    *-------------------------------------------------*
6290 MCURVAT: ! ***** MCURVAT SUBROUTINE for iterating the local bend radius **
6300            ! ***** at the top roll nominal contact in multipass bending   **
6310            !    *-------------------------------------------------*
6320 ! THE ITERATION USES (1) SIMPLE BISECTION METHOD (2) NORMAL METHOD
6330 !
6340 ! ***** To define a test function to end the iteration *****
6350 !
6360             DEF FNR2(R,RRfinish,MiEI) = 1/R-MiEI-1/RRfinish
6370            ! ---------------------------------------------!
6380 ! The FUNCTION for internal resistance to the external bending moment
6390 !
6400             DEF FNM2(Am1,Am2) = 2*b*(Am1+Am2)
6410            ! -------------------------------!
6420 !
6430 ! To decide whether the BISECTION ITERATION is used for evaluating
6440 ! the local bend radius at the top roll nominal contact. For N is
6450 ! equal to any value, other than 0, the BISECTION ITERATION is
6460 ! executed.
6470 !
6480           IF N=0 THEN GOTO 7150
6490 !
6500 ! To commence the iteraion using the BISECTION METHOD
6510 !
6520 !
6530      FOR L=1 TO 2
6540           IF L=1 THEN R=Ra1 ELSE R=Ra2
6550           GOSUB MSTRAIN
6560           GOSUB Am1VALUE
6570           GOSUB Am2VALUE
6580           Mi=FNM2(Am1,Am2) ! The internal resistance to bending moment
6590           MiEI=Mi/EI ! The springback curvature
6600 !
6610           IF L=1 THEN GOTO 6640
6620 !
6630           Mi2=Mi @ MiEI2=MiEI @ Vepsilon2=Vepsilon @ Ra2=R @ GOTO 6680
6640           Mi1=Mi @ MiEI1=MiEI @ Vepsilon1=Vepsilon @ Ra1=R
6650 !
6660      NEXT L
6670 !
6680           RTest1=FNR2(Ra1,RRfinish,MiEI1)
6690           RTest2=FNR2(Ra2,RRfinish,MiEI2)
6700           ProTest=RTest1*RTest2 ! For testing purpose
6710 !
6720           IF ProTest=0 THEN GOTO 7070
6730           IF ProTest>0 THEN GOTO 6890
6740 !
6750           IF ABS (RTest1)>ABS (RTest2) THEN GOTO 6910
6760 !
6770           Ra2=(Ra1+Ra2)/2 @ R=Ra2
6780           GOSUB MSTRAIN
6790           GOSUB Am1VALUE
6800           GOSUB Am2VALUE
6810           Mi=FNM2(Am1,Am2)
6820           MiEI=Mi/EI
6830 !
6840           RTest2=FNR2(R,RRfinish,MiEI)
6850           VR=R @ Ra2=R
6860           Vepsilon2=Vepsilon
6870           GOTO 7010
```

```
6880 !
6890            IF ABS (RTest2)>ABS (RTest1) THEN GOTO 6770
6900 !
6910            Ra1=(Ra1+Ra2)/2 @ R=Ra1
6920            GOSUB MSTRAIN
6930            GOSUB Am1VALUE
6940            GOSUB Am2VALUE
6950            Mi=FNM2(Am1,Am2)
6960            MiEI=Mi/EI
6970            RTest1=FNR2(R,RRfinish,MiEI)
6980            VR=R @ Ra1=R
6990            Vepsilon1=Vepsilon
7000 !
7010            bsA4=ABS (Ra1) @ bsA5=ABS (Ra2)
7020            IF ABS (bsA4-bsA5)<= RAccuracy THEN GOTO 7340
7030 !
7040            GOTO 6700
7050 !
7060 !
7070            IF ABS (RTest1)=0 THEN VR=Ra1 ELSE VR=Ra2
7080            GOTO 7340
7090 !
7100 !      *-------------------------------------------------------------------*
7110 ! ***** To iterate for the local bend radius without using the BISECTION *
7120 ! ***** METHOD                                                             *
7130 !      *-------------------------------------------------------------------*
7140 !
7150            GOSUB MSTRAIN
7160            GOSUB Am1VALUE
7170            GOSUB Am2VALUE
7180            Mi=FNM2(Am1,Am2)
7190            MiEI=Mi/EI
7200 !
7210            RTest=FNR2(R,RRfinish,MiEI)
7220 !
7230            IF RTest>0 THEN Ra2=R ELSE GOTO 7270
7240            RTest2=RTest
7250            GOTO 6700
7260 !
7270            NewCurve=(1+1.25)*(1/R) ! The new assumed curvature at the
7280                                    ! top roll nominal contact
7290            Ra1=R @ RTest1=RTest
7300            R=1/NewCurve
7310            EpsilonDiff0=Vepsilon
7320 !
7330            GOTO 7150
7340 !
7350   RETURN
7360 ! ++++++++++++++++++++++++++++++++++++++++++++++++++++++++++++++++++++++++
7370 !              *-----------------------------------------------------*
7380 Am1VALUE: ! *** Am1VALUE SUBROUTINE for evaluating the internal resistance*
7390            ! *** to the external bending moment in the elasctic deformation*
7400            ! *** at the top roll nominal contact                          *
7410            !  *-----------------------------------------------------*
7420 !
7430            f3=Rfinish/R-1
7440            C0=c1*Rfinish*SigmaEm/(E*f3*c2-c1*SigmaEm)
7450 !
7460            Am1=E*f3*(C0^2/2-Rfinish*C0+Rfinish^2*LOG (1+C0/Rfinish))
7470 !
7480  RETURN
7490 ! ++++++++++++++++++++++++++++++++++++++++++++++++++++++++++++++++++++++++
7500 !              *-----------------------------------------------------*
```

```
7510 Am2VALUE: ! *** Am2VALUE SUBROUTINE for evaluating the internal resistance*
7520           ! *** to the external bending moment in the elastoplastic       *
7530           ! *** deformation at the top roll nominal contact               *
7540           !  *-----------------------------------------------------------*
7550 ! 1- To define the integral functins
7560 !
7570 DEF FNIN(X) = (K*(Co+X)^n+a3*X+g)/(f3-(K*(Co+X)^n+a3*X+g))
7580 !
7590 DEF FNIN1(X) = (K*(Co+X)^n+a3*X+g)/f3
7600 !
7610 DEF FNIN2(X) = Sigma0+H*(Co+X)^n
7620 !
7630 ! 2- To define the common parameters
7640         f3=Rfinish/R-1 @ g=F2 @ N0=20 @ del=Vepsilon/N0
7650         dh=0 @ Am=0 @ Am0=0 @ Ba1=H*f3/K
7660 ! 3- To integrate the integrand [(FNIN(X))^2] using Simpson method
7670       FOR LI=1 TO N0/2 STEP 1
7680         dh0=dh+del @ dh1=dh0+del
7690         s=del*(FNIN(dh)^2+4*FNIN(dh0)^2+FNIN(dh1)^2)/3
7700         Am=Am+s @ dh=dh1
7710       NEXT LI
7720 !
7730         del1=del/2 @ dha=0
7740 A00: FOR LI=1 TO N0 STEP 1
7750         dha0=dha+del1 @ dha1=dh0+del1
7760         sa1=del1*(FNIN(dha)^2+4*FNIN(dha0)^2+FNIN(dha1)^2)/3
7770         Am0=Am0+sa1 @ dha=dha1
7780      NEXT LI
7790 !
7800         IF ABS ((Am0-Am)/Am)<= Tol THEN GOTO AA0
7810         Am=Am0 @ N0=N0*2 @ del1=del1/2 @ dha=0 @ Am0=0
7820 !   PRINT "Am=";Am @ PRINT "      "
7830         GOTO A00
7840 !
7850 AA0: Aa1=FNIN(Vepsilon)^2*FNIN2(Vepsilon)-FNIN(0)^2*FNIN2(0)
7860 Aa2=FNIN(Vepsilon)-FNIN(0)+2*LOG ((1-FNIN1(Vepsilon))/(1-FNIN1(0)))+(FNIN1(
Vepsilon)-FNIN1(0))
7870      Aa3=a3*Am0/f3
7880      Am2=Rfinish^2*(Aa1-Ba1*(Aa2-Aa3))/(2*a3)
7890 !
7900 RETURN
7910 ! ++++++++++++++++++++++++++++++++++++++++++++++++++++++++++++++++++++++++++++
```

APPENDIX 6.1

SURFACE FINISH MEASUREMENTS FOR ROLLERS AND BEND PLATE SPECIMENS

A6.1.1. Introduction

In the roller plate bending process, surface finish of the rolls, together with the surface finish of the plate to be roller-bent, are the main factors in determining the friction condition. The characteristic of the surface condition may also change due to wear resulting from each subsequent bending. Consequently a detailed analysis of the roll surface condition will enable a clearer understanding of the process in terms of the surface interaction, the estimation of pinch forces on the top and bottom rolls and the torque required to convey the bent plate through the pinch region.

The following measurements are thus recommended.

a- The surface condition of the rolls before the bending operations commence.
b- The surface condition of the rolls after each roll bending operation.
c- The surface condition of the rolls after roughening , if the friction effect is studied.
d- The repeat of item (b) if item (c) is undertaken.

Generally a precision surface recording instrument can be used to measure the surface finish of the rolls in situ. However, as this machine was not available, it was impossible to perform these measurements for every successive bending test. Normally, the roll surface texture will not be significantly changed if the ratio of Young's modulus of the roller material and the plate material is high. Since the rollers were made of Sanderson Kayser tool steel and the plate specimens of aluminium, this ratio is high. Consequently, the initial measurements on the rolls should give a good indication of the surface conditions throughout the aluminium specimen bendings. For this reason only the surface finish of the rollers before bending was measured.

It was difficult to carry out adequate Talysurf measurements on a large bent plate. Therefore the collection of the surface roughness history of a bent plate, in the process of bending it to an anticipated bend radius was not done. It was consequently decided to measure only the initial surface finish of the plate.

A6.1.2. Surface condition measurements of the rollers

The relevant surface conditions were the circumferential and the longitudinal surface texture of the rollers. The former would give an indication of how the asperities on the plate and the rollers during bending interaction with each other. Owing to the fact that the rollers were turned, it was impractical to measure the circumferential surface finish. The only possible alternative was to measure its roundness, which due to the large roller size could not be carried out. For this reason only the longitudinal surface finish measurements were obtained.

The longitudinal surface finish samples were measured using the following equipment :

(i) A Taylor Hobson Talysurf, model 3, seres no.RTH112/321.
(ii) A Taylor Hobson rectilinear recorder.
(iii) A Taylor Hobson talysurf adjustable average unit, series No.1707810, Res. 1000 Ω.

The measurements were taken on the longitudinal surface, at a subtending angle of 90°, at three different places along the roller length direction (fig A6.1 and A6.2). Traces of the surface finish from the rectilinear recorder were also obtained. A sample of the traces is shown on fig A6.3. The initial reason to acquire the surface traces of the rollers was to indicate the possible interactional effect of the interaction of surface asperities with those of the bendplate,

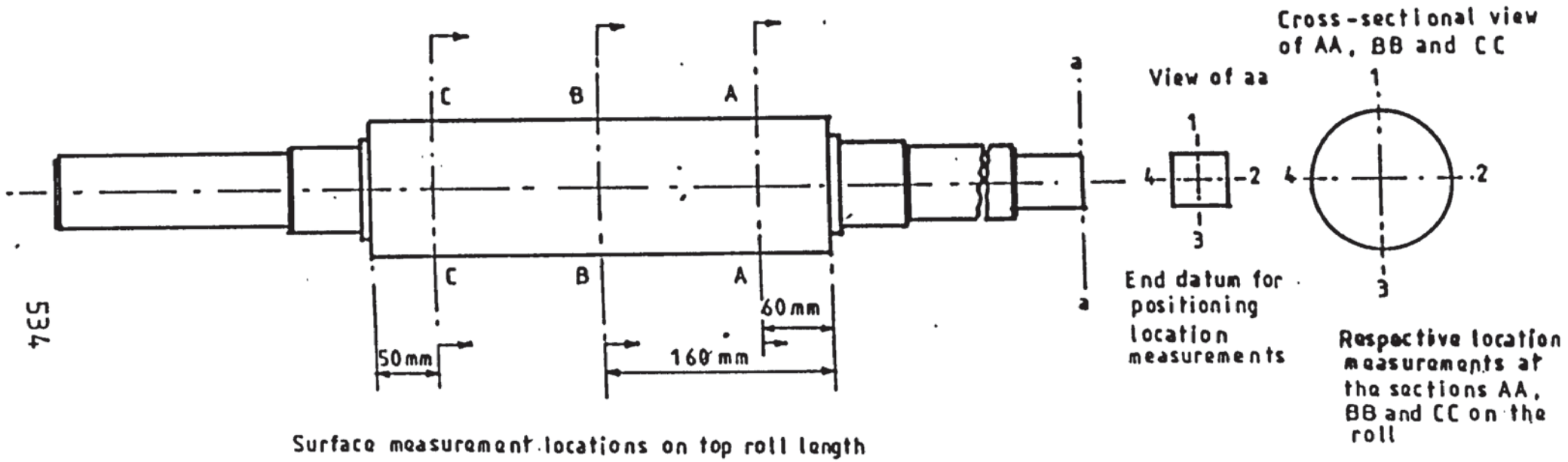

534

FIG A6.1 LONGITUDINAL POSITIONS OF SURFACE FINISH MEASUREMENTS ON TOP ROLL

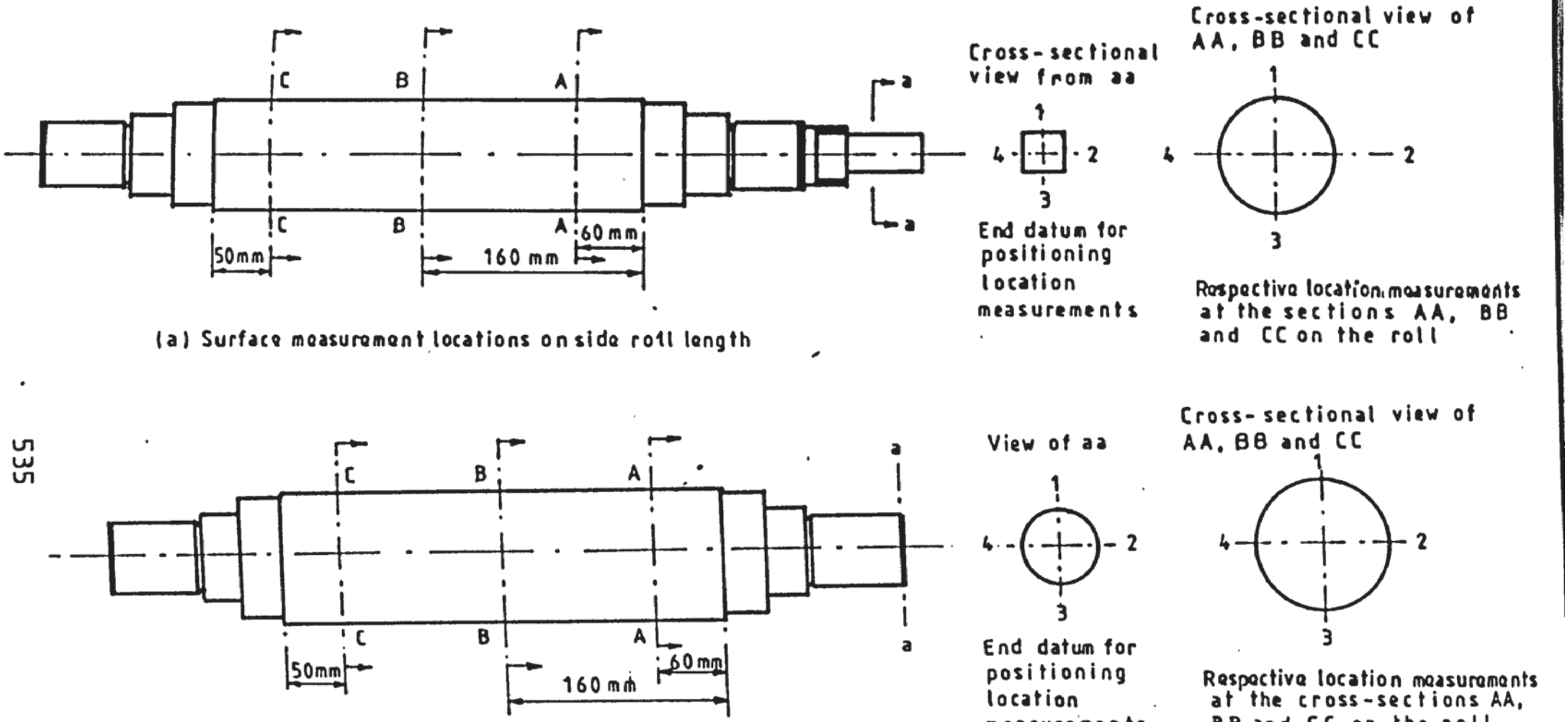

FIG A6.2 LONGITUDINAL POSITIONS OF SURFACE FINISH MEASUREMENTS ON SIDE AND BOTTOM ROLLS

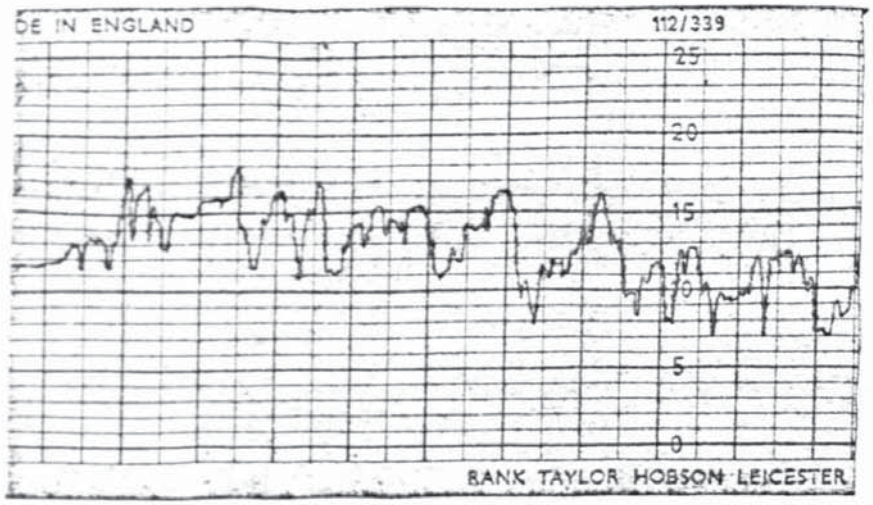

Trace at 1-A (fig A6,1) for top roll

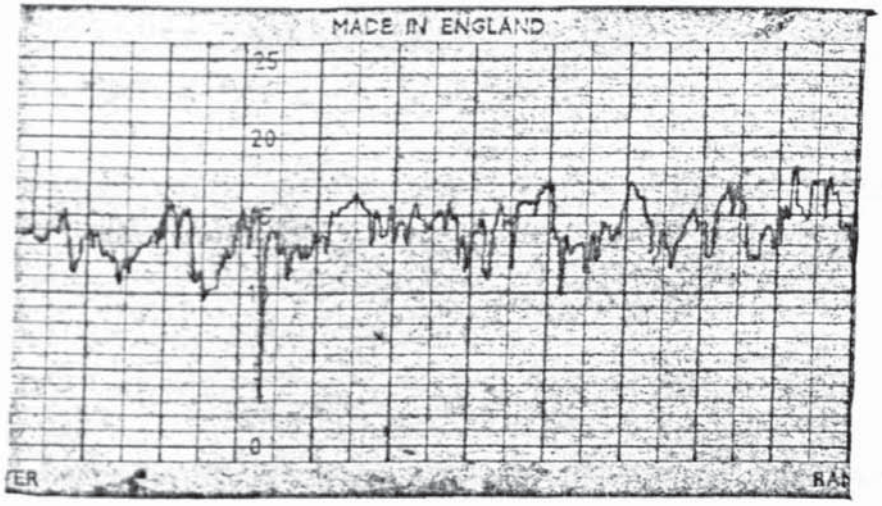

Trace at 1-B (fig A6,1) for top roll

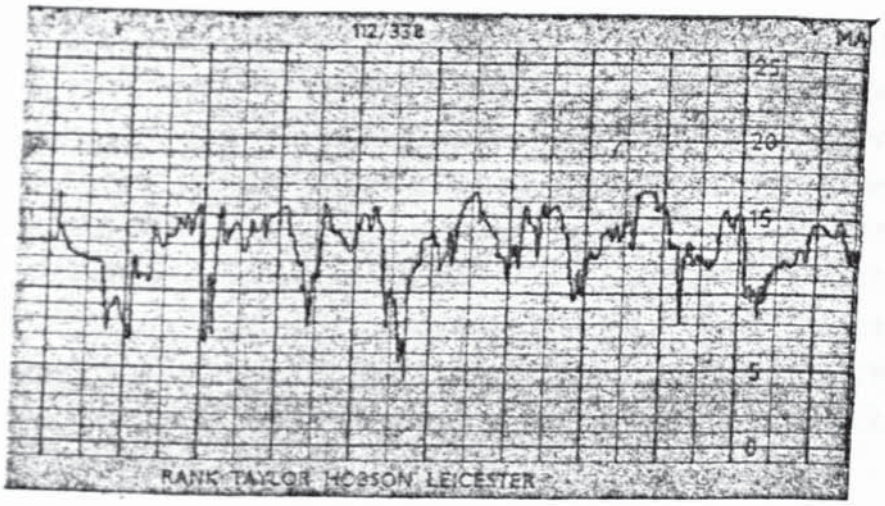

Trace at 1-C (fig A6,1) for top roll

FIG A6,3 SAMPLE OF THE ROLLER SURFACE FINISH TRACE

though it was not performed due to the inadequacy of the available equipment to obtain traces from the workpiece. The traces are therefore considered to be a record for the roller surface texture only.

Prior to the measurements, the surface of the rollers were properly cleaned using Inhibisol.

The measured CAL values are tabulated in Table A6.1.

A6.1.3. Surface finish measurements of the aluminium bend plates

The measurements were carried out using the following equipment :

(i) A portable Taylor Hobson talysurf.
(ii) A Taylor stylus unit (0.25" UNF, O.B.A. 6 mm).

Prior to all surface measurements the plate specimens were cleaned using Inhibisol.

Measurements for the narrow plates were taken along the central line in the longitudinal direction. Their lateral measurements were taken as close as possible to the positions corresponding to those of the longitudinal ones. For the wider plates, the measurements were taken along the two longitudinal lines which approximately equally divided each plate into three strips. The CAL readings for each of the widest plates were taken along the three longitudinal lines dividing the plate into equal strips. The lateral measurements for the latter two cases were also taken.

The average values of the CAL measurements for each plate and its standard deviation were calculated for either surface of each individual plate. Samples of the above values relevant

to the bend specimens are shown in Table A6.2.

Table A6.1 Surface Finish Measurements of The Rollers

The following table shows the CAL values of the surface finish measurements of the rollers. The corresponding positions on the surface of the rollers are indicated in figs A6.1 and A6.2 respectively.

Rollers	Longitudinal positions	The CAL values of the surface finish measurements (μm)			
		Measuring circumferential positions on the rolls			
		1	2	3	4
top	A	0.38	0.38	0.34	0.36
	B	0.4	0.43	0.34	0.4
	C	0.65	0.4	0.46	0.47
Bottom	A	0.6	0.55	0.55	0.52
	B	0.35	0.36	0.35	0.37
	C	0.318	0.32	0.34	0.33
Side-1 (left)	A	0.5	0.6	0.45	0.54
	B	0.34	0.27	0.275	0.29
	C	0.25	0.29	0.31	0.3
Side-2 (right)	A	0.6	0.58	0.5	0.6
	B	0.56	0.55	0.55	0.4
	C	0.525	0.5	0.53	0.5

Table A6.2 Surface Finish Measurements of The Bend Plate Specimens

The table shows the estimated mean values of the surface finish CAL measurements of HP30 aluminium bend plates. Their corresponding standard deviations are also indicated. The allocated specification for each specimen is mainly for reference purpose, see Table 7.1

Items	Spec.	Sampling No.	Data sum (μm)	Mean values (μm)	Standard deviations μm	
					Population	Sample
A	1Lo	6	0.32	0.0533	0.0047	0.0052
	1La	6	0.47	0.0783	0.0146	0.0160
	1Av	12	0.79	0.0658	0.0166	0.0173
	2Lo	8	0.455	0.0568	0.0208	0.0222
	2La	7	0.545	0.0779	0.0156	0.0168
	2Av	15	1.000	0.6667	0.0213	0.0220
B	1Lo	9	0.75	0.0833	0.0115	0.0122
	1La	9	0.91	0.1011	0.0173	0.0183
	1Av	18	1.66	0.0922	0.0172	0.0177
	2Lo	9	0.66	0.0733	0.0176	0.0187
	2La	9	0.91	0.1011	0.0251	0.0267
	2Av	18	1.57	0.0872	0.0258	0.0265
C	1Lo	10	0.59	0.059	0.0226	0.0238
	1La	10	0.75	0.075	0.0291	0.0306
	1Av	20	1.34	0.067	0.0272	0.0279
	2Lo	11	0.51	0.0464	0.0123	0.0129
	2La	11	0.75	0.0682	0.0072	0.0075
	2Av	22	1.26	0.0573	0.0148	0.0152
D	1Lo	9	0.39	0.0433	0.01	0.0106
	1La	8	0.64	0.08	0.0171	0.0183
	1Av	17	1.03	0.0606	0.0229	0.0236
	2Lo	10	0.565	0.0565	0.0059	0.0626
	2La	10	0.79	0.079	0.0024	0.0255
	2Av	20	1.355	0.0678	0.0209	0.0214
E	1Lo	12	0.55	0.0458	0.0104	0.0108
	1La	12	0.79	0.0658	0.0095	0.0996
	1Av	24	1.34	0.0558	0.0141	0.0144
	2Lo	14	0.77	0.055	0.0206	0.0214
	2La	14	1.07	0.0764	0.0111	0.0115
	2Av	28	1.84	0.0657	0.0197	0.0201

Table A6.2 Surface Finish Measurements of the bend plates (Cont)

Items	Spec.	Sampling No.	Data sum (μm)	Mean values (μm)	Standard deviations μm	
					Population	Sample
F	1Lo	8	0.45	0.0563	0.0132	0.0141
	1La	6	0.41	0.0683	0.0107	0.0117
	1Av	14	0.86	0.0614	0.0136	0.0141
	2Lo	7	0.395	0.0564	0.0205	0.0221
	2La	6	0.42	0.07	0.0153	0.0167
	2Av	13	0.725	0.0558	0.0209	0.0218
G	1Lo	9	0.505	0.0561	0.007	0.0074
	1La	10	0.69	0.069	0.0066	0.007
	1Av	19	1.195	0.0629	0.0094	0.0096
	2Lo	9	0.4	0.0444	0.0047	0.0039
	2La	10	0.625	0.0625	0.0068	0.0072
	2Av	19	1.025	0.054	0.0106	0.0109
H	1Lo	10	0.53	0.053	0.0078	0.0082
	1La	10	0.65	0.065	0.0169	0.0178
	1Av	20	1.18	0.059	0.0145	0.0148
	2Lo	10	0.46	0.046	0.0128	0.0135
	2La	10	0.525	0.0525	0.0129	0.0136
	2Av	20	0.985	0.0495	0.0133	0.0136
I	1Lo	4	0.59	0.1475	0.0115	0.0132
	1La	4	0.835	0.2088	0.0241	0.0278
	1Av	8	1.425	0.1781	0.036	0.0384
	2Lo	4	0.575	0.1438	0.0147	0.0170
	2La	5	1.31	0.262	0.0206	0.0231
	2Av	9	1.885	0.2094	0.0615	0.0653
J	1Lo	8	1.4	0.175	0.0265	0.0283
	1La	8	1.94	0.2425	0.0171	0.0183
	1Av	16	3.34	0.2088	0.0404	0.0418
	2Lo	9	1.71	0.19	0.0267	0.0283
	2La	8	2.06	0.2575	0.0171	0.0183
	2Av	17	3.77	0.2218	0.0406	0.0419

Note: In the second column, 1 and 2 represent side 1 and side 2 respectively. While Lo, La and Av represent the measurements along longitudinal and lateral directions of the plate, and the average value of each set of measurements, respectively.

APPENDIX 7.1

DERIVATION OF THE EMPERICAL EXPRESSIONS FOR SPRINGBACK AND BEND RADIUS ANALYSIS FOR THIN PLATE BENDING MODES

A7.1. Introduction

The bend radius measured in section 7.3.7 is the finished bend radius after spring back. A determination of spring back implies a knowledge of the bending mechanics prior to springback, and therefore the dimensions and finished bend radius of the plate specimen need to be measured.

The measurement of the bend radius during the bending process was rather complicated and involved the development of new instruments.

Considering the available instrumentation and the experimental technique, an empirical method to investigate the springback and the bend radius of a bend plate before springback was devised. The method required the bending forces on the rolls and the displacements of the side roll to be determined experimentally.

This particular appendix is thus devoted to the derivation of an empirical mathemetical model to determine the stated parameters by employing the experimental data from the bending conditions. It was noted that some initial bending conditions provided a simpler expression than others. Some cases demanded that a computer programme be written, using numerical iteration based on the experimental results.

The analysis was carried out using cartesian co-ordinates.

A7.2. Assumptions

The following analysis is performed by assuming that :

(i) the deflection of the rollers,

and

(ii) the deformation of rollers surfaces

are negligible.

In addition, the contact between roll and bendplate is assumed to be along the central plane of the plate.

A7.3. Definition of contact angle, θ, between a roll and the bendplate (fig A7.1)

The contact angle, θ, is defined as the angle subtended by a line through the instantaneous centre of a roll and its contact point with the bend-plate and the vertical line through the instantaneous centre of the specified roll.

From the experimental measurements, the contact angle, θ_t, of the top roll and bendplate is expressed as

$$\theta_t = \tan^{-1}(H_t/V_t) \qquad \text{(A7.1a)}$$

The contact angle, θ_b, of the bottom pinch roll is expressed as

$$\theta_b = \tan^{-1}(H_b/V_b) \qquad \text{(A7.1b)}$$

Whilst the final contact angle, θ_s, of the side roll with the bendplate is expressed as follows :

$$\theta_s = \tan^{-1}(H_s/V_s) = \tan^{-1}[(P_s\tan\psi - N_s)/(P_s + N_s\tan\psi)] \qquad \text{(A7.1c)}$$

where, H, V are the respective horizontal and vertical force components measured by the loadcells.

N_s is the bending load measured by the side roll loadcell.

P_s is the axial load measured on the side roll loadcell.

Suffices b, s and t indicate the bottom, side and top roll respectively.

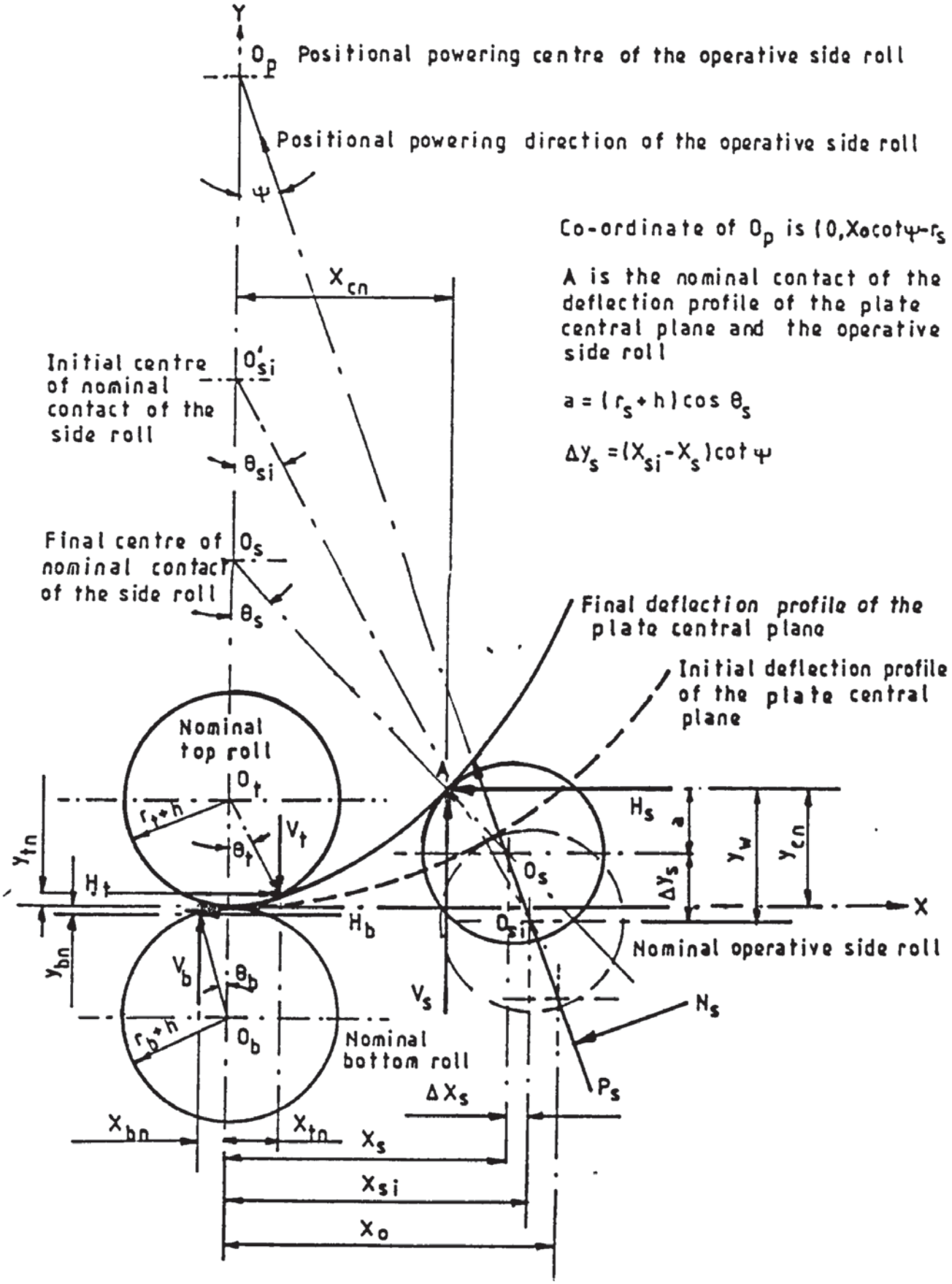

Measured data from experiment:-
Geometrical data are X_{si}, X_s , Δy_s
Force components are P_s , N_s , V_t , H_t , V_b , H_b

FIG A7.1 ROLL GEOMETRY AND FORCES IN BENDING AN INITIALLY CURVED PLATE

A7.4. Displacement of the active side roll in the bending process (fig A7.1)

A7.4.1. Vertical displacement

Let θ_{si} be the initial side roll contact angle and θ_s be its corresponding finished contact angle. If y_∂ is the vertical distance of the initial centre of the active side roll to its contact point with the bendplate, then

$$y_\partial = \Delta y_s + (r_s + h)\cos\theta_s \qquad \text{(A7.2a)}$$

where, r_s is the radius of the side roll and h is half of the bent plate thickness.

In which Δy_s is a measured quantity which is given in (7.10).

The net vertical displacement, $y_{\partial n}$, is thus expressed as

$$y_{\partial n} = \Delta y_s + (r_s + h)\cos\theta_s - (r_s + h)\cos\theta_{si} \qquad \text{(A7.2b)}$$

Expression (A7.2b) can subsequently be stated as follows.

$$y_{\partial n} = \Delta x_s \cot\psi + (r_s + h)\{\cos[\tan^{-1}(H_s/V_s)] - \cos\theta_s\} \qquad \text{(A7.2)}$$

where, $\Delta x_s = x_{si} - x_s$,

x_s is the horizontal distance of the vertical line through the instantaneous centre of the side roll and the vertical line through the centres of the pinch rolls.

x_{si} is the corresponding distance for the initial centre of the side roll.

A7.4.2. Horizontal displacement, $x_{\partial n}$

The geometrical analysis from fig A7.1 gives

$$x_{\partial n}=(x_{si}-x_s)+(r_s+h)\{\sin[\tan^{-1}(H_s/V_s)]-\sin\theta_{si}\} \qquad (A7.3)$$

in which x_{si}, x_s and H_s, V_s are all experimental results (see sections 7.2 and 7.3).

A7.5. Estimation of the initial contact angle, θ_{si}, between side roll and bendplate (fig A7.2)

If r_f is the initial radius of the curved plate, the co-ordinate of the centre of the contact between the plate and side roll, i.e. O_{si}', is thus at $(0, r_f)$.

Let $O_p(0, x_0\cot\psi-r_s-h)$ be the centre of the positional powering direction of the side roll, $(x_0, -r_s-h)$ be the positional centre of the side roll before bending of a straight plate, and $[x_{si}, (x_0-x_{si})\cot\psi-r_s-h]$ be the positional co-ordinate of the instantaneous centre of the side roll.

A7.5.1. Positional equation of the side roll

The positional equation of the powering direction of the side roll can be expressed as :

$$y=(x_0-x)\cot\psi-r_s-h \qquad (A7.4)$$

If (x_i,y_i) is the instantaneous centre of the active side roll, expression (A7.4) can be rewritten as :

$$y_i=(x_0-x_i)\cot\psi-r_s-h \qquad (A7.4a)$$

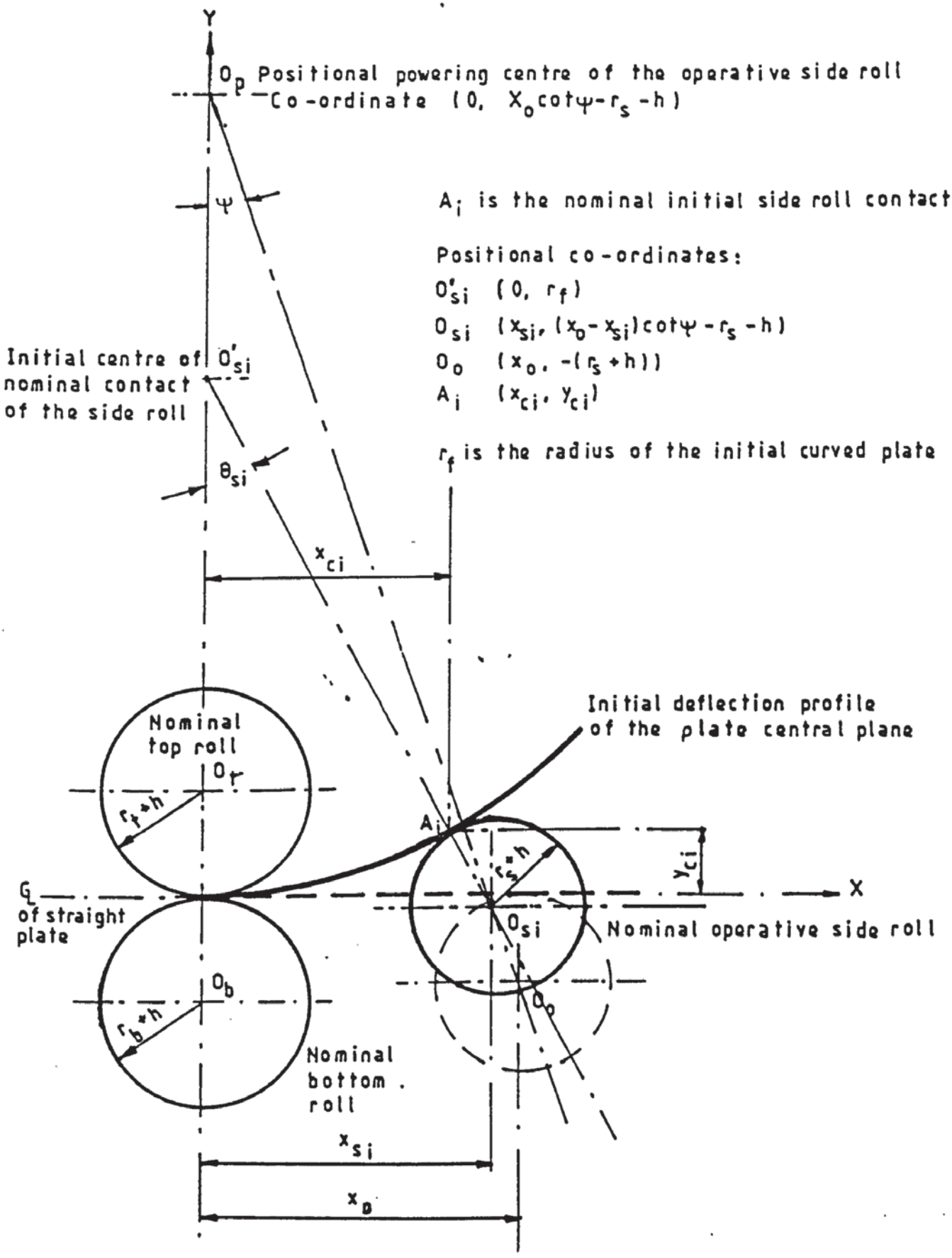

FIG A7.2 ROLL GEOMETRY AND INITIAL CONTACT ANGLE OF SIDE ROLL IN BENDING AN INITIALLY CURVED PLATE

At the start of bending, $x_i=x_{si}$, $y_i=y_{si}$ and h is obtained from experiment.

A7.5.2. Equation of the initial shape of the bendplate

Taking the bendplate to have an initial radius of curvature r_f, its circle equation is thus expressed as follows :

$$x^2+(y-r_f)^2=r_f^2 \qquad \text{(A7.5)}$$

The positional circle equation of the active side roll at the start of the bending is :

$$(x-x_{si})^2+[y-(x_0-x_{si})\cot\psi+r_s+h]^2=(r_s+h)^2 \qquad \text{(A7.5a)}$$

A7.5.3. Contact point

The contact point (X, Y) in equations (A7.5) and (A7.5a) must be the same. If this point is taken as (x_{ci}, y_{ci}), equation (A7.5) can thus be expressed as :

$$y_{ci}-r_f=\pm(r_f^2-x_{ci}^2)^{1/2} \qquad \text{(A7.5b)}$$

Since the positive quantity of the r.h.s. of this equation is not compactible to the actual physical operation of the bending process, y_{ci} is taken as :

$$y_{ci}=r_f-(r_f^2-x_{ci}^2)^{1/2} \qquad \text{(A7.5c)}$$

Substituting y_{ci} into equation (A7.5b) and then (A7.5a) gives

$$(x_{ci}-x_{si})^2+[r_f-(r_f^2-x_{ci}^2)^{1/2}-(x_0-x_{si})\cot\psi+r_s+h]^2=(r_s+h)^2 \qquad \text{(A7.5d)}$$

Equation (A7.5d) can be solved for $x_{ci}=x_{cn}$ through an iterative technique, and $y_{ci}=y_{cn}$ is thus evaluated from equation

(A7.5c).

Since the tangent of the contact angle, θ_{si}, is the first derivative of either (A7.5) or (A7.5a) at (x_{ci}, y_{ci}), then

$$\theta_{si}=\tan^{-1}[-x_{ci}/(y_{ci}-r_f)]=\tan^{-1}\{(x_{si}-x_{ci})/[y_{ci}-(x_0-x_{si})\cot\psi+r_s+h]\}$$

(A7.6)

A7.5.4. Complete expressions for the vertical and horizontal displacements

Substituting the expression of the initial contact angle, θ_{si}, into equations (A7.2) and (A7.3), the complete expressions for the vertical and horizontal displacements are :

$$y_{\partial n}=(x_{si}-x_s)\cot\psi+(r_s+h)\{\cos[\tan^{-1}(H_s/V_s)]-\cos[\tan^{-1}[x_{ci}/(r_f-y_{ci})]]\}$$

(A7.7)

and

$$x_{\partial n}=(x_{si}-x_s)+(r_s+h)\{\sin[\tan^{-1}(H_s/V_s)]-\sin[\tan^{-1}[x_{ci}/(r_f-y_{ci})]]\}$$

(A7.8)

A7.6. Bending of a straight-flat plate (plate axis initially along X-axis) [fig A7.3]

For this case the initial contact angle, θ_{si}, subtended with the vertical line through the centre of active side roll, is zero.

A7.6.1. Using chart values of H_t and V_t

Refering to fig A7.3, it can be shown that the horizontal

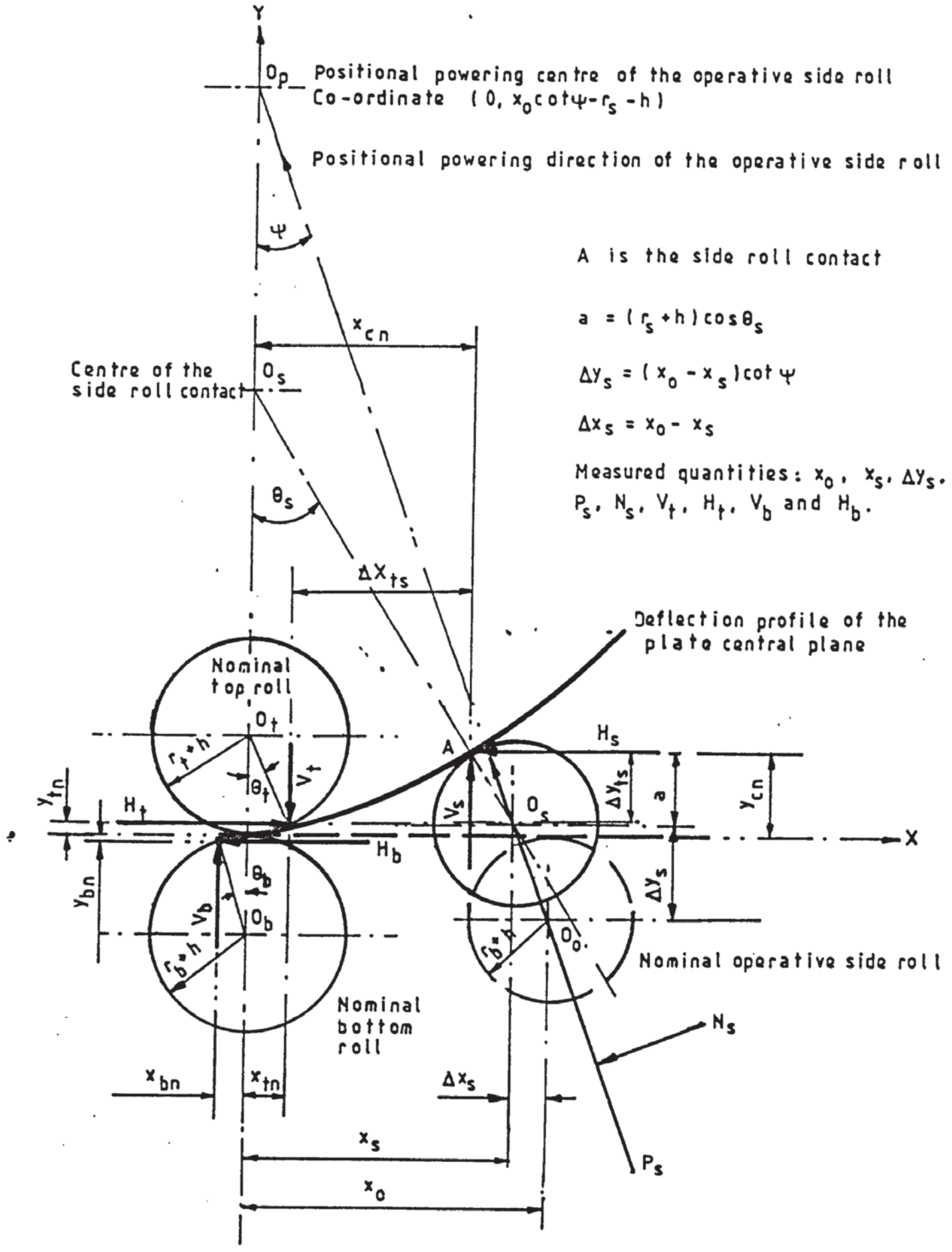

FIG A7.3 ROLL GEOMETRY AND FORCES IN BENDING AN INITIALLY FLAT PLATE

distance, Δx_{ts}, between the side roll and the top roll contacts, at the instance that the bending process is completed, can be expressed as follows :

$$\Delta x_{ts}=x_s-(r_s+h)\sin[\tan^{-1}(H_s/V_s)]-(r_t+h)\sin[\tan^{-1}(H_t/V_t)] \qquad \text{(A7.9)}$$

and the corresponding vertical distance, Δy_{ts}, of the side roll as :

$$\Delta y_{ts}=(x_0-x_s)\cot\psi+(r_s+h)\{\cos[\tan^{-1}(H_s/V_s)]-(r_t+h)\cos[\tan^{-1}(H_t/V_t)]\} \qquad \text{(A7.10)}$$

Assuming the contact point, of the top pinch roll and the bendplate, is at (x_{tn}, y_{tn}), the external bending moment, M_t, about this point in the x-y plane, can thus be expressed as :

$$M_t=H_s\Delta y_{ts}+V_s\Delta x_{ts}=H_b\Delta y_{bt}+V_b\Delta x_{bt} \qquad \text{(A7.11)}$$

where, $(\Delta x_{bt}, \Delta y_{bt})$ is the corresponding bending arms, about the top roll contact, of the force components, (H_b, V_b), on the bottom roll.

The spring back curvature, $1/R_3$, is then given by :

$$1/R_3=M_t/EI=(H_s\Delta y_{ts}+V_s\Delta x_{ts})/EI \qquad \text{(A7.12)}$$

where, E is material Young's modulus and I is the second moment of area of the plate.

Substituting the corresponding quantities in equation (A7.12) from expressions (A7.9) and (A7.10) gives the complete expression for $1/R_3$ in terms of the measured quantities of x_0, x_s, r_s, h, r_t, H_s and V_s.

In addition, the bend radius, R_1, at the top roll contact point before spring back, can subsequently be evaluated in terms of the finished bend radius, R_2, and R_3 as :

$$1/R_1=1/R_2+1/R_3 \qquad \text{(A7.13)}$$

It can be seen that the evaluation does not require any iteration. The evaluation is purely by substitution of the appropriate experimental measurements.

A7.6.2. When chart values of H_t and V_t are not used

In this case, $x_{tn}=(r_t+h)\sin\theta_t$ and $y_{tn}=(r_t+h)(1-\cos\theta_t)$ are unknown and require evaluation.

From the second expression above, the top roll contact angle, θ_t, can be written as :

$$\theta_t=\cos^{-1}[1-y_{tn}/(r_t+h)]$$

From this, the horizontal distance, of the contact point of the top roll, from where X=0, can therefore be expressed as :

$$x_{tn}=(r_t+h)\sin[\cos^{-1}[1-y_{tn}/(r_t+h)]] \qquad \text{(A7.14)}$$

Hence the horizontal bending arm, Δx_{ts}, from the top roll contact to the contact of the side roll and bendplate, can be stated as :

$$\Delta x_{ts}=x_s-(r_s+h)\sin[\tan^{-1}(H_s/V_s)]-(r_t+h)\sin\{\cos^{-1}[1-y_{tn}/(r_t+h)]\} \qquad \text{(A7.15)}$$

and the corresponding vertical bending arm as :

$$\Delta y_{ts}=(x_0-x_s)\cot\psi+(r_s+h)\{\cos[\tan^{-1}(H_s/V_s)]-1\}-y_{tn} \qquad \text{(A7.16)}$$

It also leads to the determination of the corresponding horizontal and vertical bending arm, i.e. Δx_{bt} and Δy_{bt}, from the top roll contact to the contact of the bottom pinch roll and bendplate. The expressions are as follows :

$$\Delta x_{bt}=(r_b+h)\sin[\tan^{-1}(H_b/V_b)]+(r_t+h)\sin\{\cos^{-1}[1-y_{tn}/(r_t+h)]\} \quad \text{(A7.17)}$$

and,

$$\Delta y_{bt}=(r_b+h)\{1-\cos[\tan^{-1}(H_b/V_b)]\}+y_{tn} \quad \text{(A7.18)}$$

After substituting the corresponding parameters in (A7.15), (A7.16), (A7.17) and (A7.18) into expression (A7.11), rearrangement gives :

$$\begin{aligned}&\Delta y_{tn}(H_b+H_s)+(r_t+h)\sin\{\cos^{-1}[1-y_{tn}/(r_t+h)]\}\\&=H_s\{(x_0-x_s)\cot\psi+(r_s+h)\{\cos[\tan^{-1}(H_s/V_s)]-1\}\}\\&\quad+V_s\{x_s-(r_s+h)\sin[\tan^{-1}(H_s/V_s)]\}-H_b\{(r_b+h)\{1-\cos[\tan^{-1}(H_b/V_b)]\}\}\\&\quad-V_s(r_b+h)\sin[\tan^{-1}(H_b/V_b)]\end{aligned} \quad \text{(A7.19)}$$

The iteration of equation (A7.19) gives y_{tn} and x_{tn} and are thus determined by using equation (A7.14).

After (x_{tn}, y_{tn}) is determined, the springback curvature, $1/R_3$, and the bend curvature, $1/R_1$, can thus be obtained by substituting the values of the x_{tn} and y_{tn} into the following expressions.

$$1/R_3=\Big\{H_s\{(x_0-x_s)\cot\psi+(r_s+h)\{\cos[\tan^{-1}(H_s/V_s)]-1\}-y_{tn}\}$$

$$+V_s\{x_s-(r_s-h)\sin[\tan^{-1}(H_s/V_s)]-x_{tn}\}\Big\}/EI \qquad \text{(A7.20)}$$

and,

$$1/R_1=1/R_2+1/R_3 \qquad \text{(A7.21)}$$

respectively.

A7.7. Bending of an initially curved plate

From fig A7.1, the top roll contact is at (x_{tn}, y_{tn}). The equilibrium consideration of the external bending moment, M_t, about this contact point is taken as :

$$M_t=H_s\Delta y_{ts}+V_s\Delta x_{ts}=H_b\Delta y_{bt}+V_b\Delta x_{bt} \qquad \text{(A7.22)}$$

From the geometry on the figure, it can be shown that

$$O_tO_b=r_b+r_t+2h$$

and

$$\Delta y_{bt}=y_{bn}+y_{tn}=O_tO_b-(r_b+h)\cos\theta_b-(r_t+h)\cos\theta_t$$

The latter can further be expressed as

$$\Delta y_{bt}=r_b+r_t+2h-(r_b+h)\cos\theta_b-(r_t+h)\cos\theta_t \qquad \text{(A7.23)}$$

A7.7.1. When $r_t=r_b=r_p$, V_t and H_t, H_b and V_b are measured

For this case expression (A7.23) can be rewritten as

$$\Delta y_{bt}=(r_p+h)\{2-\cos[\tan^{-1}(H_b/V_b)]-\cos[\tan^{-1}(H_t/V_t)]\} \qquad \text{(A7.24)}$$

The above equation is the vertical bending moment arm from the bottom roll contact to the contact of the top roll. The corresponding horizontal bending moment arm, Δx_{bt}, is expressed as follows.

$$\Delta x_{bt}=(r_p+h)\{\sin[\tan^{-1}(H_b/V_b)]+\sin[\tan^{-1}(H_t/V_t)]\} \quad \text{(A7.25)}$$

The corresponding bending arms, i.e. $(\Delta y_{ts}, \Delta x_{ts})$, from the top roll contact to the side roll contact, at (x_{cn},y_{cn}), are as follows :

$$\Delta y_{ts}=y_{cn}-(r_s+h)\sin[\tan^{-1}(H_s/V_s)]-(r_p+h)\sin[\tan^{-1}(H_t/V_t)]\} \quad \text{(A7.26)}$$

and

$$\Delta x_{ts}=x_S-(r_s+h)\sin[\tan^{-1}(H_s/V_s)]-(r_p+h)\sin[\tan^{-1}(H_t/V_t)]\} \quad \text{(A7.27)}$$

Substituting either expressions (A7.24) and (A7.25) or expressions (A7.26) and (A7.27) into $1/R_3=M_t/EI$ gives the elastic recovery curvature, at the top roll contact, due to the release of the loading, as

$$1/R_3=(r_p+h)\Big(H_b\{2-\cos[\tan^{-1}(H_b/V_b)]-\cos[\tan^{-1}(H_t/V_t)]\}$$

$$+V_b\{\sin[\tan^{-1}(H_b/V_b)]+\sin[\tan^{-1}(H_t/V_t)]\}\Big)/EI \quad \text{(A7.28a)}$$

or,

$$1/R_3=\Big[H_s\{x_{cn}-(r_p+h)\sin[\tan^{-1}(H_t/V_t)]\}$$

$$+V_s\{y_{cn}-(r_p+h)(1-\cos[\tan^{-1}(H_t/V_t)])\}\Big]/EI \quad \text{(A7.28b)}$$

Subsequently the radius of curvature of the bend, before spring back, at the contact point, can be evaluated by substituting either (A7.28a) or (A7.28b) into expression (A7.13).

Its evaluation does not require any iteration.

A7.7.2. When H_t and V_t are not measured

Following the derivation for the similar case in bending a straight flat plate (see section A7.5), it can be shown that the expressions (A7.14) to (A7.18) are also applicable for this particular condition. The substitution of the relevant expressions into (A7.22) generates the following expression.

$$H_s(y_{cn}-y_{tn})+V_s\{x_{cn}-(r_p+h)\sin(\cos^{-1}[1-y_{tn}/(r_p+h)])\}$$

$$=(r_p+h)\Big\{V_b\sin[\tan^{-1}(H_b/V_b)]+h_b(1-\cos[\tan^{-1}(h_b/V_b)])$$

$$+V_b\sin\{\cos^{-1}[1-y_{tn}/(r_p+h)]\}\Big\}+H_by_{tn} \qquad \text{(A7.29)}$$

Substituting the iterated values of $x_{tn}=x_{ci}$ and $y_{tn}=y_{ci}$ from expressions (A7.5) and (A7.5c) into the above expression, enables the values of y_{tn} to be obtained through the iterative technique using (A7.29). The value of x_{tn} can subsequently be obtained using the following expressions :

$$1/R_3=\{H_s(y_{cn}-y_{tn})+V_s(x_{cn}-x_{tn})\}/EI \qquad \text{(A7.30)}$$

and

$$1/R_1=1/R_2+\{H_s(y_{cn}-y_{tn})+V_s(x_{cn}-x_{tn})\}/EI \qquad \text{(A7.31)}$$

respectively.

A7.8. Bending of a very thin plate

Expressions (A7.29), (A7.20) and (A7.21) are the general expressions for determining the corresponding parameters. It can be seen that for the condition of $H_b=0$ the contact of the bottom pinch roll and the plate is at $X=0$. It thus simplifieds the expression (A.29) to

$$(r_p+h)V_b\sin\{\cos^{-1}[1-y_{tn}/(r_p+h)]\}$$

$$=H_s(y_{cn}-y_{tn})+V_s\{x_{cn}-(r_p+h)\sin(\cos^{-1}[1-y_{tn}/(r_p+h)])\} \quad \text{(A7.32)}$$

In this case the bending is similar to bending a thin cantilever plate with an initial radius of curvature of r_f.

A7.9. Summary of the analysis

From the above analysis, the following conclusions can be drawn :

(a) It is possible to study experimentally the springback and the bend radius of a bend plate before springback takes place using the present instrumentation and the experimental set-up. However, it requires the incorporation of the derived mathematical model with certain measured data.

(b) The experimental data required for the mathematical model are :

1- The force components on the pinch rolls and active side roll (for determining the contact angle).
2- The horizontal distances of the centres of the bottom pinch roll and the active side roll, before and after bending.
3- The vertical displacement of the centre of the active side roll.

If no other data is available, a numerical iteration to analyse the results is required. The estimation of the springback, and the bend radius of a bendplate before springback, will be easier, if the force components on the top roll are also experimentally determined.

(c) The evaluation of the springback and the bend radius of the plate before springback takes place is more complex in bending a pre-bent plate with initial bend radius of r_f.

ACKNOWLEDGEMENTS

To :

Professor D H Sansome, whom I wish to express my thanks for initiating this interesting and challenging project, his encouragement and discussion during the period of his supervision.

Dr K Baines, whom I wish to express my thanks for helping to get an extension for the research grant so as to allow for the completion of the mathematical model, for his patience to discuss and read the manuscripts of the thesis, for his continuous interest in the research and its further development.

Dr I M Cole, whom I wish to express my thanks for his reading of the final draft of the thesis.

I am grateful to the Science and Engineering Research Council for their financial support and to Head Wrightson Teesdale Ltd. (HWT) for their co-operative support in the research.

I would also like to thank :

Mr. R Wright, formerly Technical Director of HWT, and Mr. M Stoddart, Production Engineer at HWT, for their assistance and discussion during the design stage of the model plate bender.

Mr. M J Scattergood, the Departmental Technical Superintendent of the Department of Mechanical and Production Engineering, Aston University, for his permission to use the departmental facilities out-side the normal working hours.

Members of the technical staff in the Department of Mechanical and Production Engineering for their assistance and friendship, especially Messrs T Rudge, P McGuire, F Fletcher, G Yardley, K Harrison and B Marshall.

My colleague, Mr. V Kumar for checking the typed-scripts.

To all my past and present colleagues, I wish to express my appreciation for their companionship and friendship during my period of loneliness.

Finally, I wish to express my thanks and deep appreciation to Dr. R F LeFeuvre and Mr. W E Marshall, both at Newcastle Upon Tyne Polytechnic, for their continuous encouragement and friendship throughout the years.

Supervisor : Dr. K. Baines

Advisor : Dr. I. M. Cole

REFERENCES

Plasticity :

1. Avitzur, B.,
"Metalforming : The application of limit analysis", Marcel Dekker Inc., New York, 1980.

2. Drucker, D. C.,
"Relation of experiments to mathematical theories of plasticity", J. Appl. Mech., Trans ASME, 1949, 16.

3. Dubey, R. N. and Hillier, M. J.,
"Yield criteria and Bauschinger effects for a plastic solid", J. Basic Engg., Trans ASME, 1972, March, 228-230.

4. Finzi, L.,
"On the principle of Haar and von Karman in statically determinate problems of plasticity", J. Appl. Mech., Trans ASME, 1957, Sept., 461-463.

5. Ford, H. and Alexander, J. M.,
"Advanced mechanics of materials", 2nd ed., Ellis Horwood, 1977.

6. Handelman, G. H., Lin, C. C., and Prager, W.,
"On the mechanical behaviour of metals in the strain-hardening range", Quart. Appl. Maths, 1947, 4, 397-407.

7. Hencky, H.,
"The new theory of plasticity, strain hardening, and creep, and the testing of the inelastic behaviour of metals", J. Appl. Mech., APM-55-18, 1934, 1, 151-155.

8. Hill, R.,
"A variational principle of maximum plastic work in classical plasticity", Quart. J. Mech. Appl. Maths, 1948, 1, 18-28.

9. Hill, R.,
"A theory of the yielding and plastic flow of anisotropic metals", Proc. Roy. Society, Series A, London, 1948, 193, 281-297.

10. Hill, R.,
"A comparative study of some variational principles in the theory of plasticity", J. Appl. Mech., 1950, 17, 64-66.

11. Hill, R.,
"Mathematical theory of plasticity", Clarendon Press, Oxford, 1951.

12. Hill, R.,
"On the state of stress in plastic-rigid body at the yield point", Phil. Mag., 1951, 42, 868.

13. Hill, R.,
"A new method for determining the yield criterion and plastic potential of ductile metals", J. Mech. Phys. Solids, 1953, 1, 271-276.

14. Hill, R.,
"A general method of analysis for metal working processes", J. Mech. Phys. Solids, 1963, 11, 305-326.

15. Hodge, P. and Prager, W.,
"A variational principle for plastic materials with strain-hardening", J. Maths Physics, 1948, 27, 1-10.

16. Hundy, B. B. and Green, A. P.,
"A determination of plastic stress-strain relations", J. Mech. Phys. Solids, 1954, 3, 16.

17. Johnson, W. and Mellor, P. B.,
"Engineering plasticity", Von Nostrand Reinhold, London, 1980.

18. Lahoti, G. D. and Kobayashi, S.,
"On Hill's general method of analysis for metal-working processes", Int. J. Mech. Sci., 1974, 16, 521-540.

19. Lode, W.,
"Der Einfluss der mittleren Hauptspannung auf das Fliessen der Metalle", Forschungsarbeiten aus dem Gebiete des Ingenieurwesens, No.303, VKI-Verlag, Berlin, 1928.

20. Marin, J.,
"The mechanical behaviour of engineering materials", Prentice Hall, Englewood Cliffs, N. J., 1962.

21. Mendelson, A.,
"Plasticity : theory and application", Macmillian, New York, 1964.

22. Nadai, A.,
"Plasticity, a mechanics of the plastic state of matter", McGraw Hill, New York, 1931, 75.

23. Nadai, A.,
"Theory of strength of materials", J. Appl. Mech., 1934, 1, 111-129.

24. Nadai, A.,
"Theory of flow and fractures of solids", Vol 2, McGraw Hill, New York, 1963.

25. Osgood, W. R.,
"Combined stress tests on 24S-T aluminium alloy tubes", J. Appl. Mech., Trans ASME, 1947, 69, A-147.

26. Prager, W.,
"On isotropic materials with continuous transition from elastic to plastic state", Proc. 5th Int. Congr. Appl. Mech., Cambridge, Mass., 1938, 234-237.

27. Prager, W.,
"Strain hardening under combined stress", J. Appl. Phys., 1945, 16, 837-840.

28. Prager, W.,
"The stress-strain law of the mathematical theory of plasticity - a survey of recent progress", J. Appl. Mech., Trans ASME, 1948, 15.

29. Sowerby, R. and Uko, D. K.,
"A review of certain aspects of the Bauschinger effects in metals", Mat. Sci. Engg., 1979, 41, 43-58.

30. Taylor, G. I. and Quinney, H.,
"The plastic distortion of metals", Phil Trans Roy. Society, Series A, 1931, 230, 323-362.

31. Washizu, K.,
"Variational methods of elastic and plasticty", 2nd ed., Pergaman, New York, 1975.

Roll bending

32. Bala, S. R. and Malik, L.,
"Roll forming to higher strain levels successful", Welding and Metal Fabrication, 1983, March, 100.

33. Bassett, M. B. and Johnson, W.,
"The bending of plate using a three roll pyramid type plate bending machine", J. Strain Analysis, 1966, 1, 5, 398.

34. Hanson, N. E. and Jannerup, O.,
"Modelling of elastic-plastic bending of beams using a roller bending machine, ASME paper No.78WA/Prod 6, 1979.

35. Ludowig, G. and Zicke, G.,
"Steuen Von CNC-Walzrundmaschinen durch simulation", Industrie Anzeiger, Nr 95, 1981, 25, 11, 34.

36. Ludowig, G. and Zicke, G.,
"Biegen von blechen auf CNC-Walzrundmaschinen". Bänder Bleche Rohre, 1985, 22, 5(S), 116.

37. Roggendorff, S. and Haeusler, J.,
"Plate bending : three rolls and four rolls compared", Welding and Metal Fabrication, 1979, Jul./Aug., 353.

38. Winship, J. T.,
"Basics of roll bending", Amer. Mach., 1983, 127(2), 105.

Plate/Beam bending

39. Ashwell, D. G. and Greenwood, E. D.,
"The pure bending of rectangular plates", Engineering, 1950, 21, 50-53, 77-78.

40. Ashwell, D. G.,
"The anticlastic curvature of rectangular beams and plates", J. Roy. Aero. Society, 1950, 54, 708-715.

41. Barlow, D. A.,
"Yield criteria and the bending of wide beams", J. Mech. Phys. Solids, 1954, 2, 259-264.

42. Barten, H. J.,
"On the deflection of a cantilever beam", Quart. Appl. Maths, 1944, 2, 168-171.

43. Benscotter, S. U.,
"A theory of torsion bending for multicell beams", J. Appl. Mech., 1954, March, 25-34.

44. Berger, H. M.,
"A new approach to the analysis of large deflections of plates", J. Appl. Mech., 1955, Dec., 465-472.

45. Bisshopp, K. E. and Drucker, D. C.,
"Large deflection of cantilever beams", Quart. Appl. Maths, 1945, 3, 3, 272-275.

46. Botros, B. M.,
Springback is sheet metal forming after bending", Trans ASME, paper No.67-WA/Prod-17, 1967.

47. Coan, J. M.,
"Large deflection theory for plates with small initial curvature loaded in edge compressiom", J. Appl. Mech., 1951, Jun., 143-151.

48. Conway, H. D.,
"The large deflection of simply supported beams", Phil. Mag., 7th ser., 1947, 38, 905-911.

49. Conway, H. D.,
"The approximate analysis of certain boundary-value problems", J. Appl. Mech., Trans ASME, 1960, 27, 275-277.

50. Conway, H. D. and Farnham, K. A.,
"Anticlastic curvature of strips of variable thickness", Int. J Mech. Sci., 1965, 7, 451-458.

51. Dadras, P. and Majlessi, S. A.,
"Plastic bending of work hardening materials", J. Engg. Ind., Trans ASME, 1982, 104, 224-230.

52. Danese, G.,
"New mathematical method on the distortion of metal sheets subjected to plastic bending", Microtecnic, 1958, 12, 6, 313-322.

53. Datsko, J. and Yang, C. T.,
"Correlation of bendability of materials with their tensile properties", J. Engg. Ind., Trans ASME, 1960, Nov., 309-314.

54. Deverall, L. I. and Thorne, C. J.,
"Some thin plate problems by the sine transform", J. Appl. Mech., 1951, Jun., 151-156.

55. Deverall, L. I.,
"Solution of some problems in bending of thin clamped plates by means of the method of Muskhelishvilli", J. Appl. Mech., Trans ASME, 1957, 27, 295-298.

56. Drucker, D. C.,
"The effect of shear on the plastic bending of beams", J. Appl. Mech. 1956,, Dec., 509-514.

57. Eason, G.,
"The elastic, plastic bending of simply supported plate", J. Appl. Mech., 1961, Sept., 395-401.

58. El-Domiaty, A. and Shabaik, A. H.,
"Bending of work-hardening metals under the influence of axial load", J. Mech. Working Tech., 1984, 10, 57-66.

59. Frisch-Fay, R.,
"Large deflections of cantilever under two concentrated loads", J. Appl. Mech., Trans ASME, Ser. E, 1962, 29, 200-205.

60. Fung, Y. C. and Wittrick, W. H.,
"The anticlastic curvature of a strip with lateral thickness variation", J. Appl. Mech., 1954, Dec., 351-358.

61. Gaydon, F. A.,
"An analysis of the plastic bending of a thin strip in its plane", J. Mech. Phys. Solids, 1953, 1, 103-112.

62. Gerard, G.,
"Effect of bend width upon minimum bend radii", J. Aero. Sci., 1946, 13, 4, 161-182.

63. Green, A. E.,
"On Reissner's theory of bending of elastic plates", Quart. Appl. Maths, 1949, 7, 2, 223-228.

64. Grover, R. L. and Chou, S. I.,
"Solution of plane stress and plane bending problems by boundary integral equations",5th Tran. Int. Conf. Struct. Mech. React. Tech., Berlin, 1979, Aug., Paper M11/1.

65. Hodge, P. G.,
"Interaction curves for shear and bending of plastic beams", J. Appl. Mech., 1957, 27, 453-456.

66. Hoffman, O. and Sachs, G.,
"Introduction to the theory of plasticity for engineers", McGraw Hill, New York, 1953, 266-272.

67. Holl, D. L.,
"Analysis of plate examples by difference methods and the superposition principles", J. Appl. Mech., 1936, 3, A81-89.

68. Holl, D. L.,
"Cantilever plate with concentrated edge load", J. Apple. Mech., 1937, 4, A8-10.

69. Horrock; D. and Johnson, W.,
"On anticlastic curvature with special reference to plastic bending : A literatute survey and some experimental investigations", Int. J. Mech. Sci., 1967, 9, 835-861.

70. Jaramillo, T. J.,
"Deflections and moments due to a concentrated load on a cantilever plate of infinite length", J. App. Mech., Trans ASME, 1950, 72, 67-72.

71. Johnson, W. and Yu, T. X.,
"Springback after the biaxial elastic-plastic pure bending of rectangular plate - I", Int. J. Mech. Sci., 1981, 23, 619-630.

72. Johnson, W. and Yu, T. X.,
"On the range of applicability of results for the spring back of an elastic/perfectly plastic rectangular plate after subjecting it t biaxial pure bending - II", Int. J. Mech. Sci., 1981, 23, 631-637.

73. Johnson, W. and Yu, T. X.,
"The large elastic deflection of thin strip in V-die bending and the onset of plasticity", Proc. Int. Mech. Engrs, 1984, 198c, 4.

74. Leissa, A. W. and Niedenfuhr, F. W.,
"A study of the cantilevered square plate subjected to a uniform loading", J. Aerospace Sci., 1962, 29, .1, 162-169.

75. Leissa, A. W. and Niedenfuhr, F. W.,
"Bending of a square plate with two adjacent edges free and the others clamped or simply supported", AIAA Journal, 1963, 1, 1, 116-120.

76. Lin, T. H., Lin, S. R. and Mazelsky, B.,
"Elastoplastic bending of rectangular plates with large deflection", J. Appl. Mech., Trans ASME, 1972, Dec., 979-981.

77. Lubahn, J. D. and Sachs, G.,
"Bending of an ideal plastic metal", Trans ASME, 1950, 72, 201-208.

78. MacGreger, C. W.,
"Deflection of a long helical gear tooth", Mech. Engg, 1935, 57, 225-227.

79. Majlessi, S. A. and Dadras, P.,
"Pure plastic bvending of sheet laminates under plane strain condition", Int. J. Mech. Sci., 1983, 25, 1-14.

80. Martin, G. and Tsang, S.,
"The plastic bending of beams considering die deflection effects", J. Engg. Ind., Trans ASME, 1966, Aug., 237-250.

81. Nash, W. A.,
"Several approximate analysis of the bending of a rectangular cantilever plate by uniform normal pressure", J. Appl. Mech., 1952, 19, 33-36.

82. Ohashi, Y. and Murakami, S.,
"Large deflection in elastoplastic bending of a simply supported circular plate under a uniform load", J. Appl. Mech., Trans ASME, 1966, Dec.,866-870.

83. Ohashi, Y. and Kamiya, N.,
"On the bending of thin plates of material having a non-linear stress-strain relation", Int. J. Mech. Sci., 1967, 9, 183-193.

84. Osgood, W. R.,
"Plastic bending", J. Aero. Sci., 1944, 11, 213-226.

85. Osgood, W. R.,
"Plastic bending-Further considerations", J. Aero. Sci., 1945, 12, 253-272.

86. Osgood, W. R.,
"Plastic bending-Approximate solution", J. Aero. Sci., 1945, 12, 408-420.

87. Phillips, A.,
"Bending with axial force of curved bars in plasticity", J. Appl. Mech., 1952, 19, 327-330.

88. Plass, H. J., Gaines, J. H. and Newsom, C. D.,
"Application of Reissner's variational principle to cantilever plate deflection and vibration problems", J. Appl. Mech., Trans ASME, series E, 1962, 29, 127-135.

89. Prescott, J.,
"The equations of equilibrium of an elastic plate under normal pressure", Phil. Mag., 6th ser., 1922, 43, 67-125.

90. Ramachandra Rao, B. S.,
"Generalized orthogonality relations for the flexure of rectangular plates and a cantilever problem for semi-infinite plates", J. Struct. Mech., 1981, 9, 1, 51-70.

91. Reissner, E.,
"On the theory of bending of elastic plates", J. Math. Phys., 1944, 23, 184-191.

92. Reissner, E.,
"The effect of transverse shear deformation on the bending of elastic plates", J. Appl. Mech., 1945, Jun., A69-77.

93. Reissner, E.,
"On bending of elastic plates", Quart. Appl. Maths, 1947, 5, 1, 55-68.

94. Reissner, E.,
"Upper and lower bounds for deflections of laminated cantilever beams including the effect of transverse shear deformation", J. Appl. Mech., Trans ASME, 1973, Dec., 988-991.

95. Reissner, E.,
"Dynamic response of an elastic plate strip to a moving line load", AIAA Journal, 1963, 1, 2, 354-360.

96. Rohde, F. V.,
"Large deflections of a cantilever beam with uniformly distributed load", Quart. Appl. Maths, 1953, 11, 337-338.

97. Sangdahl, G. S., Aul, E. L. and Sachs, G.,
"An investigation of stress and strain states occuring in bending rectangular bars", Proc. Soc. Exper. Stress Analysis, 1948, 6, I, 1-18.

98. Seames, A. E. and Conway, H. D.,
"A numerical procedure for calculating the large deflections of straight and curved beams", J. Appl. Mech., Trans ASME, 1957, 27, 289-294.

99. Shaffer, B. W. and House, R. N.,
"The significance of zero shear stress in the pure bending of a wide curve-bar", J. Aero. Sci., 1957, April, 307-308.

100. Shaffer, B. W. and House, R. N.,
"Displacements in a wide curved bar subjected to pure elastic-plastic bending", J. Appl. Mech., 1957, 27, 447-452.

101. Shaffer, B. W. and House, R. N.,
"The elastic-plastic stress distribution within a wide curved bar subjected pure bending", J. Appl. Mech., 1955, 25, 303-310.

102. Shepherd, W. M. and Gaydon, F. A.,
"Plastic bending of a ring sector by end couples", J. Mech. Phys. Solids, 1957, 5, 296-301.

103. Stelson, K. A. and Gossand, D. C.,
"An adaptive pressbrake control using an elastic-plastic material model", J. Eng. Ind., Trans ASME, 1982, 104, 389-393.

104. Swift, H. W.,
"Plastic bending under tension", Engineering, 1948, Oct., 333-384.

105. Szilard, R.,
"Theory and analysis of plate-Classical and numerical methods", Prendice Hall, New Jersey, 1974.

106. Tabarrok, B. and Dost, S.,
"Some variational formulations for large deformation analysis of plates", Comp. Meth. Appl. Mech. Engg., 1980, 22, 279-288.

107. Thorne, C. J.,
"Square plates fixes at point", J. Appl. Mech., Trans ASME, 1948, 15, 73-79.

108. Timoshenko, S. P. and Woinowsky-Krierger, S.,
"Theory of plates and shells", 2nd ed., McGraw Hill, New York, 1981.

109. Verguts, H. and Sowerby, R.,
"The pure plastic bending of laminated sheet metals", Int. J. Mech. Sci., 1975, 17, 31-51.

110. Way, S.,
"Bending of circular plates with large deflection", J. Appl. Mech., Trans ASME paper A-56-12, 1933, 1, 627-636.

111. Weil, N. A. and Newmark, N. M.,
"Large plastic deformations of circular membranes", J. Appl. Mech., 1955, 25, 533-538.

112. Westbrook, D. R., Chakrabarti, S. and Cheung, Y. K.,
"A three dimensional finite element method for plate bending", Int. J. Mech. Sci., 1974, 16, 470-487.

113. Witmer, E. A., Balmer, H. A., Leech, J. W. and Pian, T. H. H.,
"Larger dynamic deformations of beams, rings, plates and shells", AIAA Journal, 1963, 1, 8, 1848-1857.

114. Wojno, W. and Wierzbicki, T.,
"Perturbation solution for impulsively loaded viscoplastic plates", Int. J. Non-linear Mech., 1980, 15, 211-223.

115. Yu, T. X. and Johnson, W.,
"The pressbrake bending of rigid/linear work-hardening plates", Int. J. Mech. Sci., 1981, 23, 307-318.

116. Yu, T. X. and Johnson, W.,
"The large elastic-plastic deflection with springback of a circular plate subjected to circumferential moments", J. Appl. Mech., Trans ASME, 1982, 49, 507-651.

Surface contact stresses/friction

117. Archard, J. F.,
"Contact and rubbing of flat surfaces", J. Appl. Phys., 1953, 24, 8, 981-988.

118. Bentall, R. H. and Johnson, K. L.,
"Slip in the rolling contact of two dissimilar elastic rollers", Int. J. Mech. Sci., 1967, 9, 389.

119. Bentall, R. H. and Johnson, K. L.,
"An elastic strip in plane rolling contact", Int. J. Mech. Sci., 1968, 10, 637.

120. Conway, H. D. and Engel, P. A.,
"Contact stresses in slabs due to round rough indenters", Int. J. Mech. Sci., 1969, 11, 709-722.

121. Goodman, L. E.,
"Contact stress analysis of normally loaded rough spheres, J. Appl. Mech., Trans ASME, 1962, 29, 515-522.

122. Greenwood, J. A. and Tabor, D.,
"The properties of model friction junctions", Proc. Phys. Soc., 1958, 71, 989.

123. Greenwood, J. A.,
"The area of contact between rough surfaces and flats", J. Lub. Tech., Trans ASME, 1967, Jan., 81-91.

124. Hahn, H. T. and Levinson, M.,
"Indentation of an elastic layer(s) bounded to a rigid cylinder-I. Quasi-static case without friction", Int. J. Mech. Sci., 1974, 16, 489-502.

125. Hahn, H. T. and Levinson, M.,
"Indentation of an elastic layer(s) bounded to a rigid cylinder-II. Unidirectional slipping with coulomb friction", Int. J. Mech. Sci., 1974, 16, 503-514.

126. Heilmann, P. and Rigney, P. A.,
"Sliding friction of metals", Proc. 7th Leeds-Lyon Symp. on Tribology, held in Inst. Tribology, Dept. Mech. Eng., University of Leeds, 1980, 9-12th Sept., 15-19.

127. Johnson, K. L.,
"Aspect of friction", Proc. 7th Leeds-Lyon Symp. on Tribology, held in Inst. Tribology, Dept. Mech. Eng., University of Leeds, 1980, 9-12th Sept., 2-12.

128. Kragelsky, I. V. and Demkin, N. B.,
"Contact area of rough surfaces", Wear, 1960, 3, 170-187.

129. Ling, F. F.,
"On asperity distributions of metallic surfaces", J. Appl. Phys., 1958, 29, 8, 1168-1174.

130. McFarlane, J. S. and Tabor, D.,
"Adhesion of solids and the effect of surface films", Proc. Roy. Society, Series A, 1950, 202, 224-243.

131. Mindlin, R. D.,
"Compliance of elastic bodies in contact", J. Appl. Mech., Trans ASME, 1949, 16, 259-268.

132. O'Conner, J. J.,
"Compliance under a small torsional couple of an elastic plate pressed between two identical elastic spheres", J. Appl. Mech., Trans. ASME, 1966, 13, 377-383.

133. Poristsky, H.,
"Stresses and deflections of cylindrical bodies in contact with application to contact of gears and of locomotive wheels", J. Appl. Mech., 1950, 17, 191-201.

134. Smith, J. O. and Liu, C. K.,
"Stresses due to tangential and normal loads on an elastic solid with application to some contact stress problems", Trans ASME, J. Appl. Mech., 1953, 50, 157-166.

135. Soong, T. C. and Li, C.,
"The rolling contact of two elastic-layers covered cylinders driving a loaded sheet in nip", Trans ASME, J. Appl. Mech., 1983, 48, 889-894.

136. Soong, T. C. and Li, C.,
"The steady rolling contact of two elastic layer bonded cylinders with a sheet in the nip", Int. J. Mech. Sci., 1981, 23, 263-273.

137. Tabor, D.,
"Junction growth in metallic friction : the role of combined stresses and surface contamination", Proc. Roy. Society, Series A, 1959, 251, 378-393.

138. Timoshenko, S. P. and Goodier, J. N.,
"Theory of elasticity", McGraw Hill, New York, 1970.

139. Tsukizoe, T. and Hisakado, T.,
"On the mechanism of contact between metal surfaces - the penetrating depth and the average clearance", Trans ASME, J. Basic Eng., 1965, 87, 666-673.

140. Tu, Y. O. and Gazis, D. C.,
"The contact problem of a plate pressed between two spheres", J. Appl. Mech., 1964, 31, 659-666.

141. Yoshimoto, G. and Tsukizoe, T.,
"On the mechanism of wear between metal surfaces", Wear, 1957, 1, 472-490.

General

142. Ryder, G. H.,
"Strength of materials", 3rd ed., Macmillan, 1971.

143. Press & Shear Machinery Co. Ltd.,
"Two roll plate rolling and curving", Ind. Equipment News (UK). 1974, Mid-March, 54.

144. Ford, H.,
"Researches into the deformation of metals by cold rolling", Proc. Inst. Mech. Engrs., 1948, 159, 121.

145. Holman, J. P.,
"Experimental methods for engineers". 2nd ed., McGraw Hill, New York, 1971, P329.

146. Nadai, A.,
"Plasticity", McGraw Hill, New York, 1931, P251.

147. Rowe, G. W.,
"Elements of metal working theory", Edward Arnold 1979.

148. Watts, S. B. and Ford, H.,
"An experimental investigation of the yielding of strip between smooth dies", Proc. Inst. Mech. Engrs., 1953, 1B, 448-453.

149. Watts, S. B. and Ford, H.,
"On the basic yield stress curve for a metal", Proc. Inst. Mech. Engrs., 1955, 169, 1141-1149.

150. Hua, M.,
"The mechanics of continuous roller bending of plates", Initial Progress Report, Department of Production Technology and Production Management, Aston University, 1983 ,May.

151. Sengupta, A.K., Fogg, B. and Ghosh, S.K.,
"On the mechanism behind the punch-bank surface conformation in stretch-forming and deep-drawing", J. Mech. Working Technology, 1981, 5, 3-4, 181-210.